UNIVERSITATEA BABEŞ-BOLYAI

Facultatea de Chimie şi Inginerie Chimică

Theoretical studies in cluster chemistry – OR - Synthesis – a Ph adjustment of Ph.D.

Student: Adrian M.V. Brânzanic

Advisor: Prof. Radu Silaghi-Dumitrescu

Ph.D. thesis

Cluj-Napoca, 2020

Motto:

I am not in sympathy with the attitude which favours the repression of certain possible working hypotheses because they are perhaps erroneous, and so may possess no lasting value. Certainly I endeavoured as far as possible to guard myself from error, which might indeed become especially dangerous upon these dizzy heights, for I am entirely aware of the risks of these investigations. However, I do not consider scientific work as a dogmatic contest, but rather as a work done for the increase and deepening of knowledge.[*]

Carl Gustav Jung

---

[*] Carl Gustav Jung, *Psychology of the Unconscious*, translated by Beatrice M. Hinkle, republished by Dover Publications, INC, Mineola, New York, 2018, p. XLVI.

Celui din Milet

Contents

1 Introduction

Motto:

"It is only a slight exaggeration to say

that good physics has at times

been spoiled by poor philosophy."[*]

Werner Heisenberg

---

[*] Werner Heisenberg, *The nature of elementary particles*, Physics Today, March, 1976, p. 32-39.

1.1 The four sapiential stages

Knowledge can be revealed in different forms - and depending on the sharpness of the thought employed in order to open the abyss of truth, knowledge can be perceived at various levels of depth. According to Plato, there are four stages at which this perception of knowledge can occur (cf. Figure 1). The shallowest of them is termed είκασια (eikasia), representing a state which can be perceived only through images and reflections. The term itself derives from the word *εικών* (eikon), which can be translated to *image, face* or *reflection* (the same word represents the etymological root of the modern English word “icon”). As a first step involving the act of perceiving knowledge, it deals with images and their generation. The rather superficial character of this step is best emphasized in Plato’s words when he states that “the visible Universe is an εικών of the intelligible one, which comprise the είδη (eide = ideas)”, and that “time is an image of eternity”. The second step deals with the sensorial perception of the image and it is associated with the view developed from this process. This stage of perceiving is referred to as πίστις (pistis), a term which can be translated to *belief, faith, conviction* (the etymology of the word “piety” can be traced to the Latin equivalent of πίστις, *pietas*). These two steps differ from the next two the same way believing differs from comprehending*. Consequently, the third step represents understanding and is termed διάνοια (dianoia). It also refers to *discursive thinking* and, in general, represents the type of knowledge that can be achieved with the help of sciences. Lastly, the fourth step is επιστήμη (episteme), which represents the true nature of things. This type of knowledge is in opposition to that of δόχα (doxa), which represents *opinions*, and, furthermore, Plato distinguishes επιστήμη from πρακτική (praktike = the science of action) and ποιητική (poietike = the productive science, art, poetry) as being of a pure theoretical nature. He puts the latter two terms at the same level with διάνοια, while he places the first one, δόχα, between the act of knowing the true things, i.e. επιστήμη, and ignorance, to which he refers the act of knowing about untrue things. Thus, the act of achieving an epistemic type of knowledge implies mining through the previous three levels of perception. Although at the dianoic level of knowledge a three-fold degeneracy occurs, Plato’s reasoning emphasizes the need of passing through διάνοια in order to reach επιστήμη, avoiding, thus, the other two, πρακτική and ποιητική. In other words, a symmetry breaking is required in order to remove the dianoic degeneracy such that the epistemic level of knowledge can be achieved, a symmetry breaking that quite resembles the Jahn-Teller effect of fame in modern physical

---

* Heisenberg, p.32. Cf. section 1.4.

chemistry. If in the latter (Jahn-Teller) case the geometry of a molecule is distorted along one of its symmetry axis such that a more energetically favorable state is achieved, in the former, the 3rd level of knowledge is distorted along the "διάνοια axis" such that a deeper kind of knowledge (i.e. επιστήμη) can be achieved.

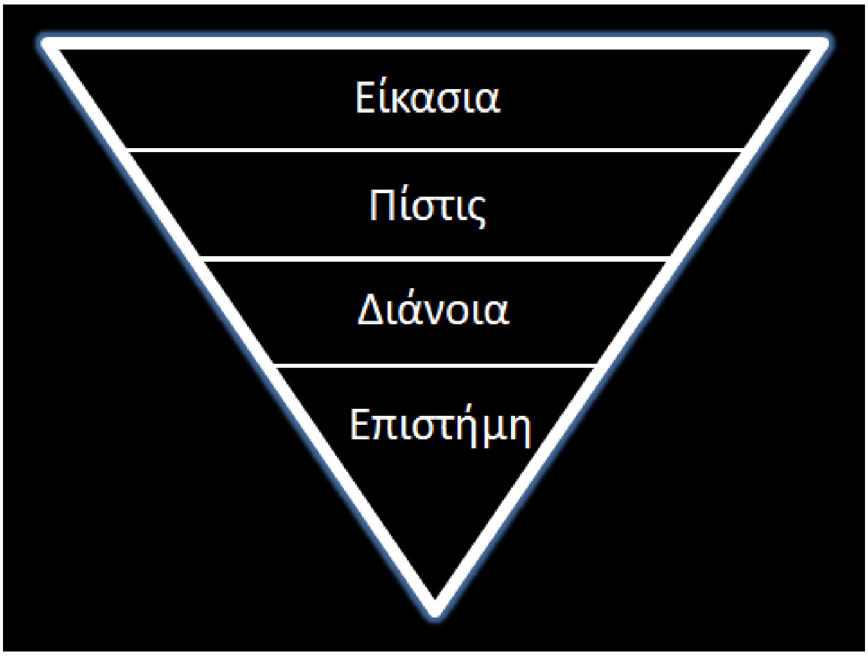

Figure 1. The four stages of the perception of knowledge cf. Plato

The subtle difference between διάνοια and επιστήμη is exemplified in an enlightening manner by Werner Heisenberg in his *"Philosophical Problems of Quantum Physics, p.32",* where he notes: "*Consider a man, whom we believe we know well, suddenly committing some misdeed which is at first quite incomprehensible. Those who know all the details of the case can then explain the reasons for his action. Thus we are in a position to deal with all the arguments, one after the other, and eventually, after a thorough investigation of these arguments we may understand the wrong he committed. This understanding corresponds to διάνοια. Or alternatively we may suddenly realize that this man* ***had*** *to act as he did. This sort of recognition can be described Plato's επιστήμη.*" Interestingly by the manner in which the outcome is revealed, the *sudden* epistemic recognition of the truth, which Heisenberg details in his example, resembles the *spontaneous* breaking of symmetry that implies the Jahn-Teller effect. Thus, in a ludic fashion, it can be asserted that the epistemic Jahn-Teller metaphor discussed above shares soil with Heisenberg's philosophic view. Regarding the role of modern science, Heisenberg stresses that the physical explanation of Nature is a discussion aimed to distinguish διάνοια from επιστήμη. Regardless if the latter stage is achieved or not, it emphasizes the exclusion of the first two steps of knowledge from the domain in which scientific reasoning should manifest itself.

1.2 The *eide*

Returning to the deepest level of perception of things, Plato believes that in order to reach the epistemic level of knowledge, the true nature of things needs to be known. In his view, the είδη (eide) constitutes the true nature of things that, like in the above-mentioned example regarding the intelligible Universe, are hindered behind appearance. The concept of είδη, of the indivisible and eternal entities that lay within the kernel of things, was developed in contrast with the pre-Socratic philosophy which, bearing Heraclitus as exponent, viewed change and fluctuation as the essence of Nature (cf. the famous Heraclitian aphorism *Πάντα ῥέι* = Everything flows). Consequently in this line of thought, as everything changes there is no true nature of things, the only constant in Nature being change itself. This fluctuation restricts the achievement of the epistemic level of knowledge and constrains the view of the world within the borders of illusion and temporal truths that are susceptible to fade as time prolongs. In this framework, the highest act of knowing is represented by a πίστις → διάνοια transition. Plato rejected this framework as the fundamental view of the world and concluded that, in order to achieve the true form of knowledge (i.e. επιστήμη), the core of reality should not be subject to change. Interestingly, he refutes the somehow similar atomistic views of Democritus for being materialistic and in a suggestive metaphor he compares its followers to the Titans, while the Olympians are represented by the seekers of επιστήμη by means of transcending to a suprasensible picture of reality through the use of the είδη. Indeed a godly clash that dislocated the highest act of knowing from a πίστις → διάνοια transition to a διάνοια → επιστήμη transition…

The είδη represent the essence of things, the *ideas* that are the fundament of every object. They are of suprasensible nature, meaning that they cannot be grasped through sensorial means. Nevertheless, they can be reached through various rational processes, such as recollection (ανάμνεσις) and different forms of dialectics (διαλεκτική). For instance, one of the first dialectical processes consisted in a regression from a hypothesis towards an unhypothesized principle, αρχή. Later, the dialectical process involved a collection/reunion (συναγωγή) followed by a primer division (διαίρεσις) which continues via a second, specific division (διαφορά) downwards the ultimate, indivisible έιδος. Examples of eide are found in each class of things such as mathematics, in natural and artificial objects, in relations or even ethics, beauty, goodness. Some of the είδη play a more important role. For instance, for Plato the greatest kinds of είδη are the *Being*, the *Same*, the *Different*, the *Movement* and the *Rest*. By their nature, the είδη are transcendent and form the class of objects by which epistemic knowledge can be revealed. Their collection forms the *τόπος νοητός,* the intelligible place, are represented as the first concentric circle in Figure 2:

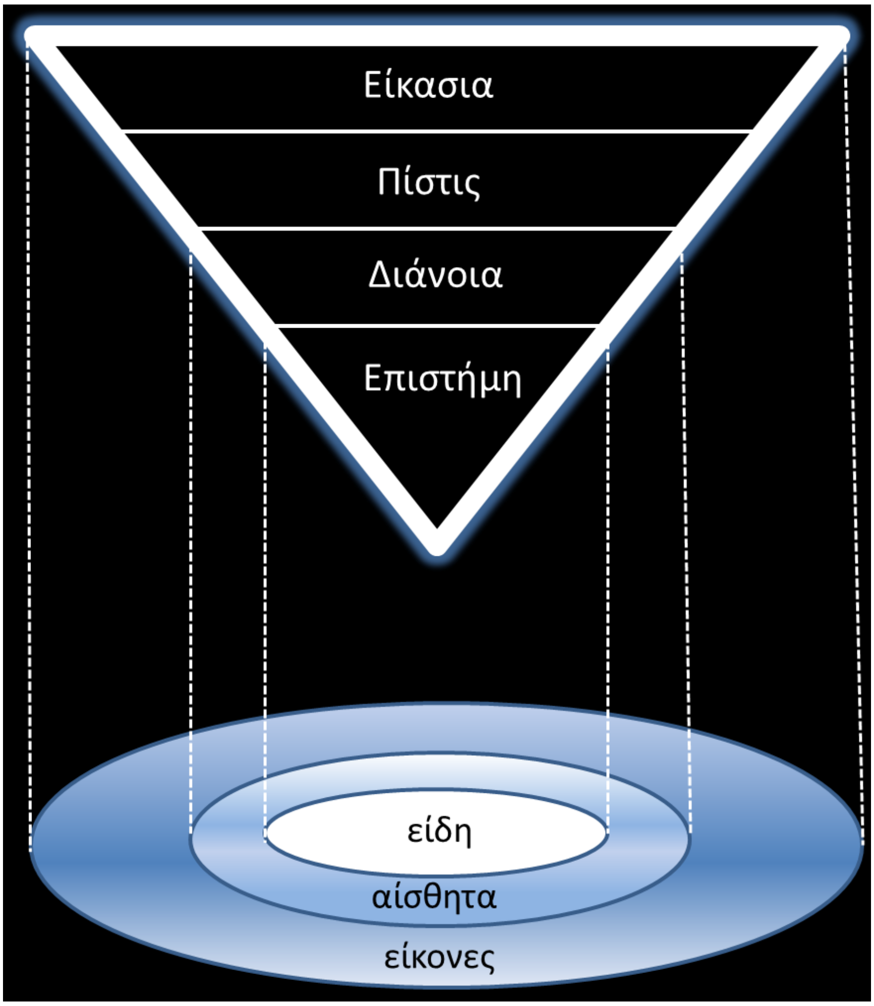

Figure 2. The classes of objects characteristic for different types of knowledge and their corresponding topos: *τόπος νοητός* in white*;* *κόσμος* and its illusory extension in blue.

Αἴσθησις (aisthesis) represents the sensible nature of things and the objects by which it can be perceived are referred to as *αἴσθητα* (aistheta). They are the source of sensation which, in itself, was regarded as the transition of a sensible entity from its potency (*δύναμις)* to its act (*ἐνέργεια*). Thus, the sensibles, *αἴσθητα,* are objects that are capable of being perceived. They cannot lead to an epistemic level of knowledge but are limited to a dianoic level of knowledge (cf. Figure 2) and therefore can only express opinions. They can still, however, retrieve a deeper level of knowledge than the *είκονες* (eikones) which represent the images, reflections and shadows of things that are therefore restricted to *είκασια* and *πίστις* levels of truth. The topos of the sensibles (second concentric circle in Figure 2) bears a name that, through its modern meaning, also emphasizes the alteration that the ancient Greek concepts suffered through the ages: *κόσμος* (cosmos).

The transition from έιδος to αίσθησις is achieved through the intermediate class of the *μέταξύ* (metaxy) which, like the eide, are also eternal. The process itself was referred to as *μέθηξισ* (methexis) which means *participation*. The difference between the eide and metaxy consists in the plurality nature which the later adopt. Such metaxy objects are represented by the objects of mathematics and geometry. For instance, the ideal numbers (αριτμόι ειδητική) are of such character and can modulate the transition between the world of the suprasensible and material world. In some aspects, this picture is not that different from our today’s scientific method, which starts from empirical investigations of material objects and then baths in mathematics in order to build models that can offer prediction. At this stage, more often than not, the similarity ends. The process is no longer descended towards the eide, but rather, in a boomerang manner, is redirected back towards the material world. Perhaps this is one of the crucial differences between us and the Elders. Often enough we restrain our mathematical endeavors to the practical aspects of reality and to its predictability. Blinded by the tempting shine of practical predictions, we ignore the underlying mysteries of the suprasensible world; we too often *shut up and calculate.*

1.3 About this thesis

1.3.1 Manifesto

"Lessing, the most honest of theoretical men, dared to state openly that searching for the truth meant more to him than truth itself; thereby the fundamental secret of science is revealed, much to the astonishment, indeed annoyance, of the scientifically minded. Admittedly, alongside this isolated recognition (which represents an excess of honesty, if not of arrogance), one also finds a profound delusion which first appeared in the person of Socrates, namely the imperturbable belief that thought, as it follows the thread of causality, reaches down into the deepest abysses of being, and that it is capable, not simply of understanding existence, but even of correcting it. This sublime metaphysical illusion is an instinct which belongs inseparably to science, and leads it to its limits time after time, at which point it must transform itself into art; which is actually, given this mechanism, what it has been aiming at all along."[*]

"The regions of science lie far asunder. Their ways of handling their subject matters are fundamentally different. This disintegrated multiplicity of disciplines is still meaningfully maintained today only through the technical organization of universities and faculties and through the practical aims of the disciplines. Yet the rootedness of the sciences in their essential ground has atrophied. In all its areas, science today is a technical, practical matter of gaining information and communicating it. No awakening of the spirit at all can proceed from it as science. Science itself needs such an awakening."[†]

This thesis represesnts the zeroth order term of an attempt towards such an awakening.

1.3.2 Structure

This PhD endeavor can be regarded as a diastole-systole ontological breathing effort. Within the diastole step (left side of Figure 3) a transcendent dive is done into the matter of things by which, in the systole step (right side of Figure 3), a transcendental extraction of available truth is presented as means to justify the original contribution to Science that this PhD offers.

---

[*] Nietzsche, p. 73 (English). Cf. section 1.4.

[†] Heidegger, *Introduction to Metaphysics*, p. 51 (English). Cf. section 1.4.

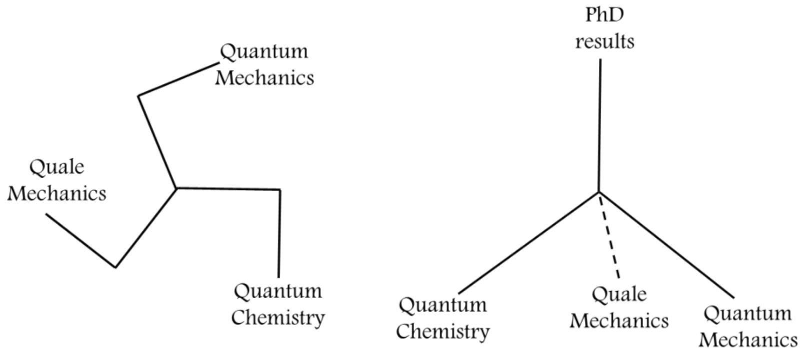

Figure 3. Scheme of current PhD thesis ontological breath.

The present Ph.D. thesis may be argued to entail an *Apollonian-Dionysian* duality. An *Apollonian* character pertains to the majority of the text (metallaboranes, the majority of the study on sulfite reductase), while the philosophical discussions, encountered mainly in the first two chapters of this thesis and in its epilogue, are of *Dionysian* character. The result of the achieved *Apollonian-Dionysian fusion* is best emphasized in the *4.2 Pars ballistica: Why does sulfite reductase employ siroheme?* subchapter which, by revealing the reason behind sulfite reductase's choice for the siroheme, may be viewed as the apex of this thesis in the terms illustrated in Figure 1. In terms of the levels of truth that were surpassed, the question *why does sulfite reductase employ siroheme?* has reached its level where, with regards to the available truth remaining to be unveiled by this question (i.e. none), an epistemic character may be asserted. The *Dionysian* emerges as a thesis which is soon-after complemented by an *Apollonian* antithesis. For instance, in chapter 4.2, the role of siroheme within the sulfite reductase enzyme was first envisioned (i.e a *Dionysian* way) in the thesis that siroheme enhances the enzyme's electron transfer ability; its antithesis would imply that siroheme inhibits those processes. In *Apollonian* manner, the electron transfer ability of sulfite reductase was computed - showing that the reason behind the enzyme's choice for siroheme is an interplay of both thesis and antithesis, as some electron transfer routes were found to be inhibited while others promoted. Thus, a unification of a thesis and its antithesis was achieved which, technically stated, represents a *synthesis*. The title of this dissertation emphasizes this development. Furthermore, it alludes to a need to resurrect the philosophical part of the scientific endeavor and states that such a resurrection is done within its pages. The *Ph in Ph.D. is thus adjusted*. We express this by the metaphorical use of the chemical concept of pH such that the title of this dissertation embodies the "acidity" of the problematic use of Philosophy in Science.

1.4 Chapter Bibliography

1. Francis E. Peters, *Greek Philosophical Terms,* New York University Press, New York, USA, **1967.** The Romanian translation by D. Stoianovici: Francis E.Peters, *Termenii filozofiei grecesti*, Editura Humanitas, Bucuresti, Romania, **2007**.
2. Werner Heisenberg, *Philosophical problems of Quantum Physics,* translated by F.C. Hayes, reprint published by Ox Bow Press, Woodbridge, Connecticut, USA, **1979.**
3. Martin Heidegger, *Introducere in metafizica*, translated by G. Liiceanu and T. Kleininger, Editura Humanitas, Bucuresti, Romania, **2011**. Translated in English by G. Fried and R.Polt: Martin Heidegger, *Introduction to Metaphysics*, Yale University Press, USA, **2000.**
4. Martin Heidegger, *Fiinta si Timp*, translated by G. Liiceanu and C. Cioaba, Editura Humanitas, Bucuresti, Romania, **2006.**
5. Martin Heidegger, *Conceptele fundamentale ale metafizicii*, translated by P. G. Sandu, Editura Humanitas, Bucuresti, **2019.**
6. Vasile Frateanu, *Tratat de metafizica*, Editura ASCR, Cluj-Napoca, Romania, **2014**.
7. Friedrich Nietzsche, *Nasterea Tragediei*, translated by L. Pricop, Editura Cartex, Bucuresti, 2018. English translation by R. Speirs: Friedrich Nietzsche, *The Birth of Tragedy and Other Writings*, Cambridge University Press, Cambridge, UK, **2007.**
8. Stephen W. Hawking, *Scurta istorie a timpului*, translated by M. Ciodaru, Editura Humanitas, Bucuresti, **2001.**
9. Roger Penrose, *Cycles of Time*, Vintage Random House, London, UK, **2010.**

2 The elements

Motto:

"Chemistarum studium in sensuabilus insensualem

illam veritatem a suis compedibus liberare."[*]

Dorneus

---

[*] "It is the study of the Chemists to liberate that unsensual truth from its fetters in things of sense." Cited by C.G. Jung in *Aion. Researches into the Phenomenology of the Self*, second edition, translated by F.C. Hull, Princeton University Press, 1968, pag.201.

2.1 Elements of Quantum Mechanics

The godly clash between materialism and the suprasensible picture of the world recurred at the dawn of the 20th century. This time, the Titans had the Newtonian Mechanics at their disposal, while the young Olympians were forging their new approach in order to extend the old mechanics: the approach which soon became coined Quantum Mechanics. It is quite a funny historical coincidence when one recalls Newton's reference to the standing on the shoulders of Giants as the reason for his far-reaching sight (i.e. the *nanos gigantum humeris insidentes* metaphor). Although far-reaching, his sight could not help him foresee that by standing on the shoulders of Giants he will become himself a Giant* in Plato's godly clash metaphor.

By the end of the 19th century, the Newtonian Mechanics had reached an undisputed status as governing ontological tool by which humankind could ultimately grasp the true nature of the physical reality and, therefore, nature itself. Indeed, the *titanic* endeavor pursued by Newton's intellectual descendants such as Lagrange and Hamilton (who upgraded Newton's Mechanics) or Maxwell (who managed to provide a unitary description of the magnetic and electrical forces and therefore unite them under a common electromagnetic interaction) had managed to unveil the vast majority of mysteries hidden beneath the known-at-that-time aspects of Nature. There were, however, still some exotic phenomena such as the spectra of the black-body radiation and the emissions of atoms that were still not fully understood but were believed to be soon comprehensible by the virtue of Newtonian Mechanics. This atmosphere within the scientific world is perhaps best emphasized by the advice that Planck had received with regards to the study of physics: to abandon it as there is nothing left to be discovered beside these soon to be solved exotic issues.

Nevertheless, Planck can be regarded as an *Olympian-Titanic* chimera that, by still holding ground within the realm of Newtonian Mechanics, managed to provide a pivotal foot ground in the darkness lying ahead towards the suprasensible nature of what will later become Quantum Mechanics. Indeed, as it is often recalled, Planck's solution for the black-body radiation problem was the first shot in the dark; a shot that by hitting its target submitted the foundation of Classical Mechanics into a crisis. It was so because, in developing his explanation, Planck had hypothesized that the oscillating atoms constituting

---

*The etymology of the word *giant* is found in the Latin *Gigantes*, which denotes the Roman equivalent of the Greek Titan gods.

the walls of the black-body can transfer light only in discrete quantities of an elementary unit of light – a quanta. This was against Newtonian dogma that saw no reason for which this process should not be done in incremental amounts of light. Thus, while Newtonian Mechanics suggested a continuous range of energy by which the black-body radiation could be emitted, Planck's shot in the dark implied the opposite, that it can be emitted only in amounts of energy which were an integer multiple of an elementary energy.

It was in 1901 that Planck published his results, and the general impression under which they were received was skeptical. Planck's shot in the dark seemed as a fortunate accident and was regarded as a provisional result that was expected to be corrected and sustained within the Newtonian dogma. Planck himself tried to reconcile the two antagonistic approaches but it was too late. The shot in the dark he had taken provoked an avalanche. In 1905, in his *annus mirabilis*, Einstein further employed Planck's quanta hypothesis in order to explain the photoelectric effect. In doing so, Einstein brought confusion with regards to an aspect that was thought to be clearly understood, that is, the undulatory nature of light. Historically, Newton managed to establish the field of Optics by considering light as being of corpuscular nature. This was later shown to be incorrect by Huygens who, by treating light as an undulatory phenomenon, managed not only to reproduce the results of Newton's Optics, but also could provide explanations where the former failed: namely in the process of the diffraction of light. Thus the particle-like behavior of light, which was thought of as a particular description embodied in the general undulatory theory provided by Huygens, was revived by Einstein in his reasoning behind the photoelectric effect. The fundamental mystery that laid behind this effect consisted in the nature of the dependence that the ejected electrons displayed when removed from a light-ionized material. Namely, the number of such electrons (accountable by the intensity of the current that they were developing when connected to an electric circuit) was dependent on the frequency of the incident ionizing light and independent of its intensity. This was contrary to what one might expect from the undulatory behavior of light. Indeed, if light was to be of wave-like nature, the number of ejected electrons ought to be dependent on its intensity. This is so because the intensity of light is directly linked to the amount of energy it possess and thus to the amount of energy available to kick electrons out of their hosting material. The dependence on frequency, however, implied that only some specific amounts of energy can yield electron ejections. Einstein managed to explain this frequency dependence by employing Planck's quantas of light as elementary particles constituting light itself. Thus, light appeared to behave in some situations as a wave and in others as particle. This aspect became known as the wave-particle duality of light.

The charge distribution within atoms was eventually clarified in 1911 when Rutherford, by scattering radiation upon atoms, managed to prove that atoms concentrate their positive charge in a point-like center, which is surrounded by a uniformly distributed negative charge. The positively charged nucleus was thus shown to be composed of protons and to be minute in comparison to the entire atomic volume, while the electrons formed the negatively charged medium that surrounded it and accounted for the vast majority of the atomic volume. In 1913 Bohr rationalized Rutherford's discovery in terms of stationary orbits that the electrons would adopt in their trajectories around the nucleus (stationary - with regard to the electromagnetic exchange that an electron ought to have with the surrounding medium when adopting these favorable orbits). From classical electrodynamics it was expected that an electron orbiting a nucleus would emit electromagnetic radiation due to being under a constant influence of the electrostatic force (and thus subject to acceleration; classical electrodynamics implies that an electric charge in accelerated movement would emit electromagnetic radiation). The loss of energy due to the radiating process would be responsible for a decrease of the electron's kinetic energy which would cause an imbalance in the favor of the centripetal electrostatic force. Ultimately, the electron would be doomed to collapse unto the nucleus. Bohr hypothesized that there ought to be some special orbits within which this radiative process would cease to exist (i.e. stationary states) and managed to explain the emission spectra of the hydrogen atom in terms of transitions between these stationary states. For instance, transitioning from a lower-energy stationary orbit to a higher-energy one, energy in the form of electromagnetic radiation would need to be added. Oppositely, an electron would output electromagnetic radiation when descending from a high-energy orbit to a lower-lying one. For all other infinite possible trajectories that an electron might adopt when orbiting the nucleus, the classical electromagnetic dogma would still hold as the electron would lose energy by emitting radiation but now, in its descend, would be caught in the safety-net of its proximal stationary orbit. Thus the planetary model of the atom was established and another anomaly was explained in terms of discrete phenomena (i.e. fixed values corresponding to interorbital transitions) as opposed to the continuous, incremental approaches adopted in classical physics. Furthermore, Bohr also showed that the stationary orbits that he hypothesized contained an amount of angular moment which was an integer multiple of the constant that Planck had devised in his discrete description of the black-body radiation spectrum. It was the same Planck's constant that Einstein also used in explaining the photoelectric effect and that was now appearing in the motion adopted by the electron in the favorable, stationary trajectories inside atoms.

The wave-particle dual character of light was extended by de Broglie in 1924 to particles. It was in his PhD thesis where he showed that, under convenient circumstances, the electrons should behave like waves and diffract similarly to how light normally does. The same constant of Planck's appeared again. This time, however, it became clearer what it really is: the embodiment of the wave-particle duality itself, as it showed that for any given object, the amount of wave-like character that the object possess (provided by its wavelength measure λ) and the amount of its particle-like character (provided by its momentum p) is constant:

$$\hbar = \lambda \cdot p$$

Equation 1.

The first mathematical formulation of Quantum Mechanics was established in 1925 by Heisenberg. The approach he adopted marks the end of the chimeric quantum-classical era (marked as the period of the Old Quantum Theory) and the dawn of the pure Olympian era of the Quantum Theory (also referred to as the New Quantum Theory). Heisenberg abandoned the concept of electron trajectories and relied solely on the observable quantities that were available from experiments. These were the energies of what Bohr called stationary states and Heisenberg associated them to virtual oscillators that were within the atom. He then coupled these virtual oscillators in terms of the transition energies known from atomic emission spectra. The revolutionary approach consisted in working with quantities which were associated with two states and not with one. For instance, when concerned with the trajectory of an electron within a stationary orbit, one might be interested in quantities such as velocity, position or momentum in terms of the energy associated with the respective stationary orbit. In other words, in quantities associated with a state. Heisenberg neglected these quantities and treated the known experimental data in terms of energies that coupled virtual oscillators corresponding to Bohr's stationary orbits, i.e. quantities associated with two states. In doing so, he stumbled upon a new quantum multiplication rule which, also to his dismay, was non-commutative in nature. Soon after he urged Heisenberg to publish his new approach, Born recognized that the non-commutative character of this new multiplication rule was similar to the non-commutative nature of some less familiar, exotic mathematical objects that he had encountered at some point earlier in his life: matrices. By this time, however, Heisenberg departed to Copenhagen, at Bohr's institute. Thus, Born had to ask his other prominent assistant, Pauli, to help him formulate in terms of matrices Heisenberg's approach. Convinced that the path of matrices will be just a mathematical complication, Pauli refused. He expressed this by warning Born that he will spoil Heisenberg with his mathematical endeavors. Nevertheless, Born was not disheartened and managed to spark the interest of one of his other pupils, Jordan. Together, in the same year (1925), they published the first formulation of quantum mechanics in terms of matrices. Heisenberg joined Jordan and Born, and together published, still in 1925, the paper that marked the birth of Matrix Mechanics. It was still 1925 and now Pauli redeemed himself by adopting and finally mastering the new matrix formulation. In doing so, he managed to discover two new fundamental quantum concepts: the two-valued nature of the electron with respect to a non-classical coordinate (which in the following year was observed experimentally and denoted as the *spin* of the electron) and the Exclusion Principle.

The following year, 1926, further marked the development of Quantum Theory. Firstly, Schrödinger adopted de Broglie's wave description of electrons and conceived in terms of wavefunctions a new approach to the quantum phenomena. His work on this subject marked the birth of Wave Mechanics. Then Born, again quick in reactions, provided within the same year the interpretation of Schrödinger's wavefunction as the amplitude that when squared retrieves the probability of finding in a certain location the quantum object that it describes. Subsequently, Heisenberg formulated the Uncertainty Principle, which states that some quantum quantities cannot be simultaneously precisely known. Such quantities became reffered to as complementary objects and could be identified by possessing mathematical descriptors which did not commute with each other. If the descriptors of two quantities commuted, then both quantities could simultaneously be known with precision. For instance, the position x and momentum p of particle cannot be simultaneously known. Similarly, there is an uncertainty between the adopted energy in an interval of time:

$$\begin{cases} \Delta x \Delta p \geq \frac{\hbar}{2} \\ \Delta E \Delta t \geq \frac{\hbar}{2} \end{cases}$$

Equation 2.

From 1926 to 1928, Dirac had managed to synthesize the newly developed quantum theories and then further provided his own crucial contributions to their development. He firstly demonstrated the equivalency between the matrix and the wavefunction formulations of Quantum Theory (together with the work of Jordan which became known as the Dirac-Jordan Transformation Theory; the equivalency, however, was also demonstrated independently by Schrödinger). He then managed to provide a connection, in terms of Poisson brackets, between Quantum Theory and the classical Hamiltonian Dynamics. His attempt to reconcile Quantum Theory with the Theory of Relativity led him to develop what was afterwards known as the Dirac equation. The relativistic treatment employed on Quantum Theory yielded, via this equation, in a natural way the concept of spin and also predicted the existence of antimatter.

At this point the ingredients for the foundation of a rigorous theory describing the quantum phenomena were set. The accomplished theory became known as Quantum Mechanics which, like other fundamental theories, is axiomatic in nature. The set of axioms adopted within Quantum Mechanics were based on the earlier results of the matrix and wave formulations and is comprised of six axioms.

The first axiom implies that each quantum state is characterized by a wavefunction, Ψ, which upon squaring retrieves the probability density associated with that state. All available information regarding the particular state is embedded within the wavefunction. For instance, if one might be interested in the position of particle within a certain state, the square of the wavefunction describing that state would map the space adopted by that state in terms of a probability of finding the particle in each point of the space occupied by the state. This axiom descends from Schrödinger's Wave Mechanics and Bohr's interpretation of the wavefunction.

The second axiom states that observable quantities are represented by mathematical operators that act upon the wavefunction. From a mathematical standpoint, these operations are done in a specific abstract space known as the Hilbert space. This axiom incorporates the essence of the earlier matrix formulation.

The third axiom assures that the evolution in time of a quantum state is described by the time-dependent Schrödinger equation:

$$i\hbar\frac{\partial\Psi}{\partial t} = \hat{H}\Psi$$

Equation 3.

where Ψ is the wavefunction describing the quantum state and $\hat{H}$ is the Hamiltonian operator.

The fourth axiom states that the result of a single experiment retrieves only one eigenvalue of the operator associated with the quantity sought by the experiment.

An eigenvalue problem implies that the outcome of an operator acting on a function will be the same function times a constant. If the function is represented by a wavefunction Ψ and the operator is generally noted as $\hat{O}$, then the eigenvalue problem can be written as:

$$\hat{O}\Psi = \omega_i\Psi$$

Equation 4.

where ω_i represents the entire set of constants that are solutions to the eigenvalue problem. The constants themselves are named eigenvalues and their set, referred to as spectrum, are specific for each operator. For instance, if the wavefunction describes the hydrogen atom, a Hamiltonian operator acting upon it will retrieve the (eigen)energies of the system: the energy of the 1s orbital, of 2s , 2p and so on. Thus, the fourth axiom implies that when trying to measure an electronic state within the H atom, for instance, one would obtain one of its available eigenstates (not two, not more). Both this and previous axioms are assumed from Schrödinger's wave-mechanical considerations.

The fifth axiom implies the existence of a spin degree of freedom for each quantum particle. This comes from experimental evidence. Like mentioned earlier, the relativistic treatment of quantum mechanics, however, retrieves the spin concept in a natural way.

The sixth axiom states that a wavefunction describing a set of bosons (=particles that possess an integer spin number) has to be symmetric while a wavefunction describing a set of fermions (=particles possessing a half-integer spin number) has to be antisymmetric. This implies that when exchanging the positions of two bosons, the wavefunction describing them remains the same:

$$\Psi_{1-2}^{bosons} = \Psi_{2-1}^{bosons}$$

Equation 5.

while for fermionic particles it changes sign:

$$\Psi_{1-2}^{fermions} = -\Psi_{2-1}^{fermions}$$

Equation 6.

This last axiom comes from experimental considerations which also provided the basis of Pauli's spin statistics.

Quantum phenomena are not restricted to discrete phenomena. In fact, the specific quantum discreteness appears only in bounded systems while for non-bounded ones particles can adopt a continuous range of states similar to the way they do in Classical Mechanics. For instance, an electron bounded to a nucleus will adopt a discrete range of energetic levels, while as a free-particle, such as in scattering experiments, the same electron can adopt a continuous range of energy states. In Quantum Mechanics the *Natura non facit saltus* classical dogma becomes *Natura ligatum facit saltus et natura liberum non facit saltus.*

An example encapsulating quantum phenomena can be given in the form of the Casimir effect. When two metal rods are placed in vacuum very close to each other (cf. the black bars in Figure 4), they experience an attractive interaction which, although small in magnitude, turns out to be far greater than if caused by gravitational attraction alone. The reason why they attract has been interpreted in a few ways – but among these is a pure quantum mechanical effect. Thus, in fact, the bars are not attracted to each other, but are being pushed to each other. This Casimir effect may thus be seen as an interplay of continuous and discrete states of matter embedded in Heisenberg's Uncertainty Principle. Due to the latter, vacuum may be interpreted to not be empty after all. Due to the complementary nature of energy and time, as shown in Equation 2, the uncertainty of one measure is coupled to the other. Thus for brief amounts of time, when Δt becomes very small, a significant fluctuation of energy, ΔE, may appear. The way in which this increase of energy manifests itself is by spontaneously generating pairs of particles and antiparticles that will exist for limited amount of time, Δt of Equation 2, after which they will annihilate themselves by recombining. The reaction between a particle and its antiparticle converts the full amount energy stored inside them in the form of mass, into pure energy in the form of photons. For instance, when an electron collides with a positron, two isoenergetic photons are released, each bearing a 0.51 MeV energy corresponding to the electron mass converted into energy via Einstein's $E = mc^2$. For a minute amount of time Δt corresponding via Equation 2 to the 1.02 MeV amount of ΔE, a pair of electron and positron will appear. Out of nowhere 1.02 MeV of energy is borrowed for the positron-electron generation, which will be repaid when the 1.02 MeV resulting from their annihilation returns back to nowhere. These transactions are allowed only during the Δt amount of time corresponding to the required particle-antiparticle energy. Do to the recurring generation-annihilation processes, the ground state energy of vacuum is higher than zero. Its inherent fluctuations cause a continuous range of energetic states that can be adopted. In the case of the Casimir rods, these positron-electron generation and annihilation processes occur in the vacuum outside rods as well in the vacuum between the two rods (cf. upper half of Figure 4). There is, however, a dramatic difference between the ways these processes manifest themselves outside the rods and between the rods. Confined within the region between the rods, the generated particles behave like textbook examples of particle-in-the-box systems and, similar to electrons confined in atoms, can only adopt a discrete set of energies. For the regions outside the rods, particles are no longer confined as they are limited only in one direction by a rod. Consequently, they can adopt a continuous range of energies (lower half of Figure 4). Now, for each discrete energy state resulting between the rods, there will be an associated pressure exerted upon the rods. The pressure results from the occasional collisions between the particles corresponding to the discrete states and the walls of the rods. For each such discrete state between the rods, there will be an isoenergetic state outside the rods which will balance the rods by manifesting an equal amount of pressure from outside the rods. Furthermore, within the outside region there will be a continuous range of states between those corresponding to the discrete levels present between the rods. Consequently, the pressures associated with these non-discrete values of energies will not be balanced by corresponding pressures between the rods simply because the energies required by such pressures cannot be developed in a confined space (i.e. a bounded system). Thus, the overall pressure appearing outside the rods will exceed the one appearing between the rods and therefore will push the rods towards each other. The Casimir concept can be further elaborated to interpret gravitation itself, as done by Sernelius.[1]

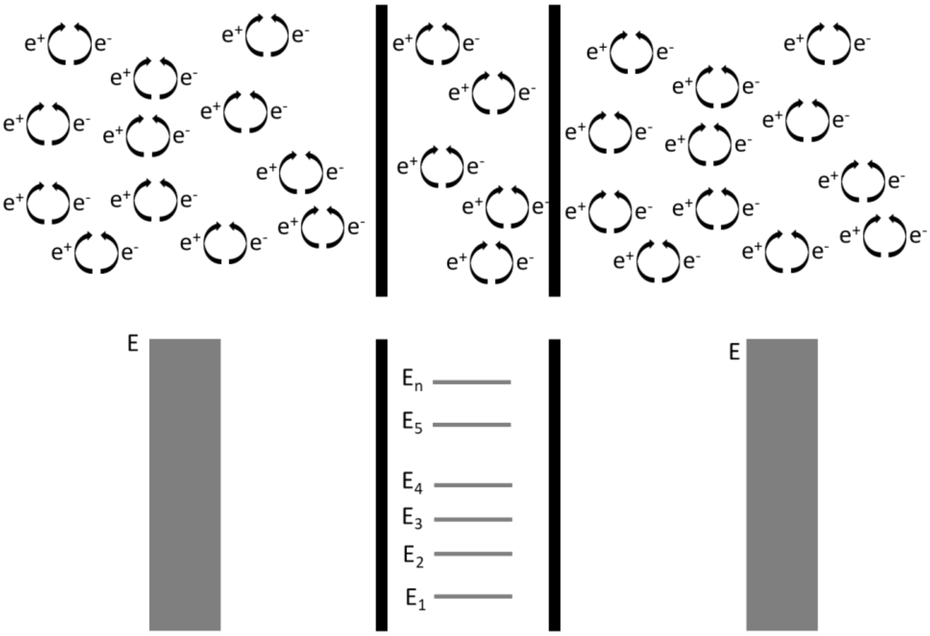

Figure 4. The Casimir effect.

2.2 Elements of Quale Mechanics

By the term *Quale Mechanics* we refer to the qualitative aspects of *Quantum Mechanics* that are susceptible of metaphysical considerations. This infant domain that we propose here can serve as a first hand approximation that can ease the understanding of fundamental quantum mechanical concepts. Beyond this, *Quale Mechanics* can be regarded as a polydentate ligand that chelates the axiomatic system of *Quantum Mechanics* onto *Metaphysics* and thus offering a funneling of the rigid axiomatic QM system into a domain that is fertile with regards to interpretations.

Quantum Mechanics (QM) represents the most accurate mathematical framework which can be employed in order to describe and predict the natural phenomena occurring at the atom-size dimensions of reality. It represents the scaffold on which Quantum Theory (QT) resides the weight of its interpretations and the spring from which fields of quantic phenomena branch into technological applications.

A proposed hierarchical structure of Quantum Theory is presented in Figure 5. At the core of this classification lies the mathematical apparatus specific to this theory, coined "Quantum Mechanics". This mathematical theory starts from an axiomatic system, dubbed the Quantum Mechanical Axiomatic System (QMAS), which is further developed into theorems and statements. Each mathematical proposition constructed within this framework adds to the size of the group. This growth can be pictured as an *encapsulated expansion*, as each new statement will extend the size of the group, but it will not bring any new information that was not hindered within the group's essence (i.e. the QMAS). Mathematics is the tool that processes the QMAS inherent truth into aspects specific to certain situations.

Quantum Theory is a generalization of Quantum Mechanics, not in a mathematical sense (because Quantum Mechanics is regarded as a closed system), but in the sense that the former is a global group in which the latter is part as a subgroup. For the QM case it can be asserted that an epistemological level of knowledge can be achieved because any complex "why" type of a question can be mathematically traced to its fundamental axioms. From the QM point of view there is no other truth laying beyond its axiomatic system and, although it can always be extended, it can be as closed (mathematical) system because all further-to-be-generated truth can be derived from previous generated truth and so on, further down to the zero-level unquestionable set of truths: to the QMAS. Within QM there is no other type of truth that is not *genetically* related to the QMAS.

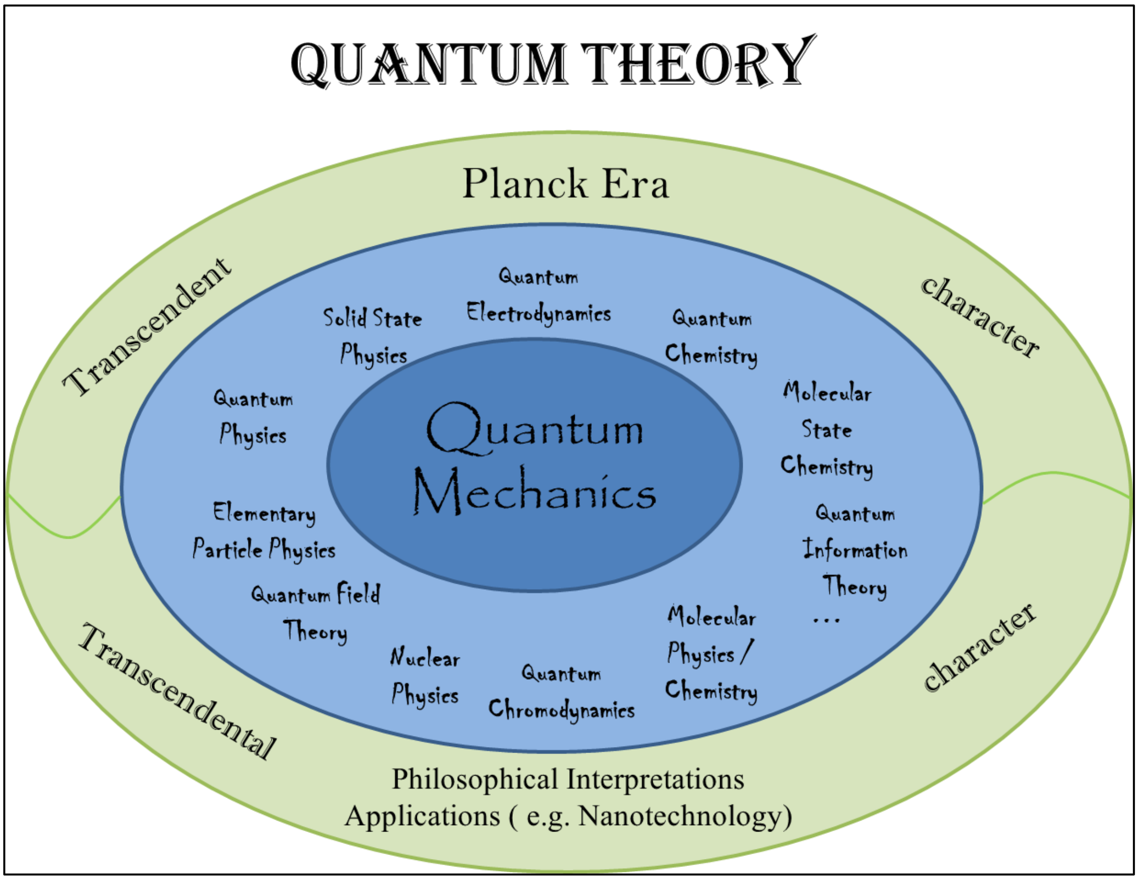

Figure 5. A hierarchical structure of Quantum Theory at the core of which lies the mathematical apparatus in the form of Quantum Mechanics. The second layer represents the further sprung quantum based scientific domains. The third layer denotes the two orientations the theory has: facing towards human perception and comfort are, respectively, its philosophical interpretation and its applications; facing toward its transcendent truth is the Planck Era of the Universe.

On the other hand, the global Quantum Theory group also comprises that part of intellectual activity that casts the “why” question on the very essence of Quantum Mechanics (i.e. QMAS), namely the philosophical aspect of the “Interpretation of QM” subgroup. Applying the philosophical drill on the QMAS leads to its transcendence into a domain in which it can no longer be expected that an epistemological level of knowledge can be achieved. There is a two-folded reason why it can be stated that this has not been achieved, which may be presented in a Kantian manner as follows:

- From a transcendental point of view, i.e. from the point of view starting from the QMAS and heading towards the human preceptor (the observer), it has not been answered which of the QM interpretations (Copenhagen, Bohm - de

Broglie) is correct. As a matter of fact, recently it has been shown that neither of interpretations known to date can be correct.[2]

- From a transcendent point of view, i.e. from the point view departing on the opposing side from the QMAS towards a deeper essence of truth, it can be stated that all effects (including the QMAS itself) in the Universe can be traced back, cause by cause, to a cause that will eventually had to be taken place prior the Planck time, in a time in which all human-conceived theories are no longer valid.

From a philosophical perspective, the Planck Era of the Universe can be regarded as the matrix of *mystery* and the primeval source of what Lucian Blaga refers to as "*luciferian knowledge"*. Through this term, the philosopher considers that type of knowing by which "*through the initial act, it (i.e the luciferian knowledge) considers its object cleaved in two, in one part which reveals itself and in one which conceals itself. The object of luciferian knowledge is always a mystery, a mystery which through its signs, on the one hand, reveals itself and on the other conceals itself*."[*] In Blaga's philosophical system, the *luciferian knowledge* is complemented by the *paradisiac knowledge*. The terminology used by Blaga is strictly restricted to its etymological sense. Namely *luciferian* is used with its original sense, that of *bringer of light* (the etymology of the word is found in the Latin words *lux,* meaning light, and *fero,* meaning carrier, bearer). On the other hand, the *paradisiac* term borrows its mythological sense and reflects the *illo tempore* condition "when" everything was in good order, everything in equilibrium and furthermore everything was *known*. Perhaps an example can elucidate the meaning and usage of these two terms. Let us consider a celestial object that can be visible on a night sky. We assume that no astronomical instruments are at our disposal so that, in observing the celestial object, we rely solely on our eyesight. In this configuration, the celestial body can be regarded as a mysterious object subject to a luciferian type of knowledge in the sense that the light arriving from it offers positivistic aspects regarding its location and brightness, but simultaneously the same arrived light is the factor that obscures the object's essence. Thus, although some aspects of its being are revealed, its nature remains hindered to us and we cannot know exactly if the celestial body is, for instance, a star or planet Venus. In blagian words, the sign by which the celestial object manifests itself simultaneously reveals and conceals its characteristic aspects. This line of thought can be extended as the technological and theoretical instruments required for understanding the

---

[*] Blaga, p.253 (personal translation). Cf. section 2.5.

celestial body evolve. For instance, it might be shown that the object is in fact a star and now the mystery is further descended to the question “how does it produce the light by which it is seen?” Upon understanding that the respective light is produced by nuclear fusion, the mystery is shrunk to the question “why does nuclear fusion produce light?”. This can be understood from the perspective of the Special Theory of Relativity (STR), which provides the equivalency between matter and energy together with the law that governs their transformation (i.e. $E=mc^2$). From STR’s perspective, the now acquired information is of an epistemological level because this transformation law can be decomposed to STR’s axiomatic system. For instance, one such axiom would be that light travels at constant speed in all relative reference systems. Within the STR framework the question “why does light travel at a constant speed regardless of reference system?” is an invalid question because its domain of applicability lies outside that of STR. Thus, from STR’s perspective, the knowledge has reached an επιστήμη level that corresponds to a paradisiac type of knowledge as all that can be known, within STR’s boundaries, is known. Pushing the question outside the STR domain would require a further (more profound?) theory in which, now, the STR-epistemic knowledge would be degraded to, at best, a διάνοια level.

Now we are left with the impression that the pursuit of knowledge itself could be painted via encircled cycles which, by concentrically collapsing within themselves, provide the transition towards more fundamental stages. This picture in itself implies a fundamental axiom that governs all axiomatic systems of each theoretical stage: that within each stage there are at least two levels of knowledge, one corresponding to επιστήμη and one to διάνοια. Perhaps at one point, a stage in which all available knowledge is of επιστήμη nature and thus, this axiom among axiom might also lose its domain of applicability. Nevertheless, each of the aforementioned steps employed in the transition between the stages of acquired knowledge, from simply observing the celestial body all the way to the axioms of Special Relativity, correspond to what Blaga refers to as the *the crisis of the object.* The act of questioning the *paradisiac* pillars of the theory triggers a crisis that, by deepening the foundation of the *paradisiac* theory into mystery, becomes the basis of the new *luciferian* knowledge.

Converged to the Planck Era is also the metaphysical endeavor towards fundamentals. In this case, similar to the space bordering a black hole’s horizon that generates* Hawking

---

[*] In terms of the same uncertainty considerations explained for the Casimir effect (cf. Figure 4) , the vacuum surrounding a black hole will generate pairs of particles and antiparticles. At the black hole’s horizon, i.e. the region of space from which nothing can escape its gravitational attraction, the pairing will be disrupted: one of

radiation “out of nothing”, the space-time region corresponding to the Planck Era can be seen engulfed within the fundamental question of metaphysics: *why is there entity instead of nothingness?* The domain of this question covers all that is, was and will be within the Universe and ends where it can no longer be asserted about anything as being Being: the Planck Era. As put by Heidegger: *“The domain of this question is limited only by what simply is not and never is: by Nothing. All that is not Nothing comes into the question, and in the end even Nothing itself—not, as it were, because it is something, an entity, for after all we are talking about it, but because it "is" Nothing.*”[*] . The true Nothing is that out of which the Big Bang presumably commenced (as explained for the Casimir effect, the vacuum is not really empty, is not a *nothing)*. Furthermore, the Plank Era is the only era which is limited at one end by Nothing and at the other by something in which entities exist. By continuing this line of thought, we can identify two types of eras from now on. One of them (a single era in this category) starts from the end of the Planck Era and lasts for as much as needed for an entity to come into existence. Thus, this era belongs to something that has entity and, being the first of this kind, is limited on one side by the Planck era and at the other by something that has entities. From here onwards, all eras, no matter how divided, will always be delimited by entity-containing eras. How does that first entity come into existence? Physically, it just transitioned from the previous era in the form of the primeval radiation and can be imagined as a collision of two photons generating matter in the form of particle-antiparticle pairs. By having converted energy into mass, space and time come as byproducts of this process (from the General Theory of Relativity it is known that space and time cannot exist in the absence of matter, just as well as matter cannot exist in a framework outside space and time), and from now onwards the space-time stage is set for all entities to exist. Metaphysically, existence implies the transition from *Being* to *Entity,* the manifestation of a *Being* through *Entity.* To better understand the difference between the two latter terms we can follow one the subtle examples provided by Heidegger:

“Over there, on the other side of the street, stands the high school building. An entity. We can scour every side of the building from the outside, roam through the inside from basement to attic, and note everything that can be found there: hallways, stairs, classrooms,

---

the generated particle will be intialy oriented towars the black hole and by passing through its horizon will not be able to return to its partner particle and annihilate; the paired particle, initially being oriented oppositely to the black hole, will have the chance to evade its gravitational sink. The net result is called the Hawking radiation (being formed from the evaded particles). The swallowed antiparticles will eventually lead to the black hole’s evaporation.

[*] Heidegger, *Introduction to Metaphysics,* p.2 (English); p.11 (Romanian). Cf. section 1.4.

and their furnishings. Everywhere we find beings, and in a very definite order. Where now is the Being of this high school? It is, after all. The building is. The Being of this entity belongs to it if anything does, and nevertheless we do not find this Being within the entity.

Moreover, Being does not consist in our observing entity. The building stands there even if we do not observe it. We can come across it only because it already is. In addition, the Being of this building does not at all seem to be identical for everybody. For us, as observers or passers-by, it is not what it is for the students who sit inside, not just because they see it only from the inside but because for them this building really is what it is and how it is. One can, as it were, smell the Being of such buildings, and often after decades one still has the scent in one's nose. The scent provides the Being of this entity much more directly and truly than it could be communicated by any description or inspection. On the other hand, the subsistence of the building does not depend on this scent that is hovering around somewhere."[*]

For the ancient Greeks, *being* meant either something standing in itself, when referred to by *φύσις* (fusis), either something constant, enduring, when referred to through the word *οὐσία* (ousia). To exit from such a state meant to no longer be and the word use to describe this was *ἐξίστασθαι* (existasthai).[†] To bring a being into existence means to transpose it into an entity. Thus, the original, Greek meaning of existence implied to no longer be. Similar to how in the quantum mechanical language, upon measurement a wavefunction expressed in the Hilbert space collapses into one of its eigenstates expressed in the real space (i.e. fourth QM axiom), in the language of metaphysics bringing a being into existence collapses it into entity. Similar to how a wavefunction cannot be directly observed, but only grasped through its manifestation upon collapsing into to real space (and further observed via a quantity derived from its square modulus), the metaphysical *being* cannot be physically reached but only grasped through its entity manifestation. Both *being* and wavefunction, however, can be reached and tangled through the human intellect. Both are of suprasensible nature and are susceptible in collapsing into sensible manifestations (cf. Figure 6).

---

[*] Heidegger, *Introduction to Metaphysics*, p. 35-36 (English); p 54-55 (Romanian). Cf. section 1.4.

[†] Perhaps the etymology of the English word "exit" might be traced to the Greek *ἐξίστασθαι*.

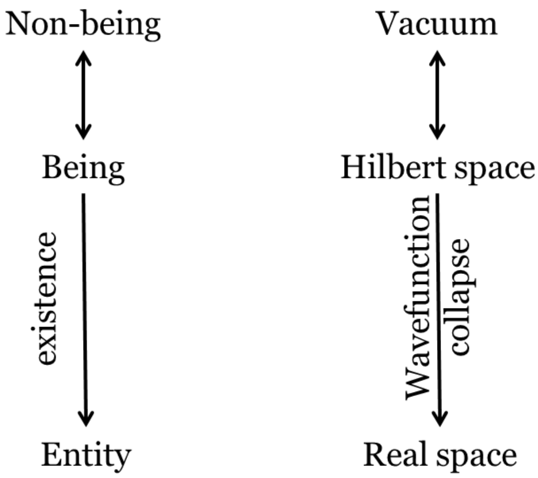

Figure 6. Parallel between Metaphysics (left) and Quantum Mechanics (right).

In its uniqueness, the *Being* is only matched by the *non-Being.*[*] The two concepts find themselves in a complementary relationship similar to the complementary quantities appearing in the uncertainty relationship responsible for the vacuum generation of virtual particles and antiparticles.

Being of suprasensible nature, the *Being* can be asserted within the *τόπος νοητός* (topos noetos*)* and therefore sharing ground with the eide. The *entity* on the other hand, is by the virtue of its sensible nature an object within the *κόσμος (*cosmos*)* and therefore sharing ground with the aistheta. Thus a third parallel represented by the eide-aistheta binomial can be traced to the previous two parallels. Now, the fully deterministic wavefunction expressed within the Hilbert space can be translated to an ancient Greek as a sort of eidos belonging to the *τόπος νοητός* that by collapsing, in a similar way to which the eide enter in *participation* (methexis), can be observed within the real space similar to how an aistheton is sensed within the *κόσμος.*

---

[*] Heidegger, *Introduction to Metaphysics* , p. 80-84(English); p. 112-117 (Romanian). Cf. section 1.4.

2.4 Elements of Computational Chemistry

2.4.1 Introduction

As suggested by its name, the field of computational chemistry comprises that domain of knowledge that interfaces the science of chemistry with that of computer science.

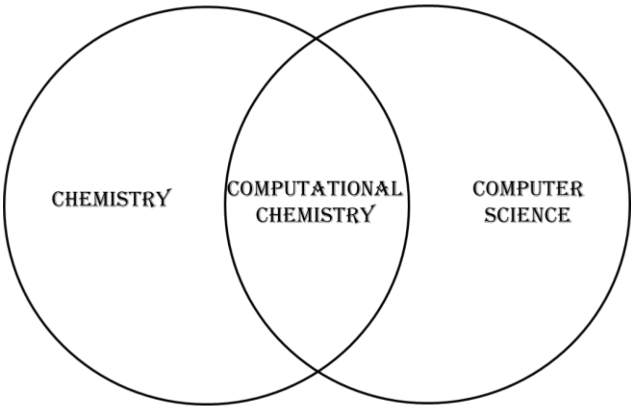

Figure 7. Realm of computational chemistry.

The resonance of these two domains is threefold or, if we are to adopt the jargon used in this field, triple degenerated. Namely, the domain of computational chemistry comprises:

a) the field of method development that deals with the deduction of either some sort of quantum mechanical equations that can be used to approximate the chemical reality, or the development of classical mechanical based models such as force-fields.

b) the field of software development that deals with programming and code development.

c) the field of applications that use the quantum/classical methods in some special developed software in order to address real-life chemical problems.

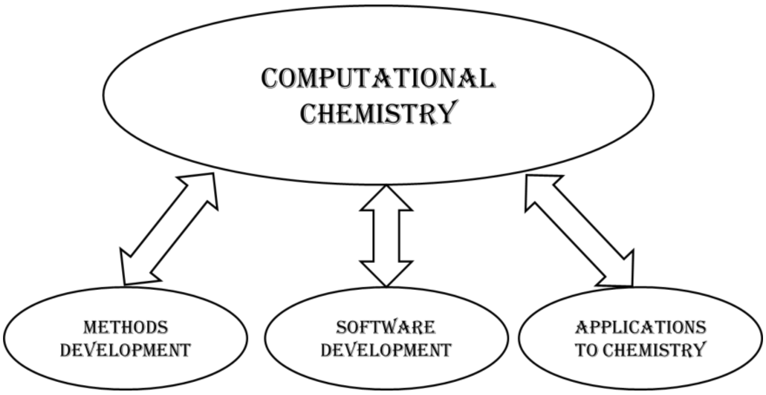

Figure 8. The three branches of computational chemistry.

Based on the type of physics adopted, all computational chemistry methods can be categorized in two main groups:

a) methods that use classical mechanics and, thus, are derived from the Newton's equation of motion. These methods are all collected under the name of "Molecular Mechanics"
b) methods that use quantum mechanics and are developed from the Schrödinger equation. These methods form what is known as "Quantum Chemistry".

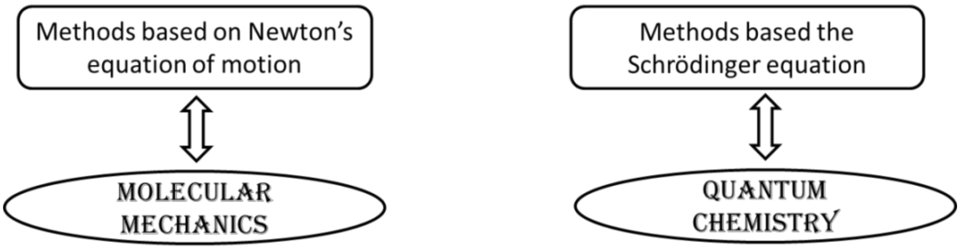

Figure 9. Classes of methods in computational chemistry.

2.4.2 Molecular Mechanics

In the molecular mechanics approach, all atoms are treated as spheres and all chemical bonds as resorts. The forces acting between the atoms of a studied system are computed via a potential that, in its turn, is computed with the help of a pre-parameterized forcefield. A usual molecular mechanical potential (*V*) has the following form:

$$V = \sum_{bonds} \frac{1}{2} k_b (r - r_0)^2 + \sum_{angles} \frac{1}{2} k_\theta (\theta - \theta_0)^2 + \sum_{improper} \frac{1}{2} k_\chi (\chi - \chi_0)^2 + \sum_{dihedrals} k_\varphi [1 + \cos(n\varphi - \delta)] + \sum_{i>j} \frac{q_i q_j}{4\pi\varepsilon_0 r_{ij}} + \sum_{i>j} \varepsilon_{ij} \left[\left(\frac{\sigma_{ij}}{r_{ij}}\right)^{12} - \left(\frac{\sigma_{ij}}{r_{ij}}\right)^{6} \right]$$

Equation 7.

The first term of the potential describes the stretching of all the chemical bonds present in the system, with k_b being a preparameterized constant, *r* the distance between the atoms involved in the chemical bond, and r_0 the equilibrium bond length. This is actually a direct application of the Hooke's law for the potential V_{Hooke} of a spring:

$$V_{Hooke} = \frac{k}{2} x^2$$

Equation 8.

where k is a constant of proportionality and x is the displacement of the spring. Similarly, the second term in Equation 7 deals with the bending of angles; θ represents the angle between three atoms, θ_0 the equilibrium bond angle and k_θ is pre-parameterized constant. The third term is needed in order to ensure planarity of some particular groups (such as, for example, carbon atoms in aromatic rings) - and ensues as a consequence of the inability of the previous terms to correctly describe the planarity in such compounds. Consequently, this term describes the positive contribution to the total energy of those out-of-plane motions. The fourth term describes the bending of the dihedral angle between 4 non-planar atoms (similarly, χ is the dihedral angle, χ_0 the equilibrium dihedral angle and k_χ a pre-parameterized constant). The fifth term represents the electrostatic interactions and is provided by the classical Coulomb law. Thus, $q_{i,j}$ represents the charge of atom *i* or *j*, r_{ij} the distance between them, and ε_0 is the vacuum permittivity. The last term of Equation 7 consists of the Lennard-Jones potential that describes long-range interactions such as van der Waals and dispersion interactions. The ε_{ij} term is a pre-parameterized constant, σ_{ij} represents the distance at which this potential is zero between atom *i* and *j*, and r_{ij} is the distance between the two atoms. The $\left(\frac{\sigma_{ij}}{r_{ij}}\right)^{12}$ term accounts for the Pauli exclusion based repulsion found at close range, while the $\left(\frac{\sigma_{ij}}{r_{ij}}\right)^{6}$ term for the long-range attractive van der Waals and dispersion interactions.

The forcefield consists of a set of constants (the “k”-s in Equation 7) that are given for each type of atom within a specific chemical system. For instance, if a forcefield is parameterized for organic molecules, it will possess parameters not only for the most widely encountered atoms, but also for the types of bonding that they can supply. Thus, a C=C double bond will have different parameters from a simple C-C bond. This type of computation starts with the assignment of the forcefield parameters on each atom comprising the studied system. The potential interaction between each two atoms that are present in the system is subsequently computed via Equation 7. From the obtained potential, one can compute the forces (*F*) acting on each atom, via Newton’s equation of motion, as shown below:

$$F = -\nabla V = ma = m\frac{d^2r}{dt^2}$$

Equation 9.

with ∇ being the nabla operator, m the mass of the atom, a the acceleration, r the spatial dislocation and t the time. Having the forces computed for each atom, their trajectory in space can be further computed with the aid of, for example, the Verlet algorithm that computes the future position of an atom, $r(t+\Delta t)$, starting from its current position, $2r(t)$, its previous position, $r(t-\Delta t)$ and by the amount of force acting on it, i.e. the final $\left(\frac{F_{(t)}}{m}\right)\Delta t^2$ term:

$$r(t+\Delta t) = 2r(t) + r(t-\Delta t) + \left(\frac{F_{(t)}}{m}\right)\Delta t^2$$

Equation 10.

Molecular mechanical methods enable the treatment of very large atomic ensembles, such as biological systems. Protein-protein interactions or protein-environment interactions and, likewise, other large biomolecules can be investigated. As an example from the literature, the respiratory complex I has been investigated[3] at the molecular mechanical level to describe the dynamics of the complex. However, the electron transfer mechanism involved in this complex could not have been treated at this level of theory. This is a general feature and the most important limitation of the molecular mechanical methods: electron-dependent phenomena, such as charge transfer and chemical reactions, cannot be treated with these methods. This limitation comes from the way these methods were built, namely treating the atoms as spheres and neglecting their constituent parts. Nevertheless, this approximation allows the treatment of very large systems because the equations describing them at this level can be solved very fast/easy from the computational point of view. In order to describe the electron transfer mechanism employed by this complex, quantum chemical methods had to be invoked. Contrary to the classical methods, these quantum chemical methods describe the motion of all electrons and nuclei and, thus, are well-suited for treating electron transfer phenomena occurring in this complex, as well as, in general, chemical reactions.

2.4.3 Quantum Chemistry

The covalent bond is an effective stabilized *Fermi heap* which in turn is a manifestation of the *exchange interaction* resulting from the antisymmetric character that an electronic wavefunction requires. The exchange interaction represents the kernel of Chemistry and its treatment is called Quantum Chemistry. The ongoing chapter is meant to provide the explanatory details behind this statement.

All quantum chemical methods trace back to the Schrödinger equation (cf. Equation 11), which states that by applying the Hamiltonian operator upon the wavefunction describing the state of the system, the same wavefunction will be retrieved alongside with the energy of that state, E.

$$\widehat{H}\Psi = E\Psi$$

Equation 11.

In quantum formalism, the state of a system is described by a mathematical entity dubbed wavefunction, Ψ, while observables are described by mathematical operators. The energy of a system can be determined experimentally and therefore it is an observable. The operator associated with this observable is called the Hamiltonian, H, and can be extended in the following form:

$$\widehat{H} = -\sum_{i}\frac{\hbar}{2m_e}\nabla_i^2 - \sum_{i}\frac{\hbar}{2m_k}\nabla_k^2 - \sum_{i}\sum_{j}\frac{e^2 Z_k}{r_{ik}} + \sum_{i<j}\frac{e^2}{r_{ij}} + \sum_{k<l}\frac{e^2 Z_k Z_L}{r_{kl}}$$

Equation 12.

The first term represents the total kinetic energy of the electrons present in the system, the second the kinetic energy of the nuclei, the third one represents the attractive electron-nucleus interactions, while the last two terms represent the repulsive electron-electron and nucleus-nucleus interactions.

Although appearing straightforward, with the exception of some very simple models the Schrödinger equation cannot be precisely solved. Concerning chemistry, this equation can be precisely solved only for the hydrogen atom and the hydrogen-like ions. Any step forward in complexity, i.e. any extra electron added to the system, requires approximations. Thus, it can be stated that quantum chemistry represents the struggle to approximate the Schrödinger equation such that chemical phenomena can be studied with it.

Quantum chemical methods can be further classified in different categories. Onwards we will present and briefly discuss some of such categories risen from classifications based on the numerical approach adopted in order to solve the Schrödinger equation (i.e. 2.4.3.3 Variational vs. perturbational methods), their covariance with regards to the Lorentz transformation (in other words, (2.4.3.4) Non-relativistic vs. relativistic methods), on the system environment (cf. 2.4.3.6 Vacuum vs. Solvent environment), on the periodicity of the system (cf. 2.4.3.5 Standard vs. Periodic) and by considering whether or not there is an electron exchange between the studied system and the exterior (cf. 2.4.3.7 Stationary vs. Non-stationary / equilibrium vs. non-equilibrium).

2.4.3.1 *The wavefunction*

All quantum chemical computations start from a trial wavefunction that is being improved during the computation process. This wavefunction is built starting from basic one-electron functions that are specific for each particular element. Usually, these one-electron functions are parameterized versions of the hydrogen solutions of the Schrödinger equation. Hence, these basic functions are also called orbitals, as they resemble the familiar *s*, *p*, *d* (cf. Figure 10) and *f* orbitals (that are, again, analytical solutions of the Schrödinger equation for the hydrogen atom).

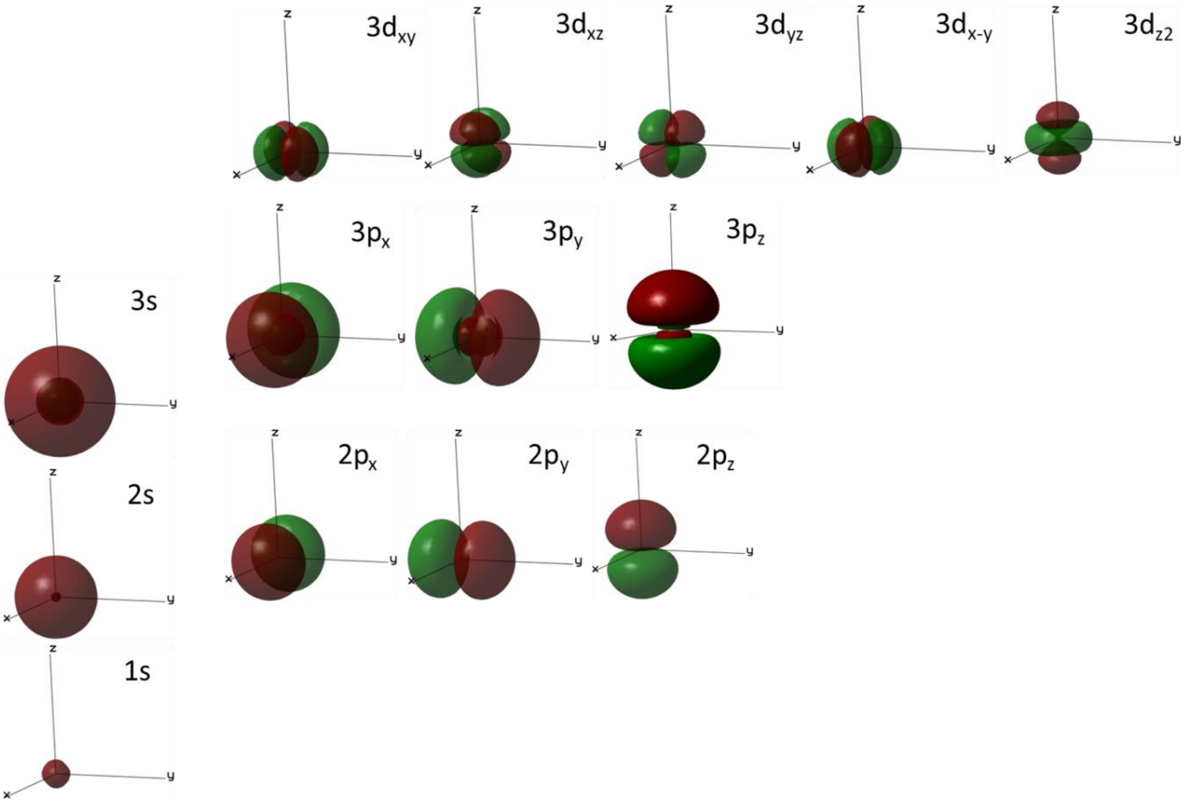

Figure 10. The *s***,** *p* and *d* atomic orbitals of the C atom computed at the B3LYP/def2-SV(P) level of theory.

In a molecular system, these basic orbitals are combined with each other using the linear combination of atomic orbitals approximation (LCAO) to construct the initial molecular orbitals of the molecular system and, thus, its trial wavefunction. In LCAO, a certain molecular orbital φ can be obtained from the linear combination of the *i* basis set functions with each χ_i being weighted by a c_i coefficient:

$$\varphi = \sum_i c_i \chi_i$$

Equation 13.

As an example, let us assume that a basis set consisting of orbitals for the carbon and hydrogen atom is available and from these orbitals a trial wavefunction of the benzene molecule is needed. The minimal requirements are to provide s orbitals for the hydrogen atoms and *s* and *p* for the carbon atoms - and then the benzene molecular orbitals can be constructed. For instance, the benzene HOMO (cf. Figure 11) can be constructed from three p_z carbon orbitals aligned in phase for left-hand side of the molecule in Figure 11, and other three p_z orbitals coming from the other carbon atoms (right-hand side of the benzene molecule in Figure 11) that are in phase among themselves but in antiphase with the left-hand side orbitals. Similarly, all the molecular orbitals are constructed and thus, the trial wavefunction is obtained. The task of the future computation is to adjust the c_i coefficients that come in the linear combination (cf. Equation 13) such that a wavefunction that closely resembles the true wavefunction is obtained. In general, if higher-angular momentum orbitals (*d*, *f* and *g*) are used, they will provide extra flexibility in constructing the molecular orbitals and will yield a better description of the system. Of course, this comes at a higher computational cost.

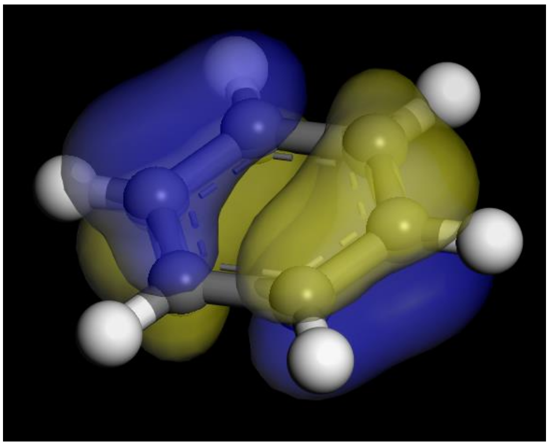

Figure 11. Benzene HOMO.

Collections of such initial functions are called basis sets. The difference between the basis sets is always a result of the different parameterization scheme that was employed when they were developed. The struggle is always to give a feasible ratio between the accuracy of the basis sets and the computational cost.

The atomic orbitals comprising quantum chemical basis sets are usually of Slater type (n=1 in Equation 14) or Gaussian type (n=2 in Equation 14) which have the following general form:

$$\chi(r) = f(x, y, z)e^{-ir^n}$$

Equation 14.

where *r* is the distance relative to the center of the atomic orbital and *f(x,y,z)* is a polynomial function that modulates the shape of the atomic orbital.

2.4.3.2 *The Hamiltonian*

The modeling of the Hamiltonian part of the Schrödinger equation is a subject of great interest in the field of quantum chemistry. There are, basically, four main groups in which the hamiltonians related to quantum chemistry can be divided: the Hartree-Fock method, the post Hartree-Fock methods, the semiempirical methods and, last but not least, the density functional based methods.

2.4.3.2.1 The Hartree-Fock method and the exchange interaction

Hartree was the first to provide an iteration scheme by which the Schrödinger equation could be numerically solved, while Fock further developed this method in order to correctly account for the Pauli exclusion type of interactions, which are also referred to as exchange interactions. The equations involving this method can be numerically solved, but the method itself is fundamentally wrong as it does not take into account the correlation of the electron's movement with regards to other electrons. Instead, the electrostatic effect induced by the presence of other electrons is smeared out and now the energy of an electron is not computed by taking into account its interaction with each individual other electron but by computing its interaction with the electrostatic mean-field generated by the other electrons. Nevertheless, the method provides a good ground state description of chemical systems found in their equilibrium geometry. Although not that popular in present days, the Hartree-Fock method is ubiquitous in quantum chemical textbooks as a starting point that provides a first attempt to solve, albeit by means of approximations, the Schrödinger equation for real life chemical problems. The reason behind this ubiquity lies not only in the historical development of quantum chemistry, but also as means to provide a working paradigm for further improved methods. For instance, in perturbation theory methods, the HF method provides the starting wavefunction that will sequentially be further improved. Also, the popular Kohn-Sham version of Density Functional Theory borrows the molecular orbital approach used in HF (i.e. Kohn-Sham orbitals).

There are two types of approximations that can be employed in order to treat a physical system in quantum mechanical terms. The first way is to simplify the Hamiltonian and therefore ignore some physical properties, while the second way consists in simplifying the wavefunction. Hartree chose the latter and constructed the wavefunction of a composite system as the product of the wavefunctions of each individual component of the system. This became known as the Hartree product:

$$\Psi = \prod_n \varphi_n$$

Equation 15.

Ψ denotes the wavefunction of the entire system, while φ_n denotes the wavefunctions of its components. For instance Ψ can account for the total electronic wavefunction of an atom while φ_n *for* each of its comprising orbitals. This is the simplest way to write such a wavefunction. It might seem odd how a total wavefunction written in terms of the product of some components is simpler than a total wavefunction written, for instance, in terms of the the sum of its components. The problem arises when the total wavefunction is squared in order to obtain the probability density. Beside the square terms (i.e. φ_n^2), a wavefunction expressed as a sum of its constituting components would yield coupling terms (i.e. $\varphi_n \varphi_m$) which would further increase the computational effort. Expressed as a product, the squaring of a wavefunction would yield only φ_n^2 terms and thus its evaluation can be made faster.

The root of the Hartree-Fock theory's downfall, namely neglecting of the electron correlation interaction, lies in the in the Hartree product itself. From the theory of probabilities it is known that the probability of uncorrelated events is accounted by the product of the probabilities of each individual event. The Hartree product is nothing more than the translation of this probabilistic fact in the language of wavefunctions and atomic orbitals. Thus by virtue of the product approximation, Equation 15 accounts for uncorrelated events and when transposed to the electronic structure language, this means that the electronic movement of each electron will not be correlated with the movement of the other present electrons.

Another problem arising when writing a wavefunction in terms of a Hartree product is that it does not account for the antisymmetric character that an electronic wavefunction should possess. From Pauli's spin statistics it is known that a wavefunction describing an assembly of fermions should change its sign when the order of two such particles is interchanged. For instance, the electronic wavefunction of the helium atom

$$\Psi^{He} = 1s_{\alpha}^{1}1s_{\beta}^{1}$$

Equation 16.

can be written as:

$$\Psi^{He} = 1s_{\alpha}(1)1s_{\beta}(2)$$

Equation 17.

by which it is noted that the first electron (1) is placed in the $1s_{\alpha}$ spinorbital while the second (2) is placed in the $1s_{\beta}$ spinorbital. Pauli's antisymmetric requirement of such a fermionic system implies that when interchanging electron (1) with electron (2) the wavefunction becomes:

$$-\Psi^{He} = 1s_{\alpha}(2)1s_{\beta}(1)$$

Equation 18.

This is certainly not the case of a wavefunction expressed by the Hartree product:

$$\Psi = \varphi_1\varphi_2\varphi_3 \dots \varphi_n = \varphi_2\varphi_1\varphi_3 \dots \varphi_n \neq -\Psi$$

Equation 19.

The Hartree approximation would not encounter such symmetry-caused problems if the electrons were to be bosons. Indeed, for an assembly of bosons, Pauli's spin statistics dictates that the total wavefunction should preserve its sign once the order of two bosons are interchanged. Nevertheless, Vladimir Fock was the first to observe that an efficient way to fulfil the wavefunction antisymmetric requirement is to expand the Hartree product in terms of a Slater determinant:

$$\Psi = \frac{1}{\sqrt{n!}} \begin{vmatrix} \varphi_1(1) & \varphi_2(1) & \cdots & \varphi_n(1) \\ \varphi_1(2) & \varphi_2(2) & \cdots & \varphi_n(2) \\ \vdots & \vdots & \ddots & \vdots \\ \varphi_1(n) & \varphi_2(n) & \cdots & \varphi_n(n) \end{vmatrix}$$

Equation 20.

The prefactor $\frac{1}{\sqrt{n!}}$ is needed in order to assure that the wavefunction is normalized. We can check the validity of this notation by expressing the helium electronic wavefunction in terms of a Slater determinant:

$$\Psi^{He} = \frac{1}{\sqrt{2}} \begin{vmatrix} 1s_{\alpha}(1) & 1s_{\beta}(1) \\ 1s_{\alpha}(2) & 1s_{\beta}(2) \end{vmatrix} = \frac{1}{\sqrt{2}} \left[1s_{\alpha}(1) 1s_{\beta}(2) - 1s_{\alpha}(2) 1s_{\beta}(1) \right]$$

Equation 21.

By interchanging electron (1) with electron (2) the wavefunction becomes:

$$\Psi^{He}_{1\leftrightarrow 2} = \frac{1}{\sqrt{2}} \begin{vmatrix} 1s_{\alpha}(2) & 1s_{\beta}(2) \\ 1s_{\alpha}(1) & 1s_{\beta}(1) \end{vmatrix} = \frac{1}{\sqrt{2}} \left[1s_{\alpha}(2) 1s_{\beta}(1) - 1s_{\alpha}(1) 1s_{\beta}(2) \right]$$

Equation 22.

From Equation 21 and Equation 22 can be concluded that:

$$\Psi^{He}_{1\leftrightarrow 2} = -\Psi^{He}$$

Equation 23.

and thus the electronic antisymmetric character of the electronic wavefunction required by the Pauli's spin statistic is fulfilled.

By the virtue of the Born-Oppenheimer approximation, the electronic Hamiltonian, $\hat{H}_{el}$, can be decoupled from the nuclear Hamiltonian and thus expressed as:

$$\hat{H}_{el} = -\frac{1}{2} \sum_{i} \nabla_i^2 - \sum_{i,N} \frac{Z_N}{r_{iN}} + \sum_{i<j} \frac{1}{r_{ij}}$$

Equation 24.

where the $-\frac{1}{2}\sum_i \nabla_i^2$ term accounts for the kinetic energy of all electrons, $-\sum_{i,N} \frac{Z_N}{r_{iN}}$ for the electrostatic interaction between each *i* electron and *N* nuclei (with Z being the charge of the nucleus and r_{iN} the electron-nucleus distance) and finally the $\sum_{i<j} \frac{1}{r_{ij}}$ wich represents the electron-electron electrostatic interaction. The electronic Hamiltonian can further be divided into a one-electron Hamiltonian and a two-electron Hamiltonian. The former accounts for the

dynamics of each individual electron in the electrostatic field of the present nuclei and as if the other electrons were not present. This electron-nuclei Hamiltonian, $\hat{h}_{e-N}$, can be noted as:

$$\hat{h}_{e-N} = -\frac{1}{2}\sum_{i} \nabla_i^2 - \sum_{i,N} \frac{Z_N}{r_{iN}}$$

Equation 25.

The expectation value of this Hamiltonian retrieves the total one-electron energy E_{e-N} of the system:

$$E_{e-N} = -\sum_{i,N} \left\langle \Psi \middle| \frac{1}{2}\nabla_i^2 + \frac{Z_N}{r_{iN}} \middle| \Psi \right\rangle$$

Equation 26.

The total energy of the system is then corrected by including the two-electron interactions in the form of the $\hat{h}_{e-e}$ Hamiltonian:

$$\hat{h}_{e-e} = \sum_{i<j} \frac{1}{r_{ij}}$$

Equation 27.

which retrieves the electron-electron energy term E_{e-e}:

$$E_{e-e} = \sum_{i<j} \left\langle \Psi \middle| \frac{1}{r_{ij}} \middle| \Psi \right\rangle$$

Equation 28.

Equation 28 represents the crux problem of quantum chemistry. From the perspective of Blaga's philosophy, its treatment can be regarded as a *luciferic* endeavor because the treatment of this problem retrieves the core quantum chemical concept, in the form of the *exchange interaction,* and simultaneously pushes further into the unknown the (exact) electronic behavior. The trade-off, however, proves fruitful from the practical point of view as the driving force of the entire chemistry can be emphasized in this manner, while the uncorrelated movement of the electrons can later be recovered by other methods. Thus a significant part of the mystery that is concealed under the *luciferic* endeavor of Equation 28 can further be unveiled.

In order to emphasize this endeavor, we will first express the two-electron energy (Equation 28) of the He ground state, ε, and abandon for a moment the Dirac notation:

$$\varepsilon = \left\langle \Psi^{He} \left| \frac{1}{r_{12}} \right| \Psi^{He} \right\rangle = \int \left[\Psi^{He} \frac{1}{r_{12}} \Psi^{He} \right] d\tau$$

Equation 29.

with the $d\tau = dxdydzd\omega = drd\omega$. The first three differentials represent the spatial dimensions (*dr*) of the wavefunction while ω represents its spin dimension. By inserting Equation 21 the following occurs:

$$\varepsilon = \frac{1}{2} \int \left[[1s_\alpha(1)1s_\beta(2) - 1s_\alpha(2)1s_\beta(1)] \frac{1}{r_{12}} [1s_\alpha(1)1s_\beta(2) - 1s_\alpha(2)1s_\beta(1)] \right] d\tau$$

$$\varepsilon = \frac{1}{2} \int \left[[1s_\alpha(1)1s_\beta(2) - 1s_\alpha(2)1s_\beta(1)] \left[\frac{1s_\alpha(1)1s_\beta(2)}{r_{12}} - \frac{1s_\alpha(2)1s_\beta(1)}{r_{12}} \right] \right] d\tau$$

$$\varepsilon = \frac{1}{2} \int \left[\frac{1s_\alpha(1)1s_\beta(2) \cdot 1s_\alpha(1)1s_\beta(2)}{r_{12}} - \frac{1s_\alpha(2)1s_\beta(1) \cdot 1s_\alpha(1)1s_\beta(2)}{r_{12}} \right.$$
$$\left. - \frac{1s_\alpha(1)1s_\beta(2) \cdot 1s_\alpha(2)1s_\beta(1)}{r_{12}} + \frac{1s_\alpha(2)1s_\beta(1) \cdot 1s_\alpha(2)1s_\beta(1)}{r_{12}} \right] d\tau$$

$$\varepsilon = \frac{1}{2} \int \left[\frac{[1s_\alpha(1)]^2 [1s_\beta(2)]^2}{r_{12}} - 2 \frac{1s_\alpha(1)1s_\alpha(2)1s_\beta(1)1s_\beta(2)}{r_{12}} + \frac{[1s_\alpha(2)]^2 [1s_\beta(1)]^2}{r_{12}} \right] d\tau$$

Equation 30.

Now $\int [1s_\alpha(1)]^2 d\tau$ represents the probability density to find electron (1) in the $1s_\alpha$spinorbital. Thus the quantity

$$\int \frac{[1s_\alpha(1)]^2 [1s_\beta(2)]^2}{r_{12}} d\tau = \int [1s_\alpha(1)]^2 \frac{1}{r_{12}} [1s_\beta(2)]^2 d\tau = J_{12}$$

Equation 31.

represents the Coulombic interaction between the electronic densities of electrons (1) and (2). On the other hand, because $1s_\alpha$ and $1s_\beta$ are orthogonal $\int 1s_\alpha(1)1s_\beta(1)d\tau = 0$ and thus

$$\varepsilon = \frac{1}{2}(J_{12} - 2\cdot 0 + J_{21}) \xleftrightarrow{J_{12}=J_{21}} \varepsilon = J_{12}$$

Equation 32.

As expected from classical electrodynamic considerations, two electrons placed in the same orbital exhibit a repellent Coulombic interaction. Things, however, become more quantum mechanical when the open-shell electronic structure of the first He excited state is analyzed. By emphasizing the presence of two unpaired electrons, we note the wavefunction of the first excited state as $\ddot{\Psi}^{He}$:

$$\ddot{\Psi}^{He} = \frac{1}{\sqrt{2}}\begin{vmatrix} 1s_\alpha(1) & 2s_\alpha(1) \\ 1s_\alpha(2) & 2s_\alpha(2) \end{vmatrix} = \frac{1}{\sqrt{2}}[1s_\alpha(1)2s_\alpha(2) - 1s_\alpha(2)2s_\alpha(1)]$$

Equation 33.

and its associated eigenenergy with η

$$\eta = \left\langle \ddot{\Psi}^{He} \middle| \frac{1}{r_{12}} \middle| \ddot{\Psi}^{He} \right\rangle = \int \left[\ddot{\Psi}^{He} \frac{1}{r_{12}} \ddot{\Psi}^{He}\right] d\tau$$

Equation 34.

which can be expanded as:

$$\eta = \frac{1}{2}\int \left[[1s_\alpha(1)2s_\alpha(2) - 1s_\alpha(2)2s_\alpha(1)]\frac{1}{r_{12}}[1s_\alpha(1)2s_\alpha(2) - 1s_\alpha(2)2s_\alpha(1)]\right] d\tau$$

$$\eta = \frac{1}{2}\int \left[[1s_\alpha(1)2s_\alpha(2) - 1s_\alpha(2)2s_\alpha(1)]\left[\frac{1s_\alpha(1)2s_\alpha(2)}{r_{12}} - \frac{1s_\alpha(2)2s_\alpha(1)}{r_{12}}\right]\right] d\tau$$

$$\eta = \frac{1}{2}\int \left[\frac{1s_\alpha(1)2s_\alpha(2)\cdot 1s_\alpha(1)2s_\alpha(2)}{r_{12}} - \frac{1s_\alpha(2)2s_\alpha(1)\cdot 1s_\alpha(1)2s_\alpha(2)}{r_{12}} \right.$$
$$\left. - \frac{1s_\alpha(1)2s_\alpha(2)\cdot 1s_\alpha(2)2s_\alpha(1)}{r_{12}} + \frac{1s_\alpha(2)2s_\alpha(1)\cdot 1s_\alpha(2)2s_\alpha(1)}{r_{12}}\right] d\tau$$

$$\eta = \frac{1}{2}\int \left[\frac{[1s_\alpha(1)]^2[2s_\alpha(2)]^2}{r_{12}} - 2\frac{1s_\alpha(1)2s_\alpha(1)1s_\alpha(2)2s_\alpha(2)}{r_{12}} + \frac{[1s_\alpha(2)]^2[2s_\alpha(1)]^2}{r_{12}} \right] d\tau$$

Equation 35.

Because now the integration with respect to spin is done only over α spinorbitals, the coupling term of Equation 35 no longer vanishes. The new integral can be noted as

$$\int 1s_\alpha(1)2s_\alpha(1)\frac{1}{r_{12}}1s_\alpha(2)2s_\alpha(2)d\tau = K_{12}$$

Equation 36.

and is referred to as the exchange integral because it accounts for both electrons being exchanged in both available orbitals. The electron-electron interaction becomes:

$$\eta = \frac{1}{2}(J_{12} - 2 \cdot K_{12} + J_{21}) \xleftrightarrow{J_{12}=J_{21}} \eta = J_{12} - K_{12}$$

Equation 37.

Thus the Coulombic interaction of the two parallel electrons formally placed in two different orbitals becomes reduced by the exchange interaction accounted by Equation 36. In other words, the classical electrodynamic interaction of two spin-parallel electrons becomes corrected by a pure quantum mechanical interaction. This exchange interaction is different in nature not only to the classical concepts of forces but also from their quantum mechanical equivalents. For instance, the quantum electrodynamic interaction (i.e. the quantum equivalent of the classical electromagnetic force) is one of the four fundamental *forces* and is consequently driven by the exchange of a virtual particle (a virtual photon in this case) between the two electromagnetically interacting particles. The pure quantum exchange *K*, on the other hand, is not mediated by any virtual particle but rather is a direct consequence of the antisymmetric requirement that a fermionic wavefunction possesses. While quantum mechanical forces are mediated by exchange-particles between charged[*] particles, the *exchange interaction, K,* is the exchange itself devoid of mediating exchange-particles and thus simply is a manifestation of the wavefunction constrained under symmetry considerations.

---

[*] Electric charge in the case of Quantum electrodynamics (QED) which governs atomic forces by the exchange of virtual photons. Or color charges in the case of Quantum chromodynamics (QCD) that governs nuclear forces by exchanging virtual gluons.

In order to provide a better grasp on the way the exchange interaction manifests itself, we first need to expand the spin-orbital notation so that the spin dimension is explicitly included. Thus we note

$$1s_\alpha(1) = 1s(1)\alpha(1)$$
$$1s_\beta(1) = 1s(1)\beta(1)$$

Equation 38.

Also, we further expand the wavefunction notation and now include as a subscript the orbitals which are harbored by electrons. Thus, the ground state of the He atom can now be rewritten as:

$$\begin{aligned}\Psi_{1s}^{He} &= \frac{1}{\sqrt{2}}[1s(1)\alpha(1)1s(2)\beta(2) - 1s(2)\alpha(2)1s(1)\beta(1)] \\ &= \frac{1}{\sqrt{2}}1s(1)1s(2)[\alpha(1)\beta(2) - \alpha(2)\beta(1)]\end{aligned}$$

Equation 39.

with the probability density of finding both opposite-spin electrons placed in the same *1s* orbital being:

$$\begin{aligned}\int |\Psi_{1s}^{He}|^2 d\tau &= \frac{1}{2}\int [1s(1)]^2[1s(2)]^2 dr \int [\alpha(1)\beta(2) - \alpha(2)\beta(1)]^2 d\omega \\ &= \frac{1}{2}\int \{[\alpha(1)]^2[\beta(2)]^2 - 2[\alpha(1)\beta(1)\alpha(2)\beta(2)] + [\alpha(2)]^2[\beta(1)]^2\} d\omega \\ &= \frac{1}{2}(1 - 0 + 1) = 1\end{aligned}$$

Equation 40.

Because the orbitals, as well as the spin variables, each form an orthonormal set, $\int[1s(1)]^2 dr = \int[1s(2)]^2 dr = 1$ and $\int \alpha(1)\beta(1)d\omega = \int \alpha(2)\beta(2)d\omega = 0$. Thus, the probability of finding two spin-opposite electrons in the 1s orbital is equal to unity. Now we can follow the same treatment of a state $\ddot{\Psi}_{1s}^{He}$ in which both electrons share the same spin and are placed in the same orbital:

$$\ddot{\Psi}_{1s}^{He} = \frac{1}{\sqrt{2}}\begin{vmatrix} 1s_{\alpha}(1) & 1s_{\alpha}(1) \\ 1s_{\alpha}(2) & 1s_{\alpha}(2) \end{vmatrix} = \frac{1}{\sqrt{2}}[1s(1)\alpha(1)1s(2)\alpha(2) - 1s(2)\alpha(2)1s(1)\alpha(1)]$$

$$= \frac{1}{\sqrt{2}}[1s(1)1s(2) - 1s(2)1s(1)]\alpha(1)\alpha(2)$$

Equation 41.

The probability density of this state is:

$$\int \left|\ddot{\Psi}_{1s}^{He}\right|^2 d\tau = \frac{1}{2}\int [1s(1)1s(2) - 1s(2)1s(1)]^2 dr \int [\alpha(1)]^2[\alpha(2)]^2 d\omega$$

$$= \frac{1}{2}\int \{[1s(1)]^2[1s(2)]^2 - 2[1s(1)1s(2)1s(2)1s(1)] + 1s(2)^2 1s(1)^2\} dr$$

$$= \frac{1}{2}\int \{[1s(1)]^2[1s(2)]^2 - 2[1s(1)]^2[1s(2)]^2 + [1s(2)]^2[1s(1)]^2\} dr$$

$$= \frac{1}{2}(1 - 2 - 1) = 0$$

Equation 42.

where again $\int [1s(1)]^2 dr = \int [1s(2)]^2 dr = 1$. Thus the probability of a state in which both electrons share the same orbital while having the same spin orientation is zero. Again the antisymmetric requirement that the Pauli spin statistics impose on the fermionic wavefunction leads to profound consequences. The periodic table of the elements is a testimony to this antisymmetry requirement. As there are only two possible spin alignments that an electron can adopt, there can only be two electrons sharing the same orbital while engaging in an antiparallel alignment: a third electron would necessary be parallel to one of them and eventually develop zero probability density in the respective region of the populated orbital. Thus, the only available option for a third electron is to occupy an excited state. Thus chemistry commences.

When placed in two different orbitals, the two He electrons can engage in both parallel and antiparallel alignments. For the parallel alignment, we have:

$$\ddot{\Psi}_{1s2s}^{He} = \frac{1}{\sqrt{2}}[1s(1)\alpha(1)2s(2)\alpha(2) - 1s(2)\alpha(2)2s(1)\alpha(1)]$$

$$= \frac{1}{\sqrt{2}}[1s(1)2s(2) - 1s(2)2s(1)]\alpha(1)\alpha(2)$$

Equation 43.

The probability density associated with this state is non-vanishing:

$$\begin{aligned}\int \left|\ddot{\Psi}^{He}_{1s2s}\right|^2 d\tau &= \frac{1}{2}\int [1s(1)2s(2) - 1s(2)2s(1)]^2 dr \int [\alpha(1)]^2[\alpha(2)]^2 d\omega \\ &= \frac{1}{2}\int \{[1s(1)]^2[2s(2)]^2 - 2[1s(1)2s(2)1s(2)2s(1)] + 1s(2)^2 2s(1)^2\} dr \\ &= \frac{1}{2}(1 - 0 + 1) = 1\end{aligned}$$

Equation 44.

with $\int [\alpha(1)]^2 d\omega = \int [\alpha(2)]^2 d\omega = 1$ and $\int 1s(1)2s(1)dr = \int 1s(2)2s(2)dr = 0$. Continuing in the same manner with antiparallel alignment we find:

$$\begin{aligned}\Psi^{He}_{1s2s} &= \frac{1}{\sqrt{2}}\begin{vmatrix} 1s_\alpha(1) & 2s_\beta(1) \\ 1s_\alpha(2) & 2s_\beta(2) \end{vmatrix} = \frac{1}{\sqrt{2}}[1s(1)\alpha(1)2s(2)\beta(2) - 1s(2)\alpha(2)2s(1)\beta(1)] \\ &= \frac{1}{\sqrt{2}}[1s(1)2s(2)\alpha(1)\beta(2) - 1s(2)2s(1)\alpha(2)\beta(1)] = ?\end{aligned}$$

Equation 45.

We reached a dead end using this notation as we can no longer separate the spatial part of the wavefunction from its spin part. We can write another wavefunction associated with this state by keeping in mind that it has to be antisymmetric. Because the wavefunction is written as the product between a spatial part and a spin part, only one of these two parts has to be antisymmetric with regards to the swapping of the two electrons in the two available orbitals so that the overall wavefunction remains antisymmetric. If both spatial and spin part are antisymmetric, the resulting wavefunction will be overall symmetric and therefore incorrect from the Pauli's spin statistics perspective (the situation being similar when both parts are symmetric). We observe from the previous written wavefunctions that in paramagnetic configurations the spatial part of the wavefunction is antisymmetric while the spin part is symmetric. In the diamagnetic configuration the opposite occurs and thus we expect that, similarly, the Ψ^{He}_{1s2s} wavefunction should possess a symmetric spatial part and an antisymmetric spin part. The spatial part of the wavefunction can now be written in a generalized symmetric manner as $\frac{1}{\sqrt{2}}[1s(1)2s(2) + 1s(2)2s(1)]$. With the inclusion of an antisymmetric spin part in the form $\frac{1}{\sqrt{2}}[\alpha(1)\beta(2) - \alpha(2)\beta(1)]$, the total wavefunction Ψ^{He}_{1s2s} becomes:

$$\Psi_{1s2s}^{He}=\frac{1}{2}[1s(1)2s(2)+1s(2)2s(1)][\alpha(1)\beta(2)-\alpha(2)\beta(1)]$$

Equation 46.

and we can see that this wavefunction, as well, corresponds to a non-vanishing electron density:

$$\begin{aligned}\int|\Psi_{1s2s}^{He}|^2d\tau &=\frac{1}{4}[1s(1)2s(2)+1s(2)2s(1)]^2[\alpha(1)\beta(2)-\alpha(2)\beta(1)]^2\\ &=\frac{1}{4}\int\{[1s(1)]^2[2s(2)]^2+2\cdot 1s(1)2s(1)1s(2)2s(2)\\ &+[1s(2)]^2[2s(1)]^2\}dr\int\{[\alpha(1)]^2[\beta(2)]^2+2\cdot\alpha(1)\alpha(2)\beta(1)\beta(2)\\ &+[\alpha(2)]^2[\beta(1)]^2\}d\omega=\frac{1}{4}(1+2\cdot 0+1)(1-2\cdot 0+1)=1\end{aligned}$$

Equation 47.

Now we can compare the spatial part of $\ddot{\Psi}_{1s2s}^{He}$ and Ψ_{1s2s}^{He} and compute the value of the wavefunction (i.e. the wavefunction amplitude) in a spatial point shared by both electrons. By noting the coordinates of electron (1) as (x_1,y_1,z_1) and similarly (x_2,y_2,z_2) for electron (2), we can compute the wavefunction amplitude in a point (x,y,z) where the two coordinates overlap:

$$\begin{aligned}\frac{\ddot{\Psi}_{1s2s}^{He}}{\alpha(1)\alpha(2)} &=\frac{1}{\sqrt{2}}[1s(x_1,y_1,z_1)2s(x_2,y_2,z_2)-1s(x_2,y_2,z_2)2s(x_1,y_1,z_1)]\\ &\xRightarrow{\substack{x_1=x_2=x\\ y_1=y_2=y\\ z_1=z_2=z}}\frac{1}{\sqrt{2}}[1s(x,y,z)2s(x,y,z)-1s(x,y,z)2s(x,y,z)]=0\end{aligned}$$

Equation 48.

Thus, the probability of finding the two spin-parallel electrons in the same region of space is zero. As a consequence of the antisymmetric nature of the wavefunction associated this paramagnetic state, the two electrons will avoid each other in their motion. This will cause an overall increase of the average value of the distance between them which in turn will lead to an overall decrease of the electrostatic repulsion that the two electrons will experience. Each electron is said to be surrounded by a *Fermi hole* because the probability density of each electron to be in superimposed on the other electron drops to zero, causing thus a hole in the probability density map of both electrons. The presence of Fermi holes is the cause of the electrostatic correction that appears in the form of the exchange integral *K* when two electrons share the same spin orientation.

Similarly, the wavefunction amplitude of two antiparallel electrons placed in two different orbitals can be computed as:

$$\frac{\Psi_{1s2s}^{He}}{\frac{1}{\sqrt{2}}[\alpha(1)\beta(2)-\alpha(2)\beta(1)]} =$$
$$= \frac{1}{\sqrt{2}}[1s(x_1,y_1,z_1)2s(x_2,y_2,z_2)+1s(x_2,y_2,z_2)2s(x_1,y_1,z_1)]$$
$$\xrightarrow[z_1=z_2=z]{\substack{x_1=x_2=x\\ y_1=y_2=y}} \frac{1}{\sqrt{2}}[1s(x,y,z)2s(x,y,z)+1s(x,y,z)2s(x,y,z)] = \frac{2}{\sqrt{2}}[1s(x,y,z)2s(x,y,z)]$$
$$= 2[1s(x,y,z)2s(x,y,z)]$$

Equation 49.

The opposite effect occurs when the two electrons are antiparallel as now the amplitude of one electron over the region belonging to the other electron is twice in magnitude to that it would normally had if no other electrons would be present at all. Electrons (and fermions in general) tend to clump together if their spins are antiparallel aligned and are said to form *Fermi heaps*. Their formations represent the prime reason behind covalent bonding and thus it can be asserted that the covalent bond is a stabilized Fermi heap.

Hartree-Fock theory incorporates the exchange interaction by making use of the so-called Fock operator, $\hat{f}$:

$$\hat{f} = \hat{h}_{e-N} + \sum_i \left(\hat{J}_i - \hat{K}_i\right)$$

Equation 50.

which is given by the one-electron operator $\hat{h}_{e-N}$ (provided by Equation 25), the Coulomb operator $\hat{J}_i$ and by the exchange operator $\hat{K}_i$. The last two operators act on a given electron present in a φ_1 spinorbital by including the presence the other electron in a φ_2 spinorbital. Being given by:

$$\hat{J}_1\varphi_1 = \left[\int \frac{\varphi_2^*\varphi_2}{r_{12}}d\tau\right]\varphi_1$$

Equation 51.

the Coulomb operator is said to be local because of its multiplicative nature and because it assures that for any random point *r* in space there is an uniquely defined potential On the other hand, for the exchange operator given by:

$$\hat{K}_1\varphi_1 = \left[\int \frac{\varphi_2^*\varphi_1}{r_{12}}\,d\tau\right]\varphi_2$$

Equation 52.

the locality is no longer preserved, as the orbital upon which it acts appears under the integral. The non-locality of the exchange operator implies that the value of region surrounding a point *r* is needed in order for a property value to be computed in that certain point *r*.

2.4.3.2.2 Post Hartree-Fock methods

Although capturing in its description the subtle quantum mechanically exchange correlation, the Hartree-Fock method fails to accurately describe chemical systems mainly because its two fundamental limitations. On the one hand, although corrected by the determinant approach, the Hartree product premise will exclude electron correlation as it treats the movement of all electrons as uncorrelated events (cf. Equation 15 and the paragraph discussing it). Its second drawback comes from its monodeterminant nature which accounts for the Hartree-Fock failure in describing systems that are in resonant states and, thus, possess a characteristic determinant for each resonance.

The electron correlation problem is in fact a collection of different types of phenomena that contributes to the dependence of an electron's movement to the motion of the other present electrons. The fact that the Hartree-Fock method neglects the majority of these phenomena has led Löwdin to define the energy stabilization resulting from the much more ordered, correlated movement of electrons as the difference between the real, exact energy of the system and the energy computed at the Hartree-Fock level of theory. However, we have seen that Hartree-Fock theory can actually account for one type of correlation, namely from the exchange correlation resulting from the presence of Fermi holes around each electron. The electron correlation resulting from the Coulombic interactions that would describe the movement of each electron in the explicit presence of the other electrons is known as the dynamical correlation part of the electron correlation problem. The quantum mechanical nature, in terms of superposition of states, can drive an interaction between the superposed states present in the resonant systems and therefore will further impose constrains to the electron motion – it will further correlate it. This part of the electron correlation problem is referred to as the non-dynamical part of the electron correlation problem. Added to this, there is a fourth phenomenon that contributes to the electron correlated motion: the static correlation which is magnetic in nature and accounts for an unpaired electron's spatial constrains due to its ferromagnetic, antiferromagnetic or superexchange interaction with another unpaired electron present in a different site of the system.

The dynamical correlation energy can be recovered by the perturbational theory-based methods (cf. section 2.4.3.3). Typical for quantum chemistry are the MPn methods, which stand for the names of their original contributors – Møller and Plesset – and with n standing for the n-th term of the Taylor expansion (cf. Equation 76) up to which terms are included the perturbation treatment.

In order to account for the non-dynamical correlation effects, all states participating in the superposition need to be explicitly included. Such states are usually denoted as references of the superimposed system and for this reason the method employs an explicit determinant for each configuration is known as the Multireference method (MR, or MRSCF when the self-consistent field (SCF) variational approach complements it). For instance, in the case of the B atom, the ground state electronic configuration implies the presence of a single electron in the *2p* subshell:

$$\Psi^{B} = 1s^{2}2s^{2}2p^{1}$$

Equation 53.

which can actually populate each/any of the triply degenerated $2p_x$, $2p_y$ and $2p_z$ orbitals. A MR wavefunction will take the following form for B ground state configuration:

$$\Psi_{MR}^{B} = \frac{1}{\sqrt{3}}\Psi_{p_x}^{B} + \frac{1}{\sqrt{3}}\Psi_{p_y}^{B} + \frac{1}{\sqrt{3}}\Psi_{p_z}^{B}$$

Equation 54.

where each Ψ_p^B wavefunction is described by a determinant in the Equation 20 form in which the last electron is placed in the x, y or z *2p* orbital.

The states involved in the superimposed state can also include excited states. Such methods are referred to as Configuration Interaction (CI) methods and, similar to the MR methods, exhibit a multideterminant wavefunction comprised of a weighted sum of determinants describing, together with the ground state, each excited state. The MRCI methods employ both the reference expansion of the MR methods as well as the configuration expansion of the CI methods. The span of orbitals involved in the excited states which are near-degenerate, or close to the ground state, form the set of the so-called active orbitals. They are opposed to the inactive orbitals which denote the populated non-frontier orbitals. While the active orbitals are allowed to be populated by one, two or none electrons, the inactive orbitals are always kept doubly occupied. The rest of the virtual orbitals that result from the basis set used to construct molecular orbitals are referred to as external orbitals. The Complete Active Space (CAS) approach includes the sets of inactive and active orbitals in the multideterminant expansion of the wavefunction into the SCF procedure resulting the CASSCF method. In the Restrictive Active Space variant, RASSCF, virtual orbitals from the external orbital domain are also included in the expansion. Both methods account for the non-dynamical part of the electron correlation problem but still lack the treatment of its dynamical part. This, however, can be corrected by including, again, perturbation theory. Its conjunction with the CAS approach, this led to the CASPT2 method, which starts from a CASSCF solution and then applies a second-order perturbation correction such that the dynamical correlation is retrieved.

A full-CI is said to be achieved when all possible excitations that can be accounted by the used basis set are taken into consideration. Such a treatment is adopted by the Coupled Cluster method (CC) which uses an exponential ansatz to expand the Hartree-Fock wavefunction in terms of all possible excitations. The Coupled Cluster wavefunction, Ψ_{cc}, is written as:

$$\Psi_{cc} = e^{T}\Psi_{HF}$$

Equation 55.

with Ψ_{HF} denoting the Hartree-Fock wavefuntion and T being the cluster operator which in turn is given by all coupled excitation that can occur in the studied system:

$$T = T_1 + T_2 + T_3 + \cdots + T_n$$

Equation 56.

in which T_1 represents all single-electron excitation, T_2 all excitation involving 2 electrons and so on up to the case of all n possible excited electrons. The truncation of Equation 55 at different levels of T yields different practical variants of the Coupled Cluster theory. For instance, when all the electronic excitations are restricted at the T_1 and T_2 level the CCSD (single and double excitation including CC) variant is obtained. Likewise, if the triple excitations are also included, the CCSD(T) method is said to be used.

These post Hartree-Fock methods, together with the Hartree-Fock method itself, are generally referred to as *ab initio* methods because they start *from the beginning*, from the Schrödinger equation.

2.4.3.2.3 Semiempirical methods

The semiempirical methods derive from the *ab initio* methods but they avoid the direct computations of some parts of the Hamiltonian by providing an experimentally or previous calculated value for this explicit term. The simplifications adopted by these methods drastically reduce the computational effort at the expense of loss of chemical accuracy. Nevertheless, the semiempirical methods provide a compromise between the size of the studied system and the accuracy under which it is studied. They prove to be useful when properties relating to the motion of electrons within large biological systems need to be computed. For instance, electron excitations or electron transfer processes that cannot be described by molecular mechanics can be tackled by the some semiempirical methods.

The J and K integrals appearing in the Hartree-Fock theory are tackled by semiempirical methods by the use of their estimated values *a priori* the computation. One direction of developing semiempirical approaches consists in neglecting the integrals accounting for interactions between atoms separated by significant distances. A second direction implied the adoption of some parameters that were set to reproduce experimental data. Historically, the semiempirical methods did not only allow the tackling of large systems relevant from the chemical point of view, but also, in an era when computational power was far more scarcely available and when geometry optimization procedures were not yet well established, managed to provide the exploring ground for the computation of the analytical derivatives required to account for the nuclear motion. This not only allowed the computation of the relaxed geometry that a molecule might adopt, but also facilitated the development of procedures that search for transition states.

2.4.3.2.4 Density functional theory

Density functional theory (DFT) methods are by far the most popular of the quantum chemical methods. Their characteristic feature is that instead of working directly with the wavefunction, they works with the electronic density. This gives two main advantages: reduces the computational cost and can also describe the correlation effects. The drawback, however, is that DFT can no longer precisely account for the exchange interaction (i.e. Pauli exclusion effects). Compromises, however, were made to include DFT with Hartree-Fock methods such that a good approximation of the correlation could be obtained from the former and a good approximation of the exchange interaction could be obtained from the latter. Such methods are referred to as hybrid DFT methods and one of the most popular used versions is the so called B3LYP method.

In DFT, the problem of finding the correct wavefunction is avoided by replacing the wavefunction itself with its direct observable effect: the probability density of finding the electron. For short the electron density which, defined in a point *r*, takes the following form:

$$\rho(r) = \sum_i n_i |\varphi_i(r)|^2$$

Equation 57.

where $\rho(r)$ denotes the electron density in point *r*, $\varphi_i(r)$ is the orbital that overlaps the point *r*, and n_i represents the number of electrons by which the $\varphi_i(r)$ is populated. The integration of the total electron density retrieves the number of electrons *N* present in the system:

$$\int \rho(r) dr = N$$

Equation 58.

Interestingly, the position of nuclei in a molecular system can be determined solely from the electronic density. This is because, being effectively positive point charges, the nuclei conglomerates electronic density around them due to the attractive Coulombic interactions. Mathematically, the electronic density as a function of position would exhibit a maximum when reaching positions of nuclei and therefore the derivative of such a function in a nuclear position equals to zero. Furthermore, the charge of the nucleus can be determined from the slope of such a function when computed in the position right next to that of the nucleus. The slope of this function is known to be equal to *-2Z,* with Z being the nuclear charge. For a spherical average density $\bar{\rho}(r)$ surrounding a nucleus position it can be noted that:

$$\frac{\partial \bar{\rho}(r)}{\partial r} = -2Z\rho(r)$$

Equation 59.

Thus the information regarding the position and charge of nuclei is actually stored in the electronic density of the molecular assembly. The potential of all K nuclear-electron attraction, V_{e-N}, can be expressed in terms of electron density in the following way:

$$V_{e-N} = -\sum_{K} \int \frac{Z_k \rho(r)}{r} dr$$

Equation 60.

while the self-repulsion V_{e-e} of the entire electronic density can be provided by

$$V_{e-e} = \frac{1}{2} \iint \frac{\rho(r_1)\rho(r_2)}{|r_1 - r_2|} dr_1 dr_2$$

Equation 61.

The first analytical form for the evaluation of the kinetic energy (*T*) of an electron derived from its electron density probability was first provided in 1927 by Thomas and independently by Fermi in what is referred to as the first density theory approach:

$$T = \frac{3}{10} \sqrt[3]{9\pi^4} \int \sqrt[3]{\rho^5(r)} dr$$

Equation 62.

This early DFT variant represented by the Thomas-Fermi model found success in solid-state physics where its simplicity was counterbalanced by the ability to treat large systems. On the chemical field, however, the Thomas-Fermi model failed to properly describe molecular systems and for this reason little advance was done in the development of density functional theory until the 1960'.

It was 1964 when Hohenberg and Kohn proved that for a given ground state of a system the electronic density can be used as a full descriptor of the system in the same way as the wavefunction is used in *ab initio* methods. In their approach, the electronic density was treated as a uniform electron gas that interacts with an external potential mimicking the nuclear attraction potential. This external potential has the form of Equation 60 and can be expressed as following: each *i* electron will develop a potential $v(r_i)$ with all *K* nuclei given by:

$$v(r_i) = -\sum_{K} \frac{Z_k}{r_{iK}}$$

Equation 63.

which summed of all present *i* electrons retrieves the total external potential *V*:

$$V = \sum_{i} v(r_i)$$

Equation 64.

Now, the expectation value of this external potential was shown to be expressible in terms of the electron density as:

$$\langle \Psi | V | \Psi \rangle = \int v(r) \rho(r) dr$$

Equation 65.

Thus, the external potential can be seen via Equation 65 as function of the electron density which in term can be seen via Equation 57 as a function of the wavefunction. A function of a function is known as a functional, hence the *functional* term in DFT.

To fully describe the electron gas, the internal potential developed between the repelling electrons needed to also be accounted. This internal potential was said to be given by an unknown functional $F^{HK}[\rho]$ that retrieves the ρ electron density that is the outcome of a wavefunction that in terms retieves the smallest value of the expectation value of the electronic kinetic energy and the Coulombic

$$F^{HK}[\rho] \equiv \min_{\Psi \to \rho} \langle \Psi | T + V_{e-e} | \Psi \rangle$$

Equation 66.

Because the Hohenberg-Kohn theorem stated, in other words, that such a functional should exist, without knowing its precise form the Hohenberg-Kohn potential (V^{HK}) was delivered as the sum of the two external and internal potentials:

$$V^{HK} = \int v(r)\rho(r)dr + F^{HK}[\rho]$$

Equation 67.

The following year, Kohn together with Sham adopted a further bold and in the same time weird approach. The electron gas was treated as a fictitious gas in which the electrons do not interact among themselves but only interact with the nuclei via a modified potential, v_x , that would retrieve the same behavior as if the electrons would interact among themselves. The advantage of this approach consists in that by treating the electron gas as non-interactive system the problematic integrals that normally would appear in *ab initio* methods (i.e. Equation 28) are avoided and a one-electron Schrödinger-type equation can be written in the form:

$$\left(-\frac{1}{2}\Delta + v_x\right)\phi_i = \varepsilon_i \phi_i$$

Equation 68.

which can be solved similarly to the nonproblematic Equation 26. Furthermore, Equation 68 is solved in terms of a new type o electronic orbitals, ϕ_i, which are referred to as Kohn-Sham orbitals and are the DFT equivalents of the φ_i *ab initio* molecular orbitals.

The problem, however, of this approach is that it transfers the *ab initio* struggle of finding a correct wavefunction to a DFT struggle of finding a correct Hamiltonian that would account for this fictitious v_x potential. In blagian terms, the DFT *luciferic* endeavor provoked a displacement of the *object of crisis* as now the process of revealing the *paradisiac knowledge* is set within the realm of the Hamiltonian. Nevertheless, the *luciferic* endeavor continued, as the Kohn-Sham approach provided a kinetic energy term T^{KS} in the form:

$$T^{KS} = -\frac{1}{2}\sum_i \langle \phi_i | \Delta \phi_i \rangle$$

Equation 69.

where the expression of the total energy could be provided by the electronic density in terms of the Kohn-Sham approach. The total energy of a fictitious Kohn-Sham electron gas E^{KS} is accounted by the kinetic energy of the comprising non-interacting electrons (cf. Equation 69), by the external potential provided by the Hohenberg-Kohn approach (cf. Equation 65), the electron gas self-interaction (while the electrons themselves are assumed to not interact with each other in their motion, the resulting electronic cloud would still possess a self-interaction provided by Equation 61) and …everything left out by not being described by these terms… namely, the coulombic correlation and exchange correlation energies. These two last terms are collected under the same term E_{XC} and now the total Kohn-Sham energy can be written as:

$$E^{KS} = T^{KS} + \int v(r)\rho(r)dr + V_{e-e} + E_{XC}$$

Equation 70.

Similar to the luciferic process of revealing the true nature of a celestial body, given as an example in section 1.1, the mysterious electron-electron interaction is pushed further down into terms still unknown after several aspects of their *mystery* had been revealed (or at least acceptably tackled). From here onwards, the task of finding the correct form of the E_{XC} term became the main DFT priority. Unfortunately however, there is only one case known in which this exchange-correlation potential can be provided exactly, namely for the harmonic helium atom. Although in itself a fictitious system, the harmonic helium atom can be used as a reference system to test developed DFT methods with respect to an exact DFT solution. For any other system, empirical, trained and other type of guesses have been employed to determine the functional form of E_{XC}. Each one of them (and further combination of them) marks the plethora of DFT acronyms that attempt to provide a working functional form of E_{XC}. The empirisation of this process has gone so far that it is by no means incorrect to regard the Kohn-Sham variant of DFT as a semiempirical quantum chemical method. Regardless of ontological aspects, the impact that the DFT revitalisation had on chemistry can be best accounted by the Nobel Prize that Kohn had received in 1998 for his involvement in the DFT development.

2.4.3.3 *Variational vs. perturbational methods*

There are two main mathematical frameworks by which the solutions of the Schrödinger equation for chemistry-relevant systems can be approached… approximately.

The first mathematical approach is based on the variational principle and for this reason the methods adopting this mathematical philosophy are referred to as variational based methods. The variational principle states that for a given random wavefunction Ψ_{random}, the corresponding energy associated with this state, E, will be larger or equal to that of the ground state, E_0. Mathematically this is expressed via Equation 71:

$$E = \frac{\langle \Psi_{random} | \hat{H} | \Psi_{random} \rangle}{\langle \Psi_{random} | \Psi_{random} \rangle}$$

$$E \geq E_0$$

Equation 71.

Although apparently trivial, this principle generates a crucial consequence that lies at the heart of the variational-based mathematical machinery. Since the energy associated with a trial wavefunction will always lead to a state higher in energy than the ground state (if by luck the trial wavefunction is the exact wavefunction then the ground state energy would be retrieved), then the direction by which the wavefunction can be improved (in order to approach the true wavefunction) will always imply a decrease in energy. Thus, given a random wavefunction that needs to be corrected, one needs to always pursue the changes to its structure that lead to a decrease of energy (while changes leading to an increase of energy should be avoided). Basically, this approach consists in constructing a trial wavefunction of the system under interest and corrects it with various iterative algorithms that follow the decrease of the energy until the desired threshold difference of energy in two successive iterative steps is obtained.

The variational principle still holds for some cases involving excited states. Namely, the variational principle can still be applied when Ψ_{random} is orthogonal to all the states encountered between it and the lower, desired $\Psi_{excited.}$ Different variational approaches schemes exist. For instance, the Ritz variational method, which represents the trial wavefunction as a linear combination of its underlying basis functions, and the Hylleraas variational principle.

The second numerical approach to solve the Schrödinger equation is based on the Taylor expansion of the ground state in terms of a perturbing parameter. The methods adopting this mathematical approach form what is referred to as perturbation theory. First of all, this theory requires that the Hamiltonian and wavefunction of the unperturbed system are predetermined (and consequently the eigenenergies of the system's eigenstates) by a variational based method. Perturbation theory can refine the results obtained by variational based methods and can further incorporate physical aspects that were previously neglected. As an example, we briefly mention here that Hartree-Fock is a variational based method that completely neglects the electron correlation phenomenon and that by applying perturbation theory the effect of the electron correlation is incorporated (approach known as MP2 theory). Similarly, CASPT2 is a perturbational refinement of the variational based CASSCF method.

Having a known system characterized by a wavefunction Ψ^0 that once acted upon by a $\widehat{H}^{(0)}$ Hamiltonian retrieves the system energy E_0, the perturbation theory approach can commence by applying a slight perturbation so that the system is slightly moved from its initial state. The philosophy behind perturbation theory implies the refinement of a system's wavefunction by accounting for its modification under the action of a perturbing factor. For instance, the hydrogen atom can be considered as an initial, unperturbed system that is subsequently perturbed by an external electric field. Nevertheless, the Schrödinger equation of the initial, unperturbed system can be noted for all its inherent k eigenstates as:

$$\widehat{H}^{(0)}\Psi_k^{(0)} = E_k^{(0)}\Psi_k^{(0)}$$

Equation 72.

If the perturbing factor is accounted by a $\widehat{H}^{(1)}$ Hamiltonian, then the Hamiltonian of the perturbed system, $\widehat{H}$, can be summed to:

$$\hat{H} = \hat{H}^{(0)} + \hat{H}^{(1)}$$

Equation 73.

In order to stand on its feet, perturbation theory requires that the perturbing Hamiltonian, $\hat{H}^{(1)}$¸ is minute compared to the Hamiltonian of the unperturbed system, $\hat{H}^{(0)}$. One way by which this requirement can be assured to be fulfilled implies the introduction of a perturbation parameter, λ, that modulates the perturbing Hamiltonian, $\hat{H}^{(1)}$:

$$\hat{H}(\lambda) = \hat{H}^{(0)} + \lambda\hat{H}^{(1)}$$

Equation 74.

The λ parameter can vary between 0 and 1, and although for most of its values it might not correspond to physical realities, it serves as a useful tool for the mathematical trick that can be employed in order to express the energy and the wavefunction of the perturbed system in power series. The return to the physical reality can be done by inserting λ=1 in the final equation. The Schrödinger equation of the perturbed system can be noted as:

$$\hat{H}(\lambda)\Psi_k(\lambda) = E_k(\lambda)\Psi_k(\lambda)$$

Equation 75.

with the k indices referring to the eigenstates of the perturbed Hamiltonian (as opposed to the unperturbed eigenstates indexed by *n*). For instance, k=0 refers to the ground state of the perturbed system, k=1 for the first excited state and so on.

Now, the Taylor series of the perturbed energy of a k eigenstate as a function of the perturbing parameter λ can be expanded as:

$$E_k(\lambda) = E_k^{(0)} + \lambda\frac{\partial E_k^{(0)}}{\partial\lambda} + \frac{\lambda^2}{2!}\frac{\partial^2 E_k^{(0)}}{\partial\lambda^2} + \frac{\lambda^3}{3!}\frac{\partial^3 E_k^{(0)}}{\partial\lambda^3} + \cdots$$

or

$$E_k(\lambda) = E_k^{(0)} + \lambda E_k^{(1)} + \lambda^2 E_k^{(2)} + \lambda^3 E_k^{(3)} + \cdots$$

Equation 76.

Similarly, the wavefunction of the perturbed system can also be expanded as a function of λ:

$$\Psi_k(\lambda) = \Psi_k^{(0)} + \lambda \frac{\partial E_k^{(0)}}{\partial \lambda} + \frac{\lambda^2}{2!}\frac{\partial^2 E_k^{(0)}}{\partial \lambda^2} + \frac{\lambda^3}{3!}\frac{\partial^3 E_k^{(0)}}{\partial \lambda^3} + \cdots$$

or

$$\Psi_k(\lambda) = \Psi_k^{(0)} + \lambda\Psi_k^{(1)} + \lambda^2\Psi_k^{(2)} + \lambda^3\Psi_k^{(3)} + \cdots$$

Equation 77.

Having assumed that the perturbation is minute, it is safe to consider just the first few terms of the Taylor expansion in order to obtain a refined energy (and wavefunction) of the studied system. For instance, the zero$^{\text{th}}$ term of Equation 76, representing the eigenenergies of the initial unperturbed (known) system is

$$E_k^{(0)} = \left\langle \Psi_k^{(0)} \middle| \hat{H}^{(0)} \middle| \Psi_k^{(0)} \right\rangle$$

Equation 78.

The first term of the energy correction is the expectation value of the perturbing Hamiltonian computed with the wavefunction of the initial, unperturbed system:

$$E_k^{(1)} = \left\langle \Psi_k^{(0)} \middle| \hat{H}^{(1)} \middle| \Psi_k^{(0)} \right\rangle$$

Equation 79.

The first term of the wavefunction correction is found to be expressed as:

$$\Psi_{\mathrm{k}}^{(1)} = \sum_{k \neq n} \frac{\left\langle \Psi_k^{(0)} \middle| \hat{H}^{(1)} \middle| \Psi_n^{(0)} \right\rangle}{E_k^0 - E_n^0} \Psi_{\mathrm{n}}^{(0)}$$

Equation 80.

where $\Psi_n^{(0)}$ represents an eigenfunction of the unperturbed system differing from the *k*th eigenfunction. For instance, if ground state values are being sought, i.e. *k*=0, n represents all the excited states of the unperturbed system.

The second energy correcting term is given by:

$$E_k^{(2)} = \sum_{k \neq n} \frac{\left\langle \Psi_k^{(0)} \middle| \hat{H}^{(1)} \middle| \Psi_n^{(0)} \right\rangle^2}{E_k^0 - E_n^0}$$

Equation 81.

Two correction terms for the energy expression and one for the wavefunction usually provide enough accuracy in chemical relevant systems. This can be emphasized by the above expression of $E_k^{(2)}$ when the ground state energy is being corrected, i.e. k=0. As each excited state is by definition higher in energy than the ground state, the denominator of Equation 81 is always negative and thus the entire $E_k^{(2)}$ term will decrease the intial, unperturbed (togheter with the first order energy correction) energy. This, by virtue of the variational principle, assures that the inclusion of the second correction term improves the accuracy of the system's computed energy. The correction can, of course, be extended to higher terms. Interestingly, perturbation theory is an odd example in which the inclusion of higher order terms in the truncation of the Taylor series does not necessarily improve the quality of the result, but they rather worsen it. This is in part due to the convergence problems that usually are encountered in the series expressed by the perturbation theory.

There are several variants of perturbation theory employed in the field of quantum chemistry. We restrict the discussion by briefly mentioning the Rayleigh-Schrödinger theory, the Hylleraas approach (that is a continuation of the Hylleraas variational method), the Brillouin-Wigner perturbation theory or the time-dependent formulated Raimes perturbation theory.

2.4.3.4 *Non-relativistic vs. relativistic methods*

Standard quantum chemical methods do not account for the relativistic effects accompanying high-velocity electrons. Thus, one of the reasons behind the incompatibility of quantum mechanics and the theory of relativity lies in the lack of relativistic correction within Schrödinger's equation. Furthermore, the same Schrödinger equation is invariant with regards to the Galilean transformation, which accounts for the classical dependence of the motion of a body in two reference systems that, in turn, are in motion relative to each other, but fails to be invariant with regards to the Lorentz transformation, which is the relativistic version of the Galilean transformation (cf. Figure 12). The invariance with regard to a transformation implies that no coordinate system is treated preferentially, i.e. that the form of the theory's governing equations remains the same in both reference systems. If applied to two reference systems moving at low velocities (compared to the speed of light), the Schrödinger equation retains its form in both systems of reference (i.e. is invariant with regard to the Galilean transformation). However, relative to a stationary reference system, the Schrödinger equation changes its form when applied to a reference systems moving at relativistic velocities.

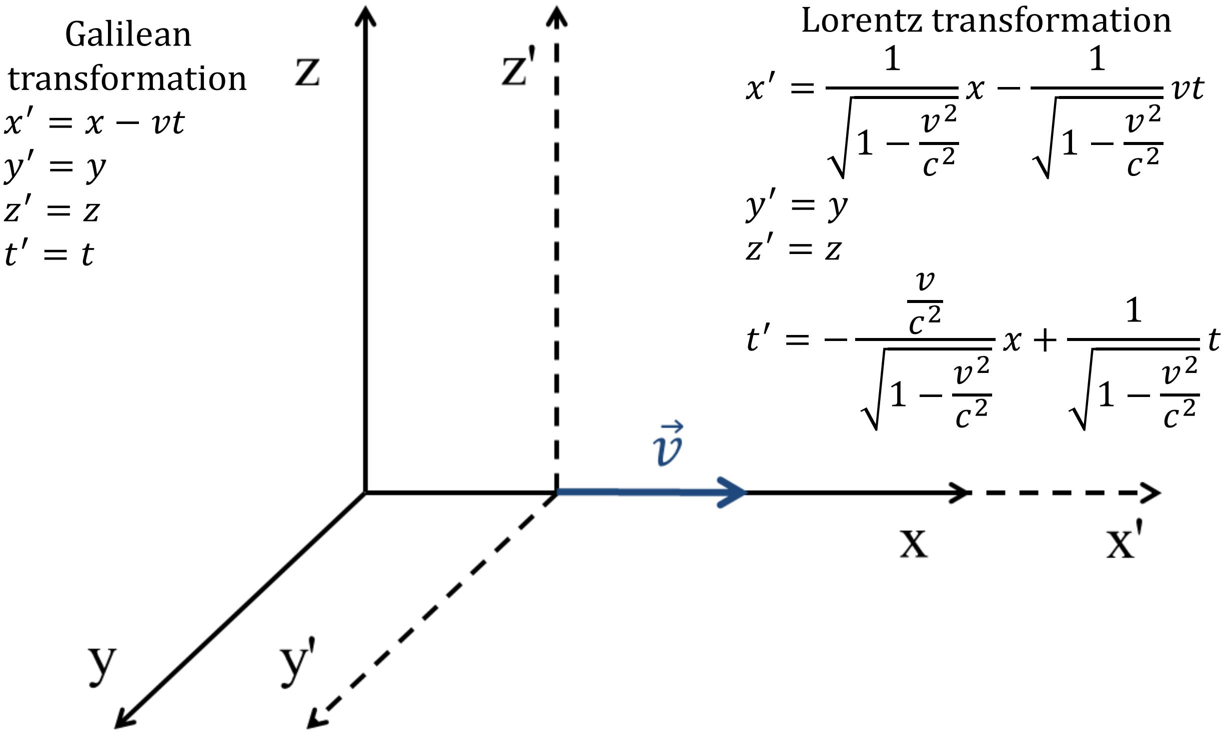

Figure 12. The Galilean and Lorentz transformations of the coordinates of a moving, ***x'y'z'***, reference system relative to a standing ***xyz*** reference system. The motion of ***x'y'z'*** is set along the x axis of ***xyz*** at a ***v*** velocity. When $v \ll c$ the Galilean transformation is recovered from the Lorentz transformation.

Dirac prophesized that relativistic effects will not be important in chemistry. However, his prophecy did not survive the passage of time, as later on it was becoming clearer that the electronic structure of heavy elements cannot be correctly described as long as relativistic effects are neglected. For instance, the core electrons of heavy elements are subject to electrostatic potentials so high that the electrons become accelerated to speeds comparable to the speed of light. Why does this affect in any way the chemistry of that element? One dry and direct answer is that the standard Schrödinger equation (and all approximations further derived from it) breaks down at velocities comparable to the speed of light. Another way to answer this question is to recall that one of the most interesting results of the special theory of relativity is the spatial contraction experienced by a moving body in the framework of a static reference system. From the temporal point of view, this effect is antagonistic and now the time experienced by a moving body will become dilated in the framework of a resting reference system. Both results come as direct consequences of the Lorentz transformation and have to following mathematical expressions:

$$length_{rest} = length_{moving}\sqrt{1-\frac{v^2}{c^2}}; \quad and \quad time_{rest} = \frac{time_{moving}}{\sqrt{1-\frac{v^2}{c^2}}}$$

Equation 82.

The lengths covered by an *1s* electron will be contracted in the framework of a heavy nucleus and thus it can be expected that the atomic orbital itself will become more contracted due to this relativistic effect. In general, the contraction of an orbital is directly tied to its energetic stabilization and thus it is expected that core atomic orbitals will become more stabilized in heavy atoms. The consequences of this relativistic perturbation of electronic structures of heavy elements are best exemplified the case of the Au atom. Its characteristic yellow color is an effect of the disturbance in its electronic structures caused by the relativistic core electrons. It the absence of the relativistic phenomenon, the Au atom would exhibit a silvery colour.[4]

In order to further clarify how these relativistic effects occur in some atoms we will estimate the speed of the *s* electrons present in C and Au atoms. First, the electron speed will be computed in a classical manner and later the computed speed will be revisited by a relativistic approach.

In quantum theory the expectation value of the kinetic energy, $\langle E_{kin}\rangle$, is related to that of the potential energy, $\langle E_{pot}\rangle$, by the Virial theorem:

$$\langle E_{kin}\rangle = \frac{1}{2}s\langle E_{pot}\rangle$$

Equation 83.

The coupling term, s, is related to the potential energy by $E_{pot} = ax^s$ where a is a constant of proportionality. In the case of an electron found in the electric potential of a nucleus, the potential energy has the usual form:

$$E_{pot} = \frac{1}{4\pi\varepsilon_0}\frac{q_1 q_2}{x}$$

Equation 84.

The entire $\frac{q_1 q_2}{4\pi\varepsilon_0}$ quantity can be regarded as a constant and thus Equation 84 can be noted as $E_{pot} = ax^{-1}$. By inserting the obtained $s = -1$ into Equation 83 yields:

$$E_{kin} = -\frac{1}{2}E_{pot}$$

$$E_{tot} = E_{kin} + E_{pot} = E_{kin} - 2E_{kin} = -E_{kin}$$

and

$$E_{kin} = -E_{tot}$$

Equation 85.

The total energy of a free particle, i.e. in the absence of a potential, is always positive, while that of a particle bound by a potential is always negative. In other words, the total energy of bounded states is always positive and those of free states are always negative. This comes as consequence of the anthropic conventions regarding electric charges and their interactions to each other (same-charge particles repel and always give a positive potential while different charged particles attract and always yield a negative potential, cf. Equation 84). Thus, for bound states, it can be noted that $E_{tot} < 0$.

The dependence the electron's velocity on the energy of a bound state can be roughly estimated from the classical expression of the kinetic energy:

$$E_{kin} = \frac{m_0 v^2}{2}$$

Equation 86.

with m_0 representing the resting mass of the electron. The speed, v, can obtained as:

$$v = \pm\sqrt{\frac{2E_{kin}}{m_0}} = \pm\sqrt{\frac{-2E_{tot}}{m_0}} \quad ; \quad E_{tot} < 0$$

Equation 87.

A standard quantum chemical computation retrieves the energy of a system, E_{comp}, expressed in atomic units. In this system of measurement the mass of the electron is by definition equal to unity, i.e. $m_0 \equiv 1$, and the speed of light takes the approximate value $c \cong 137$.

We now approximate the computed energy as equal to the total energy, i.e. $E_{tot} = E_{comp}$, and thus, by adopting the atomic units of measurement and retaining only the physically acceptable solution (the + solution), the speed of an electron in an energetic state, E_{comp}, relative to the speed of light can be estimated by:

$$\frac{v}{c} = \frac{\sqrt{-2E_{comp}}}{137}; \quad E_{comp} < 0$$

Equation 88.

In classical mechanics the mass of a moving body remains constant regardless of velocity. For this reason the relationship between the kinetic energy of a moving body and its momentum, p, has a simple form:

$$\left\{\begin{array}{c} E_{kin} = \frac{mv^2}{2} \\ p = mv \\ m = m_0 \end{array}\right. \rightarrow \quad E_{kin} = \frac{p^2}{2m}$$

Equation 89.

The relation between the kinetic energy and momentum takes a slightly more complicated form in relativistic mechanics, due to the dependence of the mass of a body to its velocity. Indeed, the mass of a body is no longer a constant quantity, but becomes a variable proportional to the velocity. This dependence takes the following form:

$$m = \frac{m_0}{\sqrt{1 - \frac{v^2}{c^2}}}$$

Equation 90.

where m is the mass of a body moving at speed v, c represents the speed of light, and the m_0 the mass of the object when stationary, i.e. its resting mass. Now, the relativistic expression of the momentum, p, becomes:

$$p = \frac{m_0 v}{\sqrt{1 - \frac{v^2}{c^2}}}$$

Equation 91.

For a body moving in an environment of a free of any potential, the kinetic energy accounts for the entire energy of the system, which in turn can expressed by Einstein's famous $E = mc^2$ equation. With m expressed by Equation 90, the kinetic energy becomes:

$$E_{kin} = \frac{m_0 c^2}{\sqrt{1 - \frac{v^2}{c^2}}}$$

Equation 92.

Einstein's equation implies an equivalency between mass and energy and for this reason, in the special theory of relativity, a stationary particle outside of any exterior potential will still possess an *internal* energy in the form of its mass. This energy can be noted as E_{rest} and will take the simple form (which can also be obtained from Equation 92 by inserting $v=0$):

$$E_{rest} = m_0 c^2$$

Equation 93.

By taking the difference of Equation 92 and Equation 93, we obtain the *pure* kinetical term:

$$E_{kin} - E_{rest} = \frac{m_0 c^2}{\sqrt{1 - \frac{v^2}{c^2}}} - m_0 c^2 = m_0 c^2 \left(\frac{1}{\sqrt{1 - \frac{v^2}{c_2}}} - 1 \right)$$

Equation 94.

In order to express the velocity as a function of energy, we first need to retrieve *v* from under the radical. We can try this by squaring Equation 93:

$$(E_{kin} - E_{rest})^2 = {m_0}^2 c^4 \left(\frac{1}{\sqrt{1 - \frac{v^2}{c^2}}} - 1 \right)^2$$

$${E_{kin}}^2 - 2E_{kin}E_{rest} + {E_{rest}}^2 = \frac{{m_0}^2 c^4}{1 - \frac{v^2}{c^2}} - 2\frac{{m_0}^2 c^4}{\sqrt{1 - \frac{v^2}{c^2}}} + {m_0}^2 c^4$$

Equation 95.

but we still remain with a coupling term between the kinetic and the Equation 95 resting energy, that still implies a radical expression. However, we can now note the following identities:

$${E_{kin}}^2 = \frac{{m_0}^2 c^4}{1 - \frac{v^2}{c^2}}; \quad E_{kin}E_{rest} = \frac{{m_0}^2 c^4}{\sqrt{1 - \frac{v^2}{c^2}}}; \quad {E_{rest}}^2 = {m_0}^2 c^4$$

Equation 96.

and by taking just the difference between the square of the kinetic energy and the square of the resting energy we avoid carrying the radical expression along our equations:

$$E_{kin}{}^2 - E_{rest}{}^2 = \frac{m_0{}^2c^4}{1-\frac{v^2}{c^2}} - m_0{}^2c^4 = m_0{}^2c^4\left(\frac{1}{1-\frac{v^2}{c^2}} - 1\right)$$

$$= m_0{}^2c^4\left(\frac{1-1+\frac{v^2}{c_2}}{1-\frac{v^2}{c^2}}\right) = m_0{}^2c^4\left(\frac{\frac{v^2}{c_2}}{1-\frac{v^2}{c^2}}\right) = \frac{m_0{}^2c^4\frac{v^2}{c_2}}{1-\frac{v^2}{c^2}}$$

$$= \frac{m_0{}^2v^2c^2}{1-\frac{v^2}{c^2}} = m^2v^2c^2 = p^2c^2$$

Equation 97.

and thus:

$$E_{kin}{}^2 - E_{rest}{}^2 = p^2c^2$$

$$E_{kin}{}^2 = p^2c^2 + E_{rest}{}^2$$

$$E_{kin}{}^2 = p^2c^2 + m_0{}^2c^4$$

Equation 98.

which represents the relativistic expression that connects the momentum of a moving particle to its kinetic and resting energy. We now collect the main measures involved in the dynamics of a relativistic particle in Equation 99.

$$\left\{\begin{aligned} E_{kin} &= \frac{m_0c^2}{\sqrt{1-\frac{v^2}{c^2}}} \\ p &= \frac{m_0v}{\sqrt{1-\frac{v^2}{c^2}}} \\ m &= \frac{m_0}{\sqrt{1-\frac{v^2}{c^2}}} \end{aligned}\right. \quad \rightarrow \quad E_{kin}{}^2 = p^2c^2 + m_0{}^2c^4$$

Equation 99.

We are now interested in expressing the relativistic velocity of a moving body in terms of its momentum, which in turn will be expressed in terms the kinetic energy of the system. Then we can obtain an expression involving the total energy of a state and thus make use a of a standard quantum chemical computation in order to estimate the speeds of the C and Au *s* electrons with the use of relativistic formula. We do this by squaring the expression of the relativistic momentum (Equation 91) and then express the velocity in terms of momentum:

$$p^2 = \frac{m_0^2 v^2}{1 - \frac{v^2}{c^2}} = \frac{m_0^2 v^2 c^2}{c^2 - v^2} \leftrightarrow p^2 c^2 - p^2 v^2 = m_0^2 v^2 c^2$$

$$p^2 c^2 = m_0^2 v^2 c^2 + p^2 v^2 = v^2 (m_0^2 c^2 + p^2)$$

Equation 100.

From here we extract *v:*

$$v = \pm \sqrt{\frac{p^2 c^2}{m_0^2 c^2 + p^2}}$$

Equation 101.

We retain the positive solution because only it represents a physically meaningful case and now express the speed of an relativistic electron relative to the speed of light as:

$$v = \frac{1}{c} \sqrt{\frac{p^2 c^2}{m_0^2 c^2 + p^2}}$$

Equation 102.

Because the standard computational approach that we will use is derived from the non-relativistic Schrödinger equation, the total state energy that will be computed will not include the electron rest energy term (E_{rest}). We can correct this by adding the resting energy term as follows: we note the energy computed via the quantum chemical approach as E_{comp} and observe that this quantity represents the relativistic total energy of the state, E_{tot}, deprived of the relativistic resting energy of the electron, E_{rest}:

$$\left|E_{comp}\right| = |E_{tot}| - |E_{rest}|$$

or

$$|E_{tot}| = \left|E_{comp}\right| + |E_{rest}|$$

Equation 103.

Because E_{comp} and E_{tot} have negative values while E_{rest} is a positive, we express this as:

$$E_{tot} = E_{comp} - E_{rest}$$

Equation 104.

The kinetic energy relates to E_{tot} via Equation 85 and thus we have:

$$E_{kin} = -E_{comp} + E_{rest}$$

Equation 105.

By squaring we obtain:

$$E_{kin}^2 = E_{comp}^2 - 2E_{comp}E_{rest} + E_{rest}^2$$

Equation 106.

which equated to Equation 98 leads to:

$$E_{comp}^2 - 2E_{comp}E_{rest} + E_{rest}^2 = p^2c^2 + {E_{rest}}^2$$

Equation 107.

from which we obtain the following expressions that we can use to compute *v*:

$$p^2c^2 = E_{comp}^2 - 2E_{comp}E_{rest}$$

$$p^2 = \frac{E_{comp}^2 - 2E_{comp}E_{rest}}{c^2}$$

Equation 108.

In the atomic units of measurement, we have $E_{rest} = 137^2$ and Thus Equation 102 becomes:

$$\begin{cases} v = \dfrac{1}{137}\sqrt{\dfrac{p^2c^2}{137^2 + p^2}} \\ p^2c^2 = E_{comp}^2 - 2 \cdot 137^2 E_{comp} \\ p^2 = \dfrac{E_{comp}^2 - 2 \cdot 137^2 E_{comp}}{137^2} \end{cases}$$

Equation 109.

Now that we have obtained an approximate expression for the relativistic case as well, we proceed by performing some simple and fast quantum chemical calculations (using the DFT approach under the B3LYP functional in conjunction with the DND basis set) to obtain the electronic structures of the carbon and gold atoms. Table 1 collects the results of these calculations together with the electron velocities computed with the above-discussed classical and relativistic formulae.

In the case of the C atom, the computed electron velocities do not even approach the same order of magnitude as the speed of light, and therefore the relativistic effects accompanying these electrons can safely be discarded. In the Au case however, up to the *3s* atomic orbital the computed electron velocities have the same order of magnitude as the speed of light. Thus, the relativistic effects in the electronic structure of the Au atom cannot be neglected.

Table 1. Electron velocities in C and Au *s* orbitals computed via Equation 88 and Equation 109. Velocities are expressed relative to the speed of light, *c*. E_{tot} represents the atomic orbital energy computed at the B3LYP/DND level of theory.

Atom	state	E_{tot}	v/c	
		a.u.	classical	relativistic
C	1s	-10.320	0.033	0.033
	2s	-0.474	0.007	0.007
Au	1s	-2685.004	0.535	0.484
	2s	-453.142	0.220	0.216
	3s	-109.751	0.108	0.108
	4s	-25.978	0.053	0.053
	5s	-3.334	0.019	0.019
	6s	-0.198	0.005	0.005

Now there is a quite interesting observation regarding the electronic velocities values computed with our classical (cf. Equation 88) and relativistic (cf. Equation 109) approaches. For low velocities, the two approaches retrieve the same results, but for the high velocities encountered in the Au *1s* and *2s* atomic orbitals the relativistic values are lower than the classical values. One might be puzzled why the relativistic velocities are lower than the classical one since, as we previously stated, the relativistic effects cause a stabilization of the Au core electrons. This was stated in our phenomenological explanation of this effect in terms of relativistic spatial contractions. This effect was quantitatively proven already in the late '70s in the case of Au and Hg atoms, where it was shown[4] that the relativistic effects cause a strong stabilization of the core orbitals which in turn shift the valence orbitals at energy levels that cause the specific gold color in Au atoms and stabilizes the Hg *6s* to the point that filling it makes it behave "almost as a rare gas". Since an orbital stabilization by definition means an increase of the absolute value of its energy, which in turn increases the absolute value of the kinetic energy as well (as shown in the virial theorem discussion at the beginning of this subchapter) the electron velocity is expected to increase as well. This expectation is valid in classical domains, but in the relativistic area this can no longer be the case because here the acquired extra kinetic energy, besides the increase of velocity, can be also accounted as an increase of mass. Thus, for the relativistic domain it is safer to restrict the effect of the kinetic energy increase to an increase of the momentum. This increase of momentum could happen with a simultaneous increase of mass and velocity, or with an increase of one at the expense of the other (when compared to the non-relativistic case). So, are the relativistic effects causing a decrease of velocity compared to the classical determined velocities determined for the same energetic state? Our results from Table 1 imply a positive answer. We can prove this for any general case by expressing the same amount of momentum of a particle in both classical and relativistic manners:

$$p_{classic} = p_{relativistic}$$

$$m_0 v_{classic} = \frac{m_0 v_{relativistic}}{\sqrt{1 - \frac{v_{relativisic}^2}{c^2}}} = \frac{m_0 v_{relativistic}}{\gamma}$$

$$v_{classic} = \frac{v_{relativistic}}{\gamma}$$

Equation 110.

Because no particle can exceed the speed of light, $\gamma = \sqrt{1 - \frac{v_{relativisic}^2}{c^2}} < 1$ and it can be concluded that $v_{classic} > v_{relativistic}$.

Thus for a given energetic state, the computed electron velocity will be always smaller when the relativistic effects are considered than when they are neglected.

This is valid for the case when one computed energy value is translated into electron velocity via our classical and relativistic approaches. In reality, the relativistic effects will stabilize the state and thus different energy states would be obtained when the relativistic effects are turned on.

The relativistic effects accompanying a core electron can also be viewed through the lens of Heisenberg's uncertainty principle:

$$\Delta x \Delta p \geq \frac{h}{4\pi}$$

Equation 111.

The relativistic contraction can be accounted as an decrease of Δx, which, being in an inverse proportionality relation with the momentum, would cause an increase of Δp. When approaching the speed of light, the rate of velocity increase would be diminished compared to the rate of the mass increase.

An increase of the electron speed up to luminous velocities also alters the temporal aspects of its dynamics (cf. Equation 82). If, again, the reference system of the nucleus is considered static with regards to the moving reference system of the electron, the time intervals will become dilated in the nucleus reference system. From the Heisenberg uncertainty principle

$$\Delta E \Delta t \geq \frac{h}{4\pi}$$

Equation 112.

the time dilatation means an increase of Δt which in turn leads to a decrease of ΔE. In cases when the energy variation has a lowest lying energy limit, E_o, such as in the case of quantum bounded states (i.e. atoms), this decrease of certainty in the energy measurements also causes the decrease of the energy mean value. Thus, it can be expected that relativistic effects would decrease the energy mean values of states associated with high-speed electrons. In other words, the observed energy stabilization of relativistic electrons contained in atoms can be rationalized through the uncertainty principle.

All this was done by using a non-relativistic Hamiltonian, yet we still managed to grasp a sense of the relativistic effects that appear in heavy atoms. The correct way to do it implies a relativistic Hamiltonians and now we will follow the way in which such an expression was for the first time obtained. The kinetic energy of a relativistic system can be re-expressed from Equation 99 as:

$$E_{kin} = \pm c\sqrt{p^2 + {m_0}^2 c^2}$$

Equation 113.

By adding a potential energy term, V, the total energy of the system, E, is expressed as:

$$E = \pm c\sqrt{p^2 + {m_0}^2 c^2} + V$$

Equation 114.

If the system itself is comprised of an electron of mass m_0 that moves in the field of an electromagnetic potential $V = q\Phi$ (with q representing the electron charge and Φ accounts for the field), the momentum of the electron will be influenced by the field (which will be accounted by function A of the field) and Equation 114 can be written as:

$$E = \pm c\sqrt{\left(p - \frac{q}{c}A\right)^2 + {m_0}^2 c^2} + q\Phi$$

$$(E - q\Phi)^2 = c^2\left[\left(p - \frac{q}{c}A\right)^2 + {m_0}^2 c^2\right]$$

Equation 115.

now the quantum mechanical momentum and time-dependent energy operators can be introduced:

$$\left(i\hbar\frac{\partial}{\partial t}-q\Phi\right)^2=c^2\left[\left(-i\hbar\nabla-\frac{q}{c}\boldsymbol{A}\right)^2+{m_0}^2c^2\right]$$

Equation 116.

and by attaching the systems wavefunction, Ψ, the Schrödinger-Fock-Klein-Gordon equation is obtained:

$$\left(i\hbar\frac{\partial}{\partial t}-q\Phi\right)^2\Psi=c^2\left[\left(-i\hbar\nabla-\frac{q}{c}\boldsymbol{A}\right)^2+{m_0}^2c^2\right]\Psi$$

Equation 117.

From here on, Dirac took the next steps and rewrote Equation 117 as follows:

$$\left(\frac{i\hbar\frac{\partial}{\partial t}-q\Phi}{c}\right)^2-\left[\left(-i\hbar\nabla-\frac{q}{c}\boldsymbol{A}\right)^2+{m_0}^2c^2\right]=0$$

Equation 118.

And by making the following notations he obtained:

$$\pi_0=\frac{i\hbar\frac{\partial}{\partial t}-q\Phi}{c};\quad \pi_\mu=-i\hbar\nabla-\frac{q}{c}\boldsymbol{A};\quad \mu=x,y,z$$

$$\pi_0^2-\sum_{\mu=x,y,z}\pi_\mu^2+{m_0}^2c^2=0$$

Equation 119.

Dirac regarded this as an a^2-$b^2=0$ equation and expanded it as $(a+b)(a-b)=0$, from which he could then force out in terms of some unknown coefficients, α_μ and α_0, the following form:

$$\left(\pi_0+\sum_{\mu=x,y,z}\alpha_\mu\pi_\mu+\alpha_0m_0c\right)\left(\pi_0-\sum_{\mu=x,y,z}\alpha_\mu\pi_\mu-\alpha_0m_0c\right)=0$$

Equation 120.

He then analyzed these unknown coefficients, and by noting that they must satisfy the anticommutation relationships $\alpha_\mu^2 = 1;\ \ \alpha_\mu\alpha_\nu + \alpha_\nu\alpha_\mu = 1;\ \ with\ \ \mu \neq \nu$ he concluded that these coefficients must be some sort of matrices (as no numbers can satisfy these conditions). He then managed to expressed them in terms of Pauli matrices, σ_{x}, σ_{y}, σ_{z} :

$$\alpha_x = \begin{pmatrix} 0 & \sigma_x \\ \sigma_x & 0 \end{pmatrix} = \begin{pmatrix} \begin{pmatrix} 0 & 0 \\ 0 & 0 \end{pmatrix} & \begin{pmatrix} 0 & 1 \\ 1 & 0 \end{pmatrix} \\ \begin{pmatrix} 0 & 1 \\ 1 & 0 \end{pmatrix} & \begin{pmatrix} 0 & 0 \\ 0 & 0 \end{pmatrix} \end{pmatrix}$$

$$\alpha_y = \begin{pmatrix} 0 & \sigma_y \\ \sigma_y & 0 \end{pmatrix} = \begin{pmatrix} \begin{pmatrix} 0 & 0 \\ 0 & 0 \end{pmatrix} & \begin{pmatrix} 0 & -i \\ i & 0 \end{pmatrix} \\ \begin{pmatrix} 0 & -i \\ i & 0 \end{pmatrix} & \begin{pmatrix} 0 & 0 \\ 0 & 0 \end{pmatrix} \end{pmatrix}$$

$$\alpha_z = \begin{pmatrix} 0 & \sigma_z \\ \sigma_z & 0 \end{pmatrix} = \begin{pmatrix} \begin{pmatrix} 0 & 0 \\ 0 & 0 \end{pmatrix} & \begin{pmatrix} 1 & 0 \\ 0 & -1 \end{pmatrix} \\ \begin{pmatrix} 1 & 0 \\ 0 & -1 \end{pmatrix} & \begin{pmatrix} 0 & 0 \\ 0 & 0 \end{pmatrix} \end{pmatrix}$$

$$\alpha_0 = \begin{pmatrix} \begin{pmatrix} 1 & 1 \\ 1 & 1 \end{pmatrix} & \begin{pmatrix} 0 & 0 \\ 0 & 0 \end{pmatrix} \\ \begin{pmatrix} 0 & 0 \\ 0 & 0 \end{pmatrix} & \begin{pmatrix} -1 & -1 \\ -1 & -1 \end{pmatrix} \end{pmatrix}$$

$$\boldsymbol{\sigma_x} = \begin{pmatrix} \mathbf{0} & \mathbf{1} \\ \mathbf{1} & \mathbf{0} \end{pmatrix}, \boldsymbol{\sigma_y} = \begin{pmatrix} \mathbf{0} & \boldsymbol{-i} \\ \boldsymbol{-i} & \mathbf{0} \end{pmatrix} \boldsymbol{\sigma_x} = \begin{pmatrix} \mathbf{1} & \mathbf{0} \\ \mathbf{0} & \mathbf{-1} \end{pmatrix}$$

Equation 121.

By noting $\sum_{\mu=x,y,z} \alpha_\nu \pi_\nu \equiv \boldsymbol{\alpha} \cdot \boldsymbol{\pi}$**,** Equation 120 takes the following form:

$$(\pi_0 + \boldsymbol{\alpha} \cdot \boldsymbol{\pi} + \alpha_0 m_0 c)(\pi_0 - \boldsymbol{\alpha} \cdot \boldsymbol{\pi} - \alpha_0 m_0 c) = 0$$

Equation 122.

Each bracket is, on its own, equal to 0. Furthermore, each bracket quantity is in the form of an operator that should act on the same wavefunction, Ψ:

$$(\pi_0 + \boldsymbol{\alpha} \cdot \boldsymbol{\pi} + \alpha_0 m_0 c)\Psi = 0$$

Equation 123.

$$(\pi_0 - \boldsymbol{\alpha} \cdot \boldsymbol{\pi} - \alpha_0 m_0 c)\Psi = 0$$

Equation 124.

Now, Dirac expanded and stated that while Equation 123 describes the electron, Equation 124 should describe something which is similar to the electron but in the same time also opposed in nature to the electron. No such particles were known at that time of his predictions, but soon such a particle was indeed found by Andersson at the precise energy value predicted by Dirac (the particle was discovered in experiments involving collisions of subatomic particles; the energy predicted by Dirac refers to the collision energy required to observe such particle). The particle had the same rest mass as the electron, but with a positive charge. This positive electron became known as the *positron.*

By expanding π_0 of Equation 123, the following is obtained:

$$\left(\frac{i\hbar\frac{\partial}{\partial t} - q\Phi}{c} + \boldsymbol{\alpha} \cdot \boldsymbol{\pi} + \alpha_0 m_0 c\right)\Psi = 0$$

$$\left(i\hbar\frac{\partial}{\partial t} - q\Phi - c\boldsymbol{\alpha} \cdot \boldsymbol{\pi} - \alpha_0 m_0 c^2\right)\Psi = 0$$

Equation 125.

And by rearranging, the time-dependent Dirac equation of the electron is obtained:

$$i\hbar\frac{\partial\Psi}{\partial t} = (q\Phi + c\boldsymbol{\alpha} \cdot \boldsymbol{\pi} + \alpha_0 m_0 c^2)\Psi$$

Equation 126.

which for stationary states becomes:

$$(E - q\Phi - c\boldsymbol{\alpha} \cdot \boldsymbol{\pi} - \alpha_0 m_0 c^2)\Psi = 0$$

Equation 127.

Symmetrically, the same equations can be obtained for the positron:

$$i\hbar\frac{\partial\Psi}{\partial t} = (q\Phi - c\boldsymbol{\alpha}\cdot\boldsymbol{\pi} - \alpha_0 m_0 c^2)\Psi$$

Equation 128.

$$(E - q\Phi + c\boldsymbol{\alpha}\cdot\boldsymbol{\pi} + \alpha_0 m_0 c^2)\Psi = 0$$

Equation 129.

The Dirac equation lies at the foundation of all relativistic quantum chemical methods. Besides the prediction of antiparticles, the further development of the Dirac equation in terms of bispinors retrieved in a natural way the *spin* concept that the non-relativistic quantum mechanics had to postulate in order to account for the experimentally discovered inherent electron magnetic moment. The Dirac equation also overcomes the relativistic limitation of the Schrödinger equations as it is invariant with regards to the Lorentz transformation.

2.4.3.5 *Standard vs. Periodic*

The usual way to deal with the scaling problem when one wants to increase the size of a studied system is to somehow truncate the system in different regions and apply different levels of theory within each region. The level's accuracy (and therefore computational cost) of each region may be assigned in terms of the region's relevance towards the investigated issue. However, if the increased system comprises a periodically repeating central unit, then the system's translational symmetry can be exploited in order to compute desired wavefunction-derived properties. Such methods that tackle the system size-extensivity through the virtue of translational symmetry can be referred to as *periodic methods* (e.g. periodic Hartree-Fock, periodic DFT).

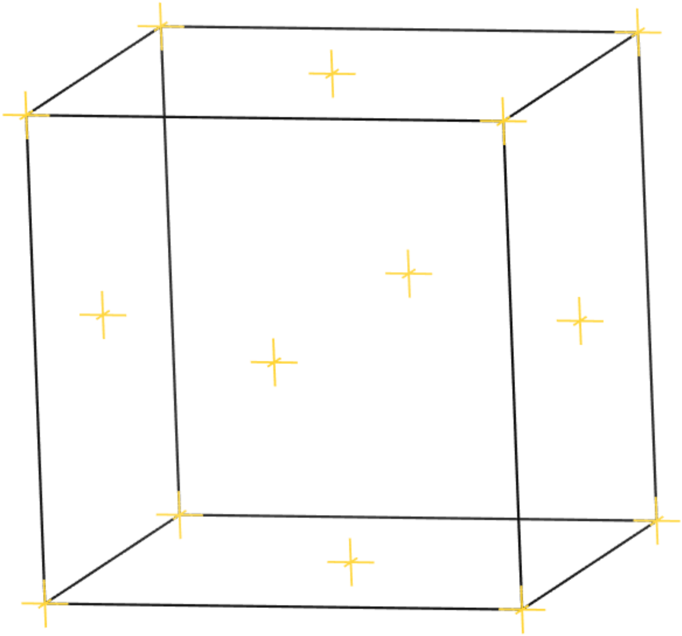

Figure 13. The Au face-centered cubic unit cell. The positions of Au atoms within the cubic cell are marked in yellow crosses.

One of the common areas of research where the periodic methods are of most use is the science of solid state materials. In general, all materials that possess a crystal or crystal-like structure can be subjected to a periodic approach. For instance, Figure 13 captions the repeating unit that is encountered in solid state Au. This is formed by a cube that has Au atoms placed on the middle of each of its face and on all of its vertices – a structure that is referred to as a face-centered cubic unit cell. The solid state structure of Au is formed by repeating the unit cell in all three directions. As an example, a nano-sized fragment from a bulk Au is represented in Figure 14, where the unit cell (cf. Figure 13) was repeated 5 times along each spatial dimension.

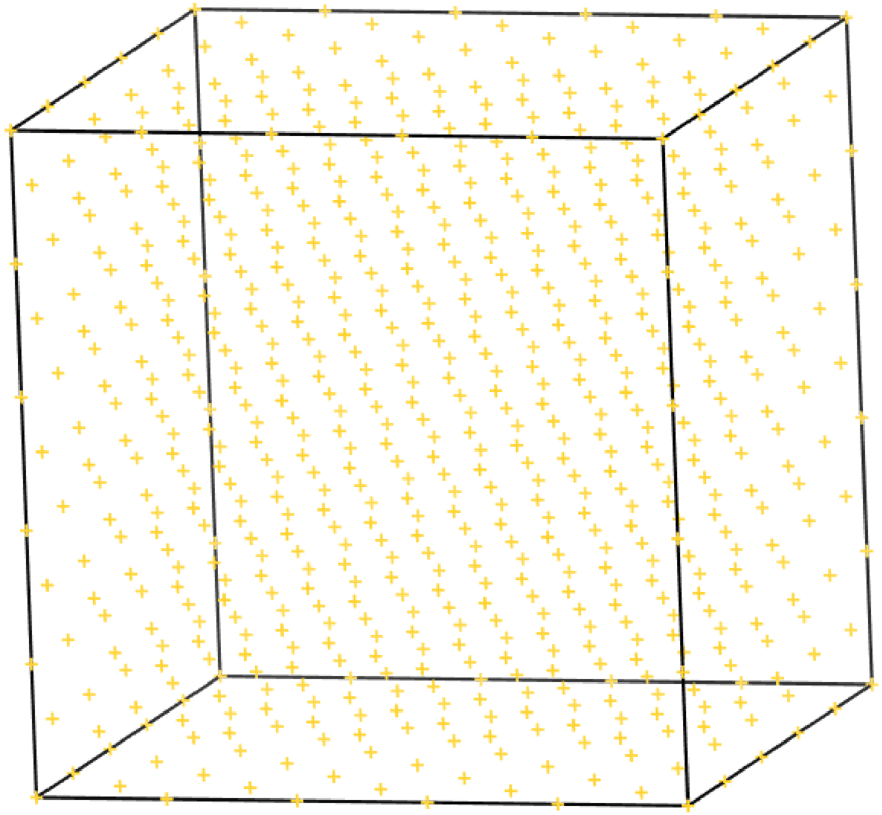

Figure 14. A 5x5x5 supercell of Au unit cells.

As each position of the unit cell (*r*) is occupied by the same atomic species, the potential takes the same value, $V_{(r)}$, in each such point. When measured along a edge of the unit cell, the potential will decrease as we move away from position *r* until we reach the middle of the distance between positions *r* and *r+1*. From here onwards the potential will increase until we reach position *r+1*. The same behavior will remain valid if we continue to positions *r+2, r+3* ... *r+n*. The distance between the consecutive positions corresponds to the unit cell length, *L*. Thus, a simple way to note the translational symmetry manifested in the (electromagnetic) potential is:

$$V_{(r+L)} = V_{(r)}$$

Equation 130.

This periodicity characterizing the variation of the potential constrains the wavefunction to adopt a form in which its amplitude varies in a similar, periodic, way along each direction axis. Such wavefunctions are known from the solutions of the Schrödinger equation applied to a free particle and are called planewave solutions. The planewave wavefunctions adapt easily to periodic systems by adjusting their maximum amplitude on the positions occupied by atoms. The general form that they adopt is given by the Bloch theorem which can be basically distilled to:

$$\Psi_{(k,r+L)} = e^{ikL}\Psi_{(k,r)}$$

Equation 131.

with k being a vector that assures that a translation between two consecutive points can be modulated by a phase factor e^{ikL}. This newly introduced quantum number also denotes the type of atomic orbital that is used to construct the wavefunction. For instance, in the Au case, there is a planewave function generated by a *3d* atomic orbital, one for *6s* and so on. The sum of each atomic orbital over all atoms present in the periodic structure is known as the electronic band of that particular orbital.

2.4.3.6 *Vacuum vs. Solvent environment*

Quantum chemical calculations retrieve results for isolated systems which can be accounted for systems in vacuum or, at most, in gas phase. If interested in the interactions present, for example in solutions, of a solvated molecule with the surrounding solvent molecules, one would have to explicitly add the solvent molecules in order to account for the solvation effects accompanying the solute once its solvation process commences. The problem encountered now relates to the number of solvent molecules that would nee to be added within the model in order to attain a realistic grasp of the solvation effects present in the studied system. One may add a few layers of solvent molecules around the solute and then adopt the periodical approach (similar to 2.4.3.5) by which a translational symmetry is imposed within the solvent region afar from the solvated molecule. This approach might work for small molecules; however, for larger solute systems a high computational cost would incur as the number of explicitly added solvent molecules would need to be very large.

Another way to deal with the solvation problem is to exclude the solvent molecules from the model and to retain their electrostatic effect on the solute. As each solvent molecule is characterized by a dielectric constant (that accounts for the bulk polarity of the solvent), the entire region surrounding the solute molecule can be modelled as a dielectric continuum that is characterized by the dielectric constant of the solvent molecule. There is a computational advantage for a solvent-implied approach as the number of atoms that need to be quantum-chemically accounted is restricted to those of the solute molecule.

The idea to use a dielectric continuum in order to compute the solvation effects can be traced all the way back to the 1920s when Max Born approximated the solvation energy of an ion in a solvent *s* by:

$$\Delta G_s^{ion} = -\frac{\varepsilon - 1}{\varepsilon} \cdot \frac{Q^2}{2R}$$

Equation 132.

where ΔG_s^{ion} represents the solvation free energy of an ion in solvent s, ε denotes the dielectric constant of the solvent, Q is the charge of the ion and R the effective ion-radius.

The dielectric constant, also known as permittivity, measures the polarizability of a dielectric material (=an insulator that is polarized when subjected to an electric field). The vacuum has the lowest possible polarizability and its value is set by definition to 1 (i.e. $\varepsilon_0 = 1$). Higher polarizabilities correspond to higher ε values. For instance, the permanently polar molecule H_2O has a dielectric constant ε=80. In the extreme limit, when $\varepsilon \to \infty$, a dielectric becomes a conductor. A dielectric medium surrounding two immersed charges will screen their interaction. As each individual charge will now have to electrostatically interact and polarize the dielectric medium, the two charges can now interact only via the residue charge that is not involved in the interaction with the dielectric medium. The more polarizable the dielectric medium is, the more charge is available for interacting with the immersed charged and thus less residual charge remains available for the *transdielectric* interaction between the two immersed charges. In the conductor limit, the screening becomes complete as now, at infinite polarizability, the medium will have at its disposal any opposing charge available to interact with the immersed charge. At the opposite limit, in vacuum, there is no available dielectric charge that could interact with the two charges and thus the vacuum screening effect is zero.[*]

---

[*] This is true for small electric fields. For large electric fields like those present between the nucleus and *1s* electrons (especially in heavy atoms), quantum electrodynamic effects will cause the interparticle vacuum to manifest itself as a weak dielectric that will slightly screen the nucleus-electron interaction. The cause of this manifestation is rooted in the Heisenberg uncertainty principle and is due to the spontaneous vacuum generation of particle-antiparticle pairs that will exist for a short amount of time before they annihilate. The amount of time available for the pair existence depends on the type of particles that are generated. This dependence is governed by Equation 112 and thus the more massive (i.e. more energy containing) the particle pairs are, the shorter the

In order to quantitatively describe the screening effect of a dielectric medium, we can start by defining a measure τ that accounts for the amount of residual charge that is left to interact with the other charge through the screening dielectric medium. This measure is similar to the optical transmittance of a medium, just like the screening effect of the dielectric resembles the optical absorbance of a medium. As discussed above, the more polarizable a dielectric is, the more efficient its screening effect is and thus less amount of residual charge, τ, is available for the *transdielectric* interaction. Thus τ is in an inverse proportionality relation with the polarizability of the dielectric medium, $\tau \sim \frac{1}{\varepsilon} \to \tau = \frac{k_\varepsilon}{\varepsilon}$. By choosing $k_\varepsilon = \varepsilon_0$ we assure that τ is in general a subunitary measure whose upper limit value $\tau_{max} = \tau_0 = 1$ (when everything passes through the medium, i.e. in vacuum) and the lower limit value $\tau_{min} = \tau_{conductor} = 0$ (when nothing passess through the medium, i.e. perfect conductor). Thus, $\tau = \frac{\varepsilon_0}{\varepsilon}$. The amount of screened charge is represented by the difference between the amount of charge that can interact through vacuum (i.e. all of it, τ_0) and the amount of residual charge left to interact through the dielectric medium, τ. Therefore, a screening parameter σ can be written as:

$$\tau_0 - \tau = 1 - \frac{\varepsilon_0}{\varepsilon} = 1 - \frac{1}{\varepsilon} = \frac{\varepsilon - 1}{\varepsilon} = \sigma$$

Equation 133.

Which represents the first fraction from Born's equation (cf. Equation 132).

A closer inspection of Equation 132 reveals two limiting cases. The first case represents the solvation of the ion in vacuum, which is accounted by a dielectric constant, of $\varepsilon = 1$. In such a case, the solvation free energy takes the value of zero (which verifies the validity of Born's equation, as no energy change should accompany an ion that is *solvated* from vacuum to vacuum).

$$\Delta G_s^{ion} = -\frac{1-1}{1} \cdot \frac{Q^2}{2R} = 0 \equiv \Delta G_{vacuum}^{ion}$$

Equation 134.

---

time interval between their generation and annihilation is. It so happens that the timescale of electron-positron pair generation is long enough to actually screen the nucleus-*1s* interaction (in the same way, more massive, shorter-living pairs of particles, belonging to the meson family, can screen the nucleon-nucleon interaction from within the nucleus).

The second case is encountered when the value of the dielectric constant is increased up to the point that becomes characteristic for conducting materials. In the perfect conductor limit, $\varepsilon \to \infty$, the solvation free energy becomes:

$$\lim_{\varepsilon\to\infty} \Delta G_s^{ion} = \left(-\frac{Q^2}{2R}\right) \lim_{\varepsilon\to\infty} \frac{\varepsilon - 1}{\varepsilon} = -\frac{Q^2}{2R} \equiv \Delta G_{perfect\ conductor}^{ion}$$

Equation 135.

Born's formulation works at a qualitative level. However, soon after, in the 1930's, better estimations of the solvation appeared. Thus, Onsager developed a formulation in terms of the dipole moment of the solvated molecule, μ:

$$\Delta G_s^{dipole} = -\frac{\varepsilon - 1}{\varepsilon + 1/2} \cdot \frac{\mu^2}{2R^3}$$

Equation 136.

while Kirkwood generalized the solvation free energy formalism in terms of multipole expansion:

$$\Delta G_s = -\frac{1}{2}\sum_{l=1}^{\infty} f_l(\varepsilon)\frac{M_l^2}{R^{2l-1}}$$

Equation 137.

with

$$f_l(\varepsilon) = \frac{\varepsilon - 1}{\varepsilon + x_l}; \quad x_l = \frac{l-1}{l}$$

Equation 138.

where *l* is the multipole expansion order, i.e *l*=1 for charge, *l*=2 for dipole , *l*=3 for tripole and so on. M_l represents the multipole expansion term (again *l*=1 for charge, *l*=2 for dipole , *l*=3 for tripole etc). Thus, the Born and Onsager formulations become the first two terms of the Kirkwood's expansion. As no experimental procedure was available for multipole measurements, Equation 137 could not be verified until computational protocols that could compute these terms became affordable.

The first computational approaches appeared in the 1980's in the form the self-consistent reaction field (SCRF) method. Later on, the polarizable continuum model (PCM) was developed and at the beginning of the 1990's the conductor-like screening model (COSMO) was proposed. This led to a conductor-like correction of the PCM model (C-PCM) and to the development of the more accurate COSMO-Real Solvent (COSMO-RS) and the COSMO-Segment Activity Coefficient model (COSMO-SAC). For the rest of the subchapter the COSMO variants will be briefly presented as they were used in the development of this thesis.

COSMO is a dielectric continuum model in which the solvation energy is computed by embedding a solute molecule in a perfectly conducting medium. The embedded molecule generates a cavity within the conductor medium, and the solutes' energy correction due to its immersion, ΔE, is computed via:

$$\Delta E = -\frac{1}{2}\sum_{i,j} \frac{q_i q_j R}{\sqrt{R^4 + 2Rr_i r_j + r_i^2 r_j^2}}$$

Equation 139.

where $q_{i,j}$ are the charges of each atom contained in the molecule, R the radius of cavity and $r_{i,j}$ the distances of each atom from the center of the cavity. There is a specific procedure by which the cavities are built as a function of each atom present in the solute molecule. The COSMO approach was extended for non-spherical cavities and thus offered a higher flexibility. Another specific differentiating aspect of the COSMO method, when compared with other continuum models, lies in the adoption of Equation 138 as a scaling factor for the boundary conditions under which Equation 139 is solved. COSMO offers results that agree at the quantitative scale with experimental data. However, its major downfall is represented by its incapacity to distinguish two different solvents that possess the same dielectric constant.

The solvation free energy, $\Delta G_{i/S}^{*sol}$, is defined as the change in free energy accompanying the immersion of a solute molecule, *i,* from an ideal gas state to a fixed position within a solute, *S*, at constant temperature and pressure conditions. The asterix in the notation denotes that the atomic positions within the solute molecule are kept fixed during the solvation process.

The activity coefficient of a solute, i, in a solution S is denoted as $\gamma_{i/s}$ and can be determined from:

$$\ln \gamma_{i/S} = \frac{\Delta G_{i/S}^{*solvation} - \Delta G_{i/i}^{*solvation}}{RT} + \ln \frac{c_S}{c_i}$$

Equation 140.

where $\Delta G_{i/S}^{*solvation}$ represents the solvation free energy resulting from the immersion of the solute i from vacuum to solution S, while $\Delta G_{i/i}^{*solvation}$ accounts for the free energy resulting from the immersion of the solute molecule i from gas phase to its liquid phase. Thus, the first term accounts for the polarization induced by the solvent molecules on the solute molecule, while the second term accounts for the polarization induced by the solute molecules on the solute molecule. R represents the gas constant, T the temperature while C_S and C_i represent the molar concentrations of the solvent and solute, respectively.

Equation 140 can be rewritten in terms of a computationally more easily available energy measure dubbed the restoration free energy, which accounts for the energy gain by a molecule when transferred from an ideal conductor medium to the real solvent. Thus, Equation 140 can be rewritten as:

$$\ln \gamma_{i/S} = \frac{\Delta G_{i/S}^{*restoration} - \Delta G_{i/i}^{*restoration}}{RT} + \ln \frac{c_S}{c_i}$$

Equation 141.

Further on, the $\ln \frac{c_S}{c_i}$ can be replaced by the so-called Staverman-Guggenheim combinatorial term that offers a better accounting for effects appearing in the cavity formation step:

$$\ln \gamma_{i/S}{}^{SG} = \ln \frac{\phi_i}{x_i} + \frac{z}{2} q_i \ln \frac{\theta_i}{x_i} + l_i + \frac{\phi_i}{x_i} \sum_j x_j l_j$$

$$\phi_i = \frac{x_i q_i}{\sum_j x_j l_j}; \quad \theta_i = \frac{x_i r_i}{\sum_j x_j l_j}; \quad l_i = \frac{z}{2}[(r_i - q_i) - (r_i - 1)]$$

Equation 142.

where x_i represents the mole fraction of component i, r_i the normalized parameter for i, q_i the normalized surface parameter of I, and z is a coordination number usually set to z=10. All parameters are known, and by varying the mole fraction of the solute, x_i, the Staverman-Guggenheim combinatorial term modulates the variation of its activity constant in terms of its concentration in solution.

By rewriting everything in terms of restoration free energy, the energies are computed relative to a standard represented by the perfect conductor. The author of the COSMO-RS method quite often quotes this process as an equivalency to setting a North Pole with regards to which all solvents can be mapped. Nevertheless, the first step of the computational protocol implies a COSMO computation of the solute molecule in a perfect conductor environment, i.e. by setting$\varepsilon \to \infty$.[*] Then the solute molecule is computed in e vacuum. The energetic difference between the two states accounts for the electrostatic component of the restoration energy. In order grasp a more realistic picture of this process, besides the electrostatic interaction between the solute-solvent molecules, their dispersion interaction need to also be included. This is done by asserting a dispersion constant ζ between molecular surfaces and accounting the dispersion in terms of surface available for interaction. Thus:

$$\begin{cases} \Delta G_i^{solv\ \varepsilon\to\infty} = \Delta E_i^{electrostatic} + \Delta E_i^{dispersion} \\ \Delta G_S^{solv\ \varepsilon\to\infty} = \Delta E_S^{electrostatic} + \Delta E_S^{dispersion} \end{cases}$$

Equation 143.

$$\Delta E^{electrostatic} = E^{\varepsilon\to\infty} - E^{vacuum}$$

$$\Delta E^{dispersion} = \zeta A$$

Equation 144.

$$\begin{cases} \Delta G_i^{solv\ \varepsilon\to\infty} = E_i^{\varepsilon\to\infty} - E_i^{vacuum} + \zeta_i A_i \\ \Delta G_S^{solv\ \varepsilon\to\infty} = E_S^{\varepsilon\to\infty} - E_S^{vacuum} + \zeta_S A_S \end{cases}$$

Equation 145.

In COSMO-RS, a standard molecular surface is defined as the unit surface in terms of which all further molecular surfaces will be expressed. This unit of surface is referred to as

---

[*] In practice this is done by inserting the upper limit value of ε that the software can work with. For instance, in Materials Studios the upper limit is ε=10000. The scaling factor for this values becomes $f_l(\varepsilon) = \frac{\varepsilon-1}{\varepsilon+x_l}$=0.9998.

the standard surface area segment and is noted with $a_{eff.}$ Thus, a molecular surface A will be meshed in n segments of a_{eff} , $A = n_i a_{eff}$. A quantum chemical COSMO calculation will retrieve a molecular electrostatic potential that will be directly mapped onto the segmented molecular surface. Each segment will host an amount of electric charge, q, which, relative to the unit surface, can be expressed as a surface charge density σ:

$$\sigma = \frac{q}{a_{eff}}$$

Equation 146.

Each molecule possesses a characteristic distribution of charged segments. This specific molecular information can be arranged by accounting for all the $n(\sigma)$ segments possessing a certain σ charge density and expressing it in terms of the total number of segments hosted by the molecular surface (or, equivalently, as the fraction between the molecular surface $A(\sigma)$ that possesses a σ charge density and the total area of the molecular surface, A):

$$p(\sigma) = \frac{n(\sigma)}{n} = \frac{A(\sigma)}{A}$$

Equation 147.

The obtained ratio has the form of a probabilistic measure as it accounts for the probability to find, within the n segments of a molecular surface, a segment with a σ charge density (or, equivalently, the chance to find a charge density σ on the molecular surface A). This probability measure can be accounted for all the σ values that a molecular surface may possess and can be expressed graphically as a function of the σ values. Such a chart offers a distinctive molecular fingerprint and for this reason $p(\sigma)$ is referred to as the *sigma profile* of a molecule.

In order to account for real liquids, the perfect conductor medium needs to be removed so that now the solute molecules could interact with the solvent molecule. Or, in a mesh sense, the segments of the solute molecule could interact with the segments of the solute molecule. Firstly, the conductor medium is downgraded to a dielectric continuum that will mirror the charge density of both solute and solvent segments. At this point, there is no energetic difference between the obtained state and the one embedded in the perfect conductor as each segment of each molecule will be perfectly screened by its generated antisegment. This is, however, the last quantum chemical standing point of the COSMO based theories. Next, all the segment-antisegment pairs are decoupled and treated as a thermodynamic assembly and allowed to interact with each other. Whenever a segment will encounter its antisegment, there will be no departure from the screening conductor state and therefore no energy will be gained or lost. All other intersegment interactions will account for each scenario in which the solute and solvent could interact in their liquid mixture. The energy of these interactions represents the energy needed to depart from a state in which the solute and solvent are perfectly screened (i.e. immersed in a perfect conductor medium) to the state in which the solute and solvent real interaction is achieved. Because this energy term comes from the interaction of misfitting (in absolute values) segments, it is usually denoted as the *misfit energy* and we will denoted as $E^{segment\ misfit}$. This energy term, however, is equivalent with the restoration energy term discussed in Equation 141. In other words:

$$\Delta G_{i,S}^{*restoration} = E_{i,S}^{segment\ misfit}$$

Equation 148.

Thus a link was constructed from quantum chemically derived solute-solvent molecular properties to a macroscopic thermodynamic property of their liquid mixture. From here onwards a plethora of parameterizations cascades towards two equations of the same "*bipolar personality*"-like theory: COSMO-RS/SAC.

Amazed by the success of the COSMO-RS/SAC methods to predict thermodynamic properties relevant to fluid mixtures, one can only hear the words of John von Neumann echoing between each of their successful prediction: *"With four parameters I can fit an elephant, and with five I can make him wiggle his trunk."*

2.4.3.7 *Stationary vs. Non-stationary / equilibrium vs. non-equilibrium*

All quantum chemical considerations referred up until now share common ground from the time evolution perspective. Namely, they all are applied to stationary conditions (systems that are considered constant in time, hence independent of time). For instance, the solutions of the Schrödinger equation describing the hydrogen atom, that are used as basis function in the vast majority of cases, are themselves solutions of a time-independent problem. However, processes that are in a continuous state of change need to be described by time-dependent approaches. One such approach is to start from the time-dependent Schrödinger equation, while a different approach entails the Green's functions perspective. Within the time-dependent approach, a time-dependent solution offers a glimpse, a static projection of an otherwise dynamic phenomenon.

Density functional theory was eventually generalized in 1984 for time-dependent processes in the form of TD-DFT (time-dependent density functional theory). As a direct descendent of the time-dependent Schrödinger equation, the TD-DFT approach allows the treatment of non-stationary phenomena (systems that change in time). The approach starts by extending the Hamiltonian, $\hat{H}(t)$, with an external potential that is variable in time, $\hat{V}_{ext}(t)$:

$$\hat{H}(t) = \hat{T} + \hat{V} + \hat{V}_{ext}(t)$$

Equation 149.

In Equation 149, $\hat{T}$ represents the kinetic energy operator while $\hat{V}$ the potential energy operator associated with the coulombic interactions within the system. The exterior potential, $\hat{V}_{ext}(t)$, can be, for example, an electromagnetic pulse that can cause the system to depart from its ground state and adopt various excited states. The Schrödinger equation relating a time dependent Hamiltonian also adopts a time-dependent form:

$$\hat{H}(t)\Psi(t) = i\hbar\frac{d}{dt}\Psi(t)$$

Equation 150.

In general, TD-DFT is used by the quantum chemical community to study the excited states of molecules as this approach is less computationally expensive than the CI methods. This external potential, however, can be accounted for many more time-dependent phenomena - such as the rotational and vibrational excitation of molecules in the context of adiabatic movement of nuclei, low-energy ion-atom collision, and also the interaction of atoms with laser fields. Although less often encountered, the TD-DFT external potential can also be employed for the study of single molecular conductances. This, however, is more often dealt with by using Green's functions based methods.

Green's functions were developed in the classical context of electrodynamics where they were defined as inverses of differential operators. They were revived in the context of quantum theory by Julian Schwinger in his pioneering work regarding Quantum

Electrodynamics (QED). Greenhs functions yield so-called propagator solutions which, as suggested by the name, account for the propagation of a system and thus can be used to describe electron flow phenomena. The Green's function $G(x,x')$ of the Schrödinger equation can be noted as

$$[E-\hat{H}]G(x,x')=\delta(x-x')$$

Equation 151.

where E is the energy of the system, H the Hamiltonian operator, $G(x,x^{'})$ the Green's function describing the system propagation from *x* to *x'*, and $\delta(x-x')$ is the Dirac function.

Green's function based methods are also the workhorses of an interesting field of research which developed for the last 3 decades: the science of single molecule electronics, an interdisciplinary field that overlaps organic chemistry, electrochemistry, electronics, nanotechnology, solid state physics and quantum chemistry. The core of this field lies in a pure quantum mechanical concept, namely in the quantum tunneling effect. This phenomenon explains how some processes, which in a normal, classical view of the world, would require a certain amount of energy in order to happen, do actually happen even at lesser amounts of energy.

Quantum tunneling is a subtle consequence of Heisenberg's uncertainty principle (cf. Equation 111) and is usually explained in terms of the wave-particle duality. For instance, nuclear alpha emission was for the first time explained by George Gamov by invoking[5] the wavelike character of the α-particles. The quantum tunneling effect, however, can also be visualized from the particle-like perspective in following way. A moving particle possessing a momentum p smaller than the momentum needed to overpass a potential barrier $p_{barrier}$ will possess a position uncertainty Δx and an uncertainty in the momentum, Δp (cf. left side of Figure 15). When approaching the potential barrier the uncertainty in the particle's position decreases as there is a lesser amount of space available for delocalization. By virtue of Equation 111, the decrease of uncertainty in the particle's position will lead to an increase of the particle's momentum uncertainty. When close to the potential barrier, the amount of Δp accumulated at the expense of the decreased Δx can be enough to sustain the barrier overpass (right side of Figure 15). The same line of thought can be followed through the energy-time variant (cf. Equation 112) of the uncertainty principle. Now, the potential barrier is regarded as the energy required to overpass it. The closer the particle moves towards the potential barrier, the lesser amount of time it will have left until it will reach it. This in turn restrains the amount of time available for *detemporalisation* and thus allows an increase of the particle's energy uncertainty. Again, when close to it, the particle can accumulate sufficient ΔE to overpass the potential barrier, $E_{potential}$. With this particle-like view in mind, one might talk of *quantum overpassing* the same way one talks about *quantum tunneling* when adopting the wavelike view.

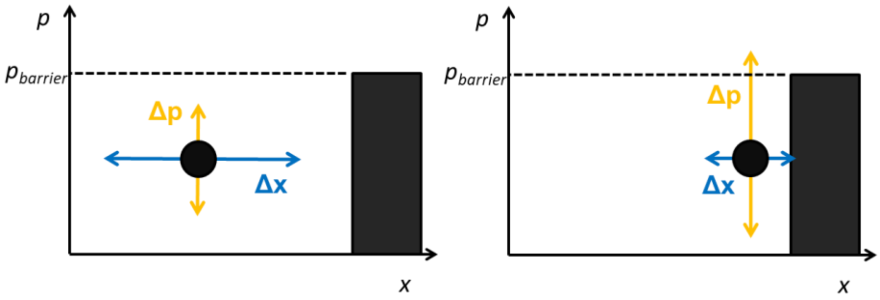

Figure 15. The quantum overpassing of a potential barrier.

Exploiting this phenomenon can lead to interesting applications. In biological systems involved in electron transfer processes, ranging from anaerobic and aerobic processes to photosynthesis, all such electron transfers entail quantum tunneling effects. In modern experimental science, single molecular electronics is a field of research which, by exploiting this quantum tunneling effect, searches for medium sized molecules that can be used as junctions between nanosize electrodes (cf. Figure 16.):

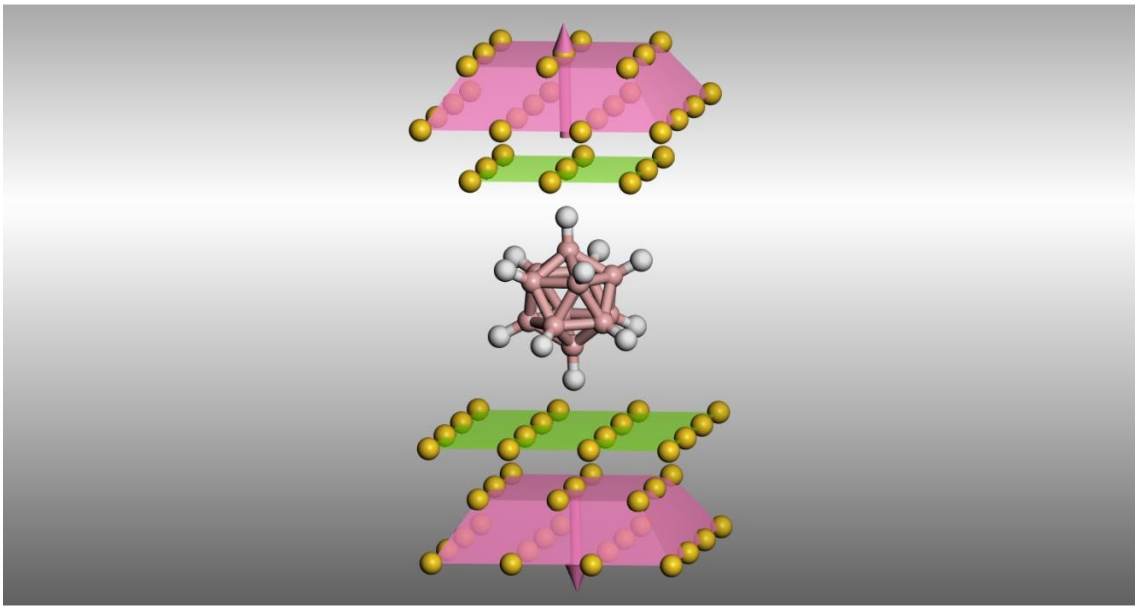

Figure 16. An icosahedral $B_{12}H_{12}$ borane as a molecular junction sandwiched between two Au electrodes.

The term junction implies that the molecule can adhere to the surface of both electrodes and, most importantly, conduct electric current from one electrode to the other. This electric current, although still a transfer of electrons, has a different regime of functioning than that occurring in the metallic electrodes. Molecular orbitals are involved in both cases, but the difference arises from their number (cf. Figure 17). In the metallic case, the number of orbitals involved is practically infinite - and this allows them occupy a continue range or energetic states. The part of this range of continuous energetic states that are occupied with electrons takes the name of “band”. On the other hand, in a molecular structure (such as single-molecule junctions) the number of molecular orbitals is much smaller: although on the order of thousands, it is still minor in comparison to metallic systems. One way to picture the difference is to consider an uncountable number of orbitals involved in the metallic band and a countable, albeit large, number of orbitals involved in molecular systems. Nevertheless, the crucial difference that appears between the two regimes lies in the continuity of the energetic states that they possess. Thus, molecular structures have a discrete range of energetic states, while the metallic having a continuous one.

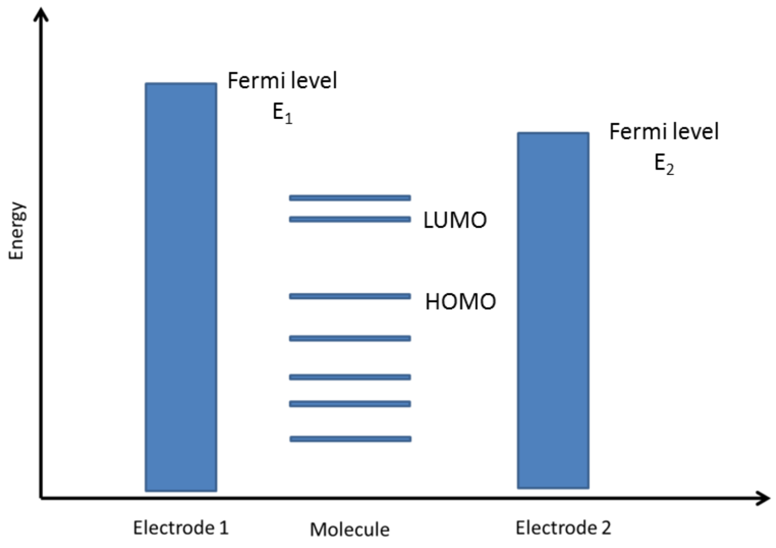

Figure 17. Energy bands associated with two metal electrodes, depicted on the extremities, and a molecular orbital diagram, depicted in the middle.

In most cases, the nanosize electrodes are comprised of metals. Thus, when considering molecular junctions between metallic assemblies, one has to think of an interplay between the previously mentioned regimes of electric currents in terms of favorable overlaps between isoenergetic states. With metal electrodes possessing a continuous range of states, one has to modulate the molecule that is used as junction in such a way that its energetic states lies in the band of the electrodes. More details regarding the theoretical aspects of some Green's functions based methods are provided in section 4.2.

2.5 Chapter Bibliography

1. Lucian Blaga, *Trilogia Cunoasterii*, Editura Humanitas, Bucuresti, Romania, **2013.**
2. Lucjan Piela, *Ideas of Quantum Chemistry*, second edition, Elsevier,**2014.**
3. Christopher J. Cramer, *Essentials of Compuational Chemistry*, second edition, John Wiley & Sons Ltd, UK, **2004.**
4. Peter Atkins, Ronald Friedman, *Molecular Quantum Mechanics,* fifth edition, Oxford University Press, Oxford, UK, **2011.**
5. Malcolm Longair, *Quantum Concepts in Physics*, Cambridge University Press, Cambridge, UK, **2013.**
6. Attila Szabon, Neil S. Ostlund, *Modern Quantum Chemistry*, republished by Dover Publications, INC, Mineola, New York , USA, **2015.**
7. Hans A. Bethe, Edwin E. Salpeter, *Quantum Mechanics of One- and Two-Electron Atoms*, republished by Dover Publications, INC, Mineola, New York , USA, **2008.**
8. Mihai V. Putz, Fanica Cimpoesu, Marilena Ferbinteanu,*Structural Chemistry*, Springer, **2018.**
9. Leonard Susskind, Art Friedman, *Quantum Mechanics*, published by Basic Books, USA, **2014.**
10. Leonard Susskind, Art Friedman, *Special Relativity and Classical Field Theory*, published by Allen Lane, UK, **2017.**
11. Bjorn O. Roos, Roland Lindh, Per Ake Malmqvist, Valera Veryazov, Per-Olof Widmark, *Multiconfigurational Quantum Chemistry*, John Wiley & Sons Ltd, **2016.**
12. Isaiah Shavitt, Rodney J. Bartlett, *Many-Body Methods in Chemistry and Physics*, Cambridge University Press, Cambridge, UK, **2009.**
13. Eberhard Engel, Reiner M. Dreizler, *Density Functional Theory- An Advanced Course*, Springer, **2011.**
14. Richard Dronskowski, *Computational Chemistry of Solid State Materials*, Wiley, **2005**.
15. Andreas Klamt, *Cosmo-RS. From Quantum Chemistry to Fluid Phase Thermodynamics and Drug Design*, Elsevier, **2005.**
16. Jean-Pierrre Launay, Michel Verdaguer, *Electrons in Molecules*, Oxford University Press, Oxford, revised ed., **2018.**
17. Herbert M. Fried, *Green's Functions and Ordered Exponentials*, Cambridge Univeristy Press, Cambridge, UK, **2002.**
18. Bo E. Sernelius, *Gravitation as a Casimir effect*, International Journal of Modern Physics A, **2009**, (24), 8-9, 1804-1812

3 Theoretical studies of hydrogen-rich metallaboranes

Motto:

“Even if our preferred “polyhedral series” thesis
is found to have no theoretical basis and is simply
the unlikely result of quite a number of coincidences,
it should at least serve as a convenient memory aid
in the teaching of this subject.”[*]

Robert E. Williams

---

[*] Fragment from the seminal paper in which Williams formulates the *most spherical deltahedron* paradigm. Cf. R. E. Williams, *Inorg. Chem.*, **1971**, 10, 210–214.

3.1 Introduction

The boron atom can be regarded as an electron deficient element. This comes as a consequence of the ground state of its electronic structure that forms an electronic last shell comprised of four orbitals (i.e. 2s, $2p_x$, $2p_y$, $2p_z$) that can be populated by the just three available electrons. From this electron deficiency perspective, the boron atom is similar to the majority of the transition metal elements and, likewise, boron atoms tend to aggregate in clusters rather than to adopt the planarity present in the rich organic chemistry of its neighboring element, the carbon atom.

Because of their high reactivity, the neutral boranes required special techniques in order to have their molecular formulas determined.[6] This was first possible in the 1930s when Stock, in his pioneering work,[7] synthesized and determined the stoichiometry of the B_2H_6, B_4H_{10}, B_5H_9, B_5H_{11}, B_6H_{10} and $B_{10}H_{14}$. However, their structure and bonding still remained unclear because of their unsuspected stoichiometry. For instance the dimer B_2H_6 (cf. Figure 18) shares the same number of hydrogen atoms as the ethane, C_2H_6, but has two less electrons. The BH_3 molecule itself was behaving ’anomalous´ as it preferred to dimerize to the the same B_2H_6. Although this suggested that the boron atom might be tetravalent (like the carbon atom) in these small molecules, there was still striking evidence from the halogenated versions (i.e. BCl_3, BF_3) that B, as normally expected, is trivalent in nature.

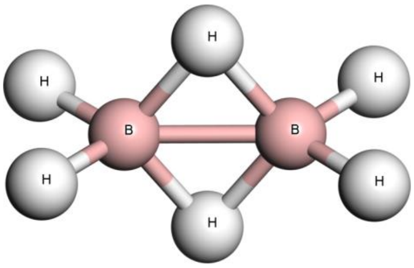

Figure 18. The structure of the B_2H_6 molecule.

The first prediction of the correct structure of B_2H_6 (as shown in Figure 18) appeared earlier in 1921 in a proposal made by Dilthey.[8] However, his interpretation was marginalized by the scientific community until the 1940s when data obtained from infrared spectroscopy[9] supported his interpretation. Although at first this evidence was accepted with reluctance, the final and conclusive proof was brought by X-ray[10] and electron-diffractions studies.[11]

This newly encountered bonding scheme, in which within the same molecule (B_2H_6) the H atom was present in the classical monovalent form but also in an apparent divalent form, led Pitzer to propose the "protonated double bond" concept in 1945.[12] Later, in 1954, Lipscomb introduced[13] the concept of three-center two-electron (3c-2e) bonding by which he was able the explain the bridging H atoms within the B_2H_6 molecule. For this contribution, Lipscomb will be awarded the Nobel Prize in chemistry in 1976. The then known structures of the neutral boranes led Lipscomb to consider all boranes, beside the square pyramidal B_5H_9 molecule, to possess structures based on icosahedral fragments.[10] Later on, after more experimental borane structure became known, Williams corrected[14] Lipscomb's consideration and proposed, in 1971, the concept of "most spherical" deltahedra by which he explained the structural variation of borane compound as the number of BH vertices is increased. A deltahedron is a polyhedron that contains only triangular faces, i.e. in the shape of the Greek letter delta – Δ. Examples of deltahedra commonly adopted by boranes are provided in Figure 19.

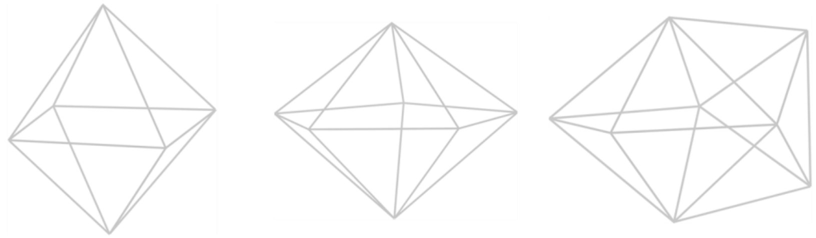

Octahedron
6 vertices

Pentagonal bypiramid
7 vertices

Bidisphenoid
8 vertices

Tricapped trigonal prism
9 vertices

Bicapped square antiprism
10 vertices

Icosahedron
12 vertices

Figure 19. Structures of the 6-10 and 12 most spherical deltahedra usually adopted by borane compounds.

Insights behind the borane's reason to adopt polyhedral arrangements were first brought in 1955 by the work of Longuet-Higgins and Roberts in which[15] the electronic structure of the icosahedral $B_{12}H_{12}$ molecule was computed by hand with the aid of molecular orbital methods. They concluded that the borane icosahedron has 12 bonding molecular orbitals that keep the icosahedral framework together and that the dianion form, $B_{12}H_{12}^{2-}$, would possess the necessary number of electrons to populate them. Thus they predicted that $B_{12}H_{12}^{2-}$ rather than the neutral $B_{12}H_{12}$ will be the stable form. Five years later, in 1960, this prediction was confirmed by the experiments of Hawthorne and Pitochelli[16] after they previously prepared the salts of the $B_{10}H_{10}^{2-}$.[17] A remarkable aspect that both of these new boranes exhibited was the enhanced chemical stability that they possessed, as compared to the previously known BH compounds. Their structures were determined by X-ray diffraction methods, which revealed that the $B_{12}H_{12}^{2-}$ adopts[18] the icosahedral geometry while the $B_{10}H_{10}^{2-}$ that of the bicapped square antiprism[19] (cf. Figure 19). Soon thereafter, the entire $B_nH_n^{2-}$ (n=6-12) series was synthesized and had their structure precisely characterized by X-ray diffraction experiments.[20]

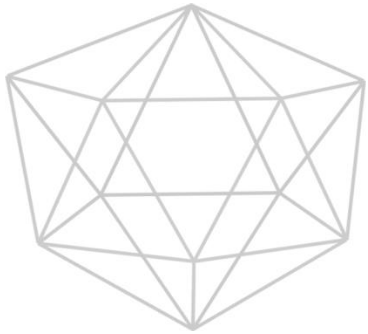

Figure 20. The 11-vertex edge-coalesced icosahedron. The deltahedron is oriented such that its single 6 degree vertex is placed on the top vertex.

The deltahedron paradigm earlier proposed by Williams has now been validated, as it was shown that all $B_nH_n^{2-}$ (n=6-12) structures share the geometries of their corresponding most spherical deltahedra (cf. Figure 19). All structures were comprised only of triangular faces and had their B atoms places in the degree 4 or 5 vertices. The single exception to this behavior was seen in the case of the $B_{11}H_{11}^{2-}$ compound, which, beside degree 4 and 5 vertices, encompassed a degree 6 vertex (cf. Figure 20). King and Diujvestijn later, in 1990, proved[21] that the reason behind this exception within the $B_{11}H_{11}^{2}$ should not be sought in a perhaps exotic behaviour of the B atom, but in the inherent geometric limitations of the 9 vertices deltahedra: that they cannot be built without the aid of an 6 degree vertex.

By replacing two BH vertices with CH units (i.e. 1 electron richer fragment) the neutral analogues of the borane clusters were obtained in the form of the $C_2B_3H_5$, $C_2B_4H_6$ and $C_2B_5H_7$ molecules.[22,23] The synthesis of these structures can be regarded as the dawn of the carborane chemistry.[23] The newly synthesized carboranes shared the same chemical stability as their boranes correspondent. The comparison to the instability of the originally known B-H hydrides suggested that a chemical stabilization might occur in the polyhedrally-structured new boranes. Such kind of stabilization was already known in organic chemistry to occur when certain numbers of electrons are adopted by some ring structures. This enhanced molecular stability caused by the favorable electronic delocalization is known as *aromaticity* and explains for instance why, although sharing the same hexagonal arrangement, the benzene (C_6H_6) molecule is much more stable than cyclohexane (C_6H_{12}). This aromaticity concept was extended to the tridimensional polyhedral boranes in the late 1970s. King and Rouvray used graph theory based methods to demonstrate the analogy between the planar electron delocalization appearing in organic chemistry and the three-dimensional electron delocalization occurring in polyhedral boranes.[24] In the meantime Aihara explicitly proposed[25] the presence of a three-dimensional aromaticity within the polyhedral borane structures. An interesting approach was then taken by Stone and Alderton in 1982.[26] By approximating the deltahedral boranes to spheres and applying the tensor surface harmonic theory, they generated the skeletal orbital of borane deltahedra. These orbital solutions are the correspondents of the spherical harmonic solutions generated by Schrödinger's approach, i.e. the atomic orbitals.

3.2 The Wade-Mingos rules

Beside the $B_nH_n^{2-}$ and $C_2B_{n-2}H_n^{2-}$ series that have been to a certain degree rationalized, there were still the Lipscomb icosahedral fragments that remained unclarified. In the same seminal paper in which the *most spherical deltahedron* paradigm was proposed,[14] Williams also delivered the rationale by which the structural relationship between the known boranes could be made. Although he did not provide a theoretical basis for his rationale, the scheme he proposed arranged the known structures in a geometry-based logic order.

The $B_nH_n^{2-}$ and $C_2B_{n-2}H_n^{2-}$ series adopted closed polyhedra (cf. Figure 19) and hence they were referred to as *closo* structures (from the latin word *clausa*, meaning closed). Beside them, there were the structures that had opened faces. The ones resembling nest-like structures were commonly referred to as *nido* structures (from the Latin word *nidus,* meaning nest). The structures that were even more opened resembled spider nets and for this reason they became known as *arachno* structures (from the Greek work άράχνιον, meaning spider web). Both categories of opened structures featured an extra number of H atoms. The *nido* structures adopted a B_nH_{n+4} general formula while the *arachno* one a B_nH_{n+6} formula. These "extra" H atoms were always bridging units similar to the ones encountered in the B_2H_6 molecule (Figure 18) Williams proposed that a *nido* structure could be obtained from a *closo* structure by the removal of one of its BH vertex and by capping with bridging H atoms the edges of the resulting opened face. Thus a B_nH_{n+4} *nido* structure could be obtained from a $B_{n+1}H_{n+1}^{2-}$ *closo* structure. Similarly, a B_nH_{n+6} *arachno* structure could be obtained from a $B_{n+2}H_{n+2}^{2-}$ by the removal of two BH vertices.

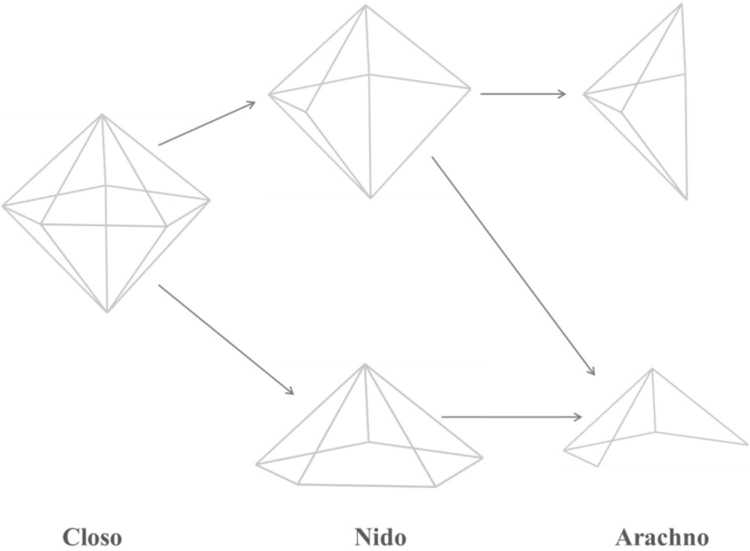

Figure 21. The structural relationship between the *closo, nido* and *arachno* geometries.

An example of this procedure is given in Figure 21. The 7 vertices pentagonal bipyramid is the geometry adopted by the $B_7H_7^{2-}$ molecule and it represents a *closo* structure (left side of Figure 21). There are two types of vertices available within this geometry, namely equatorial vertices (the five vertices that form the pentagonal belt) and apex vertices (the two vertices place on top and below the pentagonal belt). Consequently, there are two possible positions from which a vertex can be removed from the pentagonal bipyramid in order to obtain a 6 vertices *nido* structure. These two possible *nido* structures are shown in the middle of Figure 21, with the structure obtained by removal of an equatorial *closo* vertex shown on top and the one obtained by removal of an apex vertex shown below. The further removal of a vertex leads to the two corresponding *arachno* structures shown on the right side of Figure 21. The *arachno* geometry shown on top has a unique generation path (i.e. by the removal of two equatorial vertices from the *closo* parent), while the one shown below can be obtained from alternating the types of vertices that are removed from the parent *closo* structure and thus there are two paths by which it can obtained (i.e. removal of an apex vertex followed by the removal of an equatorial vertex and vice versa).

Wade provided[27] the theoretical basis that could explain, in terms of electronic structure, the observations that forged Williams's scheme. It was the same year, 1971, and there is a low chance that Wade even knew of Williams work as his paper was received for refereeing two months earlier than Williams' paper. Nevertheless, Wade argued that, because of the symmetries of the $B_nH_n^{2-}$ series, there were always n+1 skeletal bonding molecular orbitals (MO) obtained from the 3n atomic orbitals (AO) provided by each of the n BH vertex. The n+1 MO will be populated by 2n+2 electrons and thus it can be stated that each *closo* structure will be characterized by 2n+2 skeletal electrons, i.e. electrons involved in cluster bonding. He then argued that the symmetries of these internal MOs will remain unaffected if a removed BH^{2+} vertex will be replaced by 4 H^+ at the site of the removal (i.e. on the edges of the opened face). Now two of these 4 H atoms will balance the charge of the leaving BH^{2+} unit and, because the obtained tetragonal face remains with two vacant edges, two extra H can be harbored such that the dianionic nature of the parent *closo* is balanced. Thus, it became clear why the *nido* substances could be obtained as neutral molecules as opposed to the *closo* species which were always obtained in salts in the form of dianions. In terms of electronic structure, a *nido* structure comprised of n vertices will share the number of electrons of its parent n+1 *closo*. In other words, the number of skeletal electrons adopted by a *nido* species will be 2(n+1)+2= 2n+4. The same rationale can be further applied to the *arachno* species. By considering that two vertices need to be removed from a parent *closo*, an *arachno* species will adopt a total of 2(n+2)+2= 2n+6 skeletal electrons. Thus, the *closo, nido* and *arachno* series could be rationalized based on their electron structure or, how it will be further referred, based on their inherent *skeletal electron count.*

Later, in 1983 Mingos generalized[28] Wade's rationale in his *polyhedral skeletal electron pair* approach and provided a simple view by which the structural diversity of polynuclear molecules (e.g. metalla(car)boranes, organometallic polyhedral compounds etc.) could be understood. Thus, the relationship between the electronic structure and the geometries of polyhedral systems became known to be governed by the rationale provided by Wade and Mingos - the Wade-Mingos rules (cf. Figure 25).

By the virtue of the *isolobal principle,*[29] the BH vertex of a polyhedral borane can be substituted by a M(ligand)$_x$ unit (M=transitional metal). The obtained species are known as *metallaborane* sturctures. Their synthesis[30] became a testimony for the ever-growing richness of the borane chemistry. The structural determinations of these metallaboranes proved that some of these structures adopt geometries that are topological different from the *most spherical deltahedra*. Such structures became known as *isocloso* because they shared closed deltahedral but adopted a different geometry. Related to this disobedient geometry was an also disobedient skeletal electron count, as these *isocloso* molecules adopted a 2n paradigm.

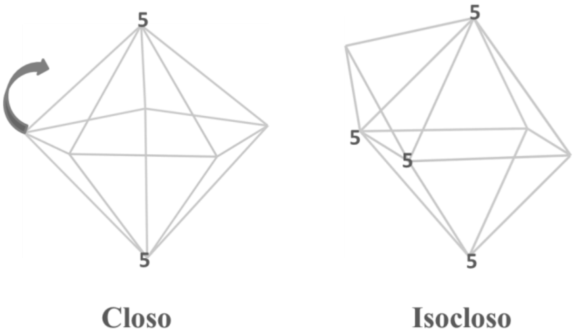

Figure 22. The *closo* 7 vertices bicapped pentagon (left) and its *isocloso* correspondent, the capped octahedron (right). The degree 5 vertices are emphasized.

The *isocloso* structures are related to their corresponding *closo* structures by the rearrangement of some of the polyhedron's vertices such that their connectivity (i.e. the degree of the vertex) is increased. These inversions are obtained by so called diamond-square-diamond fluxional arrangements and were first observed in 9 and 10 vertices systems.[30] For the sake of clearance and simplicity this process will be exemplified for the 7 vertex polyhedron. As seen in Figure 22, the 7 vertices *isocloso* structure is obtained from the autocapping of equatorial vertex of the bicapped pentagonal *closo* followed by a squaring of the equatorial belt. The obtained capped octahedron *isocloso* structure possesses two extra degree 5 vertices.

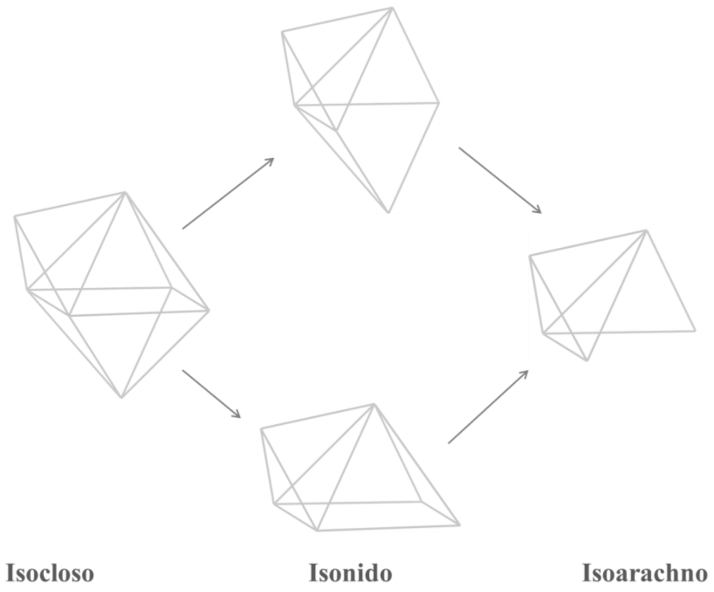

Figure 23. The structural relationship between the *isocloso*, *isonido* and *isoarachno* geometries.

The isocloso 2n skeletal electron count can be rationalized by considering the capping vertex as an electron donor unit that provides the underlying central polyhedron with skeletal electrons. The remaining central octahedron obeys the *closo* electron count and thus acquires 2*6+2 skeletal electrons. Relative to the full polyhedron (i.e. 7 vertices), this translates to a 2(n-1)+2 electron count, which is precisely the 2n electron count specific to the *isocloso* structures. The iso- series can be expanded similar to the *closo* series. Thus an isonido structure can be obtained (cf. Figure 23) either by the removal of an equatorial vertex of the underlying octahedron (middle-top of Figure 23) or by an apex vertex (middle-bottom of Figure 23). Both isonido structures will share an 2n+2 electron count (cf. Figure 25). The removal of an extra vertex which is different from the capping vertex, leads to one possible *isoarachno* structure (cf. right side of Figure 23) that will possess a 2n+4 skeletal electron count (cf. Figure 25).

The dawn of the new millennium marked the discovery of a yet another surprise of the metallaborane chemistry. The group of Fehlner[31] had managed to obtain highly flattened dimetallaborane molecules which featured their metal vertices in the antipodal positions of axial squashed polyhedra. These structures were flattened enough so that the antipodal metal vertices could adhere in bonding (cf. left side of Figure 24). Because of their less spherical and more oblate adopted geometries, these new structures were coined *oblatocloso*. Their apparent electron count also suggested a violation of the Wade-Mingos rules as they were adopting a 2n-4 electron count. Similarly to the *closo* and *isocloso* series, the *oblatonido* and *oblatoarachno* can be obtained from the parent *oblatocloso* (cf. Figure 24) having an 2n-2, respectively 2n electron count (cf. Figure 25).

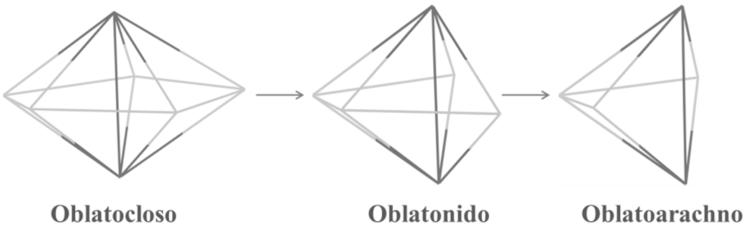

Figure 24. The structural relationship between the *oblatocloso, oblatonido* and *oblatoarachno* geometries.

However, as King has already pointed[32] in 2006, the 2n-4 electron count of the *oblatocloso* series is the result of a blind applications of the Wade-Mingos rules. Within these highly flattened *oblato* structures the metal vertices behave differently than in their corresponding *closo* and *isocloso* structures. In the latter cases, the Wade-Mingos rules implies that each metal vertex will possess three sp^3d^5 hybrid orbitals oriented towards the ligand(s) (and involved in metal-ligand bonding), three oppositely oriented towards the cluster (and available for cluster bonding), while the remaining three orbitals are tangent to the polyhedral surface and thus are nonbonding in character. In *oblato* structures the polyhedron surfaces become less spherical and now the previously nonbonding orbitals can become involved in cluster bonding. Their involvement in cluster bonding leads to the formation of simple of multiple metal-metal bonds.

$$\begin{array}{ccc} closo: 2n+2 & nido: 2n+4 & arachno: 2n+6 \\ isocloso: 2n & isonido: 2n+2 & isoarachno: 2n+4 \\ oblatocloso: 2n-4 & oblatonido: 2n-2 & oblatoarachno: 2n \end{array}$$

Figure 25. The Wade-Mingos rule for the closo, isocloso and oblatocloso classes of structures.

The applications of the Wade-Mingos rules in the *iso-* and *oblato-* families of metallaborane cluster is not as straightforward as in the classical main group (car)borane chemistry. Their rationalization requires extensive theoretical endeavour. Consequently, this chapter will deal with the theoretical investigations of some of such examples, namely of the hydrogen-rich dimetallaboranes contain 5, 6, 7 and 8 polyhedral vertices.

3.3 Theoretical methods

Geometry optimizations were carried out on the $Cp_2M_2B_nH_n$ n=5-8 systems (M = Ir, Ru, Os, Re, Mo, W, Ta for n = 6, 7 and with the extra Pd,Pt, Rh included for the n = 5, 8) at the B3LYP/6-31G(d)[33–35] level for all atoms except the metal, for which the SDD (Stuttgart–Dresden ECP plus DZ) basis set[36] was chosen. The lowest energy $Cp_2M_2B_5H_9$ structures were then reoptimized at a higher level, i. e., M06L/6-311G(d,p)/SDD.[37] The natures of the stationary points after optimization were checked by calculations of the harmonic vibrational frequencies.[38] If significant imaginary frequencies were found, the optimization was continued by following the corresponding normal modes to insure that genuine minima were obtained. Usually this resulted in reduction of the molecular symmetry.

All calculations were performed using the Gaussian 09 package[39] with the default settings for the SCF cycles and geometry optimization, namely the fine grid (75,302) for numerically evaluating the integrals, 10^{-8} hartree for the self-consistent field convergence, maximum force of 0.000450 hartree/bohr, RMS force of 0.000300 hartree/bohr, maximum displacement of 0.001800 bohr, and RMS displacement of 0.001200 bohr. Wiberg bond indices (WBIs) for the M-M interactions in the optimized $Cp_2M_2B_4H_8$ structures determined using NBO analysis[40] were used since they are well-established as means for evaluating M-M interactions in polyhedral dimetallaboranes[41] as well as other binuclear and trinuclear transition metal complexes.[42] Relevant structures, the total and relative energies (including zero-point corrections), and the relevant interatomic distances for all calculated systems are given in section 6.1.

Structures are numbered as **M_2B_5-x** where x is the relative order of the structure on the energy scale. Only the lowest energy and thus potentially chemically significant structures are considered in detail in this chapter.

Most of the $Cp_2M_2B_5H_9$ structures reported in this chapter have a terminal hydrogen atom on each boron atom and four bridging hydrogen atoms. In the Tables, the locations of the bridging hydrogen atoms are designated as M_2, MB, and B_2 for hydrogen atoms bridging metal-metal edges, metal-boron edges, and boron-boron edges, respectively, of the underlying polyhedron. For each particular metal system there is also provided a table in which the skeletal electron count is detailed. The metal atoms are expected to adopt a valence shell expanded in a 9 sp^3d^5 manifold. Three of these orbitals are oriented towards the cyclocpentadienyl ligand (Cp) and consequently become involved in metal-ligand bond formation. Opposed to them, other three orbitals are oriented towards the center of the cluster and thus become involved in cluster bond formation. The remaining three orbitals are tangent to the cluster's spherical surface and thus become of non-bonding nature. Upon coordination, the Cp ligand is considered to accept one electron from the metal atom so that it can adopt the 6 π electrons required for an aromatic stabilization (similar to the benzene molecule). These considerations lead to a simple formula by which the number of electrons donated by an CpM vertex for cluster bond formation can be calculated: out of the *g* valence electrons, 1 electron will be donated to the Cp ligand and 6 electrons will be harboured in the three non bonding orbitals - leaving, thus, a number of *g*-1-6 = *g-7* available for cluster bond donation. However, as already pointed in section 1.1, in flattened metallaborane molecules the initial non-bonding orbitals can become involved in metal-metal bond formation if the two metal atoms are brought in the vicinity of each other. In such cases, the *g-7* rule becomes corrected by the addition of the extra electrons brought by the multiple metal-metal bond formation.

3.4 5 vertices

Historically, the pentaborane represented a high research interest due to its possible military application. After Stone had synthesized and characterized[7] the structure of the B_5 containing molecule in the early 1930's, it became clear that the pentaborane also contains and extra amount of H atoms within its molecular structure. Similarly to the diborane (cf. Figure 18), the 3c-2e B-H-B bonding scheme was adopted by the pentaborane. However, in the latter case, 4 extra bridging H atoms were harbored on the open square face of the central B_5H_5 square pyramidal framework (cf. left side of Figure 26). This led to a general B_5H_9 nido molecular formula that was also referred to as the *pentaborane-9* molecule. Besides the nido pentaborane, there was another pentaborane specie found in lesser amount in the reaction mixture. This species contained 6 extra H atoms and thus had a B_5H_{11} stoichiometry. This *pentaborane-11*, as it was also referred to, possessed the structure of a square pyramid that had one of its basal edges removed. This led the cluster to become even more opened and now the 6 extra H atoms were divided in 3 bridging atoms and 3 terminal atoms. The overall arachno structure is depicted on the right side of Figure 26. Both molecules became of military interest because of their high amount of stored H, which made plausible candidates as fuels for hydrogen-burning missiles. Because of their lower molecular mass, they also possessed higher heats of combustion than the equivalent hydrocarbons. However, the exhaust substances were toxic and, together with the low stability of these molecules, led to the abandonment of their use as rocket fuels. Nevertheless, by the time of this abandonment, tons of pentaborane had already been obtained.

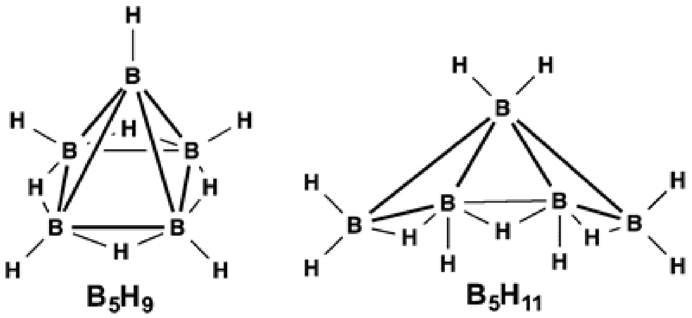

Figure 26. Structures of the two known pentaboranes B_5H_9 and B_5H_{11}.

The structural relationship between the 5-vertices polyhedra is shown in Figure 27. The most spherical 5-vertices deltahedron is represented by the trigonal bipyramid (cf. left side of Figure 27) and it is adopted by the 12 skeletal electron containing $C_2B_3H_5$ molecule.[43] The addition of two extra skeletal electrons can lead to the formation of two possible nido geometries. By removing an equatorial-axial edge, the edge-bridged tetrahedron can be obtained (cf. middle-bottom of Figure 27). Removal of an equatorial-equatorial edge followed by a rearrangement of the initial apical vertices can lead to the formation a tetragonal pyramid (cf. middle-top of Figure 27) such as that adopted by the pentaborane-9 molecule. The addition of 2 extra skeletal electrons leads to further removal of a basal-basal edge and to the formation of the open arachno structure such as that of the pentaborane 11 molecule (cf. right side of Figure 27).

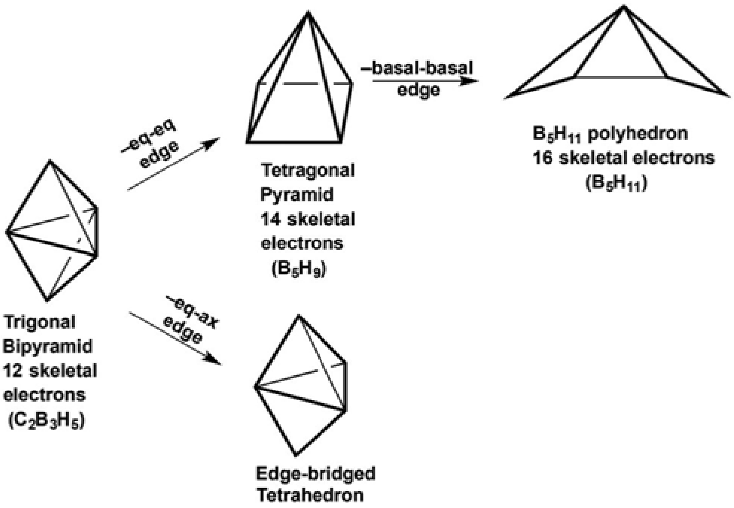

Figure 27 . The relationship between the five-vertex polyhedra and the number of skeletal electrons.

The planar pentagon and the tetragonal pyramid were the initial geometries (cf. Figure 28) from which the structures subjected to geometry optimization computations were constructed. The CpM vertices were substituted in all possible ways and the extra four hydrogen atoms were then incorporated as edge-capping atoms on the edges of the tetragonal/pentagonal open face or on the metal–metal edge. This led to 35 different starting geometries to be optimized for each metal family.

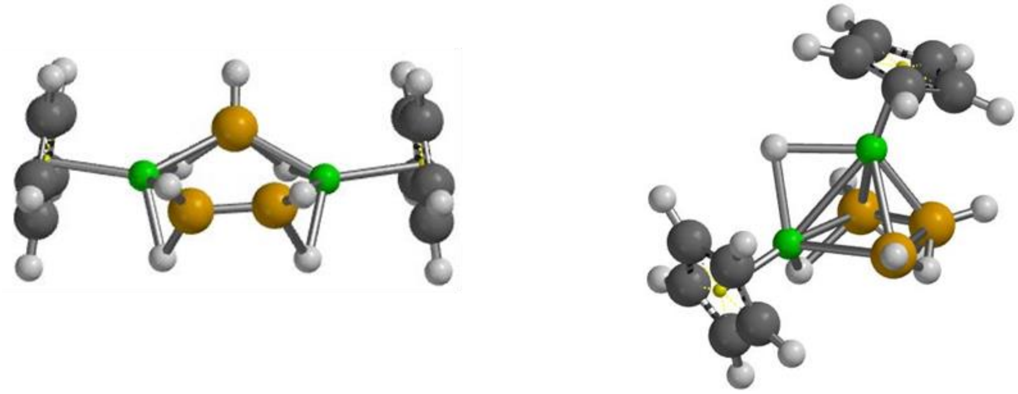

Figure 28. Initial geometries of the $Cp_2M_2B_3H_7$ (M = Pd, Pt) structures and the number of their isomers. Left: the pentagon (32 isomers). Right: the tetragonal pyramid (3 isomers).

3.4.1 $Cp_2M_2B_3H_7$ (M = Pd, Pt) systems

Each metal vertex of the $Cp_2M_2B_3H_7$ (M = Pd, Pt) molecules donates 3 electrons for cluster bonding (cf. Table 2). Added with the 6 electrons provided by the BH vertices and the 4 electrons donated by bridged hydrogen atoms, the total skeletal electron count in these systems rises to 16 Wadean electrons.

Table 2. Skeletal electron count of the $Cp_2M_2B_3H_7$ (M = Pd, Pt) and B_5H_{11} systems.

Molecule	Fragment	Nr. of fragments	e$^-$ donated by fragment	Total e$^-$ donated
$Cp_2Pd/Pt_2B_3H_7$	CpPd/Pt	2	10-6-1=3	6
	BH	3	2	6
	H	4	1	4
	Skeletal electron count			**16**
B_5H_{11}	BH	5	2	10
	H	6	1	6
	Skeletal electron count			**16**

In terms of Wade-Mingos rules, a five vertex cluster possessing 16 skeletal electrons represents a 2n+6 arachno scenario. This implies that the $Cp_2M_2B_3H_7$ (M = Pd, Pt) are isoelectronic with the pentaborane-11 molecule (cf. Table 2). Indeed, the most stable $Cp_2M_2B_3H_7$ (M = Pd, Pt) structures share the same geometry (cf. Figure 29 and Table 3) with the pentaborane-11 molecule (cf. Figure 26). In the metallaborane molecules, the two CpM groups are located in vertices having different degrees of connection. Thus, one CpM group replaces a four-degree BH_2 group in the apical position and the other one replaces a three-degree BH_2 group. In the global ground-state, this basal position occupied by the one CpM vertex is actually located at the cluster's arachno opening. The geometry of the $Cp_2M_2B_3H_7$ (M = Pd, Pt) clusters can be obtained by increasing the distance between two basal vertices of a square pyramid up to a distance at which they can be considered as non-bonded vertices. In the case of pentaborane-11, this distance has been determined by means of X-ray diffraction techniques to be 3.091 Å.[44] In the computed $Cp_2M_2B_3H_7$ (M = Pd, Pt) structures, this arachno opening possesses a distance of ~3 Å between the two non-bonded basal vertices.

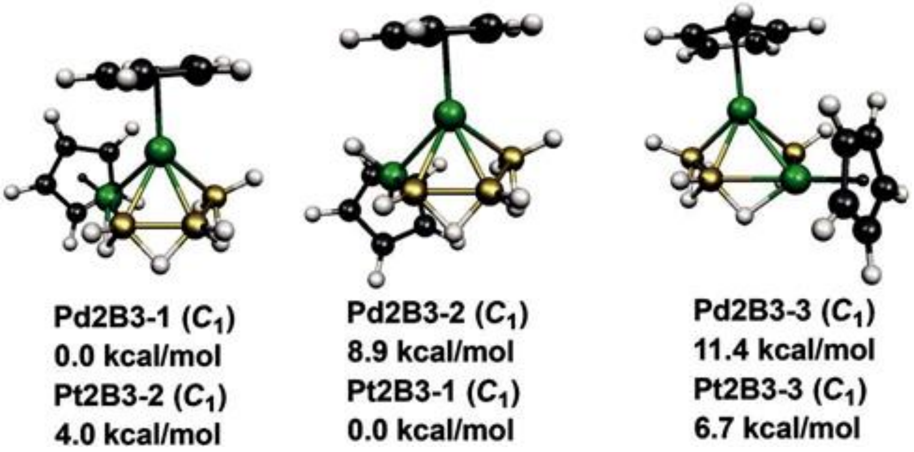

Figure 29. The three $Cp_2M_2B_3H_7$ (M = Pd, Pt) structures within 12 kcal mol^{-1} of the global minima.

Table 3. The three optimized $Cp_2M_2B_3H_7$ (M = Pd, Pt) structures within 12 kcal/mol of the global minima with relative energies in kcal/mol.

Structure	Hydrogen	$Cp_2Pd_2B_3H_7$				$Cp_2Pt_2B_3H_7$			
(symmetry)	Bridges	ΔE	Pd–Pd	WBI	Pd–BH_2	ΔE	Pt–Pt	WBI	Pt–BH_2
Pd2B3-1/Pt2B3-2	MB/$2B_2$	0.0	2.604	0.33	3.086	4.0	2.668	0.39	3.261
Pd2B3-2/Pt2B3-1	M_2/$2B_2$	8.0	2.634	0.31	3.233	0.0	2.683	0.39	3.356
Pd2B3-3/Pt2B3-3	MB/$2B_2$	11.4	2.575	0.29	2.960	6.7	2.631	0.35	2.992

3.4.2 $Cp_2M_2B_3H_7$ (M = Rh, Ir) systems

Proceeding to the M = Rh and Ir cases of the $Cp_2M_2B_3H_7$ structures, the total electron count drops to 14 Wadean electrons as now each metal vertex donates 2 electrons for cluster bond formation. The resulting electronic structure corresponds to a 2n+4 *nido* scenario, which is isoelectronic with the pentaborane-9 molecule (cf. Table 4).

Table 4. Skeletal electron count of the $Cp_2M_2B_3H_7$ (M = Rh, Ir) and B_5H_9 systems.

Molecule	Fragment	Nr. of fragments	e^- donated by fragment	Total e^- donated
$Cp_2Rh/Ir_2B_3H_7$	CpRh/Ir	2	9-6-1=2	4
	BH	3	2	6
	H	4	1	4
		Skeletal electron count		**14**
B_5H_9	BH	5	2	10
	H	4	1	4
		Skeletal electron count		**14**

Again, the Rh/Ir metallaborane adopts the same geometry (cf. Figure 30) as its isoelectronic pentaborane counterpart (cf. Figure 26). Namely, a tetragonal pyramid is adopted - a structure which, in contrast with the pentaborane-11 and the M = Pd, Pt variants, has all its basal vertices connected (i.e. a textbook *nido* geometry). The same geometry is adopted by all the isomers (cf. Figure 30 and Table 5) that possess a structural energy relevant for the experimental point of view (i.e. being less than 20 kcal/mol above the global minimum). Interestingly, the Rh containing metallaborane has been previously synthetized with the permethylated version of the cyclopentadienyl as ligand.[45] This methylation of the ligand does not affect the electron structure of the core cluster. However, the permethylated version is preferred from the experimental point view. This is because of the extra steric repulsion that is induced by the methyl groups avoids dimerization reactions. Nevertheless, the experimental structure has the same geometry as the pentaborane-9 molecule and as the here-computed $Cp_2Rh_2B_3H_4$ global minimum.

The locations of the metal vertices differ among the low-energy structures. While in the case of M_2B_3-1 and M_2B_3-3 one CpM vertex is placed in the apical position and the other in the basal position (similar to the Pd/Pt structures), for the M_2B_3-2 and M_2B_3-4 both metal vertices are located at the base of the pyramid.

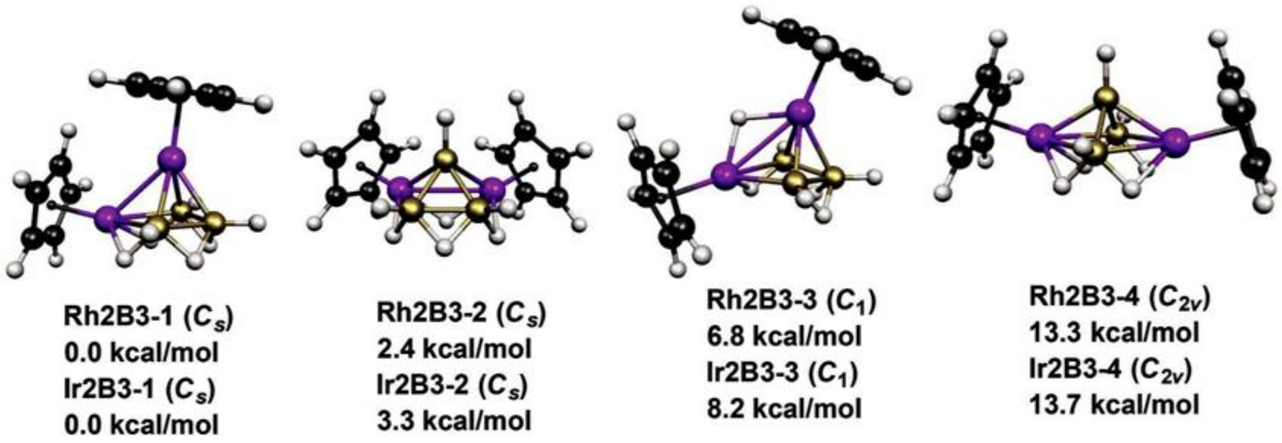

Rh2B3-1 (C_s)
0.0 kcal/mol
Ir2B3-1 (C_s)
0.0 kcal/mol

Rh2B3-2 (C_s)
2.4 kcal/mol
Ir2B3-2 (C_s)
3.3 kcal/mol

Rh2B3-3 (C_1)
6.8 kcal/mol
Ir2B3-3 (C_1)
8.2 kcal/mol

Rh2B3-4 (C_{2v})
13.3 kcal/mol
Ir2B3-4 (C_{2v})
13.7 kcal/mol

Figure 30. The four $Cp_2M_2B_3H_7$ (M = Rh, Ir) structures within 30 kcal mol^{-1} (M = Rh) or 20 kcal mol^{-1} (M = Ir) of the global minima.

Besides the crystal structure determined by X-ray diffraction analysis, in solution the presence of a second isomer has been signaled by NMR analysis. The structure of this second isomer is similar to the computed Rh_2B_3-3, which shares the same geometry as that of Rh_2B_3-1 but differs only by the location of one bridging hydrogen atom. While in the solid state all bridging hydrogen atoms are placed between basal vertices (cf. Rh_2B_3-1), in the Rh_2B_3-3 case one hydrogen atom is located between the metal centers, i.e. between the apex and a basal vertices. The computed energy difference of the two isomers is just 6.8 kcal/mol. The lowest-lying structures were also computed with the permethylated version of the cyclopentadienyl ligand. In this case, the energy difference between the two isomers dropped to 1.6 kcal/mol. This emphasizes the fluxionality of the two structures. In the permethylated case, however, the global ground state is a structure in which both metal vertices are placed in basal positions. This structure has not been seen experimentally - as it is probably hindered by kinetic aspects of its formation reaction. Indeed, one might expect a higher energy barrier for the interchange of metal and boron from the apical to the basal position than the energy barrier that a hydrogen atom encounters when being transmuted from a basal-basal bridging position to an apex-basal one.

Table 5. The four optimized $Cp_2M_2B_3H_7$ (M = Rh, Ir) structures within 30 kcal/mol (M = Rh) or 20 kcal/mol (M = Ir) of the global minima with relative energies in kcal/mol. All of these structures have central M_2B_3 tetragonal pyramids.

Structure		Hydrogen	$Cp_2Rh_2B_3H_7$			$Cp_2Ir_2B_3H_7$		
(symmetry)	Metal Location	Bridges	ΔE^a	Rh–Rh	WBI	ΔE^a	Ir–Ir	WBI
M2B3-1 (C_s)	Apex-Base	$2MB/2B_2$	0.0(2.1)	2.616	0.40	0.0(0.8)	2.686	0.42
M2B3-2 (C_s)	Base-Base	$M_2/3MB$	2.4(0.1)	2.744	0.30	3.3(0.0)	2.797	0.33
M2B3-3 (C_1)	Apex-Base	$M_2/MB/B_2$	6.8(3.7)	2.705	0.29	8.2(4.4)	2.764	0.31
M2B3-4 (C_{2v})	Base-Base	4MB	13.3(5.9)	3.621	0.13	13.7(6.2)	3.660	0.10

3.4.3 $Cp_2M_2B_3H_7$ (M=Ru,Os) systems

In the Ru and Os case each metal vertex donates a single skeletal electron and thus a total of 12 Wadean skeletal electrons are accumulated (cf. Table 6). This electron count is specific to the trigonal bipyramid geometry, as is the case, for example, in the $C_2B_3H_5$ carborane (cf. Table 6). Indeed, the lowest--energy structures (cf. Figure 31) are found to obey the Wade-Mingos rules with the metal atoms located at degree 4, equatorial vertices.

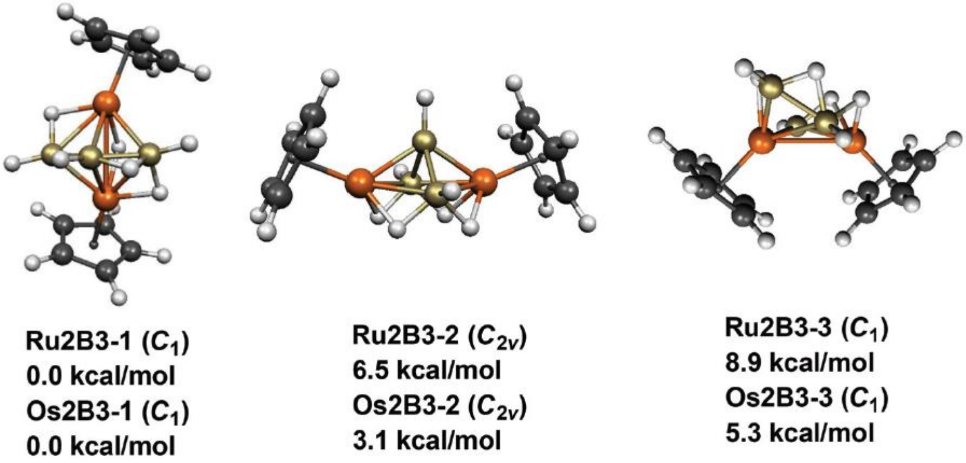

Figure 31. The three $Cp_2M_2B_3H_7$ (M = Ru, Os) structures within 9 kcal mol^{-1} of the global minima.

Table 6. Skeletal electron count of the $Cp_2M_2B_3H_7$ (M = Ru, Os) and $C_2B_3H_5$ systems.

Molecule	Fragment	Nr. of fragments	e^- donated by fragment	Total e^- donated
$Cp_2Ru/Os_2B_3H_7$	CpRu/Os	2	8-6-1=1	2
	BH	3	2	6
	H	4	1	4
		Skeletal electron count		**12**
$C_2B_3H_5$	BH	3	2	6
	CH	2	3	6
		Skeletal electron count		**12**

There are also other types of polyhedra found among the low-energy structures. As seen in Figure 31 and Table 7, the tetragonal pyramid is found as the second lowest-energystructure for both metal cases (6.5 kcal/mol above the ground state in the Ru case and 3.1 kcal/mol in the Os case). In both systems, the metal atoms are located in diagonal basal positions. The M2B3-3 structures possess a central B_2M_2 tetrahedron to which the third boron atom is bridged between the two metal vertices.

Table 7. The three optimized $Cp_2M_2B_3H_7$ (M = Ru, Os) structures within 9 kcal/mol of the global minima with relative energies in kcal/mol.

Structure (symmetry)	Polyhedron	Hydrogen Bridges	$Cp_2Ru_2B_3H_7$			$Cp_2Os_2B_3H_7$		
			ΔE	Ru–Ru	WBI	ΔE	Os–Os	WBI
M2B3-1 (C_1)	Trigonal bipyramid	M_2/2MB/B_2	0.0	2.788	0.33	0.0	2.857	0.36
M2B3-2 (C_{2v})	Tetragonal pyramid	4MB	6.5	3.090	0.31	3.1	3.530	0.28
M2B3-3 (C_1)	Edge-cap Tetrahed	2MB/B_2	8.9	2.750	0.37	5.3	2.810	0.39

3.4.4 $Cp_2Re_2B_3H_7$ systems

Each CpRe vertex is an effective 0 electron donor (cf. Table 8). This might induce the impression that the $Cp_2Re_2B_3H_7$ are highly electron deficient. However, this apparent electron depletion is removed when the multiple Re=Re bonding are invoked in order to explain their electronic structure. Thus, the short Re-Re distance coupled with higher that 0.4 Wiberg bond indices (cf. Table 9) infers the presence of formal Re=Re double bonds. This extra double bond contributes with two extra electrons to the global cluster bonding and thus raises the total skeletal electron count to 12 Wadean electrons. Such Re-Re surface bonding had been previously indicated, with the use of similar computational methods, in other Re-containing clusters.[46,47] Nevertheless, on the basis of the Wade-Mingos rules, the 12 Wadean electron count corresponds to a closo structure. Indeed, the trigonal bipyramid , i.e. a typical closo structure, is found among the lowest energy lying isomers in the case of Re_2B_3-3 and Re_2B_3-4 that lye just 4 kcal/mol above the ground state. The most stable isomers adopts a central edge-bridged tetrahedron geometry that is also shared by the Re_2B_3-2, Re_2B_3-6 and Re_2B_3-7 isomers (cf. Figure 32). This geometry is still a closo structure and can be interpreted as following: a central Re=Re double bond to which a three-electron donor BH_2 fragment coordinates on one of its side and a five electron donor μ-B_2H_5 fragment on its opposing side. The double Re=Re bond is suggested (cf. Table 9) by the short intermetallic distance, ~2.7 Å, corroborated with the higher WBI values of ~0.8. These WBI values are twice to those found in the Os-Os bond (cf. Table 7), a case which is interpreted as formal single bond. The resulting electronic configuration leads to a total 18 electron count on each Re atom and 12 Wadean electrons for cluster bonding.

Table 8. Skeletal electron count of the $Cp_2Re_2B_3H_7$ systems.

Molecule	Fragment	Nr. of fragments	e^- donated by fragment	Total e^- donated
$Cp_2Re_2B_3H_7$ (closo)	CpRe	2	7-6-1=0	0
	BH	3	2	6
	H	4	1	4
	Re=Re	1	2	2
	Skeletal electron count			**12**
$Cp_2Re_2B_3H_7$ (nido)	CpRe	2	7-6-1=0	0
	BH	2	2	6
	H	4	1	4
	Re≡Re	1	4	4
	Skeletal electron count			**14**

Interestingly, the $Cp_2Re_2B_3H_7$ systems also adopt nido geometry in the form of tetragonal pyramid. This geometry is encounter in the case of the Re_2B_3-5 isomer that lies just 4.8 kcal/mol above the ground state. The shorter Re-Re distance and higher WBI suggest former triple bonding between the metal centers. This adds two extra electrons to cluster bonding and leads to a total of 14 Wadean electrons that represents a 2n+4 (nido) scenario.

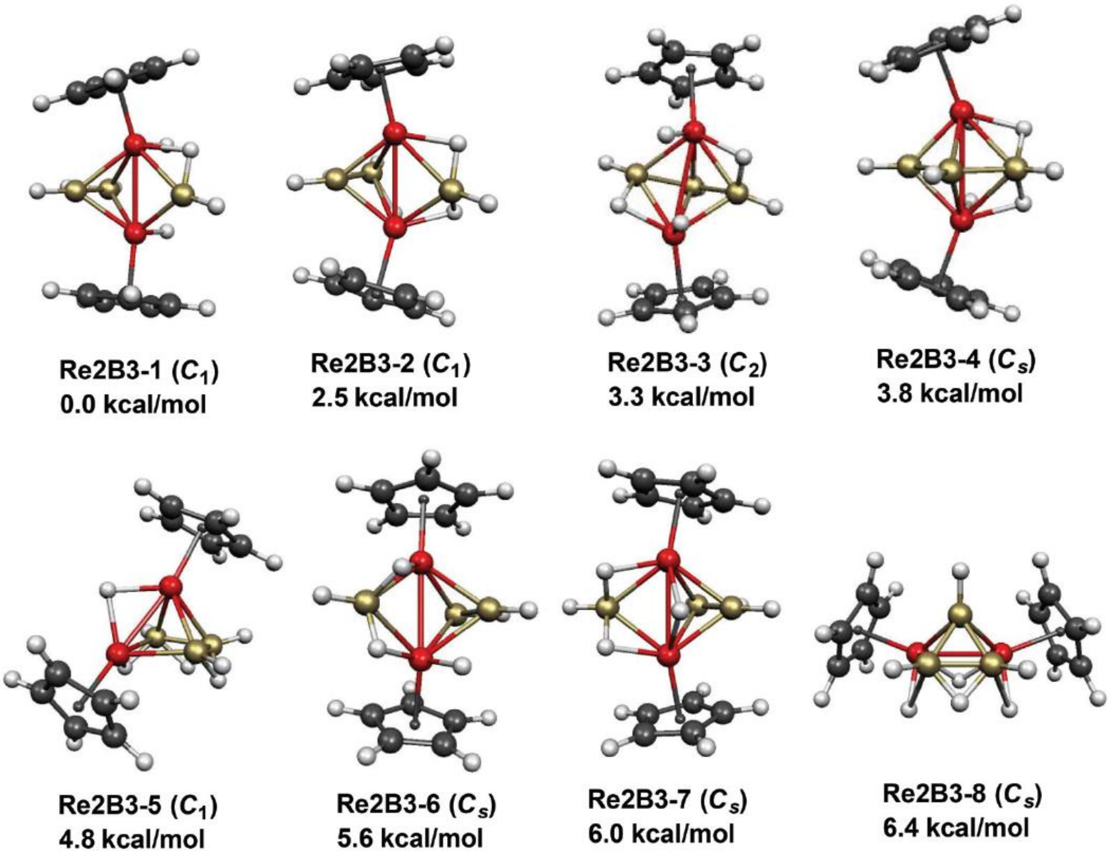

Figure 32. The eight $Cp_2Re_2B_3H_7$ structures within 10 kcal mol^{-1} of the global minimum.

Table 9. Optimized $Cp_2Re_2B_3H_7$ structures within 10 kcal mol^{-1} of the global minimum.

Structure (symmetry)	Relative energy	Hydrogen Bridges	Re-Re			Polyhedron
			Location	Å	WBI	
Re2B3-1 (C_1)	0.0	2ReB/B_2	2 deg 4	2.593	0.89	Edge-bridge tetrahedron
Re2B3-2 (C_1)	2.5	3ReB/B_2	2 deg 4	2.670	0.73	Edge-bridge tetrahedron
Re2B3-3 (C_2)	3.3	2ReB	Eq-eq	2.967	0.56	Trigonal bipyramid
Re2B3-4 (C_s)	3.8	2ReB	Eq-eq	2.975	0.58	Trigonal bipyramid
Re2B3-5 (C_1)	4.8	Re_2/ReB/2B_2	Apex-base	2.452	1.35	Tetragonal pyramid
Re2B3-6 (C_s)	5.6	2ReB/B_2	2 deg 4	2.637	0.84	Edge-bridge tetrahedron
Re2B3-7 (C_s)	6.0	Re_2/ReB/2B_2	2 deg 4	2.629	0.70	Edge-bridge tetrahedron
Re2B3-8 (C_s)	6.4	Re_2/ReB/2B_2	Base-base	2.442	1.40	Tetragonal pyramid

3.4.5 $Cp_2M_2B_3H_7$ (M=Mo,W) systems

The trigonal bipyramid is the most common geometrical motif found among the Mo and W complexes (cf. Figure 33). Out of the six lowest lying structures, five of them possess this geometry and share their metal atoms in apical vertices. The short intermetallic distances correlated with high WBI (cf. Table 11) suggest that, in four out of these five structures, the metal-metal interactions can be interpreted as formal M≡M, (M = Mo, W), triple bonds. The presence of a triple bond implies extra 4 electrons that are being donated for cluster bonding. Summing them to the 6 electrons donated by the BH vertices and the 4 electrons by the bridging H atoms, a total of 14 donated electrons are accumulated. However, each metal vertex is an effective -1 electron donor, acting thus as an electron acceptor. Consequently the total electron count drops to 12 skeletal electrons (cf. Table 10) which represents the electron count specific to trigonal bypiramid (i.e. closo) geometry as dictated by the Wade-Mingos rules. These four structures differ only by the positions which the bridging H atoms adopt. The other trigonal bipyramidal structures depart from the Wade-Mingos paradigm as they now possess larger M-M bond lengths associated with lower WBI that can no longer be interpreted as triple bonds and thus the four extra electrons needed for the 12 skeletal electron count is no longer achieved. The other low-lying structures (Mo2B3-2/W_2B_3-1) share a geometry similar to that of Re_2B_3-1, Re_2B_3-2, Re_2B_3-6, Re_2B_3-7 and Ru_2B3-3 systems. These structures can be obtained by the breaking of an apical-equatorial edge of and trigonal bipyramid.

Table 10. Skeletal electron count of the $Cp_2M_2B_3H_7$ (M = Mo, W) systems.

Molecule	Fragment	Nr. of fragments	e^- donated by fragment	Total e^- donated
$Cp_2Mo/W_2B_3H_7$	CpMo/W	2	6-6-1=-1	-2
	BH	3	2	6
	H	4	1	4
	M≡M	1	4	4
		Skeletal electron count		**12**

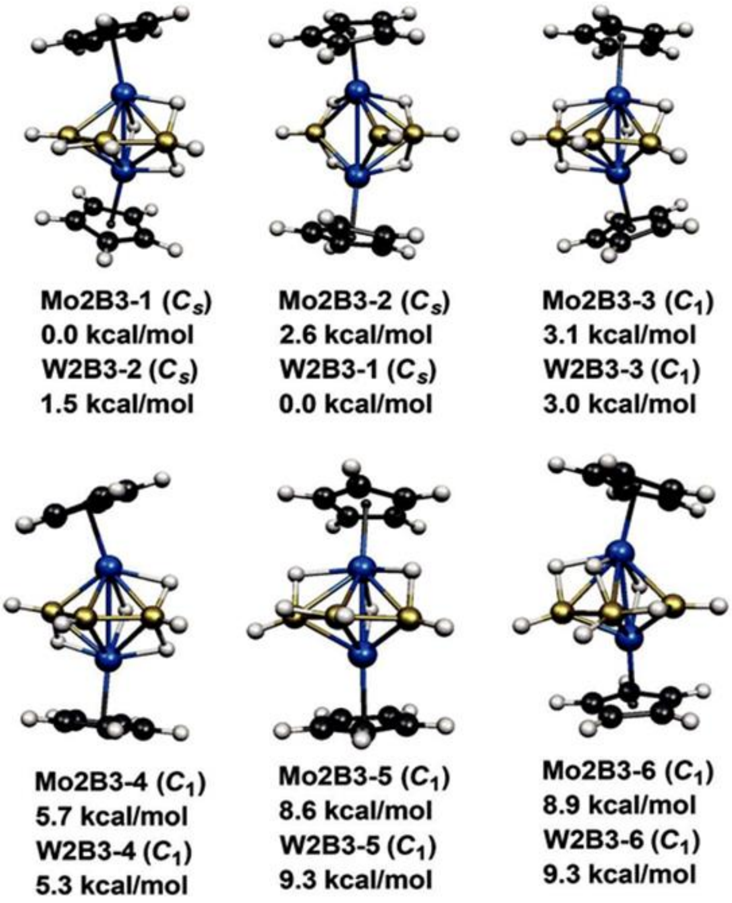

Figure 33. The six $Cp_2M_2B_3H_7$ (M = Mo, W) structures within 10 kcal mol^{-1} of the global minima.

Table 11. Optimized $Cp_2M_2B_3H_7$ (M = Mo, W) structures within 10 kcal/mol of the global minima with relative energies in kcal/mol.

Structure		Hydrogen	$Cp_2Mo_2B_3H_7$			$Cp_2W_2B_3H_7$		
(symmetry)	Polyhedron	Bridges	ΔE	Mo-Mo	WBI	ΔE	W-W	WBI
Mo2B3-1/W2B3-2 (C_s)	Trigonal bipyramid	M_2/2MB/B_2	0.0	2.521	1.51	1.5	2.556	1.50
Mo2B3-2/W2B3-1 (C_s)	Edge-cap Tetrahed	4MB	2.6	2.739	1.07	0.0	2.762	1.05
Mo2B3-3/W2B3-3 (C_1)	Trigonal bipyramid	M_2/3MB	3.1	2.500	1.53	3.0	2.538	1.53
Mo2B3-4/W2B3-4 (C_1)	Trigonal bipyramid	M_2/3MB	5.7	2.759	1.00	5.3	2.780	1.01
Mo2B3-5/W2B3-5 (C_1)	Trigonal bipyramid	M_2/2MB/B_2	8.6	2.500	1.46	9.3	2.536	1.45
Mo2B3-6/W2B3-6 (C_1)	Trigonal bipyramid	M_2/2MB/B_2	8.9	2.513	1.36	9.3	2.545	1.36

3.4.6 The single $Cp_2Ta_2B_3H_7$ structure

In the case of Ta complexes, the isomers lying above the ground state are predicted to be high in energy and thus harder to be obtained experimentally. As seen in Figure 34, the $Cp_2Ta_2B_3H_7$ ground state adopts the trigonal bipyramid geometry with both metal atoms placed in equatorial positions. The Ta=Ta bond length and WBI suggest (cf. Table 13) the presence of a formal double bond between the metal vertices. Also, Ta often adopts a 16 electron configuration which would make a CpTa vertex an effective 0 electron donor. In this scenario (cf. Table 12), the total skeletal electron count adds to the same 12 Wadean electrons needed so that, based on the Wade-Mingos rules, the trigonal bipyramid is obtained.

Table 12. Skeletal electron count of the $Cp_2Ta_2B_3H_7$ systems.

Molecule	Fragment	Nr. of fragments	e^- donated by fragment	Total e^- donated
$Cp_2Ta_2B_3H_7$	CpTa	2	5-4-1=-2	0
	BH	3	2	6
	H	4	1	4
	Ta=Ta	1	2	2
	Skeletal electron count			**12**

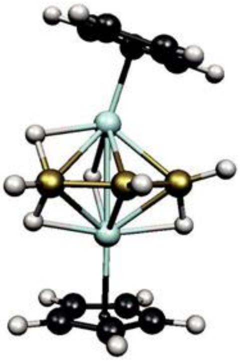

Figure 34. The single $Cp_2Ta_2B_3H_7$ structure lying ~24 kcal mol^{-1} in energy below the next lowest energy structure.

Table 13. The global minimum $Cp_2Ta_2B_3H_7$ structure lying ~24 kcal mol^{-1} in energy below the next lowest energy structure.

Structure (symmetry)	Relative energy	Hydrogen Bridges	Ta-Ta			Polyhedron
			Location	Å	WBI	
Ta2B3-1 (C_1)	0.0	Ta_2/3TaB	Eq-eq	2.737	1.11	Trigonal bipyramid

3.5 6 vertices

The process of generating an n-vertex nido polyhedron by the removal of a boron vertex from an (n + 1) vertices deltahedron can be applied not only to the most spherical closo deltahedra, but also to the (n + 1) vertices isocloso and oblatocloso deltahedra. Figure 35 illustrates such processes of vertex removal from seven-vertex deltahedra to give various versions of open six- vertex polyhedra. Thus, the pentagonal bipyramid is the most spherical seven-vertex deltahedron. Removal of a degree 5 vertex from the pentagonal bipyramid gives the pentagonal pyramid. Removal of a degree 4 vertex from the capped octahedron gives a tetragonal prism capped on a triangular face. The closest seven-vertex deltahedron to an oblatocloso deltahedron is a squashed pentagonal bipyramid with the antipodal degree 5 vertices for the metal atoms. Removal of a degree 4 vertex from such a deltahedron generates a bicapped tetrahedron if the original pentagonal bipyramid is squashed enough to have the axial metal atoms within bonding distance.

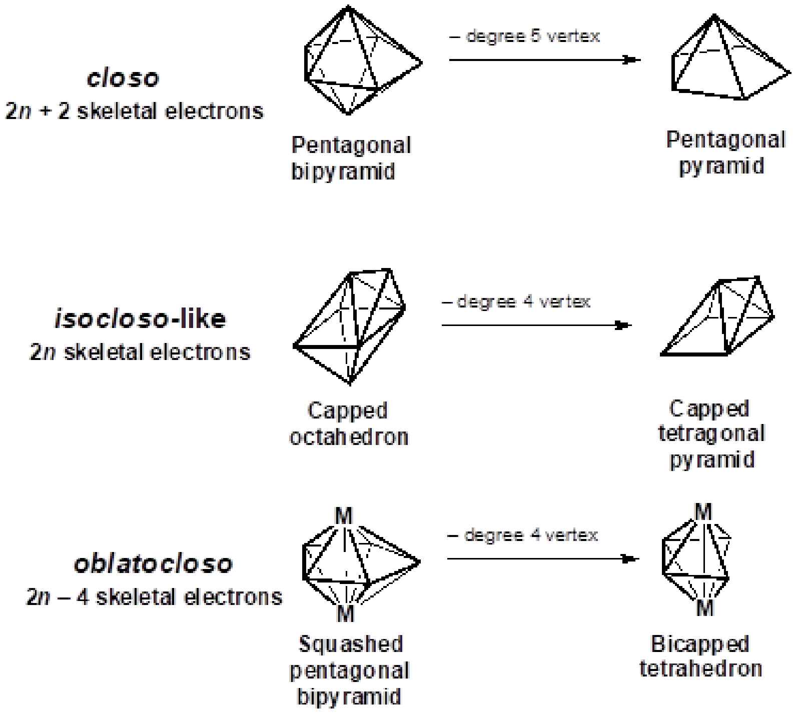

Figure 35. Removal of a vertex in various ways from seven-vertex deltahedra analogous to *closo*, *isocloso*, and *oblatocloso* deltahedra.

The initial $Cp_2M_2B_4H_8$ structures were constructed by the systematic substitution of the two metal atoms on the vertices of the polyhedra shown in Figure 36. The extra four hydrogen atoms are considered as edge-capping atoms on the edges of the tetragonal/ pentagonal open face or on the metal−metal edge. This leads to 45 different starting geometries to be optimized for each metal system.

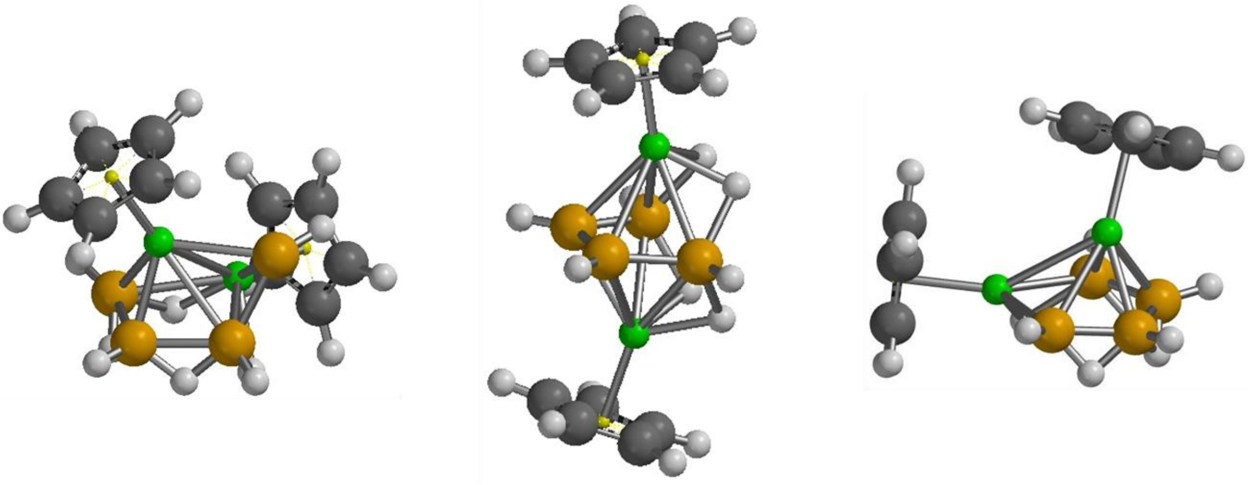

Figure 36. Initial geometries of the $Cp_2M_2B_4H_8$ structures and the number of their isomers. Left: the capped tetragonal pyramid (16 structures). Middle: the 1 equatorial vertex depleted pentagonal bipyramid (7 isomers) Right: the pentagonal pyramid (22 isomers).

3.5.1 $Cp_2Ir_2B_4H_8$ systems

Being isolobal with a BH fragment, each CpIr vertex donates two electrons for cluster bonding. Added to the eight electrons donated by the BH vertices and to the four electrons donated by the bridging H atoms, a total of 16 wadean electrons are accumulated for cluster bonding (cf. Table 14). This makes the $Cp_2Ir_2B_4H_8$ system isoelectronic with the B_6H_{10} hexaborane (cf. Table 14) and, likewise, possessing an electron count specific to nido structures, it adopts the geometry of a pentagonal pyramid (cf. Figure 37). Five isomers are found within the 22 kcal/mol interval above the ground state. They all share the same pentagonal pyramid geometry and vary in terms of location of the metal vertices and bridging H atoms. The first four isomers possess the same framework (i.e. with one metal vertex in the apical position) and have the H atoms permuted on different basal edges. In the case of the ground state structure, one of the bridging H becomes a terminal H linked to the basal Ir vertex. In all four isomers the Ir-Ir bond lengths are ~2.7 Å and have corresponding WBI of ~0.4 (cf. Table 15), which leads to their interpretation as formal single bonds. The fifth isomer lays 15.2 kcal/mol above the ground state and differs from the first four isomers by having the two metal vertices in nonadjacent basal positions. Its Ir-Ir distance reaches 3.7 Å and with the WBI dropping to 0.09 it is emphasized the lack of bonding interaction between them.

Table 14. Skeletal electron count of the $Cp_2Ir_2B_4H_8$ (M = Pd, Pt) and B_5H_{11} systems.

Molecule	Fragment	Nr. of fragments	e^- donated by fragment	Total e^- donated
$Cp_2Ir_2B_4H_8$	CpIr	2	9-6-1=2	4
	BH	4	2	8
	H	4	1	4
	Skeletal electron count			**16**
B_6H_{10}	BH	6	2	12
	H	4	1	4
	Skeletal electron count			**16**

The Ir_2B_4-1 computed structure corresponds to that of the experimentally known $Cp^*_2Ir_2B_4H_8$ compound.[48,49] Both adopt the pentagonal pyramid geometry with one metal vertex placed in the apex of the pyramid and one in the basal position.

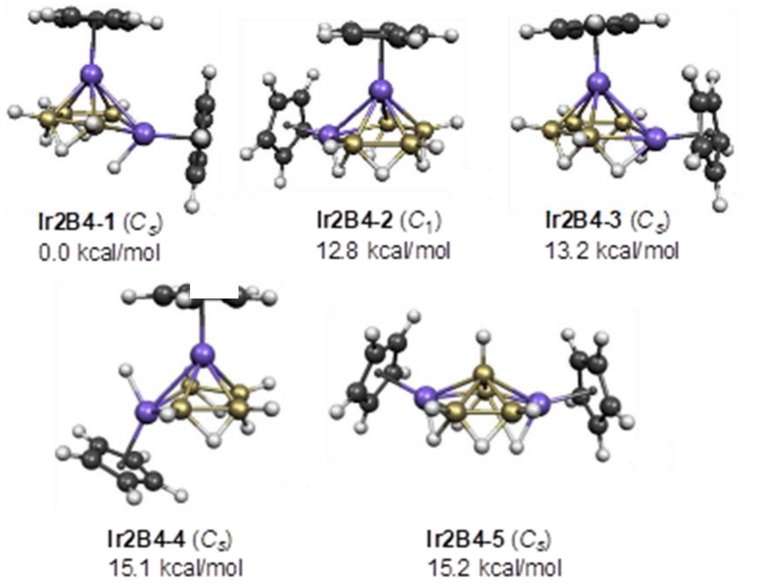
Ir2B4-1 (C_s) 0.0 kcal/mol
Ir2B4-2 (C_1) 12.8 kcal/mol
Ir2B4-3 (C_s) 13.2 kcal/mol
Ir2B4-4 (C_s) 15.1 kcal/mol
Ir2B4-5 (C_s) 15.2 kcal/mol

Figure 37. The five $Cp_2Ir_2B_4H_8$ structures within 22 kcal/mol of the global minimum.

Table 15. Optimized $Cp_2Ir_2B_4H_8$ structures within 22 kcal/mol of the global minimum with relative energies in kcal/mol.

Structure (symmetry)	Relative energy	Hydrogen Bridges	Ir-Ir Location	Ir-Ir Å	Ir-Ir WBI	Polyhedron
Ir2B4-1 (C_s)	0.0	$3B_2$	Apex-base	2.712	0.35	Pentagonal pyramid
Ir2B4-2 (C_s)	12.8	$2IrB/2B_2$	Apex-base	2.715	0.40	Pentagonal pyramid
Ir2B4-3 (C_s)	13.2	$2IrB/2B_2$	Apex-base	2.696	0.39	Pentagonal pyramid
Ir2B4-4 (C_s)	15.1	$4B_2$	Apex-base	2.736	0.35	Pentagonal pyramid
Ir2B4-5 (C_1)	15.2	$2IrB/2B_2$	Base-base	3.742	0.09	Pentagonal pyramid

3.5.2 $Cp_2M_2B_4H_8$ (M = Ru, Os) systems

Each CpM vertex donates 1 electron in the M = Ru, Os systems. This leads to a skeletal electron count of 14 Wadean electrons (cf. Table 16) that corresponds to a closo scenario. Thus, an octahedral geometry would be expected to be found as the ground state of the $Cp_2M_2B_4H_8$ (M = Ru, Os) systems. However, it was shown experimentally[50] that in fact, in the permethylated version, the Ru containg complex (i.e. $Cp^*{}_2Ru_2B_4H_8$) adopts a different geometry, namely a tetragonal pyramid with the sixth vertex capping one of the triangular faces. Our computations found the same geometry to be the ground state and also agree with the positions of the metal vertices. Thus, in the ground state structure the metal vertices are adjacently placed in the basal position of the underlying pyramid (cf. Figure 38). All four basal edges are bridged by the "extra" H atoms. As shown in Table 17, the M-M distances are 2.858 Å in the Ru system and 2.889 Å in the Os containing system. For both metal cases the WBI are ~0.3.

Table 16. Skeletal electron count of the $Cp_2M_2B_4H_8$ (M = Ru, Os) systems.

Molecule	Fragment	Nr. of fragments	e^- donated by fragment	Total e^- donated
$Cp_2Ru/Os_2B_4H_8$	CpRu/Os	2	8-6-1=1	2
	BH	4	2	8
	H	4	1	4
	Skeletal electron count			**14**

In both metal systems, the next favorable isomer is at about 8 kcal/mol above the ground state. This isomer also adopts the capped tetragonal pyramid geometry but different metal positions. One CpM vertex is located in the apical position the tetragonal pyramid and the other one in the basal position. The M-M distances are shorter: 2.738 Å in the Ru system and 2.799 Å in the Os one, with corresponding WBI of ~0.4. The "extra" H atoms bridge the same basal positions as in the ground state structure.

The Wade-Mingos suggested octahedral geometry is present in higher energy isomers. Thus, the Ru_2B_4-6 isomer adopts the octahedral geometry at 15.1 kcal/mol above the ground state. The CpM vertices are placed in adjacent equatorial positions. Three Ru-B edges are bridged by H atoms while the fourth "extra" H atom forms an unsymmetrical bridge across the Ru-Ru bond (the H is placed at 1.64 Å from one Ru and at 2.04 Å from the second Ru atom). In the Os equivalent, i.e. the Os_2Ru_2-3 isomer at 10.3 kcal/mol from the ground state, the fourth H atom is even less symmetrically bridged between the metal vertices. Now, the bridging H is at 1.63 Å from one Os vertex and 2.48 Å from the second Os vertex. Thus, the resulting asymmetry is so pronounced that the fouth "extra" H atom can better be described as terminal atom.

Table 17. Optimized $Cp_2M_2B_4H_8$ (M = Ru, Os) structures within 17 kcal/mol of the global minimum with relative energies in kcal/mol.

Structure (symmetry)	Polyhedron	Hydrogen Bridges	$Cp_2Ru_2B_4H_8$			$Cp_2Os_2B_4H_8$		
			ΔE	Ru–Ru	WBI	ΔE	Os–Os	WBI
Ru2B4-1/Os2B4-1 (C_s)	Cap Tetrag Pyr	M_2/2MB/B_2	0.0	2.828	0.30	0.0	2.889	0.32
Ru2B4-2/Os2B4-2 (C_1)	Cap Tetrag Pyr	2MB/B_2	8.6	2.738	0.39	7.6	2.799	0.40
Ru2B4-3/Os2B4-4 (C_1)	Cap Tetrag Pyr	M_2/2MB/B_2	12.6	2.874	0.29	12.2	2.939	0.30
Ru2B4-4/Os2B4-6 (C_1)	Cap Tetrag Pyr	M_2/MB/2B_2	13.2	2.732	0.33	14.4	2.783	0.36
Ru2B4-5/Os2B4-5 (C_1)	Cap Tetrag Pyr	M_2/3MB	13.4	2.733	0.34	13.4	2.790	0.36
Ru2B4-6/Os2B4-3 (C_1**)**	Octahedron	M_2/3MB	15.1	2.762	0.36	10.3	2.794	0.46
Ru2B4-7/Os2B4-7 (C_2)	Octahedron	M_2/3MB	16.2	2.838	0.29	14.7	2.902	0.31

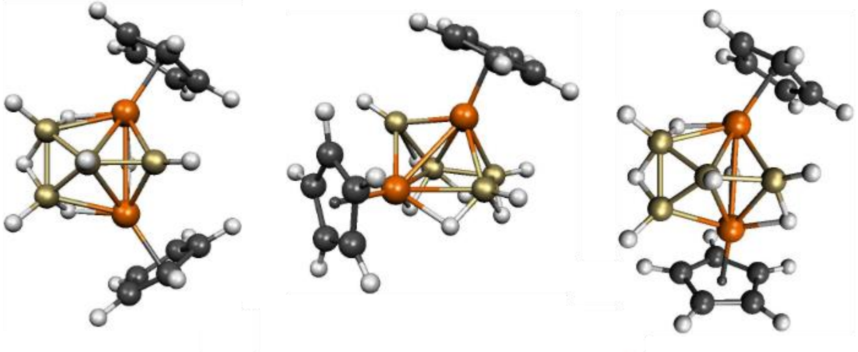

Ru2B4-1 (C_s)
0.0 kcal/mol
Os2B4-1 (C_s)
0.0 kcal/mol

Ru2B4-2 (C_1)
8.6 kcal/mol
Os2B4-2 (C_1)
7.6 kcal/mol

Ru2B4-3 (C_1)
12.6 kcal/mol
Os2B4-4 (C_1)
12.2 kcal/mol

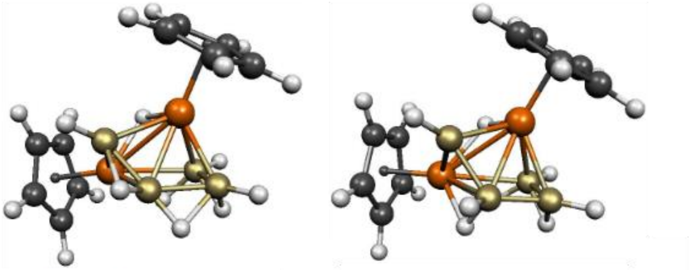

Ru2B4-4 (C_1)
13.2 kcal/mol
Os2B4-6 (C_1)
14.4 kcal/mol

Ru2B4-5 (C_1)
13.4 kcal/mol
Os2B4-5 (C_1)
13.4 kcal/mol

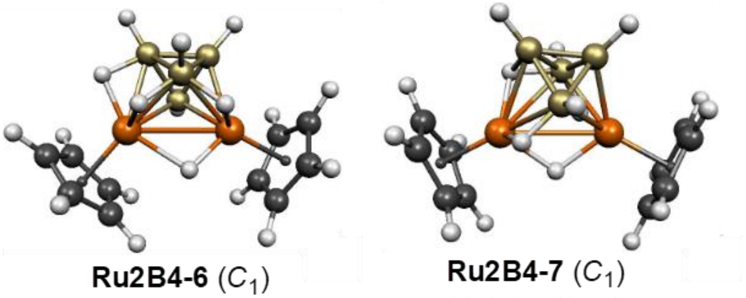

Ru2B4-6 (C_1)
15.1 kcal/mol
Os2B4-3 (C_1)
10.3 kcal/mol

Ru2B4-7 (C_1)
16.2 kcal/mol
Os2B4-7 (C_1)
14.7 kcal/mol

Figure 38. The seven $Cp_2M_2B_4H_8$ (M = Ru, Os) structures within 17 kcal/mol of the global minimum.

3.5.3 $Cp_2Re_2B_4H_8$ systems

Each CpRe vertex is an effective 0 electron donor. Consequently, the total electron count of the $Cp_2Re_2B_4H_8$ system comprises 12 Wadean electrons. This makes the Re system isoelectronic with the $Os_6(CO)_{18}$ complex, which is known to possess the geometry of a bicapped tetrahedron.[51] The same geometry is found to be adopted by the $Cp_2Re_2B_4H_8$ ground state (cf. Figure 39 and Table 19).

Table 18. Skeletal electron count of the $Cp_2Re_2B_4H_8$ and $Os_6(CO)_{18}$ systems.

Molecule	Fragment	Nr. of fragments	e^- donated by fragment	Total e^- donated
$Cp_2Re_2B_4H_8$ (biccaped tetrahedron)	CpRe	2	7-6-1=0	0
	BH	4	2	8
	H	4	1	4
	Skeletal electron count			**12**
$Os_6(CO)_{18}$	$Os(CO)_3$	6	2	12
	Skeletal electron count			**12**
$Cp_2Re_2B_4H_8$ (capped tetrahedral pyramid)	CpRe	2	7-6-1=0	0
	BH	4	2	8
	H	4	1	4
	Re=Re	1	2	2
	Skeletal electron count			**14**
$Cp_2Re_2B_4H_8$ (pentagonal pyramid)	CpRe	2	7-6-1=0	0
	BH	4	2	8
	H	4	1	4
	Re≡Re	1	4	4
	Skeletal electron count			**16**

The $Cp_2Re_2B_4H_8$ computed ground state can be interpreted as a fluxional system comprised of the just 2.6 kcal/mol separated Re_2B_4-1 and Re_2B_4-2 isomers. The Re-Re bond is surrounded on one side by a B_4H_4 chain in the structure of the Re_2B_4-1 isomer. Two of the “extra” H atoms are found on one end of the B_4H_4 and each bridges a Re-B bond. The remaining two “extra” are each coordinated to one metal vertex. The resulting assembly can be regarded as a doubly distorted tetrahedron (formed by an elongated Re-Re edge, four equal Re-B edges resulting from the interaction of the Re atoms with the two inner B atoms of the B_4H_4 chain, and a shortened B-B edge) that is capped by the two B ends of the B_4H_4 chain. In the Re_2B_4-2 isomer the B_4H_4 chain breaks in two B_2H_2 fragments and now the two terminal H atoms approach the B atoms such that now they become bridging units. The M-M bond length and WBI in this fluxional system (i.e. ~2.8 Å and 0.5 WBI) is similar those found in the $Cp_2Re_2B_nH_n$ (n=6-10) *oblatocloso* series and can be interpreted as formal single bonds. The third higher energy structure lies 10.2 kcal/mol above the ground state. It adopts the same bicapped tetrahedral geometry and shares similar Re-Re bond parameters (i.e. 2.846 Å and 0.48 WBI). The main aspect differing it from the ground state is the migration of a bridging H atom from a Re-B to a B-B bond. The computed ground state of the $Cp_2Re_2B_4H_8$ system corresponds with the experimentally determined[52] $Cp^*_2Re_2B_4H_8$ compound. It shares the same geometry and atom arrangement. The computed 2.834 Å Re-Re distance is very close to the 2.809 Å determined by experiments.

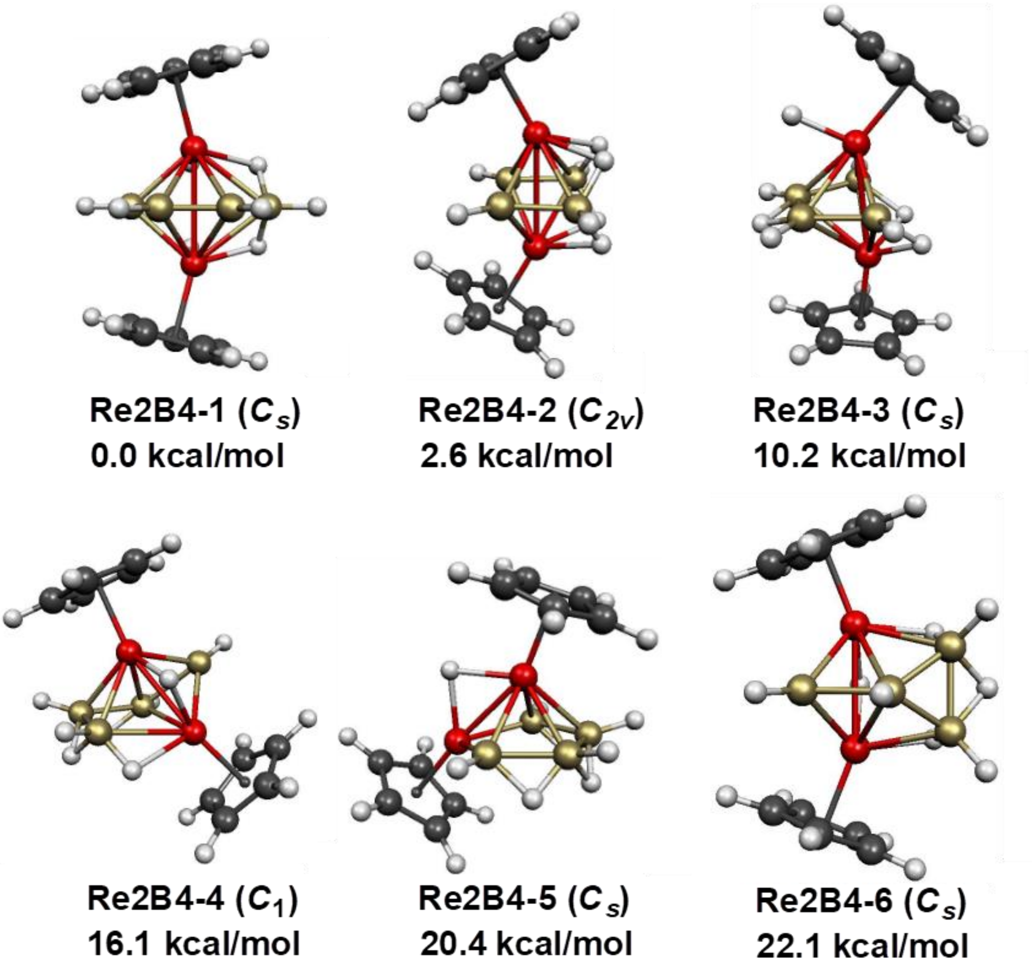

Re2B4-1 (C_s)
0.0 kcal/mol

Re2B4-2 (C_{2v})
2.6 kcal/mol

Re2B4-3 (C_s)
10.2 kcal/mol

Re2B4-4 (C_1)
16.1 kcal/mol

Re2B4-5 (C_s)
20.4 kcal/mol

Re2B4-6 (C_s)
22.1 kcal/mol

Figure 39. The six $Cp_2Re_2B_4H_8$ structures within 25 kcal/mol of the global minimum.

Table 19. Optimized $Cp_2Re_2B_4H_8$ structures within 25 kcal/mol of the global minimum with relative energies in kcal/mol.

Structure	Relative	Hydrogen	Re-Re			
(symmetry)	energy	Bridges	Location	Å	WBI	Polyhedron
Re2B4-1 (C_s)	0.0	4ReB	2 Apical	2.832	0.49	Bicap tetrahedron
Re2B4-2 (C_{2v})	2.6	4ReB	2 Apical	2.806	0.52	Separate B_2 ligands
Re2B4-3 (C_s)	10.2	$2ReB/B_2$	2 Apical	2.846	0.48	Bicap tetrahedron
Re2B4-4 (C_1)	16.1	$Re_2/2ReB/B_2$	Apex-base	2.596	0.78	Cap Tetrag Pyr
Re2B4-5 (C_s)	20.4	$Re_2/3B_2$	Apex-base	2.458	1.18	Pentagonal Pyramid
Re2B4-6 (C_s)	22.1	$Re_2/2ReB/B_2$	Base-base	2.721	0.84	Cap Tetrag Pyr

The next isomers are interesting from the presence of M-M multiple bonds. Similar to the Ru/Os ground states (cf. Figure 38 and Table 17), the Re_2B_4-3 and Re_2B_4-6 isomers adopt the geometry of a capped tetrahedral pyramid and have bond lengths and WBIs that suggest formal double bonding between the Re vertices. The extra double bond increases their skeletal electron count to 14 Wadean electrons (cf. 3rd entry of

Table **18**) and thus make them isoelectronic with the $Cp_2M_2B_4H_8$ (M=Ru, Os) systems (cf. Table 16). The Re_2B_4-5 isomer adopts the pentagonal pyramid geometry (similar to the Ir systems; cf. Figure 37) and its bond length of 2.458 Å and WBI of 1.18 suggest a formal triple bond between the metal vertices. The extra Re≡Re triple bond adds 4 extra Wadean electron (cf. 4th entry of

Table **18**) and thus the Re_2B_4-5 isomer becomes isoelectronic with the $Cp_2Ir_2B_4H_8$ (cf. Table 14).

3.5.4 $Cp_2M_2B_4H_8$ (M = Mo, W) systems

The ground states of both $Cp_2M_2B_4H_8$ (M=Mo,W) systems also form fluxional states. The same bicapped tetrahedral geometry found in the Re ground state is also adopted by the Mo and W systems (cf. Figure 40). The fluxionality of their ground states implies the migration of the four “extra” H atoms. The WBI of the M-M ground states are double (cf. Table 21) to the one found in the Re ground state (cf. Table 19). These values suggest the presence of metal-metal double bond in the Mo and W ground states. The 2 extra electrons provided by this double bond balance the 2 electrons accepted by the CpM vertices. Thus, a total of 12 Wadean electrons are accumulated (cf. 1st entry of Table 20) for cluster bonding.

This makes the $Cp_2M_2B_4H_8$ (M = Mo, W) systems isoelectronic with the $Cp_2Re_2B_4H_8$ ground state and the $Os_6(CO)_{18}$ system (cf. 1st and 2nd entries of Table 18).

Table 20. Skeletal electron count of the $Cp_2M_2B_4H_8$ (M = Mo, W) systems.

Molecule	Fragment	Nr. of fragments	e^- donated by fragment	Total e^- donated
$Cp_2Mo/W_2B_4H_8$ (bicapped tetrahedron)	CpMo/W	2	6-6-1= -1	-2
	BH	4	2	8
	H	4	1	4
	M=M	1	2	2
	Skeletal electron count			**12**
$Cp_2Mo/W_2B_4H_8$ (tetragonal pyramid)	CpMo/W	2	6-6-1= -1	-2
	BH	6	1	6
	H	4	1	4
	M≡M	1	4	4
	Skeletal electron count			**14**

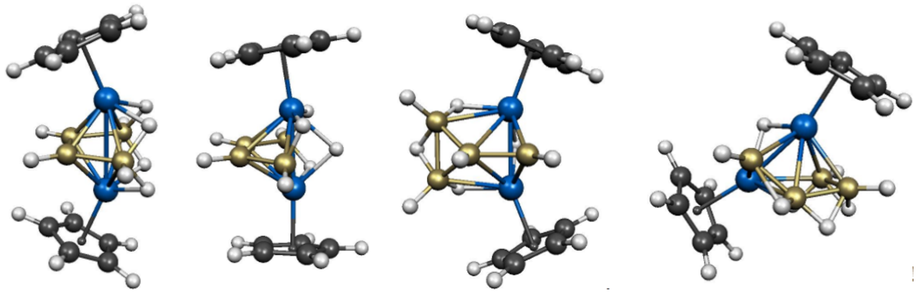

Mo2B4-1 (C_{2v})
0.0 kcal/mol
W2B4-2 (C_{2v})
0.7 kcal/mol

Mo2B4-2 (C_{2v})
1.1 kcal/mol
W2B4-1 (C_{2v})
0.0 kcal/mol

Mo2B4-3 (C_s)
8.4 kcal/mol
W2B4-3 (C_s)
9.8 kcal/mol

Mo2B4-4 (C_{2v})
21.3 kcal/mol
W2B4-4 (C_{2v})
23.1 kcal/mol

Figure 40. The four $Cp_2M_2B_4H_8$ (M = Mo, W) structures within 25 kcal/mol of the global minimum.

The next two isomers, M_2B_4-3 and M_2B_4-4, adopt the geometry of the capped tetragonal pyramid, which is similar to the geometry adopted by the Ru and Os ground states (cf. Figure 40 and Figure 38). The decrease of M-M bond lengths and increase of their corresponding WBI (cf. Table 21) suggest the presence of metal-metal triple bonds. In this case, the M≡M bond donates 4 electrons which leads to a total count of 14 Wadean electrons (cf. 2nd entry of Table 20). Indeed, these isomers become isolectronic with the Ru and Os systems (cf. Table 16) and hence the similarity of the geometry that is being adopted.

Table 21. Optimized $Cp_2M_2B_4H_8$ (M = Mo, W) structures within 25 kcal/mol of the global minimum with relative energies in kcal/mol.

Structure		Hydrogen	$Cp_2Mo_2B_4H_8$			$Cp_2W_2B_4H_8$		
(symmetry)	Polyhedron	Bridges	ΔE	Mo-Mo	WBI	ΔE	W-W	WBI
Mo2B4-1/W2B4-2 (C_{2v})	Bicap tetrahedron	4MB	0.0	2.997	0.87	0.7	3.035	0.88
Mo2B4-2/W2B4-1 (C_1)	Bicap tetrahedron	M_2/3MB	1.1	2.604	0.95	0.0	2.632	0.97
Mo2B4-3/W2B4-3 (C_s)	Cap Tetrag Pyr	M_2/2MB/B_2	8.4	2.495	1.51	9.8	2.528	1.52
Mo2B4-4/W2B4-4 (C_1)	Cap Tetrag Pyr	M_2/2MB/B_2	21.3	2.476	1.39	23.1	2.518	1.34

3.5.5 $Cp_2Ta_2B_4H_8$ systems

There are three most stable isomers in the $Cp_2Ta_2B_4H_8$ systems and all of them adopt the bicapped tetragonal pyramid geometry (cf.Figure 41). The Ta_2B_4-2 isomer lies at 14.9 kcal/mol above the ground state while the Ta_2B_4-3 isomer at 19.4 kcal/mol (cf.Table 23). The unusual feature of these two last isomers is the positioning of one of their constituting Ta atom in a degree 4 vertex. This is opposed to the commonly encountered case, present also in the ground state case, in which both Ta atoms are located at degree 5 vertices. The Ta_2B_4-1 structure is similar to the $Cp_2M_2B_4H_9$ (M=Re, Mo, W) ground state but it is lacking their fluxional character.

Table 22. Skeletal electron count of the $Cp_2Ta_2B_4H_8$ systems.

Molecule	Fragment	Nr. of fragments	e^- donated by fragment	Total e^- donated
$Cp_2Ta_2B_4H_7$	CpTa	2	5-4-1=0	0
	BH	4	2	8
	H	4	1	4
	Skeletal electron count			**12**
B_5H_{11}	BH	5	2	10
	H	6	1	6
	Skeletal electron count			**16**

The presence of a triple Ta≡Ta bond would provide the necessary 12 Wadean electrons that the Re, Mo and W systems accumulated. However, the WBI value of the Ta-Ta interaction within the ground state is not in favor of this hypothesis, but rather suggests the presence formal single Ta-Ta bond. Nevertheless, the 12 skeletal electron count can be achieved by considering that Ta would thrive for the 16 electrons configuration rather than the usual 18 electrons configuration. This would make the CpTa vertex an effective 0 electron donor and thus the 12 Wadean electrons configuration can be achieved (cf. Table 22).

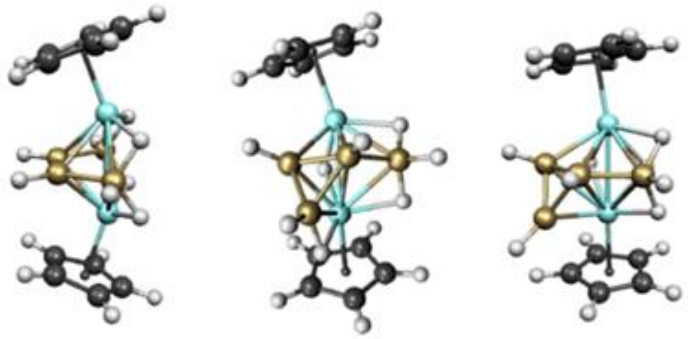

Ta2B4-1 (C_{2v}) **0.0 kcal/mol** **Ta2B4-2 (C_1)** **14.9 kcal/mol** **Ta2B4-3 (C_s)** **19.4 kcal/mol**

Figure 41. The three $Cp_2Ta_2B_4H_8$ most stable isomers.

Table 23. Optimized $Cp_2Ta_2B_4H_8$ structures within 22 kcal/mol of the global minimum with relative energies in kcal/mol.

Structure (symmetry)	Relative energy	Hydrogen Bridges	Ta-Ta Location	Ta-Ta Å	Ta-Ta WBI	Polyhedron
Ta2B4-1 (C_{2v})	0.0	4TaB	2 deg 5	2.977	0.76	Bicap tetrahedron
Ta2B4-2 (C_1)	14.9	Ta_2/3TaB	Deg5/Deg4	2,724	1.10	Bicap tetrahedron
Ta2B4-3 (C_s)	19.4	$2Ta_2$/2TaB	Deg5/Deg4	2.686	1.07	Bicap Tetrahedron

3.6 7 vertices

The eight-vertex deltahedra that can be used to generate suitable seven-vertex polyhedra for the hydrogen-rich systems by vertex removal include the bisdisphenoid and the hexagonal bipyramid (cf. Figure 42).

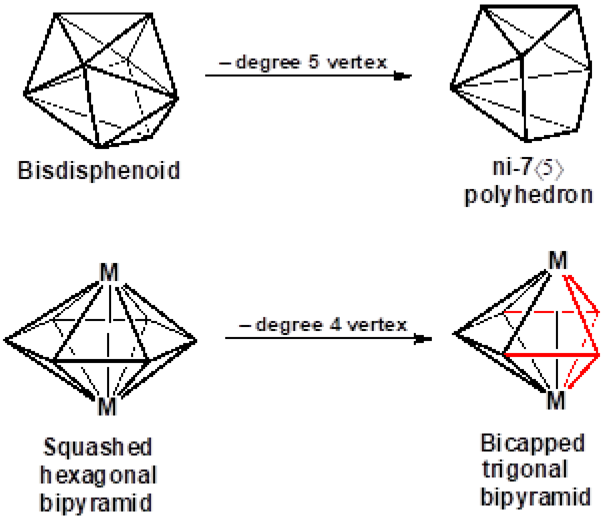

Figure 42. Generation of seven-vertex polyhedra for the hydrogen-rich $Cp_2M_2B_5H_9$ structures by vertex removal from an eight-vertex deltahedron. The capping vertices and associated edges in the bicapped trigonal bipyramid are shown in red for clarity. Note that the equatorial vertices of the underlying M_2B_3 trigonal bipyramid form an M_2B triangle including the M-M interaction that was an internal bond in the original squashed hexagonal bipyramid.

Removal of a degree 5 vertex from the bisdisphenoid gives a polyhedron having three degree 3 vertices, three degree 4 vertices, one degree 5 vertex, and a pentagonal open face (cf. top of Figure 42). This polyhedron does not have an obvious name; it will be designated here as ni-7⟨5⟩ using the nomenclature of Williams[53] to designate a seven-vertex nido (ni) polyhedron with a pentagonal open face (⟨5⟩). The hexagonal bipyramidal structure from which the polyhedron for some of the $Cp_2M_2B_5H_9$ structures is derived has the metal atoms at the two antipodal degree 6 vertices and is squashed to give an oblate deltahedron with the antipodal metal atoms within bonding distance. Removal of a degree 4 equatorial vertex from a squashed hexagonal bipyramid brings the internal metal-metal bond to the polyhedral surface (cf. bottom of Figure 42). Therefore, the resulting seven-vertex polyhedron does not have an open face but instead remains a deltahedron with all triangular faces. This deltahedron is a bicapped trigonal bipyramid with BH groups capping both M_2B triangular faces of the underlying M_2B_3 trigonal bipyramid.

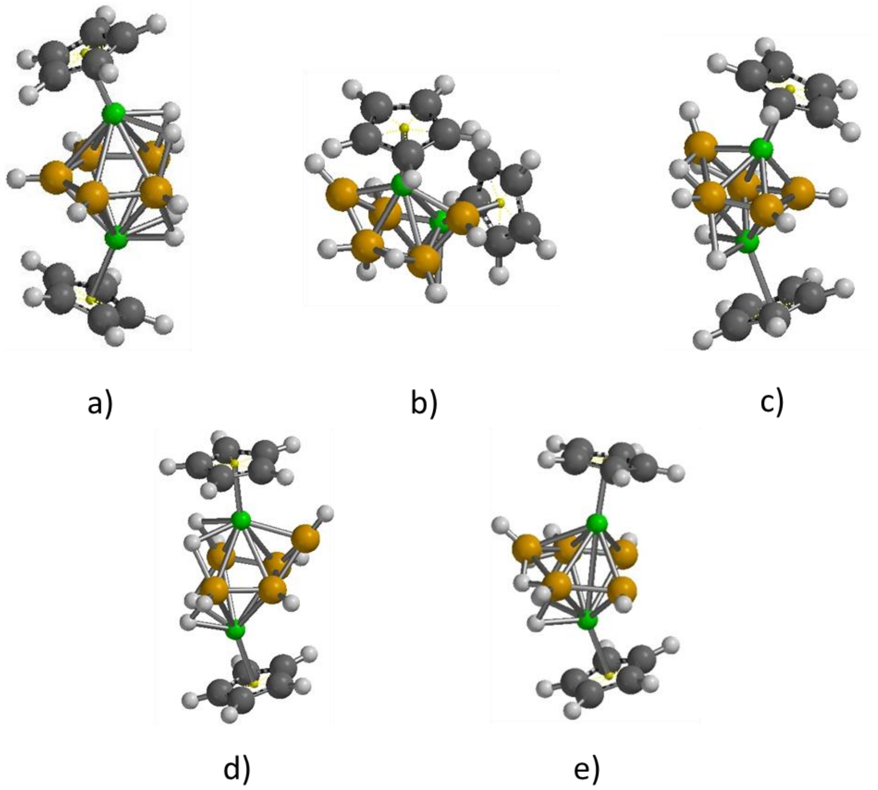

Figure 43. Initial geometries of the $Cp_2M_2B_5H_9$ structures and the number of their isomers. a) the 1-vertex depleted 8 vertices hexagonal bipyramid (10 structures). b) the 1-vertex depleted 8 vertices dicapped octahedron (8 isomers). c) the 1-vertex depleted 8 vertices bidisphenoid (12 isomers). d) the 1-vertex depleted 8 capped pentagonal bipyramid (21 isomers). e) the 1-vertex depleted 8 vertices bicapped octahedron (Cs symmetry) (14 isomers).

The initial $Cp_2M_2B_5H_9$ structures were constructed by systematic substitution of two metal atoms in the ni-7⟨5⟩ polyhedron and the bicapped trigonal bipyramid as well as three other seven-vertex polyhedra obtained by vertex removal from the capped pentagonal bipyramid and the bicapped octahedron (cf. Figure 43). The extra four hydrogen atoms are considered as edge-capping atoms on the edges of the tetragonal/ pentagonal open face or on the metal-metal edge. This leads to 81 different starting geometries to be optimized for each metal system.

3.6.1 $Cp_2Ir_2B_5H_9$ systems

The $Cp_2Ir2B_5H_9$ systems harbor 18 Wadean electrons (cf. Table 24) which, for the 7 vertices polyhedra, accounts for a nido structure (14 = 2n + 4; n = 7). Indeed, all 6 most stable isomers adopt (cf. Figure 44) a nido structure in the form of a ni-7<5> geometry. This polyhedron is obtained by removing a degree 5 vertex from the most spherical 8 vertices containing polyhedron. There are only 2.4 kcal/mol separating the two most stable isomers and in both structures the Ir atoms are placed in a degree-5 and degree 4 vertices, i.e. the maximum degree vertices available in the ni-7<5> polyhedron. Here, as well as in the Ir_2B_5-4 and Ir_2B_5-5 cases, the metal vertices are in adjacent positions and form interactions that possess WBIs ranging from 0.28 to 0.37 (cf. Table 23). Together with their characteristic bond lengths of 2.71 and 2.85 Å, these interactions can be regarded as formal Ir-Ir single bonds. The Ir_2B_5-3 and Ir_2B_5-6 isomers have the metal vertices placed in non-adjacent positions at ~3.6 Å distance from each other. The lower 0.08 WBI emphasize the nonbonding interactions of their metal vertices. The “extra” four H atoms bridge just Ir-B and B-B bond within the Ir_2B_5-2 structure. In the other five isomers there is always a terminal H atom connected to an Ir atom.

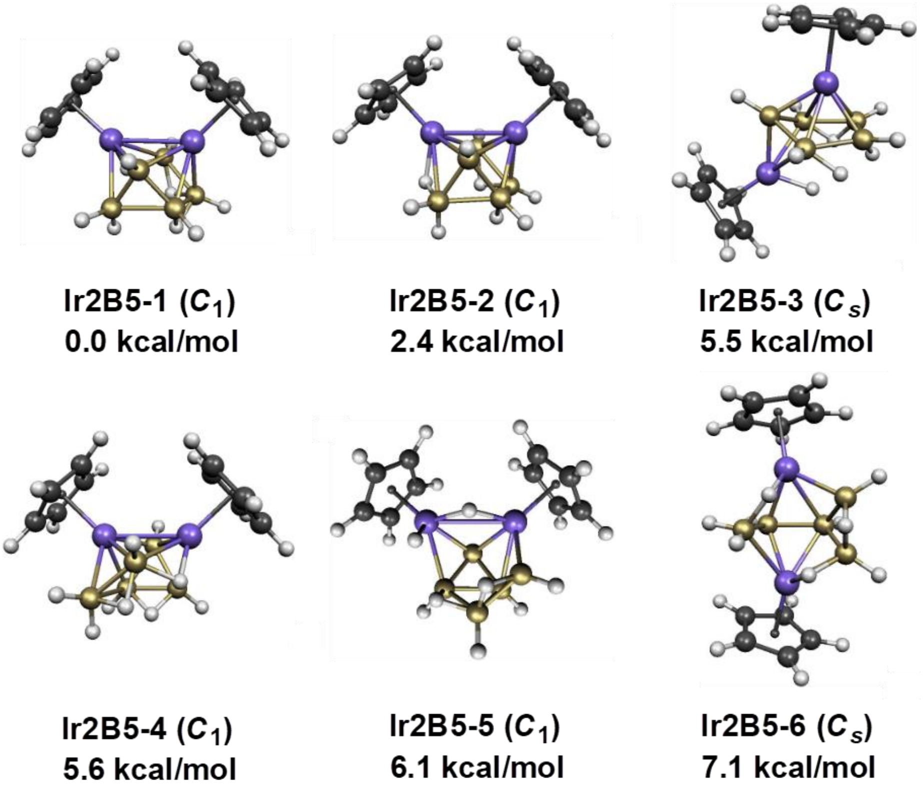
Ir2B5-1 (C_1)
0.0 kcal/mol

Ir2B5-2 (C_1)
2.4 kcal/mol

Ir2B5-3 (C_s)
5.5 kcal/mol

Ir2B5-4 (C_1)
5.6 kcal/mol

Ir2B5-5 (C_1)
6.1 kcal/mol

Ir2B5-6 (C_s)
7.1 kcal/mol

Figure 44. The six $Cp_2Ir_2B_5H_9$ structures within 10 kcal/mol of the global minimum.

Table 24. Skeletal electron count of the $Cp_2Ir_2B_5H_9$.

Molecule	Fragment	Nr. of fragments	e^- donated by fragment	Total e^- donated
$Cp_2Ir_2B_5H_9$	CpIr	2	9-6-1=2	4
	BH	5	2	10
	H	4	1	4
	Skeletal electron count			**18**

Table 25. Optimized $Cp_2Ir_2B_5H_9$ structures within 10 kcal/mol of the global minimum with relative energies in kcal/mol.

Structure (symmetry)	Relative energy	Hydrogen Bridges	Ir-Ir vertices			Polyhedron
			Degrees	Å	WBI	
Ir2B5-1 (C_1)	0.0	IrB/B_2	5,4	2.731	0.36	ni-7⟨5⟩
Ir2B5-2 (C_1)	2.4	$IrB/3B_2$	5,4	2.717	0.36	ni-7⟨5⟩
Ir2B5-3 (C_s)	5.5	$3B_2$	5,3	3.605	0.09	ni-7⟨5⟩
Ir2B5-4 (C_1)	5.6	$IrB/2B_2$	5,4	2.722	0.37	ni-7⟨5⟩
Ir2B5-5 (C_1)	6.1	$Ir_2/2B_2$	4,3	2.847	0.28	ni-7⟨5⟩
Ir2B5-6 (C_s)	7.1	$2IrB/B_2$	4,4	3.582	0.08	ni-7⟨5⟩

3.6.2 $Cp_2M_2B_5H_9$ (M = Ru, Os) systems

As each CpM (M = Ru, Os) vertex donates 1 electron for cluster bonding, a total of 16 skeletal electron are accumulated in the $Cp_2M_2B_5H_9$ systems. (cf. Table 26). According to the Wade-Mingos rules, this represents a closo scenario - and for the 7-vertices polyhedra this would mean that the pentagonal bipyramid would be the expected ground state geometry. However, in the hydrogen-rich paradigm a non-deltahedral face is required for the accommodation of the 4 “extra” H atoms. The geometries that can fulfil this requirement, and that are found in the most favorable $Cp_2M_2B_5H_9$ (M = Ru, Os), are the ni-7<5> and the tricapped tetrahedron (cf.Figure 42).

Table 26. Skeletal electron count of the $Cp_2M_2B_5H_9$ (M = Ru, Os) systems.

Molecule	Fragment	Nr. of fragments	e^- donated by fragment	Total e^- donated
$Cp_2Ru/Os_2B_5H_9$	CpRu/Os	2	8-6-1=1	2
	BH	5	2	10
	H	4	1	4
	Skeletal electron count			**16**

The three most stable isomers are the same for both metal systems and all lie within a 1 kcal/mol interval from each other (cf. Table 27). As shown in Figure 45, the Ru_2B_4-1 isomer and its Os_2B_4-3 equivalent adopt the geometry of the tricapped tetrahedron. Similar to the Ir systems, the remaining two isomers adopt the ni-7<5> geometry and have the metal vertices placed in adjacent positions. In the M_2B_5-4 (M = Ru, Os) case the same tricapped tetrahedron is adopted at ~3 kcal/mol above the ground state and, as opposed to the previous isomers, the metal vertices are located in nonadjacent positions. The M_2B_5-5 isomers lie at 4.2 kcal/mol above the ground state in the Ru case and at 7.5 kcal in the Os systems and share the ni-7<5> geometry. Similar to the M_2B_5-2 isomers, the metal vertices are placed in nonadjacent postitions. The differing aspect, however, consists in having 5 bridging H atoms in contrast with the usual 4 bridging H adopted by the M_2B_5-2 isomer.

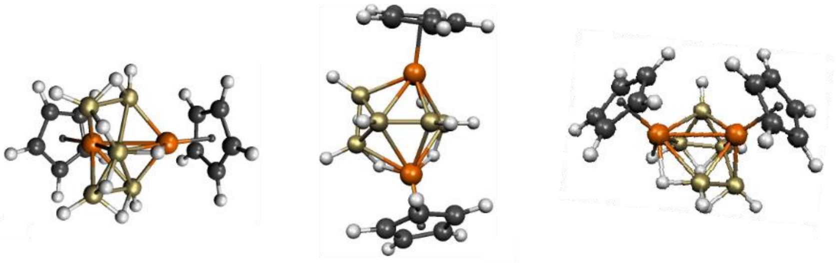

Ru2B5-1 (C_s)
0.0 kcal/mol
Os2B5-3 (C_s)
0.7 kcal/mol

Ru2B5-2 (C_1)
0.2 kcal/mol
Os2B5-2 (C_1)
0.7 kcal/mol

Ru2B5-3 (C_1)
0.2 kcal/mol
Os2B5-1 (C_1)
0.0 kcal/mol

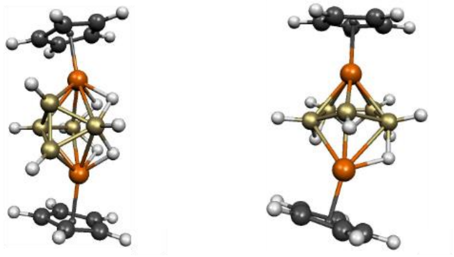

Ru2B5-4 (C_s)
2.5 kcal/mol
Os2B5-4 (C_s)
3.0 kcal/mol

Ru2B5-5 (C_s)
4.2 kcal/mol
Os2B5-5 (C_s)
7.5 kcal/mol

Figure 45. The five lowest energy $Cp_2M_2B_5H_9$ (M = Ru, Os) structures.

The $Cp_2Ru_2B_5H_9$ system possesses a very complicated potential energy surface. For instance, 12 of its most stable isomers are found within the 10 kcal/mol above the ground state (cf. Table 83 in sections 6.1.2.2). Within the same 10 kcal/mol range there are only 4 isomers of the $Cp_2Os_2B_5H_9$ system.

Table 27. The five lowest energy $Cp_2M_2B_5H_9$ (M = Ru, Os) structures with relative energies in kcal/mol.

Structure (symmetry)	Polyhedron	Hydrogen bridges	$Cp_2Ru_2B_5H_9$			$Cp_2Os_2B_5H_9$		
			ΔE	Ru–Ru	WBI	ΔE	Os–Os	WBI
Ru2B5-1/Os2B5-3 (C_s)	Bicap trig bipy	$MB/4B_2$	0.0	2.731	0.33	0.7	2.782	0.36
Ru2B5-2/Os2B5-2 (C_1)	ni-7⟨5⟩	$3MB/B_2$	0.2	3.519	0.17	0.7	3.567	0.16
Ru2B5-3/Os2B5-1 (C_1)	ni-7⟨5⟩	$2MB/2B_2$	0.2	2.747	0.42	0.0	2.801	0.45
Ru2B5-4/Os2B5-4 (C_s)	Tricap tetrahed	4MB	2.5	3.568	0.10	3.0	3.604	0.09
Ru2B5-5/Os2B5-5 (C_s)	ni-7⟨5⟩	$2MB/3B_2$	4.2	3.670	0.15	7.5	3.716	0.16

3.6.3 $Cp_2Re_2B_5H_9$ systems

As each CpRe is an effective 0 electron donor, a total of 14 Wadean electrons are accumulated (cf. Table 28) in the $Cp_2Re_2B_5H_9$ systems. The 14 electron count corresponds to a 2n isocloso regime. The isocloso geometry for a 7-vertices system is represented by the capped octahedron geometry and, indeed, the first three most stable computed isomers share the capped the octahedral geometry (cf. Figure 46). In the Re_2B_4-1 and Re_2B_4-2 isomers, a degree 3 BH vertex caps a Re_2B face and thus each Re atom becomes a degree 5 vertex. The Re-Re bond lengths and WBI (~2.91 Å respectively ~0.4) are representative for formal single bonds (cf. Table 29). In the Re_2B_4-3 isomer the BH vertex caps a ReB_2 face. The bond parameters are similar to the previous two isomers and suggest formal single bond between the metal vertices.

Table 28. Skeletal electron count of the $Cp_2Re_2B_5H_9$ systems.

Molecule	Fragment	Nr. of fragments	e^- donated by fragment	Total e^- donated
$Cp_2Re_2B_5H_9$	CpRe	2	7-6-1=3	0
	BH	5	2	10
	H	4	1	4
	Skeletal electron count			**14**

The bicapped tetrahedron is also found among the most stable isomers of the $Cp_2Re_2B_5H_9$ systems. The Re_2B_5-4 isomer adopts this geometry at 10 kcal/mol above the ground state. Its structure can be interpreted as a central Re_2B_3 tetragonal pyramid capped by two BH vertices. This central Re_2B_3 framework is similar to the nido square pyramidal geometry of the B_5H_9 pentaborane. The latter possesses 14 Wadean electrons and thus is isolectronic with the $Cp_2Re_2B_5H_9$ systems.

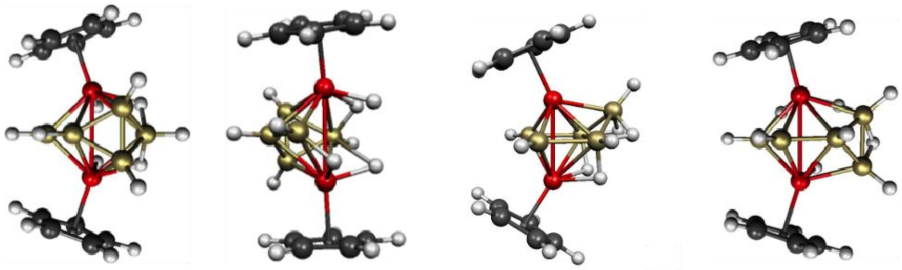

Re2B5-1 (*C*$_s$) **0.0 kcal/mol**

Re2B5-2 (*C*$_s$) **3.2 kcal/mol**

Re2B5-3 (*C*$_s$) **7.4 kcal/mol**

Re2B5-4 (*C*$_s$) **10.0 kcal/mol**

Figure 46. The four $Cp_2Re_2B_5H_9$ structures within 17 kcal/mol of the global minimum.

Table 29. Optimized $Cp_2Re_2B_5H_9$ structures within 17 kcal/mol of the global minimum with relative energies in kcal/mol.

Structure (symmetry)	Relative energy	Hydrogen Bridges	Re-Re vertices			Polyhedron
			Degrees	Å	WBI	
Re2B5-1 (*C*$_s$)	0.0	4ReB	5,5	2.907	0.41	Capped octahedron
Re2B5-2 (*C*$_s$)	3.2	4ReB	5,5	2.917	0.45	Capped octahedron
Re2B5-3 (*C*$_s$)	7.4	2ReB/2B_2	5,4	2.825	0.44	Capped octahedron
Re2B5-4 (*C*$_s$)	10.0	2ReB/B_2	5,5	2.956	0.47	Bicap tetrag pyramid

3.6.4 $Cp_2M_2B_5H_9$ (M=Mo,W) systems

The Mo and W systems share a surprisingly simple potential energy surface in the vicinity of the ground state (cf. Table 85 from section 6.1.3.4). The Mo_2B_5-2 isomer lies at 24.1 kcal/mol above the ground state while the W_2B_5-2 isomer at 23.1 kcal/mol (cf.Table 31). As seen in Figure 47, the ground state adopts the geometry of a bicapped trigonal bipyramid polyhedron. As each CpM vertex is an effective -1 electron donor the total skeletal electron count of these systems reaches 12 Wadean electrons (cf. 1st entry of Table 30). If the capping BH vertices are considered electron donor units and not accounted as polyhedral vertices, then the remaining trigonal bipyramid framework, i.e. a closo geometry, can be rationalized by the 12 Wadean electron count, i.e. 12 = 2n + 2, for n = 5 vertices (cf. 2nd entry of Table 30).

Table 30. Skeletal electron count of the $Cp_2M_2B_5H_9$ (M = Mo, W) systems.

Molecule	Fragment	Nr. of fragments	e^- donated by fragment	Total e^- donated
$Cp_2Mo/W_2B_5H_9$	CpMo/W	2	6-6-1=-1	-2
	BH	5	2	10
	H	4	1	4
		Skeletal electron count		**12**
M_2B_3 underlying trigonal pyrdamid	CpMo/W	2	6-6-1=-1	-2
	BH	3	2	6
	BH (cap)	2	2	4
	H	4	1	4
		Skeletal electron count		**12**

Both Mo and W systems had been previously synthetized in their permethylated $Cp^*_2M_2B_4H_9$ (M = Mo, W) versions.[54–56] Our computations found for the ground state of these systems the same geometry as the one reported based on experimental endeavors. The remarkable agreement between the two approaches can be emphasized by the comparison of the experimentally determined and DFT computed Mo-Mo distance: 2.809 Å vs. 2.802 Å. In the W case, theseare, 2.817 Å and 2.836 Å, respectively.

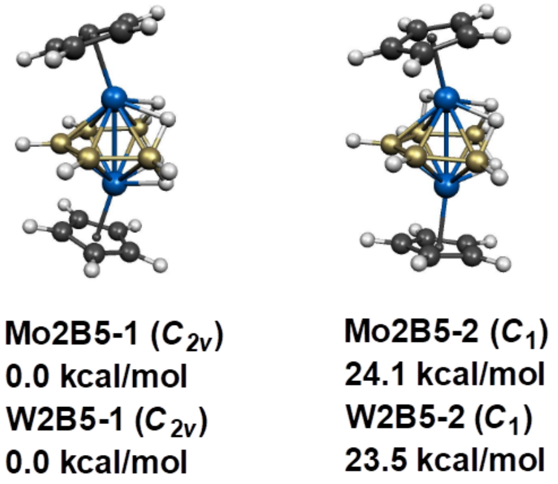

Figure 47. The two $Cp_2M_2B_5H_9$ (M = Mo, W) structures within 40 kcal/mol of the global minimum.

Table 31. Optimized $Cp_2M_2B_4H_8$ (M = Mo, W) structures within 40 kcal/mol of the global minimum with relative energies in kcal/mol.

Structure		Hydrogen	$Cp_2Mo_2B_5H_9$			$Cp_2W_2B_5H_9$		
(symmetry)	Polyhedron	bridges	ΔE	Mo–Mo	WBI	ΔE	W–W	WBI
Mo2B5-1/W2B5-1 (C_{2v})	Bicap trig bipy	4MB	0.0	2.802	0.71	0.0	2.836	0.74
Mo2B5-2/W2B5-2 (C_1)	Bicap trig bipy	4MB	24.1	2.783	0.64	23.5	2.819	0.65

3.6.5 $Cp_2Ta_2B_5H_9$ systems

The Wade-Mingos rules applied for the $Cp_2Ta_2B_5H_9$ systems yield a total of 10 skeletal electrons available for cluster bonding. This is because, at first sight, each CpTa vertex is an effective -2 electron donor (cf. 1st entry of Table 32). However, as shown in Figure 48, the geometry adopted is the same bicapped trigonal bipyramid as seen in the M = Mo, W systems (cf. Figure 47). The interpretation of a Ta atom as adopting the 16 electron configuration rather than the usual 18 electron configuration makes the respective CpTa vertex an effective 0 electron donor (cf. 2nd entry of Table 32). In this interpretation, the total skeletal electron count is adjusted to the 12 Wadean electron characteristic of the $Cp_2M_2B_5H_9$ (M = Mo, W) systems.

Table 32. Skeletal electron count of the $Cp_2Ta_2B_5H_9$ systems.

Molecule	Fragment	Nr. of fragments	e^- donated by fragment	Total e^- donated
$Cp_2Ta_2B_5H_9$	CpTa	2	5-6-1=-2	-4
	BH	5	2	10
	H	4	1	4
	Skeletal electron count			**10**
$Cp_2Ta_2B_5H_9$	CpTa (18e config.)	1	5-6-1=-2	-2
	CpTa (16e config.)	1	7-6-1=0	0
	BH	5	2	10
	H	4	1	4
	Skeletal electron count			**12**

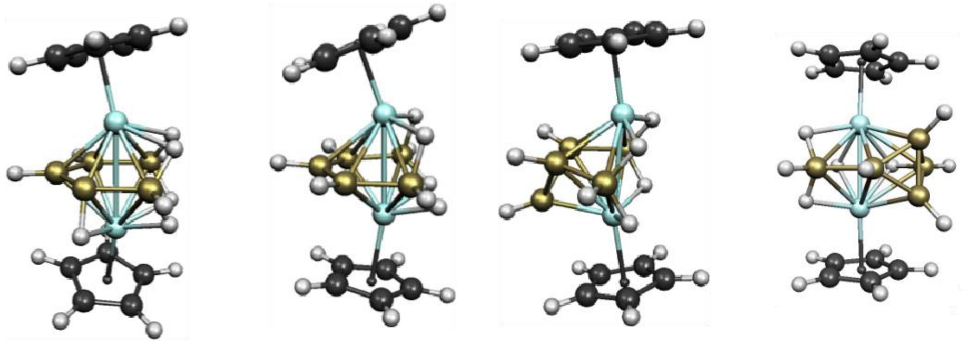

Ta2B5-1 (C_1) **0.0 kcal/mol**

Ta2B5-2 (C_s) **3.8 kcal/mol**

Ta2B5-3 (C_s) **6.7 kcal/mol**

Ta2B5-4 (C_s) **9.2 kcal/mol**

Figure 48. The four $Cp_2Ta_2B_5H_9$ structures within 11 kcal/mol of the global minimum.

Table 33. Optimized $Cp_2Ta_2B_5H_9$ structures within 11 kcal/mol of the global minimum with relative energies in kcal/mol.

Structure (symmetry)	Relative energy	Hydrogen Bridges	Ta-Ta vertices Degrees	Å	WBI	Polyhedron
Ta2B5-1 (C_s)	0.0	4TaB	6,6	3.056	0.55	Bicap trig bipy
Ta2B5-2 (C_s)	3.8	4TaB	6,6	2.893	0.69	Bicap trig bipy
Ta2B5-3 (C_s)	6.7	4TaB	6,5	2.941	0.88	Tricapped tetrahedron
Ta2B5-4 (C_s)	9.2	4TaB	5,5	2.717	1.12	Capped octahedron

3.7 8 vertices

The initial $Cp_2M_2B_6H_{10}$ structures were constructed by systematic substitution of the two metal atoms on the vertices of the ni-8<5> polyhedron and the B_8H_{12} framework (cf. Figure 49) as well as into three other eight-vertex polyhedra obtained by vertex removal from the capped pentagonal bipyramid and the bicapped octahedron (cf. Figure 50). The extra four hydrogen atoms are considered as edge-capping atoms on the edges of the open face or on the metal-metal edge. This leads to 187 different starting geometries to be optimized for each metal.

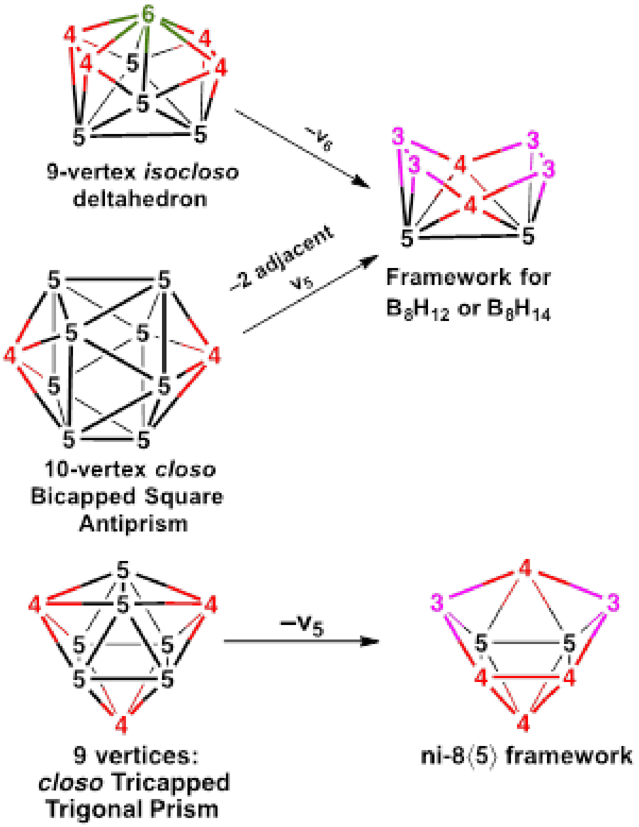

Figure 49. (a) Generation of the 8-vertex framework for either B_8H_{12} or B_8H_{14} by removal of the degree 6 vertex from the *isocloso* 9-vertex deltahedron or by removal of two adjacent degree 5 vertices from the *closo* 10-vertex deltahedron, namely the bicapped square antiprism; (b) Generation of the ni-8⟨5⟩ framework by removal of a degree 5 vertex from the *closo* 9-vertex deltahedron, namely the tricapped trigonal prism.

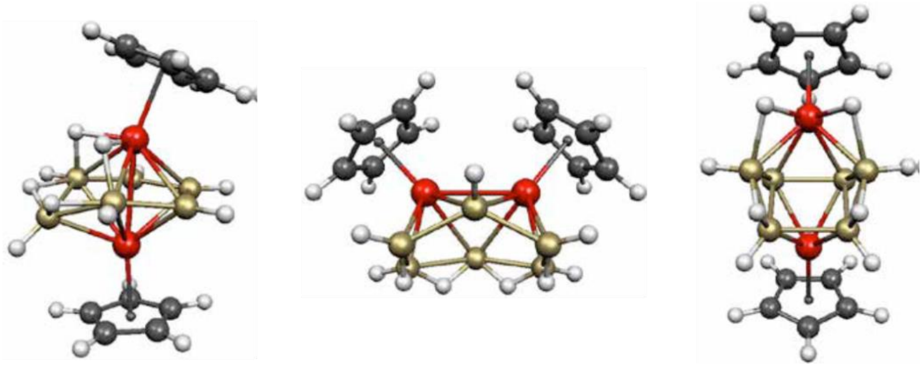

Figure 50. Initial geometries of the $Cp_2M_2B_6H_{10}$ structures and the number of their isomers. Left: the 1-vertex depleted 9 vertices *oblatocloso* (11 structures). Middle: the 1-vertex depleted 9 vertices *isoclocloso* (77 isomers) Right: the 1-vertex depleted 9 vertices *closo* (99 isomers).

3.7.1 $Cp_2M_2B_6H_{10}$ (M = Pd, Pt) systems

The CpM (M = Pd, Pt) vertices donate a total of 6 electrons for cluster bonding as each metal vertex is an effective 3 electron donor unit. Added to the 12 electrons donated by the 6 BH vertices and the 4 electrons brought the by the "extra" H atoms, a total of 22 Wadean electrons are accumulated (cf. Table 35) within the $Cp_2M_2B_6H_{10}$ (M = Pd, Pt) systems. According to the Wade-Mingos rules, this represents a 2n + 6 (n = 8) arachnno scenario. Both metal systems adopt the same ground state geometry which incorporates an open hexagonal face (cf. Figure 51) and is similar to the geometry of the arachno B_8H_{14} system (cf. Figure 49). In this ar-8<6> structure, the metal atoms are adjacently located at degree 3 vertices in the open hexagonal face. The typical M-M distances and WBI (cf. Table 35) suggest a formal single bond between the metal vertices.

Table 34. Skeletal electron count of the $Cp_2M_2B_6H_{10}$ (M = Pd, Pt) and B_8H_{14} systems.

Molecule	Fragment	Nr. of fragments	e^- donated by fragment	Total e^- donated
$Cp_2Pd/Pt_2B_6H_{10}$	CpPd/Pt	2	10-6-1=3	6
	BH	6	2	12
	H	4	1	4
	Skeletal electron count			**22**
B_8H_{14}	BH	8	2	16
	H	6	1	6
	Skeletal electron count			**22**

The Pd_2B_6-2 and its Pt correspondent Pt_2B_6-3 isomers share the ground state geometry but differ in terms of CpM locations. Here they are placed in opposing rather than adjacent degree 3 vertices and have no direct bonding interaction. This is emphasized by the low WBI 0.03 (cf. Table 35). The "extra" four H atoms bridge two M-B and two B-B edges. The third Pd isomer lies at 14.4 kcal/mol above the ground state and adopts a different geometry in the form of the nido structure ni-8<5>. The metal vertices are placed in nonadjacent positions and the "extra" 4 H atoms cap the pentagonal open face. In the Pt system, this geometry is more favorable and, by lying at just 5.8 kcal/mol above the ground state, it becomes the second most favorable isomer of the $Cp_2Pd_2B_6H_{10}$ systems.

Pd2B6-1 (0.0) (*C_s*)
Pt2B6-1 (0.0) (*C_s*)

Pd2B6-2 (13.6) (*C_2*)
Pt2B6-3 (10.4) (*C_2*)

Pd2B6-3 (14.4) (*C_1*)
Pt2B6-2 (5.8) (*C_1*)

Figure 51. The three lowest energy $Cp_2M_2B_6H_{10}$ (M = Pd, Pt) structures within 12 kcal/mol (M = Pd) or 20 kcal/mol (M = Pt) of the lowest energy structure with relative energies (kcal/mol) in parentheses.

Table 35. Relative energies (kcal/mol), metal-metal distances (Å), and metal-metal Wiberg Bond Indices for the three lowest energy $Cp_2M_2B_6H_{10}$ (M = Pd, Pt) structures.

Structure		Hydrogen	$Cp_2Pd_2B_6H_{10}$			$Cp_2Pt_2B_6H_{10}$		
(symmetry)	Polyhedron	bridges	ΔE	Pd–Pd	WBI	ΔE	Pt–Pt	WBI
Pd2B6-1/Pt2B6-1 (C_s)	B_8H_{14}	$M_2/3B_2$	0.0	2.622	0.26	0.0	2.676	0.32
Pd2B6-2/Pt2B6-3 (C_2)	B_8H_{14}	$2MB/2B_2$	13.6	4.521	0.03	10.4	4.503	0.03
Pd2B6-3/Pt2B6-2 (C_1)	ni-8⟨5⟩	$MB/3B_2$	14.4	3.834	0.09	5.8	3.836	0.07

3.7.2 $Cp_2M_2B_6H_{10}$ (M=Rh,Ir) systems

Each metal vertex of the $Cp_2M_2B_6H_{10}$ (M = Rh, Ir) systems donates 2 electrons for cluster bonding. This adds up to a total of 20 Wadean electrons (cf. 1st entry of Table 36) which represent the electron count needed by a nido structure (20=2n+4, n=8) as is the case of the B_8H_{12} molecule(cf. 2nd entry of Table 36). Both metal systems share a complicated potential energy surface: Rh has 12 isomers within the 10 kcal/mol interval above the ground (cf.Table 90 from section 6.1.4.2) state while Ir hosts its 12 most stable isomers within a 13 kcal/mol interval above the ground state (cf. Table 91 from section 6.1.4.2).

Table 36. Skeletal electron count of the $Cp_2M_2B_6H_{10}$ (M = Rh, Ir) and B_8H_{12} systems.

Molecule	Fragment	Nr. of fragments	e^- donated by fragment	Total e^- donated
$Cp_2Rh/Ir_2B_6H_{10}$	CpRh/Ir	2	9-6-1=2	4
	BH	6	2	12
	H	4	1	4
	Skeletal electron count			**20**
B_8H_{12}	BH	8	2	16
	H	4	1	4
	Skeletal electron count			**20**

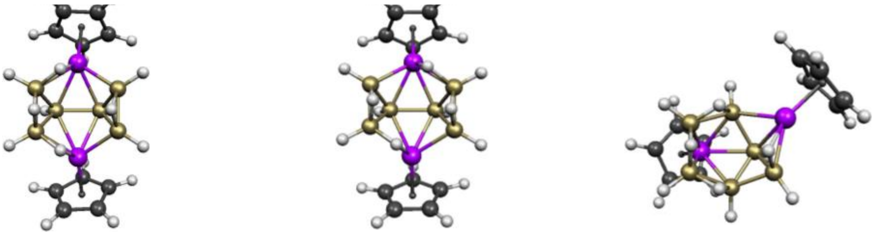

Rh2B6-1 (0.0) (C_s) **Ir2B6-1** (0.0) (C_s)

Rh2B6-2 (0.8) (C_2) **Ir2B6-2** (0.4) (C_2)

Rh2B6-3 (2.3) (C_1) **Ir2B6-6** (5.2) (C_1)

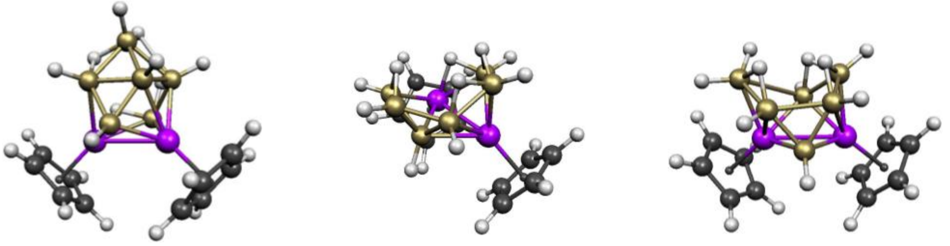

Rh2B6-4 (2.4) (C_1) **Ir2B6-4** (4.0) (C_1)

Rh2B6-5 (4.8) (C_1) **Ir2B6-5** (4.1) (C_1)

Rh2B6-6 (5.0) (C_1) **Ir2B6-3** (3.0) (C_1)

Figure 52. The six lowest energy $Cp_2M_2B_6H_{10}$ (M = Rh, Ir) structures within 6 kcal/mol (M = Rh) or 7 kcal/mol (M = Ir) of the lowest energy structure with relative energies (kcal/mol) in parentheses.

The M_2B_6-1 and M_2B_6-2 isomers form a fluxional state in both metal systems (cf. Figure 52 and Table 37). Both isomers share the geometry of the nido B_8H_{12} molecule (cf. Figure 49) and have their metal atoms placed on the open hexagonal face in opposing degree 4 vertices(cf. Figure 52 and Table 37). The fluxionality implies the movement of the 4 “extra” H atoms on this hexagonal face. This structures corresponds to the $Cp^*_2Rh_2B_6H_{10}$ structure determined by X-ray crystallography.[57] The computed Rh-Rh distance of 3.858 Å is in excellent agreement with the experimental determined 3.85 Å. The H NMR investigations of this compound also suggested the presence of a fluxional state involving the movement of the bridging H atoms across the open hexagonal face.

Table 37. Relative energies (kcal/mol), metal-metal distances (Å), and metal-metal Wiberg Bond Indices for the six lowest energy $Cp_2M_2B_6H_{10}$ (M = Rh, Ir) structures.

Structure		Hydrogen	$Cp_2Rh_2B_6H_{10}$			$Cp_2Ir_2B_6H_{10}$		
(symmetry)	Polyhedron	bridges	ΔE	Rh–Rh	WBI	ΔE	Ir–Ir	WBI
Rh2B6-1/Ir2B6-1 (C_s)	B_8H_{12}	$2MB/2B_2$	0.0	3.858	0.08	0.0	3.883	0.07
Rh2B6-2/Ir2B6-2 (C_2)	B_8H_{12}	$2MB/2B_2$	0.8	3.855	0.07	0.4	3.884	0.07
Rh2B6-3/Ir2B6-6 (C_1)	B_8H_{12}	$MB/3B_2$	2.3	3.957	0.07	5.2	3.967	0.07
Rh2B6-4/Ir2B6-4 (C_1)	ni-8⟨5⟩	$MB/3B_2$	2.4	2.670	0.33	4.0	2.730	0.36
Rh2B6-5/Ir2B6-5 (C_1)	B_8H_{12}	$MB/3B_2$	4.8	2.673	0.32	4.1	2.732	0.36
Rh2B6-6/Ir2B6-3 (C_1)	ni-8⟨5⟩	$3B_2$	5.3	2.681	0.30	3.0	2.735	0.34

The next lowest-lying structure also adopts this nido-B_8H_{12} geometry but locates its metal vertices in different positions. M_2B_6-4 and Rh_2B_6-4/ Ir_2B_6-4 adopt a different nido arrangement in the form of the ni-8<5> polyhedron.

3.7.3 $Cp_2M_2B_6H_{10}$ (M = Ru, Os) systems

Table 38 summarizes the total 18 Wadean electrons that are accumulated in the Ru and Os systems. This count would normally lead to closo structure. However, the most spherical 8 vertices polyhedron, i.e. the bidisphenoid, does not have a non-deltahedral face that could harbor the “extra” H atoms. For this reason, instead of adopting the bidsiphenoid geometry, the $Cp_2M_2B_6H_{10}$ (M=Ru,Os) systems adopt open faced polyhedral. There is a rich variety of the geometries available for the Ru and Os systems available in the 10 kcal/mol interval above the ground state (cf. Figure 53). All these structure place their metal vertices in adjacent positions at distances ranging from 2.75 Å to 2.88 Å in the Ru systems and from 2.79 to 2.99 Å in the Os systems. Their corresponding WBI range between 0.3 and 0.39, in Ru systems and in slightly higher values ranging from 0.33 to 0.58 in Os systems (cf. Table 39).

Table 38. Skeletal electron count of the $Cp_2M_2B_6H_{10}$ (M = Ru, Os) systems.

Molecule	Fragment	Nr. of fragments	e^- donated by fragment	Total e^- donated
$Cp_2Ru/Os_2B_6H_{10}$	CpRu/Os	2	8-6-1=1	2
	BH	6	2	12
	H	4	1	4
	Skeletal electron count			**18**

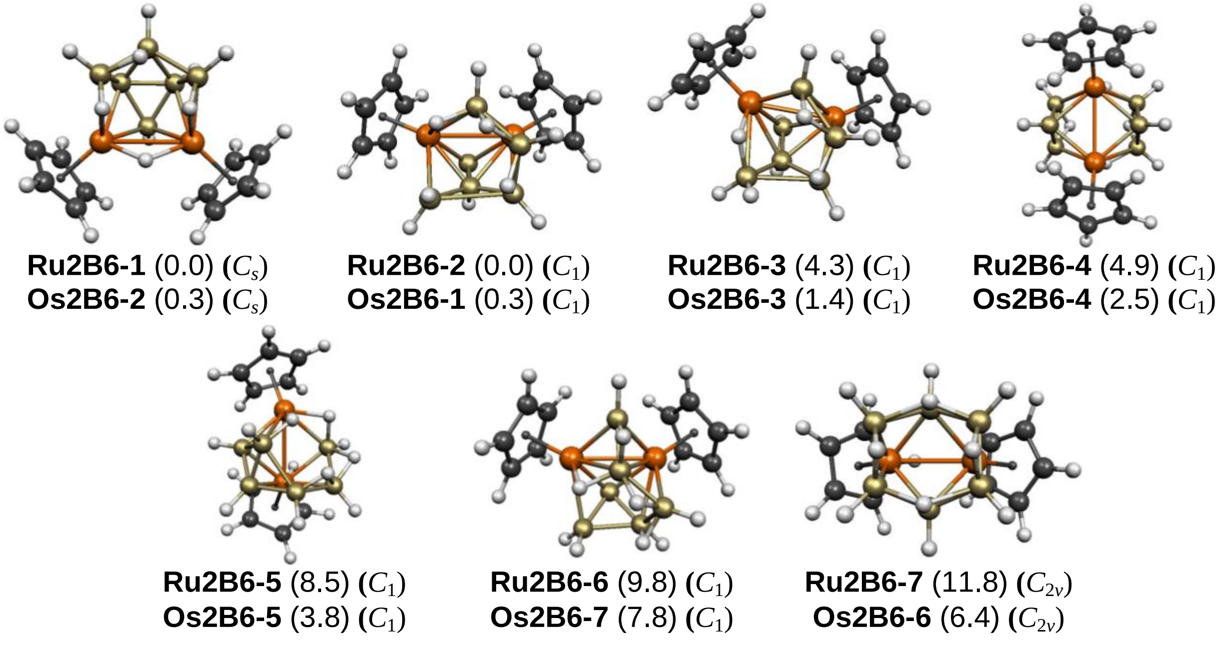

Ru2B6-1 (0.0) (C_s)
Os2B6-2 (0.3) (C_s)

Ru2B6-2 (0.0) (C_1)
Os2B6-1 (0.3) (C_1)

Ru2B6-3 (4.3) (C_1)
Os2B6-3 (1.4) (C_1)

Ru2B6-4 (4.9) (C_1)
Os2B6-4 (2.5) (C_1)

Ru2B6-5 (8.5) (C_1)
Os2B6-5 (3.8) (C_1)

Ru2B6-6 (9.8) (C_1)
Os2B6-7 (7.8) (C_1)

Ru2B6-7 (11.8) (C_{2v})
Os2B6-6 (6.4) (C_{2v})

Figure 53. The seven lowest energy $Cp_2M_2B_6H_{10}$ (M = Ru, Os) structures within 12 kcal/mol (M = Ru) or 10 kcal/mol (M = Os) of the lowest energy structure with relative energies (kcal/mol) in parentheses.

Table 39. Relative energies (kcal/mol), metal-metal distances (Å), and metal-metal Wiberg Bond Indices for the seven lowest energy $Cp_2M_2B_6H_{10}$ (M = Ru, Os) structures.

Structure (symmetry)	Polyhedron	Hydrogen bridges	$Cp_2Ru_2B_6H_{10}$ ΔE	 Ru–Ru	 WBI	$Cp_2Os_2B_6H_{10}$ ΔE	 Os–Os	 WBI
Ru2B6-1/Os2B6-2 (*C*$_s$)	ni-8⟨5⟩	M_2/2MB/B_2	0.0	2.879	0.30	0.3	2.921	0.33
Ru2B6-2/Os2B6-1 (*C*$_1$)	B_8H_{12} + M-M	MB/B_2	2.8	2.754	0.36	0.0	2.797	0.38
Ru2B6-3/Os2B6-3 (*C*$_1$)	B_8H_{12} + M-M	MB/B_2	4.3	2.747	0.34	1.4	2.790	0.37
Ru2B6-4/Os2B6-4 (*C*$_s$)	B_8H_{12}	4B_2	4.9	2.765	0.39	2.5	2.819	0.41
Ru2B6-5/Os2B6-5 (*C*$_1$)	isoni-8⟨5⟩	2MB/2B_2	8.5	2.785	0.37	5.8	2.838	0.39
Ru2B6-6/Os2B6-7 (*C*$_1$)	$3v_3+3v_4+v_5+v_6$	MB/2B_2	9.8	2.752	0.34	7.8	2.800	0.37
Ru2B6-7/Os2B6-6 (*C*$_{2v}$)	B_8H_{12}	2B_2/2B_3	11.8	2.639	0.54	6.4	2.676	0.58

3.7.4 $Cp_2Re_2B_6H_{10}$ systems

With each Cp Re being an effective 0 electron donor, a total of 16 Wadean electrons are accumulated for cluster bonding in the $Cp_2Re_2B_6H_{10}$ systems (cf Table 40). There are only two isomers within the the 12 kcal/mol interval above de ground state (cf. Figure 54). The Re_2B_6-1 isomer adopts the geometry of the tricapped trigonal bipyramid and has three degree 3 vertices. The Re_2B_6-2 isomer can be regarded as a bicapped octahedron. Both isomers may be deemed to be oblatoarchno structures obtained from an oblatocloso $Cp_2Re_2B_8H_{10}$ structure by the removal of two adjacent BH vertices. Futhermore, the Re-Re WBI values (cf. Table 41) suggest formal single bond and thus no extra electrons are added to the total skeletal electron. Thus, the total skeletal electron count is representative for the oblatoarchno 2n (n = 8) count (cf. Table 40).

Table 40. Skeletal electron count of the $Cp_2Re_2B_6H_{10}$ systems.

Molecule	Fragment	Nr. of fragments	e^- donated by fragment	Total e^- donated
$Cp_2Re_2B_6H_{10}$	CpRe	2	7-6-1=3	0
	BH	6	2	12
	H	4	1	4
	Skeletal electron count			**16**

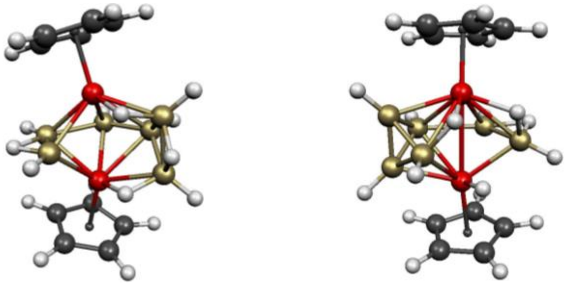

Re2B6-1 (0.0) (C_s) **Re2B6-2** (2.5) (C_s)

Figure 54. The two lowest energy $Cp_2Re_2B_6H_{10}$ structures within 12 kcal/mol of the lowest energy structure with relative energies (kcal/mol) in parentheses.

Table 41. Relative energies (kcal/mol), metal-metal distances (Å), and metal-metal Wiberg Bond Indices for the two lowest energy $Cp_2Re_2B_6H_{10}$ structures.

Structure	Relative	Hydrogen	Re-Re vertices			
(symmetry)	energy	Bridges	Degrees	Å	WBI	Polyhedron
Re2B6-1 (C_s)	0.0	2ReB/B_2	6,5	2.834	0.47	Tricap trigonal bipyramid ($3v_3$)
Re2B6-2 (C_1)	2.5	1ReB/B_2	6,6	2.819	0.46	Bicapped octahedron ($1v_3$)

3.7.5 $Cp_2M_2B_6H_{10}$ (M = Mo, W) systems

With each CpM vertex being an effective -1 electron donor, the $Cp_2M_2B_6H_{10}$ (M = Mo, W) systems possess a total of 14 Wadean electrons (cf. Table 42). This corresponds to a 14 = 2n - 2 count (n = 8 vertices) which is the electron count specific to oblatonido structures. The M_2B_6-1 and M_2B_6-2 isomers are separated by ~3.5 kcal/mol and share the geometry of a bicapped octahedron (cf. Figure 55 and Table 43). They differ between themselves only by the distribution of the 4 bridging H atoms on the opened face. The M_2B_6-3 isomer lies at 7.2 kcal/mol above the ground state in the Mo systems and at 6.7 kcal/mol in the Os systems. It adopts a geometry that can be interpreted as an octahedron fused, via a face, to a trigonal bypiramid.

Table 42. Skeletal electron count of the $Cp_2M_2B_6H_{10}$ (M = Mo, W) systems.

Molecule	Fragment	Nr. of fragments	e^- donated by fragment	Total e^- donated
$Cp_2Mo/W_2B_6H_{10}$	CpMo/W	2	6-6-1=-1	-2
	BH	6	2	12
	H	4	1	4
		Skeletal electron count		**14**

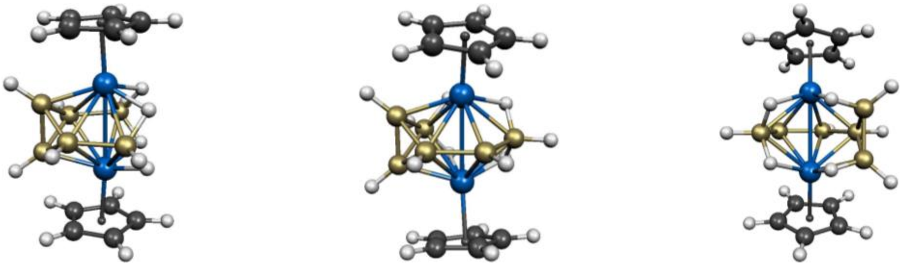

Mo2B6-1 (0.0) (C_{2v})
W2B6-1 (0.0) (C_{2v})

Mo2B6-2 (3.5) (C_s)
W2B6-2 (3.4) (C_s)

Mo2B6-3 (7.2) (C_s)
W2B6-3 (6.7) (C_s)

Figure 55. The three lowest energy $Cp_2M_2B_6H_{10}$ (M = Mo, W) structures within 13 kcal/mol (M = Mo) or 14 kcal/mol (M = W) of the lowest energy structure with relative energies (kcal/mol) in parentheses.

The permethylated version of $Cp^*{}_2W_2B_6H_{10}$ was determined experimentally. Our computed W_2B_6-1 structure is in agreement with the experimentally obtained of $Cp^*{}_2W_2B_6H_{10}$ structure.[58]

Table 43. Relative energies (kcal/mol), metal-metal distances (Å), and metal-metal Wiberg Bond Indices for the three lowest energy $Cp_2M_2B_6H_{10}$ (M = Mo, W) structures.

Structure (symmetry)	Polyhedron	Hydrogen bridges	$Cp_2Mo_2B_6H_{10}$			$Cp_2W_2B_6H_{10}$		
			ΔE	Mo–Mo	WBI	ΔE	W–W	WBI
M2B6-1 (C_{2v})	bicap octahed	4MB	0.0	2.940	0.60	0.0	2.972	0.62
M2B6-2 (C_s)	bicap octahed	4MB	3.5	2.931	0.62	3.4	2.966	0.63
M2B6-3 (C_s)	tribipy+ octahed	4MB	7.2	2.899	0.58	6.7	2.921	0.62

3.7.6 $Cp_2Ta_2B_6H_{10}$ systems

Each CpTa vertex is an effective -2 electron donor. However, the lower-lying $Cp_2Ta_2B_6H_{10}$ isomers possess high WBI (cf. Table 45) that suggest the presence of formal double bond between the Ta vertices. This extra bond adds 2 extra electrons to the total skeletal electron count and thus a total of 14 Wadean electrons are accumulated. This electron count is similar to that of the Mo and W systems (cf. Table 42) and, not surprisingly, their oblatonido arrangement is also found in the $Cp_2Ta_2B_6H_{10}$ ground state (cf. Figure 56). The Ta_2B_6-2 isomer is basically degenerated with the ground state as it lies just 0.2 kcal/mol above it. Its geometry is different and rather unusual: it has 5 bridging H atoms and one "bare" B vertex. The Ta-Ta WBI suggests formal single bond in this isomer. The 14 skeletal electron count still stands as now there is one extra electron donated by the fifth bridging H atom and one extra electron coming from the "bare" B vertex (which is in effective 3 electron donor, opposed to the 2 electron donor BH vertex). The remaining lower-lying isomers also share unfamiliar polyhedral geometries.

Table 44. Skeletal electron count of the $Cp_2Ta_2B_6H_{10}$ systems.

Molecule	Fragment	Nr. of fragments	e^- donated by fragment	Total e^- donated
$Cp_2Ta_2B_6H_{10}$	CpTa	2	5-6-1=-2	-4
	BH	6	2	12
	H	4	1	4
	Ta=Ta	1	2	2
	Skeletal electron count			**14**

Table 45. Relative energies (kcal/mol), metal-metal distances (Å), and metal-metal Wiberg Bond Indices for the five lowest energy $Cp_2Ta_2B_6H_{10}$ structures.

Structure	Relative	Hydrogen	Ta-Ta vertices			
(symmetry)	energy	Bridges	Degrees	Å	WBI	Polyhedron
Ta2B6-1 (C_{2v})	0.0	4TaB	6,6	2.892	0.87	Bicapped octahedron
Ta2B6-2 (C_1)	0.2	4TaB/B_2	7,7	3.080	0.51	$2v_3+3v_4+v_5+v_6+v_7$
Ta2B6-3 (C_s)	1.7	4TaB/B_2	5,5	3.159	0.49	$3v_3 + 2v_4 + 3v_5$
Ta2B6-4 (C_1)	6.7	3TaB/B_2	7,6	2.990	0.68	$2v_3+3v_4+v_5+v_6+v_7$
Ta2B6-5 (C_1)	7.3	4TaB	6,4	3.250	0.36	$2v_3+3v_4+2v_5+v_6$

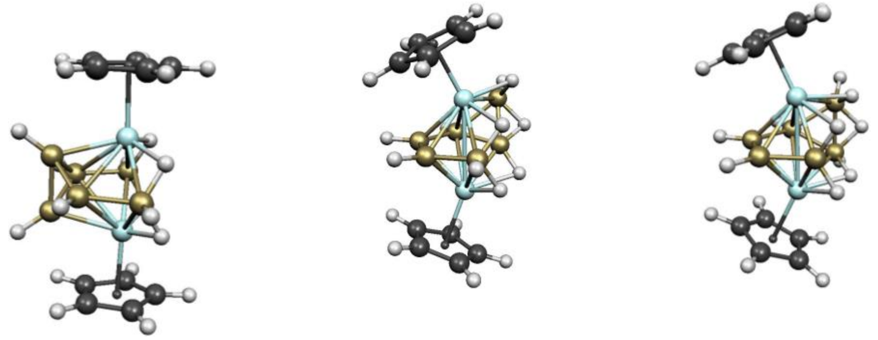

Ta2B6-1 (0.0) (C_{2v}) **Ta2B6-2** (0.2) (C_1) **Ta2B6-3** (1.7) (C_1)

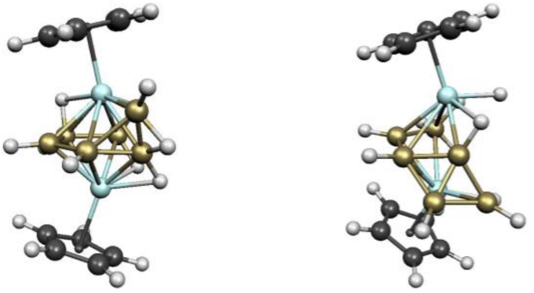

Ta2B6-4 (6.7) (C_1) **Ta2B6-5** (7.3) (C_1)

Figure 56. The five lowest energy $Cp_2Ta_2B_6H_{10}$ structures within 13 kcal/mol of the lowest energy structure with relative energies (kcal/mol) in parentheses.

3.8 Computed structures matching the *a priori* known metallaboranes

Throughout this chapter there where 34 predicted hydrogen-rich metallaborane structures: 10 structures for the 5-vertices systems, 7 structures for the 6-vertices systems, 7 structures for the 7-vertices systems and 10 structures for the 8-vertices systems. By the time of our computed predictions, there were 8 known experimental structures. Table 46 collects these previously known metallaborane structures alongside their corresponding ground states revealed by the computations within this chapter. The adopted geometries and metal-metal bond lengths are provided for both experimental and theoretical characterized structures. Furthermore, the references leading to the papers in which both experimental and theoretical determined structures were published is also provided. All the computed ground states match the experimentally known hydrogen-rich dimetallaboranes.

Table 46. *A priori* known structures and their corresponding computed ground states.

			A priori experimentally determined structure			**Computationally determined structure**		
#	V	Metallaborane	Geometry	M-M (Å)	Ref.	Geometry	M-M (Å)	Ref.
1	5	$Cp^{*}{}_{2}Rh_2B_3H_7$	Tetragonal pyramid	2.689	45	Tetragonal pyramid	2.689	59
2	6	$Cp^{*}{}_{2}Ir_2B_4H_8$	Pentagonal pyramid	2.738	48,49	Pentagonal pyramid	2.712	60
3		$Cp^{*}{}_{2}Ru_2B_4H_8$	Capped tetragonal pyramid	2.855	50	Capped tetragonal pyramid	2.828	60
4		$Cp^{*}{}_{2}Re_2B_4H_8$	Bicapped tetrahedron	2.809	52	Bicapped tetrahedron	2.832	60
5	7	$Cp^{*}{}_{2}Mo_2B_5H_9$	Bicapped trigonal bipyramid	2.809	54,55,61	Bicapped trigonal bipyramid	2.802	62
6		$Cp^{*}{}_{2}2W_2B_5H_9$	Bicapped trigonal bipyramid	2.817	56	Bicapped trigonal bipyramid	2.836	62
7	8	$Cp^{*}{}_{2}Rh_2B_6H_{10}$	B_8H_{12}	3.850	57	B_8H_{12}	3.858	63
8		$Cp^{*}{}_{2}W_2B_6H_{10}$	Bicapped octahedron	2.959	58	Bicapped octahedron	2.970	63

3.9 Predicted metallaborane structures confirmed *a posteriori* by experiments

The first experimental study concerning the synthesis of novel hydrogen-rich dimetallaboranes (i.e. structures that were not experimentally known when the results of our computations were published) appeared in 2017 in the the journal *Inorganic Chemistry*.[64] Here, the eight-vertices Ir complex, $Cp^{*}{}_{2}Ir_2B_6H_{10}$, was synthesized and its structure was characterized by X-ray crystallography and NMR investigations. The experimentally obtained crystal structure corresponds to our Ir_2B_6-1 ←→ Ir_2B_6-2 fluxional ground state that was computed in our 2016-published *Datlon Transactions* paper.[63] The crystal structure revealed that, similar to its Rh counterpart, $Cp^*_2Ir_2B_6H_{10}$ adopts the geometry of the B_8H_{12} molecule and has its metal vertices placed in opposing vertices. The bridging H atoms that were shown in our study to cause a fluxionality of the ground state by their movement on the polyhedron's open face were found to be terminal atoms connected to the Ir vertices. This might not come as a big surprise since our predicted structures were computed in gas-phase while the experiments were done in solution and solid state. Thus, the minute energy difference between the states related with different positions of the bridgind H atoms that appears in gas-phase can be removed is solution due to the molecule's interaction with the surrounding medium.

Table 47. *A posteriori* determined structres and their corresponding computed ground states.

			Computationally predicted structure			**A posteriori experimentally determined**		
#	V	Metallaborane	Geometry	M-M (Å)	Ref.	Geometry	M-M (Å)	Ref.
1	6	$Cp^*_2Mo_2B_4H_8$	Bicapped tetrahedron	2.997	60	Bicapped tetrahedron	N/A	65
2		$Cp^*_2W_2B_4H_8$	Bicapped tetrahedron	2.632	60	Bicapped tetrahedron	N/A	65
3	8	$Cp^*_2Ir_2B_6H_{10}$	B_8H_{12}	3.883	63	B_8H_{12}	3.851	64

The second study that experimentally investigated some previous unknown hydrogen-rich dimetallaboranes appeared in 2018 in the journal *Organometallics*.[65] The authors managed to synthetize the Mo and W six vertices systems, i.e the $Cp^*_2M_2B_4H_x$ with x = 8 or 10. The authors claim to have obtained the hydrogen saturated $Cp^*_2M_2B_4H_{10}$ M = Mo, W (i.e. with 6 "extra" H atoms) and not the $Cp^*_2M_2B_4H_8$ (M = Mo, W) which was the expected[66] intermediate in their studied reaction. However, due to the experimental limitation, no direct evidence of the actual obtained hydrogen-rich metallaborane could be provided. The claim of their study relies on the structural determination of a precursor of the $Cp^*_2M_2B_4H_x$ with x = 8 - 10, the $(Cp^*MCO)_2B_4H_6$. Their entire argument relies on the implicit assumption that, once the two CO groups depart from the cluster, the generated 4 electron gap should be balanced by 4 electrons donated by 4 incoming extra H atoms. Hence, they conclude, the total number H atoms of the molecular formula should be 10. However, the authors fail to acknowledge that by no means the addition of 4 extra H atoms is the only way by which the cluster can balance its 4 electron deficiency caused by the leaving of the 2 CO units. More likely, the cluster will form a double M=M bond (yielding extra 2 electrons for cluster bonding) and coordinate only 2 extra H atoms (that donate the remaining 2 electrons that are required). The presence of M=M (M = Mo, W) double bonds in the $Cp^*_2M_2B_4H_8$ (M = Mo, W) were already predicted by our study relating these systems.[60] Furthermore, the formation of this extra double bond is also clearly stated by their computational results. As this leads to the contradiction of claim, the authors simply ignore the outcome of this result.

The higher so-called thermodynamic stability of $Cp^*_2M_2B_4H_{10}$ based on the higher HOMO-LUMO gap is an artificial argument. The implied stability is actually the chemical stability of the molecule and gives no information about the thermodynamics of the formation reaction. The HOMO-LUMO gap provides information regarding the molecule's reactivity and not about its formation.

Table 48. Skeletal electron count of the $(CpMoCO)_2B_4H_6$, $Cp_2Mo_2B_4H_8$ and $Cp_2Mo_2B_4H_{10}$ molecules.

Molecule	Fragment	Nr. of fragments	e^- donated by fragment	Total e^- donated
$(CpMoCO)_2B_4H_6$	CpMo	2	6-6-1=-1	-2
	BH	4	2	8
	H	2	1	2
	CO	2	2	4
	Mo=Mo	0	2	0
	Skeletal electron count			**12**
$Cp_2Mo_2B_4H_8$	CpMo	2	6-6-1=-1	-2
	BH	4	2	8
	H	4	1	4
	CO	0	2	0
	Mo=Mo	1	2	2
	Skeletal electron count			**12**
$Cp_2Mo_2B_4H_{10}$	CpMo	2	6-6-1=-1	-2
	BH	4	2	8
	H	6	1	6
	CO	0	2	0
	Mo=Mo	0	2	2
	Skeletal electron count			**12**

Starting from the CO-devoid cluster, the Mo system will have to pass through the H8 format in order to arrive at the H10 variant. We already know that the H8 structure is the ground state of the Mo systems and thus it is expected that addition of the extra 2 H would require an energetic cost in order to pass through transition state.

Thus, it is not clear which of the candidates is actually the intermediate. Either way, its core structure is the one predicted by us. The experimentalists provide no conclusive proof that H10 is what they found.

3.10 Conclusions

Between 2014 and 2016 we published 4 papers regarding the structures of the five vertices,[59] six vertices,[60] seven vertices[62] and eight vertices[63] hydrogen-rich dimetallaboranes of the Pt, Pd, Rh, Ir, Ru, Os, Re, Mo, W and Ta transition metals, rationalizing their isomer hypersurface and indicating correlations between gropund state preferences and classical structural rules such as Wade-Mingos.Out of the 34 predicted structures, 8 structures were experimentally known at the time of our publication (cf. Table 46.) and were found by our computation to be ground states in their corresponding potential energy surfaces.

Following the publications of our results, two experimental papers that were concerned with the synthesis of hydrogen-rich metallaboranes structures similar to those investigated in this chapter appeared in the *Inorganic Chemistry*[64] and *Organometallics*[65] journals. Here, the structures of the 6-vertices $Cp^*_2Mo_2B_4H_8$ and $Cp^*_2W_2B_4H_8$ alongside the 8-vertices $Cp^*_2Ir_2B_6H_{10}$ molecules were determined. These experimentally determined structures confirmed our $Cp_2Mo_2B_4H_8$,[60] $Cp_2W_2B_4H_8$[60] and $Cp_2Ir_2B_6H_{10}$[63] predicted structures .

4 Theoretical investigations of the sulfite reductase active site

Motto:

“That which is of importance is not to produce but to understand.

And to understand means to distinguish the

level of awakening that a being had achieved,

its capacity to perceive the sum of unreality

that enters in each phenomenon.”[*]

Emil Cioran

---

[*] Emil Cioran, *Demiurgul cel rău,* Ed. Humanitas, București, 2017, pag. 95 – personal translation. The original, French version of the paragraph, as it appears in the “Emil Cioran, *Le mauvais demiurge*, Galimard, 1969“ version reads as follows: *Ce qui importe, ce n’est pas produire mais comprendre. Et comprendre signifie discerner le degree d’éveil auquel un être est parvenu, sa capacité de percevoir la somme d’irréalité qui entre dans chaque phénomène.*

4.1 Pars energetica: The importance of the siroheme modification

4.1.1 Introduction

Sulfite reductase (SiR) is a siroheme-containing metalloenzyme that catalyzes the reduction of sulfite (SO_3^{2-}) to species containing sulfur in a lower oxidation state, such as sulfide (S^{2-}or SH^-), trithionite ($S_3O_6^{2-}$) or thiosulfate ($S_2O_3^{2-}$),[67,68] involving up to six electrons. Based on the usage of the reaction product, SiR enzymes can be classified as assimilatory (when sulfide is prepared for the incorporation into sulfur-containing amino acids and cofactors) or dissimilatory (when sulfite is used as an electron acceptor in the final reductive step of anaerobic respiration processes). Assimilatory sulfite reductases (ASiR) have a αβγ heterotrimeric structure, feature sulfide as final reaction product and are found in bacteria, archaebacteria, fungi and plants. On the other hand, the dissimilatory SiR (DSiR) have a $\alpha_2\beta_2$ heterotetrameric structure, can reduce sulfite to either trithionite or thiosulfate and are found in eubacteria and archaebacteria.[69] While ASiR and DSiR differ in terms of structure and product of reduction, they have the same type of active site, comprised of a variant of heme that belongs to the isobacteriochlorin class, named siroheme, connected via an endogenous cysteine residue to an Fe_4S_4 cubane. Siroheme differs from heme in that it contains two double bonds less, reducing the amount of conjugation of the ring system (cf. Figure 60**).** The electrons required for sulfite reduction in SiR are provided by flavoproteins and are initially funneled to the iron–sulfur cubanes that further transmit them to the siroheme iron, to which substrate is bound and subsequently reduced.[70] In addition to its catalytic activity, SiR is also known to play an important role in compacting nucleoids in plastids by binding to chloroplast DNA,[71] possibly acting as a sensor of the chloroplast's redox state, as protector of DNA against oxidative damage[72] or global regulator of nucleoid transcription[73] and replication.[74]

In ASiR, the active site is close to the surface, at the interface of the three monomers.[75] As seen in Figure 57, the siroheme is located in a surface-exposed hydrophilic cavity, with its equatorial side facing the solvent. The distal side of the heme is lined with hydrophilic amino acids that help binding the substrate, sulfite (in crystal structures, this position is often occupied by a phosphate group, as in Figure 57). On the proximal side of the heme, a cysteine residue bridges it to the cubane cofactor, which is not exposed to the solvent.

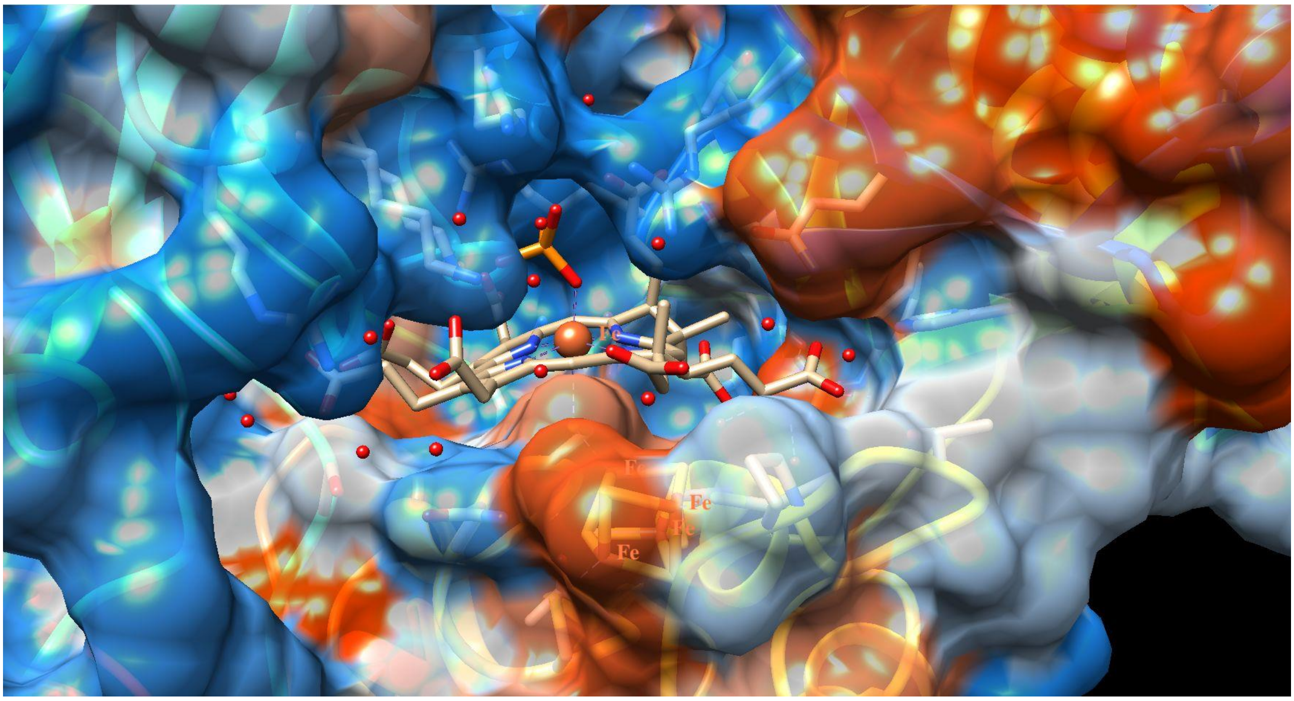

Figure 57. The ASiR active site. The amino acid side-chains are in ribbon representation with hydrophobic areas shaded in red and hydrophilic areas in blue; the siroheme is shown in stick representation. A phosphate group, as found in the enzyme's resting state, is located in a hydrophilic pocket found on the distal side of heme. The cubane cofactor, also represented in a stick manner, is buried in the enzyme. Red dots represent water molecules.

EPR measurements of the SiR active site in its resting-state reveal a high-spin ferric species (S = 5/2) associated with the siroheme center, which can be reduced to the high-spin ferrous state (S = 2) at a redox potential of –340 mV.[76] The EPR-silent Fe_4S_4 center was shown in Mössbauer spectra[77] to feature an antiferromagnetic interaction between two faces of the cubane. On each face resides a high spin ferrous ion ferromagnetically coupled to a ferric ion, adding up to a local spin S = 9/2 on one side and –9/2 on the other side. A schematic representation of SiR active site magnetic alignment is provided in Figure 58, where the orientation of the excess spin located on each iron ion is represented by a black arrow. The cubane cluster core has a 2+ charge in this oxidized resting state, and total charge of 2- after including the $4(SR)^-$ cysteine anion ligands.

The catalytic mechanism of SiR has been explored experimentally[67,78] and computationally.[79–82] However, the previous computational studies did not provide a quantitative account of the importance of the siroheme group (compared to heme), nor on the effect or participation of the coupled Fe_4S_4 cubane on the reactivity of the siroheme. On the other hand, standalone iron–sulfur cubane systems have themselves been studied extensively in both computational[83,84] and joint experimental and theoretical investigations.[85–88].Furthermore, the active site of [FeFe] hydrogenases, in which a cubane is directly connected via a cysteinate to a diiron catalytic core (as opposed to a heme in SiR), has also been subject to previous research. [89–93]

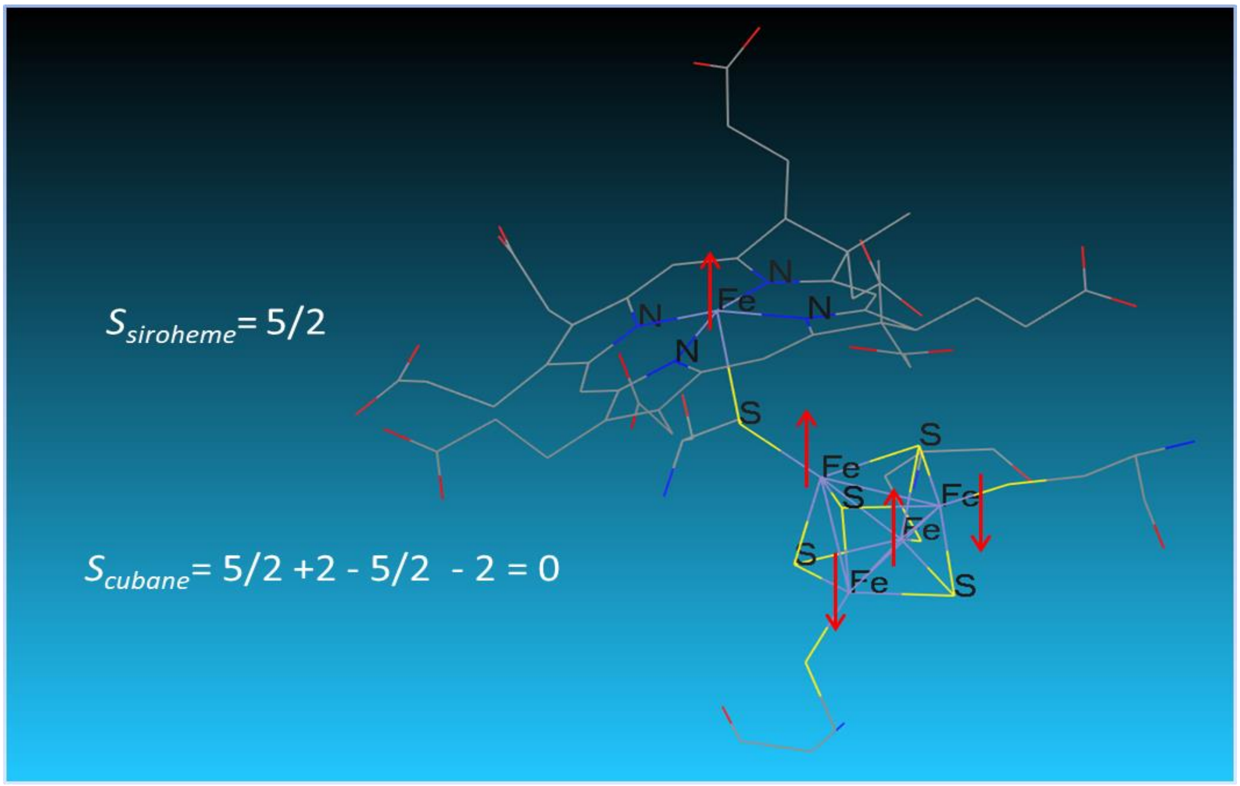

Figure 58. The SiR oxidized active site comprised of a siroheme factor (upper half) connected via a cysteine sulfide (middle) to a $Fe_4S_4^{2+}$ cofactor (lower half). Red arrows represent the orientation of the local majority spin population found on each iron ion. The figure shows one of the six possible broken-symmetry solutions that yields a total sextet located on the siroheme. Carbon atoms are depicted in grey, sulfur in yellow, oxygen in red, nitrogen in blue and iron in violet.

Besides enzymes that are involved in its own biosynthesis[94–97], siroheme is never present alone in any enzyme active site: it is always coupled to an iron–sulfur cluster. [78,98–100] Conversely, there are no examples of cubanes coupled to other types of heme in proteins, even though heme groups and iron–sulfur centers often occur together in electron transfer (for example, formate dehydrogenase-N[101] has a 90-Å long chain of redox centers involving molybdopterin–guanine dinucleotides, menaquinone, five Fe_4S_4 cubanes and two hemes; interestingly, the iron–sulfur cubanes in this case are situated along the heme plane, whereas in SiR the iron–sulfur cubane is aligned perpendicular to the siroheme). However, synthetic variants of heme–cubane systems have been constructed. While in earlier attempts no sign of catalytic activity was observed, [102,103] it was recently shown that by tuning the first sphere of interaction such that the SiR environment is reproduced, the heme-cubane system could catalyze the sulfite reduction similarly to the native, siroheme-cubane version of SiR active site.[104] Thus, by showing that siroheme is not crucial for SiR to properly function, it became even more intriguing why this enzyme employs siroheme and not the ubiquitous heme cofactor.

The effect of this siroheme modification within the SiR active site, as well the effect of the cubane on the (siro)heme system (spin-state accessibility, energetic and bond order change of the siroheme–cysteine interaction, or influence on the reaction mechanism) thus remain to be fully explored. Possible hypotheses include the control of the spin state of the substrate-binding (siro)heme iron, modulation of the trans effect of the (Fe_4S_4–bound) cysteinate, or modulation of the redox potential. Therefore, in the present study, these issues are explored using DFT methodology. However, finding a computational protocol that performs acceptably in all spin-state situations encountered in complex systems with multiple magnetic interactions and multiple redox isomerism opportunities such as SiR is not a trivial task. Hence, a benchmark test of several density functional methods was performed using a set of four bioinorganic centers, with emphasis on the difficult issue of correctly predicting spin-state preference as well as geometry. Then, a detailed description of the SiR active site models is given, investigating the available spin states and redox potentials of the (siro)heme centers, as well as the interaction of the two cofactors in terms of energy decomposition analysis (EDA)[105,106] and Mayer bond-order (MBO)[107] analysis.

4.1.2 Theoretical methods

4.1.2.1 Biological Models

A benchmark set of four models was employed, derived from biological heme and non-heme iron active sites that possess various ground state multiplicities. The peripheral substituents on the porphyrin rings in these models were replaced with hydrogen; the cysteine and histidine residues were modeled as methylthiolate and imidazole, respectively. The first model (Figure 59 (a)) consists of a pentacoordinated ferric heme with a methylthiolate axial ligand, modeling the substrate-bound form of cytochrome P450 (before reduction and before binding O_2); this state is known experimentally to be high-spin.[108] The second model (Figure 59 (b)) derives from the first one by having a water molecule coordinating to the Fe ion in the sixth position (mimicking the resting state of cytochrome P450, known experimentally to be low-spin ferric).[108] The third model (Figure 59 (c)) mimics the active site of globins and cytochrome c peroxidases (with an axial imidazole ligand) and has a water molecule bound to a ferric iron atom, known experimentally to be high-spin.[108–110] The fourth model (Figure 59 (d)) has an intermediate spin state[111] and is based on the superoxide reductase (SOR) non-heme iron site. In SOR, the ferric iron is in the same octahedral geometry as in the heme models and is surrounded by four histidine residues placed in the equatorial positions, a cysteine in the proximal position, and an NO molecule in the distal position.

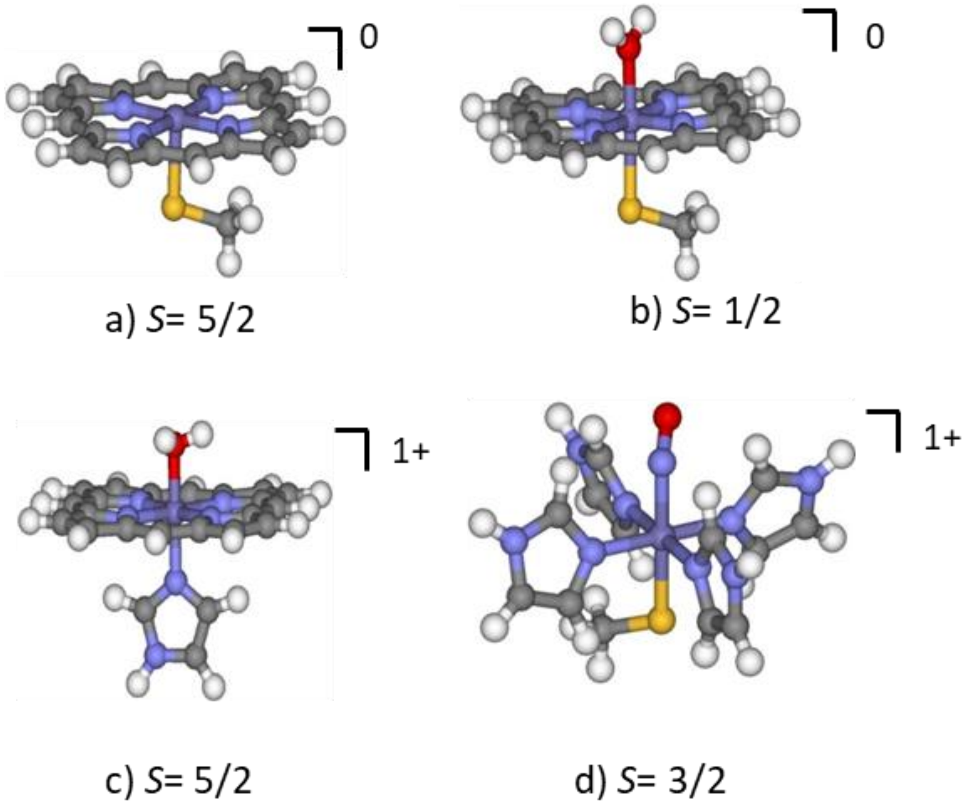

a) *S*= 5/2 b) *S*= 1/2

c) *S*= 5/2 d) *S*= 3/2

Figure 59. Bioinorganic models derived from the active sites of the following proteins: ferric cytochrome P450 with a vacant distal position (a) or aqua-bound (b), ferric hemoglobin (c) and ferrous-nitrosyl superoxide reductase (d). Ground-state overall spin (*S*) and total charge are depicted on the upper-right corner of each model. Hydrogen atoms are depicted in white, carbon in grey, sulfur in yellow, oxygen in red, nitrogen in blue and iron in violet

4.1.2.2 Heme models of the sulfite reductase active site

The siroheme system was extracted from the sulfite reductase crystal structure (PDB entry 1AOP). The peripheral substituents were replaced with hydrogen atoms for simplicity (Figure 60).

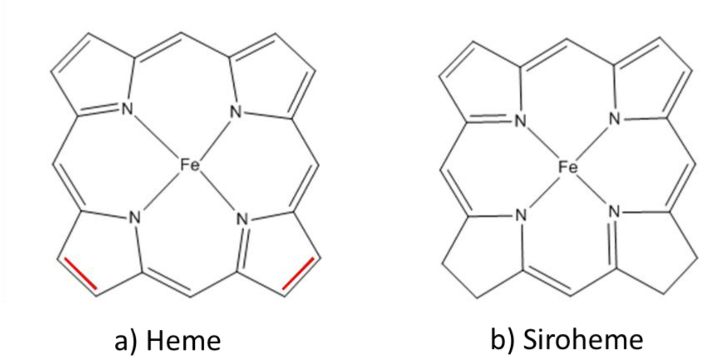

Figure 60. Heme (a) and siroheme (b) structures as employed in the present study. The extra two double bounds present in the heme variant are emphasized in red.

From these two starting structures, further models were built, in which the distal position of the iron ion was kept vacant, while the proximal position was varied, as depicted in Figure 5 (a–f).

The first model in Figure 61 comprises siroheme linked to a $[Fe_4S_4]^{2+}$ cubane via a cysteine sulfide. The other three Fe atoms of the cubane are coordinated by three cysteine residues coming from the surrounding protein environment. The cysteines are modelled as anionic methylthiolates. In the second model, the $[Fe_4S_4]^{2+}$ cubane is replaced by a Zn^{2+} ion (coordinated to four cysteine residues), so that the cubane net charge and experimentally known diamagnetic character is preserved. The third model omits the cubane cofactor altogether. Corresponding models were also built for the heme cofactor. Finally, for each model, the (siro)heme iron was modelled either as ferrous or ferric. Three spin states were employed for each charge state: $S = 0$, 1 or 2 for ferrous and $S = 1/2$, 3/2 or 5/2 for ferric. The cubane was always studied in the oxidized $[Fe_4S_4]^{2+}$ state, but we studied two different spin couplings (parallel or antiparallel alignment between the spins of the connected Fe ions on heme and in the cluster), as is described below. Thus, in total 48 models were studied.

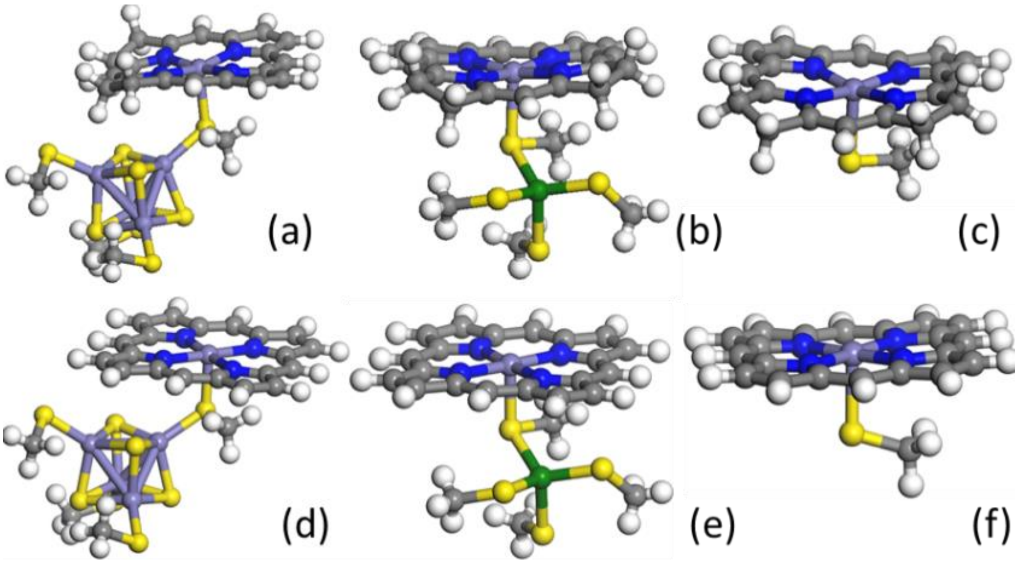

Figure 61. Models of the SiR active site, composed of siroheme connected to an iron–sulfur [4Fe-4S] cubane via a cysteinate sulfur (a). In model (b), the iron–sulfur cubane is replaced by zinc complex, $[Zn(SCH_3)_4]^{2-}$,while in model (c), the cubane complex is replaced by $[SCH_3]^{1-}$. The corresponding models with siroheme replaced by heme are shown in (d), (e) and (f). Iron atoms are depicted in violet, zinc in green, sulfur in yellow, carbon in gray and hydrogen in white.

4.1.2.3 Computational protocols

In order to choose a reliable DFT method for detailed descriptions of the SiR active site, a set of density functionals[35,112–117] available in the Turbomole software[118] were benchmarked on the models illustrated in Figure 59. These functionals use a different amount of exact Hartree–Fock exchange (HF): TPSS[119], M06-L[37] and B97-D[120] (all three 0% HF), TPSSh (10% HF),[121] B3LYP (20% HF),[34] PBE0 (25% HF),[122] M06 (27% HF),[37] BHLYP (50% HF),[123] B2PLYP (53% HF),[124] M06-2X (54%)[37] and M06-HF (100% HF).[37] Ground-state geometry optimizations[125] were performed using the resolution-of-identity approximation[126,127] and with the def2-SV(P) split-valence basis set.[128] Due to the lack of analytical gradients for B2PLYP, B3LYP geometries were used for this functional. Grimme's D3 correction for dispersion interactions[129] was used for all except the four Minnesota (M06) functionals, for which the parameterization already includes these interactions. The geometry optimizations were followed by single-point calculations with the larger triple-zeta def2-TZVP basis set[130]. Frequency calculations[131] were employed in order to check that stationary points are true local minima (except for the B97-D functional, for which analytical frequencies are not available). If significant imaginary frequencies were found, the molecular geometry was distorted along the coordinate involved the imaginary vibration and the geometry optimization was redone. The convergence criteria were set at 10^{-6} Hartree for the energy change, 10^{-3} a.u. for the maximum displacement and gradient element, while $5\cdot10^{-4}$ a.u. was set for their corresponding root mean square (RMS). Solvation free energies were calculated with the COSMO[132] approach with optimized radii for all atoms[133] and 2.0 Å for Fe[134] (and a water solvent radius of 1.3 Å), setting the dielectric constant of the continuum to $\varepsilon = 4$, mimicking a protein environment.

For models containing a cubane, the broken-symmetry approach[135,136] was adopted in order to control the assignment of spin states on each iron atom. This approach consists in converging the highest possible spin state of the system of interest (22 or 23 unpaired electrons), followed by flipping a part of the major spin population so that the desired spin state is obtained. The cubane cluster is always treated in the singlet state, formed by the antiferromagnetic coupling of a pair of an Fe(II) and an Fe(III) ion with majority spin ($S = 9/2$, which is a mainly delocalized mixed valence pair) with another similar pair with the opposite spin, as is depicted in Figure 58. Such states can be obtained in six different ways (two Fe ions can be selected from a set of four in six different ways). However, we have only studied two of these, one in which the (siro)heme Fe ion and the cluster Fe ion that is directly connected to it by the Cys bridge have the same spin (parallel alignment, shown in Figure 2) and one in which the two Fe ions have opposite spin (antiparallel alignment). A full broken-symmetry analysis will be done in future studies.

Bond orders were computed in Mayer's framework[107] and the orbital occupancy-perturbed method[137] was used to determine the contribution from each molecular orbital involved in certain bond interactions. All calculations were performed with the use of Turbomole[118], while wave-function analyses were done in Multiwfn.[138]

Redox potentials were computed following Noodleman's formulation[139] $E_{\mathrm{redox}} = \mathrm{IP} + \Delta E_{\mathrm{pr}} + \Delta E(\mathrm{SHE})$, where E_{redox} denotes the redox potential, IP the ionization potential (i.e. the energy difference between the ferric and ferrous species in vacuum), ΔE_{pr} is the difference in solvation free energy of the two species in the COSMO dielectric continuum and $\Delta E(\mathrm{SHE})$ is the potential of the standard hydrogen electrode. The value of the latter term was taken from literature[139]: $\Delta E(\mathrm{SHE}) = -4.34$ eV.

Energy decomposition analysis (EDA)[105,106] was performed as a means to separate the interaction between the two fragments divided by the $\mathrm{Fe_{(siro)heme}}$–$\mathrm{S_{Cys}}$ bond in terms of some more physical descriptive interactions. The outcome of these analyses can be regarded as heterolytic bond dissociation energies. The initial system, dubbed "supermolecule" for the purpose of EDA, is divided in two regions with the separation being made between the atoms involved in the investigated bond. The regions are referred to as "monomers" and the decomposition of the interaction between them is given by [140] $\Delta E_{\mathrm{tot}} = \Delta E_{\mathrm{ele}} + \Delta E_{\mathrm{exrep}} + \Delta E_{\mathrm{orb}} + \Delta E_{\mathrm{cor}} + \Delta E_{\mathrm{disp}}$ where ΔE_{tot} denotes the total interaction energy, ΔE_{ele} the electrostatic interaction, given by the sum of the nuclear–nuclear repulsion, one-electron attractions and two-electron repulsions, $\Delta E_{\mathrm{exrep}}$ is the sum of the exchange and repulsive interactions. This repulsive term is a consequence of the non-orthogonality manifested between orbitals belonging to the two separated monomers. ΔE_{orb} is the orbital relaxation and describes the charge transfer between monomers. ΔE_{cor} is the correlation energy, while ΔE_{disp} is the dispersion interaction. All terms include contributions from both the kinetic and potential energy. Although the partitioning of ΔE_{tot} in terms is done differently, the current EDA[140] implementation of Turbomole is similar to the ETS-NOCV[141–144] method implemented in ADF.

4.1.3 Results

4.1.3.1 Benchmarking

Eleven DFT functionals were tested on the four biological models presented in Figure 59. For each model, a score/value of 1 was assigned when the respective functional was found to reproduce the experimental spin multiplicity ground state; a value of 0 was assigned otherwise, except for the cases where the model underwent bond dissociation during the geometry optimization (in which case a –1 score was attributed). In general it is expected that local functionals will favor low-spin states while hybrid functionals will favor high-spin states. This behavior comes as a consequence of their construction design. Functionals are parameterized against test sets that mostly include closed-shell molecules, and for it is therefore expected that pure (i.e. local) functionals will favor that which they were parameterized to reproduce, that is closed-shell systems (i.e. low-spin states). Hybrid functionals are constructed in the hope to achieve a description as close as possible to reality by mixing the good description of the correlation interactions of the electrons present in the system, offered by the DFT framework, with the good description of the exchange interactions (of the same electrons) offered by Hartree-Fock theory. While DFT can handle correlation interaction, it neglects the exchange interaction. The opposite is true for Hartree-Fock theory, which explicitly accounts for the exchange interaction at the cost of completely neglecting the correlation interaction. Thus, by incorporating Hartree-Fock theory in the DFT framework, high-spin states, i.e. states involving high exchange interactions because of their unpaired electrons, can be tackled. The open question is, of course, how much mixing should be between the two theories? In general hybrid functionals were constructed to provide accurate results for a broad family of chemical systems. They might yield an acceptable overall performance but in the same time might fail to predict some specific systems. For this reason, a benchmark against biological relevant systems is required in order the find the most useful level of theory. The results for all models, with two types of basis sets (double-zeta and triple-zeta, respectively) and in two types of environment (vacuum vs. solvent), are listed in Table 53.

The high-spin state of model (a) can be expected to be correctly predicted by hybrid functionals. Indeed, this is true (cf. Table 49) for B3LYP, PBE0, M06, M06-2X and also for the double-hybrid B2PLYP functional. However, the TPSSh and M06-2X functional fail to predict the high-spin as ground state. Interestingly, the local M06-L and B97-D functionals also describe correctly the ground state of model a.

Table 49. Benchmark results for Model (a).

Functional	*S*	Def2-SV(P)		Def2-TZVP	
		Vacuum	Solv	Vacuum	Solv
		kcal/mol	kcal/mol	kcal/mol	kcal/mol
TPSS	1/2	0.00	0.00	0.00	0.00
	3/2	8.66	7.77	-8.68	9.28
	5/2	16.04	15.62	0.17	18.73
TPSSh	1/2	0.00	0.00	0.00	0.00
	3/2	4.82	3.89	5.51	-11.57
	5/2	6.46	6.18	-8.83	-8.02
B3LYP	1/2	0.00	0.00	0.00	0.00
	3/2	0.54	-0.40	15.52	15.57
	5/2	-2.07	-2.24	-0.95	-1.13
PBE0	1/2	0.00	0.00	0.00	0.00
	3/2	5.87	6.00	-7.30	7.72
	5/2	-8.58	-8.79	-22.50	-7.82
BHLYP	1/2	0.00	0.00	0.00	0.00
	3/2	-10.09	-9.70	-9.45	-8.95
	5/2	-22.47	-23.83	-25.94	-27.26
M06L	1/2	0.00	0.00	0.00	0.00
	3/2	0.43	-0.66	2.16	1.00
	5/2	-12.20	-12.70	-9.15	-9.63
M06	1/2	0.00	0.00	0.00	0.00
	3/2	-5.94	-7.04	3.69	3.76
	5/2	-20.15	-20.40	-18.94	-19.16
M06-2X	1/2	0.00	0.00	0.00	0.00
	3/2	N/A	N/A	N/A	N/A
	5/2	-27.25	-28.25	-29.61	-30.55
M06-HF	1/2	0.00	0.00	0.00	0.00
	3/2	4.14	3.20	-12.25	4.46
	5/2	5.15	4.85	-10.07	7.38
B2PLYP	1/2	0.00	0.00	0.00	0.00
	3/2	-7.73	-9.71	-10.17	-9.73
	5/2	-31.59	-32.53	-32.07	-33.01
B97-D	1/2	0.00	0.00	0.00	0.00
	3/2	1.81	0.85	3.22	2.18
	5/2	-2.15	-2.59	0.43	-0.01

On the other hand, local functionals are expected to correctly describe the low-spin state of model (b) as ground state. Among the local functionals, M06-L fails to find the low-spin as ground state. By extension, all Minnesota functionals fail as well. Remarkably, although a hybrid functional, B3LYP finds the correct ground state. The same is valid for the TPSS family and for the B97-D functional.

Table 50. Benchmark results for Model (b).

Functional	*S*	Def2-SV(P)		Def2-TZVP	
		Vacuum	Solvated	Vacuum	Solvated
		kcal/mol	kcal/mol	kcal/mol	kcal/mol
TPSS	1/2	0.00	0.00	0.00	0.00
	3/2	15.56	15.07	15.64	14.97
	5/2	22.11	22.53	24.30	24.65
TPSSh	1/2	0.00	0.00	0.00	0.00
	3/2	16.41	16.87	18.03	18.53
	5/2	12.48	12.99	14.37	14.85
B3LYP	1/2	0.00	0.00	0.00	0.00
	3/2	10.04	10.56	11.10	11.67
	5/2	2.84	3.46	2.79	3.35
PBE0	1/2	0.00	0.00	0.00	0.00
	3/2	6.94	7.71	8.49	9.28
	5/2	-3.12	-2.50	-2.31	-1.78
BHLYP	1/2	0.00	0.00	0.00	0.00
	3/2	-8.72	-7.63	-6.18	-5.07
	5/2	-18.38	-19.23	-19.23	-20.03
M06L	1/2	0.00	0.00	0.00	0.00
	3/2	11.13	11.36	12.53	12.82
	5/2	-2.45	-2.15	-0.46	-0.17
M06	1/2	0.00	0.00	0.00	0.00
	3/2	1.91	2.70	3.73	4.62
	5/2	-14.57	-14.02	-13.93	-13.38
M06-2X	1/2	0.00	0.00	0.00	0.00
	3/2	N/A	N/A	N/A	N/A
	5/2	-23.54	-24.41	-25.96	-26.70
M06-HF	1/2	0.00	0.00	0.00	0.00
	3/2	-13.68	-13.42	-13.73	-13.29
	5/2	-10.99	-10.27	-12.70	-11.86
B2PLYP	1/2	0.00	0.00	0.00	0.00
	3/2	-11.50	-9.95	-9.42	-7.66
	5/2	-29.02	-29.12	-29.62	-29.58
B97-D	1/2	0.00	0.00	0.00	0.00
	3/2	8.15	8.42	9.55	9.84
	5/2	5.61	5.14	6.92	6.22

Model (c) is the first particularly challenging model, because, as model (b), it possesses a water molecule as ligand in the distal position, but its ground state is a high-spin state, similar to model (a). This high-spin state is consequence of the low ligand-field effect that the proximal nitrogen atom has on the metal center. The opposite is valid in model (b), where the larger sulfur atom present in the proximal position has a strong ligand-field effect and destabilizes the metal e_g orbitals. Hence, the t_{2g} orbitals become fully occupied and the low-spin state conformation is obtained. The opposite happens in model (c), where the nitrogen atom induces a lower splitting between the e_g and the t_{2g} orbitals. Among the tested functionals, BHLYP together with the double hybrid B2PLYP and the Minnesota family of functionals correctly predict the ground state of model (c).

Model (d) is the second particularly challenging system, as its ground state is an intermediate-spin state. The TPSS family fails on this system while B3LYP correctly describes the ground state. Interestingly, PBE0 finds the intermediate-spin state as ground state when the double-zeta level basis set is used, but fails when the basis set is extended to the triple-zeta level. BHLYP also fails on this model. Among the Minnesota family, only M06-L predicts correctly the spin ground state. Similarly to PBE0, M06-HF also predicts correctly at the double-zeta and fails at the triple-zeta level of theory. The double hybrid, B2PLYP, and B97-D functionals also describe the ground state of model (d) correctly.

Table 51. Benchmark results for Model (c).

Functional	*S*	Def2-SV(P)		Def2-TZVP	
		Vacuum	Solvated	Vacuum	Solvated
		kcal/mol	kcal/mol	kcal/mol	kcal/mol
TPSS	1/2	0.00	0.00	0.00	0.00
	3/2	7.17	8.12	16.59	7.75
	5/2	20.82	21.58	10.22	10.34
TPSSh	1/2	0.00	0.00	0.00	0.00
	3/2	4.42	5.59	4.00	5.18
	5/2	13.29	14.18	14.15	15.05
B3LYP	1/2	0.00	0.00	0.00	0.00
	3/2	-1.94	-0.72	-3.15	-1.97
	5/2	4.06	4.94	3.39	4.24
PBE0	1/2	0.00	0.00	0.00	0.00
	3/2	-3.73	-2.20	6.61	7.96
	5/2	-2.41	-1.63	-2.35	29.93
BHLYP	1/2	0.00	0.00	0.00	0.00
	3/2	-10.68	-9.52	-18.01	-9.78
	5/2	-20.82	-20.16	-4.75	-11.15
M06L	1/2	0.00	0.00	0.00	0.00
	3/2	-5.93	-4.97	-5.34	-4.37
	5/2	-11.01	-10.40	-9.14	-8.52
M06	1/2	0.00	0.00	0.00	0.00
	3/2	-10.34	-9.07	9.53	9.93
	5/2	-16.02	-15.27	-20.60	-20.16
M06-2X	1/2	0.00	0.00	0.00	0.00
	3/2	-15.46	-14.59	-75.42	-75.00
	5/2	-26.75	-26.35	-86.90	-86.91
M06-HF	1/2	0.00	0.00	0.00	0.00
	3/2	-16.50	-15.71	-23.20	-22.66
	5/2	-21.20	-20.81	-28.46	-28.23
B2PLYP	1/2	0.00	0.00	0.00	0.00
	3/2	-15.35	-14.34	-15.28	-14.33
	5/2	-30.56	-29.98	-30.03	-29.50
B97-D	1/2	0.00	0.00	0.00	0.00
	3/2	-5.63	-4.35	-6.27	-5.03
	5/2	-2.02	-0.91	-1.53	-0.43

Table 52. Benchmark results for Model (d).

Functional	*S*	Def2-SV(P)		Def2-TZVP	
		Vacuum	Solvated	Vacuum	Solvated
		kcal/mol	kcal/mol	kcal/mol	kcal/mol
TPSS	1/2	0.00	0.00	0.00	0.00
	3/2	20.12	20.39	20.07	20.38
	5/2	26.08	27.13	27.72	28.85
TPSSh	1/2	0.00	0.00	0.00	0.00
	3/2	3.97	4.17	5.63	5.86
	5/2	14.32	15.19	16.24	17.20
B3LYP	1/2	0.00	0.00	0.00	0.00
	3/2	-9.20	-9.19	-8.55	-8.49
	5/2	0.73	0.91	1.69	1.98
PBE0	1/2	0.00	0.00	0.00	0.00
	3/2	-16.88	-17.14	7.29	8.00
	5/2	-7.10	-7.74	-5.43	-5.98
BHLYP	1/2	0.00	0.00	0.00	0.00
	3/2	0.87	0.94	-0.13	-39.06
	5/2	-25.73	-25.11	-24.63	-62.59
M06L	1/2	0.00	0.00	0.00	0.00
	3/2	-8.97	-8.93	-7.38	-7.14
	5/2	3.59	4.23	6.29	7.06
M06	1/2	0.00	0.00	0.00	0.00
	3/2	7.73	7.70	8.33	8.40
	5/2	-7.73	-6.86	-6.32	-5.45
M06-2X	1/2	0.00	0.00	0.00	0.00
	3/2	-1.97	-2.70	-1.78	-2.60
	5/2	-31.26	-33.27	-30.40	6.95
M06-HF	1/2	0.00	0.00	0.00	0.00
	3/2	-27.03	-26.88	-10.57	-10.11
	5/2	-5.50	-5.98	-16.18	-16.41
B2PLYP	1/2	0.00	0.00	0.00	0.00
	3/2	-40.67	-40.83	-39.82	-39.96
	5/2	-32.25	-33.74	-29.79	7.14
B97-D	1/2	0.00	0.00	0.00	0.00
	3/2	-7.88	-6.54	-6.38	-4.90
	5/2	6.84	8.93	8.86	11.19

As seen in Table 53, none of the tested functionals is able to predict the correct spin state for *all* models. The best-performing ones are B3LYP, B97-D and M06-L, which all gave the correct spin for three of the four models; the first two failed for model (b), while the latter failed for model (c). Other functionals fail for two or three of the models. With M06-2X, the water ligand dissociates for model (b) in vacuum. Among the three best performing functionals, M06-L fails to correctly describe the ground spin-state of all models containing sulfur in the proximal position, i.e. models relevant to the SiR active site. Consequently, we selected B3LYP for all further calculations in this report (B97-D was omitted because analytical frequencies are not available).

Table 53. Benchmark results for the various DFT functionals on the four models (a)-(d). Values were calculated with the split-valence and triple-zeta basis sets, both in vacuum (entry "v") and continuum solvation (entry "s").

Functional	def2-SV(P)									def2-TZVP									Total score
	a		b		c		d		Score	a		b		c		d		Score	
	v	s	v	s	v	s	v	s		v	s	v	s	v	s	v	s		
TPSS	0	0	1	1	0	0	0	0	**2**	0	0	1	1	0	0	0	0	**2**	***4***
TPSSh	0	0	1	1	0	0	0	0	**2**	1	1	1	1	0	0	0	0	**4**	***6***
B3LYP	1	1	1	1	0	0	1	1	**6**	1	1	1	1	0	0	1	1	**6**	***12***
PBE0	1	1	0	0	0	1	1	1	**5**	1	1	0	0	1	0	0	0	**3**	***8***
BHLYP	1	1	0	0	0	1	0	0	**3**	1	1	0	0	0	1	0	0	**3**	***6***
M06-L	1	1	0	0	1	1	1	1	**6**	1	1	0	0	1	1	1	1	**6**	***12***
M06	1	1	0	0	1	1	0	0	**4**	1	1	0	0	1	1	0	0	**4**	***8***
M06-2X	-1	1	0	0	1	1	0	0	**2**	-1	1	0	0	1	1	0	0	**2**	***4***
M06-HF	0	0	0	0	1	1	1	1	**4**	1	0	0	0	1	1	0	0	**3**	***7***
B2PLYP	1	1	0	0	1	1	1	1	**6**	0	0	0	0	1	1	1	1	**4**	***10***
B97-D	1	1	1	1	0	0	1	1	**6**	1	1	1	1	0	0	1	1	**6**	***12***

4.1.3.2 Difference in porphyrin conjugation

The *siroheme modification*, i.e. the saturation of two double bonds present in two adjacent pyrrole rings (cf. Figure 60), affects the electronic structure of the porphyrin macrocycle by interrupting its conjugation. This causes the negative charge to no longer be symmetrically distributed among the N atoms surrounding the central Fe atom. As seen in Figure 62, in the heme ring each N atom has the same partial negative charge, -0.14, which adds to a total of -0.56 negative charge surrounding the central Fe atom. In the siroheme variant, the N atoms facing the *siroheme modification* are partially depleted of negative charge (and now each of them have only -0.11 charge), while on the other two N atoms some extra charge is accumulated. Nevertheless, the total negative charge present on the N atoms of siroheme adds to -0.52, slightly less than the value discussed above for heme. This infers that the ligand field interaction of the porphyrin with the central Fe metal is decreased in the siroheme variant. Thus, it is expected that the electrostatic repulsion between the N ligands and the large electronic density associated with Fe high-spin states is also decreased by siroheme. In other words, at this point it can already be predicted that, when compared to heme, siroheme will stabilize the high-spin states associated with the Fe center. In addition, the Fe-N and N-N distances increase when the siroheme variant is adopted (cf. Table 54), which suggests that the large high-spin Fe will be better accommodated by the siroheme ring.

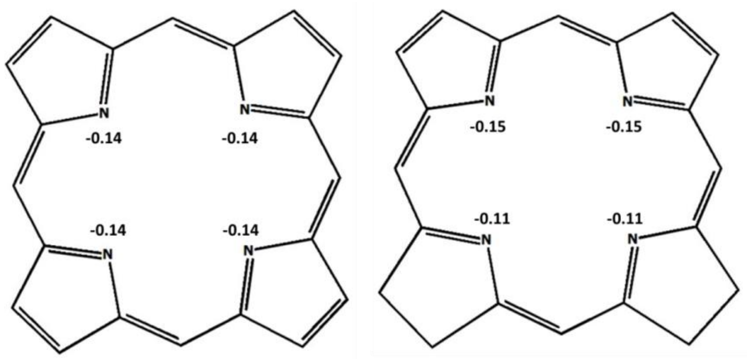

Figure 62. Mulliken charge of the nitrogen atoms comprising the heme ring (left) and siroheme (right). Values are computed at the B3LYP/def2-TZVP level of theory.

Table 54. Distances (expressed in Å) between the central (siro)heme iron and the nitrogen ligands. Values are computed at the B3LYP/def2-TZVP level of theory in the antiparallel aligned regime (cf. section 1754.1.2.3.)

		Heme-Cubane					Siroheme-Cubane				
		N1	Fe	N2	N3	N4	N1	Fe	N2	N3	N4
low-spin	N1		2.00	3.99	2.85	2.80		2.02	4.06	2.85	2.84
	Fe	2.00		2.00	2.01	2.00	2.02		2.05	2.01	2.04
	N2	3.99	2.00		2.80	2.84	4.06	2.05		2.84	2.91
	N3	2.85	2.01	2.80		4.00	2.85	2.01	2.84		4.03
	N4	2.80	2.00	2.84	4.00		2.84	2.04	2.91	4.03	
intermediate-spin	N1		2.01	4.01	2.86	2.81		2.01	4.03	2.81	2.85
	Fe	2.01		2.00	2.01	2.01	2.01		2.05	1.99	2.04
	N2	4.01	2.00		2.81	2.85	4.03	2.05		2.85	2.88
	N3	2.86	2.01	2.81		4.01	2.81	1.99	2.85		4.02
	N4	2.81	2.01	2.85	4.01		2.85	2.04	2.88	4.02	
high-spin	N1		2.09	4.13	2.92	2.92		2.09	4.15	2.91	2.92
	Fe	2.09		2.08	2.09	2.08	2.09		2.14	2.08	2.14
	N2	4.13	2.08		2.92	2.91	4.15	2.14		2.94	2.97
	N3	2.92	2.09	2.92		4.12	2.91	2.08	2.94		4.15
	N4	2.92	2.08	2.91	4.12		2.92	2.14	2.97	4.15	

4.1.3.3 Spin-state energetics of the SiR models

The computed relative stabilities of the three possible spin states of the (siro)heme Fe ion are presented in Table 55 for all models of the SiR active site. There is in general little difference between the relative energies in vacuum vs. solvent (~1 kcal/mol, occasionally up to 5 kcal/mol). Hence, only the solvated data are discussed for the remaining of the manuscript. Moreover, states with antiparallel alignment between the spins of the (siro)heme Fe and the connected Fe ion in the Fe_4S_4 cubane seem to be lower in energy than those with parallel spin (by up to 36 kcal/mol), so the ensuing analyses will focus on the former and not the latter states.

Table 55. Relative energies (kcal/mol) of the three spin states, obtained with B3LYP. All values are given relative to the low-spin state. "Fe_4S_4 anti" refers to the antiparallel spin alignment between the (siro)heme and cubane cofactors. The spin states are low spin (LS), intermediate spin (IS) and high spin (HS) i.e. S = 0, 1 and 2 for Fe(II) and 1/2, 3/2 and 5/2 for Fe(III), respectively.

Cluster model[*]		Medium	Total charge	Heme type and spin state					
				Heme			Siroheme		
				LS	IS	HS	LS	IS	HS
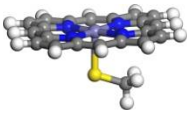 -	Fe(II)	Vacuum	-1	0.0	**-40.4**	-33.6	0.0	-4.9	**-13.6**
		Solvated	-1	0.0	**-40.7**	-38.5	0.0	-6.2	**-14.0**
	Fe(III)	Vacuum	0	0.0	15.7	**-1.1**	0.0	0.7	**-2.7**
		Solvated	0	0.0	15.7	**-1.3**	0.0	-0.4	**-2.8**
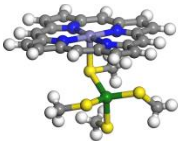 Zn	Fe(II)	Vacuum	-2	0.0	-4.3	**-8.2**	0.0	-8.8	**-16.1**
		Solvated	-2	0.0	-5.5	**-8.0**	0.0	-9.6	**-15.8**
	Fe(III)	Vacuum	-1	0.0	1.3	**-1.1**	0.0	-0.3	**-3.8**
		Solvated	-1	0.0	-0.2	**-2.3**	0.0	-1.7	**-3.9**
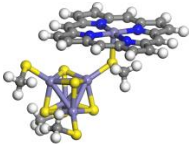 Fe_4S_4	Fe(II)	Vacuum	-2	0.0	-41.9	**-43.2**	0.0	-4.8	**-10.4**
		Solvated	-2	0.0	**-41.5**	**-41.6**	0.0	-5.6	**-10.1**
	Fe(III)	Vacuum	-1	0.0	3.1	**-6.1**	0.0	-2.7	**-6.5**
		Solvated	-1	0.0	-5.3	**-12.6**	0.0	-4.0	**-2.4**
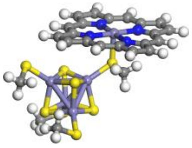 Fe_4S_4 anti	Fe(II)	Vacuum	-2	-36.1	-42.5	**-44.4**	-0.4	-5.9	**-11.2**
		Solvated	-2	-34.4	**-41.7**	**-42.5**	-0.3	-6.3	**-10.5**
	Fe(III)	Vacuum	-1	-12.1	-5.6	**-18.2**	5.6	0.6	**-8.1**
		Solvated	-1	-11.7	9.5	**-17.6**	10.6	5.2	**-3.2**

For almost all models, both functionals predict the high-spin state to be most stable, in agreement with the EPR measurements [145]. The only exception is the ferrous heme model, for

---

[*] The oxidation state refers to the (siro)heme Fe ion.

which the intermediate-spin state is more stable for the clusterless model (Figure 49f) and the two states are nearly degenerate with the cubane.

In general, the high- and intermediate-spin states are stabilized in siroheme, compared to heme, typically by 2–8 kcal/mol for the former and 1–4 kcal/mol for the latter. The prime exception is the clusterless ferrous state, for which the low-spin state is stabilized by 25–35 kcal/mol. The difference between heme and siroheme can be traced to the overall decrease of the ligand-field interaction between the central iron ion and the surrounding nitrogen atoms that comes as a consequence of the decrease in the conjugation of the ring in siroheme, i.e. aspects which were discussed in the previous paragraph.

4.1.3.4 Redox potentials

Table 56 shows the computed redox potentials for the five-coordinate heme and siroheme models. B3LYP yields strongly negative redox potentials for all models, –1.19 to –2.07 V. Compared to the experimental –0.34 V, [145] these values are too negative, reflecting a systematic error in the calculations – most likely arising from the charge and polarization of the models (the typical ε=4 mimicking the protein environment is too small for such cases where this combination of protein environment and solvation effects would yield larger values of ε); nevertheless, the relative redox potentials should be more accurate. The contribution from solvation energies is always positive (cf. Table S12), as expected since the reduced forms of the models feature a higher electrical charge. Overall, the zinc models always give the most negative redox potentials, whereas those with the cubanes give the least negative potentials. Siroheme and heme give similar potentials (within 0.2 V); for models with the cubane, siroheme gives a more negative redox potential.

Table 56. Redox potentials (V) as computed with B3LYP/def2-TZVP, using the high-spin state for each model and the antiparallel states for the complexes with cubane.

System	Heme	Siroheme	Heme–Zn	Siroheme–Zn	Heme–Fe_4S_4	Siroheme–Fe_4S_4
Potential (V)	-1.62	-1.43	-2.07	-2.05	-1.13	-1.19

4.1.3.5 $Fe_{(siro)heme}–S_{Cys}$ bond length

The $Fe_{(siro)heme}–S_{Cys}$ bond length for the various (high-spin) complexes varies between 2.28–2.41 Å cf. Table S15. It is always longer in the reduced (ferrous) systems than in the oxidized systems (by 0.01–0.07 Å), longest in the models including the cubane and shortest in the clusterless models. There are only small differences between the siroheme and heme models (less than 0.03 Å) or between models with parallel or antiparallel alignment of the spins of the connected heme and cubane Fe ions. Compared to the distance found in the crystal structure, 2.83 Å, the computed distances are always smaller. This difference is likely due to the fact that Fe is bound to a phosphate ion in the crystal structure with a very short Fe–O distance of 1.88 Å, while in our computational models the distal position is vacant.

4.1.3.6 Energy decomposition analysis (EDA)

Energy decomposition analysis was performed on the same $Fe_{(siro)heme}–S_{Cys}$ bond and the obtained results are given in Table 57.

Table 57. Energy decomposition analysis of the $Fe_{(siro)heme}–S_{Cys}$ bond. The various energy terms (kcal/mol) are described in Section 4.1.2. Computed with B3LYP in vacuum for the various models in the high-spin state, and given only for the antiparallel state of the cubane models.*

System			ΔE_{tot}	ΔE_{ele}	$\Delta E_{\mathrm{exrep}}$	ΔE_{orb}	ΔE_{cor}	ΔE_{disp}
Cluster	Heme variant	Oxidation state						
–	Heme	Fe(II)	-46.9	27640.7	-27658.0	-7.7	-12.1	-9.8
		Fe(III)	-159.2	27480.1	-27617.8	0.0	-12.5	-9.0
	Siroheme	Fe(II)	-54.3	27800.3	-27833.4	-0.1	-12.5	-8.7
		Fe(III)	-149.7	27659.3	-27787.6	-0.1	-12.0	-9.4
Zn	Heme	Fe(II)	-56.4	48162.8	-48180.0	-0.1	-17.8	-21.3
		Fe(III)	-212.0	47975.7	-48145.7	0.1	-19.0	-23.0
	Siroheme	Fe(II)	-66.2	48343.2	-48371.9	-0.2	-17.8	-19.5
		Fe(III)	-211.2	48151.4	-48318.1	0.1	-19.8	-24.8
Fe_4S_4	Heme	Fe(II)	-44.8	23.3	-24.0	0.0	-18.2	-26.0
		Fe(III)	-182.9	-101.0	-35.7	-0.1	-19.7	-26.5
	Siroheme	Fe(II)	-50.6	35.2	-36.9	-0.1	-20.6	-28.2
		Fe(III)	-172.9	-98.7	-23.3	-0.2	-21.2	-29.5

---

* For the first two clusters, $\Delta \mathrm{E}_{\mathrm{ele}}$ and $\Delta E_{\mathrm{exrep}}$ are very large but nearly cancelling, owing to a large charge density overlap. This effect is much smaller for the cubane complex, for which the negative charges are more delocalised. These effects are exaggerated as the calculations were performed in vacuum.

The strength of the $Fe_{(siro)heme}$–S_{Cys} bond is always larger in the ferric systems than in the corresponding ferrous ones, emphasizing the effect of the extra electron present in the ferrous ion, which populates an orbital that has an anti-bonding character with respect to the $Fe_{(siro)heme}$–S_{Cys} bond. The Zn models always give the strongest $Fe_{(siro)heme}$–S_{Cys} bonds (most negative ΔE_{tot}), whereas the clusterless models give the weakest bonds. Siroheme gives a stronger bond than heme for the ferrous systems but a weaker bond in the ferric systems. The difference in magnitude of the ΔE_{ele} and ΔE_{exrep} terms between the cubane and the bare and zinc models derives from the difference in size of the comprising monomers. While in the (siro)heme-cubane systems the two monomers are comparable in size and number of electrons, in the other models the (siro)heme monomers are overweighting their counterpart monomers. Thus, in the larger and more electron-rich systems, the electrostatic and exchange interactions are orders of magnitude higher in the (siro)heme monomers. The minute values of the orbital relaxation term emphasize the covalent nature of the bond (i.e. negligible charge transfer upon bond formation).

4.1.3.7 Mayer bond order analysis

Mayer bond orders (MBO) for the same $Fe_{(siro)heme}$–S_{Cys} bond are shown in Table 58 for the various models. The clusterless models always display the highest bond orders, and the cubane models the lowest. Interestingly, while in the clusterless and zinc models the bond orders are higher in ferric than in the corresponding ferrous systems, the opposite is true for the cubane models. There are only minor differences in the bond orders between the heme and siroheme systems.

Table 58. Mayer bond-order indices of the Fe(siro)heme–S_{Cys} bond. The indices are computed at the B3LYP-D3/def2-TZVP level of theory and expressed as α, β, and total electronic contribution for the high-spin states in vacuum (antiparallel alignment for the cubane model).

Model	Fe(II)			Fe(III)		
	α	β	Total	α	β	Total
Heme	0.24	0.52	0.76	0.31	0.83	1.14
Siroheme	0.27	0.54	0.81	0.31	0.83	1.15
Heme–Zn	0.26	0.46	0.72	0.30	0.69	0.98
Siroheme–Zn	0.26	0.44	0.70	0.30	0.69	0.99
Heme–Fe_4S_4	0.23	0.41	0.64	0.22	0.38	0.60
Siroheme–Fe_4S_4	0.23	0.41	0.64	0.22	0.37	0.59

The β contributions to the total bond orders are always higher than the α ones. This is because α represents the major spin population while β is the minor spin population. The major spin population will be subject to a higher exchange-driven stabilization than their minority counterpart. Owing to this increased interaction, the majority-spin orbitals become more contracted, as opposed to the minority spin-orbitals, which become more delocalized. This delocalization brings extra metallic character [146] and leads to better overlap among β-spin orbital, thus increasing their bond order.

Bonding in the iron–sulfur cubanes is dominated by effects arising from the mentioned discrepancy between the α and β spin populations. Furthermore, superexchange-mediated[147] spin-dependent delocalization is ubiquitous in these sulfur-bridged iron–iron interactions.[148]

Table 59. Mayer bond order of the two bonds involved in the superexchange interaction between (siro)heme and the cubane. The bond orders are computed at the B3LYP-D3/def2-TZVP level of theory and expressed as α, β, and total electronic contribution and shown for the high-spin states.

System			Mayer Bond Order					
Heme variant	Fe oxidation state	alignment	$\text{Fe}_{\text{(siro)heme}}$–$\text{S}_{\text{Cys}}$			S_{Cys}–$\text{Fe}_{\text{cubane}}$		
			α	β	Total	α	β	Total
Heme	Fe(II)	parallel	0.24	0.38	0.62	0.30	0.37	0.67
		antiparallel	0.23	0.41	0.64	0.44	0.30	0.74
	Fe(III)	parallel	0.27	0.51	0.79	0.27	0.33	0.60
		antiparallel	0.22	0.38	0.60	0.51	0.33	0.84
Siroheme	Fe(II)	parallel	0.24	0.36	0.60	0.31	0.39	0.70
		antiparallel	0.23	0.41	0.64	0.46	0.30	0.76
	Fe(III)	parallel	0.24	0.44	0.68	0.32	0.45	0.76
		antiparallel	0.22	0.37	0.59	0.52	0.33	0.85

Table 59 shows the total and partitioned bond orders of the $\text{Fe}_{\text{(siro)heme}}$–$\text{S}_{\text{Cys}}$ and the S_{Cys}–$\text{Fe}_{\text{cubane}}$ bonds for both the parallel and antiparallel spin alignment. With the exception of the parallel-aligned ferric heme system, the highest MBOs are always found in the S_{Cys}–$\text{Fe}_{\text{cubane}}$ bond. With parallel alignment, the β-spin orbitals are the minor spin population, exhibiting a higher spatially delocalization that permits better overlap among them, and thus an increase of β-electron density. To this, a spin delocalization comes into effect between the cubane iron and heme iron ions. Within a ferromagnetic interaction, the exclusion principle dictates that the electron delocalized among them must be of minority-spin nature, thus adding some extra β density to both bonds. Upon switching to antiparallel alignment, the α-spin electrons remain the major spin population on the heme iron while on the cubane iron ion they become the minor one. Now, for each of the two bonds, the major contribution to the bond order comes from the minority spin population of the iron ion involved in the bond, i.e. β for the cysteine–(siro)heme bond and α for the cysteine–cubane one.

When the spin of the heme Fe and the connected cubane Fe ions are antiparallelly aligned, the spin dependent delocalization is quenched[149] by the Pauli Exclusion Principle. Thus, the once delocalized β-spin electron density becomes trapped in one of the two Fe–S_{Cys} bonds. By the virtue of the same Pauli Exclusion Principle, one might expect the delocalized β-spin electron to localize in the vicinity of an α-spin excess center, i.e in the $Fe_{(siro)heme}$–S_{Cys} bond. Indeed, a closer inspection of the spin contributions found in the systems with parallel spins reveals that the β-spin populations comprise 60–65% of the total bond order in the $Fe_{(siro)heme}$–S_{Cys} bond, while the Fe_{cubane}–S_{Cys} bonds exhibit a lower β contribution, 55–60%. When switching to the antiparallel case, the percentage of β-spin contributions remains roughly the same in the $Fe_{(siro)heme}$–S_{Cys} bond (i.e. 60–65%), while the α spin dominance in terms of contribution to the total bond order, derived from their minority spin nature, is manifested in the Fe_{cubane}–S_{Cys} bond (the β contribution in this bond being reduced to ~40%). This suggests that the previously delocalized β-spin density is to a large extent quenched within the $Fe_{(siro)heme}$–S_{Cys} bond. The asymmetry generated by the local minor spin character alongside with the different geometries that the iron ions employ within the heme factor (octahedral) and the cubane factor (tetrahedral) cause, upon antiparallel quenching, the β density to reside on the more stable $Fe_{(siro)heme}$–S_{Cys} bond. Orbital occupancy-perturbed Mayer bond order calculation on the two bonds gives a quantitative view of this aspect. As seen in **Figure 63**, the molecular orbital that has the highest bonding contribution in the $Fe_{(siro)heme}$–S_{Cys} bond is more stabilized that the corresponding one found in the Fe_{cubane}–S_{Cys} bond, emphasizing the stronger interaction of the sulfur atom with the heme iron than with the cubane iron ion.

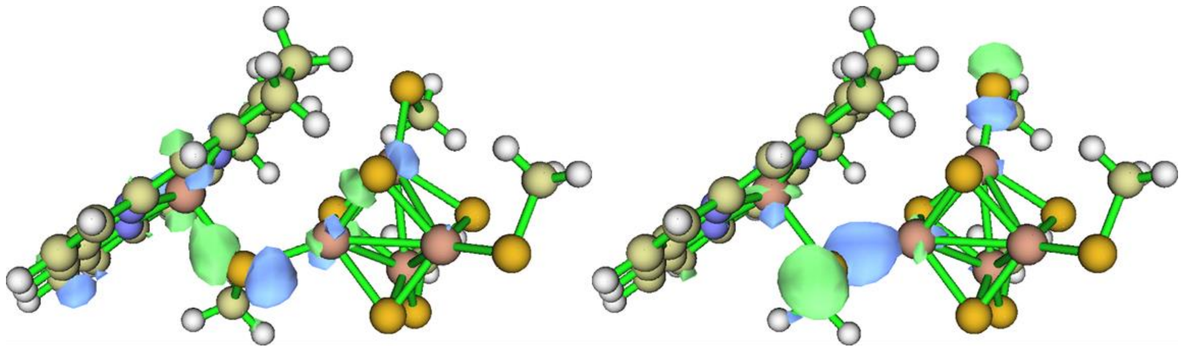

ε= -4.73 eV

ε= -4.40 eV

Figure 63. Molecular orbitals with highest bonding contribution found for the Fe$_{(siro)heme}$–S$_{Cys}$ bond (left) and Fe$_{cubane}$–S$_{Cys}$ (right) of the ferric high-spin antiferromagnetically coupled siroheme–cubane system. The corresponding orbital energies are given below the picture.

4.1.3.8 Correlation between distance, bond order and bond strength

A traditional paradigm accepted in chemistry, regarding the relationship between the distance of a bond and its strength, is that the decrease of a bond length is accompanied by a strengthening of the chemical bond.[150] Although this rule of thumb is generally valid in organic chemistry, it cannot be regarded as a universal law in chemistry,[151] as there are cases in which the shortening of the bond leads to a decrease of bond strength.[152] Such situations are encountered, for example, in the case of the C_2 molecule where the excited state of the molecule provides a shorter C=C bond while the molecule becomes less stable (i.e. the bond is weakened)[153] or in the case of Si_3N_4 ceramics where the hexagonal α- and β-phase polymorph variants are less dense but more stable than the high-pressure obtained cubic spinel variant.[154] Similar behavior departing from the classical paradigm regarding the bond length – bond strength relationship is also met in some of our models discussed so far. Figure 64 and Table 60 collect the normalized values of the distances, Mayer bond orders and bond strengths (given as the absolute value of the EDA total energy interaction, i.e. as normalized bond dissociation energy) of the bond connecting the two cofactors across all the investigated models.

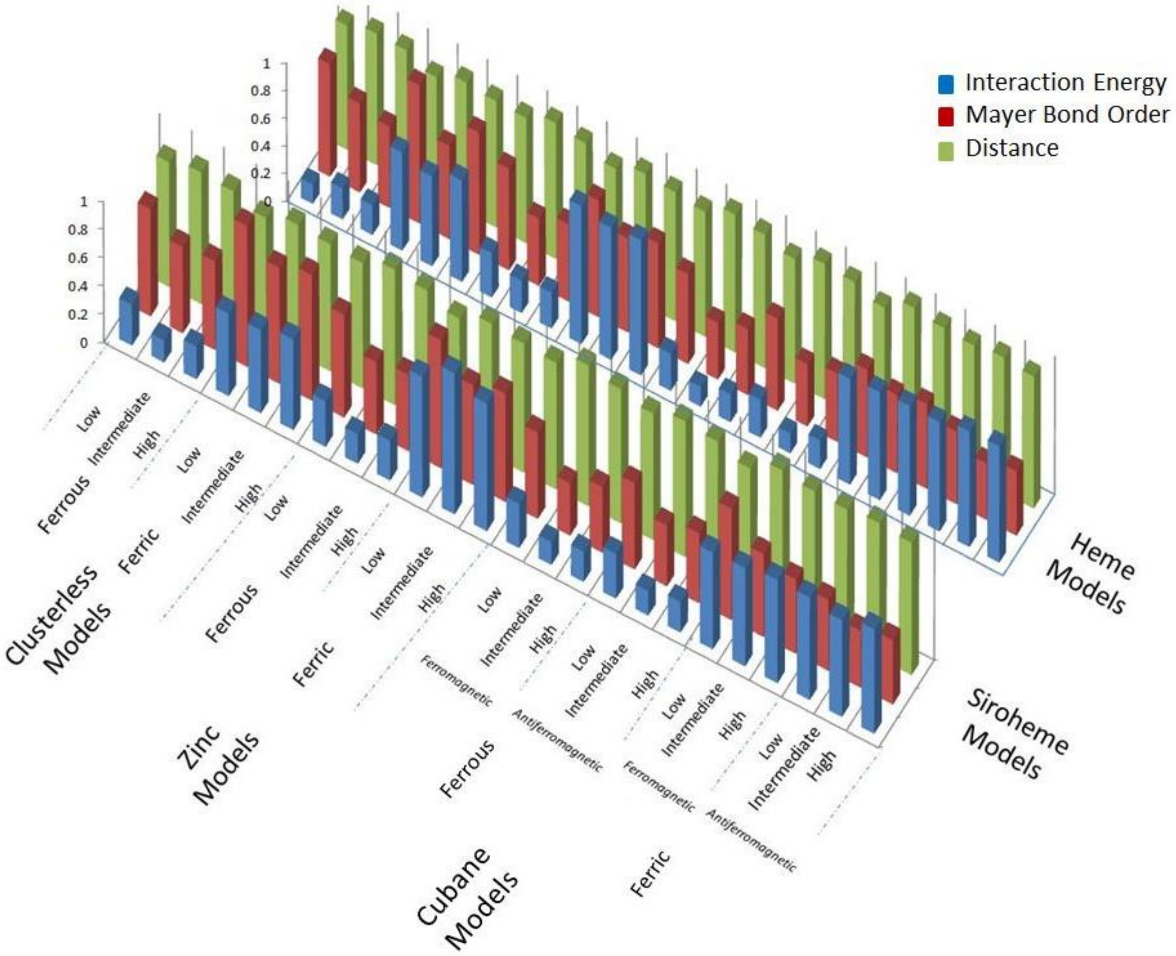

Figure 64. Interaction strength vs Mayer bond order and length of the bond connecting the two cofactors in the studied models normalized to the largest values of each type. For a detailed view, plots in which the correlation is monitored by two of the above-mentioned three parameters are provided in section 6.3.1.

Discussing these three parameters, we have to keep in mind that, from the quantum mechanical point of view, the distance and the interaction energy are observables (albeit the latter being derived from the energies (=observables) of the comprising monomers) while the bond order is a chemical concept artificially inserted in its framework. Nevertheless, MBOs are derived from a quantum mechanical observable, namely the electronic density, and they provide a quantitative measure of the phase of the wavefunction corroborated with the electronic density present between the two atom centers. In other words, a discrepancy among the behavior of the three parameters becomes less exotic when an *ab intio* perspective is adopted. A last argument in order to emphasize the naturality of the counter classical paradigm behavior can be invoked by recalling the typical potential energy surface of chemical bond (Figure 65). Indeed, the strength of the bond increases as the bond length decreases down to the equilibrium distance, after which it decreases. Thus, counter classically behavior can be expected in situations where the shortening of the bond decreases beyond the bond equilibrium distance (such as the mentioned high-pressure obtained Si_3N_4 ceramic).

A first observation that can be made upon inspecting Figure 64 is that the bond length varies less among the models than the MBO and interaction energy. Second, bond strengths are much higher in ferric systems than in ferrous ones. In clusterless models, the MBOs and bond lengths correlate in behavior: when going from low to intermediate spin, the bond length increases while the bond order decreases. Further, from intermediate to high-spin states we find in heme models a decrease in bond length which leads to additional decreases in bond order. The decrease of bond strength correlates directly with an increase in bond length in the ferrous siroheme models, but the opposite is true in the heme models. In both heme and siroheme ferric models, the lengthenig of the bond from low to intermediate-spin states correlates with a decrease in bond order and bond strength, while the shortening of the bond from intermediate- to high-spin states correlates with the increase of MBO and bond strength.

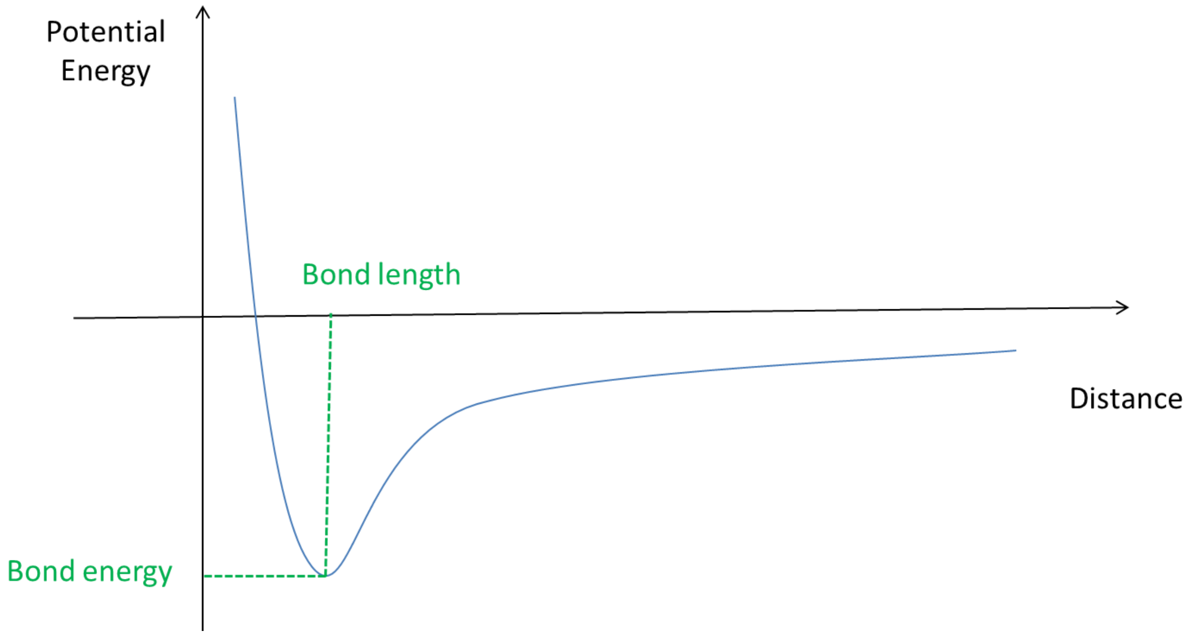

Figure 65. A typical potential energy surface for the formation of a chemical bond.

In ferrous zinc models, all three parameters correlate according to the classical paradigm. In contrast, in ferric siroheme models, lengthening of the bond (from low- to intermediate-spin state) leads to a decrease of the MBO and to a strengthening of the bond. When shortening the length, from intermediate to high-spin state, the bond order increases, but, again, the interaction energy decreases.

In cubane models, for the majority of cases, the three parameters correlate according to the classical paradigm: as the bond length increases, the bond order and bond strength decreases. Exceptions to this behavior are found in the siroheme parallel ferric models, for which shortening of the length (from intermediate- to high-spin state) is accompanied by an increase in bond strength but in decreased MBO values.

When comparing the clusterless and zinc models, the presence of the zinc center increases the length of the bond while decreasing its bond order, but contrary to classical paradigm, the strength of the bond is increased. Proceeding from zinc to cubane models, the length of the bond is further increased, but this time, both bond orders and bond strengths decrease, although they remain above the values of the clusterless models.

Table 60. Total interaction energy (kcal/mol), Mayer bond order and distances (Å) of the bond involved in the $\mathrm{Fe_{(siro)heme}}$–$\mathrm{S_{Cys}}$ bond. The experimental value of the $\mathrm{Fe_{(siro)heme}}$–$\mathrm{S_{Cys}}$ bond distance being 2.843 A.

System	*S*	ΔE_{tot}	MBO	Fe–S
		kcal/mol	-	A
Heme(Fe(II))	0	-30.3	1.05	2.232
	1	-48.5	0.83	2.366
	2	-46.9	0.76	2.349
Heme(Fe(III))	1/2	-153.9	1.29	2.147
	3/2	-140.7	0.87	2.330
	5/2	-159.2	1.14	2.282
Siroheme(Fe(II))	0	-67.8	0.98	2.241
	1	-36.7	0.79	2.355
	2	-54.3	0.81	2.323
Siroheme(Fe(III))	1/2	-136.8	1.29	2.149
	3/2	-137.4	1.06	2.325
	5/2	-149.7	1.15	2.282
Heme(Fe(II))-Zn	0	-69.7	0.95	2.256
	1	-51.3	0.63	2.442
	2	-56.4	0.72	2.361
Heme(Fe(III))-Zn	1/2	-217.0	1.09	2.186
	3/2	-206.9	0.88	2.373
	5/2	-212.0	0.98	2.321
Siroheme(Fe(II))-Zn	0	-75.6	0.94	2.249

System	S	ΔE_{tot}	MBO	Fe–S
		kcal/mol	-	A
	1	-49.1	0.66	2.430
	2	-66.2	0.70	2.360
Siroheme(Fe(III))-Zn	1/2	-199.8	1.17	2.166
	3/2	-233.3	0.91	2.367
	5/2	-211.2	0.99	2.318
Heme(Fe(II))-Fe_4S_4	0	-58.7	0.84	2.253
	1	-31.1	0.53	2.483
	2	-43.9	0.62	2.403
Heme(Fe(II))-Fe_4S_4 anti	0	-59.9	0.86	2.245
	1	-31.6	0.58	2.438
	2	-44.8	0.64	2.387
Heme(Fe(III))-Fe_4S_4	1/2	-166.0	0.82	2.213
	3/2	-169.9	0.73	2.488
	5/2	-172.6	0.79	2.409
Heme(Fe(III))-Fe_4S_4 anti	1/2	-171.8	0.68	2.373
	3/2	-181.6	0.53	2.437
	5/2	-182.9	0.60	2.379
Siroheme(Fe(II))-Fe_4S_4	0	-73.1	0.79	2.275
	1	-38.3	0.48	2.532
	2	-50.1	0.60	2.409
Siroheme(Fe(II))-Fe_4S_4 anti	0	-74.1	0.79	2.273
	1	-40.5	0.56	2.434
	2	-50.6	0.64	2.376
Siroheme(Fe(III))-Fe_4S_4	1/2	-160.4	1.02	2.201
	3/2	-162.0	0.76	2.466
	5/2	-170.9	0.68	2.391
Siroheme(Fe(III))-Fe_4S_4 anti	1/2	-169.7	0.65	2.369
	3/2	-160.0	0.52	2.428
	5/2	-172.9	0.59	2.378

4.1.4 Summary and conclusions

Models that describe the sulfite reductase (SiR) active site were employed in a computational investigation in order to assess the role of the cubane [4Fe-4S] cubane and the modified siroheme structure adapted by the SiR on the properties of its active site. In order to find a suitable DFT method that can handle the challenging electronic structure associated with the SiR active site, eleven DFT functionals were tested on four iron-containing biologically-relevant active site models. The B97-D, B3LYP and M06-L functionals offered the best performance and the latter two were further employed in (siro)heme computations.

In general, all studied models were most stable in the high-spin state, in agreement with the experiments. Siroheme stabilizes the high- and intermediate-spin states compared to heme. There are large differences in the spin-state energetics for the three models, except between the Zn and cubane models for the ferrous states.

The calculated (siro)heme redox potentials are less negative for the full cubane models than for the clusterless models. The Zn models display the opposite effect. With the cubane model, siroheme gives a more negative redox potential than heme, whereas for the other two models, the effect is opposite or dependent on the DFT functional.

Siroheme displays a stronger interaction energy between its Fe ion and the bridging sulfur cysteine than does heme for the ferrous models, whereas the opposite applies for the ferric models. On the other hand, the cubane cluster strengthens this bond for the ferric systems, compared to the clusterless models; in contrast, a Zn model overestimates the effect. For the ferrous systems, the cubane model gives the weakest interaction and the Zn model the strongest. States with opposite spins on the (siro)heme iron and the closest cubane iron are more stable than those with the same spin on these two Fe ions. The former systems have slightly stronger $\mathrm{Fe}_{\mathrm{(siro)heme}}$–$\mathrm{S}_{\mathrm{Cys}}$ bonds than the latter systems. Due to the antibonding character of the extra orbital populated in ferrous systems, the strength of the connecting bond is smaller in these systems than in the ferric ones. The orbital relaxation is minor for all systems, emphasizing the covalent nature of the interaction, with virtually no charge transfer during bond formation.

In conclusion, by substituting heme with siroheme, crucial aspects related to the SiR functionality are affected. By reducing the porphyrin conjugation, the ligand field interactions between the central Fe and the surrounding N atoms are decreased in siroheme systems. Corroborated with the asymmetric distribution of charge among the N atoms, this leads to a stabilization of the high-spin states associated with the porphyrin Fe. Furthermore, the redox potential of this center becomes more negative. The effect induced by the siroheme on the interfactor bond is, however, is antagonistic depending on the iron oxidation state: while it becomes stronger in the ferrous systems, it weakens in ferric ones.

4.2 Pars ballistica: Why does sulfite reductase employ siroheme?

4.2.1 Introduction

The active site of sulfite reductase (SiR) comprises an unusual assembly of two directly connected cofactors (cf. Figure 66): a siroheme group, which binds the substrate, and a cubane Fe_4S_4 cluster, which acts as a molecular pump that transfers to siroheme electrons provided by nearby flavoproteins.[78] Siroheme is a modified version of heme belonging to the same isobacteriochlorin class. It differs from heme in that two of the pyrrole rings are partially saturated (cf. Figure 67). This changes the nature of the π-system and rings C and D are no longer planar (see right side of Figure 66). The cubane cofactor is engulfed inside the active site pocket, while the siroheme is equatorially exposed to the surface with the partially saturated rings oriented towards the solvent.[75]

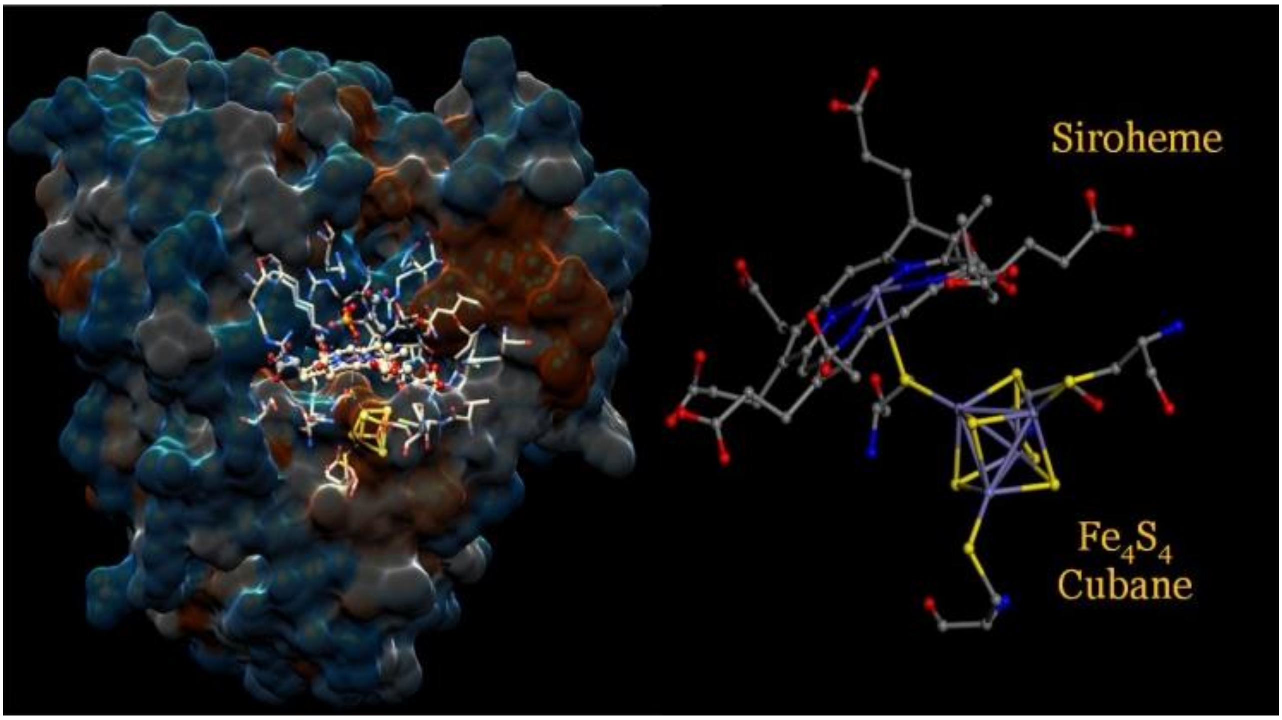

Figure 66. Left: The structure of sulfite reductase (pdb entry 1AOP) with hydrophilic areas of its surface shaded in blue and hydrophobic areas in red. The active site is represented with balls and sticks and its surrounding residues with sticks. Right: Close view of the active site comprised of siroheme and the Fe_4S_4 cubane cluster. Fe is represented in violet, N in blue, S in yellow, O in red and C in grey. Hydrogen atoms are omitted for clarity.

As also discussed in the previous sections, although heme and cubane groups are known to be simultaneously used by some enzymes,[101] the two cofactors are never covalently connected to each other directly – with the exception of the SiR active site, where a cysteine thiolate bridges one cubane Fe ion to the siroheme. Conversely, siroheme is never present alone in any enzyme active site (besides in enzymes involved in its own biosynthesis) – it is always coupled to a cubane iron–sulfur cluster.[78,98–100] While the prime role of the cubane in the SiR mechanism is to provide electrons for the reaction (six electrons are needed to reduce sulfite to S^{2-}), the choice of siroheme vs. heme in SiR has not been rationalized until the work reported in the present thesis. Structural models of the siroheme–cubane site of SiR have been synthesized, but employing heme rather than siroheme. Initially,[102,103] these models showed no catalytic activity, but more recent versions tuning the second-sphere interaction of the two cofactors with elements from the native enzyme were shown to possess catalytic activity.[104] This further emphasizes the question why SiR uses siroheme rather than heme.

In this chapter, we study how siroheme modifies the electron-transfer properties of the SiR active site compared to heme by using computational methods, providing a plausible explanation why SiR uses siroheme rather than heme.

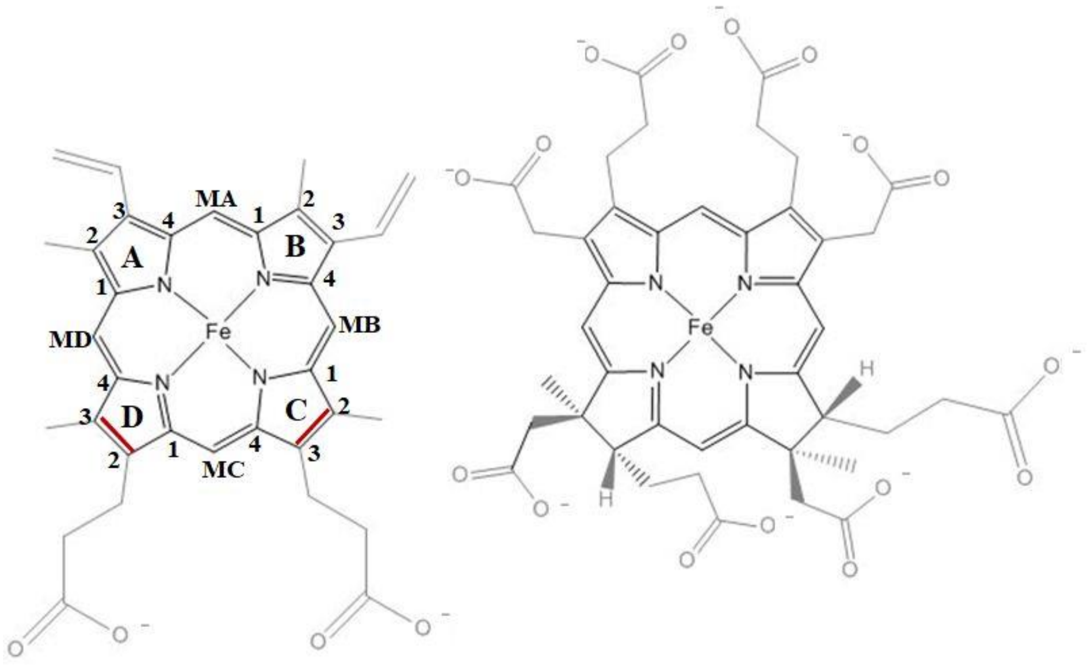

Figure 67. Structures of heme *b* (left) and siroheme (right). The peripheral substituents are shaded in grey. The extra two double bonds present in the heme ring are highlighted in red.

4.2.2 Theoretical methods

4.2.2.1 SiR active site models

The siroheme–cubane assembly was extracted from the sulfite reductase crystal structure (PDB entry 1AOP, cf. Figure 68). The peripheral substituents found on the siroheme moiety were replaced by hydrogen atoms for simplicity. The cysteine residues connecting the cubane with the siroheme cofactor and the rest of the protein were modeled as methylthiolate groups. The two single bonds that differentiates siroheme from heme were desaturated and giving the heme–cubane system (Figure 55). The (siro)heme Fe ion was modelled in the high-spin ferric state. In terms of magnetic coupling, the two cofactors were arranged with both ferro- and antiferromagnetic alignment.

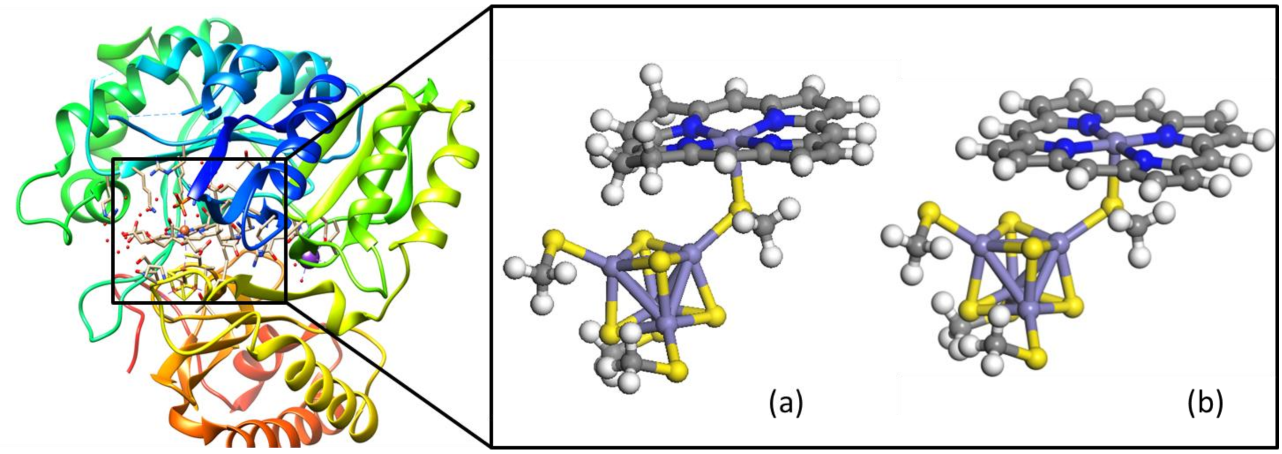

Figure 68. Left: ribbon diagram of sulfite reductase (PDB code: 1AOP). Right: close view of the modeled active site, composed of a siroheme connected to an iron–sulfur [4Fe-4S] cluster via a cysteinate sulfur (a). In model (b) the siroheme cofactor is replaced by heme. Fe is represented in violet, N in blue, S in yellow, O in red, C in grey and H in white.

4.2.2.2 Electron-transport device models

The obtained (siro)heme–cubane models, together with the corresponding isolated heme, siroheme and cubane components, were used to build electron transport devices. In such assemblies, the molecule of interest is treated as a junction that connects two metal nanorods. The molecular junction is referred to as the island part of the device, while the metal nanorods represent the electrodes. All electron-transport devices that were build consist of gold electrodes (Figure 69) in which the island part of the device is modeled either as heme (Figure 69a), siroheme (Figure 69b), heme–cubane (Figure 69c), siroheme–cubane Figure 69d). Sulfur is commonly used as the atom that connects the island to the electrode part of the device. Likewise, sulfur atoms were added in the axial positions of heme and siroheme models, faced towards the electrodes. For the (siro)heme–cubane systems, the distal axial position (bound to the (siro)heme iron) was similarly occupied by a sulfur atom, while the methyl groups were removed from all methylthiolate residues except for the one connecting the two cofactors. Thus, all island parts from each transport device were connected to the electrodes via sulfur atoms. The distances between the island part and the electrodes were set at 2.5 Å, which represents the experimentally known distance at which sulfur is known to adhere to gold electrodes.[155]

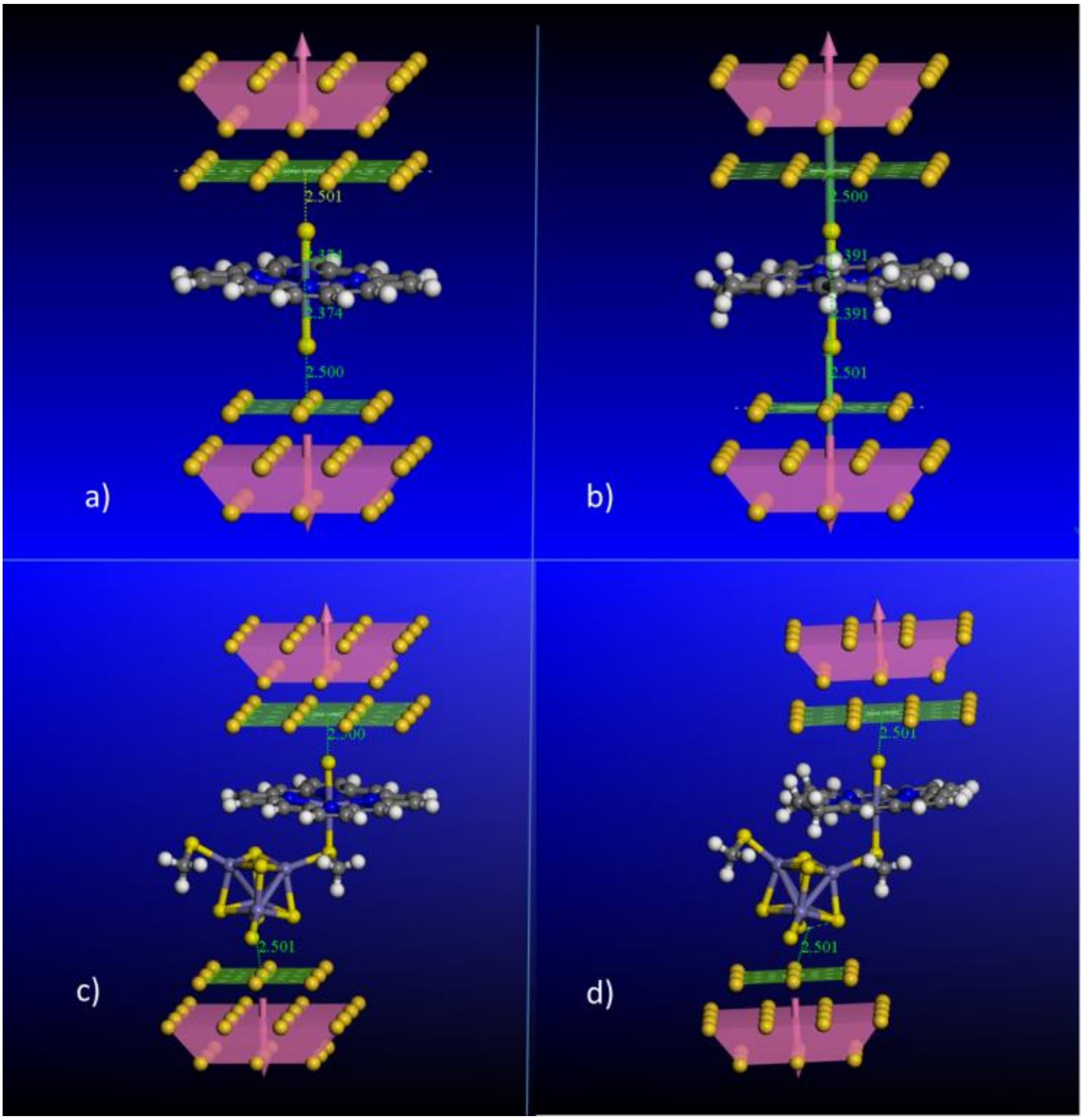

Figure 69. Heme (a), siroheme (b), heme–cubane (c) and siroheme–cubane (d) as molecular junctions connecting two Au electrodes. Au atoms are depicted in dark yellow, Fe in violet, N in blue, S in yellow, O in red, C in grey and H in white.

4.2.2.3 Computational protocols

4.2.2.3.1 Donor–acceptor treatment

DFT calculations on the SiR active site models followed a previously established protocol (cf. section 4.1.3.1). Ground-state geometry optimizations[125] were performed with the resolution-of-identity approximation[126,127] using the TPSS[119] functional, the double-zeta level def2-SV(P) split-valence basis set[128] and Grimme's D3 correction for dispersion interactions.[129] Frequency calculations[131] were employed in order to assure that stationary points are true local minima. If significant imaginary frequencies were found, the molecular geometry was distorted along the coordinate involved the in imaginary vibration and the geometry optimization was redone. On each converged structure, single-point calculations were employed with the larger triple-zeta def2-TZVP basis set[130] using the B3LYP[34] functional. Solvation free energies were calculated with the COSMO[132] approach with optimized radii for all atoms[133] and 2.0 Å for Fe[134] (and a water solvent radius of 1.3 Å), setting the dielectric constant to $\varepsilon = 4$, mimicking a protein environment. The convergence criteria were set at 10^{-6} Hartree for the change in energy, 10^{-3} a.u. for the maximum displacement and maximum gradient element, while $5\cdot10^{-4}$ a.u. was set for their corresponding root-mean-square (RMS) change.

4.2.2.3.2 Non-equilibrium Green's function coupled with DFT (NEGF-DFT).

Based on the description of the electrode parts of the electron transport device, NEGF-DFT methods can be referred to as explicit, when the transport properties are computed by directly including the electrodes in the mathematical framework, and implicit when the electrode's presence is implied through a parameter (i.e. the Fermi energy of the electrode in Equation 157).

4.2.2.3.2.1 Molecular junction treatment (explicit NEGF-DFT)

Electron transmission was computed using the non-equilibrium Green's function method coupled with DFT (NEGF-DFT). The electronic structure of the island part together with the first layer of electrode atoms was treated with standard DFT, while semiperiodic DFT[156] was employed for the rest of the electrodes. This method is restricted to pure functionals; consequently, the PBE functional was employed along with the DNP 3.5 basis set (with DFT semi-core pseudopotentials for Fe and Au).

The electron transmission from the source electrode (S) to the drain (D), $T_{SD,}$ is computed as the trace (Tr) of the matrix product of the right-hand side of Equation 152:[155]

$$T_{SD}(E) = Tr[\Gamma_S(E)G^r(E)\Gamma_D(E)G^a(E)]$$

Equation 152.

where $\Gamma_{S/D}(E)$ represents the coupling matrix between the source (S) or drain (D) and the molecular junction and $G^{r/a}(E)$ the retarded (r) respectively advanced (a) Green's function of the molecular device. The results of this approach emphasize the difference in electron transmission capabilities between the two (siro)heme-cubane models. However, a more detailed view is obtained with the aid of the implicit approach, which allows the computation of the conductance between any two atoms comprising the molecular junction.

4.2.2.3.2.2 Electron route analysis (implicit NEGF-DFT)

The Green's function, as discussed in reference,[157] is defined as

$$[E - \boldsymbol{H}(x)]G(x,x') = \delta(x,x')$$

Equation 153.

where *E* denotes the energy of the system, *G*(*x*,*x*') is the Green's function and describes the electron's propagation from *x* to *x*', δ(*x*,*x*') is Dirac's delta function**,** and ***H***(*x*) is the Hamiltonian operator with its dependence on the mass of electron, *m*, the position *x* and the potential in that point, *V*(*x*), is given by:

$$\boldsymbol{H}(x) = -\frac{1}{2m}\frac{\partial^2}{\partial x^2} + V(x)$$

Equation 154.

This equation has two general solutions. The first one is called the retarded Green's function and has the form

$$G(x - x', E) = -\frac{i}{\vartheta}e^{ik|x-x'|}$$

Equation 155

while the second, referred to as the advanced Green's function, is given by

$$G(x-x',E)=\frac{i}{\vartheta}e^{-ik|x-x'|}$$

Equation 156.

with $k=\sqrt{2m(E-V(x)}$ and $\vartheta=\frac{k}{m}$.

In order to select one of the two solutions, one can introduce an infinitesimal quantity, η, multiplied by the imaginary unit, i, and make the substitution, $E\rightarrow E\pm i\eta$, in order to obtain the retarded solution for the plus sign and the advanced solution for the negative sign.

Further developments of these equations for applications in the field of single-molecule electronics have led Yoshizawa[158] to use the following form proposed by Beratan:[159]

$$G_{rs}^{(0)R,A}(E_F)=\sum_k\frac{C_{rk}C_{sk}^*}{E_F-\varepsilon_k\pm i\eta}$$

Equation 157.

The left-hand side of Equation 157 is a notation that describes the value of Green's function at the electrode's Fermi energy level (E_F) between an atom located on site r and another located on site s. The superscript notes that this is the zero^th order Green function, the order that describes the tunneling transmission, while R and A stands for the retarded and advanced forms. The right-hand side is a sum over all molecular orbitals (MO) spread over atoms r and s. C is the coefficient corresponding to the k^{th} MO, with C^* being its complex conjugate and ε_k the energy of the k^{th} MO.

The conductance expressed in Equation 157 can be further connected to the rate constant of the electron transfer reaction (k_{et}) by the expression developed by Nitzan:[160]

$$G=\frac{8e^2}{\pi^2\Gamma_D\Gamma_AF}k_{et}$$

Equation 158.

where G is the conductance, e the charge of the electron, Γ_D the coupling between the electrode and the donor part of the junction, Γ_A the coupling between the electrode and the acceptor part of the junction, and F the thermally-averaged Franck–Condon-weighted density of states. By assuming typical experimental values for the couplings and the Franck–Condon factor it was further shown that the conductance and rate constant can be approximated as:

$$G \approx 10^{-17} k_{et}$$

Equation 159.

When implemented in the Multiwfn[138] quantum chemical software package, the $\pm i\eta$ term of Equation 157 is neglected. For this reason, positive and negative values may both be computed. In this case, one sign corresponds to the direction from site r to s and the opposite sign corresponds to the opposite direction, from s to r. Thus, only the absolute value of the computed numbers is of importance. Furthermore, the current implementation in Multiwfn is limited to closed-shell systems. For this reason, the electron-route analysis was restricted to the ferrous (siro)heme–cubane systems and approximated as a closed-shell system. Nevertheless, the high-spin states were indirectly treated by taking extra MO in the summation part of Equation 157 up to LUMO+2. Although being approximate, the investigation does not focus on exact numerical values of the particular systems, but is rather concerned with the differences between the two variants of SiR active site, for which significant error cancelation can be expected.

For this treatment, the computations were performed at the B3LYP level of theory with the 6-311G(d,p) triple-zeta basis set for all atoms except Fe, for which the SDD basis set[36] was employed. This triple-zeta basis set was used due to technical limitations of the wave-function analysis program.

All calculations were performed with the use of Turbomole,[118] Gaussian09[39] and DMol3[161] as implemented in Materials Studio,[162] while wave-function analyses were done in Multiwfn[138] and Chemissian.[163] Protein visualizations were performed with the aid of Chimera.[164]

4.2.3 Results

4.2.3.1 Intrinsic properties of the cubane cofactor

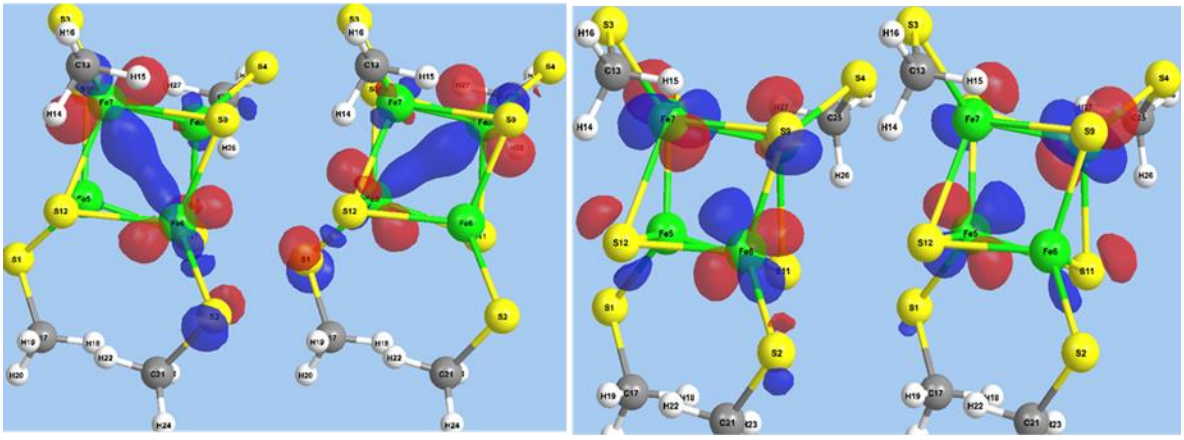

alpha beta alpha beta

HOMO LUMO

Figure 70. The HOMO (left) and LUMO (right) orbitals of the cubane cofactor computed at the B3LYP/def2-TZVP/COSMO(ε=4) level of theory.

The Fe_4S_4 cubane behaves as an electron transmitter due to the high electron-transmission capabilities and to the non-bonding nature of its frontier orbitals with respect to the Fe–S bonds:[165] the HOMO orbitals (alpha and beta) are predominantly of metallic character (cf. Figure 70) while the LUMOs are of antibonding character with respect to the Fe–Fe interaction and possess high amplitudes also on the sulfur atoms (nonbonding character). Thus, by preserving its geometry upon the successive reduction and oxidation processes associated with the electron transfer, the cubane induces steric tension neither on its electron-providing residues nor on the siroheme system.

4.2.3.2 SiR active site as a donor–acceptor molecule

The two cofactors present in the SiR active site can be regarded as a donor–acceptor system that transfers electrons from the cubane moiety (the donor) to the siroheme moiety (the acceptor). In the resting state of SiR, both cofactors are in their oxidized state, i.e. with siroheme in the ferric state and the cubane cluster in the oxidized $[Fe_4S_4]^{2+}$ state. Before electron transfer, the cubane cluster needs to be reduced to the $[Fe_4S_4]^{+1}$ state. In the (siro)heme(ox)–cubane(red) state, the HOMO is located on the cubane cofactor and the LUMO on the (siro)heme cofactor (cf. Figure 71). However, the HOMO–LUMO gap (cf. Table 61) is increased when siroheme is used – apparently detrimental to internal electron transfer.

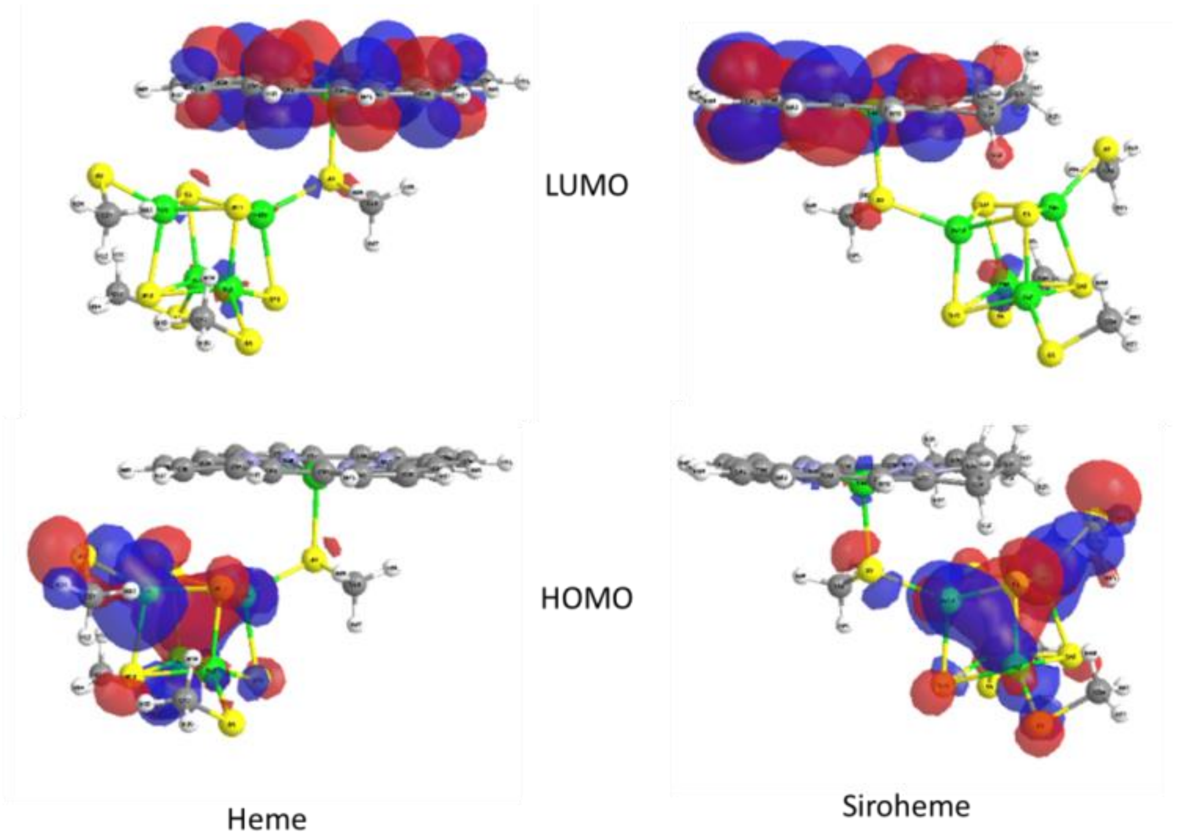

Figure 71. Frontier orbitals of the high-spin antiferromagnetically aligned heme–cubane and siroheme–cubane systems in the (siro)heme(ox)–cubane(red) state. Orbitals are computed at the B3LYP-D3/def2-TZVP/COSMO ε=4 level of theory.

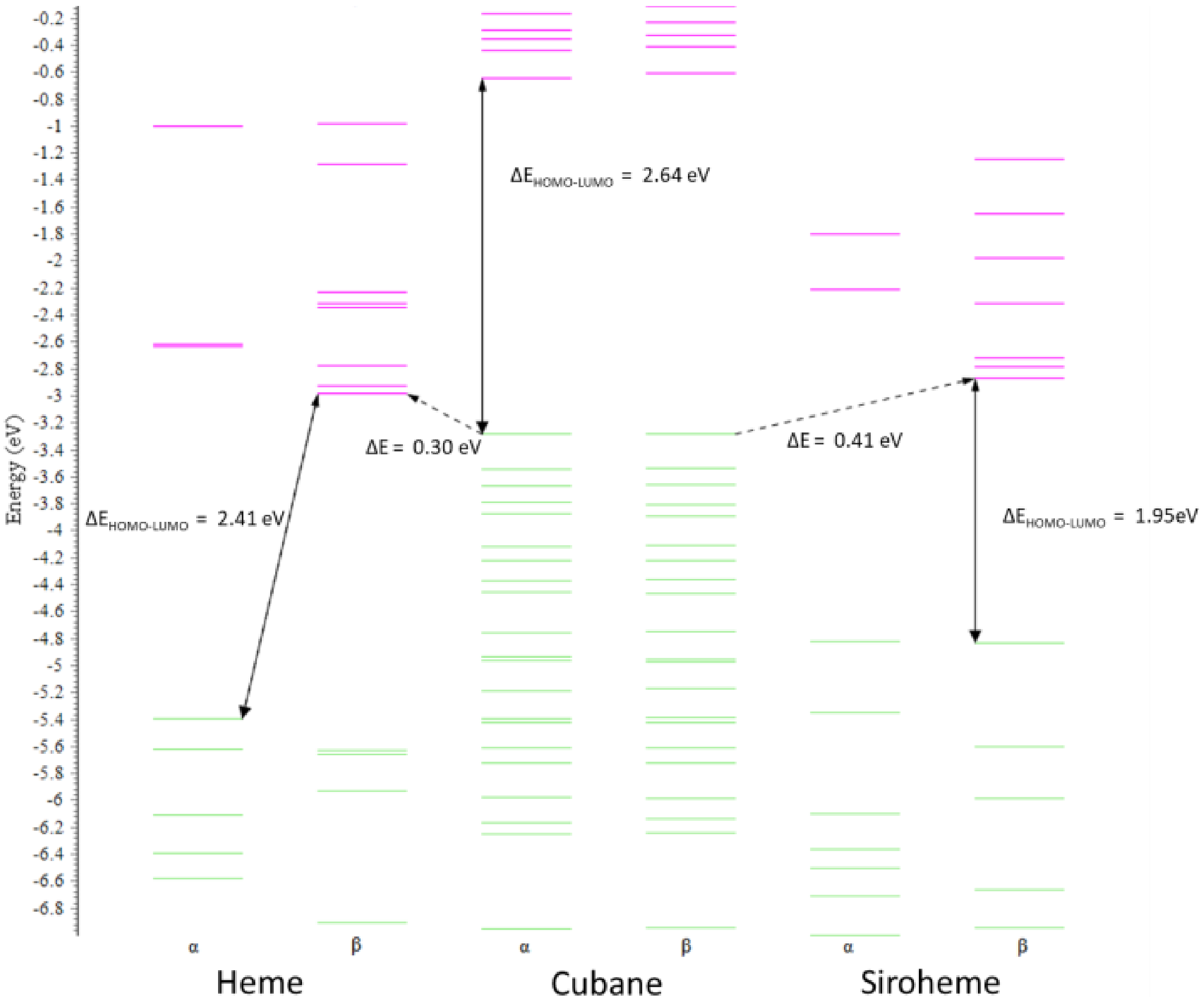

Figure 72. MO diagram of the isolated heme, cubane and siroheme fragments, computed at the B3LYP-D3/def2-TZVP level of theory for the ferric high-spin (siro)heme species and the dicationic form of the cubane cluster (reduced state). Occupied MOs are indicated in green lines while the virtual MOs in magenta.

Treated separately, the LUMO of the donor fragment has to be located at a higher energy than the LUMO of the acceptor fragment such that, when a HOMO–LUMO excitation occurs, the transferred electron will end up on the acceptor fragment. According to the molecular orbitals in Figure 72, the LUMO of the isolated cubane is 2.64 eV above its HOMO, while the heme and siroheme LUMOs are at 0.30 and 0.41 eV above it, respectively. Upon changing from heme to siroheme, the LUMO is only slightly destabilized, whereas the HOMO is strongly destabilized, leading to a decrease of the HOMO–LUMO gap from 2.41 eV in heme to 1.95 eV in siroheme. However, the smaller difference between the heme HOMO and the cubane LUMO suggests that charge transfer associated with a HOMO–LUMO transition would be diminished in the siroheme–cubane variant.

Table 61. HOMO and LUMO levels and gaps. Values are computed at the B3LYP-D3/def2-TZVP/COSMO ε=4 level of theory.

System		HOMO (eV)	LUMO (eV)	Gap (eV)
Cubane		-3.28	-0.64	**2.64**
Heme		-5.39	-2.98	**2.41**
Siroheme		-4.82	-2.87	**1.95**
Heme(ox)-Fe_4S_4(red)	ferromagnetic	-2.93	-0.94	**1.99**
	antiferromagnetic	-2.93	-0.92	**2.01**
Siroheme(ox)-Fe_4S_4(red)	ferromagnetic	-2.95	-0.70	**2.25**
	antiferromagnetic	-2.91	-0.88	**2.03**

4.2.3.3 Explicit NEGF-DFT

Computed transmissions reveal crucial differences between the two (siro)heme–cubane models in terms electron transfer mechanism (Figure 73a). Thus, when computing the transmission probabilities for the clusterless models, it is observed that the broad peaks found in the –1.6 to 1 and 1–2 eV regions are higher in the siroheme case. This suggests a higher transmission between the island part (i.e. the molecular junction) and the electrode. At the Fermi energy, the opposite is valid, with heme possessing higher electron-transport capabilities. The sharp peaks present in the –2 eV region are much higher in the siroheme case, emphasizing a higher intra-molecular electron-transfer capability.

Proceeding to the (siro)heme-cubane systems (Figure 73.b), it is observed that the peaks found in the –2 to –1.1 eV region are lowered when heme is replaced be siroheme, while the peak associated with the state found in the –2.1 eV region becomes higher. The sharpness of these peaks suggests that these states are mostly localized on the island part of the device and, thus correspond to intramolecular charge transfer. Interestingly, these peaks reveal that some states involved in the intramolecular electron transfer process are inhibited while one of them is tuned such that the transmission of the electrons is increased. The broad peaks associated with the island–electrode charge transfer become lower in the –1.1 to –0.6 eV region and near the Fermi region when siroheme replaces the heme cofactor. The opposite effect is found in the –0.6 to –0.2 eV region and for all peaks situated above 0.1 eV. Again, siroheme increases the transmission of electrons in several states associated with the island–electrode charge transfer and decreases the transmission of other states. Overall, when siroheme instead of heme is connected to the cubane cofactor, some states involved in charge transfer process are inhibited while others become more favorable.

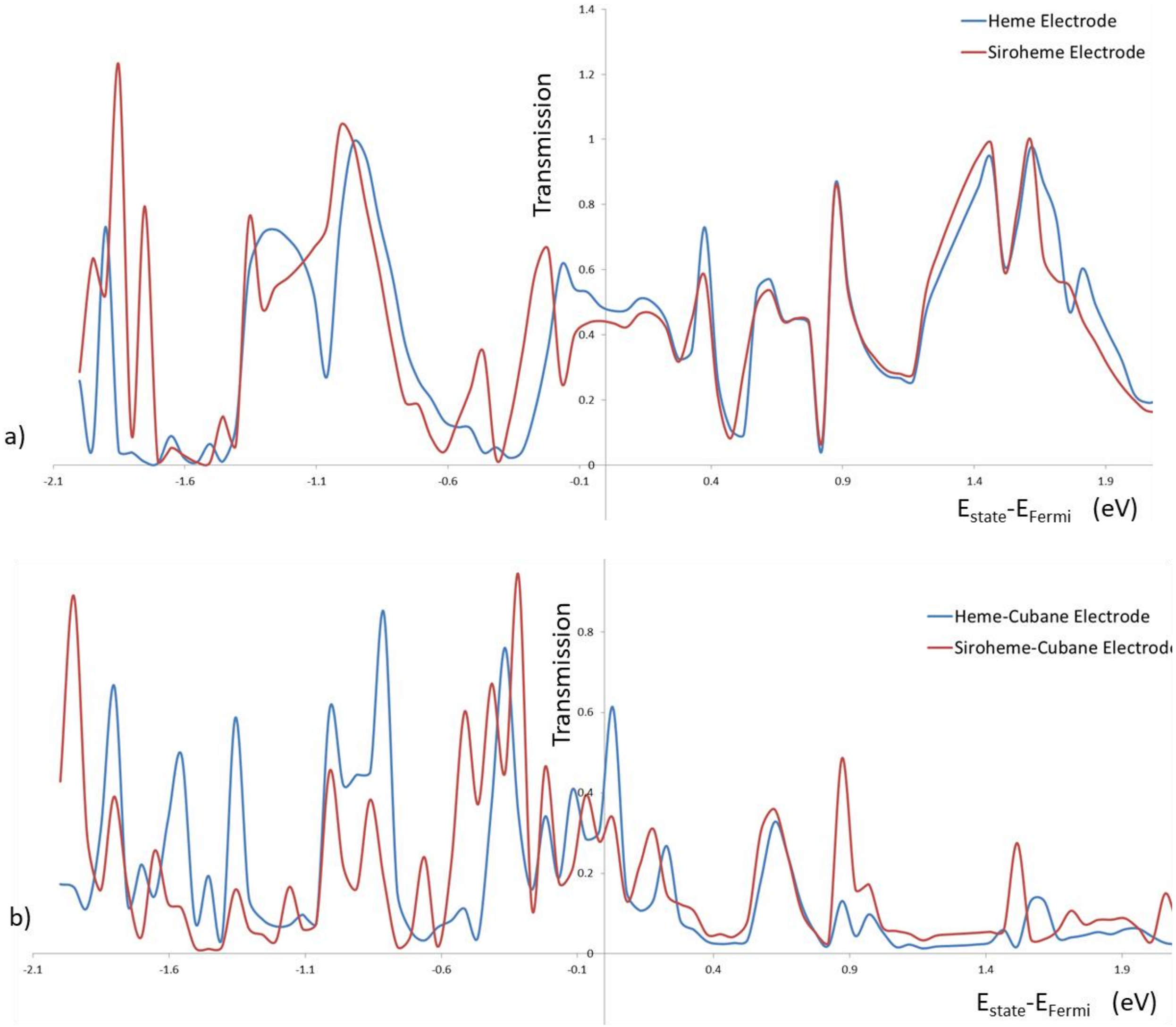

Figure 73. Electron transmission as a function of the energy associated with the electronic states involved in the charge transfer. The energy of the molecular state is expressed with reference to the electrode's Fermi energy. The blue line represents heme and the red line siroheme in a), and heme–cubane and siroheme–cubane in b). Transmissions are computed by the NEGF-DFT formalism at the PBE level with the DNP 3.5 basis set.

4.2.3.4 Implicit NEGF-DFT

By treating the SiR active site as a molecular junction (cf. Figure 74), the non-equilibrium Green's function coupled with density functional theory (NEGF-DFT) framework can be employed to compute its electron-transport properties.[156,158,166] Using this approach, an electron-route analysis was performed on four routes by which electrons can be transferred from the cubane to the (siro)heme cofactor (cf. Figure 75).

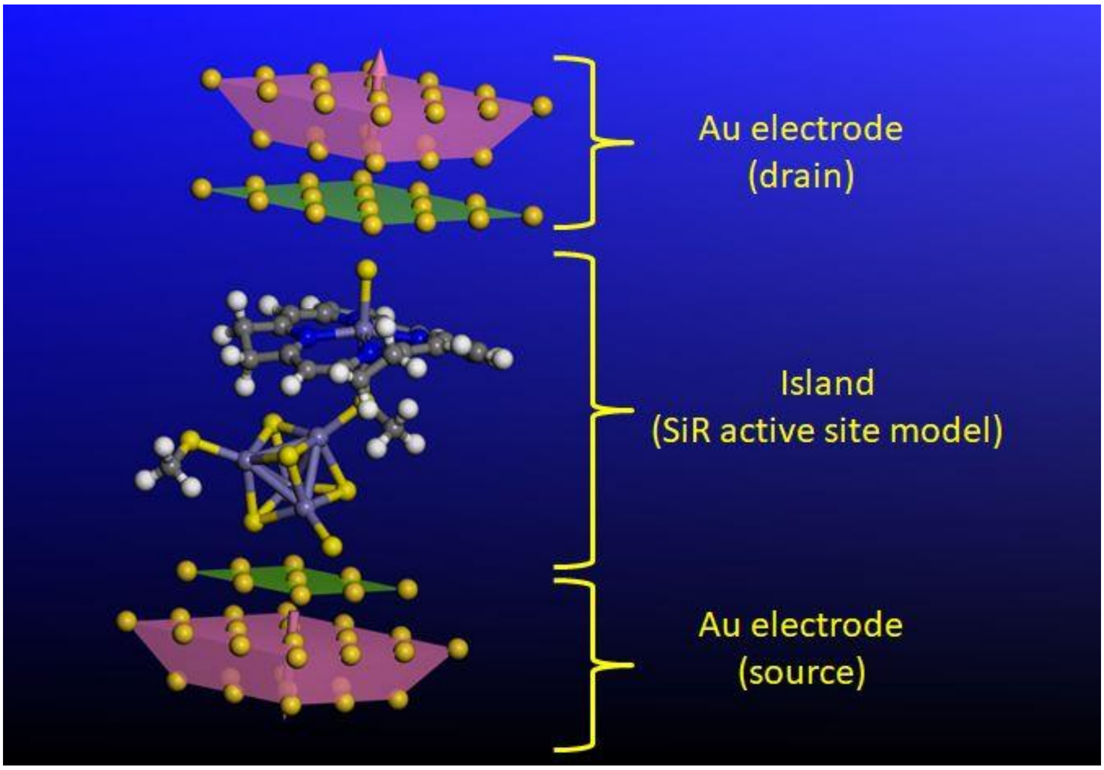

Figure 74. SiR active site as a molecular junctions connecting two Au electrodes. Au atoms are depicted in dark yellow, Fe in violet, N in blue, S in yellow, O in red, C in grey and H in white.

The first route deals with the charge transfer trough the bridging cysteinate sulfur atom (S_{bridge}), passing from the cubane iron that is involved in the interfactor bond (Fe_1) to the (siro)heme Fe ion (Fe_{heme}). The other three routes entail direct, through space,[167–169] charge transfer to Fe_{heme} via the porphyrin ring from the other three atoms of the cubane side facing (siro)heme. Both bridged and direct routes comprise two steps. In the bridged route the first step is represented by the cubane $Fe_1 \rightarrow S_{bridge}$ electron transfer and the second step by the $S_{bridge} \rightarrow Fe_{heme}$ transfer. In the direct routes the first step is represented by the cubane $Fe_2 \rightarrow$porphyrin electron transfer and the second step by the porphyrin$\rightarrow Fe_{heme}$ transfer. The bridged and direct routes differ in terms of location of the transient radical character generated by the transmitted electron: in the former case, the transient radical character is on the S_{bridge}, while in the latter case it is on the porphyrin ring.

The bridging route passes through two bonds, Fe_1–S_{bridge} and S_{bridge}–Fe_{heme} and in both models the conductance is higher in the first than in the second (cf. Table 62). For the other three routes, involving direct (through space) charge transfer between the two cofactors, different paths were considered from each cubane atom to its closest porphyrin C atoms for each path.

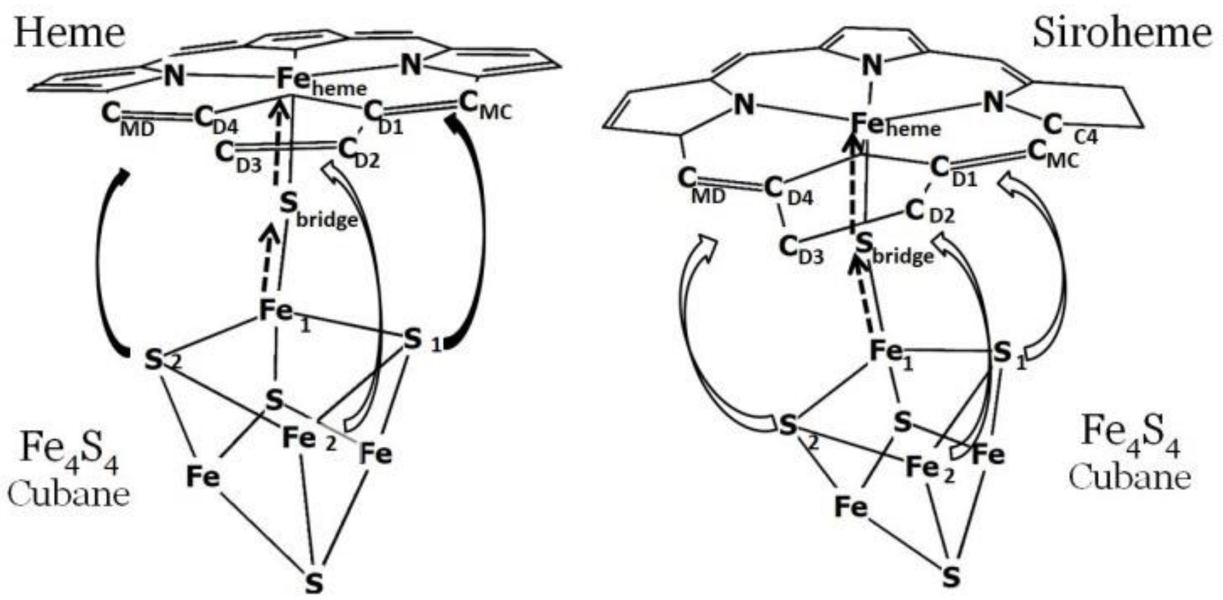

Figure 75. Electron routes investigated in the heme–cubane (left) and siroheme–cubane systems (right). The bridged route is depicted with dashed arrows, while the direct routes are shown with solid arrows. High conductance is depicted in black, while low conductance is in white. The structures were optimised at the B3LYP-D3/def2-TZVP level of theory before the electron-route analysis was performed (alternative structures are shown in 6.3.2).

In both SiR models, the electron conductance is higher in the bridged route than in the direct routes. Compared to heme, siroheme slightly decreases the conductance of the first step of the bridged route and slightly increases it in the second step. On the other hand, for the three direct routes, the total conductance is appreciably lower for siroheme than for heme. While the Fe_2→porphyrin conductance remains virtually unchanged when exchanging heme by siroheme, the routes starting from the sulfur atoms are significantly inhibited. By summing all the possible paths of each direct route this effect becomes even clearer: The average conductance in the direct routes drops from a total value of 0.7 a.u. in the heme variant to 0.1 a.u. when siroheme is used.

As can be seen in Table 62, there is no correlation between the distance of two atoms and transmission value. The difference between heme and siroheme in terms of conductance derives from the phase of the orbitals involved in the direct routes. Notably, the involved carbon atoms on the siroheme ring are sp^3 hybridized, whereas in heme they are part of the conjugated π system (i.e. sp^2 hybridized). By saturating the two double bonds involved in the direct routes, siroheme interrupts the porphyrin π system. This interruption causes the porphyrin orbitals to interact with the cubane orbitals involved in the direct routes in a less efficient manner.

Table 62. Computed conductance (*G*) for the investigated routes in the (siro)heme–cubane systems. Atom numbers are given in Figure 75; *d* represents the distance (in Å) between the two atoms. For the direct routes, the conductance of the second step (i.e. porphyrin→Fe_{heme}) is given in parenthesis.

Route	Heme–cubane				Siroheme–cubane			
	Atoms		*d*	*G*	Atoms		*d*	*G*
	#1	#2	(Å)	*a.u.*	#1	#2	(Å)	*a.u.*
bridged	Fe_1	S_{bridge}	2.4	**2.0**	Fe_1	S_{bridge}	2.3	**1.9**
	S_{bridge}	Fe_{heme}	2.2	**0.7**	S_{bridge}	Fe_{heme}	2.4	**1.0**
direct	S_1	C_{MC}	3.4	0.9(0.4)	S_2	C_{C4}	3.6	0.2(0.4)
		C_{D1}	3.3	1.3(0.1)		C_{MC}	3.2	0.1(0.1)
		C_{D2}	3.4	1.5(0.2)		C_{D1}	3.4	0.1(0.1)
direct	S_2	C_{D3}	3.4	0.9(0.2)	S_1	C_{D3}	3.7	0.3(0.2)
		C_{D4}	3.4	0.9(0.1)		C_{D4}	3.7	0.1(0.1)
		C_{MD}	3.4	0.3(0.4)		C_{MC}	4.0	0.2(0.4)
direct	Fe_2	C_{D2}	3.7	0.1(0.2)	Fe_2	C_{D2}	4.0	0.2(0.2)
		C_{D3}	3.7	0.2(0.2)		C_{D3}	3.9	0.1(0.2)

The results of the computed conductance reveal that the bridged route is always more favorable than the direct routes. This is in accordance with the well-known fact that quantum tunneling-driven charge transfer in biological systems occur over longer distances (~14 Å)[170] when the tunneling goes through the amino acids rather than when passing through vacuum.[171]

Although the conductance in the through-bond route is slightly altered when siroheme replaces heme, a much more remarkable decrease is seen for the conductance through the direct routes. This suggests that siroheme inhibits the electron transfer via the edge of the porphyrin. Avoiding these routes probably assures that the porphyrin is kept in a radical-free state, thereby reducing the risk of unwanted side-reactions such as:

- *Sulfheme formation:* the SiR active site cavity is formed only by lysine and arginine residues which are known to inhibit the sulfheme formation in (lys, arg-mutated) heme containing proteins.[172,173] Such a Lys and Arg containing environment can be linked to the enzyme's attempt to avoid sulfheme formation. Furthermore, heme radical states are invoked[174] in the sulfheme formation mechanism. In a different mechanism,[173] H_2S was shown to react with heme via HS^-, i.e. the intermediate present in the last steps of SiR's catalytic cycle.

- *Heme–solvent reactions:* being exposed to the solvent with the side involved in the direct routes, the transient heme radical could be susceptible to reacting with the solvent molecules.

- *Heme-intermediate reactions:* SiR catalyses sulfite reduction via intermediates comprising also positively charged adducts that can react with the transient negatively charged heme.[82]

Sulfheme formation in hemoglobin and myoglobin is known[175] to drastically decrease the Fe_{heme} affinity for the substrate. Similarly, the formation of this species in SiR is expected to affect the substrate binding to Fe_{heme}, an undesirable event considering the rapid six-electron reduction that the enzyme needs to undergo. Nevertheless, the purpose of SiR implies dissociation of the H_2S product at the end of the catalytic cycle and not its storage at the heme periphery (like hemeproteins that store H_2S in the sulfheme form and use it for signaling).[172] Reaction of a heme radical with water solvent can easily lead to the formation of hydroxyheme. This species is known[176] to be present in heme oxygenase's heme-degrading mechanism. Also, the displacement of an intermediate on the heme ring can drastically disturb the catalytic cycle and produce undesired products.

In the heme–cubane variant, the second steps of the direct routes (porphyrin$\rightarrow$$Fe_{heme}$) have a lower conductance than the first steps (average 0.2 vs. 0.7 a.u. respectively) and, more importantly, a lower conductance than the second step of the bridged route (i.e. $S_{bridge}\rightarrow Fe_{heme}$). The low conductance of the porphyrin $\rightarrow$ Fe_{heme} steps suggests that, once on the porphyrin, the electron delocalizes in it and the transfer to Fe_{heme} is delayed. This emphasizes that, although in the first step the direct route matches the corresponding bridged step, overall the bridged route is more efficient in transmitting electrons from the cubane to the $\text{Fe}_{\text{heme.}}$ Thus, by inhibiting the porphyrin$\rightarrow\text{Fe}_{\text{heme}}$ step, SiR avoids the futile delocalization of the transmitted electron onto the macrocycle, a delocalization that would hinder the substrate-reduction process.

4.2.4 Conclusions

Siroheme tunes the electron transfer from the cubane cofactor to the substrate such that, when compared to the heme variant of the SiR active site, the states associated with the through-vacuum charge transfer are inhibited, while the states involved in the through-bridge charge transfer are modified to increase the electron transmission (cf. Figure 76) . Thus, the role of siroheme is to block the delaying porphyrin $\rightarrow$ Fe_{heme} step in order to increase the overall charge transfer from the cubane cofactor. Furthermore, siroheme reduces the risk of porphyrin acquiring partial radical character that comes as an effect of the electrons being transmitted from the cubane via routes that involve the periphery of the porphyrin π-system. By avoiding these charge-transfer channels, the macrocycle is protected against undesired radical attack.

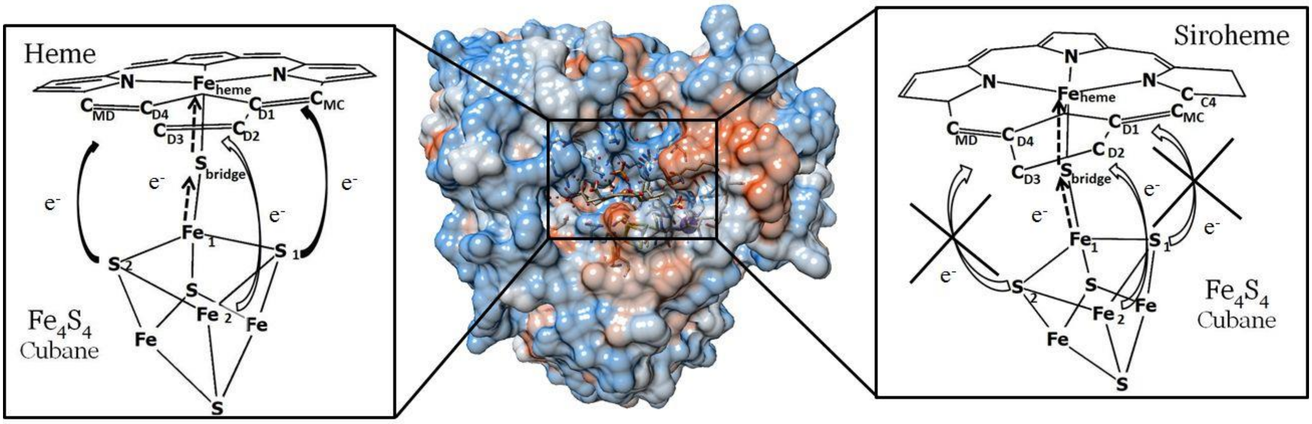

Synthetic active site

Sulfite Reductase

Biological active site

Figure 76. As opposed to heme, siroheme inhibits the charge transfer from the cubane via direct routes.

4.3 Pars mechanistica: SiR reaction mechanism

4.3.1 Introduction

The reaction mechanism by which SiR reduces sulfite (SO_3^{2-}) to sulfide (S^{2-}) has previously been proposed[82] based on experimental data regarding the known intermediates and by complementing the known information with computational obtained data of the experimentally unseen intermediates. The proposed SiR reaction mechanism is shown in Figure 77.

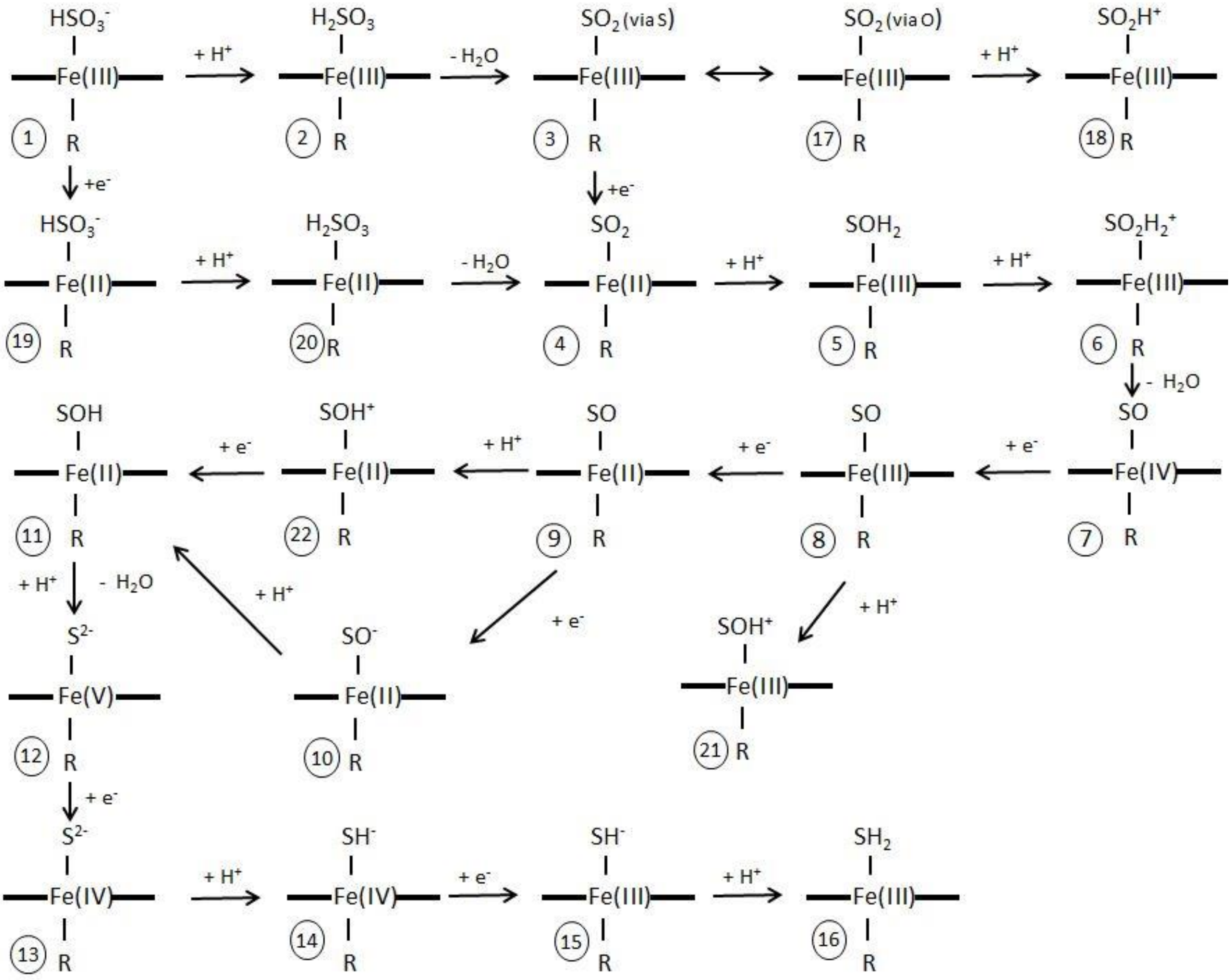

Figure 77. Sulfite Reductase reaction mechanism.

The sulfite adduct was shown to possess high proton affinities similar to other alike adducts that are known to protonate at room temperature.[82] Thus it was concluded that is reasonable to expect sulfite to arrive protonated at the active site (cf. intermediate **1** in Figure 77). Once bound to the siroheme Fe, the substrate will suffer a proton and electron addition which, followed by the elimination of a water molecule, would lead to the formation of the Fe (II)-SO_2 adduct denoted **4** in Figure 77. There are two ways by which adduct **4** can be reached and they differ by the order of in which the addition and elimination reactions are made. Thus the first way implies a protonation followed by water elimination and an electron addition (route **1-2-3-4**) while the second route starts with an electron addition followed by a proton addition and ends with the elimination of a water molecule (route **1-19-20-4**). The protonation of adduct **1** was shown to be favorable as opposed to its electron addition and thus it was concluded that route **1-2-3-4** would be the preferred way to reach intermediate **4.** Furthermore, this route implies the formation of an SO_2 adduct which in turn was shown to be bound via the oxygen atom rather than the sulfur atom (i.e intermediate **17)**. The protonation of either of these two bond isomers was found to be unfavorable and thus the **17 -> 18** step was deemed unlikely. Two protonation processes would lead to a $H_2SO_2^+$ adduct bound to a ferric siroheme (intermediate **6**) which, in turn, will eliminate a water molecule (leading to intermediate **7)**. The addition of an extra electron brings the reaction to a point from which it can continue via two possible pathways. Thus the SO adduct bound to a ferric siroheme (intermediate **8**) can be either protonated and transformed into the **21** intermediate or be reduced by an incoming electron and transformed into intermediate **9.** The former option was found to be unfavorable and thus the reaction was expected to continue via intermediate **9.** From here onwards, a succession of proton and electron additions would eventually yield the **16** reaction product in the form of a departing H_2S molecule and a ferric siroheme ready to restart the reaction cycle.[82]

However, this previously proposed SiR reaction mechanism was built based on models of intermediates that completely neglected the cubane cofactor. In order to afford the computational cost that the full active site required, it was assumed that the role of the cubane cofactor within the SiR active site is restricted to providing electrons and does not influence the reaction mechanism. In this chapter we extend the computational endeavor upon this mechanism and provide new insights to its functioning. We start by recomputing these cubane-less models at a DFT level that will make the results coherent with the rest of this chapter. We then incorporate models that contain the cubane cofactor but also an intermediate set of models in which the $[Fe_4S_4]^{2+}$ cofactor is replaced by a diamagnetic Zn^{2+} ion. This allows the differentiation of the magnetic and metallic influence of the *trans effect* on the reaction mechanism. Furthermore, different electronic states are assigned to each model and also the bond isomerism (where possible) is investigated, as detailed in section 4.3.2.

4.3.2 Theoretical methods

4.3.2.1 Models

The active site models were built starting from the crystal structure of the sulfite reductase enzyme (PDB entry: 1AOP) following the procedure described in section 4.1.2.2. The intial substrateless models are depicted in Figure 78 and are reiterations of those previously examined in Section 4.1.

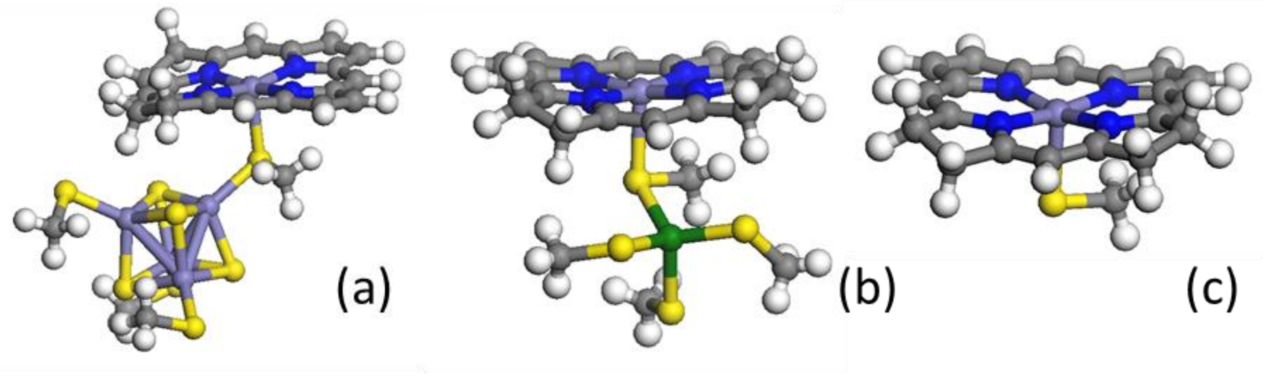

Figure 78. Substrateless models of the SiR active site, composed of siroheme connected to an iron–sulfur [4Fe-4S] cubane via a cysteinate sulfur (a). In model (b), the iron–sulfur cubane is replaced by zinc complex, $[Zn(SCH_3)_4]^{2-}$,while in model (c), the cubane complex is replaced by $[SCH_3]^{1-}$. Iron atoms are depicted in violet, zinc in green, sulfur in yellow, carbon in gray and hydrogen in white.

The first model in Figure 78 comprises a siroheme linked to a $[Fe_4S_4]^{2+}$ cubane via a cysteine sulfide. The other three Fe atoms of the cubane are coordinated by three cysteine residues coming from the surrounding protein environment. The cysteines are modelled as anionic methylthiolates. In the second model, the $[Fe_4S_4]^{2+}$ cubane is replaced by a Zn^{2+} ion (coordinated to four cysteine residues), so that the cubane net charge and experimentally known diamagnetic character is preserved. The third model omits the cubane cofactor altogether. For each model, the (siro)heme iron was modelled either as ferrous or ferric. Three spin states were employed for each charge state: S = 0, 1 or 2 for ferrous and S = 1/2, 3/2 or 5/2 for ferric. The cubane was always studied in the oxidized $[Fe_4S_4]^{2+}$ state. For each of the above series of models the substrates mentioned in Figure 77 were connected to the model's distal position. All obtained models were computed both in vacuum and solvent exposed conditions.

4.3.2.2 Computational protocols

DFT calculations on the SiR active site models followed a previously established protocol (cf. section 4.1.3.1). Ground-state geometry optimizations[125] were performed with the resolution-of-identity approximation[126,127] using the TPSS[119] functional, the double-zeta level def2-SV(P) split-valence basis set[128] and Grimme's D3 correction for dispersion interactions.[129] Frequency calculations[131] were employed in order to assure that stationary points are true local minima. If significant imaginary frequencies were found, the molecular geometry was distorted along the coordinate involved the in imaginary vibration and the geometry optimization was redone. On each converged structure, single-point calculations were employed using the B3LYP[34] functional at the same def2-SV(P) basis set level. Due to convergence issues that appeared in cubane models when the larger, def2-TZVP, triple zeta basis set was adopted the computations were restricted at the double-zeta level of theory. It was previously shown in section 4.1.3.1 that, for heme-related systems, def2-SV(P) performs as well as def2-TZVP. Solvation free energies were calculated with the COSMO[132] approach with optimized radii for all atoms[133] and 2.0 Å for Fe[134] (and a water solvent radius of 1.3 Å), setting the dielectric constant to $\varepsilon = 4$, mimicking a protein environment. The convergence criteria were set at 10^{-6} Hartree for the change in energy, 10^{-3} a.u. for the maximum displacement and maximum gradient element, while $5 \cdot 10^{-4}$ a.u. was set for their corresponding root-mean-square (RMS) change.

For models containing a cubane, the broken-symmetry approach[135,136] was adopted in order to control the assignment of spin states on each iron atom. This approach consists in converging the highest possible spin state of the system of interest (22 or 23 unpaired electrons), followed by flipping a part of the major spin population so that the desired spin state is obtained. The cubane cluster is always treated in the singlet state, formed by the antiferromagnetic coupling of a pair of an Fe(II) and an Fe(III) ion with majority spin ($S = 9/2$, which is a mainly delocalized mixed valence pair) with another similar pair with the opposite spin, as is depicted in Figure 58. Such states can be obtained in six different ways (two Fe ions can be selected from a set of four in six different ways).

Models were constructed in Materials Studio[162] and all calculations were performed with the use of Turbomole.[118]

4.3.3 Results

The relative energies obtained for all the studied models are listed in Table 63. For each model series, i.e. R=SCH_3; $Zn(SCH_3)_4$ and $[Fe_4S_4]$ $(SCH_3)_4$), energies are expressed relative to the low-spin O-bond isomers of intermediate 1. Considering the size of the data collected in Table 63 we commence this section by analyzing the linkage and redox isomerism encountered along the SiR reaction pathway and then follow the energetic implications of the three families of models on its reaction mechanism. Thus the ensuing discussions within this section will be based on Table 63, when energetic aspects are followed, while all references to atomic distances or to electronic population analyses within the studied models have Table 104 and Table 105 of section 6.3.3 as support. Furthermore, the reason behind a certain model's demise (noted as N/A in Table 63) is detailed in the *Observation* column of Table 104.

Table 63. Relative energies of reaction intermediates for the three types of SiR models of the active site.

Inter.	Bond isomer	*S*	ΔE (kcal/mol)					
			SCH_3		Zn		Fe_4S_4	
			Vacuum	Solvent	Vacuum	Solvent	Vacuum	Solvent
1	S	1/2	9.3	6.1	10.8	8.4	7.8	6.1
		3/2	19.8	17.2	N/A	N/A	N/A	N/A
		5/2	N/A	N/A	N/A	N/A	11.4	6.1
	O	1/2	0.0	0.0	0.0	0.0	0.0	0.0
		3/2	13.8	11.7	9.4	6.7	-1.4	-2.7
		5/2	6.4	5.0	3.2	2.8	-1.5	-1.8
2	S	1/2	-50.8	-24.8	-91.3	-32.8	N/A	N/A
		3/2	N/A	N/A	N/A	N/A	N/A	N/A
		5/2	N/A	N/A	N/A	N/A	N/A	N/A
	O	1/2	-61.4	-34.3	-106.8	-47.2	-90.9	-33.1
		3/2	-57.4	-31.5	-104.1	-44.7	-96.0	-38.5
		5/2	-61.7	-34.9	-110.3	-50.4	-101.4	-43.6
3	S	1/2	-63.1	-41.0	-105.1	-48.0	N/A	N/A
		3/2	N/A	N/A	N/A	N/A	-104.6	-51.9
		5/2	N/A	N/A	N/A	N/A	N/A	N/A
	O	1/2	-65.2	-42.8	-105.1	-55.8	-100.8	-50.1
		3/2	-56.0	-34.1	-121.3	-62.9	-98.0	-45.1
		5/2	-67.7	-45.8	-121.3	-62.9	-109.9	-56.7
4	S	0	-106.4	-110.0	-106.0	-109.2	-116.1	-118.8
		1	-109.9	-115.2	N/A	N/A	N/A	N/A
		2	-110.4	-115.3	-115.5	-119.6	N/A	N/A
	O	0	-104.4	-106.5	-102.6	-106.2	-121.7	-124.7
		1	-117.4	-121.6	-115.2	-120.3	-121.7	-125.4

Inter.	Bond isomer	S	ΔE (kcal/mol)					
			SCH_3		Zn		Fe_4S_4	
			Vacuum	Solvent	Vacuum	Solvent	Vacuum	Solvent
		2	-109.3	-112.7	-117.9	-122.1	-125.2	-128.6
5	S	0	-154.9	-133.4	-205.4	-160.4	-213.9	-161.6
		1	-166.3	-145.0	-216.5	-160.5	-212.1	-160.2
		2	-168.5	-146.8	-216.8	-160.5	-210.4	-157.2
	O	0	-156.9	-133.9	-206.4	-149.0	-209.5	-158.3
		1	-173.3	-150.2	-219.3	-164.1	-212.9	-160.7
		2	-171.2	-149.4	-216.8	-163.0	-210.9	-158.2
6	S	0	-136.0	-135.6	-255.0	-184.3	-243.4	-174.1
		1	-112.6	-111.8	-262.5	-188.6	-242.7	-173.4
		2	N/A	N/A	N/A	N/A	-243.4	-174.9
7	S	0	-130.7	-134.2	-253.0	-180.0	-248.5	-184.6
		1	-147.1	-149.9	-278.3	-205.5	-254.5	-190.9
		2	-133.2	-136.5	-273.3	-200.1	-234.9	-170.4
	O	0	-81.1	-82.9	-246.2	-174.5	N/A	N/A
		1	-103.3	-104.9	-275.8	-201.4	-255.0	-188.6
		2	-110.8	-112.0	-271.6	-197.7	N/A	N/A
8	S	1/2	-284.1	-267.0	-340.5	-289.0	-328.2	-280.0
		3/2	-280.6	-261.9	N/A	N/A	-322.7	-275.1
		5/2	-279.0	-260.6	-338.0	-284.0	-325.4	-276.6
	O	1/2	-282.6	-264.1	-341.2	-288.4	-327.1	-278.9
		3/2	-287.7	-268.9	N/A	N/A	-321.2	-275.5
		5/2	-286.7	-269.5	-337.8	-284.9	-325.0	-276.4
9	S	0	-330.4	-338.9	-330.0	-338.9	-350.2	-359.1
		1	-340.9	-350.2	-336.6	-344.7	-346.0	-355.1
		2	-333.9	-342.7	-334.8	-342.5	-340.2	-348.0
	O	0	-323.6	-331.9	-323.6	-240.7	-347.4	-355.8
		1	-338.1	-347.4	-335.4	-344.8	-343.8	-351.9
		2	-328.5	-338.0	-330.6	-340.8	-343.7	-352.2
10	S	1/2	-288.6	-369.1	-240.7	-350.0	-284.6	-383.0
		3/2	-280.1	-362.6	-247.9	-357.5	-273.2	-370.9
		5/2	-241.3	-317.3	-252.2	-360.6	-281.2	-379.2
	O	1/2	-289.7	-370.2	-247.5	-357.2	N/A	N/A
		3/2	-284.3	-361.5	-244.4	-352.8	N/A	N/A
		5/2	-282.3	-364.4	-254.3	-360.1	N/A	N/A
11	S	1/2	-459.6	-469.5	-460.8	-470.5	-467.2	-476.1
		3/2	-451.6	-460.6	-411.9	-416.7	-459.3	-469.4
		5/2	-450.2	-460.2	-453.0	-463.0	-461.7	-470.6
12	S	1/2	-516.5	-503.4	-576.4	-528.7	-574.3	-531.0
		3/2	-518.3	-505.6	-576.6	-529.0	-561.6	-518.2
		5/2	-512.0	-500.4	-578.9	-530.1	-567.1	-523.4
13	S	0	-556.8	-570.9	-555.0	-569.5	-580.1	-593.9

Inter.	Bond isomer	*S*	ΔE (kcal/mol)					
			SCH$_3$		Zn		Fe$_4$S$_4$	
			Vacuum	Solvent	Vacuum	Solvent	Vacuum	Solvent
		1	-576.6	-590.8	-575.8	-590.7	-587.1	-601.0
		2	-571.5	-585.2	-573.9	-587.9	-582.2	-595.5
14	S	0	-640.3	-626.7	-691.2	-642.9	-699.4	-655.9
		1	-651.1	-637.6	N/A	N/A	-699.0	-655.2
		2	-639.9	-625.9	-695.4	-648.9	-687.3	-643.6
15	S	1/2	-647.1	-659.9	-632.9	-646.3	-714.7	-728.2
		3/2	-698.5	-711.8	-625.5	-638.5	N/A	N/A
		5/2	-700.1	-714.5	-628.4	-643.0	-711.0	-724.8
16	S	1/2	-772.8	-759.5	-815.4	-770.6	-803.7	-765.6
		3/2	N/A	N/A	N/A	N/A	-806.5	-762.2
		5/2	N/A	N/A	N/A	N/A	-810.1	-765.9
18	S	1/2	-30.7	-29.8	-139.2	-62.4	-128.7	-60.6
		3/2	-29.5	-29.1	-149.5	-73.5	-129.6	-62.5
		5/2	-30.7	-29.8	-153.9	-75.2	N/A	N/A
	O	1/2	-22.0	-21.1	-159.0	-79.7	-128.9	-57.8
		3/2	-39.1	-36.6	-158.5	-79.7	-126.1	-56.7
		5/2	-29.4	-29.4	-157.8	-78.6	-131.8	-62.0
19	S	0	49.2	-24.4	86.0	-15.4	58.7	-33.1
		1	N/A	N/A	104.2	6.4	62.6	-29.6
		2	N/A	N/A	N/A	N/A	57.7	-34.0
	O	0	46.0	-22.4	87.8	-9.2	54.3	-34.8
		1	52.1	-14.8	N/A	N/A	55.4	-32.9
		2	N/A	N/A	N/A	N/A	48.5	-39.5
20	S	0	-86.1	-87.3	N/A	N/A	-105.4	-104.8
		1	N/A	N/A	N/A	N/A	N/A	N/A
		2	N/A	N/A	N/A	N/A	N/A	N/A
	O	0	-90.1	-88.7	-90.1	-91.1	-106.4	-105.2
		1	N/A	-92.3	N/A	N/A	-110.4	-110.1
		2	N/A	-101.7	N/A	N/A	-116.9	-115.8
21	S	1/2	-266.9	-269.2	-395.9	-323.4	-372.6	-309.6
		3/2	-268.3	-271.3	-396.0	-323.5	-372.4	-309.4
		5/2	-258.6	-261.1	-385.9	-312.9	-360.9	-297.2
22	S	0	-397.4	-379.4	-445.7	-392.9	-450.2	-402.5
		1	-405.7	-387.6	-464.4	-411.3	-444.6	-398.8
		2	-395.6	-377.0	-454.5	-401.0	-439.2	-391.5

4.3.3.1 Linkage isomerism in the sulfite adducts

For the ferric bisulfite adduct **1** (cf. Figure 79), binding via the oxygen is remarkably preferred (since the experimental structure of SiR features the opposite isomer),[75] but least so in the full cluster model than in the smaller ones. The cluster reduces this preference by ~ 2-3 kcal/mol; solvation also reduces it by 1-2 kcal/mol, so that the best estimate is 6 kcal/mol in favor of the O-isomer – a value which is small enough to be perturbed easily by nearby hydrogen bonding patterns.

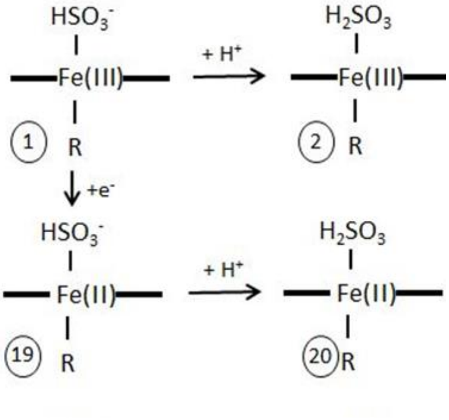

Figure 79. The HSO_3 and H_2SO_3 containing adducts involved in the SiR reactions mechanism.

Notably, in the full-cluster models the siroheme iron is predicted to be low-spin in the S-isomer and high-spin in the O-isomer of the ferric-bisulfite adduct **1**. The high-spin states are expected to feature much weaker Fe-substrate bonding: indeed, the Fe-S bond is broken in the S=5/2 state of the thiolate and in the zinc models. For the O-isomer, the Fe-O(bisulfite) bond is in the range expected of an oxygen-based ligand (1.95-2.05 Å depending on spin state). Nevertheless, one may argue that the high-spin state preference of the O-isomer in the full-cluster model is a disadvantage since it entails a more kinetically-labile binding. Together with the fact that binding via the sulfur is the more productive manner to begin a catalytic cycle where the sulfur needs to be retained to the end and liberated as hydrogen sulfide, it may be expected that SiR would eventually control linkage isomerism in sulfite binding, by employing hydrogen bonding and electrostatics above the siroheme, in order to overturn the intrinsic preference of the siroheme-cluster assembly towards a high-spin O-isomer vs a low-spin S-isomer. This finding may also be of relevance to experimental efforts towards developing small-molecule models of the SiR active site.

Qualitatively similar data were obtained for the ferrous-bisulfite models 19, hence with similar conclusions as above.

The ferric- and ferrous--sulfurous acid models follow the same pattern as the bisulfite ones – expectedly with a more marked tendency towards dissociation of the substrate-siroheme bond in the S-isomer. If this isomer is to be employed in catalytic reduction, then subsequent dehydration and/or reduction must occur very rapidly or concerted with protonation, in order to avoid loss of the substrate. On the other hand, since at this stage no electrons/energy have been invested into the substrate, its rapid on-off equilibrium would not be deleterious (unlike the perspective of an activated intermediate detaching form the siroheme *during* the cycle).

4.3.3.2 Linkage isomerism with SO_2 and SO_2H

For the (formally) ferric-SO_2 adducts (cf. Figure 80), in most of the models and most of the spin states of the S-isomer the Fe-SO_2 bond is broken upon geometry optimization – while the O-isomers are stable. Importantly, however, for the few models / spin states for which a proper comparison is possible (local minima identified for intact adducts for both isomers), the S-isomer appears slightly favored (~4-6 kcal/mol, with the exception of the thiolate model in vacuum, where the two isomers are essentially degenerate, with 1 kcal/mol in favor of the O- one). In a previous report, where we analyzed the SO_2 adduct only for a small thiolate model and using heme rather than siroheme, the O- isomer was also favored – and in fact the S-isomer was not a local minimum. The herein reported data show that in the cluster-siroheme model the S-isomer is stabilized compared to a simple heme-thiolate structure – presumably thus offering further mechanistic advantage by allowing fixation of the sulfite sulfur at the iron for further reduction and dehydration.

The SO_2 ligand is potentially available to engage in redox isomerism. The S-O bond lengths within SO_2 are at 1.49-1.50 Å in the S-isomer and at 1.56 in the O-isomer. For comparison, the computed S-O bond lengths are 1.48 Å in neutral SO_2, vs 1.56 Å in SO_2^-, 1.47 Å in SO_2^+ and 1.51 Å and 1.69 Å in SO_2H (O-S-OH and O-S-OH, respectively). Thus, the SO_2 adducts within the SiR catalytic cycle may be judged to feature a dominantly neutral ligand in the S isomer (bond lengths similar to SO_2^0 and SO_2^+ but distinctly shorter than for SO_2^-).

Also, for the S-isomer of 3, the charges and spin densities on the SO_2 ligand amount to 0.00 spin density and -0.1 charge in the small thiolate model, suggestive of a neutral ligand. In the Zn model, the charge is even smaller (0.05), while in the cluster model the charge is more than double – and the spin density is no longer zero. These latter findings still support a neutral SO_2

description of the SO_2 ligand in the S-isomer, but now with a distinctly stronger interaction in the cluster model – and a ligand more primed towards the one-electron reduced redox isomer.

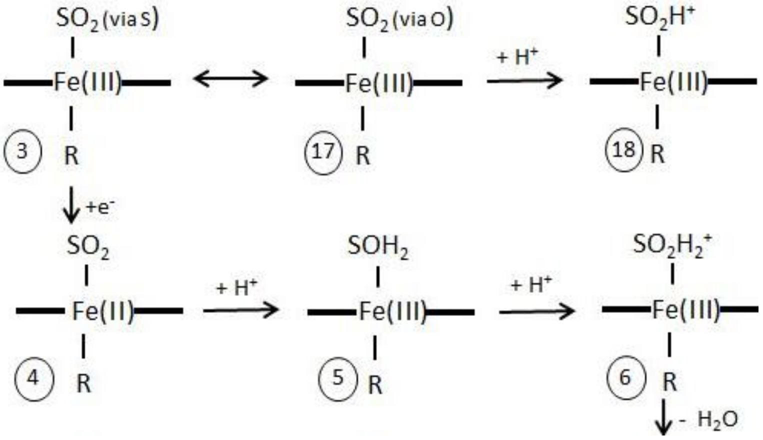

Figure 80. The SO_2 and SO_2H containing adducts involved in the SiR reactions mechanism.

Interestingly, the O-isomer features distinctly more spin density (up to 0.7) on the SO_2 ligand, and distinctly more charge (up to -0.4), depending on the model (more so in the Zn and cluster models than in the thiolate models) – suggesting a stronger component from the SO_2^- (radical) redox isomer. The longer S-O bond lengths (discussed above) also support this interpretation. While the more reduced character of the ligand would appear as an advantage for the SiR catalytic site, generation of this isomer would be a counterproductive as it would liberate the sulfur in the form of SO before fully reducing it to sulfite.

In the ferric-SO_2H complex, the O-isomer is distinctly favored by the small thiolate model – but no longer so in the larger models. Again, the cluster thus offers an advantage in favoring coordination via the sulfur. Examination of the electronic population within the SO_2H ligand reveals generally neutral or slight negative charges, with large amounts of spin densities, suggesting that the one electron fed so far into the catalytic cycle has indeed been localized at the ligand – hence a neutral SO_2H moiety (equivalent in redox state with the commonly employed reducing agent in biochemistry, dithionite) with partial SO_2H- (sulfoxylate) character (considering that the sum or partial atomic charges on SO_2H in the various models ranges from 0 to -0.3).

For the $S(OH)_2$ adduct, linkage isomerism is not an option since the oxygen atoms are already protonated. In terms of redox isomerism, we note that the ligand features total charges ranging from 0 to 0.3, and essentially zero spin density, in line with a dominant description as neutral sulfoxylic acid.

4.3.3.3 Linkage and redox isomerism with SO and SOH

In the SO complex **7**, formally the first step obtained upon dehydration of the ferric-SO_2 adduct, and described as a Fe(IV)SO$\leftarrow\rightarrow$Fe(III)-SO(+) state, the S isomer is distinctly favored in the small thiolate models(cf. Figure 81). However, in the larger models the difference is reduced to almost zero. The qualitative similarity between the zinc and the cluster models in this respect suggests that the near-degeneracy of the two isomers is not brought about by the availability of an additional redox partner which may affect the redox state of the siroheme iron, but rather, presumably, by the changes in the nature of the axial iron-thiolate bond as previously outlined.[177] Interestingly, in the various models of intermediate **7**,the SO ligand features charges of -0.3 to 0.1 (with the more negative values present in the larger models), with spin densities going up to 1.8 or very close to zero, equivalent to a neutral S=1 and S=0 states analogous to molecular oxygen. The S-O bond length is at 1.52-1.53 Å in the S isomers (compared to 1.64 Å in isolated SO^-, 1.53 Å in $^3SO^0$, 1.46 Å in SO^+) – in line with the population analysis and suggesting a structure composed of two limiting configurations – one with anionic SO and one with neutral SO). This implies either a one-electron oxidized siroheme – which indeed is visible in the strong spin density on the porphyrin atoms especially in the small thiolate models, or a redox contribution from the cluster (indeed, in some of the cluster models the spin density on the porphyrinoid ring is reduced to much smaller values). The large spin density on the siroheme ring is suggestive of a particularly unstable structure – as indeed expected for a formally Fe(IV) complex. We also note that in the O-isomers, the S-O bond length is remarkably elongated, at 1.8-2.0 Å, suggesting significant activation towards O-S bond cleavage; however, this elongation is not mirrored by significant charge transfer into the SO moiety, since its overall partial charge remains close to 0.

In model 8, formally Fe(III)-SO, the relative energies of the two isomers no longer feature strong qualitative differences between the three types of models: the two isomers are essentially degenerate, with a slight preference for the O-isomer in the larger models. The S-O bond lengths are slightly elongated compared to model **7,** suggesting that at least part of the extra electron resides on the ligand; however, the partial atomic charges and spin densities on SO are in the same ranges as for model **7**, suggesting that reduction of **7** occurs mostly within the rest of the molecule and not at the SO. This is indeed expected, since **7** was formally Fe(IV). In fact, models **8** no longer feature large amounts of spin density on the porphyrionid ring. Model **8** may thus be described as Fe(III)-SO rather than one of its possible redox isomers.

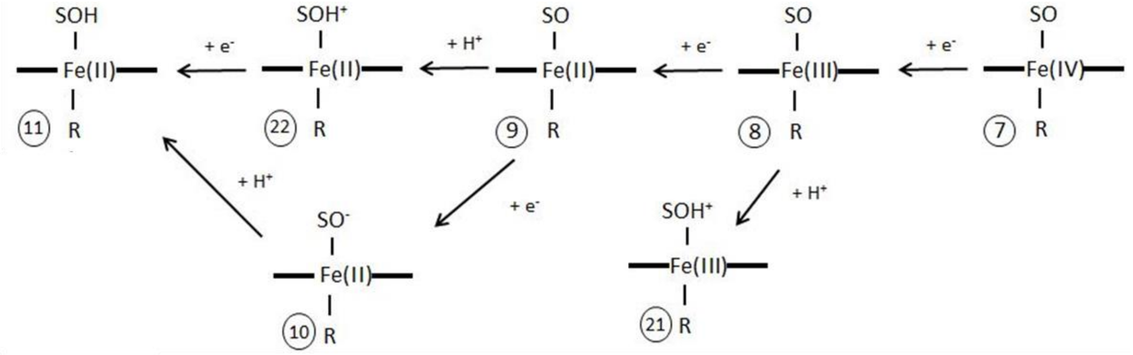

Figure 81. The SO_2 and SO_2H containing adducts involved in the SiR reactions mechanism.

For models **7** and **8** we do also note a preference for higher-spin states. This may be paralleled to the Fe(III)-O_2 complexes, whose higher-spin preferences have been invoked as reasons why ferric-dioxygen adducts are essentially unknown while ferrous-dioxygen adducts (which are dominantly low-spin, at least in heme-like settings) favor lower-spin states with stronger Fe-ligand interactions.[178]

Model **9** is an analogue of the well-known ferrous-dioxygen adduct of many hemoproteins (e.g., hemoglobin, cytochrome P450, peroxidases, heme oxygenases, nitric oxide synthases etc). The two isomers here again feature sensibly similar energies – with the clearest-cut difference at ~4 kcal/mol in favor of the S isomer, in the large cluster model in solvent. Also of note is the fact that in the larger models (but not in the other ones) the low-spin state is favored, thus reinforcing Fe-substrate/intermediate bonding. These findings are in line with mechanistic considerations requiring the sulfur coordinated to the siroheme throughout the catalytic cycle, as previously discussed – and thus again highlights a stage in the catalytic cycle where the iron-sulfur cluster disfavors the counterproductive O-coordination of the substrate and of the intermediates to the siroheme (and, here, favors a lower-spin state and hence more efficient binding of the reactive intermediate until the next catalytic steps may ensue).

The S-O bond lengths in models 9 are similar (though slightly longer, in line with slightly more negative partial atomic charges) compared to the ones in their one- and two-electron-oxidized counterparts (**7** and **8**), thus still suggestive of a dominantly neutral SO ligand, nut now with a stronger contribution from the SO- redox isomer.

For the formally Fe(II)-SO(-) model, an analogue of the well-known ferrous-superoxo/ferric-peroxo states in heme and non-heme iron proteins the two isomers were again essentially degenerate, with a slight preference for the O- one in vacuum, reversed by solvent but still in the degenerate range. The S-O bond length is now elongated up to 1.59 Å and the partial charges are up to -0.9 (with spin densities approaching 1.0), all of which suggest a structure with strong contributions from the Fe(II)-SO- as well as the Fe(III)-SO_2- redox isomers.

Structures **11** and **22** (formally Fe(II)-SOH- and Fe(II)-SOH, respectively) offer less variability across models and were not considered for linkage isomerism since the oxygen atom is already protonated and thus expected to be a much weaker ligand. These models feature neutral-to-negative charges on the SOH ligand, more towards an SOH- description in model **11** than in one-electron oxidized formal precursor, **22**.

4.3.3.4 Redox isomerism within the sulfide adducts

Models **12-14** offer an exciting opportunity to examine (formally) high-valent centers analogous to the well-known ferryl (Fe(IV)-oxo) Compound I and Compound II species of many hemoproteins. In previous cases, both redox isomerism and protonation status at the oxo ligand were shown to vary across hemoproteins. Also, an interplay between the S=1 ferryl and a neighboring radical featured on the heme or on the axial thiolate or an neighboring aminoacids in Compound I species (as opposed to Compound II, which contains ferryl without an additional radical / oxidizing equivalent) was shown to play important mechanistic roles in proteins such as cytochrome P450 (with the well-known TSR, “two-state-reactivity” theory), cytochrome c peroxidase and others.[179]

For model **12**, electronically equivalent to the above-cited Compound I species, we first note the close degeneracy of all spin states in the smaller models (and with a preference for higher-spin states rather than for the low-spin one) – and the fact that in the cluster model the low-spin state is more favored (and the solvent further strengthens this trend). In most models, the spin density on the sulfide ligand approaches 1, which we have previously shown to be reconcilable at first sight with a ferryl-like structure where the two π^* orbitals each carry 0.5 unpaired electrons – though we further showed that a description as sulfanyl is better suited. Interestingly, in some of the structures (especially in higher-spin ones and in the larger models), the sulfur spin density decreases down to 0.5, suggesting a more ionic/sulfide character. In the thiolate model, large spin densities are seen on the porphyrinoid ligand, shared significantly with the methyl-thiolate ligand in the lower-spin states but not in the high-spin state, and in line with the classical descriptions of the analogous Compound I species in Cytochrome P450 and chloroperoxidase. In the zinc model, much less spin density is delocalized onto the heme; the iron either retains this density or delocalizes it to the thiolates around the zinc. Then, in the cluster models, the porphyrinoid spin density is essentially zero. Thus, one should not expect to see a classical Compound I type species in SiR, with a porphyrin cation radical. This was perhaps expected since the nearby iron-sulfur cluster is available to store the extra oxidizing equivalent more easily that the porphyrinoid ring. The spin densities at the siroheme iron do remain similar to those in the smaller models, suggesting that the nature (and oxidation state) of the Fe=S unit ("sulfo-ferryl" as previously described) is less affected by the extra iron-sulfur cluster.

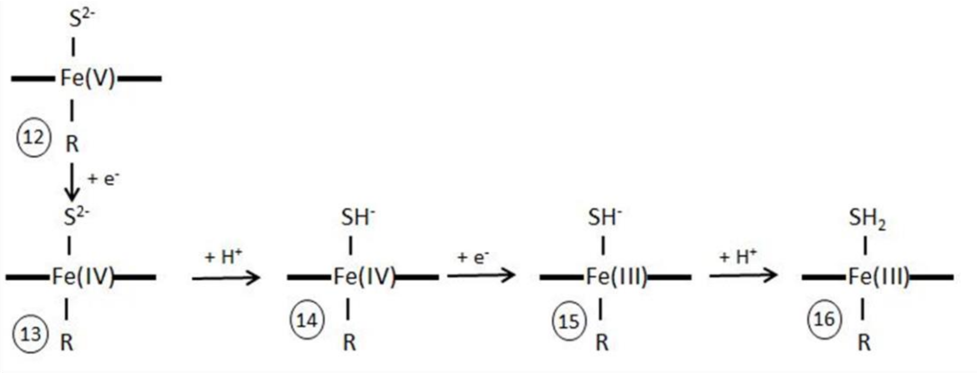

Figure 82. The sulfide containing adducts involved in the SiR reactions mechanism.

Species **13**, analogous to the ferryl Compound II species known in other hemoproteins, shows an even stronger degeneracy between the lower-spin states (by contrast heme Compound II are universally S=1)[179] – while the Fe=S moiety remains essentially the same in terms of charges and spin densities.

Species **14**, analogous to the less characterized protonated-ferryl Compound II known in hemoproteins, shows the expected trend after protonation of the sulfanyl ligand – i.e. less spin density and still reasonable amount of negative charge, in line with a dominant hydrosulfide description (and, hence, confirmation that the final step or reduction has been achieved).

4.3.3.5 Crossroads along the SiR reaction mechanism

This section discusses the thermodynamics of the various proposed pathways within the SiR catalytic cycle with emphasis on the points where the mechanism offers two branches (crossroads). Data from the most stable isomers computed in solvent are presented; vacuum data are shown in Supporting Information and discussed only where they offer notable differences towards the solvated data.

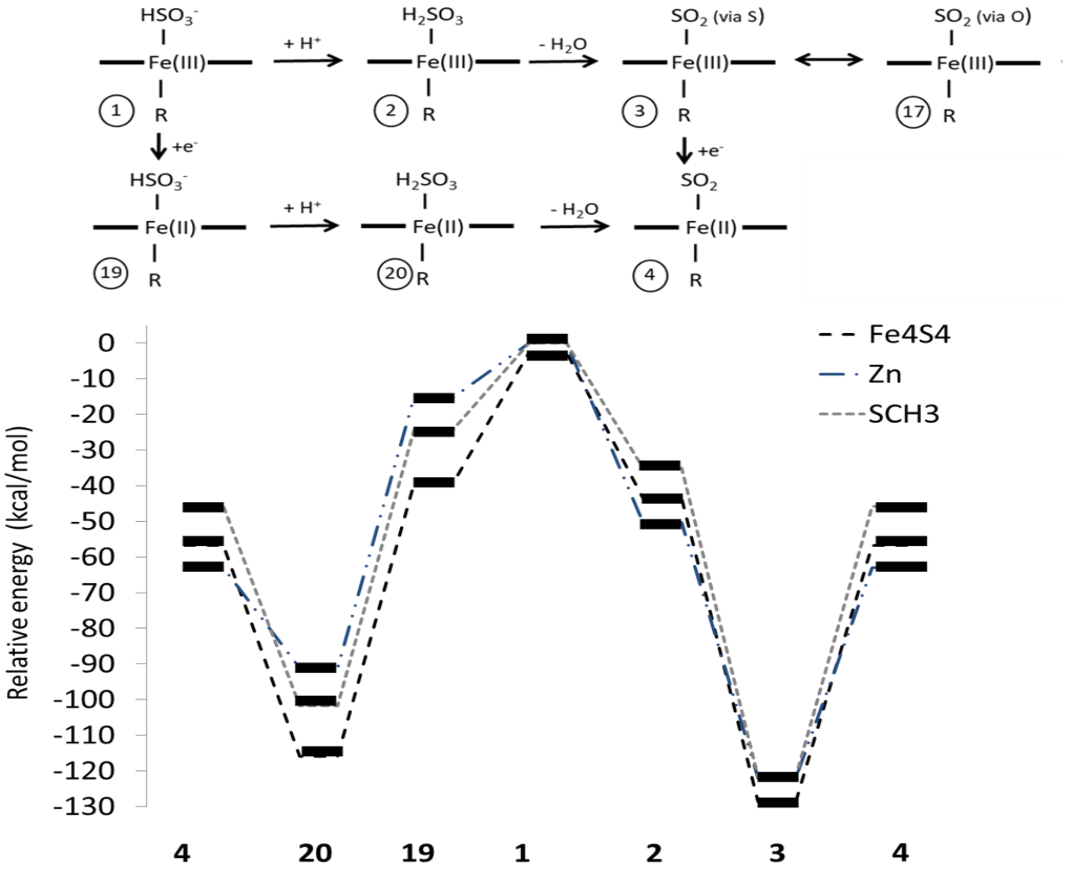

Figure 83. The **1-2-3-4** and **1-19-20-1** pathways.

The first stage of the SiR reaction mechanism implies the transformation of the HSO_3^- substrate (from intermediate **1**) into an SO_2 adduct bound to a ferrous siroheme (intermediate **4**). This can be achieved by a three-step process which involves reduction, protonation and the elimination of a water molecule from the substrate. It is not obvious in which order the protonation and reduction succeed, and for this reason two pathways implying different succession schemes had been proposed. As already mentioned in the introduction section, the first path starts with a protonation which leads to the elimination of a water molecule from the substrate and ends with an electron addition, i.e. the **1-2-3-4** path in Figure 83. The intermediates previously[82] labelled as **3** and **17** (cf. Figure 71)are numbered as one single intermediate in the present study, as they are linkage isomers; nevertheless, for the purpose of the ensuing thermodynamic considerations the original notation is retained. The second path starts with the addition of an electron followed by the addition of a proton and end with the elimination of a water molecule, i.e. the **1-19-20-4** pathway.

For all three models (thiolate, Zn, cluster), both pathways appear equally feasible. There may be a slight advantage to the **1-2-3-4** pathway, insofar as it starts with a more favorable **1->2** step than the corresponding **1→19** step of the **1-19-20-4** route. The metal cluster containing models bring an extra stabilization of the **1→2** step, with the Zn models being the most stabilizing of the two models. In the **1→19** equivalent, the effect of the Zn cluster is less stabilizing than of the simple, clusterless model. However, the Fe_4S_4 cluster adds an extra stabilizing effect when compared to the other two models and reaches a 39.5 kcal/mol stabilization. This value is comparable with the 43.6 kcal/mol involving the **1→2** (cubane) step and thus there is no real reason at this point for which SiR should prefer one route over the other. The next two steps develop a thermodynamic trap in both pathways. Thus, in the first pathway the thermodynamic trap is represented by intermediate **3,** while in the second by intermediate **20.** Both steps are favorable in terms of energy stabilization and both require energy consumption in order to reach intermediate **4.** Again, the cubane models feature the most stabilizing effect in both the **2→3** and the **19→20** steps, while the Zn model offers the least stabilizing effect in the latter step. At first glance, the **1-2-3-4** route seems more favourable as its **2→3** step implies 85 kcal/mol stabilization (in the cubane models) while **19→20** a slightly less 76.4 kcal/mol. However, the more stabilized the thermodynamic trap is, the more energy would be required for the enzyme to step out of it. Thus, the energetic advantage of the **2→3** becomes a burden in the **3→4** step as now the enzyme would require a 72 kcal/mol energy input to reach intermediate **4** via this route, compared to the lower 55.9 kcal/mol energy input required by the **20→4** step. Nevertheless, the required energy to overcome the thermodynamic trap of intermediate **3** can be supplied by the cubane cofactor. The cubane cluster modulates a 1+/2+ redox potential that, under the same level of theory, is computed to be -192.6 kcal/mol. Thus, the oxidation of $[Fe_4S_4]^+$ to $[Fe_4S_4]^{2+}$ will inject the transferred electron into the siroheme-adduct complex with an amount of energy that is more than twice the energy of the **3→4** barrier. On the other hand, by implying a proton transfer, the **20→4** step would require the enzyme to consume a high amount of energy in order to overcome the **20** thermodynamic trap.

Consequently it is more likely that the reaction mechanism would proceed via the **1-2-3-4** pathway.

Interestingly, in the vacuum models (cf. Figure 142.) the **1-19-20-4** pathway is found to be inhibited in all three types of models. The **1→19** step requires from the enzyme an ~80 kcal/mol energy input in the Zn models and ~50 kcal/mol the other two models. The **1-19-20-4** pathway offers a good example of the importance of the protein environment within the enzyme catalytic cycle.

In principle, the **3** thermodynamic trap could be evaded through a proton addition as well. This would eventually lead to intermediate **18** which, in both metal models, is slightly more stabilized than intermediate **4** (cf. Figure 72). However, even though this route would imply a lower thermodynamic barrier than the **3→4** step, it will still require the enzyme to consume energy in order to provide the proton addition (similar to the **19→4** step). Thus it is more likely that this route will also be avoided.

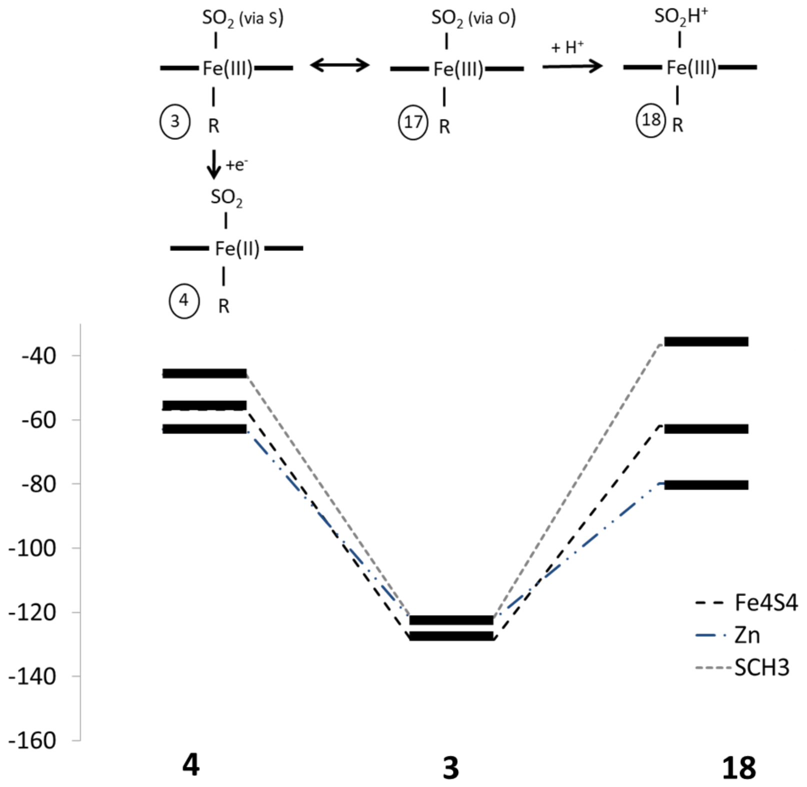

Figure 84. Intermediate **3** as a crossroad.

Arriving at intermediate **8,** the reaction can proceed via multiple paths in order to arrive to intermediate **11 - an** intermediate that, after losing a water molecule, will lead to the first sulfide-containing intermediate, **12.** In previous calculations[82] on smaller heme-thiolate (not siroheme) models, protonation of intermediate **8**leading to the formation of intermediate **21** was found to be unlikely. Similar, our vacuum computed results of the clusterless models also reveal the **8→21** step to be clearly disfavored thermodynamically. However, the metal clusters stabilize the **21** intermediate to the point that the **8→21** step becomes accessible. When computed in the solvent environment, the **8→21** step becomes accessible even in the clusterless model. Nevertheless, the 8→9 is even more favored thermodynamically and is thus proposed to be the main route within the SiR cycle, as opposed to **8→2.**

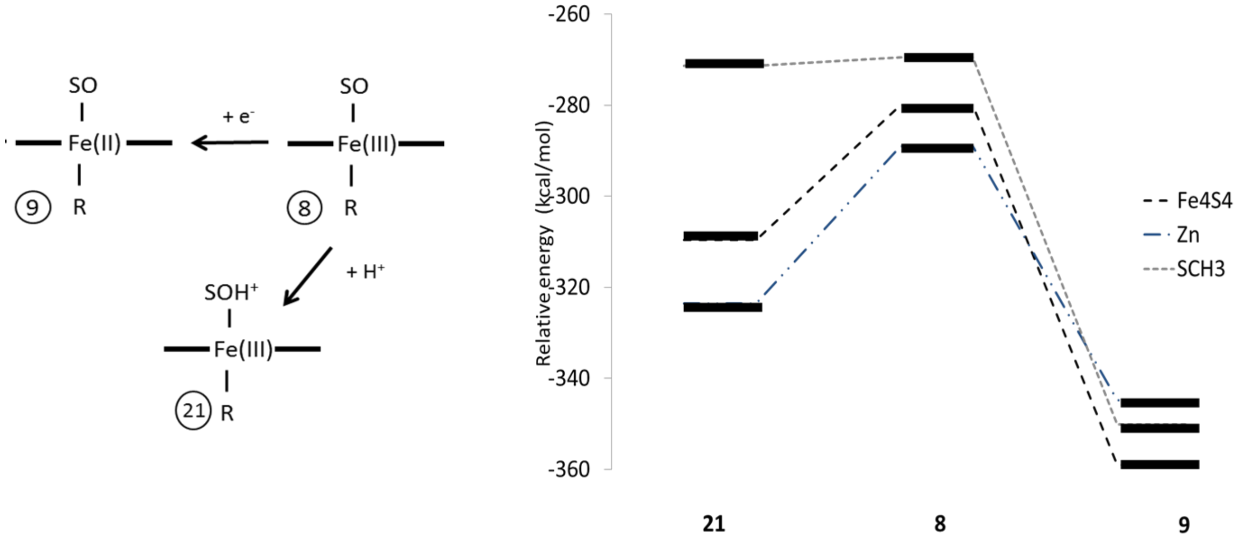

Figure 85. Intermediate **8** as a crossroad.

From intermediate **9** the reaction can proceed (cf. Figure 74) via an electron addition (i.e. intermediate **10**) or a proton addition (i.e. intermediate **22**) to reach intermediate **11.** Compared to the clusterless model, the Zn variant destabilizes intermediate **10** while the addition of the cubane stabilizes this intermediate. In the corresponding **22** intermediate of the **9-22-11** path, both metal models stabilize the intermediate when compared to the clusterless model. The protein environment facilitates the **9-10-11** path by stabilizing the **9→10** step. All three models find this step to be energy-demanding when performed in vacuum conditions. If, as suggested by Figure 74, **9-10-11** and **9-22-11** are both equally feasible (though this is also subject to the acidity of the proton donor and to the redox potential of the incoming electron), one may expect either that they both occur simultaneously, or in a concerted manner.

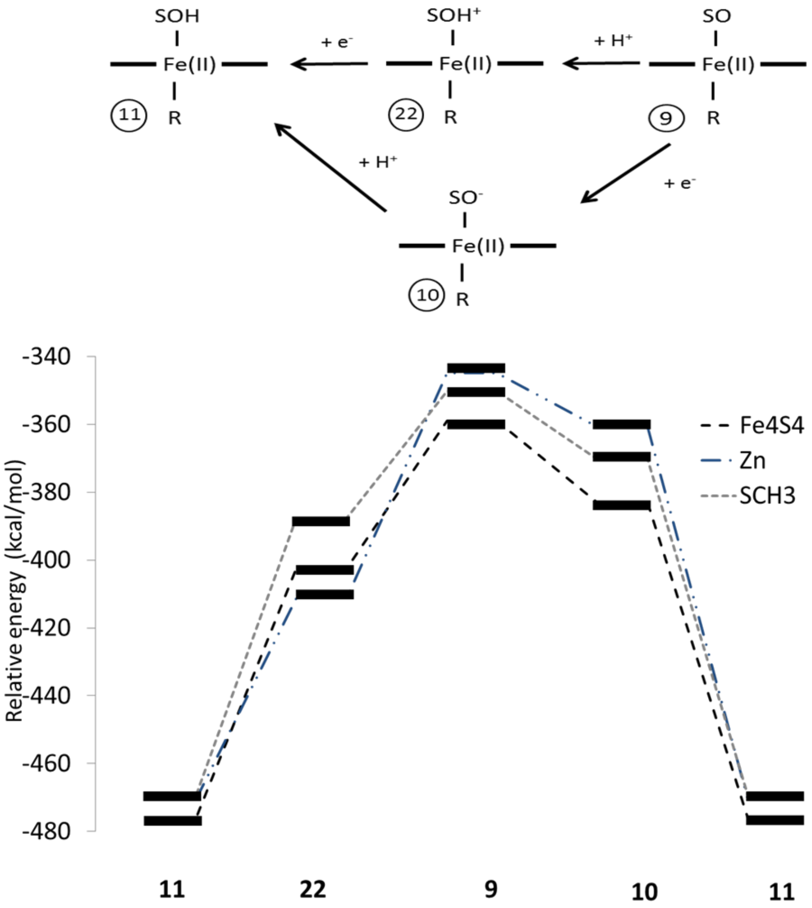

Figure 86. The **9-10-11** and **9-22-11** pathways.

4.3.4 Conclusions

Several cases of substrate linkage isomerism were identified along the SiR catalytic cycle. Among them, the sulfite adducts represent an interesting case, given that it was revealed that they prefer binding to the siroheme via the oxygen atom rather than sulfur. This is opposed to the case seen in the protein crystal structure, where the substrate coordinates via the S atom to the siroheme Fe. The cubane cluster diminishes the energetic difference between the two linkage isomers and thus it is expected to ease the protein’s effort to accommodate the S-bond isomer. This linkage isomer would be required for the catalytic cycle, as the S atom needs to be retained at the Fe until the last step of the reductive process. The tuning of hydrogen bonding by the amino acid residues present at the SiR active site pocket may further facilitate the needed bonding via S atom of these adducts. The SO_2 ligand can also engage in linkage isomerism, and also manifests a preference to binding via the O atom. With regards to this ligand, the cubane cofactor seems to play an important role as it favors the stabilization of the S-bonded isomer (while, as pointed above, it was also found to *correct* the substrate binding of the SO_2H adduct). On the othet hand, in the SO containing intermediates the two linkage isomers are essentially degenerate and the cubane cofactor fails to over-stabilize the S-bonded isomer.

Redox isomerism was noted in the sulfide containing intermediates. The key notable effect of the cubane is that the Compound I – like species, **12**, in fact has the second oxidizing equivalent on the cubane rather than of the porphyrin or on the axial thiolate. The cubane on the other hand has a lower effect on the structure of the Fe=S moiety – at most slightly altering its spin state preference.

The SiR catalytic cycle is expected to commence via the **1-2-3-4** pathway and avoid the **1-19-20-4** that implies an energetic input from the enzyme. From the same energetic consideration, the **3→8** is expected to be avoided and thus the reaction should continue via the **4-5-6** pathway. Onwards intermediate **8**, the reaction can proceed via three possible pathways: **8-9-10-11, 8-9-22-11** and **8-21-22-11.** All three involve proton and electron addition processes (and no water elimination) and differ among each other by the succession of these processes. This might offer the enzyme extra flexibility regarding the way in which the final O atom present in the substrate can be eliminated. In general the cubane cluster stabilizes intermediates and thus promotes the SiR catalytic reaction. The protein environment was noted to crucially stabilize some intermediates that were revealed to be highly energetically in vacuum conditions. Such cases were encountered in the **1→19**, **8→21** and **9→10** steps. Based on the newly obtained insights, the SiR reaction mechanism has been updated in Figure 87.

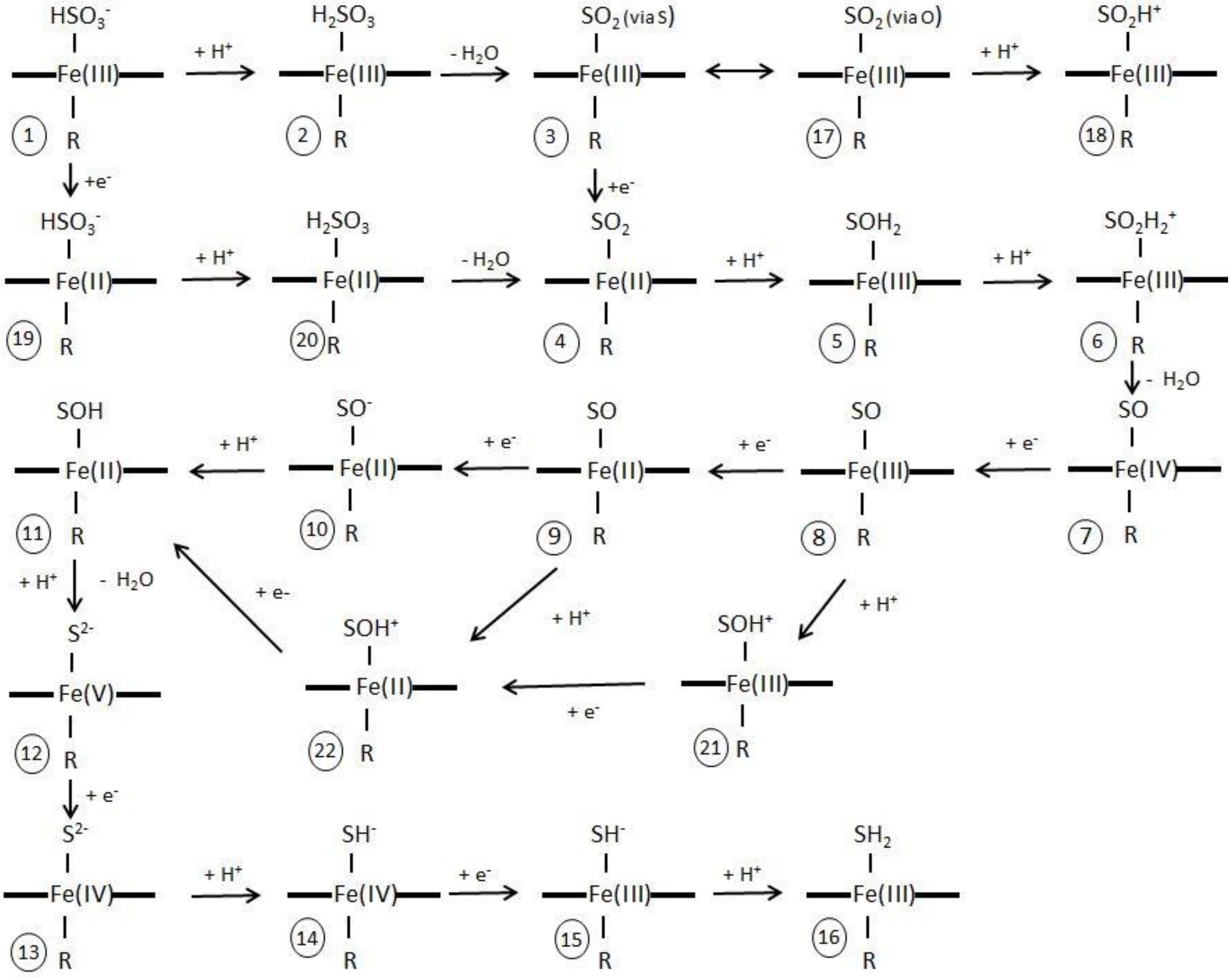

Figure 87. Updated SiR reaction mechanism.

4.4 Chapter Conclusions

We have shown that the specific porphyrin modification that the siroheme possesses, compared to the ubiquitous heme, induces effects that can be exploited by the sulfite reductase enzyme. We have first shown that by reducing its ring conjugation, siroheme reduces the ligand field interaction between its central Fe atom and the vicinal N atoms. The distribution of charge on the latter atoms becomes asymmetrical, the ligand-ligand and ligand-metal distances are increased and overall all these aspects lead to a better accommodation of the high-spin Fe species within the porphyrin ring. Also, the reduction potential of the siroheme Fe becomes more negative. The *Pars energetica: The importance of the siroheme modification* subchapter dealing with these *διάνοια* aspects has been published in the Journal of Inorganic Biochemitry.[177]

A διάνοια → επιστήμη transition has been made in the following subchapter. Here it was shown that the ultimate reason behind SiR's siroheme adoption lies in the latter's tuning capabilities of the electron transfer incoming from the cubane cofactor. Thus, by inhibiting routes that imply the edge of the porphyrin, the charge transfer rate from the cubane to the central $Fe_{siroheme}$ is increased and the porphyrin is kept in a radical-free state that, in turn, makes it less susceptible in reacting with radical intermediates and solvent molecules. The *Pars ballistica: Why does sulfite reductase employ siroheme?* subchapter dealing with this *επιστήμη* result was published in the Chemical Communications journal.[180]

The cubane cofactor was also shown to influence the SiR reaction mechanism. Thus, besides providing the electrons needed for substrate reduction, the cubane also stabilizes the SiR intermediates and in some cases corrects the binding of adducts that are likely to employ linkage isomerism. By promoting the substrate to bind via the S atom to the (siro)heme, the sulfur is retained at the active site until it is fully reduced at the end of the catalytic cycle. The obtained results of the *Pars mechanistica: SiR reaction mechanism* subchapter are currently prepared for publication; so far, we have published a paper on a very small number of the clusterless intermediate models.[80]

5 Epilogue

Motto:

“Whereof one cannot speak, thereof one must be silent.”[*]

Ludwig Wittgenstein

---

[*] Proposition 7 (and the last) of Wittgenstein’s *Tractatus Logico-Philosophicus.*

During the PhD period we have managed to publish 9 articles, cited 18 times. Our most recent one, the *ChemComm* paper, after just three months since its publication, was cited[181] by a review article when discussing the siroheme prosthetic group (as reason for its adoption).

The driving force behind this thesis' start was the understanding of the chemical bond. We have come to understand that the chemical bond belongs to that class of things that are not. Consequently, all other *unicorns*[182] derived from it, such as resonance, conjugation, hyperconjugation, covalent bonding, donor-acceptor bond, agostic interactions, π bonding etc, share the same non-existence. From the quantum mechanical point of view, chemical bonds simply do not exist, as no operator is associated with this quantity and therefore no observable quantity either. At best, chemical bond information is chopped out of the wavefunction. It is far more accurate to state that the chemical bond is an *εικών* of the wavefunction: it is the outcome of the wavefunction projection unto the chemical language. Deeper reasoning (cf. section 2.4.3.2.1) implies their viewing as local, stabilized, Fermi heaps. In general, a chemical system is better seen as an electronic density disturbed by the presence of positive nuclei. The fundamental disturbance caused by the doping of the electronic density with positive point-like nuclei is found in the system's energetic behavior: if in the absence of nuclei the electrons adopted a continuous range of energetic states, in their presence the electrons will adopt a discrete range of energetic states. This, corroborated with symmetry requirements imposed by Pauli's spin statistics, marks the point from where chemistry commence.

To emphasize the illusory character that the traditional chemical bond concept possesses we will further compare it, in a ludic manner, with the *Battle of the 300 Champions.* Fought in 546 BC between the Greek city-states of Argos and Sparta, this battle has a disputed outcome as both belligerents claimed victory at its end. Instead of engaging in a full strength battle, the combatant armies agreed to each deploy their 300 best soldiers in a death match in which victory would be acclaimed by the side that at the end of the battle will have surviving soldiers that could to tell the outcome. Both armies retreated to their cities (so that neither side could interfere in the battles itself) and the 600 champions were left alone to fight on the field of Thyrea. At the end of the battle there were only two Argos soldiers still standing - and they consequently retreated home acclaiming victory. What they overlooked, however, was an injured Spartan that, after seeing them gone, managed to survive enough to reach home and thus claim victory as well. Claiming that the chemical bond, for instance, in the O_2 molecule is the outcome of 4 electrons forming two covalent bonds is similar to stating that the Battle of the 300 Champions was fought by the 3 surviving hoplites. In both cases, the contribution of other electrons/hoplites is neglected. Similar to how the outcome of the battle is a consequence of shed blood, so is the chemical bond a consequence of annihilated wavefunction. The electronic density present between the two O atoms forming the O_2 - molecule exceeds by far the amount required by the presence of 4 electrons. The non manifesting excess simply annihilates itself by having opposing wavefunction sign in that region. But this does not mean that it is not there; its manifestation in terms of what we called chemical bond is simply canceled out. Assigning a O=O bond to the O_2 molecule resembles the forgotten blood of what became nameless soldiers that fought at Thyrea, while the “=” in O=O resembles the remembered names of surviving soldiers. Indeed, an anthropic behavior and therefore nothing more than an anthropic construct .

In the spirit of this chapter’s motto, we will not speak of things not finished but rather just mention them as directions for future studies. Thus, our further studies, sprung from this thesis, are two folded. On the metallaborane perspective, we have in preparation results of the 9 and 10 vertices containing systems. Furthermore, we intend to investigate their possible applicability as single-molecular junctions. On the sulfite reductase perspective, we have in preparation a *Pars magnetica* investigation in which the interfactorial magnetic interactions are studied. Furthermore, we plan to investigate the effect that the siroheme modification has on the interfactorial quantum entanglement. Also, a line of study is in work, where sulfite reactions with systems related to the (siro)heme are investigated at the DFT level – in collaboration with experimentalists. These are prospects that we look forward to further exploring, both because of their practical implications and because of the challenges they offer on a fundamental level and which in themselves offer strong motivation to those sharing a passion in science even when the practical applications are not immediately forthcoming; after all, as once said by Bertrand Russell, *there is much pleasure to be gained from useless knowledge.*

6 Appendix

Motto:

All things are numbers.

(Pythagorean saying)

6.1 Metallaboranes

6.1.1 5 vertices

6.1.1.1 $Cp_2M_2B_3H_7$ (M=Pd,Pt) systems

Table 64. Distances table for the lowest-lying Cp2Pd2B3H7 structures after M06L/6-311G(d,p) optimization. Included are the ZPcorrected E (a.u.), relative energy (kcal/mol), symmetry and WBI.

<table>
<tr>
<td>
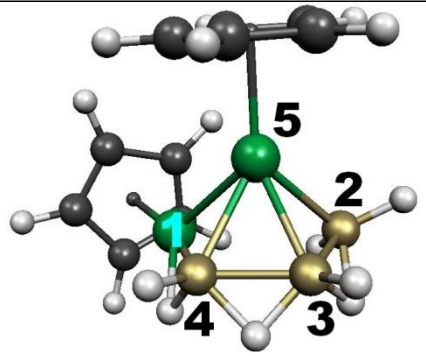

1. Pd2B3-1 -721.617401
0.0 WBI 0.33
</td>
<td>
<table>
<tr><th></th><th></th><th>1</th><th>2</th><th>3</th><th>4</th><th>5</th></tr>
<tr><td>1</td><td>Pd</td><td>0.000000</td><td></td><td></td><td></td><td></td></tr>
<tr><td>2</td><td>B</td><td>3.085625</td><td>0.000000</td><td></td><td></td><td></td></tr>
<tr><td>3</td><td>B</td><td>3.310808</td><td>1.796949</td><td>0.000000</td><td></td><td></td></tr>
<tr><td>4</td><td>B</td><td>2.217187</td><td>2.882527</td><td>1.816760</td><td>0.000000</td><td></td></tr>
<tr><td>5</td><td>Pd</td><td>2.603519</td><td>2.173146</td><td>2.105774</td><td>2.130534</td><td>0.000000</td></tr>
</table>
Pd1-H-B4 Pd1-H 1.71 B4-H 1.31
B2-H-B3 B2-H 1.34 B3-H 1.29
B3-H-B4 B3-H 1.29 B4-H 1.35
B2-H 1.19
</td>
</tr>
<tr>
<td>
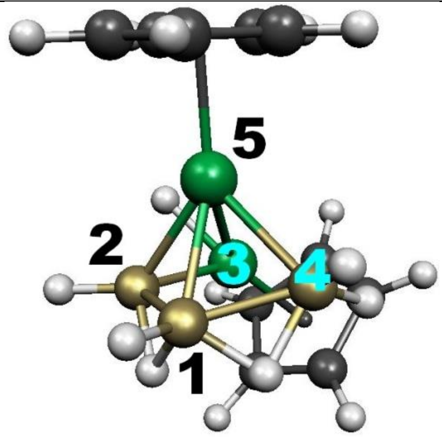

2. Pd2B3-2 -721.603220
+8.9 WBI 0.31
</td>
<td>
<table>
<tr><th></th><th></th><th>1</th><th>2</th><th>3</th><th>4</th><th>5</th></tr>
<tr><td>1</td><td>B</td><td>0.000000</td><td></td><td></td><td></td><td></td></tr>
<tr><td>2</td><td>B</td><td>1.801665</td><td>0.000000</td><td></td><td></td><td></td></tr>
<tr><td>3</td><td>Pd</td><td>3.190771</td><td>2.060173</td><td>0.000000</td><td></td><td></td></tr>
<tr><td>4</td><td>B</td><td>1.797506</td><td>2.957120</td><td>3.233373</td><td>0.000000</td><td></td></tr>
<tr><td>5</td><td>Pd</td><td>2.127885</td><td>2.091344</td><td>2.633775</td><td>2.167422</td><td>0.000000</td></tr>
</table>
Pd3-H-Pd5 Pd3-H 1.55 Pd5-H 2.66
B1-H-B2 B1-H 1.30 B2-H 1.36
B1-H-B4 B1-H 1.29 B4-H 1.34
B3-H 1.55
</td>
</tr>
<tr>
<td>
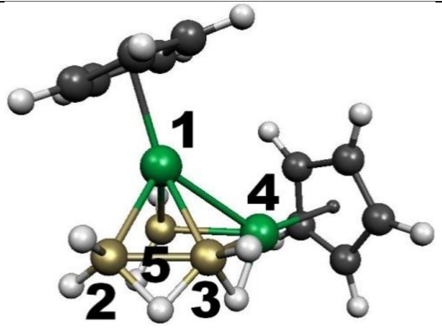

3. Pd2B3-3 -721.599168
+11.4 WBI 0.29
</td>
<td>
<table>
<tr><th></th><th></th><th>1</th><th>2</th><th>3</th><th>4</th><th>5</th></tr>
<tr><td>1</td><td>Pd</td><td>0.000000</td><td></td><td></td><td></td><td></td></tr>
<tr><td>2</td><td>B</td><td>2.187476</td><td>0.000000</td><td></td><td></td><td></td></tr>
<tr><td>3</td><td>B</td><td>2.144162</td><td>1.790523</td><td>0.000000</td><td></td><td></td></tr>
<tr><td>4</td><td>Pd</td><td>2.575369</td><td>3.551225</td><td>2.259891</td><td>0.000000</td><td></td></tr>
<tr><td>5</td><td>B</td><td>2.141670</td><td>2.959917</td><td>2.887507</td><td>2.161034</td><td>0.000000</td></tr>
</table>
Pd4-H-B3 Pd4-H 1.72 B3-H 1.33
B2-H-B3 B2-H 1.33 B3-H 1.30
B2-H 1.19
B5-H 1.19
</td>
</tr>
</table>

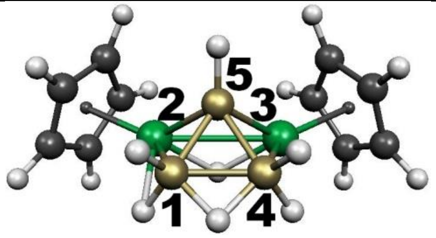 4. Pd2B3-4 -721.597436 +12.5 Cs WBI 0.24	1 2 3 4 5 1 B 0.000000 2 Pd 2.274305 0.000000 3 Pd 3.191363 2.772000 0.000000 4 B 1.808200 3.191363 2.274305 0.000000 5 B 1.789033 2.088456 2.088456 1.789033 0.000000 Pd2-H-Pd3 Pd2-H 1.73 Pd3-H 1.73 Pd2-H-B1 Pd2-H 2.06 B1-H 1.23 Pd3-H-B4 Pd3-H 2.06 B4-H 1.23 B-H-B4 B1-H 1.31 B4-H 1.31
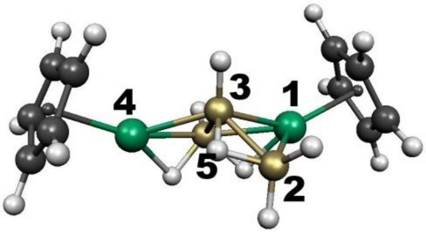 5. Pd2B3-5 -721.592367 +15.7 WBI 0.09	1 2 3 4 5 1 Pd 0.000000 2 B 2.170314 0.000000 3 B 2.180305 1.840023 0.000000 4 Pd 3.870266 3.517646 2.181764 0.000000 5 B 2.164551 2.943460 1.862634 2.095150 0.000000 Pd1-H-B5 Pd1-H 1.70 B5-H 1.36 Pd4-H-B5 Pd4-H 1.75 B5-H 1.32 B2-H-B3 B2-H 1.31 B3-H 1.30

Table 65. Distances table for the lowest-lying Cp2Pt2B3H7 structures after M06L/6-311G(d,p) optimization. Included are the ZPcorrected E (a.u.), relative energy (kcal/mol), symmetry and WBI.

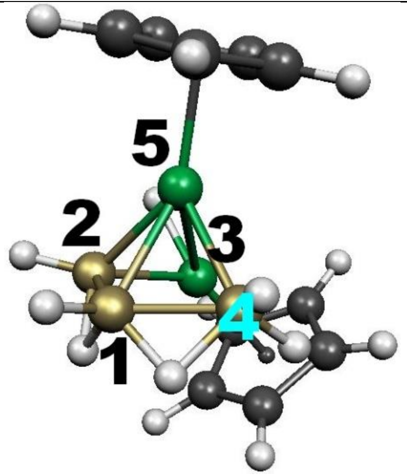 **1. Pt2B3-1 -704.550069** **0.0 WBI 0.39**	1 2 3 4 5 1 B 0.000000 2 B 1.825908 0.000000 3 Pt 3.271613 2.061276 0.000000 4 B 1.820685 2.993440 3.356315 0.000000 5 Pt 2.118914 2.106141 2.682551 2.164588 0.000000 B1-H-B2 B1-H 1.30 B2-H 1.36 B1-H-B4 B1-H 1.29 B4-H 1.34 Pt3-H 1.56 B4-H 1.19

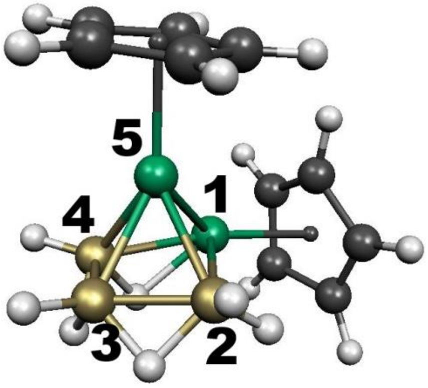 2. Pt2B3-2 -704.543691 +4.0 WBI 0.39	1 2 3 4 5 1 Pt 0.000000 2 B 3.261144 0.000000 3 B 3.395957 1.821034 0.000000 4 B 2.190555 2.916861 1.835894 0.000000 5 Pt 2.667730 2.169761 2.104002 2.118873 0.000000 Pt1-H-B4 Pt1-H 1.69 B4-H 1.37 B2-H-B3 B2-H 1.34 B3-H 1.29 B3-H-B4 B3-H 1.29 B4-H 1.35 B2-H 1.19
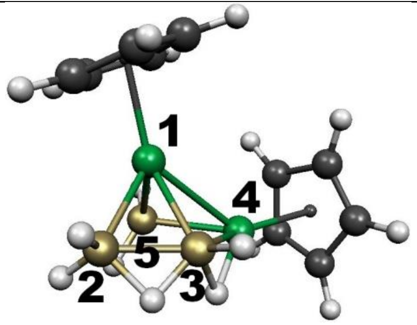 3. Pt2B3-3 -704.539359 +6.7 WBI 0.35	1 2 3 4 5 1 Pt 0.000000 2 B 2.175748 0.000000 3 B 2.122648 1.811868 0.000000 4 Pt 2.631356 3.544879 2.229566 0.000000 5 B 2.155343 2.991919 2.912852 2.173451 0.000000 Pt4-H-B3 Pt4-H 1.67 B3-H 1.43 B2-H-B3 B2-H 1.34 B3-H 1.29 B2-H 1.19 B5-H 1.19
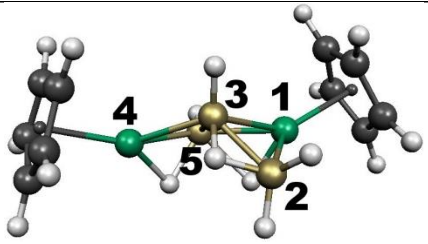 4. Pt2B3-4 -704.527206 +14.4 WBI 0.08	1 2 3 4 5 1 Pt 0.000000 2 B 2.176314 0.000000 3 B 2.189414 1.865636 0.000000 4 Pt 3.735421 3.515834 2.158830 0.000000 5 B 2.111720 3.049429 1.914473 2.017199 0.000000 Pt1-H-B5 Pt1-H 1.60 B5-H 1.77 Pt4-H-B5 Pt4-H 1.67 B5-H 1.49 B2-H-B3 B2-H 1.31 B3-H 1.30
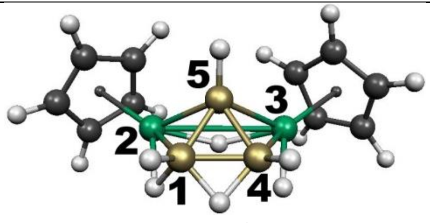 5. Pt2B3-5 -704.526146 +15.0 Cs WBI 0.19	1 2 3 4 5 1 B 0.000000 2 Pt 2.184022 0.000000 3 Pt 3.242371 3.301928 0.000000 4 B 1.736806 3.243039 2.188807 0.000000 5 B 1.747144 2.151078 2.157887 1.747875 0.000000 Pt2-H-Pt3 Pt2-H 1.79 Pt3-H 1.75 Pt2-H-B1 Pt2-H 1.69 B1-H 1.41 Pt3-H-B4 Pt3-H 1.69 B4-H 1.41 B1-H-B4 B1-H 1.33 B4-H 1.33

6.1.1.2 $Cp_2M_2B_3H_7$ (M=Rh,Ir) systems

Table 66. Distances table for the lowest-lying $Cp_2Rh_2B_3H_7$ structures after M06L/6-311G(d,p) optimization. Included are the ZPcorrected E (a.u.), relative energy (kcal/mol), symmetry and WBI.

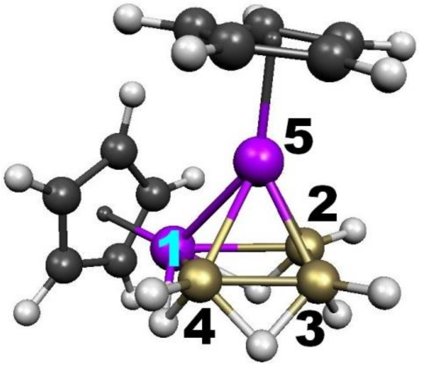 **1. -686.992314 0.0 Cs** **WBI 0.40**	1 2 3 4 5 1 Rh 0.000000 2 B 2.288707 0.000000 3 B 3.126074 1.799341 0.000000 4 B 2.292958 2.599439 1.798650 0.000000 5 Rh 2.615614 2.105862 2.090775 2.105200 0.000000 Rh1-H-B2 Rh1-H 1.72 B2-H 1.33 Rh1-H-B2 Rh1-H 1.72 B2-H 1.33 B2-H-B3 B2-H 1.35 B3-H 1.31 B4-H-B3 B4-H 1.34 B3-H 1.31
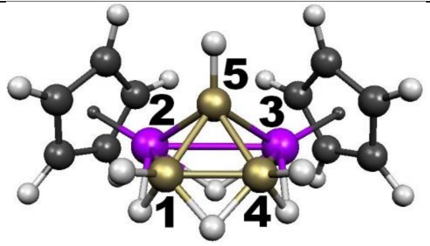 2. -686.988457 +2.4 Cs WBI 0.30	1 2 3 4 5 1 B 0.000000 2 Rh 2.210348 0.000000 3 Rh 3.111824 2.743800 0.000000 4 B 1.748600 3.111824 2.210348 0.000000 5 B 1.738504 2.125228 2.125228 1.738504 0.000000 Rh2-H-Rh3 Rh2-H 1.75 Rh3-H 1.75 Rh2-H-B1 Rh2-H 1.72 B1-H 1.33 Rh3-H-B4 Rh3-H 1.72 B4-H 1.33 B1-H-B4 B1-H 1.32 B4-H 1.32
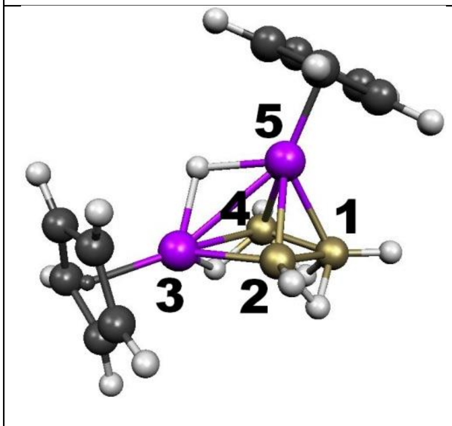 3. -686.981545 +6.8 WBI 0.29	1 2 3 4 5 1 B 0.000000 2 B 1.792678 0.000000 3 Rh 3.069735 2.089166 0.000000 4 B 1.796566 2.518671 2.314343 0.000000 5 Rh 2.115246 2.085611 2.705171 2.132937 0.000000 Rh3-H-Rh5 Rh3-H 1.71 Rh5-H 1.76 Rh3-H-B4 Rh3-H 1.74 Rh4-H 1.30 B1-H-B4 B1-H 1.30 B4-H 1.34 B1-H-B2 B1-H 1.29 B2-H 1.37

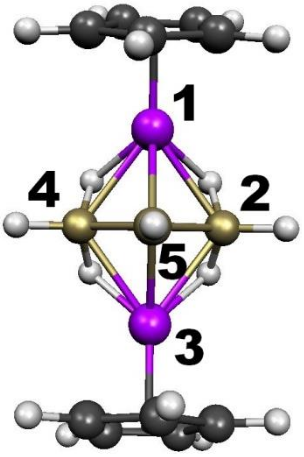

4. -686.971052 +13.3 C_{2v}
WBI 0.13

		1	2	3	4	5
1	Rh	0.000000				
2	B	2.249467	0.000000			
3	Rh	3.620600	2.247678	0.000000		
4	B	2.247678	2.664802	2.249467	0.000000	
5	B	2.119025	1.767524	2.119025	1.767524	0.000000

M-H-B M-H 1.78 B-H 1.31

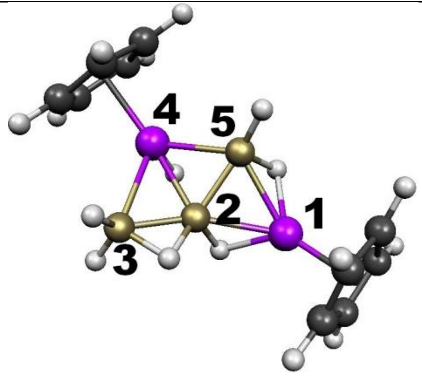

5. -686.943349 +30.7
WBI 0.14

		1	2	3	4	5
1	Rh	0.000000				
2	B	2.085602	0.000000			
3	B	3.762870	1.737832	0.000000		
4	Rh	3.691516	2.021937	2.220654	0.000000	
5	B	2.126137	1.780573	3.171653	2.078465	0.000000

Table 67. Distances table for the lowest-lying $Cp_2Ir_2B_3H_7$ structures after M06L/6-311G(d,p) optimization. Included are the ZPcorrected E (a.u.), relative energy (kcal/mol), symmetry and WBI.

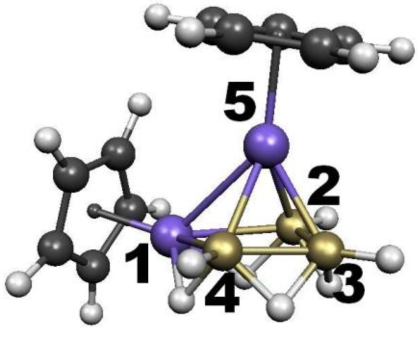

1. Ir2B3-1 -674.610910 a.u.
0.0 kcal/mol Cs WBI 0.42

		1	2	3	4	5
1	Ir	0.000000				
2	B	2.288238	0.000000			
3	B	3.154672	1.817622	0.000000		
4	B	2.292945	2.590833	1.816214	0.000000	
5	Ir	2.685530	2.103084	2.097907	2.106405	

Ir1-H-B2	Ir1-H 1.69	B2-H 1.40
Ir1-H-B4	Ir1-H 1.68	B4-H 1.40
B2-H-B3	B2-H 1.50	B3-H 1.31
B3-H-B4	B3-H 1.31	B4-H 1.35

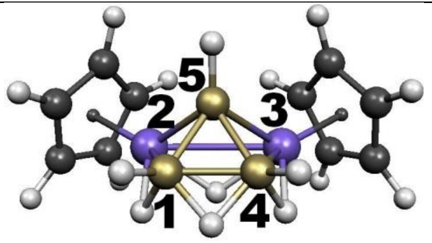

2. Ir2B3-2 -674.605693
+3.3 Cs WBI 0.33

		1	2	3	4	5
1	B	0.000000				
2	Ir	2.212843	0.000000			
3	Ir	3.125033	2.797400	0.000000		
4	B	1.740600	3.125033	2.212843	0.000000	
5	B	1.724869	2.157560	2.157560	1.724869	

Ir2-H-Ir3 Ir2-H 1.78 Ir3-H 1.78
Ir2-H-B1 Ir2-H 1.70 B1-H 1.39
Ir3-H-B4 Ir3-H 1.70 B4-H 1.39
Ir1-H- Ir4 Ir1-H 1.33 Ir4-H 1.33

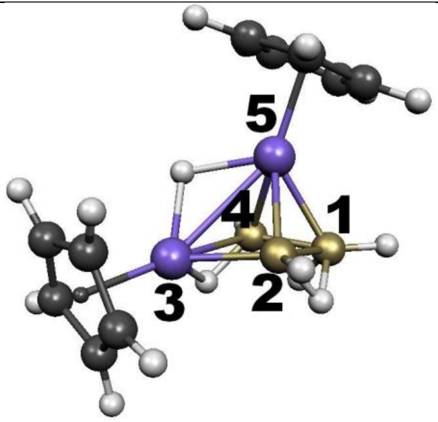

3. Ir2B3-3 -674.597810 +8.2
WBI 0.31

		1	2	3	4	5
1	B	0.000000				
2	B	1.809414	0.000000			
3	Ir	3.105776	2.101830	0.000000		
4	B	1.808662	2.533696	2.349558	0.000000	
5	Ir	2.122327	2.122282	2.763847	2.138065	

Ir3-H-Ir5 Ir3-H 1.73 Ir5-H 1.80
Ir3-H-B4 Ir3-H 1.73 B4-H 1.32
B1-H-B2 B1-H 1.28 B2-H 1.37
B1-H-B4 B1-H 1.31 B4-H 1.34

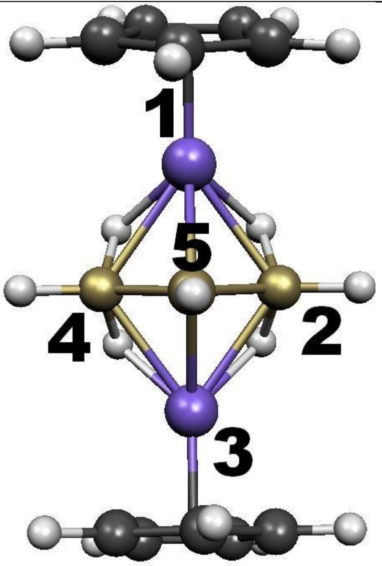

4. Ir2B3-4 -674.589126
+13.7 C_{2v} WBI 0.10

		1	2	3	4	5
1	Ir	0.000000				
2	B	2.257224	0.000000			
3	Ir	3.660401	2.255221	0.000000		
4	B	2.255221	2.638603	2.257224	0.000000	
5	B	2.161938	1.738450	2.161938	1.738450	

Ir1-H-B2 Ir1-H 1.76 B2-H 1.35
Ir1-H-B4 Ir1-H 1.76 B4-H 1.35
Ir3-H-B2 Ir3-H 1.76 B2-H 1.35
Ir3-H-B4 Ir3-H 1.76 B4-H 1.35

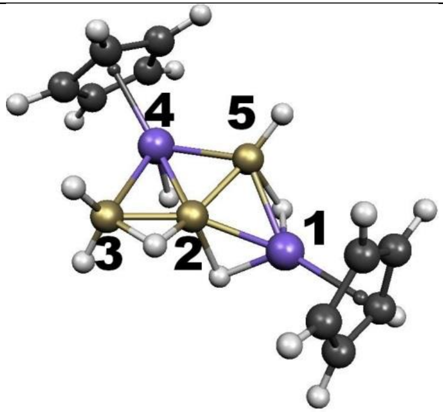 5. Ir2B3-5 -674.577540 +20.9 WBI 0.11	1 2 3 4 5 1 Ir 0.000000 2 B 2.053244 0.000000 3 B 3.729152 1.741244 0.000000 4 Ir 3.658822 2.025632 2.221878 0.000000 5 B 2.123997 1.781119 3.248526 2.065155 Ir1-H-B2 Ir1-H 1.64 B2-H 1.65 Ir1-H-B5 Ir1-H 1.64 B5-H 1.62 B2-H-B3 B2-H 1.31 B3-H 1.34 Ir4-H 1.59

6.1.1.3 $Cp_2M_2B_3H_7$ (M=Ru,Os) systems

Table 68. Distances table for the lowest-lying $Cp_2Ru_2B_3H_7$ structures after M06L/6-311G(d,p) optimization. Included are the ZPcorrected E (a.u.), relative energy (kcal/mol), symmetry and WBI.

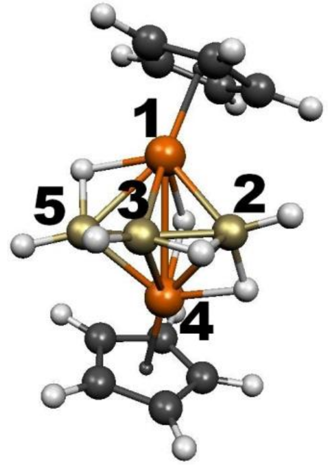 **1. Ru2B3-1 -655.655044 0.0** **WBI 0.33**	1 2 3 4 5 1 Ru 0.000000 2 B 2.087627 0.000000 3 B 2.273811 1.740950 0.000000 4 Ru 2.788496 2.161626 2.216283 0.000000 5 B 2.254602 2.881661 1.690872 2.170603 Ru1-H-Ru4 Ru1-H 1.78 Ru4-H 1.79 Ru1-H-B5 Ru1-H 1.69 B5-H 1.34 Ru4-H-B2 Ru4-H 1.73 B2-H 1.32 B2-H-B3 B2-H 1.33 B3-H 1.28
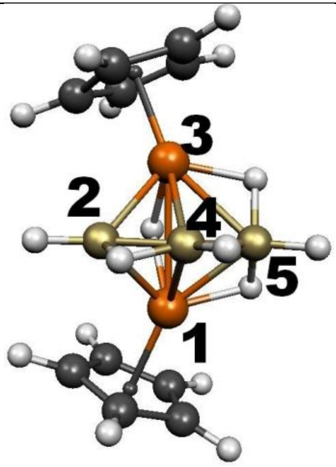	1 2 3 4 5 1 Ru 0.000000 2 B 2.162305 0.000000 3 Ru 2.790862 2.123218 0.000000 4 B 2.285484 1.650816 2.220348 0.000000 5 B 2.146021 2.863830 2.230408 1.774336 Ru1-H-Ru3 Ru1-H 1.79 Ru3-H 1.78 Ru1-H-B5 Ru1-H 1.69 B5-H 1.35 Ru3-H-B5 Ru3-H 1.69 B5-H 1.35 B2-H-B4 B2-H 1.32 B4-H 28

2. Ru2B3-2 -655.654042 +0.6
WBI 0.34

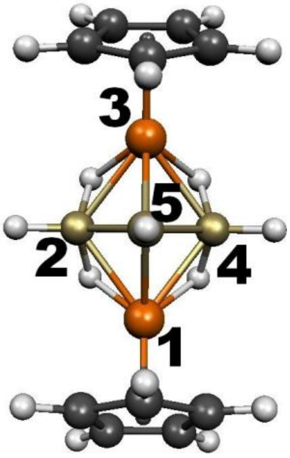

3. Ru2B3-3 -655.644692
+6.5 C_{2v} WBI 0.31

		1	2	3	4	5
1	Ru	0.000000				
2	B	2.191569	0.000000			
3	Ru	3.490200	2.191569	0.000000		
4	B	2.191509	2.633300	2.191509	0.000000	
5	B	2.068957	1.826597	2.068957	1.826524	

Ru1-H-B2 Ru1-H 1.71 B2-H 1.37
Ru1-H-B4 Ru1-H 1.71 B4-H 1.37
Ru3-H-B2 Ru3-H 1.71 B2-H 1.37
Ru3-H-B4 Ru3-H 1.71 B4-H 1.37

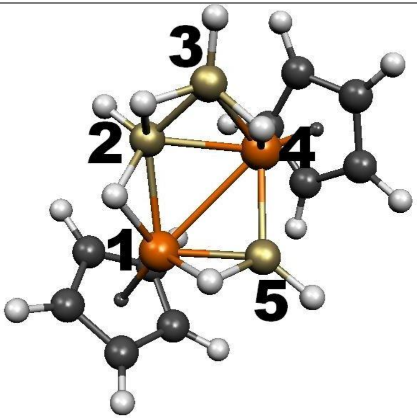

4. Ru2B3-4 -655.640794 +8.9
WBI 0.37

		1	2	3	4	5
1	Ru	0.000000				
2	B	2.170879	0.000000			
3	B	3.475032	1.755597	0.000000		
4	Ru	2.750072	2.213195	2.034963	0.000000	
5	B	2.028079	3.094321	3.407197	2.092405	

Ru1-H-B2 Ru1-H 1.70 B2-H 1.39
Ru1-H-B5 Ru1-H 1.74 B5-H 1.37
Ru4-H-B3 Ru4-H 1.78 B3-H 1.32
B2-H-B3 B2-H 1.42 B3-H 1.28

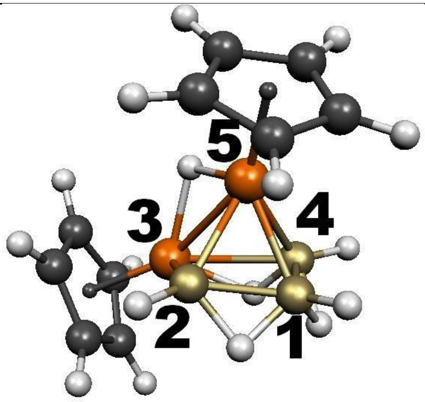

5. Ru2B3-5 -655.637966 +10.7
WBI 0.59

		1	2	3	4	5
1	B	0.000000				
2	B	1.810898	0.000000			
3	Ru	3.058189	2.184909	0.000000		
4	B	1.783592	2.636913	2.361740	0.000000	
5	Ru	2.140896	2.065130	2.612404	2.155360	

Ru3-H-Ru5 Ru3-H 1.77 Ru5-H 1.76
Ru3-H-B4 Ru3-H 1.77 B4-H 1.29
B1-H-B2 B1-H 1.29 B2-H 1.38
B1-H-B4 B1-H 1.28 B4-H 1.37

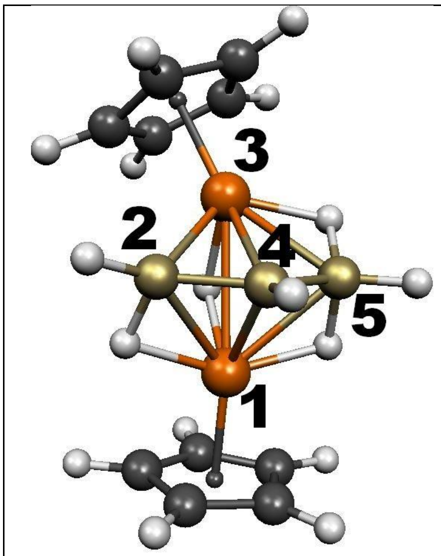 6. Ru2B3-6 -655.637855 +10.8 WBI 0.35	1 2 3 4 5 1 Ru 0.000000 2 B 2.252444 0.000000 3 Ru 2.779245 2.136590 0.000000 4 B 2.221901 1.647264 2.269262 0.000000 5 B 2.348429 2.903591 2.237051 1.648618 Ru1-H-Ru3 Ru1-H 1.76 Ru3-H 1.80 Ru1-H-B5 Ru1-H 1.73 B5-H 1.35 Ru1-H-B2 Ru1-H 1.75 B2-H 1.32 Ru3-H-B5 Ru3-H 1.76 B5-H 1.31
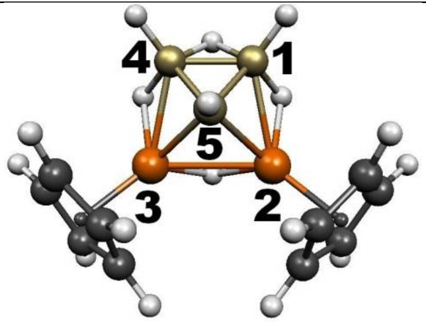 7. Ru2B3-7 -655.637608 +10.9 Cs WBI 0.72	1 2 3 4 5 1 B 0.000000 2 Ru 2.251423 0.000000 3 Ru 3.091037 2.592200 0.000000 4 B 1.730400 3.091027 2.251437 0.000000 5 B 1.736732 2.129119 2.129180 1.736732 Ru2-H-Ru3 Ru2-H 1.81 Ru3-H 1.81 Ru2-H-B1 Ru2-H 1.72 B1-H 1.34 Ru3-H-B4 Ru3-H 1.72 B4-H 1.34 B1-H-B4 B1-H 1.32 B4-H 1.32
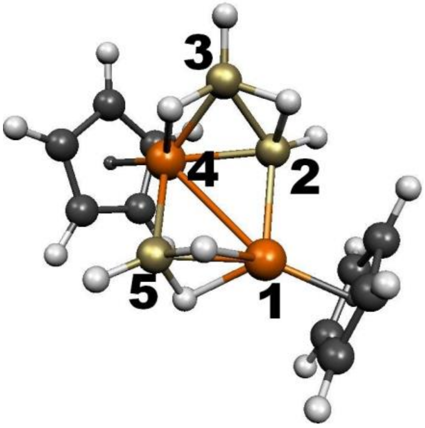 8. Ru2B3-8 -655.634610 +12.8 WBI 0.32	1 2 3 4 5 1 Ru 0.000000 2 B 2.184046 0.000000 3 B 3.410601 1.747947 0.000000 4 Ru 2.810598 2.093810 2.049231 0.000000 5 B 2.072928 3.148372 3.466984 2.187987 Ru1-H-B5 Ru1-H 1.77 B5-H 1.32 Ru1-H’-B5 Ru1-H’ 1.76 B5-H’ 1.33 Ru4-H-B3 Ru4-H 1.80 B3-H 1.30 B2-H-B3 B2-H 1.40 B3-H 1.30

Table 69. Distances table for the lowest-lying $Cp_2Ru_2B_3H_7$ structures after M06L/6-311G(d,p) optimization. Included are the ZPcorrected E (a.u.), relative energy (kcal/mol), symmetry and WBI.

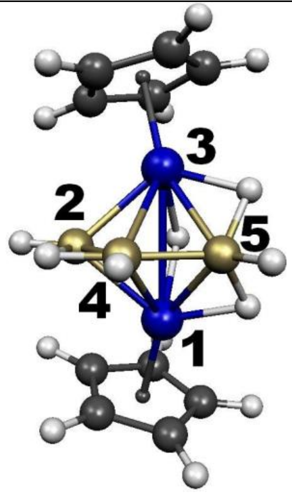 **1. -647.249915 0.0 WBI 0.36**	1 2 3 4 5 1 Os 0.000000 2 B 2.165784 0.000000 3 Os 2.857800 2.165417 0.000000 4 B 2.279764 1.656134 2.279240 0.000000 5 B 2.186676 2.835383 2.187570 1.755421 Os1-H-Os3 Os1-H 1.82 Os3-H 1.82 Os1-H-B5 Os1-H 1.70 B5-H 1.40 Os3-H-B5 Os3-H 1.70 B5-H 1.40 B2-H-B4 B2-H 1.33 B4-H 1.29
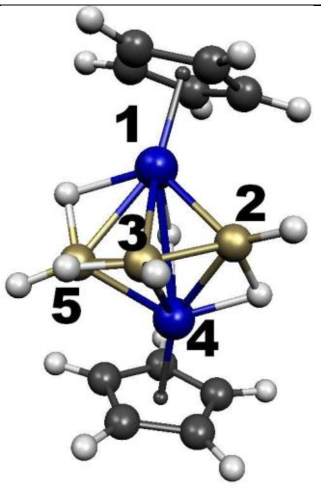 2. -647.249868 +0.03 WBI 0.34	1 2 3 4 5 1 Os 0.000000 2 B 2.113298 0.000000 3 B 2.279146 1.738894 0.000000 4 Os 2.853019 2.164346 2.262591 0.000000 5 B 2.264159 2.863320 1.689873 2.185771 Os1-H- Os4 Os1-H 1.82 Os4-H 1.82 Os1-H-B5 Os1-H 1.74 B5-H 1.35 Os4-H-B2 Os4-H 1.69 B2-H 1.38 B3-H-B5 B3-H 1.28 B5-H 1.32
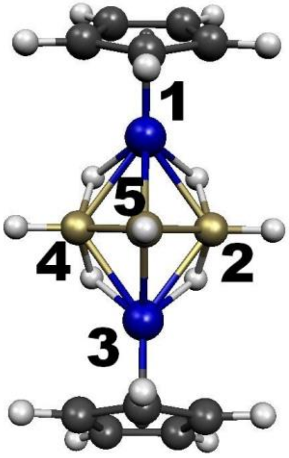 3. -647.244998 +3.1 C_{2v} WBI 0.28	1 2 3 4 5 1 Os 0.000000 2 B 2.192917 0.000000 3 Os 3.530600 2.192917 0.000000 4 B 2.192917 2.590000 2.192917 0.000000 5 B 2.099775 1.808083 2.099775 1.808083 Os1-H-B2 Os1-H 1.70 B2-H 1.43 Os1-H-B4 Os1-H 1.70 B4-H 1.43 Os3-H-B2 Os3-H 1.70 B2-H 1.43 Os3-H-B4 Os3-H 1.70 B4-H 1.43

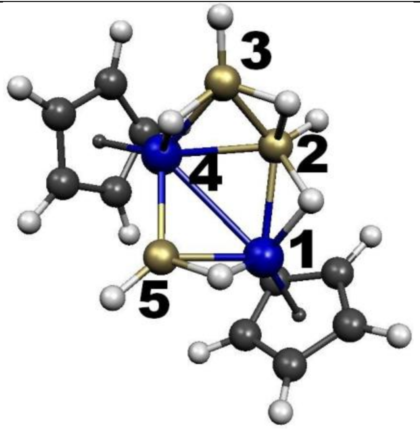 4. -647.241437 +5.3 WBI 0.39	1 2 3 4 5 1 Os 0.000000 2 B 2.159029 0.000000 3 B 3.476557 1.760191 0.000000 4 Os 2.810891 2.219346 2.059411 0.000000 5 B 2.041697 3.088352 3.431190 2.117499 Os1-H-B2 Os1-H 1.68 B2-H 1.54 Os1-H-B5 Os1-H 1.72 B5-H 1.43 Os4-H-B3 Os4-H 1.78 B3-H 1.34 B2-H-B3 B2-H 1.43 B3-H 1.27
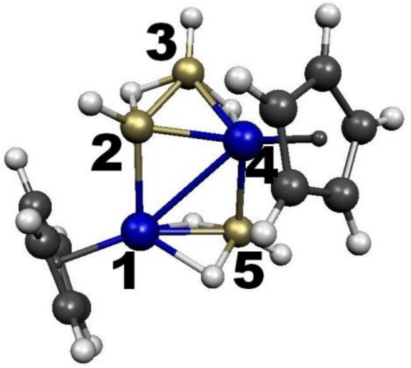 5. -647.235225 +9.2 WBI 0.36	1 2 3 4 5 1 Os 0.000000 2 B 2.189435 0.000000 3 B 3.430182 1.756662 0.000000 4 Os 2.852896 2.127492 2.062097 0.000000 5 B 2.090595 3.147365 3.463279 2.193063 Os1-H-B5 Os1-H 1.77 B5-H 1.35 Os1-H’-B5 Os1-H’ 1.78 B5-H 1.34 Os4-H-B3 Os4-H 1.80 B3-H 1.33 B2-H-B5 B2-H- 1.40 B3-H 1.30
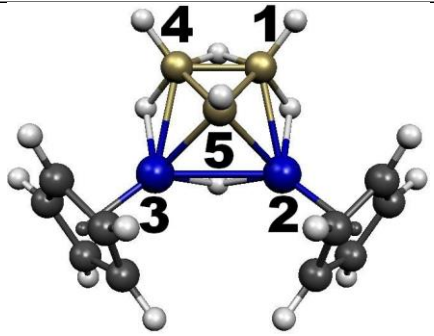 6. -647.234742 +9.5 Cs WBI 0.80	1 2 3 4 5 1 B 0.000000 2 Os 2.259357 0.000000 3 Os 3.105765 2.624600 0.000000 4 B 1.730200 3.105765 2.259357 0.000000 5 B 1.725252 2.160087 2.160087 1.725252 Os2-H- Os3 Os2-H 1.83 Os3-H 1.82 Os2-H-B1 Os2-H 1.71 B1-H 1.38 Os3-H-B4 Os3-H 1.72 B4-H 1.39 B1-H-B4 B1-H 1.33 B4-H 1.33

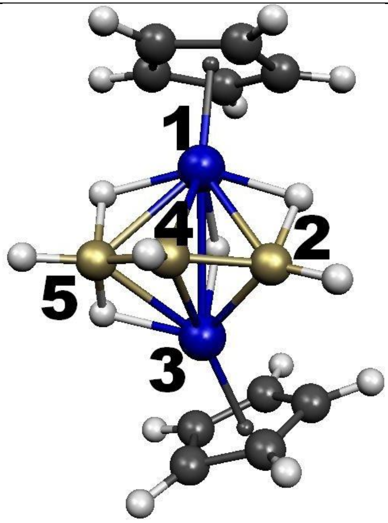

7. -647.234263 +9.8 WBI 0.37

		1	2	3	4	5
1	Os	0.000000				
2	B	2.272275	0.000000			
3	Os	2.837031	2.136613	0.000000		
4	B	2.232478	1.649876	2.293032	0.000000	
5	B	2.345122	2.889602	2.252159	1.645834	

Os1-H-Os3	Os1-H 1.81	Os3-H 1.82
Os1-H-B2	Os1-H 1.75	B2-H 1.35
Os1-H-B5	Os1-H 1.75	B5-H 1.37
Os3-H-B5	Os3-H 1.77	B5-H 1.33

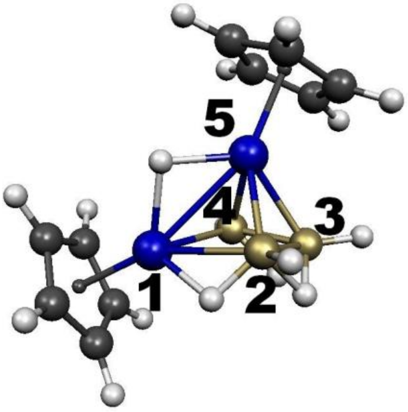

8. -647.234258 +9.8 WBI 0.64

		1	2	3	4	5
1	Os	0.000000				
2	B	2.374757	0.000000			
3	B	3.088760	1.798756	0.000000		
4	B	2.208964	2.653524	1.828613	0.000000	
5	Os	2.657812	2.163985	2.159877	2.096744	

Os1-H-Os5	Os1-H 1.79	Os5-H 1.77
Os1-H-B2	Os1-H 1.78	B2-H 1.30
B2-H-B3	B2-H 1.37	B3-H 1.28
B3-H-B4	B3-H 1.29	B4-H 1.39

6.1.1.4 $Cp_2Re_2B_3H_7$ systems

Table 70. Distances table for the lowest-lying $Cp_2Re_2B_3H_7$ structures after M06L/6-311G(d,p) optimization. Included are the ZPcorrected E (a.u.), relative energy (kcal/mol), symmetry and WBI.

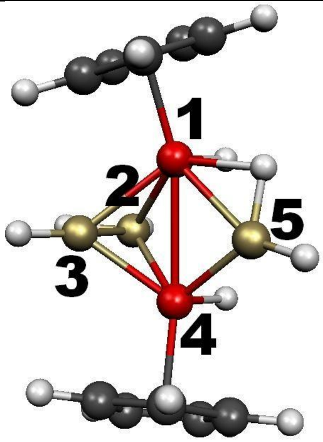

		1	2	3	4	5
1	Re	0.000000				
2	B	2.247672	0.000000			
3	B	2.239411	1.622699	0.000000		
4	Re	2.593218	2.223737	2.175292	0.000000	
5	B	2.223980	3.436494	3.369424	2.046902	

Re1-H-B2	Re1-H 1.65	B2-H 2.29
Re1-H-B5	Re1-H 1.81	B5-H 1.28
B2-H-B3	B2-H 1.31	B3-H 1.30

1. Re2B3-1 -622.432910 a.u. 0.0 WBI 0.89	
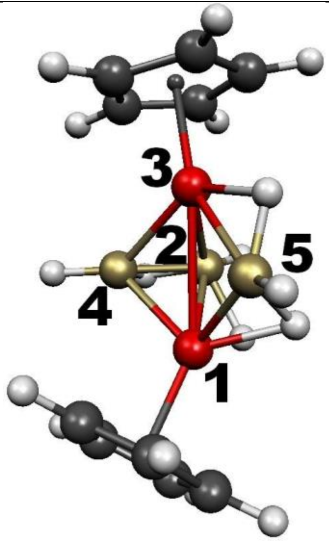 2. Re2B3-2 -622.428894 +2.5 WBI 0.73	1 2 3 4 5 1 Re 0.000000 2 B 2.299423 0.000000 3 Re 2.670359 2.223827 0.000000 4 B 2.181602 1.690647 2.168226 0.000000 5 B 2.082864 3.369576 2.290554 3.399675 Re1-H-B2 Re1-H 1.74 B2-H 1.47 Re1-H-B5 Re1-H 1.78 B5-H 1.39 Re3-H-B5 Re3-H 1.82 B5-H 1.29 B2-H-B4 B2-H 1.30 B4-H 1.35
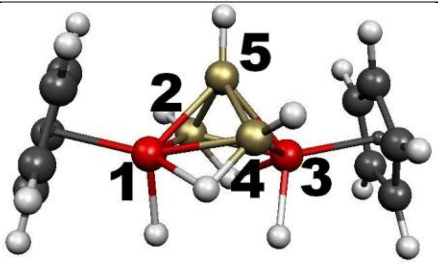 3. Re2B3-3 -622.427727 +3.3 C_2 WBI 0.56	1 2 3 4 5 1 Re 0.000000 2 B 2.159499 0.000000 3 Re 2.966840 2.136334 0.000000 4 B 2.136343 3.012671 2.159523 0.000000 5 B 2.111187 1.878558 2.111201 1.878657 Re1-H-B4 Re1-H 1.79 B4-H 1.35 Re3-H-B2 Re3-H 1.79 B2-H 1.35 Re1-H 1.67 Re3-H 1.67
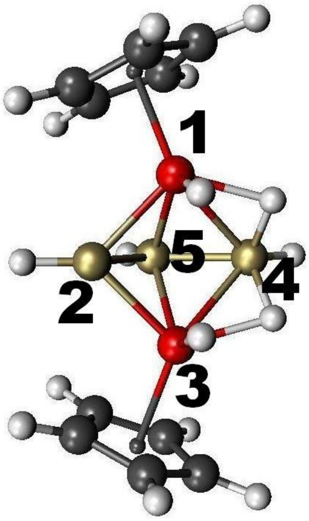 4. Re2B3-4 -622.426848 +3.8 Cs WBI 0.58	1 2 3 4 5 1 Re 0.000000 2 B 2.084750 0.000000 3 Re 2.975400 2.084746 0.000000 4 B 2.211585 3.023540 2.211557 0.000000 5 B 2.108943 1.969186 2.108872 1.831042 Re1-H-B4 Re1-H 1.75 B4-H 1.38 Re3-H-B4 Re3-H 1.75 B4-H 1.38 Re1-H 1.68 Re3-H 1.68

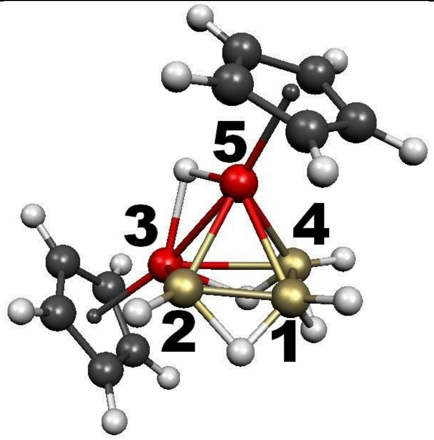 5. Re2B3-5 -622.425195 +4.8 WBI 1.35	1 2 3 4 5 1 B 0.000000 2 B 1.824625 0.000000 3 Re 3.012166 2.177716 0.000000 4 B 1.824468 2.744366 2.383180 0.000000 5 Re 2.216297 2.137221 2.452629 2.159938 Re3-H- Re5 Re3-H 1.82 Re5-H 1.81 Re3-H-B4 Re3-H 1.78 B4-H 1.35 B1-H-B2 B1-H 1.26 B2-H 1.44 B1-H-B4 B1-H 1.30 B4-H 1.36
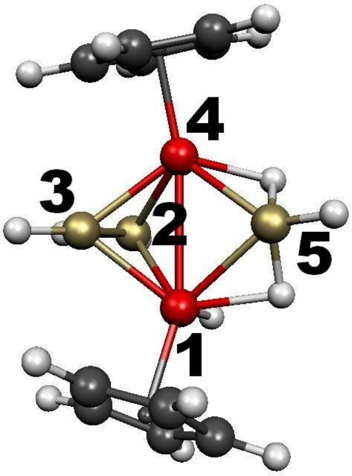 6. Re2B3-6 -622.424040 +5.6 (Cs) WBI 0.837	1 2 3 4 5 1 Re 0.000000 2 B 2.280350 0.000000 3 B 2.202071 1.650531 0.000000 4 Re 2.636747 2.235863 2.159706 0.000000 5 B 2.232787 3.372998 3.403117 2.093274 Re1-H-B5 Re1-H 1.79 B5-H 1.31 Re4-H-B5 Re4-H 1.76 B5-H 1.41 B2-H-B3 B2-H 1.30 B3-H 1.33 Re1-H 1.66
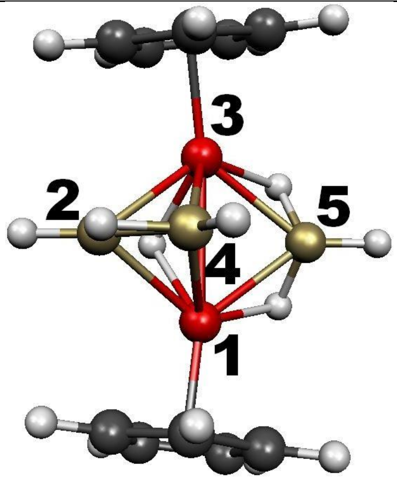 7. Re2B3-7 -622.423293 +6.0 Cs WBI 0.70	1 2 3 4 5 1 Re 0.000000 2 B 2.201935 0.000000 3 Re 2.628800 2.201984 0.000000 4 B 2.209711 1.665661 2.209479 0.000000 5 B 2.194519 3.489746 2.195042 2.856237 Re1-H- Re3 Re1-H 1.90 Re3-H 1.90 Re1-H-B5 Re1-H 1.79 B5-H 1.34 Re3-H-B5 Re3-H 1.79 B5-H 1.34 B2-H-B4 B2-H 1.33 B4-H 1.31

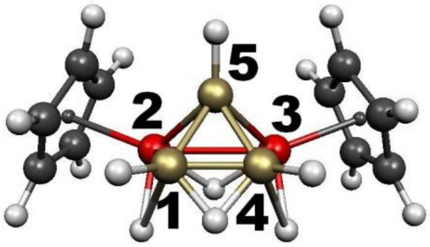 8. Re2B3-8 -622.422697 +6.4 Cs WBI 1.40	1 2 3 4 5 1 B 0.000000 2 Re 2.249149 0.000000 3 Re 3.026596 2.442803 0.000000 4 B 1.674104 3.024468 2.251670 0.000000 5 B 1.715279 2.195887 2.196462 1.713154 Re2-H- Re3 Re2-H 1.82 Re3-H 1.82 Re2-H-B1 Re2-H 1.66 B1-H 2.28 Re3-H-B4 Re3-H 1.66 B4-H 2.25 B1-H-B4 B1-H 1.31 B4-H 1.31
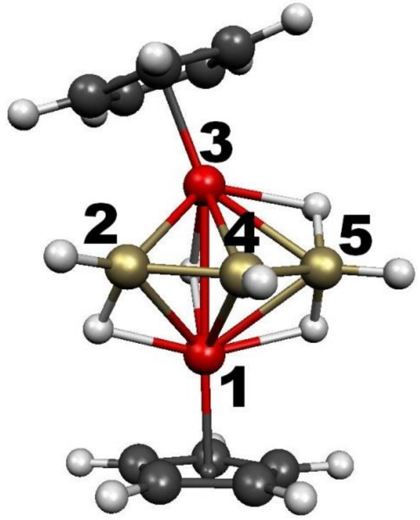 9. Re2B3-9 -622.415658 +10.8 (Cs) WBI 0.74	1 2 3 4 5 1 Re 0.000000 2 B 2.210574 0.000000 3 Re 2.684885 2.112370 0.000000 4 B 2.224032 1.748468 2.252812 0.000000 5 B 2.342656 3.027355 2.291281 1.709694 Re1-H-Re3 Re1-H 1.84 Re3-H 1.9 Re1-H-B2 Re1-H 1.76 B2-H 1.39 Re1-H-B5 Re1-H 1.84 B5-H 1.33 Re3-H-B5 Re3-H 1.86 B5-H 1.29
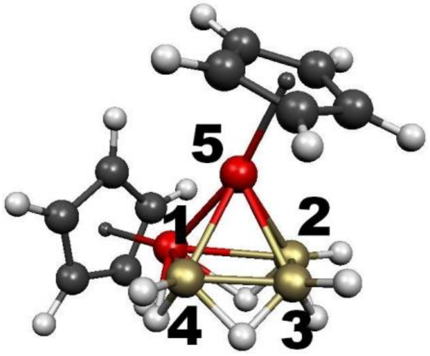 10. Re2B3-10 -622.414866 +11.3 Cs WBI 1.85	1 2 3 4 5 1 Re 0.000000 2 B 2.310214 0.000000 3 B 3.074870 1.840386 0.000000 4 B 2.312348 2.756705 1.840589 0.000000 5 Re 2.362610 2.169358 2.188911 2.168877 Re1-H-B2 Re1-H 1.79 B2-H 1.36 Re1-H-B4 Re1-H 1.80 B4-H 1.35 B2-H-B3 B2-H 1.39 B3-H 1.29 B3-H-B4 B3-H 1.29 B4-H 1.39

6.1.1.5 $Cp_2M_2B_3H_7$ (M=Mo,W) systems

Table 71. Distances table for the lowest-lying $Cp_2Mo_2B_3H_7$ structures after M06L/6-311G(d,p) optimization. Included are the ZPcorrected E (a.u.), relative energy (kcal/mol), symmetry and WBI.

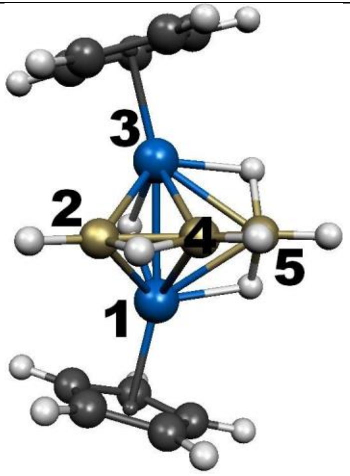

**1. Mo2B3-1 -602.205202 a.u.
0.0 kcal/mol Cs WBI 1.51**

		1	2	3	4
1	Mo	0.000000			
2	B	2.208838	0.000000		
3	Mo	2.521025	2.195478	0.000000	
4	B	2.334313	1.647130	2.283135	0.000000
5	B	2.232485	2.986099	2.270133	1.807554

Mo1-H-Mo3 Mo1-H 1.85 Mo3-H 1.86
Mo3-H- B5 Mo3-H 1.78 B5-H 1.33
Mo1-H-B5 Mo1-H 1.78 B5-H 1.32
B2-H-B4 B2-H 1.31 B4-H 1.3

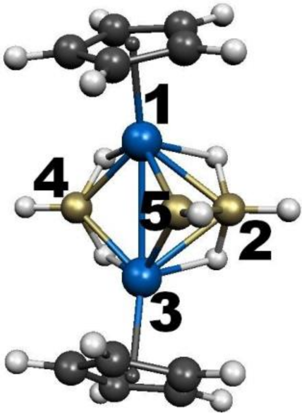

2. Mo2B3-2 -602.201032
+2.6 Cs WBI 1.07

		1	2	3	4
1	Mo	0.000000			
2	B	2.224601	0.000000		
3	Mo	2.739400	2.224601	0.000000	
4	B	2.232622	3.312813	2.232622	0.000000
5	B	2.091595	1.817785	2.091595	3.253731

Mo1-H-B2 Mo1-H 1.8 B2-H 1.37
Mo1-H-B4 Mo1-H 1.85 B4-H 1.31
Mo3-H-B2 Mo3-H 1.81 B2-H 1.37
Mo3-H-B4 Mo3-H 1.85 B4-H 1.31

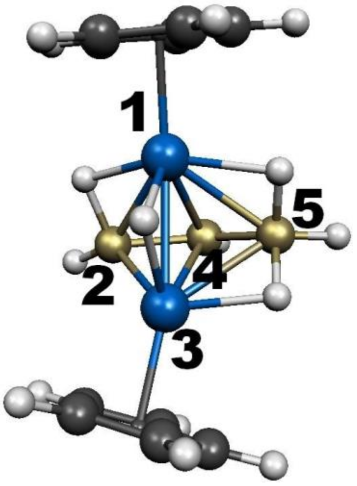

3. Mo2B3-3 -602.200268 +3.1
WBI 1.53

		1	2	3	4	5
1	Mo	0.000000				
2	B	2.254699	0.000000			
3	Mo	2.499594	2.181048	0.000000		
4	B	2.231627	1.682766	2.328636	0.000000	
5	B	2.335395	3.012209	2.352697	1.675619	

Mo1-H-Mo3 Mo1-H 1.82 Mo3-H 1.87
Mo1-H-B2 Mo1-H 1.81 B2-H 1.31
Mo1-H-B5 Mo1-H-B5 1.92 B5-H 1.27
Mo3-H-B5 Mo3-H 1.85 B5-H 1.31

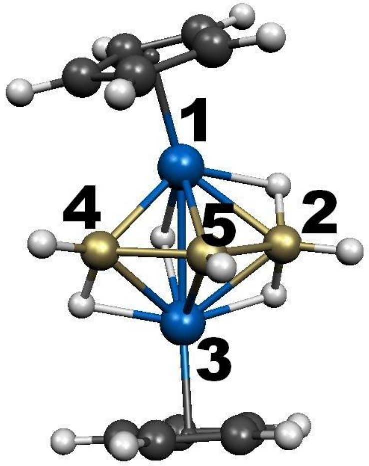

4. Mo2B3-4 -602.196157 +5.7
WBI 1.00

		1	2	3	4	5
1	Mo	0.000000				
2	B	2.221345	0.000000			
3	Mo	2.759137	2.272786	0.000000		
4	B	2.127448	3.180906	2.182075	0.000000	
5	B	2.119247	1.855653	2.173906	1.904741	

Mo1-H-Mo3   Mo1-H 1.97   Mo3-H 1.95
Mo1-H-B2   Mo1-H 1.87   B2-H 1.29
Mo3-H-B2   Mo3-H 1.8   B2-H 1.35
Mo3-H-B4   Mo3-H 1.82   B4-H 1.31

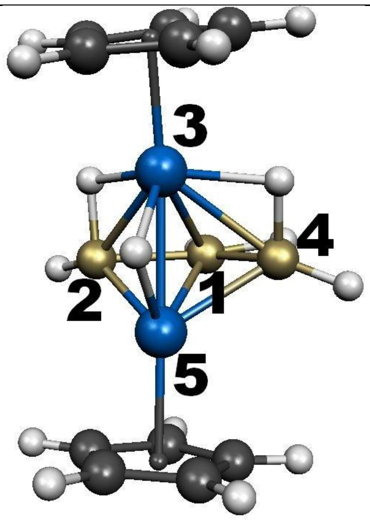

5. Mo2B3-5 -602.191516 +8.6
WBI 1.46

		1	2	3	4	5
1	B	0.000000				
2	B	1.878642	0.000000			
3	Mo	2.345514	2.282161	0.000000		
4	B	1.696849	3.095683	2.364944	0.000000	
5	Mo	2.217469	2.065060	2.500134	2.221692	

Mo3-H- Mo5   Mo3-H 1.82   Mo5-H 1.87
Mo3-H-B2   Mo3-H 1.84   B2-H 1.31
Mo3-H-B4   Mo3-H 1.79   B4-H 1.32
B1-H-B2   B1-H 1.34   B2-H 1.3

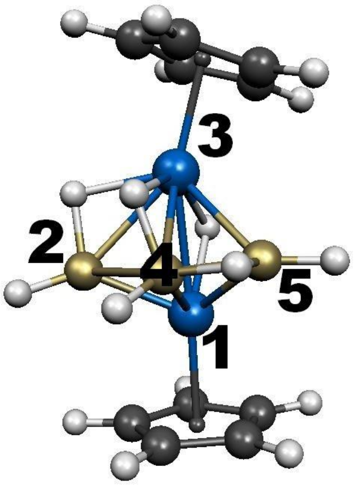

6. Mo2B3-6 -602.190959 +8.9
WBI 1.36

		1	2	3	4	5
1	Mo	0.000000				
2	B	2.048360	0.000000			
3	Mo	2.513308	2.322126	0.000000		
4	B	2.277069	2.156764	2.350410	0.000000	
5	B	2.164182	3.193773	2.318361	1.686842	

Mo1-H- Mo3   Mo1-H 1.86   Mo3-H 1.84
Mo3-H-B2   Mo3-H 1.81   B2-H 1.34
Mo3-H-B4   Mo3-H 1.85   B4-H 1.33
B4-H-B5   B4-H 1.33   B5-H 1.31

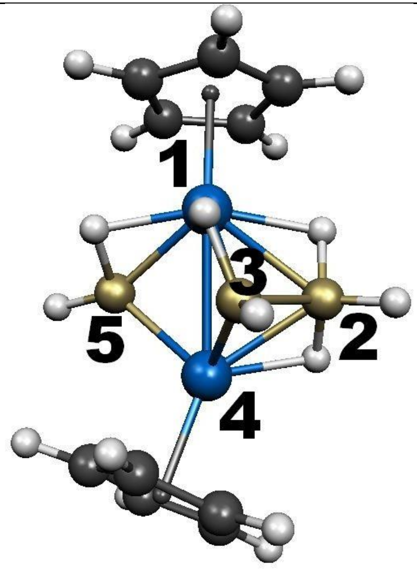

7. Mo2B3-7 -602.186609 +11.7
WBI 1.11

		1	2	3	4	5
1	Mo	0.000000				
2	B	2.352769	0.000000			
3	B	2.294930	1.871944	0.000000		
4	Mo	2.657690	2.222004	2.081299	0.000000	
5	B	2.133980	3.515805	3.095076	2.143441	

Mo1-H-B2	Mo1-H 1.89	B2-H 1.26
Mo1-H-B3	Mo1-H 1.78	B3-H 1.37
Mo1-H-B5	Mo1-H 1.83	B5-H 1.32
Mo4-H-B2	Mo4-H 1.88	B2-H 1.29

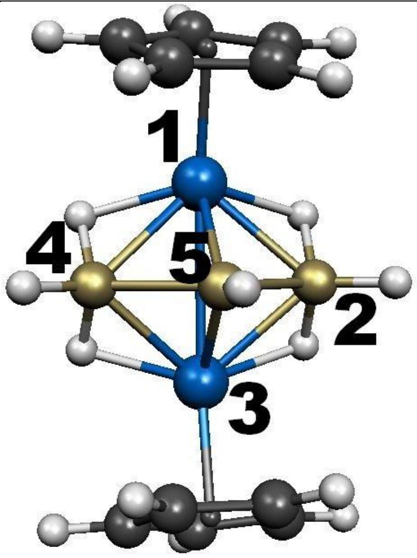

8. Mo2B3-8 -602.185979
+12.1 C_{2v} WBI 1.15

		1	2	3	4	5
1	Mo	0.000000				
2	B	2.213918	0.000000			
3	Mo	2.911200	2.213918	0.000000		
4	B	2.213880	3.245900	2.213880	0.000000	
5	B	2.109621	1.984201	2.109621	1.984168	

Mo1-H-B2	Mo1-H 1.82	B2-H 1.31
Mo1-H-B4	Mo1-H 1.82	B4-H 1.31
Mo3-H-B2	Mo3-H 1.82	B2-H 1.31
Mo3-H-B4	Mo3-H 1.82	B4-H 1.31

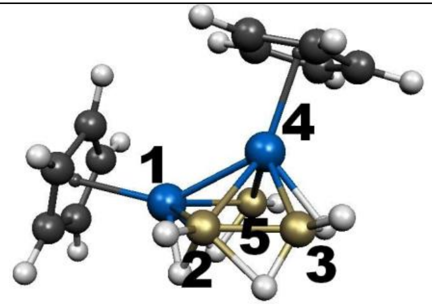

9. Mo2B3-9 -602.171797 +21.0
WBI 1.94

		1	2	3	4	5
1	Mo	0.000000				
2	B	2.237273	0.000000			
3	B	3.440791	1.763772	0.000000		
4	Mo	2.375418	2.279928	2.175859	0.000000	
5	B	2.120740	3.375697	3.539944	2.202109	

Mo1-H-B2	Mo1-B2 1.82	B2-H 1.36
Mo1-H-B5	Mo1-H 1.82	B5-H 1.32
Mo4-H-B3	Mo4-H 1.91	B3-H 1.29
B2-H-B3	B2-H 1.6	B3-H 1.24

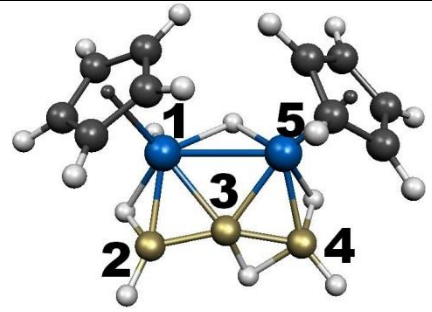

10. Mo2B3-10 -602.171199
+21.3 (Cs)   WBI 1.01

		1	2	3	4	5
1	Mo	0.000000				
2	B	2.061866	0.000000			
3	B	2.198391	1.696859	0.000000		
4	B	3.640721	3.327603	1.689144	0.000000	
5	Mo	2.661011	3.568181	2.130637	2.058366	

Mo1-H- Mo5   Mo1-H 1.93   Mo5-H 1.84
Mo1-H-B2   Mo1-H 1.83   B2-H 1.28
Mo5-H-B4   Mo5-H 1.85   B4-H 1.35
B3-H-B4   B3-H 1.26   B4-H 1.46

Table 72. Distances table for the lowest-lying $Cp_2W_2B_3H_7$ structures after M06L/6-311G(d,p) optimization. Included are the ZPcorrected E (a.u.), relative energy (kcal/mol), symmetry and WBI.

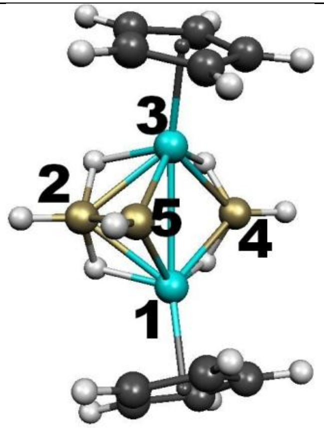

1. W2B3-1 -600.005158 a.u.
0.0 kcal/mol Cs   WBI 1.05

		1	2	3	4	5
1	W	0.000000				
2	B	2.228523	0.000000			
3	W	2.762000	2.228581	0.000000		
4	B	2.231339	3.290531	2.231261	0.000000	
5	B	2.111307	1.815766	2.111377	3.266915	

W1-H-B2   W1-H 1.79   B2-H 1.42
W1-H-B4   W1-H 1.85   B4-H 1.32
W3-H-B2   W3-H 1.79   B2-H 1.42
W3-H-B4   W3-H 1.85   B4-H 1.32

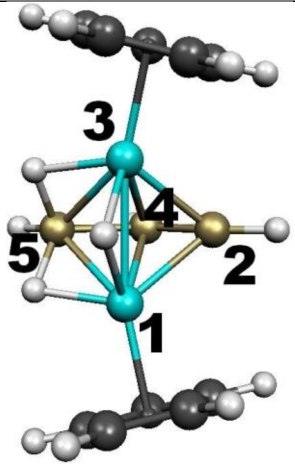

2. W2B3-2 -600.003473
+1.1 Cs   WBI 1.50

		1	2	3	4	5
1	W	0.000000				
2	B	2.213541	0.000000			
3	W	2.556102	2.209411	0.000000		
4	B	2.338541	1.658182	2.323339	0.000000	
5	B	2.246761	2.972402	2.257420	1.799184	

W1-H-W3   W1-H 1.87   W3-H 1.87
W1-H-B5   W1-H 1.79   B5-H 1.35
W3-H-B5   W3-H 1.79   B5-H 1.36
B2-H-B4   B2-H 1.31   B4-H 1.3

<table>
<tr>
<td>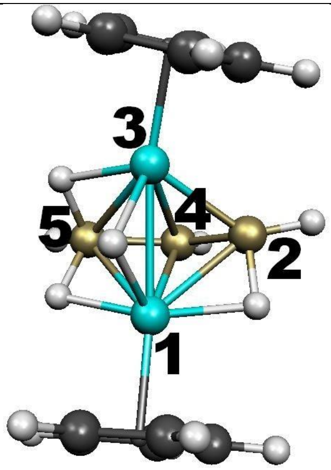
3. W2B3-3 -600.000438 +3.0
WBI 1.53</td>
<td>
<table>
<tr><th></th><th></th><th>1</th><th>2</th><th>3</th><th>4</th><th>5</th></tr>
<tr><td>1</td><td>W</td><td>0.000000</td><td></td><td></td><td></td><td></td></tr>
<tr><td>2</td><td>B</td><td>2.264922</td><td>0.000000</td><td></td><td></td><td></td></tr>
<tr><td>3</td><td>W</td><td>2.537747</td><td>2.174427</td><td>0.000000</td><td></td><td></td></tr>
<tr><td>4</td><td>B</td><td>2.261324</td><td>1.692057</td><td>2.340646</td><td>0.000000</td><td></td></tr>
<tr><td>5</td><td>B</td><td>2.346383</td><td>3.001547</td><td>2.350455</td><td>1.674504</td><td></td></tr>
</table>
W1-H-W3 W1-H 1.83 W3-H 1.88
W1-H-B2 W1-H 1.80 B2-H 1.34
W1-H-B5 W1-H 1.91 B5-H 1.29
W3-H-B5 W3-H 1.86 B5-H 1.32
</td>
</tr>
<tr>
<td>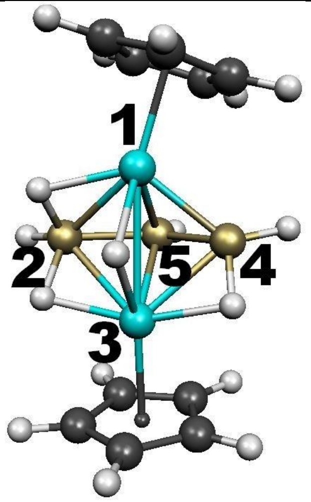
4. W2B3-4 -599.996771 +5.3
WBI 1.01</td>
<td>
<table>
<tr><th></th><th></th><th>1</th><th>2</th><th>3</th><th>4</th><th>5</th></tr>
<tr><td>1</td><td>W</td><td>0.000000</td><td></td><td></td><td></td><td></td></tr>
<tr><td>2</td><td>B</td><td>2.221126</td><td>0.000000</td><td></td><td></td><td></td></tr>
<tr><td>3</td><td>W</td><td>2.779651</td><td>2.262277</td><td>0.000000</td><td></td><td></td></tr>
<tr><td>4</td><td>B</td><td>2.135981</td><td>3.182836</td><td>2.201291</td><td>0.000000</td><td></td></tr>
<tr><td>5</td><td>B</td><td>2.138154</td><td>1.862803</td><td>2.189902</td><td>1.925052</td><td></td></tr>
</table>
W1-H-W3 W1-H 1.97 W3-H 1.95
W1-H-B2 W1-H 1.86 B2-H 1.31
W3-H-B2 W3-H 1.80 B2-H 1.39
W3-H-B4 W3-H 1.84 B4-H 1.32
</td>
</tr>
<tr>
<td>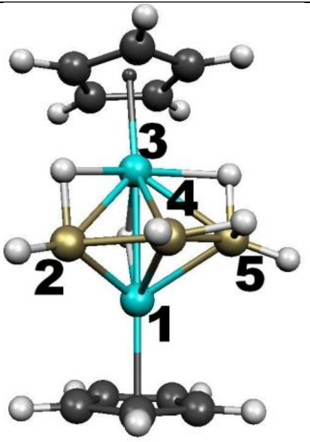
5. W2B3-5 -599.990363 +9.3
WBI 1.45</td>
<td>
<table>
<tr><th></th><th></th><th>1</th><th>2</th><th>3</th><th>4</th><th>5</th></tr>
<tr><td>1</td><td>W</td><td>0.000000</td><td></td><td></td><td></td><td></td></tr>
<tr><td>2</td><td>B</td><td>2.071279</td><td>0.000000</td><td></td><td></td><td></td></tr>
<tr><td>3</td><td>W</td><td>2.535955</td><td>2.297885</td><td>0.000000</td><td></td><td></td></tr>
<tr><td>4</td><td>B</td><td>2.230762</td><td>1.898698</td><td>2.371379</td><td>0.000000</td><td></td></tr>
<tr><td>5</td><td>B</td><td>2.229273</td><td>3.105979</td><td>2.372739</td><td>1.706202</td><td></td></tr>
</table>
W1-H-W3 W1-H 1.88 W3-H 1.83
W3-H-B2 W3-H 1.79 B2-H 1.35
W3-H-B5 W3-H 1.84 W5-H 1.33
B4-H-B5 B4-H 1.36 B5-H 1.29
</td>
</tr>
</table>

<table>
<tr>
<td>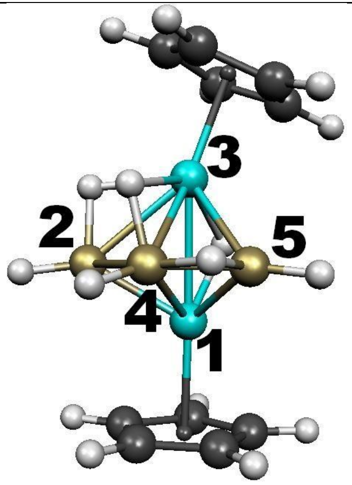

6. W2B3-6 -599.990321 +9.3
WBI 1.36</td>
<td>
<table>
<tr><th></th><th></th><th>1</th><th>2</th><th>3</th><th>4</th><th>5</th></tr>
<tr><td>1</td><td>W</td><td>0.000000</td><td></td><td></td><td></td><td></td></tr>
<tr><td>2</td><td>B</td><td>2.057212</td><td>0.000000</td><td></td><td></td><td></td></tr>
<tr><td>3</td><td>W</td><td>2.545169</td><td>2.342947</td><td>0.000000</td><td></td><td></td></tr>
<tr><td>4</td><td>B</td><td>2.290229</td><td>2.178888</td><td>2.373280</td><td>0.000000</td><td></td></tr>
<tr><td>5</td><td>B</td><td>2.180023</td><td>3.207985</td><td>2.323198</td><td>1.690980</td><td></td></tr>
</table>
W1-H-W3 W1-H 1.86 W3-H 1.86
W3-H-B2 W3-H 1.81 B2-H 1.38
W3-H-B4 W3-H 1.85 B4-H 1.36
B4-H-B5 B4-H 1.33 B5-H 1.32</td>
</tr>
<tr>
<td>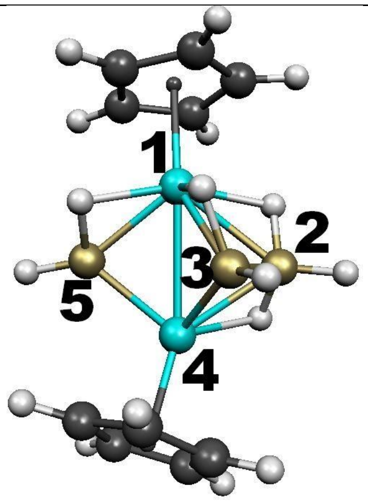

7. W2B3-7 -599.989155 +10.0
WBI 1.12</td>
<td>
<table>
<tr><th></th><th></th><th>1</th><th>2</th><th>3</th><th>4</th><th>5</th></tr>
<tr><td>1</td><td>W</td><td>0.000000</td><td></td><td></td><td></td><td></td></tr>
<tr><td>2</td><td>B</td><td>2.353487</td><td>0.000000</td><td></td><td></td><td></td></tr>
<tr><td>3</td><td>B</td><td>2.316116</td><td>1.887034</td><td>0.000000</td><td></td><td></td></tr>
<tr><td>4</td><td>W</td><td>2.682470</td><td>2.223040</td><td>2.085339</td><td>0.000000</td><td></td></tr>
<tr><td>5</td><td>B</td><td>2.145509</td><td>3.512236</td><td>3.096793</td><td>2.153925</td><td></td></tr>
</table>
W1-H-B2 W1-H 1.90 B2-H 1.26
W1-H-B3 W1-H 1.79 B3-H 1.42
W1-H-B5 W1-H 1.84 B5-H 1.33
W4-H-B2 W4-H 1.87 B2-H 1.32</td>
</tr>
<tr>
<td>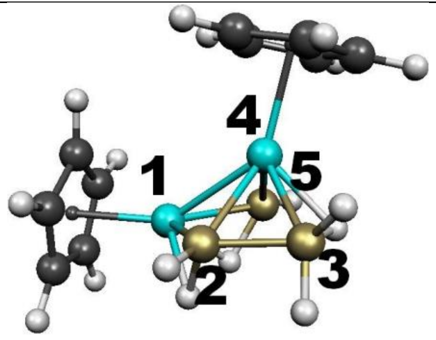

8. W2B3-8 -599.980710 +15.3
WBI 1.83</td>
<td>
<table>
<tr><th></th><th></th><th>1</th><th>2</th><th>3</th><th>4</th><th>5</th></tr>
<tr><td>1</td><td>W</td><td>0.000000</td><td></td><td></td><td></td><td></td></tr>
<tr><td>2</td><td>B</td><td>2.186047</td><td>0.000000</td><td></td><td></td><td></td></tr>
<tr><td>3</td><td>B</td><td>3.512015</td><td>1.851222</td><td>0.000000</td><td></td><td></td></tr>
<tr><td>4</td><td>W</td><td>2.441900</td><td>2.221990</td><td>2.204920</td><td>0.000000</td><td></td></tr>
<tr><td>5</td><td>B</td><td>2.146093</td><td>3.302901</td><td>3.518547</td><td>2.179670</td><td></td></tr>
</table>
W1-H-B2 W1-H 1.82 B2-H 1.40
W1-H-B4 W1-H 1.83 B4-H 1.35
W4-H-B3 W4-H 1.88 B3-H 1.32</td>
</tr>
</table>

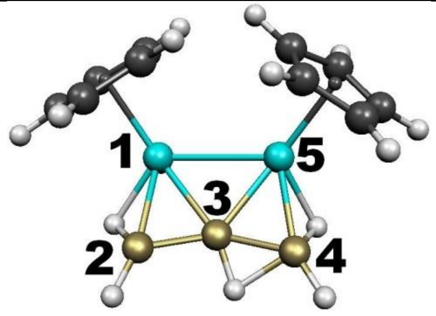

9. W2B3-9 -599.979786
+15.9 (Cs)
WBI 1.28

		1	2	3	4	5
1	W	0.000000				
2	B	2.067257	0.000000			
3	B	2.151617	1.715422	0.000000		
4	B	3.636994	3.335011	1.719896	0.000000	
5	W	2.654309	3.610881	2.154453	2.080656	

W1-H-B2 W1-H 1.85 B2-H 1.29
W5-H-B4 W5-H 1.87 B4-H 1.30
B3-H-B4 B3-H 1.23 B4-H 1.55

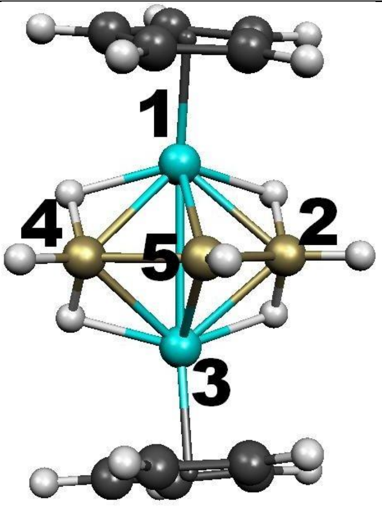

10. W2B3-10 -599.976787
+17.8 C_{2v} WBI 1.20

		1	2	3	4	5
1	W	0.000000				
2	B	2.214319	0.000000			
3	W	2.916200	2.214319	0.000000		
4	B	2.214378	3.219400	2.214378	0.000000	
5	B	2.139576	1.969239	2.139576	1.969230	

W1-H-B2 W1-H 1.82 B2-H 1.36
W1-H-B4 W1-H 1.82 B4-H 1.36
W3-H-B2 W3-H 1.82 B2-H 1.36
W3-H-B4 W3-H 1.82 B4-H 1.36

6.1.1.6 $Cp_2Ta_2B_3H_7$ systems

Table 73. Distances table for the lowest-lying $Cp_2Ta_2B_3H_7$ structures after M06L/6-311G(d,p) optimization. Included are the ZPcorrected E (a.u.), relative energy (kcal/mol), symmetry and WBI.

<table>
<tr>
<td>
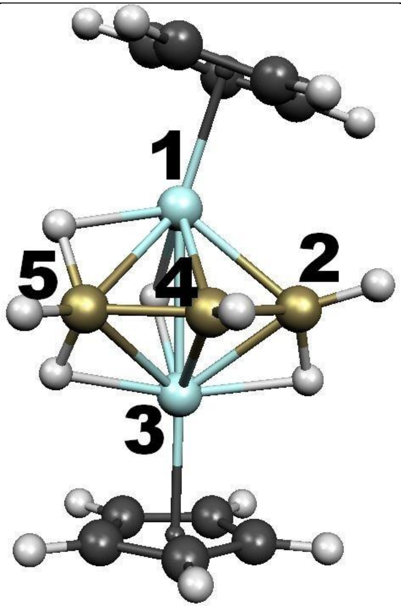

**1. Ta2B3-1 -579.846313 a.u.
0.0 kcal/mol WBI 1.11**
</td>
<td>
<table>
<tr><th></th><th></th><th>1</th><th>2</th><th>3</th><th>4</th><th>5</th></tr>
<tr><td>1</td><td>Ta</td><td>0.000000</td><td></td><td></td><td></td><td></td></tr>
<tr><td>2</td><td>B</td><td>2.300990</td><td>0.000000</td><td></td><td></td><td></td></tr>
<tr><td>3</td><td>Ta</td><td>2.737824</td><td>2.219098</td><td>0.000000</td><td></td><td></td></tr>
<tr><td>4</td><td>B</td><td>2.303440</td><td>1.758072</td><td>2.255441</td><td>0.000000</td><td></td></tr>
<tr><td>5</td><td>B</td><td>2.352154</td><td>3.108042</td><td>2.331263</td><td>1.756317</td><td></td></tr>
</table>

Ta1-H-Ta3 Ta1-H 1.97 Ta3-H 1.95
Ta1-H-B5 Ta1-H 1.89 B5-H 1.34
Ta3-H-B2 Ta3-H 1.91 B2-H 1.26
Ta3-H-B5 Ta3-H 1.94 B5-H 1.28
</td>
</tr>
<tr>
<td>
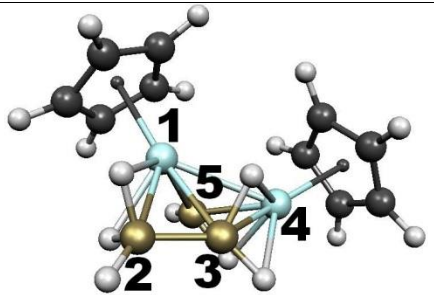

2. Ta2B3-2 -579.807993 +24.1
WBI 1.23
</td>
<td>
<table>
<tr><th></th><th></th><th>1</th><th>2</th><th>3</th><th>4</th><th>5</th></tr>
<tr><td>1</td><td>Ta</td><td>0.000000</td><td></td><td></td><td></td><td></td></tr>
<tr><td>2</td><td>B</td><td>2.265293</td><td>0.000000</td><td></td><td></td><td></td></tr>
<tr><td>3</td><td>B</td><td>2.250464</td><td>1.707198</td><td>0.000000</td><td></td><td></td></tr>
<tr><td>4</td><td>Ta</td><td>2.710531</td><td>3.679671</td><td>2.188535</td><td>0.000000</td><td></td></tr>
<tr><td>5</td><td>B</td><td>2.280465</td><td>3.615177</td><td>2.975894</td><td>2.186436</td><td></td></tr>
</table>

Ta1-H’-B2 Ta1-H’ 2.05 B2-H 1.27
Ta1-H’’-B2 Ta1-H’’ 1.99 B2-H 1.31
Ta1-Ta4-B3-H Ta1-H 2.18 Ta4-H 1.99 B3-H 1.34
Ta4-H-B5 Ta4-H 1.93 B5-H 1.32
</td>
</tr>
<tr>
<td>
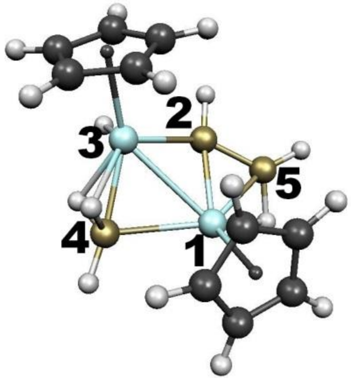

3. Ta2B3-3 -579.807752 +24.2
WBI 1.07
</td>
<td>
<table>
<tr><th></th><th></th><th>1</th><th>2</th><th>3</th><th>4</th><th>5</th></tr>
<tr><td>1</td><td>Ta</td><td>0.000000</td><td></td><td></td><td></td><td></td></tr>
<tr><td>2</td><td>B</td><td>2.201646</td><td>0.000000</td><td></td><td></td><td></td></tr>
<tr><td>3</td><td>Ta</td><td>2.807883</td><td>2.240443</td><td>0.000000</td><td></td><td></td></tr>
<tr><td>4</td><td>B</td><td>2.482109</td><td>3.393499</td><td>2.167397</td><td>0.000000</td><td></td></tr>
<tr><td>5</td><td>B</td><td>2.176156</td><td>1.655253</td><td>3.713330</td><td>4.294884</td><td></td></tr>
</table>

Ta1-H-B5 Ta1-H 1.91 B5-H 1.28
Ta3-H’-B4 Ta3-H’ 1.97 B4-H’1.28
Ta3-H’’-B4 Ta3-H’’1.98 B4-H’’ 1.27
Ta3-H 1.78
</td>
</tr>
</table>

<table>
<tr>
<td>
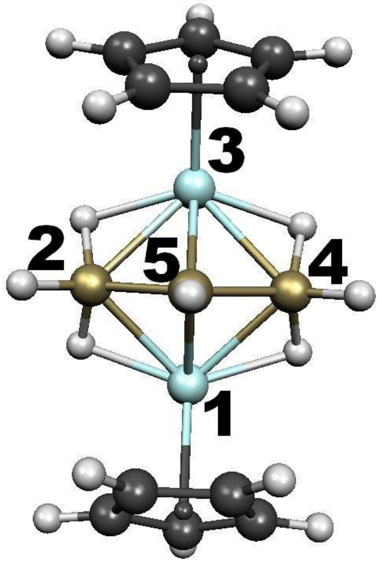

4. Ta2B3-4 -579.807450
+24.4 C_{2v} WBI 0.94
</td>
<td>
<table>
<tr><th></th><th></th><th>1</th><th>2</th><th>3</th><th>4</th><th>5</th></tr>
<tr><td>1</td><td>Ta</td><td>0.000000</td><td></td><td></td><td></td><td></td></tr>
<tr><td>2</td><td>B</td><td>2.295775</td><td>0.000000</td><td></td><td></td><td></td></tr>
<tr><td>3</td><td>Ta</td><td>3.172800</td><td>2.295775</td><td>0.000000</td><td></td><td></td></tr>
<tr><td>4</td><td>B</td><td>2.295823</td><td>3.131400</td><td>2.295823</td><td>0.000000</td><td></td></tr>
<tr><td>5</td><td>B</td><td>2.193602</td><td>1.839196</td><td>2.193602</td><td>1.839091</td><td></td></tr>
</table>
Ta1-H-B4 Ta1-H 1.88 B4-H 1.35
Ta1-H-B2 Ta1-H 1.88 B2-H 1.35
Ta3-H-B4 Ta3-H 1.88 B4-H 1.35
Ta3-H-B2 Ta3-H 1.88 B2-H 1.35
</td>
</tr>
<tr>
<td>
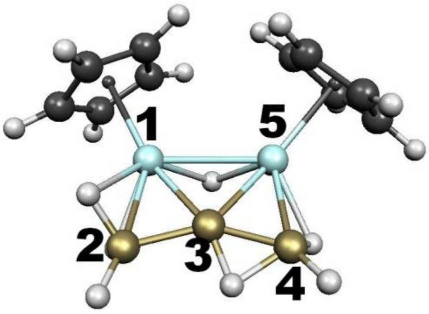

5. Ta2B3-5 -579.807176
+24.6 (Cs) WBI 1.74
</td>
<td>
<table>
<tr><th></th><th></th><th>1</th><th>2</th><th>3</th><th>4</th><th>5</th></tr>
<tr><td>1</td><td>Ta</td><td>0.000000</td><td></td><td></td><td></td><td></td></tr>
<tr><td>2</td><td>B</td><td>2.217593</td><td>0.000000</td><td></td><td></td><td></td></tr>
<tr><td>3</td><td>B</td><td>2.244243</td><td>1.753143</td><td>0.000000</td><td></td><td></td></tr>
<tr><td>4</td><td>B</td><td>3.693814</td><td>3.326241</td><td>1.679666</td><td>0.000000</td><td></td></tr>
<tr><td>5</td><td>Ta</td><td>2.661799</td><td>3.713217</td><td>2.204865</td><td>2.192724</td><td></td></tr>
</table>
Ta1-H-Ta5 Ta1-H 1.93 Ta5-H 1.98
Ta1-H’-B2 Ta1-H’ 2.01 B2-H’ 1.26
Ta1-H’’-B2 Ta1-H’’ 2.01 B2-H’ 1.31
Ta5-H-B4 Ta5-H 1.95 B4-H 1.29
B3-H-B4 B3-H 1.28 B4-H 1.39
</td>
</tr>
<tr>
<td>
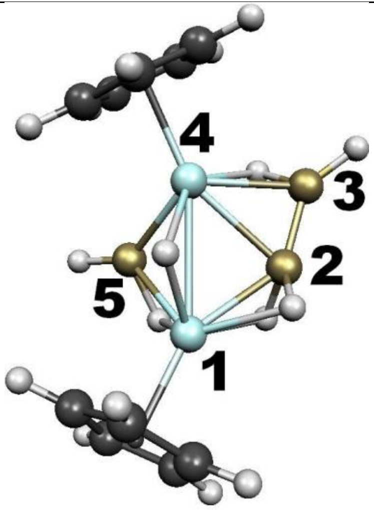

6. Ta2B3-6 -579.801970 +27.8
WBI 0.98
</td>
<td>
<table>
<tr><th></th><th></th><th>1</th><th>2</th><th>3</th><th>4</th><th>5</th></tr>
<tr><td>1</td><td>Ta</td><td>0.000000</td><td></td><td></td><td></td><td></td></tr>
<tr><td>2</td><td>B</td><td>2.159854</td><td>0.000000</td><td></td><td></td><td></td></tr>
<tr><td>3</td><td>B</td><td>3.565300</td><td>1.618323</td><td>0.000000</td><td></td><td></td></tr>
<tr><td>4</td><td>Ta</td><td>2.798648</td><td>2.367241</td><td>2.236524</td><td>0.000000</td><td></td></tr>
<tr><td>5</td><td>B</td><td>2.279271</td><td>3.119158</td><td>3.702142</td><td>2.196584</td><td></td></tr>
</table>
Ta1-H-Ta4 Ta1-H 1.89 Ta4-H 1.97
Ta1-H’-B2 Ta1-H’ 2.02 B2-H’ 1.28
Ta1-H’’-B2 Ta1-H’’ 1.91 B2-H’’ 1.33
Ta1-H-B5 Ta1-H 1.86 B5-H 1.36
Ta4-H-B3 Ta4-H 1.95 B3-H 1.31
</td>
</tr>
</table>

6.1.2 6 vertices

6.1.2.1 $Cp_2Ir_2B_4H_8$ systems

Table 74. Distances table for the lowest-lying $Cp_2Ir_2B_4H_8$ structures after M06L/6-311G(d,p) optimization. Included are the ZPcorrected E (a.u.), relative energy (kcal/mol), symmetry and WBI.

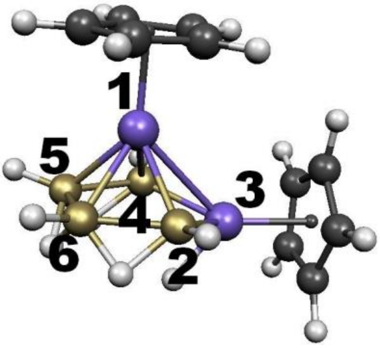 **Ir2B4-1 -700.082294 0.0 Cs** **WBI 0.35**	1 2 3 4 5 1 Ir 0.000000 2 B 2.143346 0.000000 3 Ir 2.712126 2.077293 0.000000 4 B 2.144500 2.927405 2.073673 0.000000 5 B 2.128063 2.939896 3.297450 1.822314 0.000000 6 B 2.126177 1.821716 3.300207 2.942074 1.820610 Ir3-H-B2&B4 Ir3-H 1.59 B2-H 2.26 B4-H 2.27 B2-H-B6 B2-H 1.38 B6-H 1.28 B5-H-B6 B5-H 1.32 B6-H 1.32 B4-H-B5 B4-H 1.38 B5-H 1.28
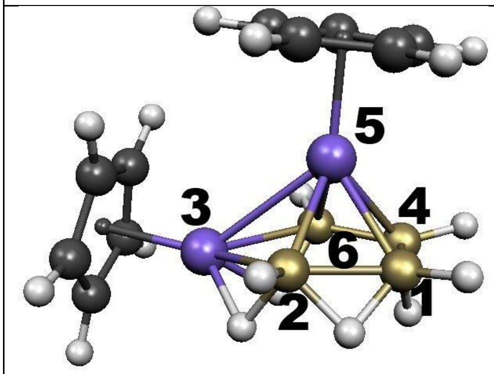 Ir2B4-2 -700.061876 +12.8 (Cs) WBI 0.40	1 2 3 4 5 1 B 0.000000 2 B 1.821498 0.000000 3 Ir 3.439797 2.267829 0.000000 4 B 1.788562 2.945368 3.371462 0.000000 5 Ir 2.127266 2.118410 2.714696 2.204359 0.000000 6 B 2.846105 3.020073 2.255335 1.636834 2.228888 Ir3-H-B2 Ir3-H 1.7 B2-H 1.38 Ir3-H-B6 Ir3-H 1.73 B6-H 1.36 B1-H-B2 B1-H 1.32 B2-H 1.33 B4-H-B6 B4-H 1.32 B6-H 1.32
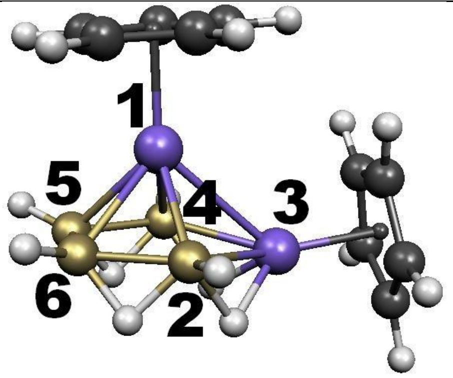 Ir2B4-3 -700.061293 +13.2 Cs WBI 0.39	1 2 3 4 5 1 Ir 0.000000 2 B 2.134175 0.000000 3 Ir 2.696437 2.279566 0.000000 4 B 2.134113 2.927109 2.282729 0.000000 5 B 2.210322 2.827641 3.512511 1.796747 0.000000 6 B 2.210025 1.798138 3.513107 2.828776 1.628901 Ir3-H-B2 Ir3-H 1.67 B2-H 1.45 Ir3-H-B4 Ir3-H 1.67 B4-H 1.45 B2-H-B6 B2-H 1.34 B6-H 1.31

	B4-H-B5 B4-H 1.34 B5-H 1.31
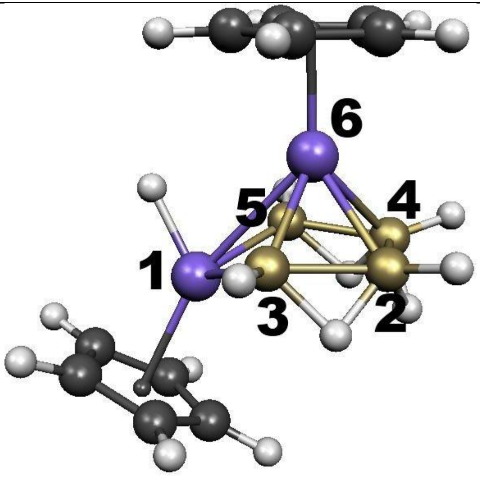 Ir2B4-4 -700.058213 +15.1 Cs WBI 0.35	1 2 3 4 5 1 Ir 0.000000 2 B 3.241769 0.000000 3 B 2.097751 1.828670 0.000000 4 B 3.223285 1.823684 2.951959 0.000000 5 B 2.052507 2.975238 2.970938 1.840441 0.000000 6 Ir 2.736110 2.127026 2.089979 2.129824 2.144318 Ir1-H-Ir6 Ir1-H 1.595 Ir6-H 2.727 B2-H-B3 B2-H 1.28 B3-H 1.4 B2-H-B4 B2-H 1.32 B4-H 1.33 B4-H-B5 B4-H 1.27 B5-H 1.41
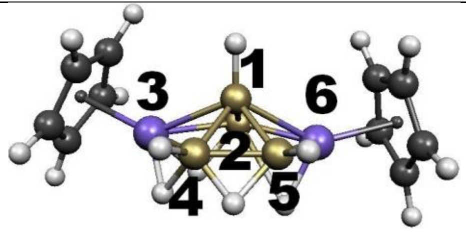 Ir2B4-5 -700.058065 +15.2 (Cs) WBI 0.09	1 2 3 4 5 1 B 0.000000 2 B 1.834974 0.000000 3 Ir 2.254680 2.173007 0.000000 4 B 1.752821 2.986244 2.227459 0.000000 5 B 1.742698 2.927993 3.383126 1.711335 0.000000 6 Ir 2.219665 2.031174 3.741753 3.250879 2.066506 Ir3-H-B2 Ir3-H 1.65 B2-H 1.52 Ir3-H-B4 Ir3-H 1.67 B4-H 1.45 B4-H-B5 B4-H 1.3 B5-H 1.37
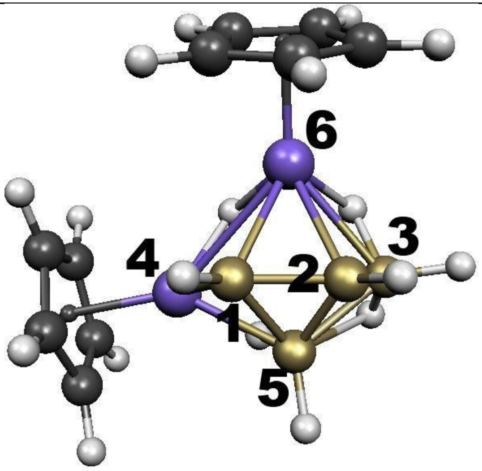 Ir2B4-6 -700.045392 +23.2 WBI 0.30	1 2 3 4 5 1 B 0.000000 2 B 1.680625 0.000000 3 B 2.866809 1.714559 0.000000 4 Ir 2.092021 3.212042 3.362022 0.000000 5 B 1.779549 1.674609 1.938970 2.247380 0.000000 6 Ir 2.226262 2.202482 2.398327 2.831086 2.907301 Ir4-H- Ir6 Ir4-H 1.71 Ir6-H 1.85 Ir4-H-B5 Ir4-H 1.63 B5-H 1.54 Ir6-H-B3 Ir6-H 1.73 B3-H 1.36 B3-H-B5 B3-H 1.20 B5-H 2.11

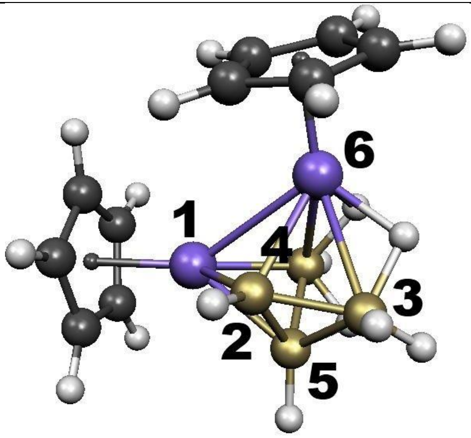 Ir2B4-7 -700.039922 +26.6 WBI 0.35	1 2 3 4 5 1 Ir 0.000000 2 B 2.072678 0.000000 3 B 3.413532 1.757255 0.000000 4 B 2.059801 2.700957 2.873632 0.000000 5 B 2.177328 1.735419 1.933903 1.825928 0.000000 6 Ir 2.753740 2.227613 2.413310 2.388859 2.924038 Ir6-H-B3 Ir6-H 1.7 B3-H 1.39 Ir6-H-B4 Ir6-H 1.7 B4-H 1.39 B3-H-B5 B3-H 1.2 B5-H 2.23 B4-H-B5 B4-H 1.3 B5-H 1.34
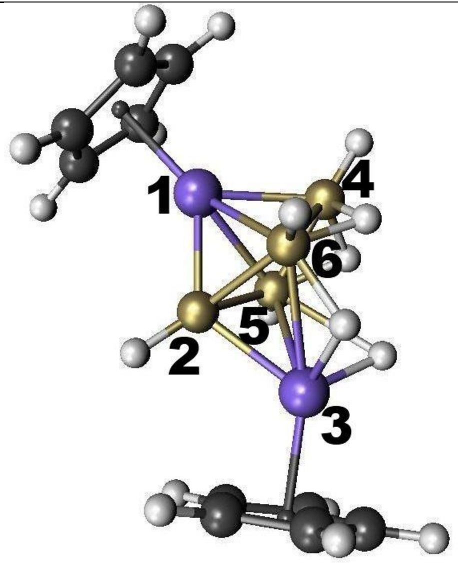 Ir2B4-8 -700.034079 +30.3 (Cs) WBI 0.10	1 2 3 4 5 1 Ir 0.000000 2 B 1.984917 0.000000 3 Ir 3.678113 2.112050 0.000000 4 B 2.089743 2.830712 3.230141 0.000000 5 B 2.195498 1.872591 2.304355 1.841472 0.000000 6 B 2.179619 1.963334 2.396008 1.842417 2.356991 Ir3-H-B5 Ir3-H 1.58 B5-H 2.24 Ir3-H-B6 Ir3-H 1.64 B6-H 1.53 B4-H-B5 B4-H 1.28 B5-H 1.37 B4-H-B6 B4-H 1.29 B4-H 1.37
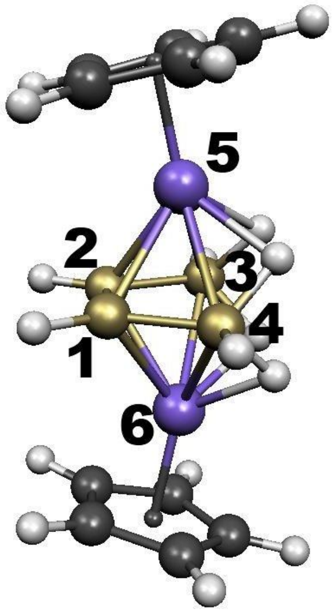	1 2 3 4 5 1 B 0.000000 2 B 1.708200 0.000000 3 B 2.828327 1.690185 0.000000 4 B 1.690185 2.828327 3.010600 0.000000 5 Ir 2.211489 2.211489 2.339056 2.339056 0.000000 6 Ir 2.211489 2.211489 2.339056 2.339056 3.453200 Ir5-H-B3 Ir5-H 1.29 B3-H 1.29 Ir5-H-B4 Ir5-H 1.29 B4-H 1.29 Ir5-H-B3 Ir5-H 1.29 B3-H 1.29 Ir6-H-B4 Ir6-H 1.29 B4-H 1.29

Ir2B4-9 -700.033303 +30.7 C_{2v} WBI 0.08	
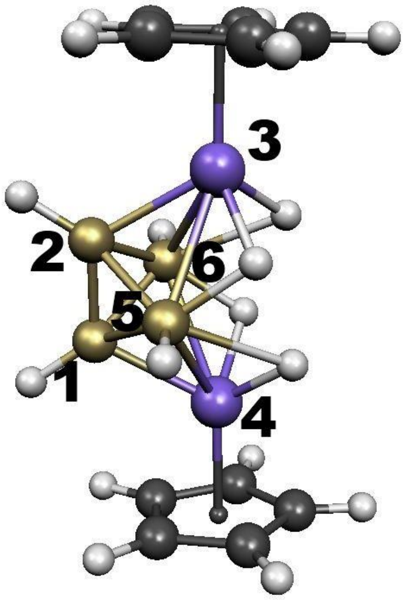 Ir2B4-10 -700.031477 +31.9 C_2 WBI 0.05	1 2 3 4 5 1 B 0.000000 2 B 1.612537 0.000000 3 Ir 3.226201 2.111165 0.000000 4 Ir 2.111165 3.226201 3.692781 0.000000 5 B 1.764474 1.779753 2.359408 2.269944 0.000000 6 B 1.779753 1.764474 2.269944 2.359408 2.328528 Ir3-H-B5 Ir3-H 1.64 B5-H 1.53 Ir3-H-B6 Ir3-H 1.58 B6-H 2.1 Ir4-H-B5 Ir4-H 1.58 B5-H 2.1 Ir4-H-B6 Ir4-H 1.64 B6-H 1.53

6.1.2.2 $M_2B_4H_8$ (M=Ru,Os) systems

Table 75. Distances table for the lowest-lying $Cp_2Ru_2B_4H_8$ structures after M06L/6-311G(d,p) optimization. Included are the ZPcorrected E (a.u.), relative energy (kcal/mol), symmetry and WBI.

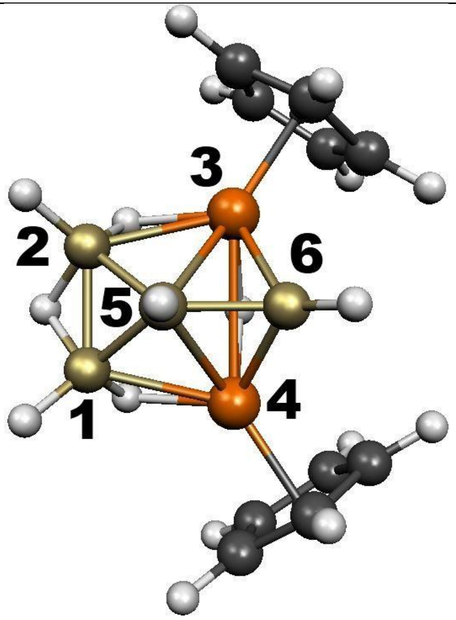 **Ru2B4-1 -681.142213 a.u. 0.0 kcal/mol Cs WBI 0.30**	1 2 3 4 5 1 B 0.000000 2 B 1.796300 0.000000 3 Ru 3.180857 2.244409 0.000000 4 Ru 2.244435 3.180931 2.828400 0.000000 5 B 1.722912 1.722964 2.223697 2.223647 0.000000 6 B 3.112005 3.112033 2.063907 2.063837 1.718841 Ru3-H-Ru4 Ru3-H 1.79 Ru4-H 1.79 Ru3-H-B2 Ru3-H 1.76 B2-H 1.31 Ru4-H-B1 Ru3-H 1.76 B1-H 1.31 B1-H-B2 B1-H 1.32 B2-H 1.32 Fehlner JACS 1999, 121, p 1275

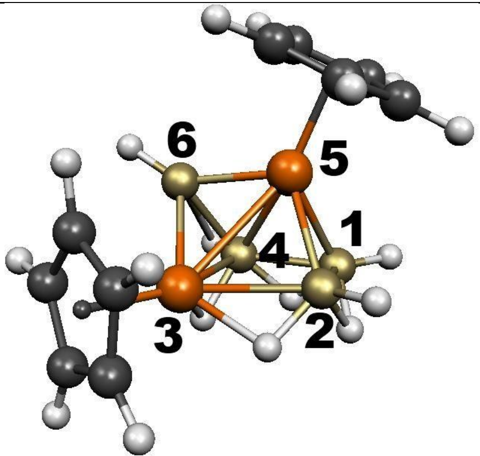

Ru2B4-2 -681.128453 +8.6
WBI 0.39

		1	2	3	4	5
1	B	0.000000				
2	B	1.809129	0.000000			
3	Ru	3.178813	2.338153	0.000000		
4	B	1.817181	2.599244	2.295943	0.000000	
5	Ru	2.109289	2.117449	2.738174	2.199603	0.00000
6	B	3.198798	3.222789	2.104647	1.901429	1.957885

Ru3-H-B2 Ru3-H 1.74 B2-H 1.31
Ru3-H-B4 Ru3-H 1.72 B4-H 1.36
B1-H-B2 B1-H 1.3 B2-H 1.37
B1-H-B4 B1-H 1.3 B4-H 1.34

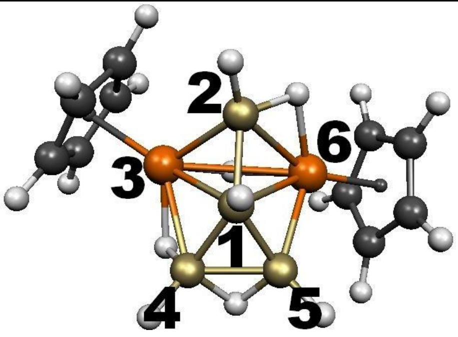

Ru2B4-3 -681.122067 +12.6
(Cs)
WBI 0.29

		1	2	3	4	5
1	B	0.000000				
2	B	1.731405	0.000000			
3	Ru	2.213465	2.119526	0.000000		
4	B	1.741357	3.147537	2.212242	0.000000	
5	B	1.685685	3.071109	3.134563	1.758454	0.000000
6	Ru	2.270550	2.169058	2.873978	3.126728	2.154360

Ru3-H-Ru6 Ru3-H 1.76 Ru6-H 1.79
Ru3-H-B4 Ru3-H 1.72 B4-H 1.34
B4-H-B5 B4-H 1.34 B5-H 1.31

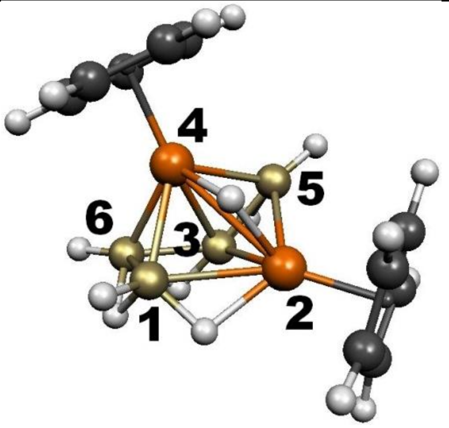

Ru2B4-4 -681.121176 +13.2
WBI 0.33

		1	2	3	4	5
1	B	0.000000				
2	Ru	2.355879	0.000000			
3	B	2.388528	2.143938	0.000000		
4	Ru	2.171369	2.731752	2.165155	0.000000	
5	B	3.290250	2.145523	1.633719	2.118031	0.000000
6	B	1.788897	3.220870	1.767074	2.103883	3.068079

Ru-H-Ru Ru2-H 1.74 Ru4-H 1.80
Ru2-H-B1 Ru2-H 1.77 B1-H 1.30
B1-H-B6 B1-H 1.36 B6-H 1.30
B3-H-B6 B3-H 1.26 B6-H 1.46

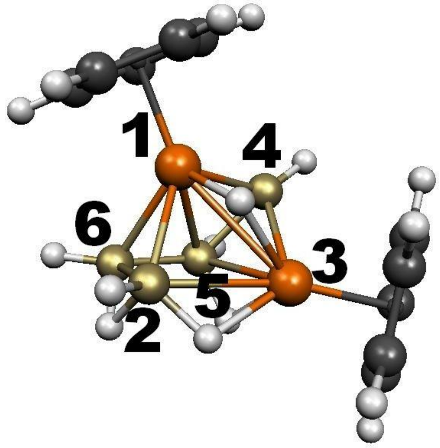

Ru2B4-5 -681.120925 +13.4
WBI 0.34

		1	2	3	4	5
1	Ru	0.000000				
2	B	2.169871	0.000000			
3	Ru	2.732765	2.442105	0.000000		
4	B	2.024147	3.308379	2.166015	0.000000	
5	B	2.229708	2.552073	2.329248	1.732868	0.000000
6	B	2.149054	1.799915	3.188529	3.017871	1.671327

Ru1-H-Ru3   Ru1-H 1.68   Ru3-H 1.89
Ru3-H-B5   Ru3-H 1.79   B5-H 1.3
Ru3-H-B2   Ru3-H 1.8   B2-H 1.3
B2-H-B6   B2-H 1.32   B6-H 1.32

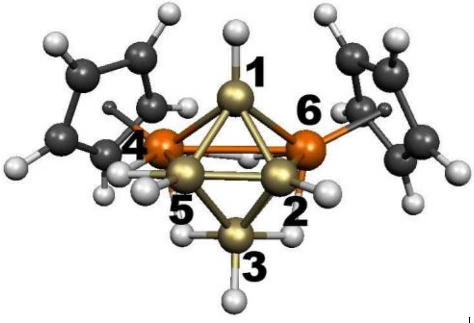

Ru2B4-6 -681.118217 +15.1
WBI 0.36

		1	2	3	4	5
1	B	0.000000				
2	B	1.728815	0.000000			
3	B	2.564541	1.773200	0.000000		
4	Ru	2.172445	3.016801	2.307160	0.000000	
5	B	1.760647	1.637691	1.897444	2.218448	0.000000
6	Ru	2.147426	2.152728	2.250564	2.762322	3.080407

Ru4-H- Ru6   Ru4-H 2.04   Ru6-H 1.64
Ru4-H-B3   Ru4-H 1.7   B3-H 1.39
Ru4-H-B5   Ru4-H 1.65   B5-H 1.39
Ru6-H-B3   Ru6-H 1.68   B3-H 1.42

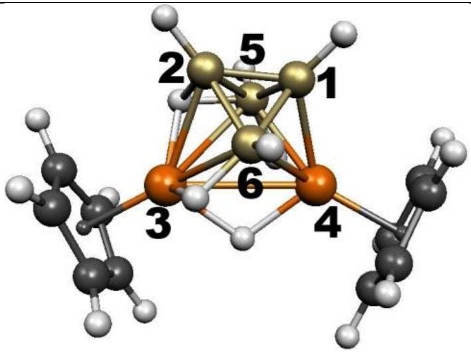

Ru2B4-7 -681.116461 +16.2
(C2) WBI 0.29

		1	2	3	4	5
1	B	0.000000				
2	B	1.655527	0.000000			
3	Ru	3.129503	2.293861	0.000000		
4	Ru	2.133062	3.058650	2.838142	0.000000	
5	B	1.725250	1.830778	2.528727	2.188818	0.000000
6	B	1.727128	1.791814	2.245492	2.252074	2.602888

Ru3-H- Ru4   Ru3-H 1.8   Ru4-H 1.72
Ru3-H-B2   Ru3-H 1.77   B2-H 1.43
Ru3-H-B6   Ru-H 1.69   B6-H 1.33
Ru4-H-B5   Ru-H 1.66   B5-H 1.43

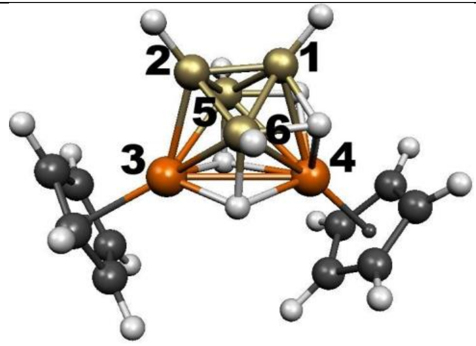

Ru2B4-8 -681.113981 +17.7 Cs
WBI 0.39

		1	2	3	4	5
1	B	0.000000				
2	B	1.673738	0.000000			
3	Ru	3.079055	2.140048	0.000000		
4	Ru	2.374226	3.189613	2.832265	0.000000	
5	B	1.814428	1.716741	2.226710	2.435871	0.000000
6	B	1.814054	1.716634	2.226026	2.442624	2.592801

Ru3-H- Ru4   Ru3-H 1.74   Ru4-H 2
Ru3-H- Ru4   Ru3-H 1.74   Ru4-H 2
B1-H-B5   B1-H 1.49   B5-H 1.46
B1-H-B6   B1-H 1.47   B6-H 1.46

Table 76. Distances table for the lowest-lying $Cp_2Os_2B_4H_8$ structures after M06L/6-311G(d,p) optimization. Included are the ZPcorrected E (a.u.), relative energy (kcal/mol), symmetry and WBI.

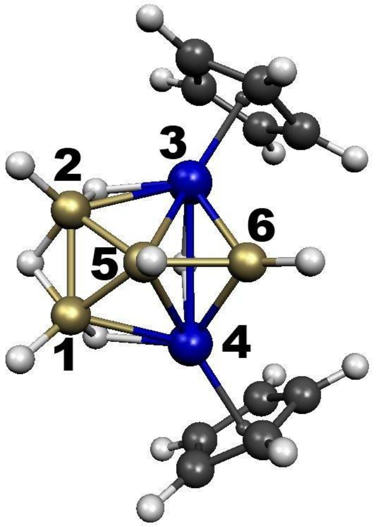

Os2B4-1 -672.740589 a.u. 0.0 kcal/mol Cs   WBI 0.32

		1	2	3	4	5
1	B	0.000000				
2	B	1.799400	0.000000			
3	Os	3.200287	2.245905	0.000000		
4	Os	2.245905	3.200287	2.888600	0.000000	
5	B	1.722774	1.722774	2.250993	2.250993	0.000000
6	B	3.122185	3.122185	2.083489	2.083489	1.744088

Os3-H-Os4   Os3-H 1.82   Os4-H 1.82
Os3-H-B2   Os3-H 1.77   B2-H 1.34
Os4-H-B1   Os4-H 1.77   B1-H 1.34
B1-H-B2   B1-H 1.33   B2-H 1.33

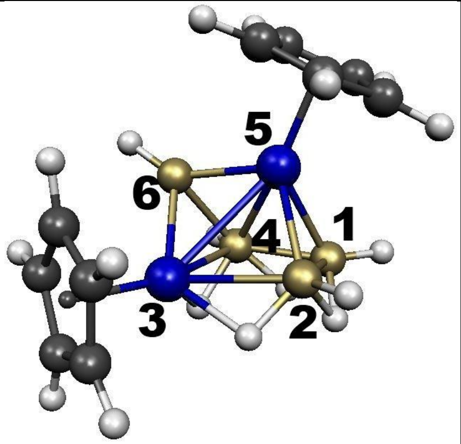 Os2B4-2 -672.728481 +7.6 WBI 0.40	1 2 3 4 5 1 B 0.000000 2 B 1.824243 0.000000 3 Os 3.205117 2.345793 0.000000 4 B 1.820507 2.602307 2.319689 0.000000 5 Os 2.131669 2.132088 2.798511 2.209356 0.000000 6 B 3.238105 3.224709 2.119802 1.927562 1.989942 Os3-H-B2 Os3-H 1.75 B2-H 1.34 Os3-H-B4 Os3-H 1.73 B4-H 1.4 B1-H B2 B1-H 1.3 B2-H 1.37 B1-H-B4 B1-H 1.3 B4-H 1.35
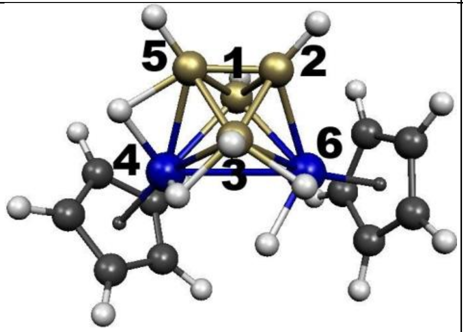 Os2B4-3 -672.724124 +10.3 WBI 0.46	1 2 3 4 5 1 B 0.000000 2 B 1.735599 0.000000 3 B 2.521144 1.764571 0.000000 4 Os 2.178450 3.048364 2.292232 0.000000 5 B 1.742718 1.645450 1.860761 2.210940 0.000000 6 Os 2.193635 2.204304 2.244174 2.794134 3.106023 Os4-H-B3 Os4-H 1.69 B3-H 1.48 Os4-H-B5 Os4-H 1.64 B5-H 1.57 Os6-H-B3 Os6-H 1.67 B6-H 1.53
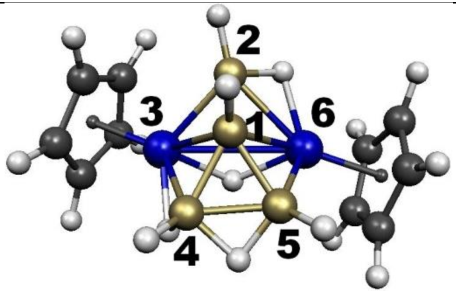 Os2B4-4 -672.721191 +12.2 (Cs) WBI 0.30	1 2 3 4 5 1 B 0.000000 2 B 1.738601 0.000000 3 Os 2.245452 2.126531 0.000000 4 B 1.742729 3.139865 2.218682 0.000000 5 B 1.693147 3.081710 3.159800 1.764792 0.000000 6 Os 2.290803 2.191433 2.938660 3.154968 2.161680 Os3-H-Os6 Os3-H 1.79 Os6-H 1.83 Os3-H-B4 Os3-H 1.73 B4-H 1.37 Os6-H-B2 Os6-H 1.72 B2-H 1.34 B4-H-B5 B4-H 1.34 B5-H 1.31

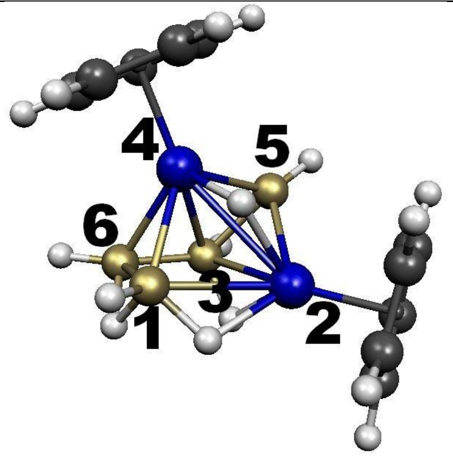

Os2B4-5 -672.719190 +13.4
WBI 0.36

```
                1          2          3          4          5
    1  B    0.000000
    2  Os   2.468582   0.000000
    3  B    2.562314   2.354221   0.000000
    4  Os   2.183871   2.790068   2.253888   0.000000
    5  B    3.318062   2.178869   1.750876   2.050461
0.000000
    6  B    1.799839   3.213126   1.675867   2.162801
3.038124
```

Os2-H-Os4   Os2-H 1.94   Os4-H 1.7
Os2-H-B1   Os2-H 1.8   B1-H 1.32
Os2-H-B3   Os2-H 1.8   B3-H 1.32
B1-H-B6   B1-H 1.32   B6-H 1.33

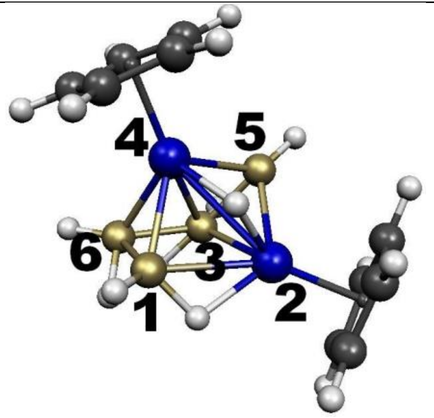

Os2B4-6 -672.717589 +14.4
WBI 0.36

```
                1          2          3          4          5
    1  B    0.000000
    2  Os   2.384387   0.000000
    3  B    2.496367   2.212049   0.000000
    4  Os   2.188924   2.782571   2.215984   0.000000
    5  B    3.283019   2.097656   1.738408   2.081920
0.000000
    6  B    1.794253   3.207447   1.780102   2.134441
3.129810
```

Os2-H-Os4   Os2-H 1.75   Os4-H 1.88
Os2-H-B1   Os2-H 1.75   B1-H 1.31
B1-H-B6   B1-H 1.33   B6-H 1.31
B3-H-B6   B3-H 1.28   B6-H 1.36

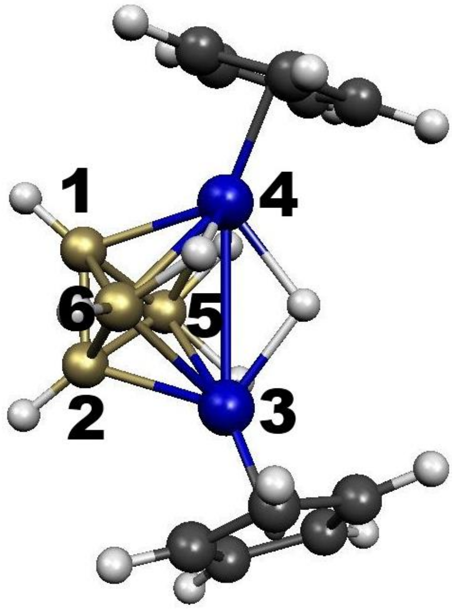

Os2B4-7 -672.717098 +14.7
(Cs)
WBI 0.31

```
                1          2          3          4          5
    1  B    0.000000
    2  B    1.663471   0.000000
    3  Os   3.088429   2.161001   0.000000
    4  Os   2.192572   3.097094   2.901772   0.000000
    5  B    1.807133   1.747600   2.251871   2.339774
0.000000
    6  B    1.754951   1.721550   2.249954   2.298028
2.559092
```

Os3-H-Os4   Os3-H 1.81   Os4-H 1.83
Os3-H-B5   Os3-H 1.66   B5-H 1.56
Os4-H-B5   Os4-H 1.71   B5-H 1.4
Os4-H-B6   Os4-H 1.71   B6-H 1.37

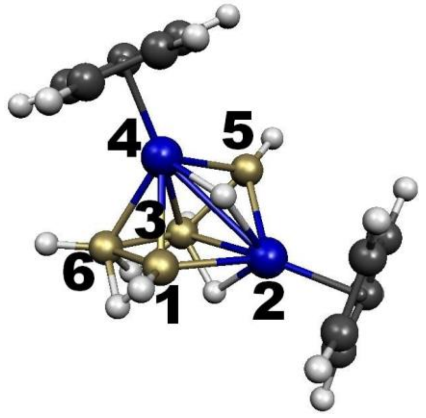 Os2B4-8 -672.713104 +17.3 WBI 0.35	1 2 3 4 5 1 B 0.000000 2 Os 2.201367 0.000000 3 B 2.500412 2.276599 0.000000 4 Os 2.205723 2.784652 2.210180 0.000000 5 B 3.203737 2.077270 1.876618 2.073447 0.000000 6 B 1.796898 3.166895 1.826963 2.149896 3.257226 Os2-H-Os4 Os2-H 1.86 Os4-H 1.74 Os2-H-B3 Os2-H 1.7 B3-H 1.41 B1-H-B6 B1-H 1.35 B6-H 1.3 B3-H-B6 B3-H 1.34 B6-H 1.31
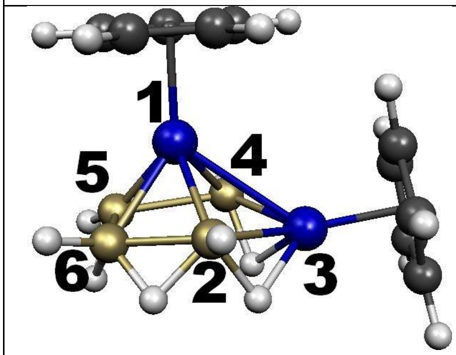 Os2B4-9 -672.708229 +20.3 (Cs) WBI 0.44	1 2 3 4 5 1 Os 0.000000 2 B 2.161645 0.000000 3 Os 2.781808 2.216041 0.000000 4 B 2.103642 2.986723 2.084169 0.000000 5 B 1.963075 2.900808 3.540139 2.158063 0.000000 6 B 2.167107 1.817682 3.524707 3.188366 1.790341 Os3-H-B2 Os3-H 1.71 B2-H 1.42 Os3-H-B4 Os3-H 1.73 B4-H 1.42 B2-H-B6 B2-H 1.4 B6-H 1.28 B5-H-B6 B5-H 1.41 B6-H 1.29
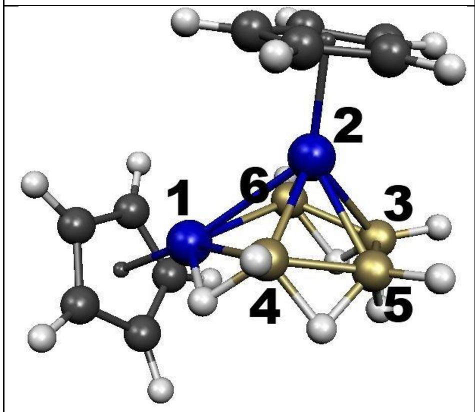 Os2B4-10 -672.706188 +21.6 WBI 0.66	1 2 3 4 5 1 Os 0.000000 2 Os 2.663550 0.000000 3 B 3.307146 2.168321 0.000000 4 B 2.379530 2.127298 3.022229 0.000000 5 B 3.361702 2.152910 1.807942 1.798806 0.000000 6 B 2.192238 2.042145 1.825607 3.198172 2.998414 Os1-H-B4 Os1-H 1.8 B4-H 1.3 B3-H-B5 B3-H 1.34 B5-H 1.33 B4-H-B5 B4-H 1.38 B5-H 1.3 B3-H-B6 B3-H 1.27 B6-H 1.46

6.1.2.3 $Cp_2Re_2B_4H_8$ systems

Table 77. Distances table for the lowest-lying $Cp_2Re_2B_4H_8$ structures after M06L/6-311G(d,p) optimization. Included are the ZPcorrected E (a.u.), relative energy (kcal/mol), symmetry and WBI.

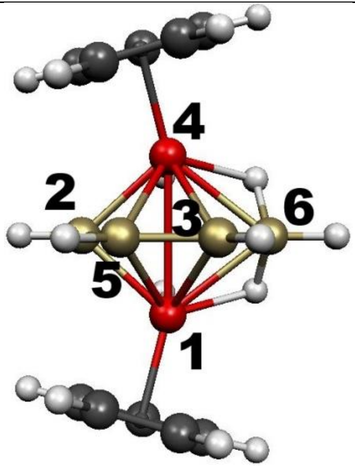 **Re2B4-1 -647.922354 0.0 Cs** **WBI 0.49**	1 2 3 4 5 1 Re 0.000000 2 B 2.110113 0.000000 3 B 2.257199 2.950254 0.000000 4 Re 2.832000 2.110113 2.257199 0.000000 5 B 2.193882 1.819983 1.637444 2.193882 0.000000 6 B 2.300610 3.377282 1.693443 2.300610 2.918674 Re1-H-B6 Re1-H 1.80 B6-H 1.33 Re4-H-B6 Re4-H 1.80 B6-H 1.33 Re1-H(-B2) Re1-H 1.67 B2-H 2.35 Re4-H(-B2) Re4-H 1.67 B2-H 2.35
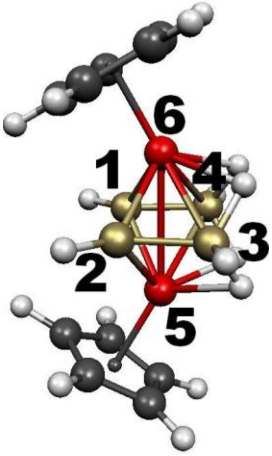 Re2B4-2 -647.918169 +2.6 C_{2v} WBI 0.52	1 2 3 4 5 1 B 0.000000 2 B 2.742778 0.000000 3 B 3.411116 1.764995 0.000000 4 B 1.757561 3.407805 3.107190 0.000000 5 Re 2.115753 2.109158 2.304033 2.309085 0.000000 6 Re 2.116270 2.108815 2.304648 2.308724 2.806100 Re5-H-B3 Re5-H 1.91 B3-H 1.28 Re5-H-B4 Re5-H 1.92 B4-H 1.27 Re6-H-B3 Re6-H 1.91 B3-H 1.28
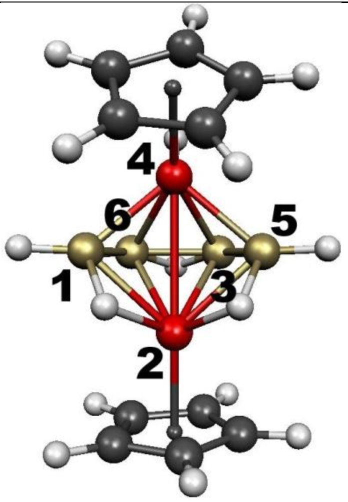 Re2B4-3 -647.906185 +10.2 C_s WBI 0.48	1 2 3 4 5 1 B 0.000000 2 Re 2.190207 0.000000 3 B 2.945230 2.291059 0.000000 4 Re 2.098172 2.846238 2.214516 0.000000 5 B 3.193659 2.175124 1.792613 2.105222 0.000000 6 B 1.791428 2.297176 1.712395 2.214017 2.947182 Re2-H-B1 Re2-H 1.72 B1-H 1.49 Re2-H-B5 Re2-H 1.72 B5-H 1.51 B3-H-B6 B3-H 1.31 B6-H 1.31

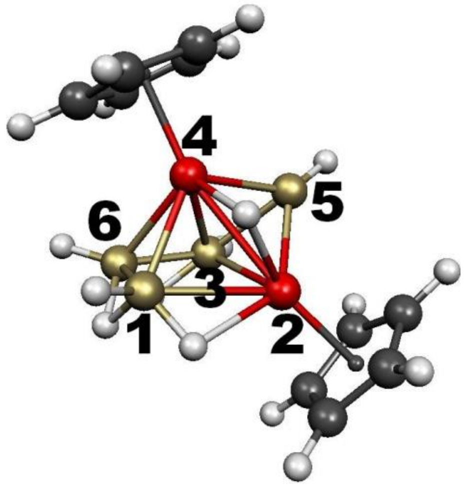 Re2B4-4 -647.896720 +16.1 WBI 0.78	1 2 3 4 5 1 B 0.000000 2 Re 2.472069 0.000000 3 B 2.727132 2.215076 0.000000 4 Re 2.240585 2.595692 2.190937 0.000000 5 B 3.546136 2.048711 2.029678 2.076789 0.000000 6 B 1.794596 3.084921 1.815088 2.201386 3.398206 Re2-H-Re4 Re2-H 1.97 Re4-H 1.79 Re2-H-B1 Re2-H 1.98 B1-H 1.24 B1-H-B6 B1-H 1.32 B6-H 1.32 B3-H-B6 B3-H 1.38 B6-H 1.28
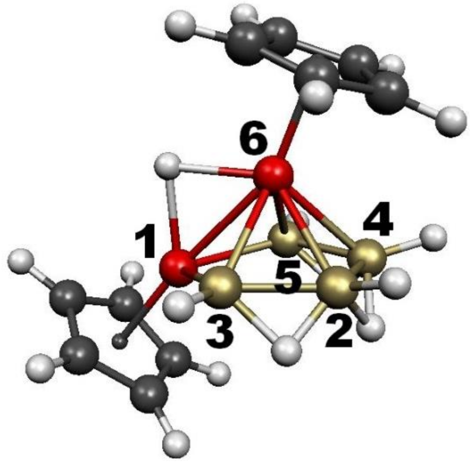 Re2B4-5 -647.889782 +20.4 Cs WBI 1.18	1 2 3 4 5 1 Re 0.000000 2 B 3.239914 0.000000 3 B 2.152152 1.805251 0.000000 4 B 3.237411 1.808518 2.998307 0.000000 5 B 2.149514 2.999868 3.172329 1.804355 0.000000 6 Re 2.457524 2.223423 2.192236 2.223342 2.195273 Re1-H-Re6 Re1-H 1.79 Re6-H 1.89 B3-H-B5 B3-H 1.41 B2-H 1.27 B2-H-B4 B2-H 1.32 B4-H 1.32 B4-H-B5 B4-H 1.27 B5-H 1.40
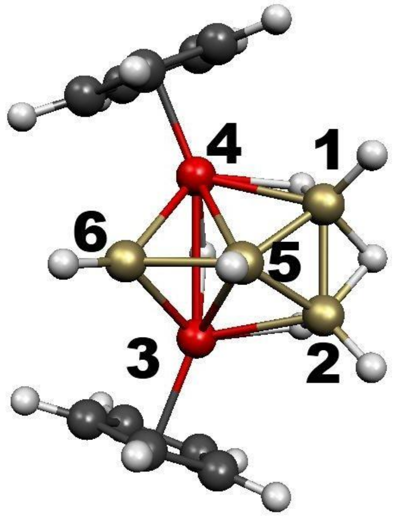 Re2B4-6 -647.887205 +22.1 Cs WBI 0.84	1 2 3 4 5 1 B 0.000000 2 B 1.779200 0.000000 3 Re 3.160820 2.269336 0.000000 4 Re 2.269347 3.160812 2.720800 0.000000 5 B 1.771982 1.772046 2.252824 2.252824 0.000000 6 B 3.279279 3.279313 2.063370 2.063370 1.909827 Re3-H-Re4 Re3-H 1.87 Re4-H 1.87 Re3-H-B2 Re3-H 1.84 B2-H 1.32 Re4-H-B1 Re4-H 1.84 B1-H 1.32 B1-H-B2 B1-H 1.32 B2-H 1.32

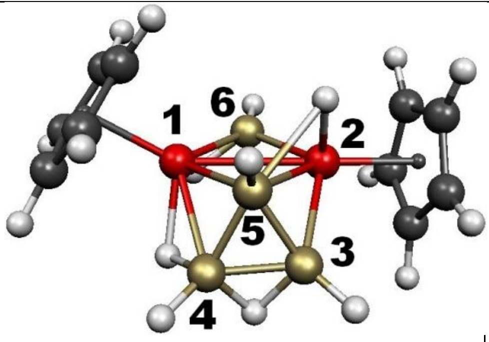

Re2B4-7 -647.881684 +25.7 (Cs)
WBI 0.85

		1	2	3	4	5	
1	Re	0.000000					
2	Re	2.677701	0.000000				
3	B	3.115424	2.205357	0.000000			
4	B	2.341592	3.116472	1.698601	0.000000		
5	B	2.220720	2.228480	1.683238	1.716170		0.000000
6	B	2.085860	2.094634	3.715298	3.780771		3.376841

Re1-H-B6   Re1-H 1.76   B6-H 1.37
Re1-H-B4   Re1-H 1.74   B4-H 1.45
Re2-H-B5   Re2-H 1.65   B5-H 2.06
B3-H-B4   B3-H 1.36   B4-H 1.29

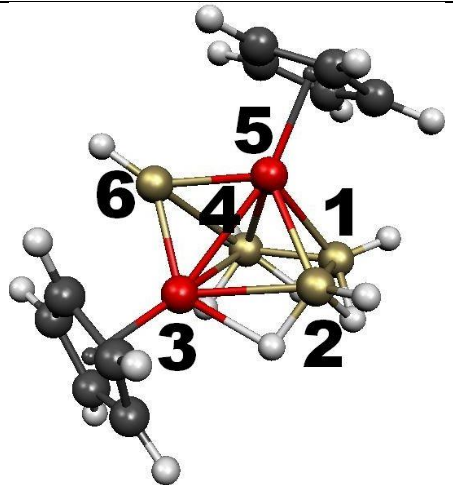

Re2B4-8 -647.881468 +25.8
WBI 1.03

		1	2	3	4	5	
1	B	0.000000					
2	B	1.798777	0.000000				
3	Re	3.165043	2.386694	0.000000			
4	B	1.822377	2.715495	2.404330	0.000000		
5	Re	2.203292	2.199339	2.626551	2.171258		0.000000
6	B	3.685049	3.442938	2.043440	2.542236		2.052463

Re3-H-B2   Re3-H 1.86   B2-H 1.28
Re3-H-B4   Re3-H 1.79   B4-H 1.36
B1-H-B2   B1-H 1.28   B2-H 1.38
B1-H-B4   B1-H 1.29   B4-H 1.38

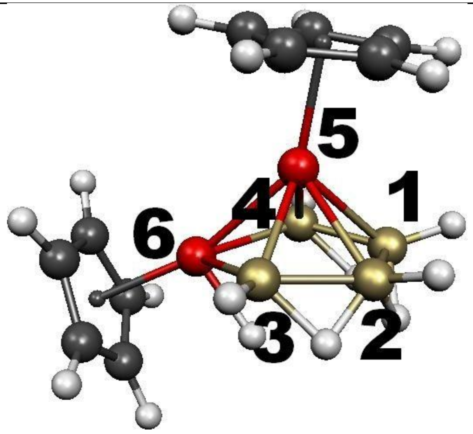

Re2B4-9 -647.881214 +25.8 Cs
WBI 1.64

		1	2	3	4	5	
1	B	0.000000					
2	B	1.808500	0.000000				
3	B	3.030232	1.810651	0.000000			
4	B	1.810719	3.030273	3.264500	0.000000		
5	Re	2.217380	2.217339	2.156480	2.156520		0.000000
6	Re	3.232654	3.232626	2.193320	2.193356		2.363690

Re6-H 1.64
B1-H-B2   B1-H 1.33   B2-H 1.33
B1-H-B4   B1-H 1.27   B4-H 1.42
B2-H-B3   B2-H 1.27   B3-H 1.48

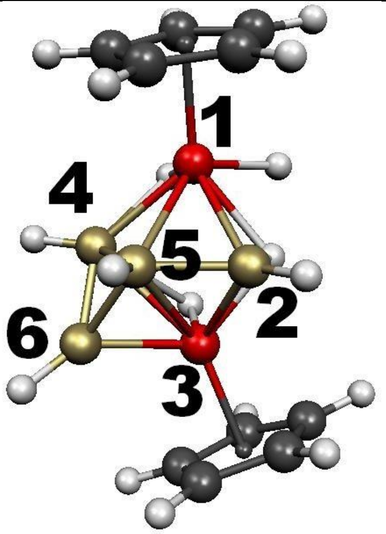 Re2B4-10 -647.881156 +25.9 WBI 0.37	1 2 3 4 5 1 Re 0.000000 2 B 2.202529 0.000000 3 Re 2.998972 2.157079 0.000000 4 B 2.128345 2.891257 2.364285 0.000000 5 B 2.248711 1.756917 2.290521 1.707475 0.000000 6 B 3.440552 3.063908 2.032551 1.686037 1.787284 Re1-B2-Re3-H Re1-H 1.99 B2-H 1.38 Re3-H 1.87 Re1-H-B4 Re1-H 1.67 B4-H 2.16
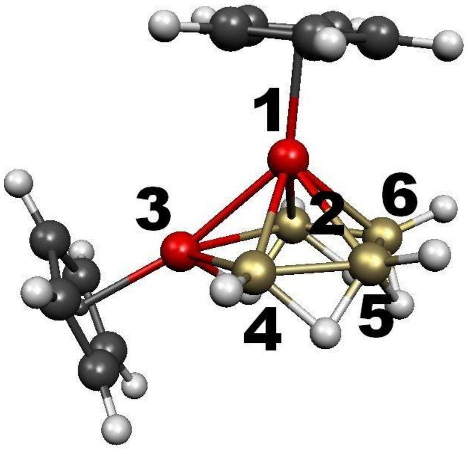 Re2B4-11 -647.879561 +26.9 WBI 1.62	1 2 3 4 5 1 Re 0.000000 2 B 2.146085 0.000000 3 Re 2.393942 2.312908 0.000000 4 B 2.178334 3.174589 2.161594 0.000000 5 B 2.217238 2.989992 3.327837 1.794984 0.000000 6 B 2.208066 1.811300 3.393634 2.987460 1.789617 Re3-H-B2 Re3-H 1.75 B2-H 1.4 B2-H-B6 B2-H 1.42 B6-H 1.27 B4-H-B5 B4-H 1.4 B5-H 1.28 B5-H-B6 B5-H 1.35 B6-H 1.31
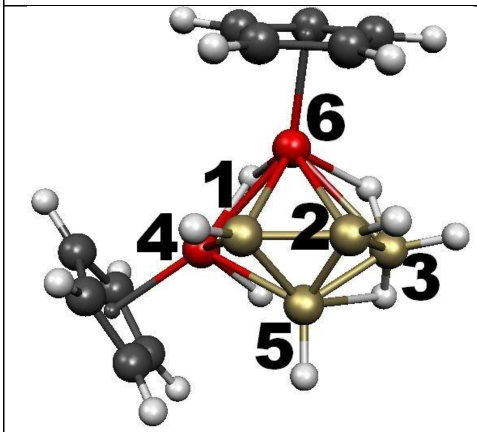 Re2B4-12 -647.879052 +27.2 WBI 1.31	1 2 3 4 5 1 B 0.000000 2 B 1.721631 0.000000 3 B 2.909699 1.740842 0.000000 4 Re 2.191905 3.275908 3.328779 0.000000 5 B 1.747424 1.634877 1.860275 2.341474 0.000000 6 Re 2.206026 2.279031 2.429880 2.451964 2.727719 Re4-H- Re6 Re4-H 1.85 Re6-H 1.81 Re6-H-B3 Re6-H 1.79 B3-H 1.37 B5-H-B3 B5-H 2.1 B3-H 1.2

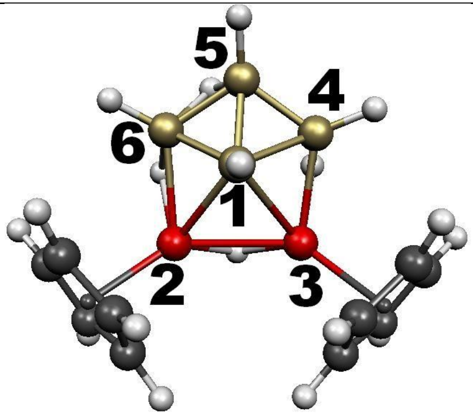

Re2B4-13 -647.871216 +32.1
(Cs)
WBI 1.54

```
                1          2          3          4          5
    1  B    0.000000
    2  Re   2.257445   0.000000
    3  Re   2.293688   2.412394   0.000000
    4  B    1.853279   3.405510   2.126701   0.000000
    5  B    1.754718   3.366196   3.310814   1.712948
0.000000
    6  B    1.774869   2.164486   3.341207   2.811304
1.714290
```

Re2-H-Re3   Re2-H 1.85   Re3-H 1.82
Re2-H-B6   Re2-H 1.74   B6-H 1.49
Re3-H-B4   Re3-H 1.79   B4-H 1.38
B5-H-B6   B5-H 1.26   B6-H 1.48

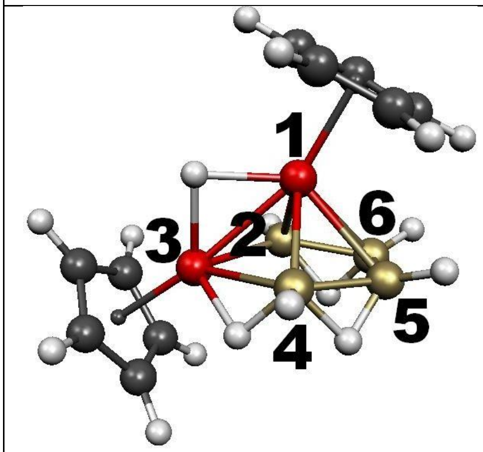

Re2B4-14 -647.865695 +35.6
(Cs)
WBI 1.30

```
                1          2          3          4          5
    1  Re   0.000000
    2  B    2.210954   0.000000
    3  Re   2.468793   2.186069   0.000000
    4  B    2.176773   3.140836   2.403098   0.000000
    5  B    2.322595   2.878410   3.432825   1.808813
0.000000
    6  B    2.355386   1.778913   3.347025   2.897742
1.631318
```

Re1-H-Re3   Re1-H 1.82   Re3-H 1.8
Re3-H-B4   Re3-H 1.75   B4-H 1.37
B2-H-B6   B2-H 1.37   B6-H 1.27
B4-H-B5   B4-H 1.36   B5-H 1.29

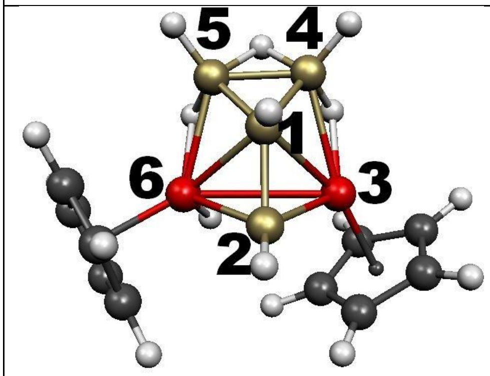

Re2B4-15 -647.862628 +37.5
(Cs)
WBI 0.51

```
                1          2          3          4          5
    1  B    0.000000
    2  B    1.757089   0.000000
    3  Re   2.246430   2.108348   0.000000
    4  B    1.727535   3.188569   2.328560   0.000000
    5  B    1.726980   3.149823   3.223083   1.796965
0.000000
    6  Re   2.263555   2.130963   2.909684   3.244002
2.245361
```

Re3-H-B4   Re3-H 1.82   B4-H 1.31
Re6-H-B5   Re6-H 1.8   B5-H 1.32
B4-H-B5   B4-H 1.28   B5-H 1.39

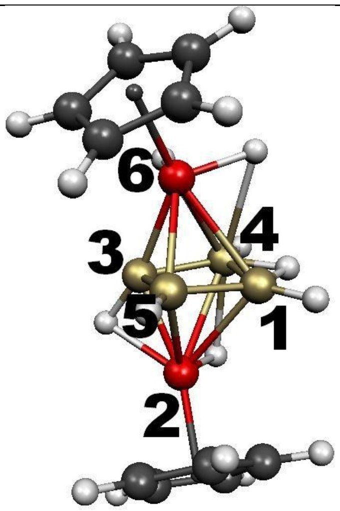

Re2B4-16 -647.858269 +40.2
WBI 0.20

		1	2	3	4	5
1	B	0.000000				
2	Re	2.298266	0.000000			
3	B	2.534675	2.189304	0.000000		
4	B	1.734292	2.453764	1.743612	0.000000	
5	B	1.775471	2.107432	1.717369	2.383535	0.000000
6	Re	2.417593	3.735873	2.229219	2.362073	2.018987

Re2-H-B3 Re2-H 1.87 B3-H 1.32
B1-H-B4 B1-H 1.27 B4-H 1.3

6.1.2.4 $Cp_2M_2B_4H_8$ (M=Mo,W) systems

Table 78. Distances table for the lowest-lying $Cp_2Mo_2B_4H_8$ structures after M06L/6-311G(d,p) optimization. Included are the ZPcorrected E (a.u.), relative energy (kcal/mol), symmetry and WBI.

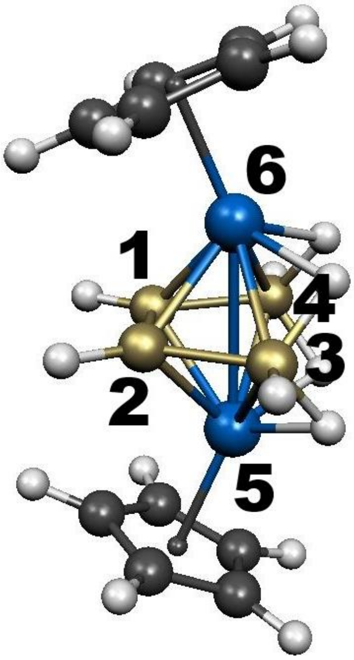

Mo2B4-1 -627.695780 a.u. 0.0 kcal/mol C_{2v} WBI 0.87

		1	2	3	4	5
1	B	0.000000				
2	B	1.882600	0.000000			
3	B	3.072854	1.837261	0.000000		
4	B	1.837261	3.072965	3.222800	0.000000	
5	Mo	2.132216	2.132272	2.261541	2.261564	0.000000
6	Mo	2.132216	2.132272	2.261541	2.261564	2.997400

Mo5-H-B3 Mo5-H 1.82 B3-H 1.34
Mo5-H-B4 Mo5-H 1.82 B4-H-1.34
Mo6-H-B3 Mo6-H 1.82 B3-H 1.34
Mo6-H-B4 Mo6-H 1.82 B4-H 1.34

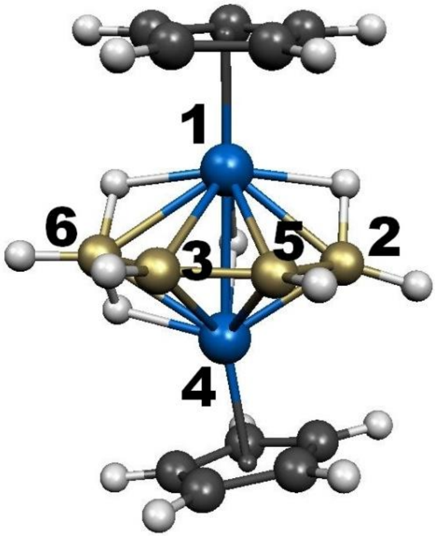 Mo2B4-2 -627.694081 +1.1 WBI 0.95	1 2 3 4 5 1 Mo 0.000000 2 B 2.249041 0.000000 3 B 2.268950 3.012179 0.000000 4 Mo 2.604112 2.169342 2.246655 0.000000 5 B 2.244564 1.745470 1.658818 2.208820 0.000000 6 B 2.349138 3.690150 1.718078 2.312124 3.027420 Mo1-H-Mo4 Mo1-H 1.93 Mo4-H 1.93 Mo1-H-B2 Mo1-H 1.85 B2-H 1.28 Mo1-H-B6 Mo1-H 1.87 B6-H 1.29 B4-H-B6 Mo-H 1.87 B6-H 1.28
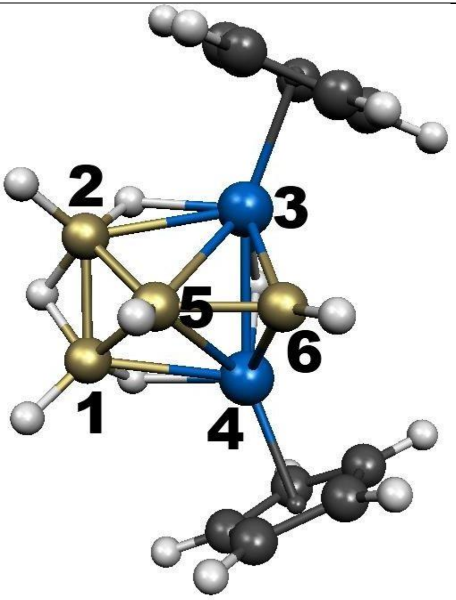 Mo2B4-3 -627.682383 +8.4 Cs WBI 1.51	1 2 3 4 5 1 B 0.000000 2 B 1.786405 0.000000 3 Mo 3.153081 2.339391 0.000000 4 Mo 2.343384 3.152095 2.494800 0.000000 5 B 1.729558 1.729842 2.295570 2.295458 0.000000 6 B 3.140128 3.139486 2.129952 2.127826 1.714327 Mo3-H-Mo4 Mo3-H 1.86 Mo4-H 1.86 Mo3-H-B2 Mo3-H 1.85 B2-H 1.3 Mo4-H-B1 Mo4-H 1.85 B1-H 1.3 B1-H-B2 B1-H 1.32 B2-H 1.32
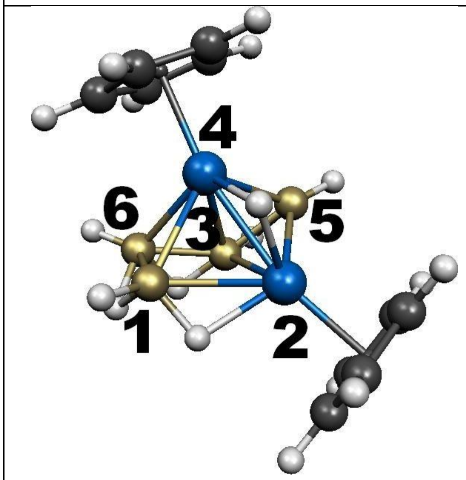	1 2 3 4 5 1 B 0.000000 2 Mo 2.408552 0.000000 3 B 2.571947 2.258855 0.000000 4 Mo 2.263682 2.475855 2.239001 0.000000 5 B 3.520812 2.191679 1.671163 2.170603 0.000000 6 B 1.772995 3.149932 1.758315 2.226707 3.123144 Mo2-H-Mo4 Mo2-H 1.84 Mo4-H 1.86 Mo4-H-B5 Mo4-H 1.85 B5-H 1.3 B3-H-B5 B3-H 1.3 B5-H 1.35

Mo2B4-4 -627.661864 +21.3 WBI 1.39	B3-H-B6 B3-H 1.4 B6-H 1.27
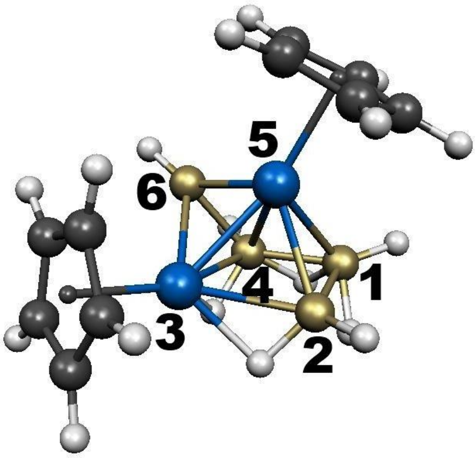 Mo2B4-5 -627.647670 +30.2 WBI 1.82	1 2 3 4 5 1 B 0.000000 2 B 1.797322 0.000000 3 Mo 3.130686 2.358747 0.000000 4 B 1.822334 2.666905 2.326749 0.000000 5 Mo 2.209737 2.269103 2.395722 2.321280 0.000000 6 B 3.143637 3.550251 2.245851 1.780172 2.084944 Mo3-H-B2 Mo3-H 1.9 B2-H 1.28 Mo3-H-B4 Mo3-H 1.89 B4-H 1.3 B1-H-B2 B1-H 1.29 B2-H 1.38 B1-H-B4 B1-H 1.34 B4-H 1.31

Table 79. Distances table for the lowest-lying $Cp_2W_2B_4H_8$ structures after M06L/6-311G(d,p) optimization. Included are the ZPcorrected E (a.u.), relative energy (kcal/mol), symmetry and WBI.

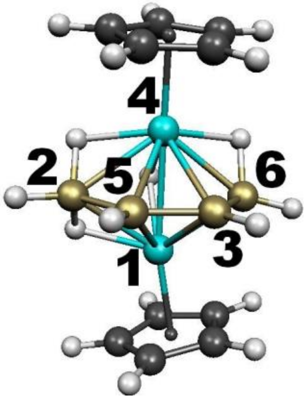 **W2B4-1 -625.500292 0.0 (Cs)** **WBI 0.97**	1 2 3 4 5 1 W 0.000000 2 B 2.261767 0.000000 3 B 2.276961 3.019006 0.000000 4 W 2.632417 2.179473 2.258581 0.000000 5 B 2.252586 1.748519 1.667065 2.226458 0.000000 6 B 2.351273 3.692469 1.715791 2.323063 3.032263 W1-H-W4 W1-H 1.94 W4-H 1.94 W1-H-B2 W1-H 1.89 B2-H 1.29 W4-H-B2 W4-H 1.88 B2-H 1.3 W4-H-B6 W4-H 1.86 B6-H 1.29

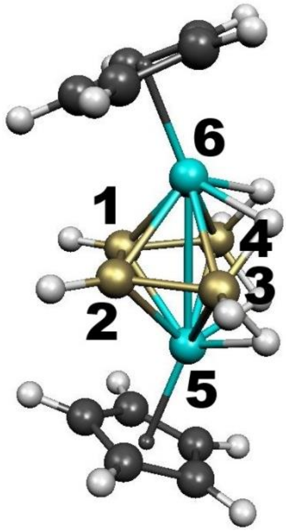

W2B4-2 -625.499140 a.u. 0.7 kcal/mol C_{2v} WBI 0.88

```
              1          2          3          4          5
    1  B    0.000000
    2  B    1.880200   0.000000
    3  B    3.057796   1.830306   0.000000
    4  B    1.830306   3.057796   3.191200   0.000000
    5  W    2.151064   2.151064   2.259983   2.259983
0.000000
    6  W    2.151064   2.151064   2.259983   2.259983
3.035000
```

W5-H-B3 W5-H 1.82 B3-H 1.37
W5-H-B4 W5-H 1.82 B4-H 1.37
W4-H-B3 W4-H 1.82 B3-H 1.37
W4-H-B4 W4-H 1.82 B4-H 1.37

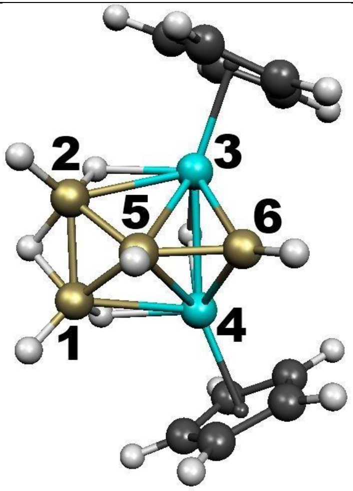

W2B4-3 -625.484708 +9.8 Cs WBI 1.52

```
              1          2          3          4          5
    1  B    0.000000
    2  B    1.791300   0.000000
    3  W    3.166471   2.344923   0.000000
    4  W    2.344939   3.166537   2.527800   0.000000
    5  B    1.731512   1.731492   2.315388   2.315440
0.000000
    6  B    3.148799   3.148772   2.138712   2.138792
1.731843
```

W3-H-W4 W3-H 1.87 W4-H1.87
W3-H-B2 W3-H 1.86 B2-H 1.31
W4-H-B1 W4-H 1.86 B1-H 1.31
B1-H-B2 B1-H 1.32 B2-H 1.32

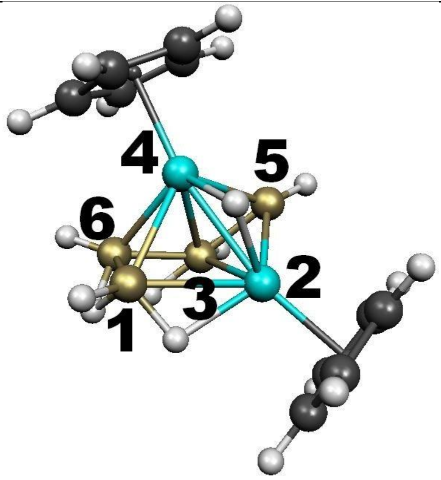

W2B4-4. -625.458073 +23.1 WBI 1.34

```
              1          2          3          4          5
    1  B    0.000000
    2  W    2.418743   0.000000
    3  B    2.628519   2.315324   0.000000
    4  W    2.275959   2.517867   2.280652   0.000000
    5  B    3.516927   2.166821   1.736968   2.147702
0.000000
    6  B    1.782607   3.162601   1.774641   2.245215
3.164283
```

W2-H-W4 W2-H 1.88 W4-H 1.86
W2-H-B1 W2-H 1.86 B1-H 1.31
B1-H-B3 B1-H 1.34 B6-H 1.3
B3-H-B6 B3-H 1.3 B6-H 1.34

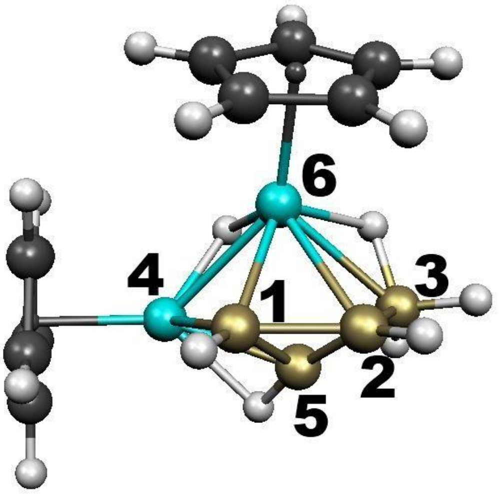 W2B4-5 -625.459872 +25.4 WBI 0.56	1 2 3 4 5 1 B 0.000000 2 B 1.756987 0.000000 3 B 3.004792 1.811614 0.000000 4 W 2.291587 3.427151 3.517672 0.000000 5 B 1.688628 1.581043 1.800980 2.222296 0.000000 6 W 2.185804 2.340526 2.420418 2.546408 2.374543 W4-H-Mo6 W4-H 1.86 W6-H 1.88 W4-H-B5 W4-H 1.96 B5-H 1.26 W6-H-B3 W6-H 1.84 B3-H 1.36
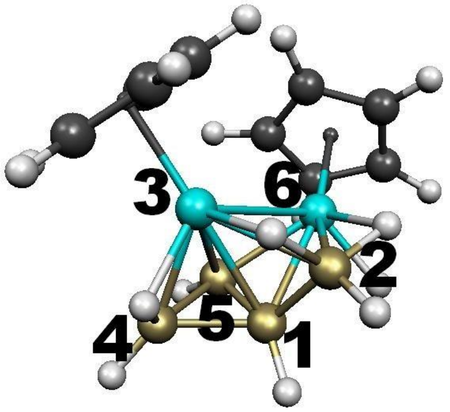 W2B4-6 -625.458073 +26.5 WBI 1.14	1 2 3 4 5 1 B 0.000000 2 B 1.747686 0.000000 3 W 2.338260 2.318737 0.000000 4 B 1.811387 3.087357 2.092723 0.000000 5 B 1.660713 2.984079 2.407399 1.821202 0.000000 6 W 2.273213 2.263326 2.733748 3.461752 2.116689 W3-H-B2 W3-H 1.78 B2-H 1.48 W3-H-B4 W3-H 1.79 B4-H 1.39 W6-H-B2 W6-H 1.84 B2-H 1.3
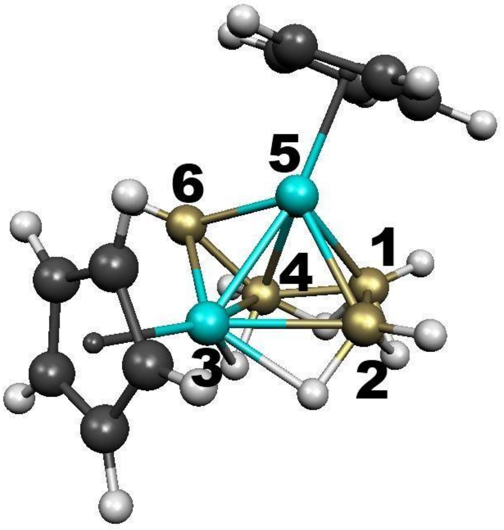 W2B4-7 -625.447061 +33.4 WBI 1.82	1 2 3 4 5 1 B 0.000000 2 B 1.815195 0.000000 3 W 3.167250 2.352371 0.000000 4 B 1.829640 2.670388 2.358519 0.000000 5 W 2.227248 2.269293 2.452318 2.326433 0.000000 6 B 3.185223 3.535723 2.242803 1.809080 2.092471 6 6 B 0.000000 W3-H-B2 W3-H 1.9 B2-H 1.3 W3-H-B4 W3-H 1.88 B4-H 1.33 B1-H-B2 B1-H 1.29 B2-H 1.39 B1-H-B4 B1-H 1.32 B4-H 1.32

6.1.2.5 $Cp_2Ta_2B_4H_8$ systems

Table 80 . Distances table for the lowest-lying $Cp_2Ta_2B_4H_8$ structures after M06L/6-311G(d,p) optimization. Included are the ZPcorrected E (a.u.), relative energy (kcal/mol), symmetry and WBI.

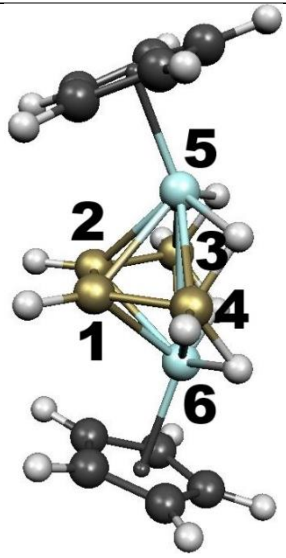 **Ta2B4-1 -605.339520 0.0 C_{2v}** **WBI 0.76**	Distance matrix (angstroms): 1 2 3 4 5 1 B 0.000000 2 B 1.720100 0.000000 3 B 3.070487 1.775805 0.000000 4 B 1.775859 3.070575 3.647800 0.000000 5 Ta 2.248299 2.248337 2.354711 2.354711 0.000000 6 Ta 2.248299 2.248337 2.354711 2.354711 2.977400 Ta5-H-B3 Ta5-H 1.91 B3-H 1.31 Ta5-H-B4 Ta5-H 1.91 B4-H 1.31 Ta6-H-B3 Ta6-H 1.91 B3-H 1.31 Ta6-H-B4 Ta6-H 1.91 B4-H 1.31
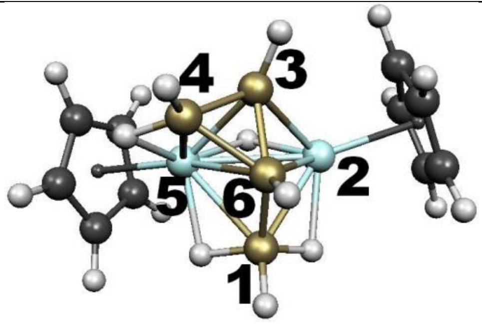 Ta2B4-2 -605.315795 +14.9 WBI 1.10	1 2 3 4 5 1 B 0.000000 2 Ta 2.307376 0.000000 3 B 3.073070 2.225809 0.000000 4 B 3.167799 3.509265 1.713773 0.000000 5 Ta 2.376118 2.724153 2.281385 2.240793 0.000000 6 B 1.796914 2.268642 1.751223 1.857470 2.431615 Ta2-H-Ta5 Ta2-H 1.9 Ta5-H 1.96 Ta2-H-B1 Ta2-H 1.9 B1-H 1.31 Ta5-H-B1 Ta5-H 1.88 B1-H 1.31 Ta5-H-B4 Ta5-H 1.94 B4-H 1.24

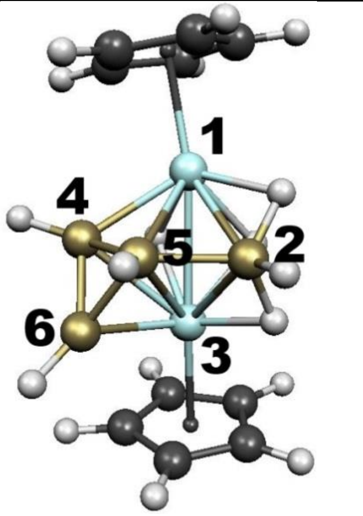

Ta2B4-3 -605.308635 +19.4
WBI 1.07

```
                  1          2          3          4          5
    1  Ta   0.000000
    2  B    2.338586   0.000000
    3  Ta   2.685514   2.451468   0.000000
    4  B    2.197678   3.062408   2.442346   0.000000
    5  B    2.340570   1.773988   2.484649   1.701823
0.000000
    6  B    3.384490   3.063331   2.235276   1.662320
1.720872
                  6
    6  B    0.000000
```

Ta1-H-Ta3   Ta1-H 1.95   Ta3-H 1.91
Ta1-H-Ta3   Ta1-H 1.96   Ta3-H 1.95
Ta1-H-B2   Ta1-H 1.93   B2-H 1.29
Ta3-H-B2   Ta3-H 1.91   B3-H 1.33

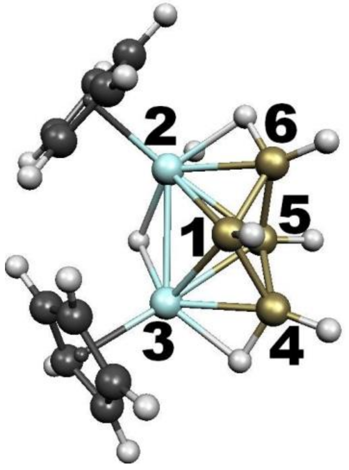

Ta2B4-4 -605.304084 +22.2 (Cs)
WBI 1.14

```
                  1          2          3          4          5
    1  B    0.000000
    2  Ta   2.379184   0.000000
    3  Ta   2.316177   2.738301   0.000000
    4  B    1.783223   3.620256   2.260163   0.000000
    5  B    1.741966   2.385581   2.338256   1.716962
0.000000
    6  B    1.762919   2.245930   3.552051   2.844320
1.755930
```

Ta2-H-Ta3   Ta2-H 1.95   Ta3-H 1.9
Ta2-H-B6   Ta2-H 1.9   B6-H 1.26
Ta3-H-B4   Ta3-H 1.91   B4-H 1.27

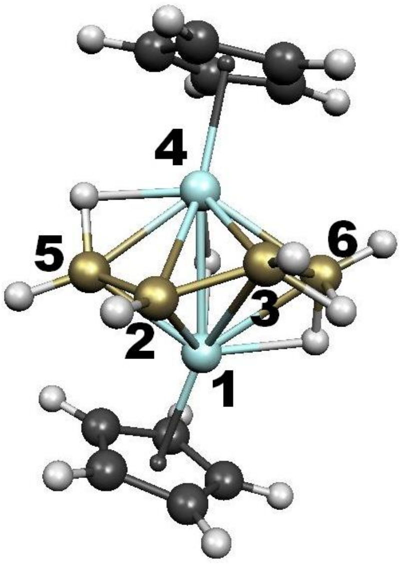

Ta2B4-5 -605.299268 +25.3

```
                  1          2          3          4          5
    1  Ta   0.000000
    2  B    2.229633   0.000000
    3  B    2.604675   1.714450   0.000000
    4  Ta   2.670151   2.435500   2.254618   0.000000
    5  B    2.328372   1.728381   3.043075   2.234300
0.000000
    6  B    2.367287   2.969174   1.729021   2.391897
3.721060
```

Ta1-H-B6   Ta1-H 1.91   B6-H 1.30
Ta4-H-B5   Ta4-H 1.89   B5-H 1.28
B3-H-B6   B3-H 1.39   B6-H 1.28

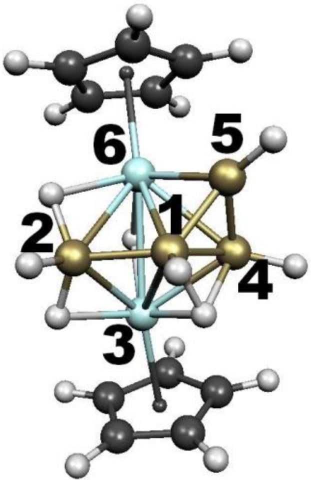 Ta2B4-6 -605.297978 +26.1 WBI 1.26	1 2 3 4 5 1 B 0.000000 2 B 1.800552 0.000000 3 Ta 2.517796 2.348286 0.000000 4 B 1.861826 3.101455 2.239551 0.000000 5 B 1.731837 3.125483 3.465848 1.697731 0.000000 6 Ta 2.407665 2.372320 2.722923 2.377830 2.162966 Ta3-H-Ta6 Ta3-H 1.87 Ta6-H 1.93 Ta3-H-B2 Ta3-H 1.88 B2-H 1.31 Ta3-H-B4 Ta3-H 1.9 B4-H 1.5 Ta6-H-B2 Ta6-H 1.89 B2-H 1.3
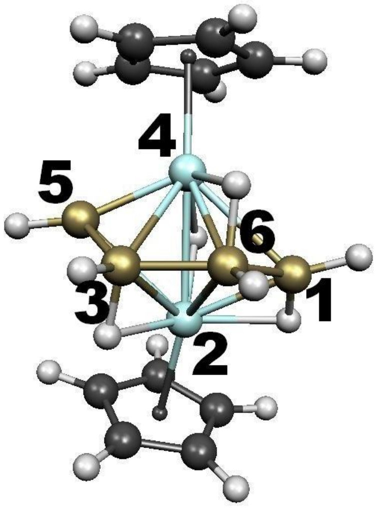 Ta2B4-7 -605.295793 +27.4 (C_2) WBI 1.13	1 2 3 4 5 1 B 0.000000 2 Ta 2.200946 0.000000 3 B 3.119414 2.321749 0.000000 4 Ta 2.598022 2.669209 2.429128 0.000000 5 B 3.861036 2.618286 1.746597 2.074182 0.000000 6 B 1.734706 2.373940 1.770039 2.400563 3.089124 Ta2-H-Ta4 Ta2-H 1.91 Ta4-H 1.94 Ta2-H-B1 Ta2-H 1.91 B1-H 1.26 Ta2-H-B3 Ta2-H 1.9 B3-H 1.3 Ta4-H-B6 Ta4-H 1.91 B6-H 1.32
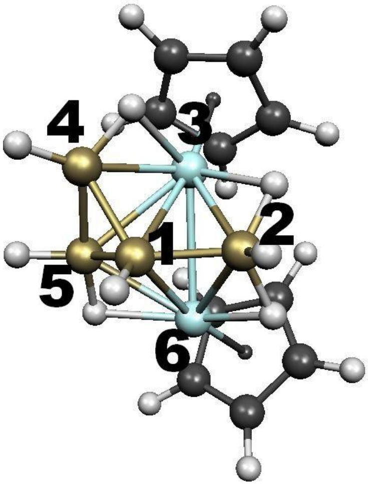 Ta2B4-8 -605.292389 +29.6 WBI 1.39	1 2 3 4 5 1 B 0.000000 2 B 1.768063 0.000000 3 Ta 2.359168 2.387011 0.000000 4 B 1.808351 3.065713 2.165397 0.000000 5 B 1.706385 3.144323 2.424616 1.846690 0.000000 6 Ta 2.299853 2.407503 2.697738 3.546609 2.278223 Ta3-H-B2 Ta3-H 1.94 B2-H 1.31 Ta3-H-B4 Ta3-H 1.89 B4-H 1.3 Ta6-H-B2 Ta6-H 1.97 B2-H 1.31 Ta6-H-B5 Ta6-H 1.88 B5-H 1.34

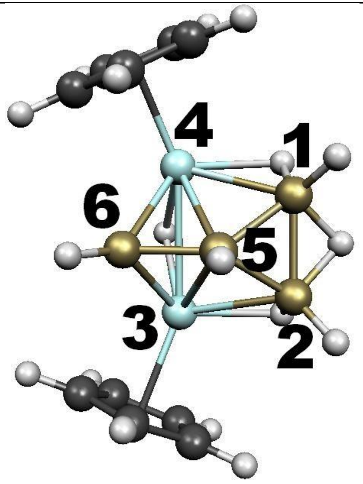

Ta2B4-9 -605.286714 +33.1 Cs
WBI 1.25

```
                 1          2          3          4          5
    1  B    0.000000
    2  B    1.827200   0.000000
    3  Ta   3.282277   2.389673   0.000000
    4  Ta   2.389673   3.282277   2.770800   0.000000
    5  B    1.760671   1.760671   2.353259   2.353259
0.000000
    6  B    3.190782   3.190782   2.186716   2.186716
1.734632
                 6
    6  B    0.000000
```

Ta3-H-Ta4 Ta3-H 1.95 Ta4-H 1.95
Ta3-H-B2 Ta3-H 1.96 B2-H 1.27
Ta4-H-B1 Ta4-H 1.96 B1-H 1.27
B1-H-B2 B1-H 1.32 B2-H 1.32

6.1.3 7 vertices

6.1.3.1 $Cp_2Ir_2B_5H_9$ systems

Table 81. Distances table for the lowest-lying $Cp_2Ir_2B_5H_9$ structures after M06L/6-311G(d,p) optimization. Included are the ZPcorrected E (a.u.), relative energy (kcal/mol), symmetry and WBI.

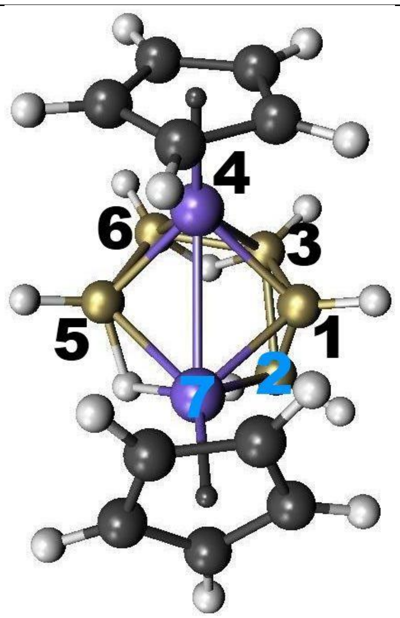

Ir2B5-1 -725.531382 a.u.
0.0 kcal/mol WBI 0.36

```
                 1          2          3          4          5
    1  B    0.000000
    2  B    1.700845   0.000000
    3  B    1.705099   2.000938   0.000000
    4  Ir   2.146441   3.310540   2.208743   0.000000
    5  B    3.008321   3.105379   2.875841   2.134447
0.000000
    6  B    2.954083   3.030634   1.812200   2.111595
1.820586
    7  Ir   2.121922   2.324391   3.194646   2.730519
2.228374
                 6          7
    6  B    0.000000
    7  Ir   3.398854   0.000000
```

Ir7-H-B5 Ir7-H 1.68 B5-H 1.39
B3-H-B6 B3-H 1.3 B6-H 1.3
B5-H-B6 B5-H 1.35 B6-H 1.3

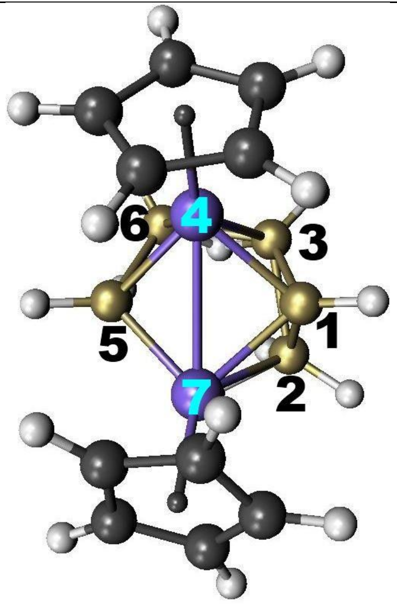

Ir2B5-2 -725.527636 +2.4
WBI 0.36

```
                 1          2          3          4          5
     1  B    0.000000
     2  B    1.732491   0.000000
     3  B    1.729402   1.937151   0.000000
     4  Ir   2.134885   3.322704   2.194551   0.000000
     5  B    3.004579   3.172228   2.880999   2.128020
0.000000
     6  B    2.978807   3.015910   1.833571   2.117840
1.806921
     7  Ir   2.123413   2.372847   3.131121   2.717462
2.105841
                 6          7
     6  B    0.000000
     7  Ir   3.277563   0.000000
```

Ir7-H-B2 Ir7-H 1.66 B2-H 1.46
B2-H-B3 B2-H 1.2 B3-H 2.31
B3-H-B6 B3-H 1.32 B6-H 1.29
B5-H-B6 B5-H 1.35 B6-H 1.3

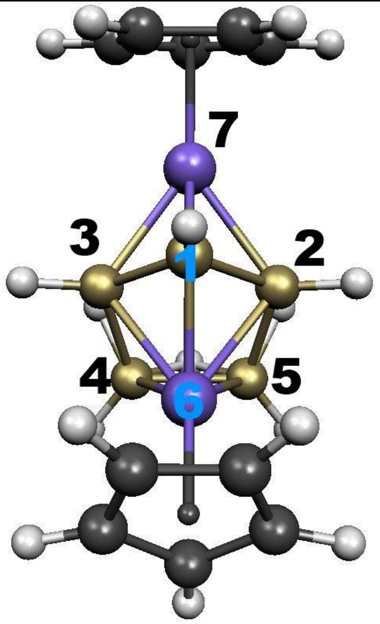

Ir2B5-3 -725.522650 +5.5 Cs
WBI 0.09

```
                 1          2          3          4          5
     1  B    0.000000
     2  B    1.824442   0.000000
     3  B    1.824442   2.647600   0.000000
     4  B    3.056335   2.863991   1.837787   0.000000
     5  B    3.056335   1.837787   2.863991   1.822400
0.000000
     6  Ir   2.074187   2.252654   2.252654   2.108049
2.108049
     7  Ir   2.011788   2.258461   2.258461   3.467149
3.467149
                 6          7
     6  Ir   0.000000
     7  Ir   3.605018   0.000000
```

B2-H-B5 B2-H 1.33 B5-H 1.28
B3-H-B4 B3-H 1.33 B4-H 1.28
B4-H-B5 B4-H 1.32 B5-H 1.32

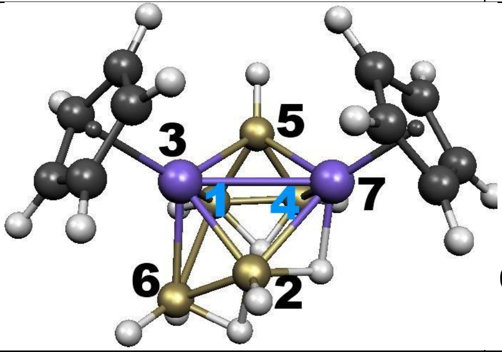

```
                 1          2          3          4          5
     1  B    0.000000
     2  B    2.983471   0.000000
     3  Ir   2.147244   2.135908   0.000000
     4  B    1.706165   3.100641   3.067360   0.000000
     5  B    1.717095   3.189158   2.139074   1.683116
0.000000
     6  B    2.479533   1.809596   2.217458   3.408007
```

Ir2B5-4 -725.522476 +5.6 WBI 0.37	3.557759 7 Ir 3.053797 2.222872 2.721531 2.202844 2.153092 6 7 6 B 0.000000 7 Ir 3.599637 0.000000 Ir7-H-B2 Ir7-H 1.66 B2-H 1.48 B1-H-B4 B1-H 1.35 B4-H 1.29 B2-H-B6 B2-H 1.31 B6-H 1.33
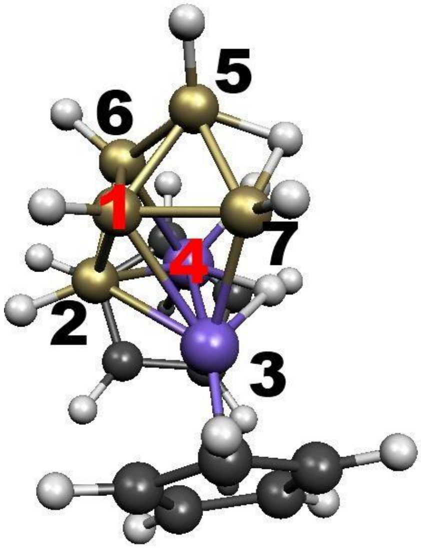 Ir2B5-5 -725.521632 +6.1 WBI 0.28	1 2 3 4 5 1 B 0.000000 2 B 1.740653 0.000000 3 Ir 2.246419 2.096637 0.000000 4 Ir 3.259398 2.115823 2.846507 0.000000 5 B 1.744291 2.952165 3.231309 3.477073 0.000000 6 B 1.823830 1.766572 3.132462 2.248336 1.833263 7 B 1.749146 2.948984 2.066096 3.649896 1.734255 6 7 6 B 0.000000 7 B 2.836083 0.000000 Ir3-H-Ir4 Ir3-H 1.76 Ir4-H 1.8 B5-H-B6 B5-H 1.29 B6-H 1.32 B5-H-B7 B5-H 1.29 B7-H 1.36
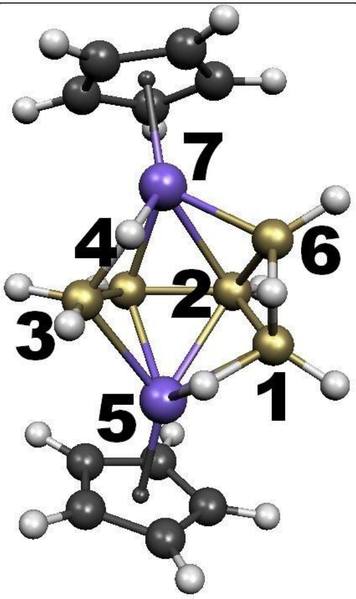 Ir2B5-6 -725.520113 +7.1 (Cs)	1 2 3 4 5 1 B 0.000000 2 B 1.747749 0.000000 3 B 3.170196 2.871986 0.000000 4 B 3.039090 1.833653 1.784919 0.000000 5 Ir 2.203988 2.249255 2.306333 2.093458 0.000000 6 B 1.708488 1.734040 3.234448 3.019276 3.324260 7 Ir 3.228817 2.245961 2.384744 2.085590 3.582047 6 7 6 B 0.000000 7 Ir 2.098043 0.000000 Ir5-H-B1 Ir5-H 1.67 B1-H 1.44

WBI 0.08	Ir7-H-B3 Ir7-H 1.66 B3-H 1.47 B1-H-B6 B1-H 1.32 B6-H 1.33
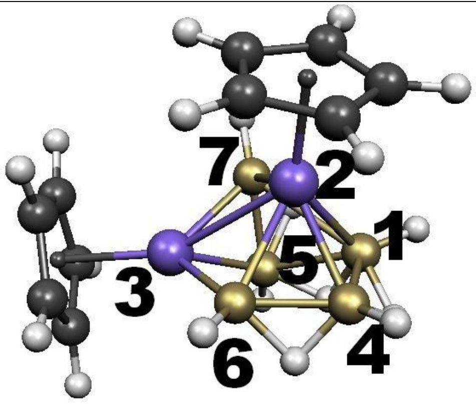 Ir2B5-7 -725.513872 +11.0 WBI 0.35	1 2 3 4 5 1 B 0.000000 2 Ir 2.120450 0.000000 3 Ir 3.265524 2.709258 0.000000 4 B 1.798667 2.141583 3.418962 0.000000 5 B 2.111015 3.022758 2.095466 3.185686 0.000000 6 B 2.763972 2.164029 2.072237 1.806829 2.928513 7 B 2.408783 2.169545 2.076174 3.497780 1.755172 6 7 6 B 0.000000 7 B 3.138175 0.000000 B1-H-B5 B1-H 1.3 B5-H 1.33 B1-H-B4 B1-H 1.35 B4-H 1.29 B4-H-B6 B4-H 1.29 B6-H 1.37
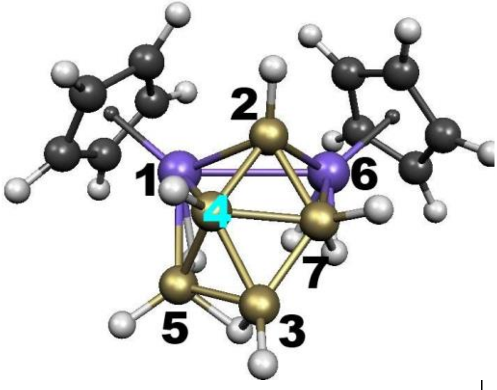 Ir2B5-8 -725.509567 +13.7 WBI 0.41	1 2 3 4 5 1 Ir 0.000000 2 B 2.159736 0.000000 3 B 3.309684 2.906746 0.000000 4 B 2.234437 1.747260 1.733333 0.000000 5 B 2.227552 3.028264 1.710602 1.753009 0.000000 6 Ir 2.775264 2.120727 3.492681 3.254964 3.625730 7 B 3.160264 1.741776 1.711038 1.802389 2.766471 6 7 6 Ir 0.000000 7 B 2.372445 0.000000 Ir1-H B5 Ir1-H 1.69 B5-H 1.4 Ir6-H- B7 Ir6-H 1.77 B7-H 1.34 B3-H-B5 B3-H 1.3 B5-H 1.34

6.1.3.2 Cp$_2$M$_2$B$_5$H$_9$ (M=Ru,Os) systems

Table 82. Distances table for the lowest-lying Cp$_2$Ru$_2$B$_5$H$_9$ structures after M06L/6-311G(d,p) optimization. Included are the ZPcorrected E (a.u.), relative energy (kcal/mol), symmetry and WBI.

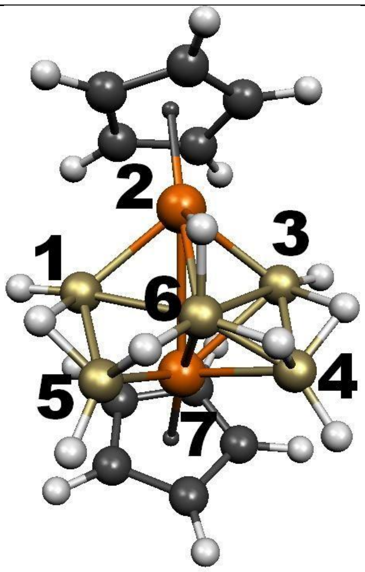 **Ru2B5-1 -706.582626 0.0** **Cs WBI 0.33**	1 2 3 4 5 1 B 0.000000 2 Ru 2.089681 0.000000 3 B 3.256791 2.087335 0.000000 4 B 3.614871 3.177316 1.822358 0.000000 5 B 1.822368 3.181432 3.617074 2.995052 0.000000 6 B 2.285465 2.159555 2.289506 1.778636 1.777977 7 Ru 2.165064 2.731262 2.161484 2.153480 2.156255 6 7 6 B 0.000000 7 Ru 2.095862 0.000000 Ru6-H-B2 Ru6-H 1.72 B2-H 1.39 B1-H-B5 B1-5 1.41 B5-H 1.28 B3-H-B4 B3-H 1.4 B4-H 1.28 B6-H-B4 B6-H 1.33 B4-H 1.33 B6-H-B5 B6-H 1.33 B5-H 1.33
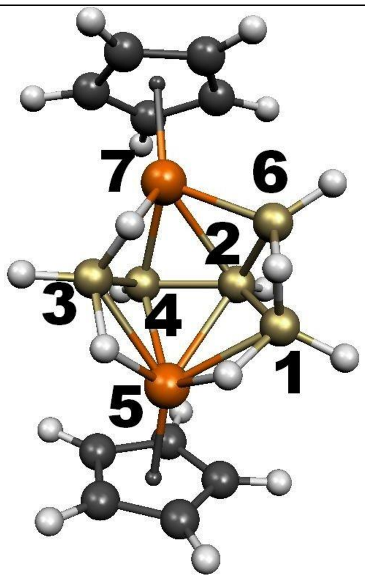 Ru2B5-2 -706.582331 +0.2 WBI 0.17	1 2 3 4 5 1 B 0.000000 2 B 1.727202 0.000000 3 B 3.235325 2.766532 0.000000 4 B 3.080516 1.754523 1.819409 0.000000 5 Ru 2.269788 2.263877 2.275920 2.150705 0.000000 6 B 1.738246 1.720969 3.172323 2.995692 3.344224 7 Ru 3.253387 2.266206 2.147257 2.069446 3.518516 6 7 6 B 0.000000 7 Ru 2.101061 0.000000 Ru5-H-B1 Ru5-H 1.71 B1-H 1.34 Ru5-H-B3 Ru5-H 1.69 B3-H 1.35 Ru7-H-B3 Ru7-H 1.73 B3-H 1.34 B1-H-B6 B1-H 1.33 B6-H 1.35

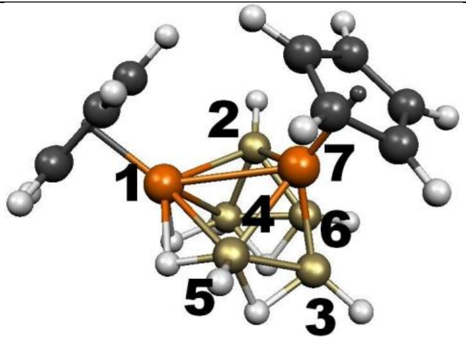

Ru2B5-3 -706.582301 +0.2
WBI 0.42

```
              1          2          3          4          5
    1  Ru   0.000000
    2  B    2.175707   0.000000
    3  B    3.355671   3.051538   0.000000
    4  B    2.250906   1.738966   3.014169   0.000000
    5  B    2.316286   3.169545   1.777531   3.203713
0.000000
    6  B    3.089770   1.738666   1.922748   1.754283
2.951048
    7  Ru   2.747291   2.068611   1.994617   3.136121
2.114729
              6          7
    6  B    0.000000
    7  Ru   2.177256   0.000000
```

Ru1-H-B4 Ru1-H 1.7 B4-H 1.35
Ru1-H- B5 Ru1-H 1.71 B5-H 1.33
B4-H-B6 B4-H 1.37 B6-H 1.31
B3-H-B5 B3-H 1.33 B5-H 1.35

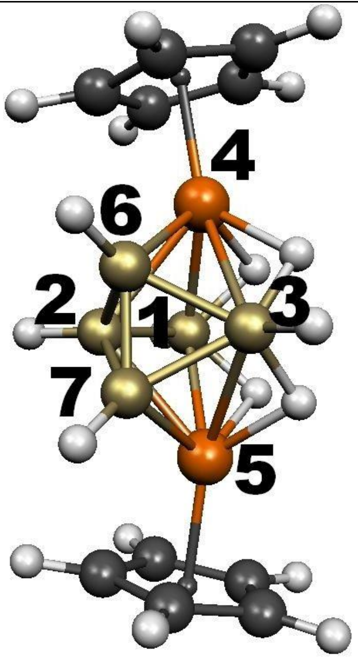

Ru2B5-4 -706.578595 +2.5
Cs WBI 0.10

```
              1          2          3          4          5
    1  B    0.000000
    2  B    1.795045   0.000000
    3  B    2.885334   2.491659   0.000000
    4  Ru   2.192968   2.292494   2.412291   0.000000
    5  Ru   2.192968   2.292494   2.412291   3.568000
0.000000
    6  B    3.036705   1.751567   1.809652   2.097853
3.201174
    7  B    3.036705   1.751567   1.809652   3.201174
2.097853
              6          7
    6  B    0.000000
    7  B    1.638600   0.000000
```

Ru4-H-B1 Ru4-H 1.68 B1-H 1.38
Ru4-H-B3 Ru4-H 1.71 B3-H 1.38
Ru5-H-B1 Ru5-H 1.68 B1-H 1.38
Ru5-H-B3 Ru5-H 1.71 B3-H 1.38

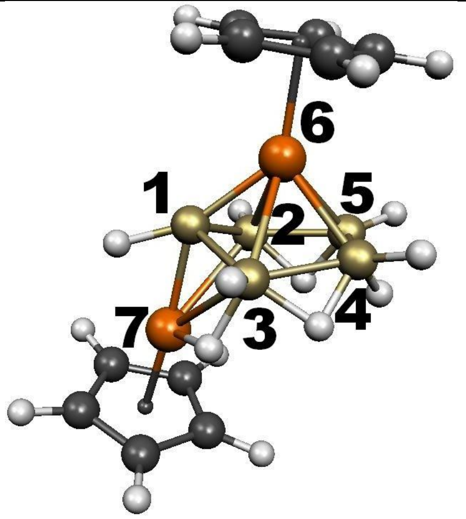

Ru2B5-5 -706.575946 +4.2
(Cs) WBI 0.15

```
               1          2          3          4          5
    1  B    0.000000
    2  B    1.713534   0.000000
    3  B    1.869522   2.790801   0.000000
    4  B    2.955567   2.894316   1.833550   0.000000
    5  B    2.856346   1.790486   2.861882   1.792517
0.000000
    6  Ru   1.952646   2.248468   2.234366   2.111645
2.123786
    7  Ru   1.960090   2.368548   2.541700   3.716581
3.585784
               6          7
    6  Ru   0.000000
    7  Ru   3.670469   0.000000
```

Ru7-H-B1 Ru7-H 1.83 B1-H 1.29
Ru7-H-B3 Ru7-H 1.75 B3-H 1.34
B2-H-B5 B2-H 1.31 B5-H 1.33
B3-H-B4 B3-H 1.35 B4-H 1.29
B4-H-B5 B4-H 1.31 B5-H 1.34

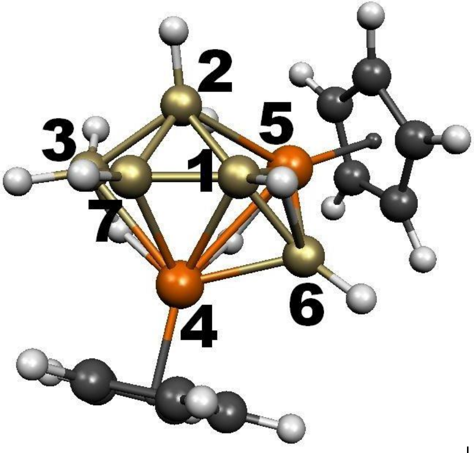

Ru2B5-6 -706.575697
+4.4 WBI 0.29

```
               1          2          3          4          5
    1  B    0.000000
    2  B    1.763517   0.000000
    3  B    2.867903   1.942406   0.000000
    4  Ru   2.251556   2.914812   2.435046   0.000000
    5  Ru   2.166951   2.314867   3.422783   2.817425
0.000000
    6  B    1.696949   3.145680   3.887757   2.125913
2.051399
    7  B    1.674222   1.719868   1.711147   2.195030
3.283962
               6          7
    6  B    0.000000
    7  B    3.034574   0.000000
```

Ru4-H- Ru5 Ru4-H 1.85 Ru5-H 1.74
Ru4-H-B3 Ru4-H 1.78 B3-H 1.32
Ru5-H-B2 Ru5-H 1.69 1.35

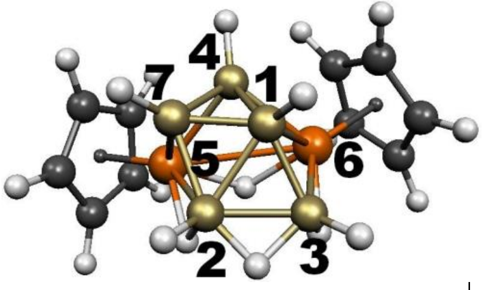

Ru2B5-7 -706.574410 +5.2

```
               1          2          3          4          5
    1  B    0.000000
    2  B    1.916369   0.000000
    3  B    1.780016   1.846712   0.000000
    4  B    1.762538   2.771990   3.028305   0.000000
    5  Ru   2.938740   2.314637   3.349550   2.134855
0.000000
    6  Ru   2.283086   3.045297   2.161294   2.101511
2.874528
    7  B    1.697361   1.787078   2.970483   1.748610
```

WBI 0.31	2.099781 6 7 6 Ru 0.000000 7 B 3.244288 0.000000 Ru5-H- Ru6 Ru5-H 1.76 Ru6-H 1.78 Ru 5-H-B2 Ru5-H 1.71 B2-H 1.37 Ru6-H-B3 Ru6-H 1.75 B3-H 1.31 B2-H-B3 B2-H 1.3 B3-H 1.33
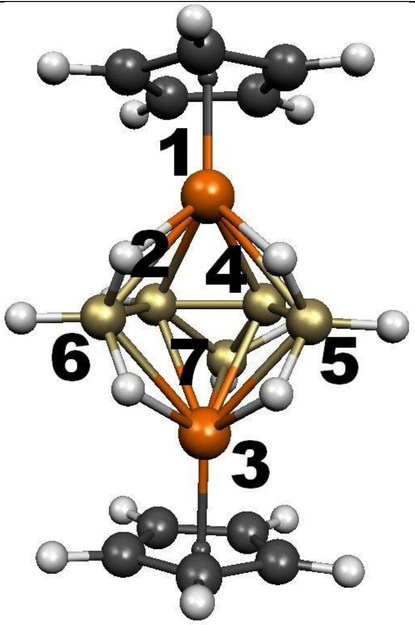 Ru2B5-8 -706.572910 +6.1 Cs WBI 0.10	1 2 3 4 5 1 Ru 0.000000 2 B 2.269208 0.000000 3 Ru 3.546548 2.295168 0.000000 4 B 2.142951 1.722580 2.257354 0.000000 5 B 2.375323 2.926052 2.422144 1.676392 0.000000 6 B 2.338701 1.702794 2.367846 2.734394 3.004026 7 B 3.429085 1.728420 2.180876 1.600605 3.046958 6 7 6 B 0.000000 7 B 3.166614 0.000000 Ru1-H-B5 Ru1-H 1.85 B5-H 1.28 Ru1-H-B6 Ru1-H 1.80 B6-H 1.29 Ru3-H-B5 Ru3-H 1.90 B5-H 1.27 Ru3-H-B6 Ru3-H 1.82 B6-H 1.29
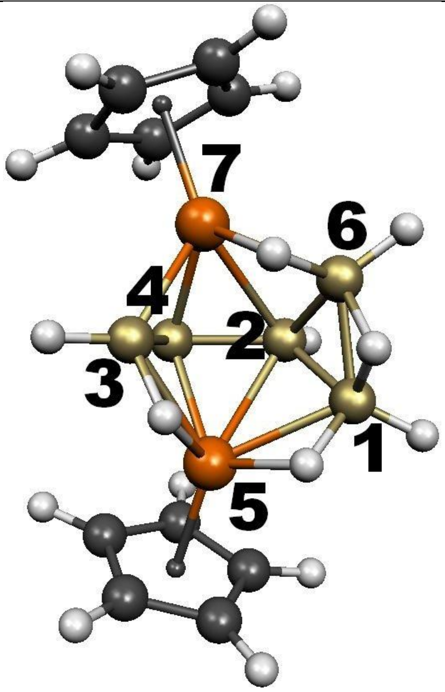 Ru2B5-9 -706.572830 +6.2	1 2 3 4 5 1 B 0.000000 2 B 1.720312 0.000000 3 B 3.315370 2.767873 0.000000 4 B 3.077954 1.736731 1.830177 0.000000 5 Ru 2.270564 2.291598 2.253292 2.139388 0.000000 6 B 1.761342 1.748016 3.103469 2.990703 3.283475 7 Ru 3.353465 2.289824 2.072242 2.057765 3.484915 6 7 6 B 0.000000 7 Ru 2.161054 0.000000 Ru5-H-B1 Ru5-H 1.71 B1-H 1.34 Ru5-H-B3 Ru5-H 1.71 B3-H 1.34 Ru7-H-B6 Ru7-H 1.71 B6-H 1.37 B1-H-B6 B1-H 1.3 B6-H 1.37

WBI 0.17

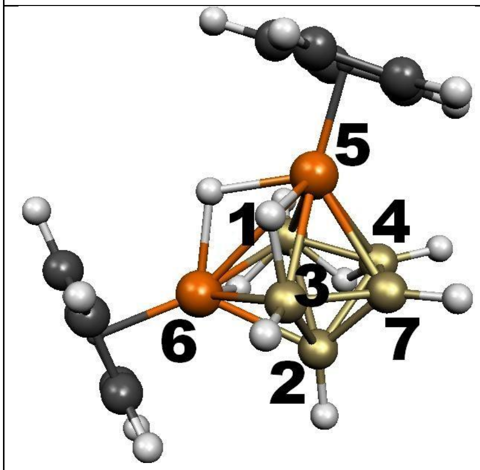

Ru2B5-10 -706.572167 +6.6
WBI 0.31

```
              1          2          3          4          5
    1  B    0.000000
    2  B    2.464952   0.000000
    3  B    3.107687   1.734418   0.000000
    4  B    1.761246   1.959953   2.800207   0.000000
    5  Ru   2.221136   2.898204   2.284959   2.216685
0.000000
    6  Ru   2.235370   2.203406   2.176022   3.169281
2.811014
    7  B    2.941990   1.663512   1.717270   1.684654
2.240094
              6          7
    6  Ru   0.000000
    7  B    3.230366   0.000000
```

Ru5-H- Ru6 Ru5-H 1.83 Ru6-H 1.73
Ru5-H-B3 Ru5-H 1.67 B3-H 1.38
Ru6-H-B1 Ru6-H 1.69 B1-H 1.33
B1-H-B4 B1-H 1.35 B4-H 1.27

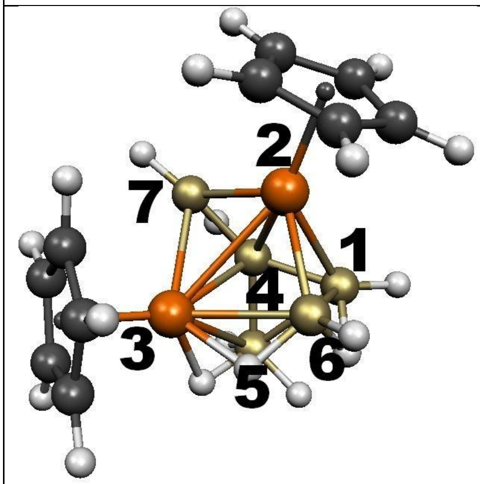

Ru2B5-11 -706.572023 +6.7
WBI 0.33

```
              1          2          3          4          5
    1  B    0.000000
    2  Ru   2.175419   0.000000
    3  Ru   3.038717   2.773246   0.000000
    4  B    1.703050   2.103242   2.227787   0.000000
    5  B    2.165656   3.525657   2.474171   1.706618
0.000000
    6  B    1.794306   2.101194   2.394612   2.590252
2.930107
    7  B    3.061476   2.064768   2.315509   1.613312
3.091487
              6          7
    6  B    0.000000
    7  B    3.370352   0.000000
```

Ru3-H-B5 Ru3-H 1.74 B5-H 1.34
Ru3-H-B6 Ru3-H 1.74 B6-H 1.31
B1-H-B6 B1-H 1.32 B6-H 1.31

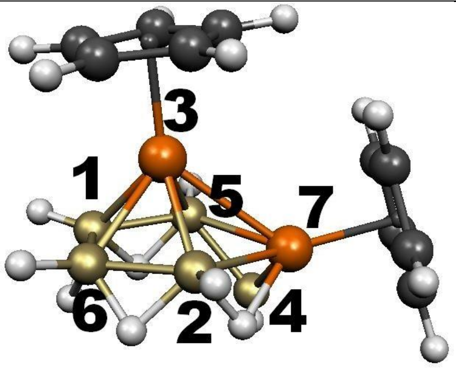 Ru2B5-12 -706.569292 +8.4 WBI 0.47	1 2 3 4 5 1 B 0.000000 2 B 2.893027 0.000000 3 Ru 2.097881 2.118733 0.000000 4 B 3.174073 3.381246 3.552201 0.000000 5 B 1.794070 2.996873 2.132072 1.834977 0.000000 6 B 1.780779 1.778115 2.112444 3.877820 2.946879 7 Ru 3.435722 2.268415 2.670881 1.879503 2.216232 6 7 6 B 0.000000 7 Ru 3.477727 0.000000 Ru7-H-B2 Ru7-H 1.70 B2-H 1.37 B2-H-B6 B2-H 1.36 B6-H 1.3 B1-H-B6 B1-H 1.36 B6-H 1.33 B1-H-B5 B1-H 1.34 B5-H 1.34
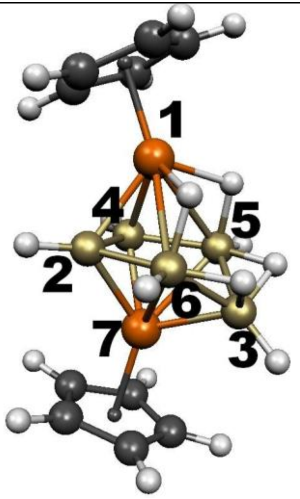 Ru2B5-13 -706.565423 +10.8 Cs WBI 0.18	1 2 3 4 5 1 Ru 0.000000 2 B 2.121536 0.000000 3 B 3.307071 3.089443 0.000000 4 B 2.122437 1.797701 3.088705 0.000000 5 B 2.391123 2.831833 1.820986 1.868278 0.000000 6 B 2.392394 1.867920 1.821914 2.831963 2.519803 7 Ru 3.362146 2.041800 2.093474 2.041611 2.260931 6 7 6 B 0.000000 7 Ru 2.259049 0.000000 Ru1-H-B5 Ru1-H 1.7 B5-H 1.38 Ru1-H-B6 Ru1-H 1.7 B6-H 1.38 B3-H-B5 B3-H 1.29 B5-H 1.35 B3-H-B6 B3-H 1.29 B6-H 1.35
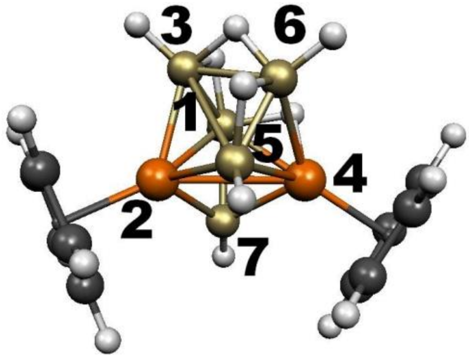	1 2 3 4 5 1 B 0.000000 2 Ru 2.163175 0.000000 3 B 1.744692 2.181252 0.000000 4 Ru 2.094093 2.729410 2.967479 0.000000 5 B 3.099887 2.267267 2.728142 2.185355 0.000000 6 B 2.584549 3.019941 2.042101 2.103916 1.785095 7 B 3.085482 2.096291 3.611394 1.976089

Ru2B5-14 -706.564653 +11.3 (C_2) WBI 0.35	1.882343 6 7 6 B 0.000000 7 B 3.166593 0.000000 Ru4-H-B1 Ru4-H 1.7 B1-H 1.38 B1-H-B3 B1-H 1.33 B3-H 1.33 B3-H-B6 B3-H 1.31 B6-H 1.3 B5-H-B6 B5-H 1.37 B6-H 1.28
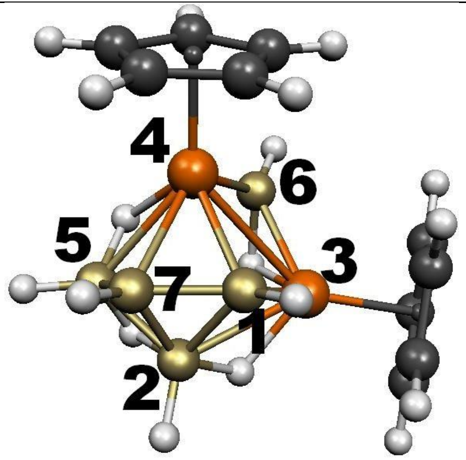 Ru2B5-15 -706.563652 +11.9 WBI 0.35	1 2 3 4 5 1 B 0.000000 2 B 1.858287 0.000000 3 Ru 2.161976 2.405429 0.000000 4 Ru 2.182897 2.909439 2.776804 0.000000 5 B 2.762656 1.817134 3.378755 2.357566 0.000000 6 B 3.178338 3.411008 2.062292 2.036511 3.234380 7 B 1.660559 1.711626 3.309747 2.233399 1.663590 6 7 6 B 0.000000 7 B 3.719920 0.000000 Ru3-H-B2 Ru3-H 1.67 B2-H 1.4 Ru3-H-B6 Ru3-H 1.70 B6-H 1.38 Ru4-H-B5 Ru4-H 1.78 B5-H 1.32 B2-H-B5 B2-H 1.47 B5-H 1.26

Table 83. Distances table for the lowest-lying $Cp_2Os_2B_5H_9$ structures after M06L/6-311G(d,p) optimization. Included are the ZPcorrected E (a.u.), relative energy (kcal/mol), symmetry and WBI.

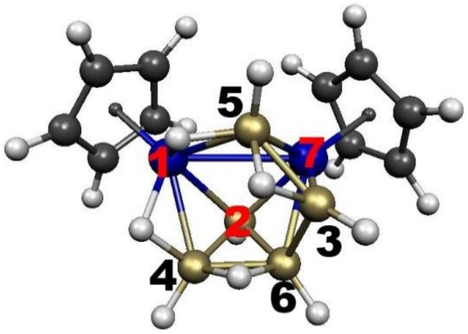 **Os2B5-1 -698.186364 a.u. 0.0 kcal/mol WBI 0.45**	1 2 3 4 5 1 Os 0.000000 2 B 2.201700 0.000000 3 B 3.392111 3.061074 0.000000 4 B 2.245086 1.729297 3.012445 0.000000 5 B 2.326049 3.165220 1.789510 3.181231 0.000000 6 B 3.120607 1.741239 1.927944 1.756576 2.952084 7 Os 2.801136 2.091149 2.015857 3.150314 2.128713 6 7 6 B 0.000000 7 Os 2.200300 0.000000

	Os1-H-B4 Os1-H 1.69 B4-H 1.41 Os1-H-B5 Os1-H 1.72 B5-H 1.36 B3-H-B5 B3-H 1.33 B5-H 1.35 B4-H-B6 B4-H 1.37 B6-H1.31
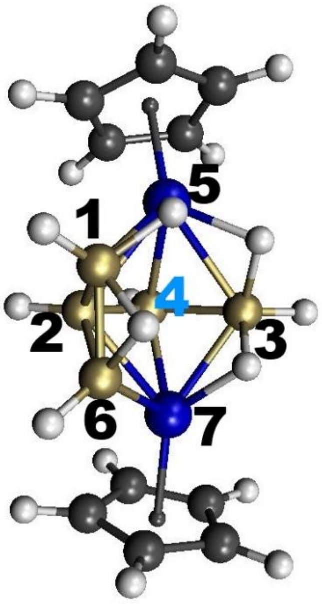 Os2B5-2 -698.185327 +0.7 (Cs) WBI 0.16	1 2 3 4 5 1 B 0.000000 2 B 1.721585 0.000000 3 B 3.214109 2.744162 0.000000 4 B 3.076648 1.756386 1.799478 0.000000 5 Os 2.276652 2.287806 2.267956 2.173083 0.000000 6 B 1.740220 1.731531 3.158913 3.005812 3.367614 7 Os 3.271089 2.290277 2.158992 2.098057 3.567574 6 7 6 B 0.000000 7 Os 2.112839 0.000000 Os5-H-B1 Os5-H 1.71 B1-H 1.38 Os5-H-B3 Os5-H 1.69 B3-H 1.42 Os7-H-B3 Os7-H 1.73 B3-H 1.37 B1-H-B6 B1-H 1.32 B6-H 1.36
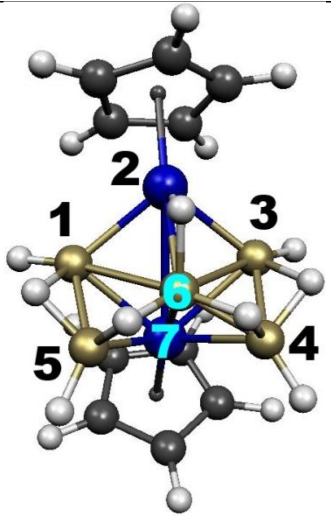 Os2B5-3 -698.185304 +0.7 Cs WBI 0.36	1 2 3 4 5 1 B 0.000000 2 Os 2.111853 0.000000 3 B 3.284106 2.111690 0.000000 4 B 3.642375 3.207260 1.837560 0.000000 5 B 1.837985 3.209198 3.643278 3.012322 0.000000 6 B 2.306240 2.182414 2.308807 1.788442 1.787723 7 Os 2.195390 2.782084 2.191858 2.165500 2.167737 6 7 6 B 0.000000 7 Os 2.116243 0.000000 Os2-H-B6 Os2-H 1.72 B6-H 1.38 B1-H-B5 B1-H 1.40 B5-H 1.28 B3-H-B4 B3-H 1.40 B4-H 1.28 B5-H-B6 B5-H 1.35 B6-H 1.32 B4-H-B6 B4-H 1.35 B6-H 1.32

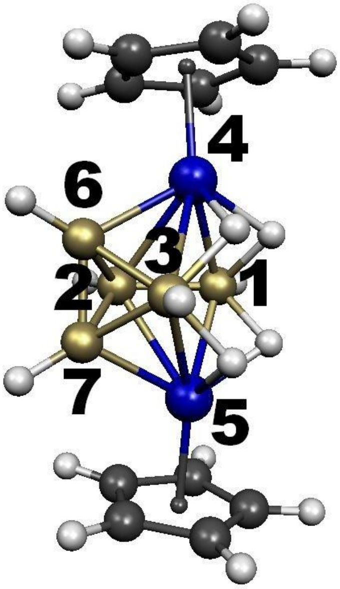

Os2B5-4 -698.181613 +3.0 Cs
WBI 0.09

```
                1          2          3          4          5
     1  B    0.000000
     2  B    1.782838   0.000000
     3  B    2.850356   2.465615   0.000000
     4  Os   2.199085   2.315806   2.408871   0.000000
     5  Os   2.199003   2.315884   2.408946   3.603500
0.000000
     6  B    3.029474   1.756530   1.796846   2.120887
3.227970
     7  B    3.029393   1.756437   1.796885   3.227825
2.121006
                6          7
     6  B    0.000000
     7  B    1.643100   0.000000
```

Os4-H-B1   Os4-H 1.69   B1-H 1.42
Os4-H-B3   Os4-H 1.71   B3-H 1.43
Os5-H-B1   Os5-H 1.69   B1-H 1.42
Os5-H-B3   Os5-H 1.71   B3-H 1.43

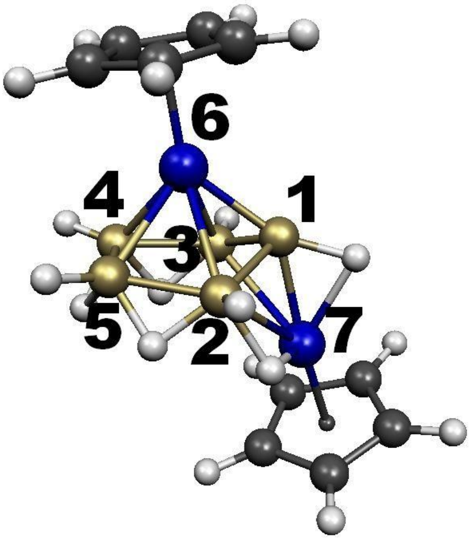

Os2B5-5 -698.174487 +7.5 (Cs)
WBI 0.16

```
                1          2          3          4          5
     1  B    0.000000
     2  B    1.835150   0.000000
     3  B    1.718192   2.752471   0.000000
     4  B    2.872610   2.862816   1.800837   0.000000
     5  B    2.945813   1.831056   2.880388   1.798044
0.000000
     6  Os   1.978696   2.256889   2.278641   2.141933
2.134953
     7  Os   1.976153   2.511590   2.372663   3.616771
3.707527
                6          7
     6  Os   0.000000
     7  Os   3.716202   0.000000
```

Os7-H-B2   Os7-H 1.71   B2-H 1.46
B2-H-B5   B2-H 1.34   B5-H 1.3
B3-H-B4   B3-H 1.32   B4-H 1.32
B4-H-B5   B4-H 1.34   B5-H 1.31

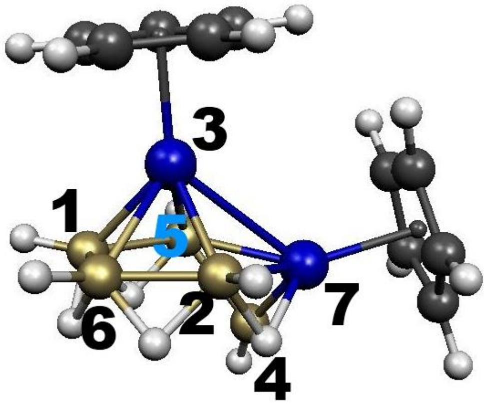

Os2B5-6 -698.169881 +10.3
WBI 0.50

```
                 1          2          3          4          5
    1  B    0.000000
    2  B    2.902903   0.000000
    3  Os   2.116646   2.126876   0.000000
    4  B    3.169790   3.377247   3.599237   0.000000
    5  B    1.807171   2.999764   2.149197   1.866582
0.000000
    6  B    1.787506   1.784545   2.134086   3.856944
2.957666
    7  Os   3.466778   2.278713   2.728650   1.902197
2.237704
                 6          7
    6  B    0.000000
    7  Os   3.499510   0.000000
```

Os7-H-B2   Os7-H 1.7   B2-H 1.42
B1-H-B6   B1-H 1.34   B6-H 1.33
B1-H-B5   B1-H 1.34   B5-H 1.35
B2-H-B6   B2-H 1.36   B6-H 1.31

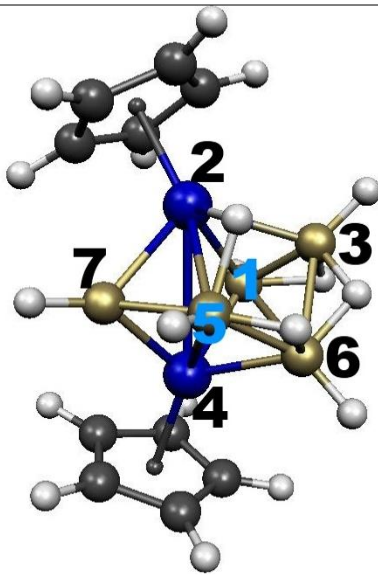

Os2B5-7 -698.169240 +10.8
WBI 0.37

```
                 1          2          3          4          5
    1  B    0.000000
    2  Os   2.187291   0.000000
    3  B    1.757316   2.203453   0.000000
    4  Os   2.121752   2.790730   3.025558   0.000000
    5  B    3.102938   2.289170   2.774064   2.185200
0.000000
    6  B    2.606285   3.052847   2.090059   2.123732
1.787322
    7  B    3.096683   2.115291   3.652775   2.009407
1.887264
                 6          7
    6  B    0.000000
    7  B    3.195395   0.000000
```

Os2-H-B5   Os2-H 1.69   B5-H 1.46
B1-H-B3   B1-H 1.36   B3-H 1.28
B3-H-B6   B3-H1.3   B6-H 1.32
B5-H-B6   B5-H 1.33   B6-H 1.32

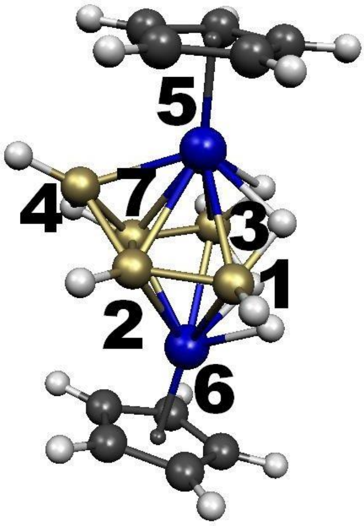

Os2B5-8 -698.167364 +11.9 (Cs)
WBI 0.09

```
                 1          2          3          4          5
    1  B    0.000000
    2  B    1.696388   0.000000
    3  B    2.973499   2.904088   0.000000
    4  B    3.149530   1.738799   3.029524   0.000000
    5  Os   2.374361   2.320065   2.423068   2.160544
0.000000
    6  Os   2.352762   2.280968   2.381900   3.465122
3.594459
    7  B    2.737529   1.725813   1.674098   1.613241
2.295049
                 6          7
    6  Os   0.000000
    7  B    2.164506   0.000000
```

Os5-H-B1   Os5-H 1.84   B1-H 1.29
Os5-H-B3   Os5-H 1.9   B3-H 1.23
Os6-H-B1   Os6-H 1.81   B1-H 1.31
Os6-H-B3   Os6-H 1.85   B3-H 1.3

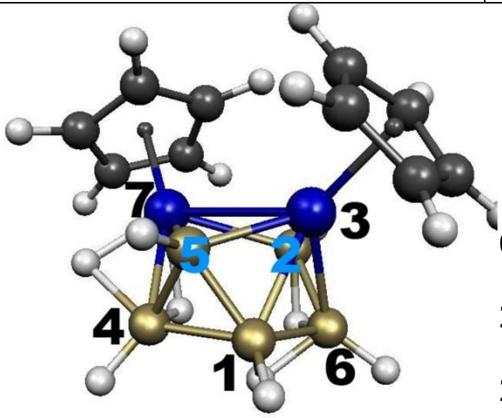

Os2B5-9 -698.160914 +16.0
WBI 0.40

```
                 1          2          3          4          5
    1  B    0.000000
    2  B    2.881085   0.000000
    3  Os   2.212476   2.056731   0.000000
    4  B    1.892971   3.097988   3.170103   0.000000
    5  B    1.726997   3.087999   2.077214   1.732645
0.000000
    6  B    1.809467   1.783025   2.107321   2.936672
2.981361
    7  Os   3.174621   2.319001   2.817389   2.152958
2.250260
                 6          7
    6  B    0.000000
    7  Os   3.381363   0.000000
```

Os7-H1-B4   Os7-H1 1.66   B4-H1 1.57
Os7-H2-B4   Os7-H2 1.74   B4-H2 1.57
B1-H-B6   B1-H 1.29   B6-H 1.4
B2-H-B6   B2-H 1.35   B6-H 1.32

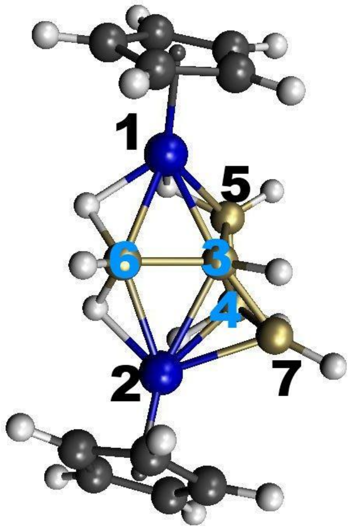 Os2B5-10 -698.157276 +18.3 WBI 0.11	1 2 3 4 5 1 Os 0.000000 2 Os 3.956173 0.000000 3 B 2.174434 2.273936 0.000000 4 B 3.386530 2.342364 1.764215 0.000000 5 B 2.162894 3.474278 1.785858 1.700063 0.000000 6 B 2.187764 2.210390 1.813990 3.055967 2.994201 7 B 3.813544 2.159861 1.653709 1.766639 2.824186 6 7 6 B 0.000000 7 B 3.058668 0.000000 Os1-H-B5 Os1-H 1.75 B5-H 1.37 Os1-H-B6 Os1-H 1.71 B6-H 1.42 Os2-H-B4 Os2-H 1.81 B4-H 1.32 Os2-H-B6 Os2-H 1.72 B6-H 1.43
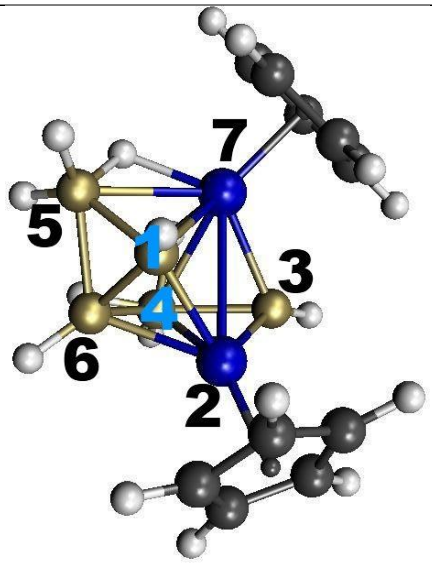 Os2B5-11 -698.155000 +19.7 WBI 0.36	1 2 3 4 5 1 B 0.000000 2 Os 2.113651 0.000000 3 B 3.183712 1.966054 0.000000 4 B 2.721918 2.165315 1.951321 0.000000 5 B 1.756879 3.460870 3.984951 2.851882 0.000000 6 B 1.742980 2.198279 3.259078 1.842167 1.927307 7 Os 2.226928 2.816273 2.206021 2.375578 2.444506 6 7 6 B 0.000000 7 Os 2.934464 0.000000 Os7-H-B5 Os7-H 1.75 B5-H 1.37 Os7-H-B4 Os7-H 1.74 B4-H 1.4 B4-H-B6 B4-H 1.3 B6-H 1.33

6.1.3.3 $Cp_2Re_2B_5H_9$ systems

Table 84. Distances table for the lowest-lying $Cp_2Re_2B_5H_9$ structures after M06L/6-311G(d,p) optimization. Included are the ZPcorrected E (a.u.), relative energy (kcal/mol), symmetry and WBI.

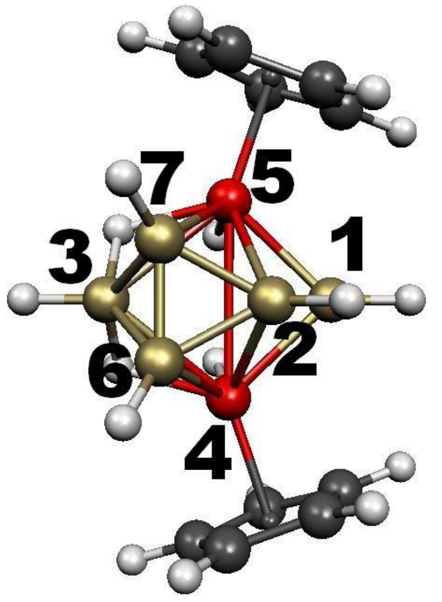

Re2B5-1 -673.388237 0.0 Cs
WBI 0.41

```
                 1          2          3          4          5
    1  B    0.000000
    2  B    1.874700   0.000000
    3  B    3.311417   2.599065   0.000000
    4  Re   2.094712   2.268232   2.344102   0.000000
    5  Re   2.094712   2.268232   2.344102   2.907000
0.000000
    6  B    3.193317   1.740761   1.810192   2.209666
3.108332
    7  B    3.193317   1.740761   1.810192   3.108332
2.209666
                 6          7
    6  B    0.000000
    7  B    1.644000   0.000000

Re4-H-B1   Re4-H 1.67   B1-H 2.54
Re4-H-B3   Re4-H 1.75   B3-H 1.4
Re5-H-B3   Re5-H 1.75   B3-H 1.4
Re5-H-B1   Re5-H 1.67   B1-H 2.53
```

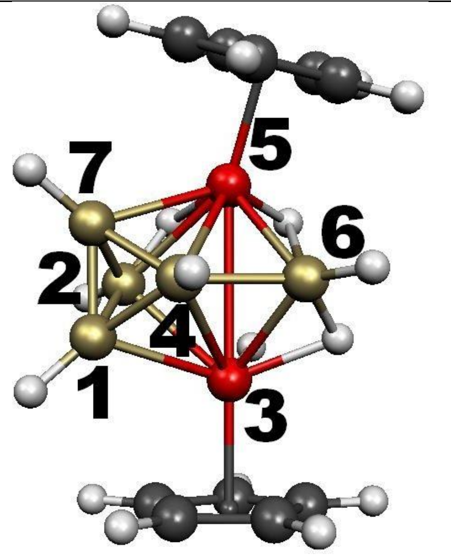

Re2B5-2 -673.383121 +3.2 (Cs)
WBI 0.45

```
                 1          2          3          4          5
    1  B    0.000000
    2  B    1.749512   0.000000
    3  Re   2.206747   2.312556   0.000000
    4  B    1.748446   2.561951   2.301607   0.000000
    5  Re   3.085720   2.312418   2.917255   2.270559
0.000000
    6  B    3.172919   3.316897   2.171778   1.815230
2.137932
    7  B    1.645274   1.774324   3.129686   1.758049
2.201754
                 6          7
    6  B    0.000000
    7  B    3.183889   0.000000

Re3-H-B2   Re3-H 1.66   B2-H 2.63
Re3-H-B6   Re3-H 1.73   B6-H 2.03
Re5-H-B2   Re5-H 1.75   B2-H 1.39
Re5-H-B6   Re5-H 1.67   B6-H 2.64
```

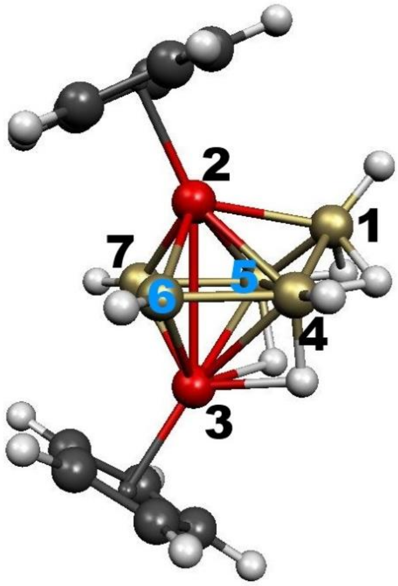

Re2B5-3 -673.376464 +7.4 Cs
WBI 0.44

```
                 1          2          3          4          5
     1  B    0.000000
     2  Re   2.163777   0.000000
     3  Re   3.244139   2.825356   0.000000
     4  B    1.830869   2.255253   2.367528   0.000000
     5  B    1.830941   2.255312   2.367583   2.627700
0.000000
     6  B    3.277632   2.042488   2.156871   1.952176
3.338437
     7  B    3.277674   2.042451   2.156840   3.338334
1.952268
                 6          7
     6  B    0.000000
     7  B    2.790900   0.000000
```

Re3-H-B4 Re3-H 1.8 B4-H 1.34
Re3-H-B5 Re3-H 1.8 B5-H 1.36
B1-H-B4 B1-H 1.29 B4-H 1.37
B1-H-B5 B1-H 1.29 B5-H 1.36

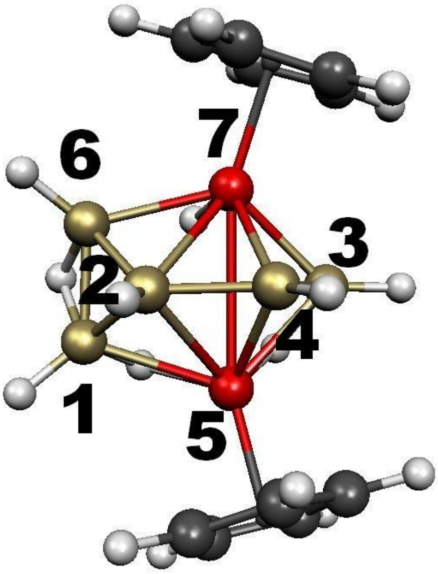

Re2B5-4 -673.372226 +10.0
(Cs) WBI 0.47

```
                 1          2          3          4          5
     1  B    0.000000
     2  B    1.743495   0.000000
     3  B    3.726445   3.112937   0.000000
     4  B    3.193767   1.801719   1.979404   0.000000
     5  Re   2.278517   2.275963   2.125253   2.152613
0.000000
     6  B    1.736208   1.724669   3.718194   3.120876
3.226400
     7  Re   3.127477   2.275003   2.084883   2.083219
2.955531
                 6          7
     6  B    0.000000
     7  Re   2.182727   0.000000
```

Re5-H-B1 Re5-H 1.76 B1-H 1.39
Re5-H-B3 Re5-H 1.7 B3-H 1.61
B1-H-B6 B1-H 1.32 B6-H 1.31

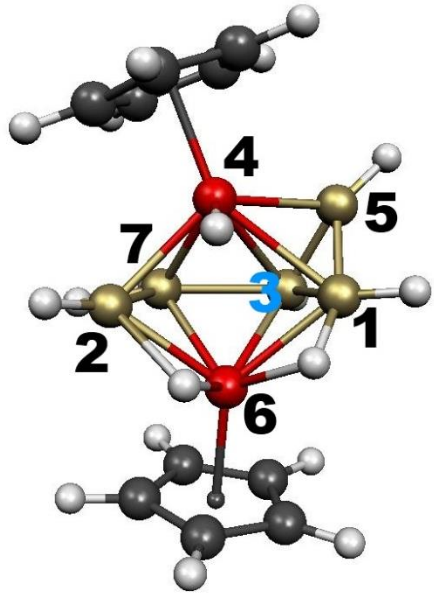

Re2B5-5 -673.360141 +17.6
WBI 0.41

```
              1          2          3          4          5
    1  B    0.000000
    2  B    3.476035   0.000000
    3  B    1.715665   3.160566   0.000000
    4  Re   2.397554   2.270056   2.328683   0.000000
    5  B    1.679653   3.944322   1.675193   2.084357
0.000000
    6  Re   2.237609   2.174257   2.202647   2.891801
3.386392
    7  B    3.177994   1.687376   2.059087   2.187337
3.182186
              6          7
    6  Re   0.000000
    7  B    2.227931   0.000000
```

Re6-H-B1   Re6-H 1.75   B1-H 1.36
Re6-H-B2   Re6-H 1.66   B2-H 2.05
B2-H-B7   B2-H 1.29   B7-H 1.39
Re4-H 1.66

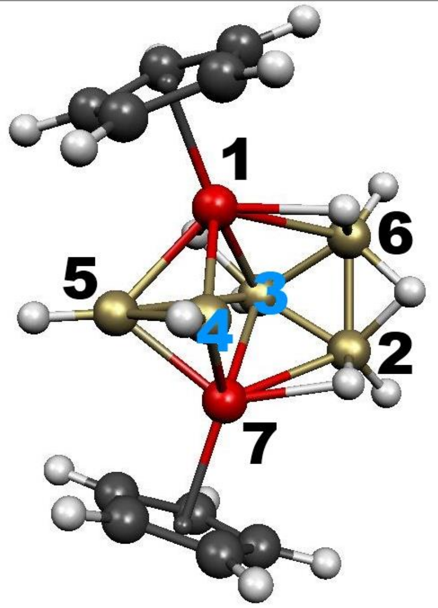

Re2B5-6 -673.346977 +25.9
WBI 0.49

```
              1          2          3          4          5
    1  Re   0.000000
    2  B    3.200118   0.000000
    3  B    2.316185   1.729539   0.000000
    4  B    2.135141   3.444037   3.340044   0.000000
    5  B    2.106530   3.744049   2.788625   1.975514
0.000000
    6  B    2.382457   1.754983   1.764523   3.564692
3.849801
    7  Re   2.835193   2.267976   2.291818   2.060737
2.052047
              6          7
    6  B    0.000000
    7  Re   3.242086   0.000000
```

Re1-H-B3   Re1-H 1.74   B3-H 1.39
Re1-H-B6   Re1-H 1.87   B6-H 1.29
Re7-H-B2   Re7-H 1.83   B2-H 1.31
B2-H-B6   B2-H 1.35   B6-H 1.29

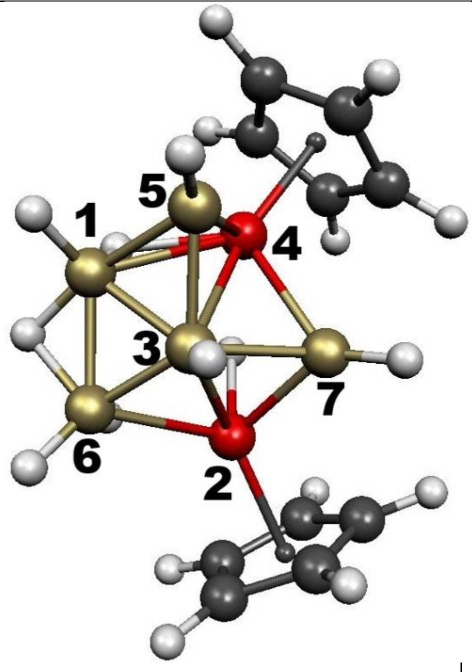

Re2B5-7 -673.339666 +30.5
WBI 0.49

```
              1          2          3          4          5
    1  B    0.000000
    2  Re   3.196659   0.000000
    3  B    1.785877   2.266542   0.000000
    4  Re   2.318705   2.867370   2.283806   0.000000
    5  B    1.874996   3.775138   1.815321   1.995427
0.000000
    6  B    1.827398   2.241077   1.758009   3.262585
3.160505
    7  B    3.326337   2.044462   1.929914   2.123751
2.761096
              6          7
    6  B    0.000000
    7  B    3.254494   0.000000
```

Re2-H-B6 Re2-H 1.84 B6-H 1.30
Re4-H-B1 Re4-H 1.83 B1-H 1.31
B1-H-B6 B1-H 1.29 B6-H 1.37

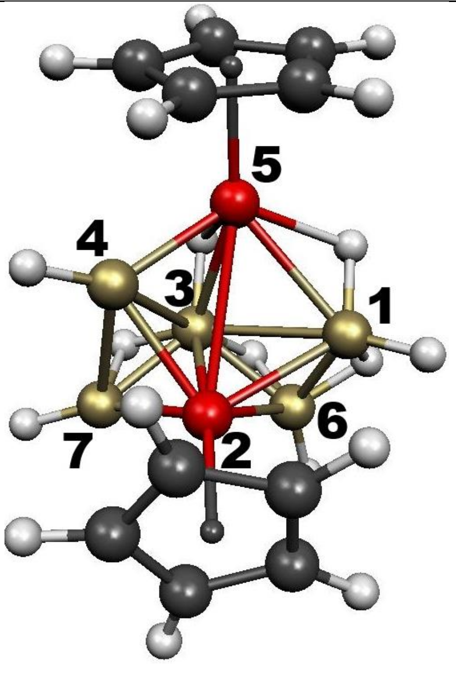

Re2B5-8 -673.332252 +35.1
WBI 0.42

```
              1          2          3          4          5
    1  B    0.000000
    2  Re   2.233646   0.000000
    3  B    2.460253   2.155954   0.000000
    4  B    3.293244   2.133131   2.420899   0.000000
    5  Re   2.342140   2.880101   2.300274   2.055460
0.000000
    6  B    1.818563   2.197361   1.815692   3.666658
3.301625
    7  B    3.636493   2.000922   1.776303   2.312936
3.472963
              6          7
    6  B    0.000000
    7  B    2.782595   0.000000
```

Re5-H-B3 Re5-H 1.80 B3-H 1.35
Re5-H-B1 Re5-H 1.81 B1-H 1.31
B3-H-B7 B3-H 1.28 B7-H 1.45
B3-H-B6 B3-H 1.35 B6-H 1.32

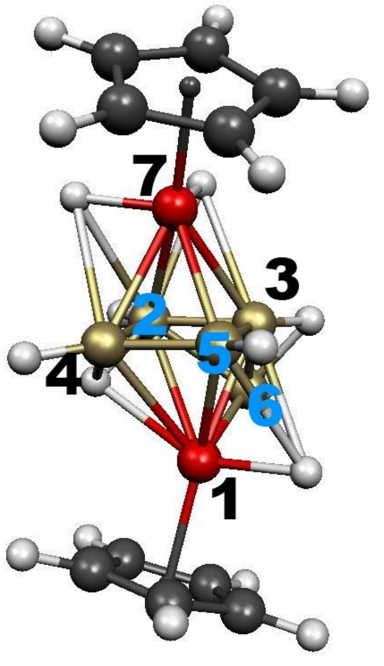

Re2B5-9 -673.331322 +35.7
WBI 0.14

		1	2	3	4	5	6	7
1	Re	0.000000						
2	B	2.474876	0.000000					
3	B	2.241332	1.750029	0.000000				
4	B	2.332503	1.892247	2.459945	0.000000			
5	B	2.195202	2.579097	1.746992	1.740803	0.000000		
6	B	2.067190	1.988793	1.662694	3.264997	3.055337	0.000000	
7	Re	3.777794	2.244693	2.202901	2.247069	2.240150	3.611498	0.000000

Re1-H-B4 Re-H 2.03 B4-H 1.37
Re7-H-B2 Re7-H 1.65 B2-H 2.3
B4-H-B2 B4-H 2.44 B2-H 2.3
B3-H-B6 B3-H 1.24 B6 -1.52

6.1.3.4 $Cp_2M_2B_5H_9$ (M=Mo,W) systems

Table 85. Distances table for the lowest-lying $Cp_2Mo_2B_5H_9$ structures after M06L/6-311G(d,p) optimization. Included are the ZPcorrected E (a.u.), relative energy (kcal/mol), symmetry and WBI.

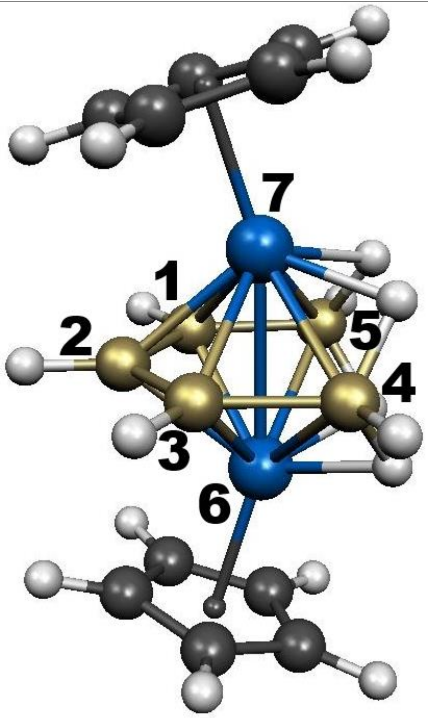

		1	2	3	4	5	6	7
1	B	0.000000						
2	B	1.712111	0.000000					
3	B	2.981403	1.712111	0.000000				
4	B	3.551135	3.040073	1.743457	0.000000			
5	B	1.743457	3.040073	3.551135	3.210205	0.000000		
6	Mo	2.207951	2.183393	2.209210	2.315884	2.314992	0.000000	
7	Mo	2.209210	2.183393	2.207951	2.314992	2.315884	2.801606	0.000000

Mo7-H-B4 Mo7-H 1.87 B4-H 1.30
Mo6-H-B4 Mo6-H 1.87 B4-H 1.30
Mo7-H-B5 Mo7-H 1.87 B5-H 1.30
Mo6-H-B4 Mo6-H 1.87 B5-H 1.30

Mo2B5-1 -653.210124 a.u. **0.00 kcal/mol C_{2v}** WBI 0.71	
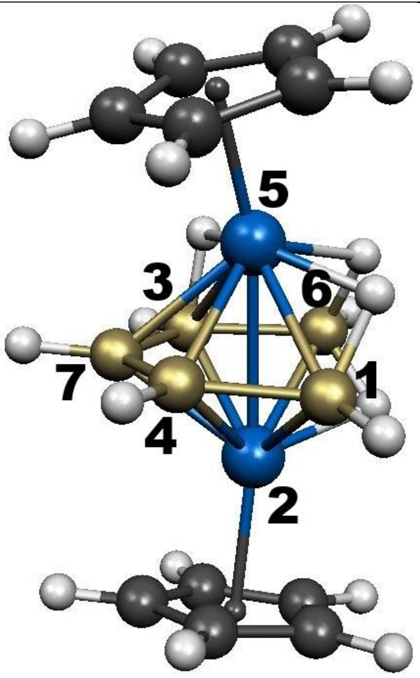 Mo2B5-2 -653.171800 +24.1 WBI 0.64	1 2 3 4 5 1 B 0.000000 2 Mo 2.106448 0.000000 3 B 3.516850 2.232504 0.000000 4 B 1.772937 2.180384 3.012152 0.000000 5 Mo 2.315317 2.782684 2.323117 2.205401 0.000000 6 B 3.081101 2.253680 1.836314 3.563085 2.407226 7 B 3.005401 2.184109 1.750773 1.693149 2.246478 6 7 6 B 0.000000 7 B 3.102916 0.000000 Mo2-H-B6 Mo2-H 1.88 B6-H 1.28 Mo5-H-B1 Mo5-H 1.81 B1-H 1.33 Mo5-H-B6 Mo5-H 1.88 B6-H 1.31 Mo5-H-B3 Mo5-H 1.89 B3-H 1.30
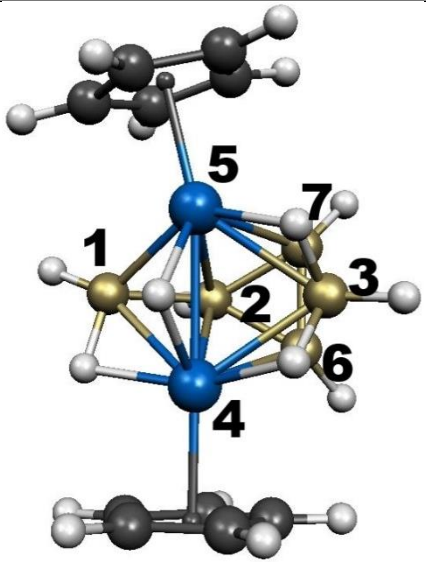 Mo2B5-3 -653.151276 +36.9 WBI 0.89	1 2 3 4 5 1 B 0.000000 2 B 1.853609 0.000000 3 B 3.592921 2.716662 0.000000 4 Mo 2.240738 2.307914 2.376865 0.000000 5 Mo 2.136532 2.273997 2.362437 2.655497 0.000000 6 B 3.241141 1.733191 1.826814 2.237908 3.027293 7 B 3.222431 1.755977 1.829293 3.077031 2.211470 6 7 6 B 0.000000 7 B 1.644656 0.000000 Mo4-H-Mo5 Mo4-H 1.88 Mo5-H 1.93 Mo4-H-B1 Mo4-H 1.89 B1-H 1.26 Mo4-H-B3 Mo4-H 1.80 B3-H 1.35 Mo5-H-B3 Mo5-H 1.82 B3-H 1.33

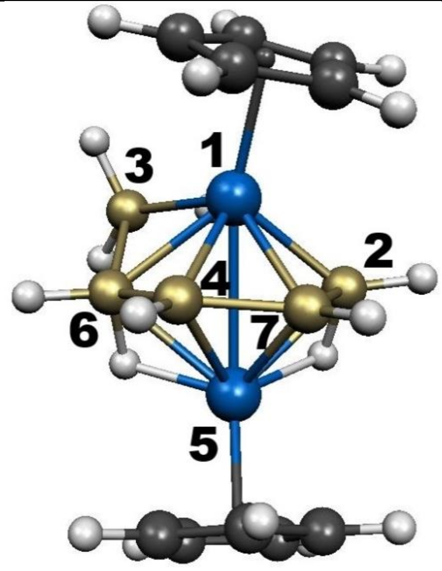

Mo2B5-4 -653.141537 +43.0 WBI 0.71

```
                1          2          3          4          5
    1  Mo   0.000000
    2  B    2.164315   0.000000
    3  B    2.265260   3.675281   0.000000
    4  B    2.139998   3.046144   3.338621   0.000000
    5  Mo   2.867977   2.283125   3.495521   2.229627
0.000000
    6  B    2.257406   3.468174   1.913955   1.813548
2.343135
    7  B    2.211628   1.812462   4.080898   1.769916
2.120494
                6          7
    6  B    0.000000
    7  B    3.086734   0.000000
```

Mo1-H-B3 Mo1-H 1.90 B3-H 1.30
Mo5-H-B2 Mo5-H 1.82 B2-H 1.30
Mo5-H-B6 Mo5-H 1.83 B6-H 1.30

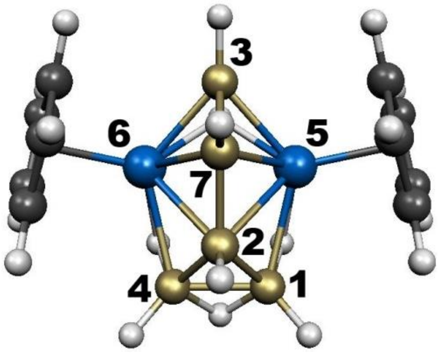

Mo2B5-5 -653.141477 +43.1 Cs WBI 0.74

```
                1          2          3          4          5
    1  B    0.000000
    2  B    1.757597   0.000000
    3  B    3.942856   3.072489   0.000000
    4  B    1.784400   1.757597   3.942856   0.000000
    5  Mo   2.315716   2.304174   2.134244   3.225939
0.000000
    6  Mo   3.225939   2.304174   2.134244   2.315716
2.826800
    7  B    3.178724   1.734295   1.815092   3.178724
2.168681
                6          7
    6  Mo   0.000000
    7  B    2.168681   0.000000
```

Mo5-H-B1 Mo5-H 1.87 B1-H 1.30
Mo6-H-B4 Mo6-H 1.87 B4-H 1.30
Mo5-H-B3 Mo5-H 1.97 B3-H 1.46
Mo6-H-B3 Mo6-H 1.97 B3-H 1.46
B1-H-B4 B1-H 1.32 B3-H 1.32

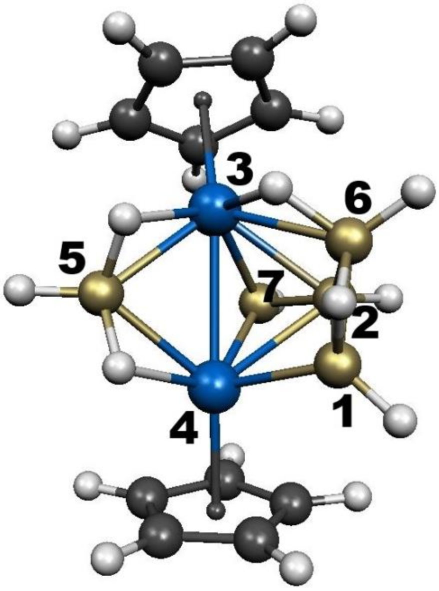

Mo2B5-6 -653.137490 +45.6
WBI 0.86

```
               1         2         3         4         5
    1  B    0.000000
    2  B    1.742470   0.000000
    3  Mo   3.170378   2.291693   0.000000
    4  Mo   2.181283   2.296178   2.692969   0.000000
    5  B    3.627801   3.609082   2.206161   2.260152
0.000000
    6  B    1.760586   1.715155   2.404810   3.149686
3.719840
    7  B    3.071514   1.715216   2.161373   2.119149
3.202106
               6         7
    6  B    0.000000
    7  B    3.174203   0.000000
```

Mo3-H-B5 Mo3-H 1.84 B5-H 1.29

Mo4-H-B5 Mo4-H 1.84 B5-H 1.29

Mo3-H-B6 Mo3-H 1.84 B6-H 1.30

B1-H-B6 B1-H 1.33 B6-H 1.31

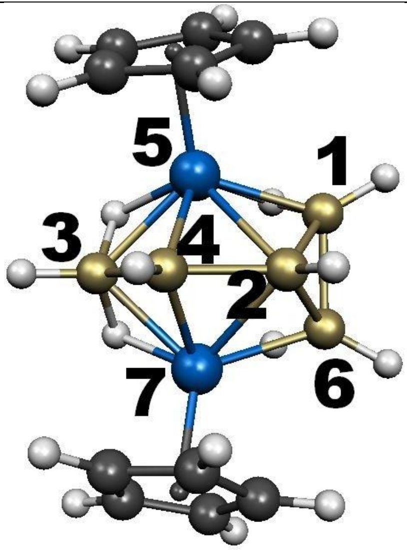

Mo2B5-7 -653.136792 +46.0
Cs WBI 0.61

```
               1         2         3         4         5
    1  B    0.000000
    2  B    1.732449   0.000000
    3  B    3.762647   3.140415   0.000000
    4  B    3.196089   1.884882   1.885539   0.000000
    5  Mo   2.178975   2.269309   2.207765   2.119895
0.000000
    6  B    1.868501   1.732483   3.762670   3.196035
3.241515
    7  Mo   3.241087   2.269659   2.206811   2.119912
3.081601
               6         7
    6  B    0.000000
    7  Mo   2.179033   0.000000
```

Mo5-H-B1   Mo5-H 1.9   B1-H 1.29

Mo5-H-B3   Mo5-H 1.8   B3-H 1.39

Mo7-H-B3   Mo7-H 1.8   B3-H 1.39

Mo7-H-B6   Mo7-H 1.9   B6-H 1.29

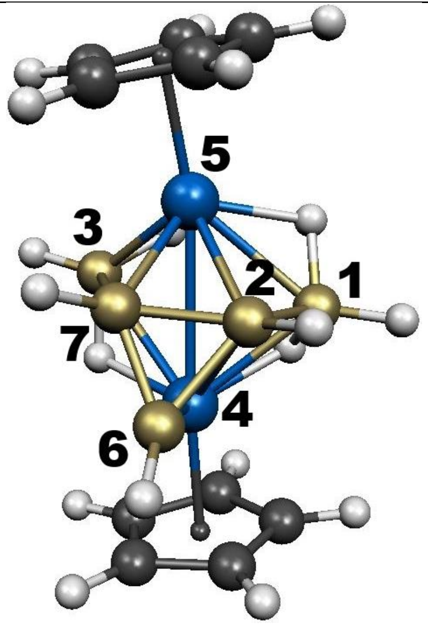

Mo2B5-8 -653.132284 +48.8
WBI 0.62

```
                   1          2          3          4          5
    1  B    0.000000
    2  B    1.773562   0.000000
    3  B    3.378121   3.432492   0.000000
    4  Mo   2.277607   2.305855   2.457417   0.000000
    5  Mo   2.312582   2.279420   2.083587   2.896164
0.000000
    6  B    3.116282   1.773049   3.607155   2.069884
3.405332
    7  B    3.032233   1.742209   2.550436   2.371283
2.147629
                   6          7
    6  B    0.000000
    7  B    1.657081   0.000000
```

Mo4-H-B1 Mo4-H 1.84 B1-H 1.30
Mo4-H-B3 Mo4-H 1.84 B3-H 1.29
Mo5-H-B1 Mo5-H 1.82 B1-H 1.33
Mo5-H-B3 Mo5-H 1.86 B3-H 1.35

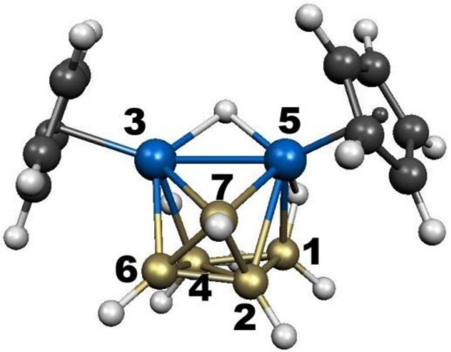

Mo2B5-9 -653.124603 +53.6
WBI 1.60

```
                   1          2          3          4          5
    1  B    0.000000
    2  B    1.768633   0.000000
    3  Mo   3.333138   2.945123   0.000000
    4  B    1.822084   1.864374   2.413249   0.000000
    5  Mo   2.307248   2.384280   2.485409   2.993965
0.000000
    6  B    2.994046   1.712392   2.177227   1.803370
3.161438
    7  B    3.098192   1.750268   2.266789   2.840074
2.137853
                   6          7
    6  B    0.000000
    7  B    1.732244   0.000000
```

Mo3-H-B4 Mo3-H 1.79 B4-H 1.38
Mo5-H-B1 Mo5-H 1.86 B1-H 1.29
Mo3-H-Mo5 Mo3-H 1.87 Mo5-H 1.83
B1-H-B4 B1-H 1.30 B4-H 1.35

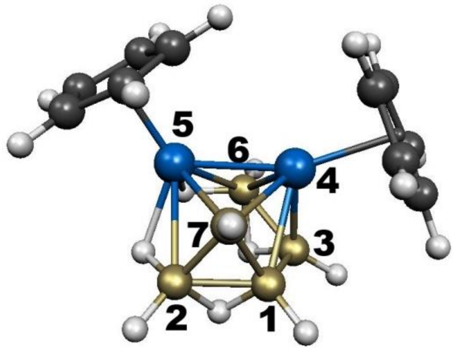

Mo2B5-10 -653.115041 +59.6
WBI 1.90

		1	2	3	4	5	6	7
1	B	0.000000						
2	B	1.784519	0.000000					
3	B	1.852340	3.057226	0.000000				
4	Mo	2.310326	3.210563	2.134709	0.000000			
5	Mo	3.003282	2.385304	3.207996	2.371736	0.000000		
6	B	2.996767	3.375882	1.759692	2.276603	2.353563	0.000000	
7	B	1.740573	1.724842	3.106546	2.188928	2.256865	3.500250	0.000000

Mo5-H-B2 Mo5-H 1.88 B2-H 1.27
Mo5-H-B6 Mo5-H 1.87 B6-H 1.30
B3-H-B6 B3-H 1.30 B6-H 1.38
B1-H-B2 B1-H 1.29 B2-H 1.37

Table 86. Distances table for the lowest-lying $Cp_2W_2B_5H_9$ structures after M06L/6-311G(d,p) optimization. Included are the ZPcorrected E (a.u.), relative energy (kcal/mol), symmetry and WBI.

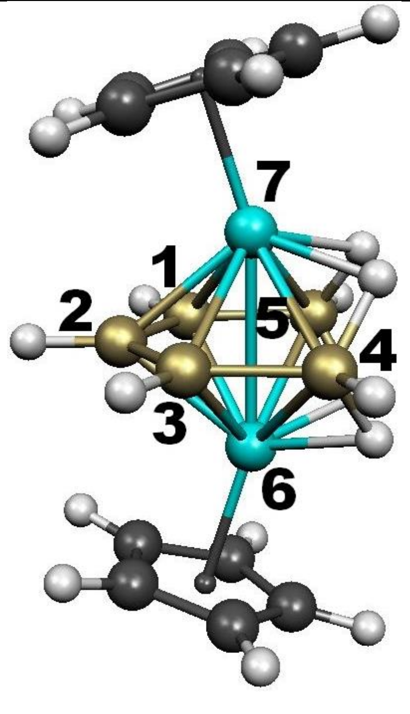

W2B5-1 -651.019914 0.0
C_{2v} WBI 0.74

		1	2	3	4	5	6	7
1	B	0.000000						
2	B	1.712842	0.000000					
3	B	2.986800	1.712842	0.000000				
4	B	3.546103	3.032637	1.742471	0.000000			
5	B	1.742471	3.032637	3.546103	3.193600	0.000000		
6	W	2.223824	2.196985	2.223824	2.317472	2.317472	0.000000	
7	W	2.223824	2.196985	2.223824	2.317472	2.317472	2.836000	0.000000

W6-H-B4 W6-H 1.87 B4-H 1.31
W6-H-B5 W6-H 1.87 B5-H 1.31
W7-H-B4 W7-H 1.87 B4-H 1.31
W7-H-B5 W7-H 1.87 B5-H 1.31

Fehlner OM 1999, 18, p 53
Ghosh IC 2009, 48, 6509

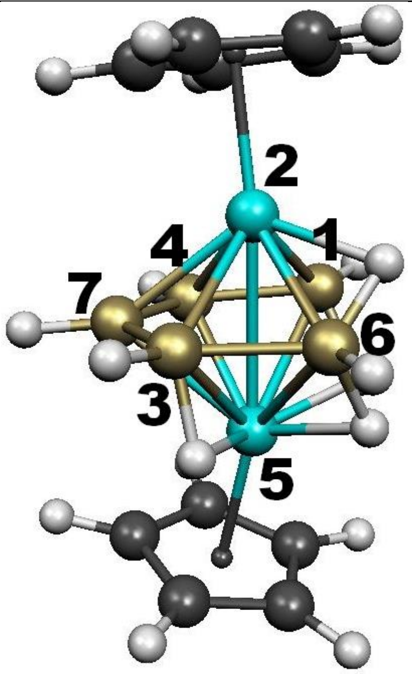

W2B5-2 -650.982518 +23.5
(C_{2v}) WBI 0.65

```
              1          2          3          4          5
    1  B    0.000000
    2  W    2.119957   0.000000
    3  B    3.521429   2.246528   0.000000
    4  B    1.774978   2.198856   3.019811   0.000000
    5  W    2.325038   2.819211   2.338308   2.215786
0.000000
    6  B    3.076639   2.256009   1.838544   3.563714
2.421691
    7  B    3.008651   2.200408   1.750179   1.699470
2.253944
              6          7
    6  B    0.000000
    7  B    3.099828   0.000000
```

W2-H-B6 W2-H 1.89 B6-H 1.28
W5-H-B1 W5-H 1.82 B1-H 1.36
W5-H-B6 W5-H 1.88 B6-H 1.33
W5-H-B3 W5-H 1.89 B3-H 1.31

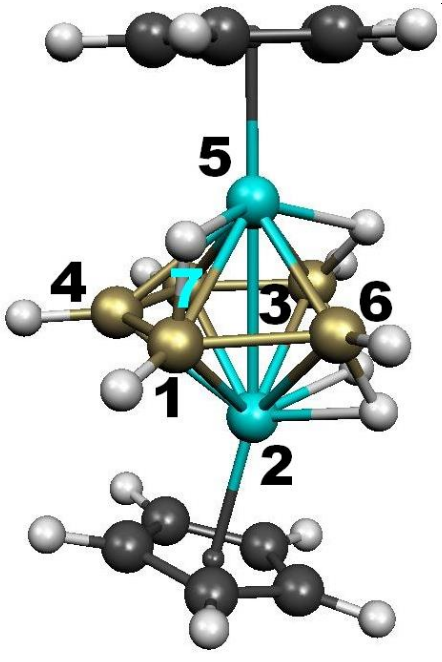

W2B5-3 -650.972909 +29.5
(C_{2v}) WBI 0.71

```
              1          2          3          4          5
    1  B    0.000000
    2  W    2.217814   0.000000
    3  B    3.581285   2.304383   0.000000
    4  B    1.775818   2.211174   2.995722   0.000000
    5  W    2.282374   2.801950   2.293985   2.249704
0.000000
    6  B    1.903152   2.277095   3.080211   3.117444
2.213524
    7  B    3.023988   2.247701   1.720401   1.676478
2.252558
              6          7
    6  B    0.000000
    7  B    3.513426   0.000000
```

W2-H-B3 W2-H 1.85 B3-H 1.32
W2-H-B6 W2-H 1.86 B6-H 1.30
W5-H-B3 W5-H 1.83 B3-H 1.33
W5-H-B1 W5-H 1.87 B1-H 1.29

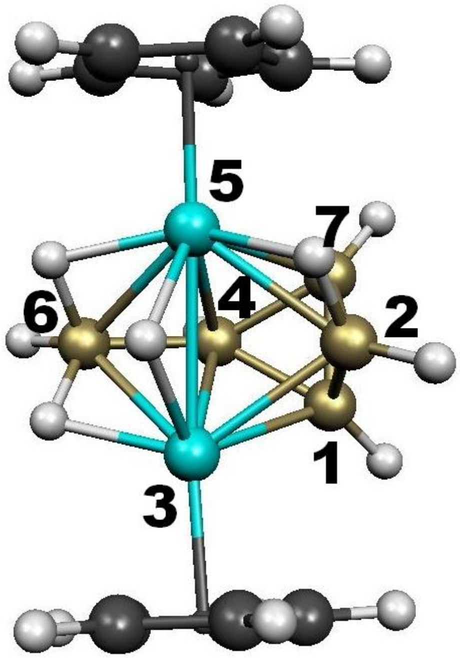

W2B5-4 -650.958648 +38.4
(Cs) WBI 0.90

```
                 1          2          3          4          5
     1  B    0.000000
     2  B    1.751270   0.000000
     3  W    2.204965   2.314985   0.000000
     4  B    1.780869   2.679007   2.319199   0.000000
     5  W    3.052616   2.317790   2.706464   2.334546
0.000000
     6  B    3.238068   3.588736   2.271163   1.809139
2.314695
     7  B    1.656603   1.796230   3.078054   1.783797
2.228687
                 6          7
     6  B    0.000000
     7  B    3.261295   0.000000
```

W5-H-B2 W5-H 1.82 B2-H 1.34
W5-H-W3 W5-H 1.9 W3-H 1.93
W5-H-B6 W5-H 1.84 B6-H 1.32
W3-H-B6 W3-H 1.84 B6-H 1.29

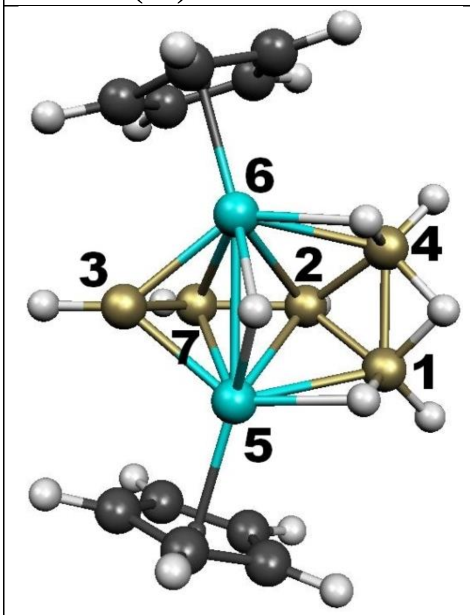

W2B5-5 -650.952962 +42.0
Cs WBI 0.91

```
                 1          2          3          4          5
     1  B    0.000000
     2  B    1.761529   0.000000
     3  B    3.996017   3.058504   0.000000
     4  B    1.820400   1.761529   3.996017   0.000000
     5  W    2.339695   2.313956   2.133550   3.228597
0.000000
     6  W    3.228597   2.313956   2.133550   2.339695
2.719000
     7  B    3.191781   1.725127   1.780750   3.191781
2.200214
                 6          7
     6  W    0.000000
     7  B    2.200214   0.000000
```

W6-H-B4 W6-H 1.93 B4-H 1.27
W6-H-W5 W6-H 1.92 W5-H 1.92
W5-H-B1 W5-H 1.93 B1-H 1.27
B1-H-B4 B1-H 1.32 B4-H 1.32

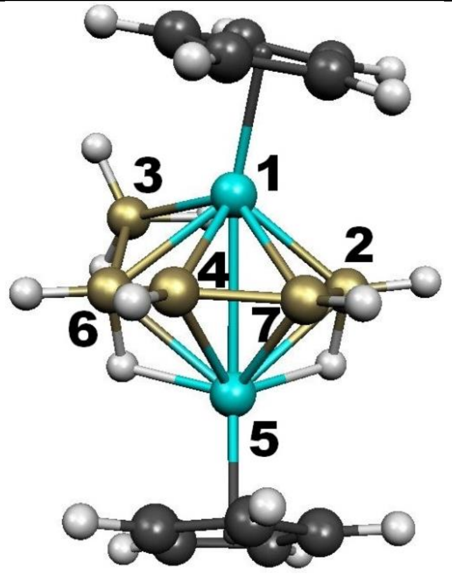

W2B5-6 -650.951407 +43.0
WBI 0.74

```
                1          2          3          4          5
    1  W    0.000000
    2  B    2.173458   0.000000
    3  B    2.257902   3.680403   0.000000
    4  B    2.156864   3.019036   3.310909   0.000000
    5  W    2.862209   2.253740   3.429930   2.226561
0.000000
    6  B    2.244637   3.445831   1.877804   1.791168
2.316848
    7  B    2.209560   1.786714   4.053426   1.754787
2.148636
                6          7
    6  B    0.000000
    7  B    3.059200   0.000000
```

W5-H-B2 W5-H 1.82   B2-H 1.32
W5-H-B6 W5-H 1.82   W6-H 1.33
B6-H-B3 B6-H 2.33   B3-H 1.19
B3-H-B2 B3-H 1.9   B2-H 2.79

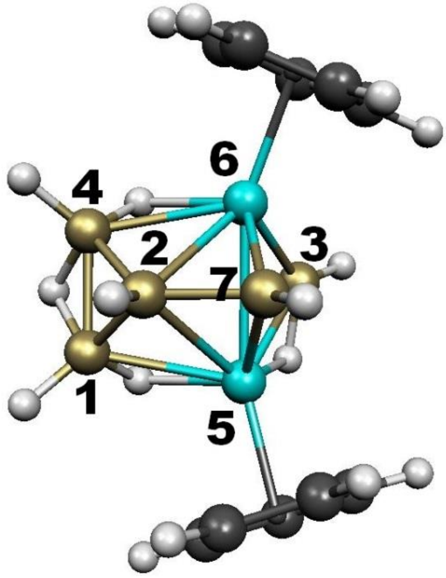

W2B5-7 -650.949324 +44.3
WBI 1.08

```
                1          2          3          4          5
    1  B    0.000000
    2  B    1.718388   0.000000
    3  B    3.713367   3.593312   0.000000
    4  B    1.787781   1.722955   3.639227   0.000000
    5  W    2.350568   2.323945   2.254861   3.199029
0.000000
    6  W    3.209578   2.322447   2.106451   2.346506
2.658188
    7  B    3.145778   1.719828   3.223675   3.127316
2.180103
                6          7
    6  W    0.000000
    7  B    2.133466   0.000000
```

W5-H-B3 W5-H 1.86   B3-H 1.28
W6-H-B4 W6-H 1.86   B4-H 1.3
W5-H-B1 W5-H 1.85   B1-H 1.32
B4-H-B1 B4-H 1.33   B1-H 1.32

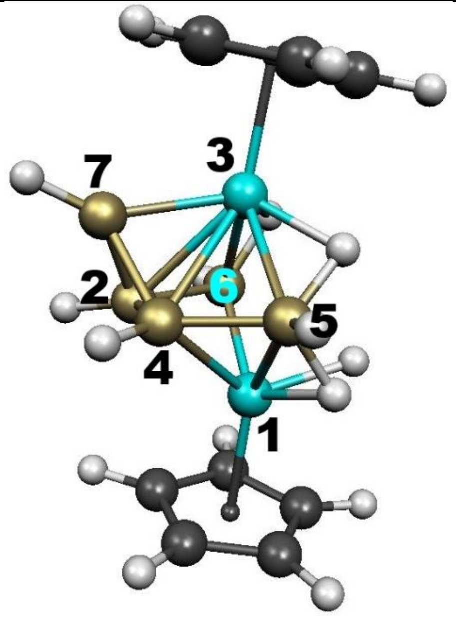

W2B5-8 -650.948745 +44.7
(Cs) WBI 0.57

```
              1          2          3          4          5
    1  W    0.000000
    2  B    2.223837   0.000000
    3  W    2.969110   2.346623   0.000000
    4  B    2.279282   1.729404   2.347230   0.000000
    5  B    2.303475   3.022992   2.312923   1.776076
0.000000
    6  B    2.133217   1.833136   2.318640   3.034716
3.422583
    7  B    3.492390   1.721553   2.078730   1.747825
3.061910
              6          7
    6  B    0.000000
    7  B    3.092766   0.000000
```

W1-H-B5 W1-H 1.84 B5-H 1.31
W1-H-B6 W1-H 1.73 B6-H 2.43
W3-H-B5 W3-H 1.82 B5-H 1.31
W3-H-B6 W3-H 1.81 B6-H 1.32

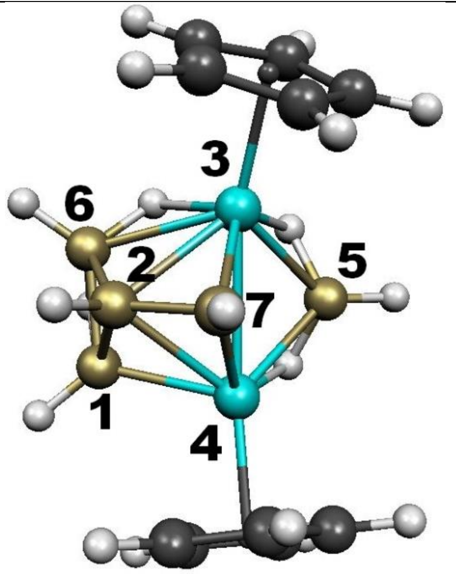

W2B5-9 -650.946715 +45.9
WBI 0.91

```
              1          2          3          4          5
    1  B    0.000000
    2  B    1.756082   0.000000
    3  W    3.186267   2.310602   0.000000
    4  W    2.187982   2.316914   2.707879   0.000000
    5  B    3.597818   3.617951   2.223893   2.247477
0.000000
    6  B    1.765162   1.717023   2.405032   3.151510
3.689446
    7  B    3.086552   1.725260   2.164186   2.135598
3.226072
              6          7
    6  B    0.000000
    7  B    3.173309   0.000000
```

W4-H-B5 W4-H 1.86 B5-H 1.3
W3-H-B5 W3-H 1.85 B5-H 1.3
W3-H-B6 W3-H 1.85 B6-H 1.31
B1-H-B6 B1-H 1.33 B6-H 1.3

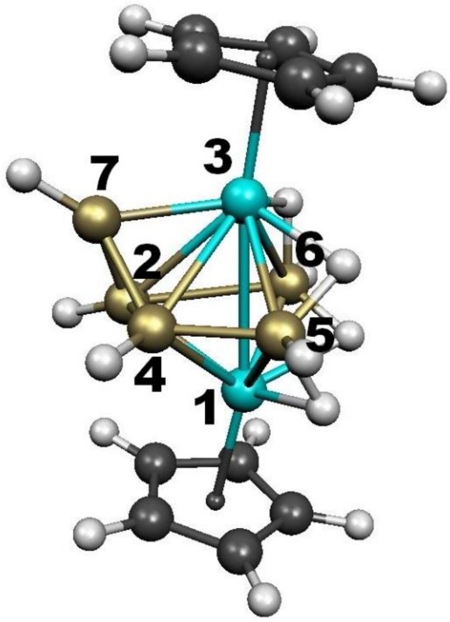

W2B5-10 -650.938404 +51.2
WBI 0.65

```
             1         2         3         4         5
    1  W    0.000000
    2  B    2.167649   0.000000
    3  W    2.884111   2.400714   0.000000
    4  B    2.304395   1.743383   2.320220   0.000000
    5  B    2.322629   3.040570   2.278117   1.769567
0.000000
    6  B    2.091146   2.731658   2.469814   3.515861
3.359592
    7  B    3.413937   1.650553   2.088811   1.778554
3.117801
             6         7
    6  B    0.000000
    7  B    3.725282   0.000000
```

W1-H-B5 W1-H 1.82 B5-H 1.35
W1-H-B6 W1-H 1.86 B6-H 1.36
W3-H-B5 W3-H 1.85 B5-H 1.3
W3-H-B6 W3-H 1.86 B6-H 1.3

6.1.3.5 $Cp_2Ta_2B_5H_9$ systems

Table 87. Distances table for the lowest-lying $Cp_2Ta_2B_5H_9$ structures after M06L/6-311G(d,p) optimization. Included are the ZPcorrected E (a.u.), relative energy (kcal/mol), symmetry and WBI.

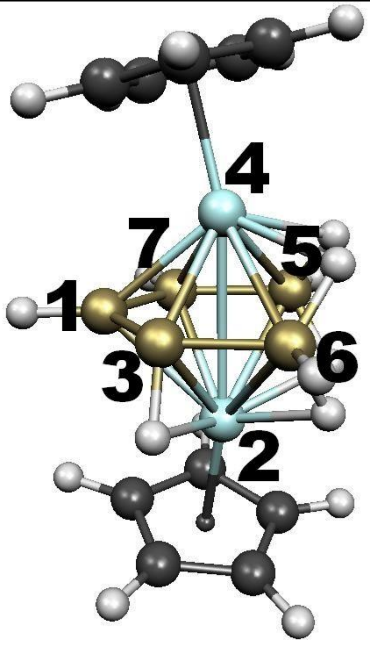

Ta2B5-1 -630.808495 a.u.
0.0 kcal/mol WBI 0.55

```
    1  B    0.000000
    2  Ta   2.331644   0.000000
    3  B    1.710861   2.206498   0.000000
    4  Ta   2.245453   3.055516   2.154995   0.000000
    5  B    3.048606   2.390878   3.378438   2.366859
0.000000
    6  B    3.184814   2.535748   1.755259   2.388036
3.217972
    7  B    1.703042   2.291121   2.865688   2.283417
1.755491
             6         7
    6  B    0.000000
    7  B    3.631451   0.000000
```

Ta2-H-B5 Ta2-H 1.925 B5-H 1.31
Ta2-H-B6 Ta2-H 1.98 B6-H 1.33
Ta4-H-B5 Ta4-H 1.97 B5-H 1.28
Ta4-H-B6 Ta4-H 1.98 B6-H 1.26

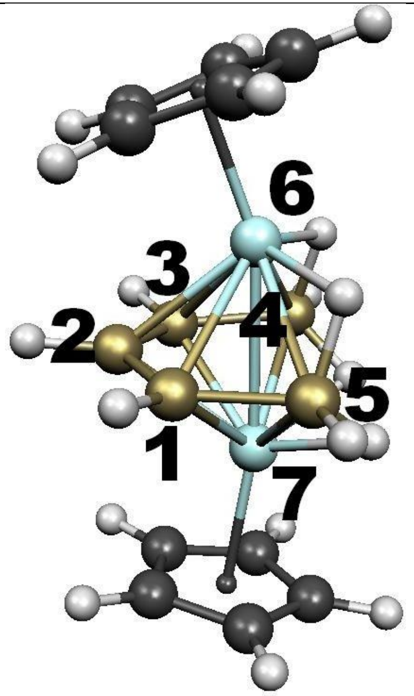

Ta2B5-2 -630.802423 +3.8 Cs
WBI 0.69

```
    1  B    0.000000
    2  B    1.650792   0.000000
    3  B    2.942702   1.650906   0.000000
    4  B    3.716721   3.058945   1.747325   0.000000
    5  B    1.747627   3.059153   3.716866   3.656803
0.000000
    6  Ta   2.413529   2.345626   2.413608   2.470007
2.470568
    7  Ta   2.252520   2.312590   2.252235   2.360442
2.360344
                  6          7
    6  Ta   0.000000
    7  Ta   2.893437   0.000000

Ta6-H-B4   Ta6-H 1.92   B4-H 1.32
Ta6-H-B5   Ta6-H 1.92   B5-H 1.32
Ta7-H-B4   Ta7-H 1.98   B4-H 1.27
Ta7-H-B5   Ta7-H 1.98   B5-H 1.23
```

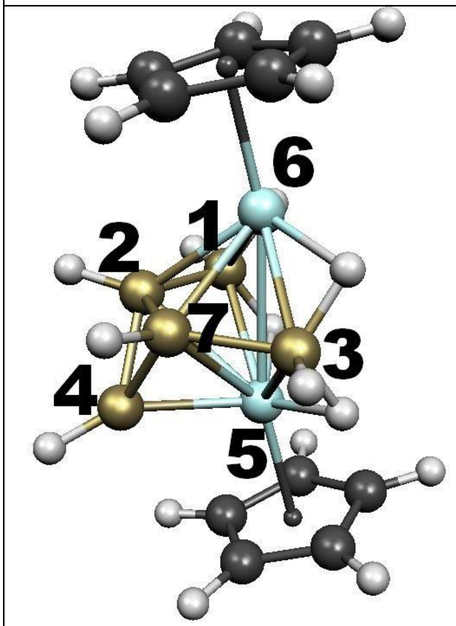

Ta2B5-3 -630.797749 +6.7 Cs
WBI 0.88

```
                  1          2          3          4          5
    1  B    0.000000
    2  B    1.810685   0.000000
    3  B    3.678493   3.113756   0.000000
    4  B    3.076301   1.755763   3.075765   0.000000
    5  Ta   2.378646   2.412705   2.376865   2.138428
0.000000
    6  Ta   2.334270   2.263594   2.334317   3.501172
2.941630
    7  B    3.114713   1.745977   1.809204   1.757978
2.413158
                  6          7
    6  Ta   0.000000
    7  B    2.262391   0.000000

Ta6-H-B1 Ta6-H 1.90   B1-H 1.29
Ta6-H-B3 Ta6-H 1.90   B3-H 1.29
Ta5-H-B1 Ta6-H 1.90   B1-H 1.27
Ta5-H-B3 Ta6-H 1.90   B3-H 1.28
```

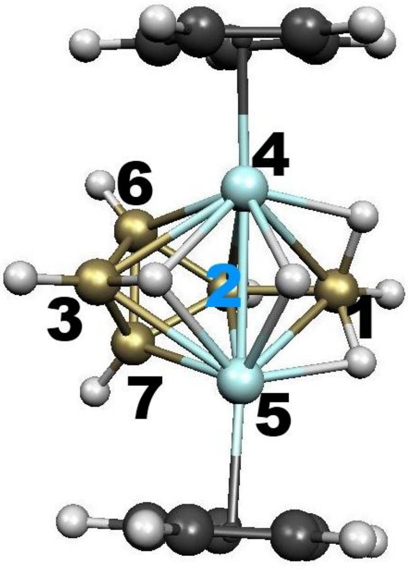 Ta2B5-4 -630.793783 +9.2 Cs WBI 1.12	1 B 0.000000 2 B 1.761570 0.000000 3 B 3.694139 2.626178 0.000000 4 Ta 2.387238 2.431096 2.479373 0.000000 5 Ta 2.387238 2.431096 2.479373 2.717200 0.000000 6 B 3.195086 1.733905 1.695281 2.315208 3.166069 7 B 3.195086 1.733905 1.695281 3.166069 2.315208 6 7 6 B 0.000000 7 B 1.716400 0.000000 Ta4-H-B1 Ta4-H 1.9 B1-H 1.29 Ta5-H-B1 Ta5-H 1.9 B1-H 1.29 Ta4-H-Ta5 Ta4-H 1.96 Ta5-H 1.96 B3-H-Ta4-Ta5 B-H 1.36 Ta4-H 2 Ta5-H 2
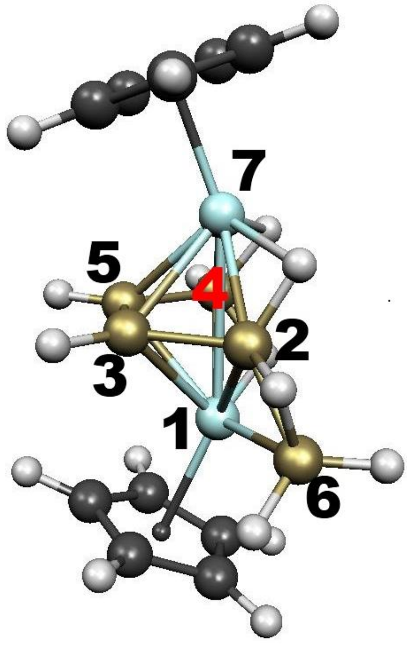 Ta2B5-5 -630.788048 +12.8 WBI 0.62	1 2 3 4 5 1 Ta 0.000000 2 B 2.224741 0.000000 3 B 2.260023 1.774259 0.000000 4 B 2.377755 3.380648 3.069042 0.000000 5 B 2.273518 2.933708 1.728611 1.787760 0.000000 6 B 2.446226 1.701690 3.023535 4.381512 4.133478 7 Ta 3.083530 2.230038 2.252932 2.350946 2.220655 6 7 6 B 0.000000 7 Ta 3.839461 0.000000 Ta1-H-B4 Ta-H 1.92 B4-H 1.3 Ta7-H-B2 Ta7-H 1.89 B2-H 1.3 Ta7-H-B4 Ta7-H 1.92 B4-H 1.3 B2-H-B6 B2-H 1.32 B6-H 1.34
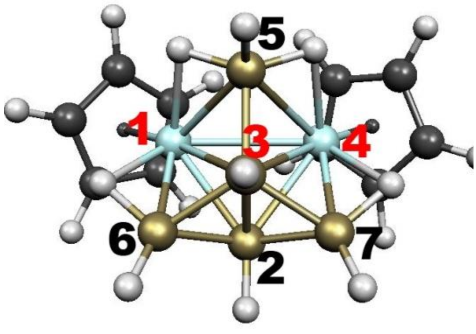	1 2 3 4 5 1 Ta 0.000000 2 B 2.329844 0.000000 3 B 2.429227 1.767591 0.000000 4 Ta 2.707288 2.333375 2.426533 0.000000 5 B 2.366617 3.110195 1.817153 2.364049 0.000000 6 B 2.205182 1.766896 1.811771 3.593706 3.117065 7 B 3.593124 1.764975 1.811844 2.208128

Ta2B5-6 -630.786628 +13.7 Cs WBI 1.39	3.122350 6 7 6 B 0.000000 7 B 2.971004 0.000000 Ta1-H-B5 Ta1-H 1.92 B5-H 1.32 Ta1-H-B6 Ta1-H 1.88 B6-H 1.28 Ta4-H-B5 Ta4-H 1.91 B5-H 1.32 Ta4-H-B7 Ta-H 1.88 B7-H 1.28
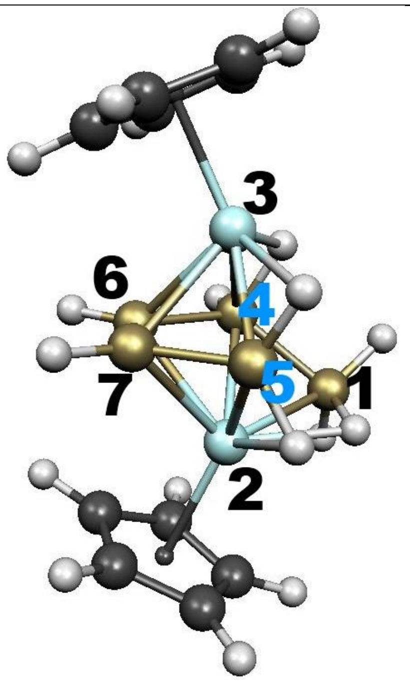 Ta2B6-7 -630.779916 +17.9 WBI 0.46	1 2 3 4 5 1 B 0.000000 2 Ta 2.338250 0.000000 3 Ta 3.595539 3.140078 0.000000 4 B 1.886737 2.344347 2.378720 0.000000 5 B 3.573906 2.165638 2.159089 3.219307 0.000000 6 B 3.349215 2.249217 2.244539 1.808387 2.820290 7 B 4.121244 2.307126 2.235529 3.074320 1.733513 6 7 6 B 0.000000 7 B 1.729512 0.000000 Ta2-H-B1 Ta2-H 1.97 B1-H 1.29 Ta2-H-B5 Ta2-H 2.03 B5-H 1.25 Ta3-H-B4 Ta3-H 1.89 B4-H 1.3 Ta3-H-B5 Ta3-H 2.05 B5-H 1.26

6.1.4 8 vertices

6.1.4.1 $Cp_2M_2B_6H_{10}$ (M=Pd,Pt) systems

Table 88. Distance table for the lowest-lying $Cp_2Pd_2B_6H_{10}$ structures after M06L/6-311G(d,p) optimization. Included are the ZPcorrected E (a.u.), relative energy (kcal/mol), symmetry and WBI.

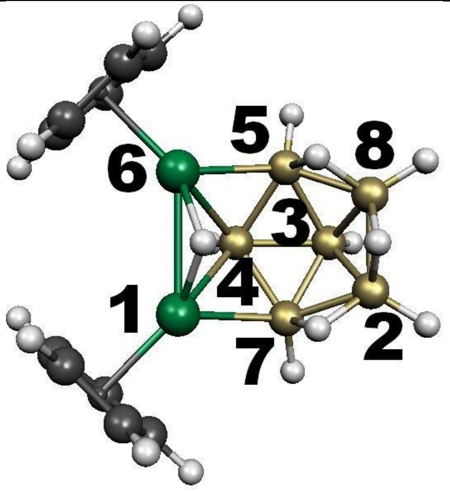

1. -798.007296 0.0 C_S
WBI 0.26

```
              1          2          3          4          5
   1  Pd   0.000000
   2  B    3.538067   0.000000
   3  B    3.460369   1.735040   0.000000
   4  B    2.182319   2.898726   1.794785   0.000000
   5  B    3.500687   2.855941   1.775715   1.799012   0.000000
   6  Pd   2.622553   4.137442   3.460351   2.182355   2.175729
   7  B    2.175729   1.767723   1.775715   1.799028   2.867734
   8  B    4.137585   1.754556   1.735034   2.898726   1.767720
              6          7          8
   6  Pd   0.000000
   7  B    3.500622   0.000000
   8  B    3.537976   2.855955   0.000000
```

Pd1-H- Pd6 Pd1-H 1.73 Pd6-H 1.73
B2-H-B7 B2-H 1.30 B7-H 1.35
B2-H-B8 B2-H 1.33 B8-8 1.33
B5-H-B8 B5-H 1.35 B8-H 1.30

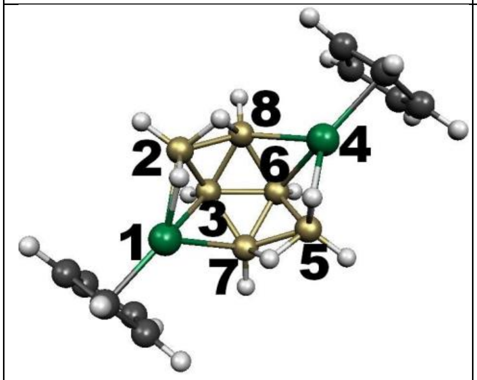

2. -797.985663 +13.6 C_2
WBI 0.03

```
              1          2          3          4          5
   1  Pd   0.000000
   2  B    2.210401   0.000000
   3  B    2.214414   1.751988   0.000000
   4  Pd   4.521384   3.499523   3.416519   0.000000
   5  B    3.499542   3.684651   2.943523   2.210407   0.000000
   6  B    3.416523   2.943523   1.775903   2.214417   1.751982
   7  B    2.209049   2.991621   1.812057   3.381315   1.754086
   8  B    3.381313   1.754083   1.753366   2.209059   2.991633
              6          7          8
   6  B    0.000000
   7  B    1.753377   0.000000
   8  B    1.812057   2.881657   0.000000
```

Pd1-H-B2 Pd1-H 1.72 B2-H 1.34
Pd4-H-B5 Pd2-H 1.72 B5-H 1.34
B2-H-B8 B2-H 1.31 B8-H 1.35
B5-H-B7 B5-H 1.31 B7-H 1.35

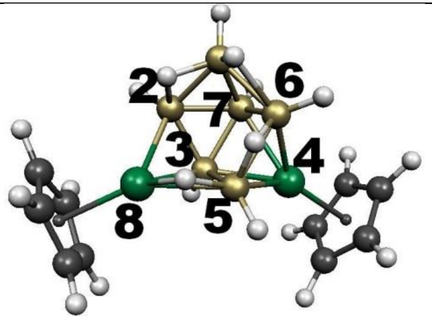

3. -797.984379 +14.4 C_1
WBI 0.09

		1	2	3	4	5
1	B	0.000000				
2	B	1.839868	0.000000			
3	B	2.920862	1.767039	0.000000		
4	Pd	3.530904	3.418897	2.100956	0.000000	
5	B	3.020137	2.802066	1.997442	2.160457	0.000000
6	B	1.850240	2.758855	2.639780	2.167750	1.935797
7	B	1.757387	1.776489	1.780267	2.173787	2.648822
8	Pd	3.467234	2.207693	2.140693	3.834987	2.270126

		6	7	8
6	B	0.000000		
7	B	1.777172	0.000000	
8	Pd	3.579341	3.384631	0.000000

Pd8-H-B5   Pd8-H 1.64   B5-H 1.38
B1-H-B2   B1-H 1.32   B2-H 1.32
B1-H-B6   B1-H 1.21   B6-H 1.80
B5-H-B6   B5-H 1.32   B6-H 1.31

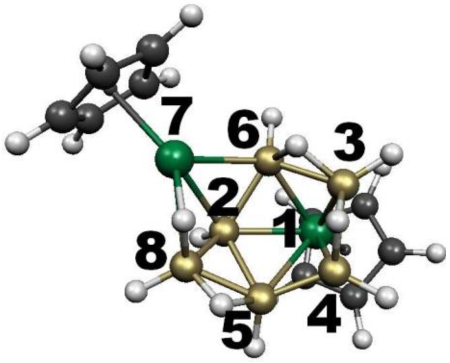

4. -797.975134 +20.2 C_1
WBI 0.06

		1	2	3	4	5
1	Pd	0.000000				
2	B	2.196270	0.000000			
3	B	2.119099	2.915945	0.000000		
4	B	2.162241	2.761725	1.811671	0.000000	
5	B	2.548678	1.894404	2.946591	1.655039	0.000000
6	B	2.141454	1.843782	1.837705	2.885909	3.041318
7	Pd	3.944688	2.191381	3.551560	4.039401	3.434397
8	B	3.602737	1.752535	3.673058	3.050687	1.742986

		6	7	8
6	B	0.000000		
7	Pd	2.196381	0.000000	
8	B	3.049582	2.235706	0.000000

Pd7-H-B8   Pd7-H 1.74   B8-H 1.33
B3-H-B4   B3-H 1.30 B4-H 1.33
B3-H-B6   B3-H 1.31   B6-H 1.31
B5-H-B8   B5-H 1.40   B8-H 1.27

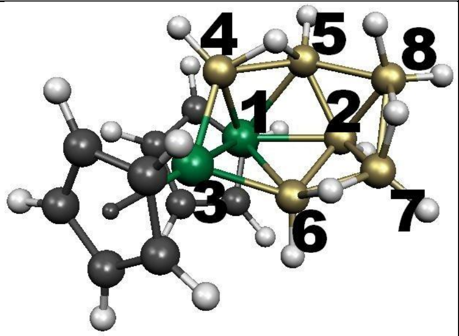

		1	2	3	4	5
1	Pd	0.000000				
2	B	2.176059	0.000000			
3	Pd	2.604134	3.404072	0.000000		
4	B	2.108252	2.905714	2.044146	0.000000	
5	B	2.215856	1.754465	3.356755	1.841512	0.000000
6	B	2.320355	1.829316	2.110669	2.834204	2.849026
7	B	3.520146	1.741784	3.512585	3.645430	2.907805
8	B	3.584454	1.763333	4.167883	3.300787	1.888063

		6	7	8

5. -797.975094 +20.3 C_1 WBI 0.25	6 B 0.000000 7 B 1.761886 0.000000 8 B 2.948172 1.842915 0.000000 B4-H-B5 B4-H 1.29 B5-H 1.31 B6-H-B7 B6-H 1.42 B7-H 1.26 B7-H-B8 B7-H 1.30 B8 1.35 B8-H 1.20
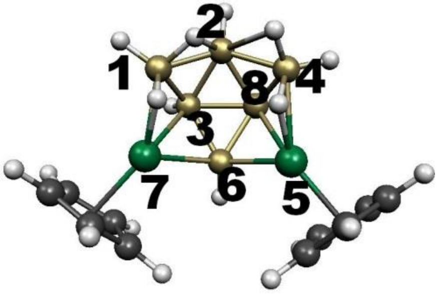 6. -797.973889 +20.9 C_1 WBI 0.07	1 2 3 4 5 1 B 0.000000 2 B 1.755183 0.000000 3 B 1.748719 1.802359 0.000000 4 B 3.172719 1.889758 3.071648 0.000000 5 Pd 4.017496 3.404677 3.393793 2.259546 0.000000 6 B 2.953152 2.870827 1.760314 3.057516 2.128257 7 Pd 2.198641 3.364418 2.210038 4.103579 3.633553 8 B 2.873054 1.750682 1.798510 1.795009 2.190920 6 7 8 6 B 0.000000 7 Pd 2.152734 0.000000 8 B 1.753947 3.348647 0.000000 Pd7-H-B1 Pd7-H 1.72 B1-H 1.34 Pd5-H-B4 Pd 5-H1.70 B4-H 1.35 B1-H-B2 B1-H 1.29 B2-H 1.33 B4-H 1.20
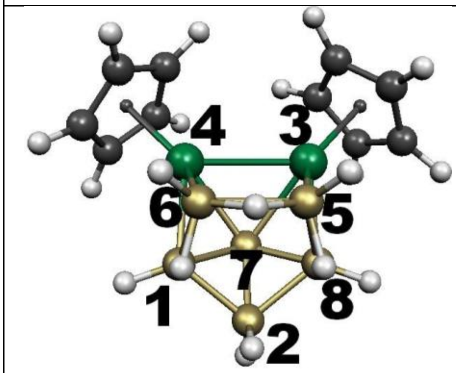 7. -797.973829 +21.0 C_S WBI 0.29	1 2 3 4 5 1 B 0.000000 2 B 1.848569 0.000000 3 Pd 3.479457 3.529997 0.000000 4 Pd 2.180275 3.528350 2.598651 0.000000 5 B 3.017997 3.019732 2.078869 3.107987 0.000000 6 B 1.818828 3.019999 3.104996 2.078438 2.050872 7 B 1.767856 1.678999 2.234428 2.233781 2.665550 8 B 2.828561 1.849614 2.181343 3.479384 1.818660 6 7 8 6 B 0.000000 7 B 2.665471 0.000000 8 B 3.018175 1.766686 0.000000 B1-H-B6 B1-H 1.33 B6-H 1.29 B5-H-B8 B5-H 1.29 B8-H 1.33 B5-H-B6 B5-H 1.29 B6-H 1.29 B2-H 1.20

Table 89. Distance table for the lowest-lying $Cp_2Pt_2B_6H_{10}$ structures after M06L/6-311G(d,p) optimization. Included are the ZPcorrected E (a.u.), relative energy (kcal/mol), symmetry and WBI.

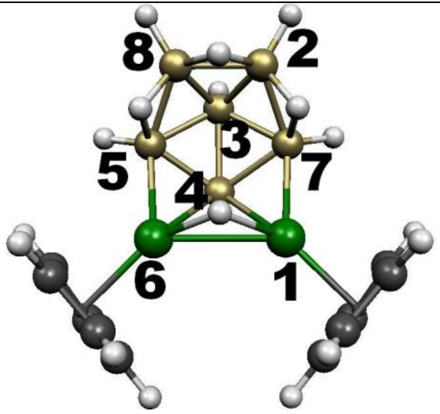

1. -780.936426 0.0 C_S
WBI 0.32

		1	2	3	4	5
1	Pt	0.000000				
2	B	3.551109	0.000000			
3	B	3.430301	1.734084	0.000000		
4	B	2.178323	2.948253	1.804452	0.000000	
5	B	3.518999	2.870864	1.781659	1.843457	0.000000
6	Pt	2.675641	4.160078	3.430306	2.178338	2.150254
7	B	2.150236	1.775318	1.781659	1.843464	2.900137
8	B	4.160127	1.755138	1.734078	2.948253	1.775314

		6	7	8
6	Pt	0.000000		
7	B	3.518977	0.000000	
8	B	3.551098	2.870874	0.000000

Pt1-H- Pt5 Pt1-H 1.75 Pt5-H 1.75
B2-H-B7 B2-H 1.29 B7-H 1.37
B8-H-B5 B8-H 1.29 B5-H 1.37
B2-H-B8 B2-H 1.33 B8-H 1.33

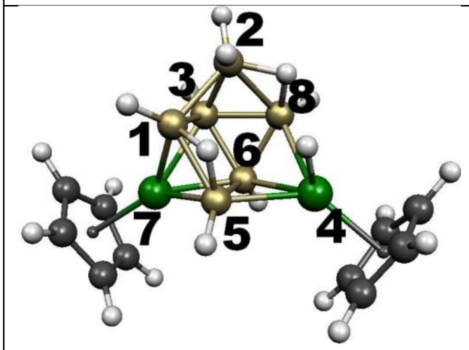

2. -780.927129 +5.8 C_1
WBI 0.07

		1	2	3	4	5
1	B	0.000000				
2	B	1.892127	0.000000			
3	B	1.797002	1.776292	0.000000		
4	Pt	3.486473	3.472296	3.387823	0.000000	
5	B	1.904246	3.084846	2.641890	2.211355	0.000000
6	B	2.620576	2.954126	1.778378	2.178105	1.968641
7	Pt	2.140939	3.546055	2.166329	3.836032	2.125948
8	B	2.777762	1.894189	1.800691	2.217819	2.816303

		6	7	8
6	B	0.000000		
7	Pt	2.115655	0.000000	
8	B	1.765679	3.436656	0.000000

B1-H-B5 B1-H 1.31 B5-H 1.31
B2-H-B8 B2-H 1.31 B8-H 1.31
Pt4-H 1.6
B2-H 1.2

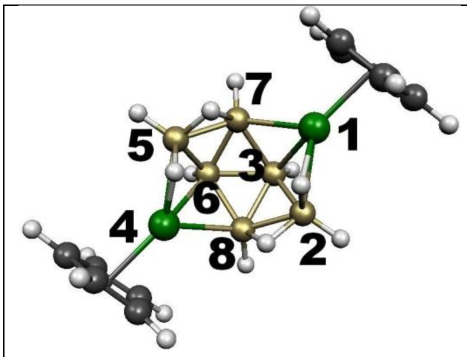

3. -780.919855 +10.4 C_2
WBI 0.03

		1	2	3	4	5	6	7	8
1	Pt	0.000000							
2	B	2.195618	0.000000						
3	B	2.219141	1.734508	0.000000					
4	Pt	4.502924	3.531295	3.415057	0.000000				
5	B	3.531295	3.736269	2.959675	2.195615	0.000000			
6	B	3.415046	2.959672	1.780204	2.219142	1.734498	0.000000		
7	B	2.194560	2.988974	1.830815	3.363974	1.756415	1.762457	0.000000	
8	B	3.363984	1.756424	1.762459	2.194577	2.988983	1.830810	2.882111	0.000000

Pt1-H- B2 Pt1-H 1.68 B2-H 1.42
Pt4-H-B5 Pt4-H 1.68 B5-H 1.42
B2-H-B8 B2-H 1.30 B8-H 1.38
B5-H-B7 B5-H 1.29 B7-H 1.67

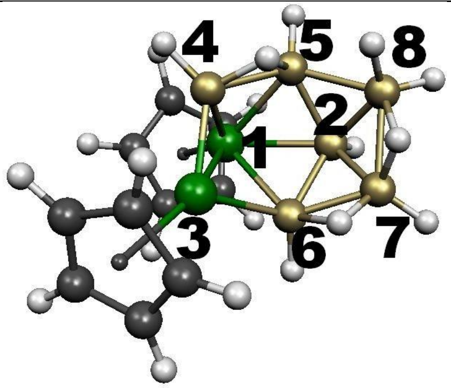

4. -780.916832 +12.3 C_1
WBI 0.32

		1	2	3	4	5	6	7	8
1	Pt	0.000000							
2	B	2.186814	0.000000						
3	Pt	2.643224	3.372381	0.000000					
4	B	2.128383	2.952724	2.051105	0.000000				
5	B	2.200817	1.764020	3.317610	1.858884	0.000000			
6	B	2.352075	1.848136	2.102004	2.923180	2.891253	0.000000		
7	B	3.540732	1.738586	3.475244	3.732288	2.949700	1.777158	0.000000	
8	B	3.585805	1.771760	4.068433	3.314898	1.902926	2.961064	1.854393	0.000000

B4-H-B5 B4-H 1.30 B5-H 1.31
B6-H-B7 B6-H 1.46 B7-H 1.25
B7-H-B8 B7-H 1.30 B8-H 1.35
B8-H 1.2

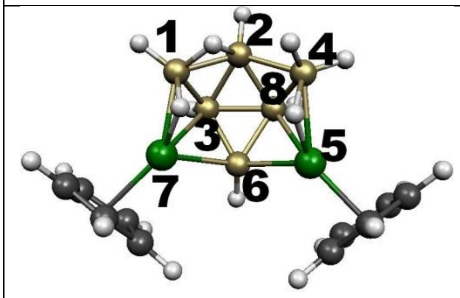

5. -780.913391 +14.5 C_1

		1	2	3	4	5	6	7	8
1	B	0.000000							
2	B	1.737544	0.000000						
3	B	1.734751	1.795747	0.000000					
4	B	3.210145	1.905539	3.079226	0.000000				
5	Pt	4.098556	3.421938	3.418868	2.254125	0.000000			
6	B	2.933490	2.862419	1.781210	3.039724	2.122697			
7	Pt	2.151368	3.322443	2.220798	4.103443	3.738700			
8	B	2.868351	1.748483	1.789848	1.791899	2.176196			

WBI 0.06	6 B 0.000000 7 Pt 2.156776 0.000000 8 B 1.778406 3.360802 0.000000 Pt5-H-B4 Pt5-H 1.64 B4-H 1.48 Pt7-H-B1 Pt7-H 1.63 B1-H 1.55 B1-H-B2 B1-H 1.30 B2-H 1.33 B4-H 1.2
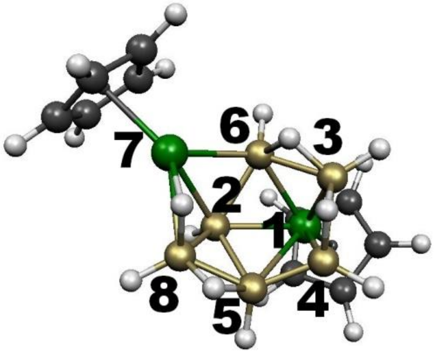 6. -780.911072 +15.9 C_1 WBI 0.07	1 2 3 4 5 1 Pt 0.000000 2 B 2.196113 0.000000 3 B 2.112960 2.969369 0.000000 4 B 2.174286 2.785778 1.822194 0.000000 5 B 2.549982 1.891096 2.957427 1.654005 0.000000 6 B 2.160784 1.910810 1.853388 2.909808 3.060548 7 Pt 3.918124 2.201748 3.568501 4.033149 3.415407 8 B 3.590508 1.737892 3.705258 3.062444 1.740784 6 7 8 6 B 0.000000 7 Pt 2.176675 0.000000 8 B 3.061391 2.224430 0.000000 Pt7-H-B8 Pt7-H 1.69 B8-H 1.41 B3-H-B4 B3-H 1.30 B4-H 1.33 B3-H-B6 B3-H 1.30 B6-H 1.32 B5-H-B8 B5-H 1.44 B8-H 1.26
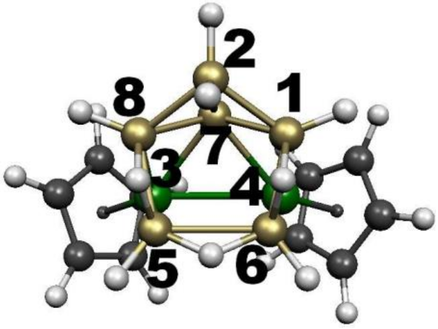 7. -780.907151 +18..4 C_S WBI 0.37	1 2 3 4 5 1 B 0.000000 2 B 1.832265 0.000000 3 Pt 3.504971 3.517525 0.000000 4 Pt 2.176739 3.513909 2.660328 0.000000 5 B 3.091911 3.051010 2.076524 3.180469 0.000000 6 B 1.841505 3.052481 3.179216 2.076063 2.180342 7 B 1.792964 1.694089 2.241521 2.239518 2.737039 8 B 2.832307 1.833506 2.178622 3.502779 1.841031 6 7 8 6 B 0.000000 7 B 2.738642 0.000000 8 B 3.093768 1.790125 0.000000 B1-H-B6 B1-H 1.33 B6-H 1.29 B8-H-B5 B8-H 1.33 B5-H 1.29 B5-H-B6 B5-H 1.30 B6-H 1.30 B2-H 1.20

6.1.4.2 $Cp_2M_2B_6H_{10}$ (M=Rh,Ir) systems

Table 90. Distance table for the lowest-lying $Cp_2Rh_2B_6H_{10}$ structures after M06L/6-311G(d,p) optimization. Included are the ZPcorrected E (a.u.), relative energy (kcal/mol), symmetry and WBI.

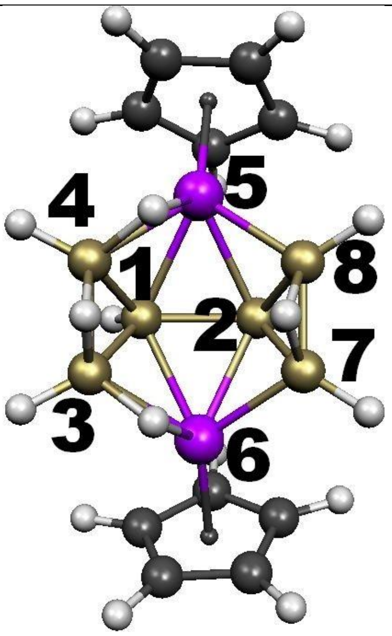 **1. -763.371780 0.0 C_S** **WBI 0.08**	1 2 3 4 5 1 B 0.000000 2 B 1.868940 0.000000 3 B 1.767888 3.059452 0.000000 4 B 1.767888 3.059452 1.708480 0.000000 5 Rh 2.206133 2.204622 3.353910 2.157973 0.000000 6 Rh 2.206133 2.204622 2.157973 3.353910 3.858324 7 B 2.996899 1.736002 3.264660 3.673584 3.299821 8 B 2.996899 1.736002 3.673584 3.264660 2.116942 6 7 8 6 Rh 0.000000 7 B 2.116942 0.000000 8 B 3.299821 1.660664 0.000000 Rh5-H-B4 Rh5-H 1.68 B4-H 1.39 Rh6-H-B3 Rh6-H 1.68 B3-H 1.39 B3-H-B4 B3-H 1.33 B4-H 1.33 B7-H-B8 B7-H 1.34 B8-H 1.34
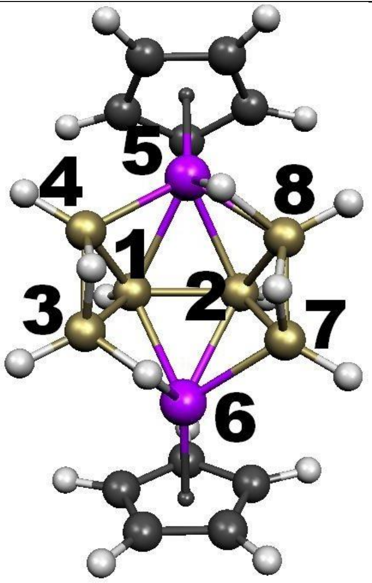 2. -763.370496 +0.8 C_2 WBI 0.07	1 2 3 4 5 1 B 0.000000 2 B 1.871585 0.000000 3 B 1.773404 3.037250 0.000000 4 B 1.727845 3.021782 1.684901 0.000000 5 Rh 2.219521 2.194381 3.298067 2.105360 0.000000 6 Rh 2.194354 2.219467 2.165787 3.344433 3.855048 7 B 3.021738 1.727825 3.271546 3.745743 3.344370 8 B 3.037278 1.773411 3.601623 3.271636 2.165728 6 7 8 6 Rh 0.000000 7 B 2.105338 0.000000 8 B 3.298104 1.684910 0.000000 Rh5-H-B8 Rh5-H 1.67 B8-H 1.41 Rh6-H-B3 Rh6-H 1.66 B3-H 1.41 B3-H-B4 B3-H 1.35 B4-H 1.33 B8-H-B7 B8-H 1.35 B7-H 1.33

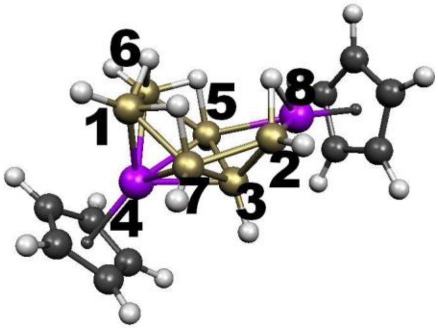

3. -763.368066 +2.3 C_1
WBI 0.07

		1	2	3	4	5
1	B	0.000000				
2	B	3.106396	0.000000			
3	B	2.933515	1.744228	0.000000		
4	Rh	2.080179	3.481774	2.205282	0.000000	
5	B	2.915178	2.910567	1.805628	2.179383	0.000000
6	B	1.802523	3.580849	2.950474	2.091839	1.823309
7	B	1.818265	1.866580	1.766935	2.150324	2.873652
8	Rh	4.051941	2.033429	2.174470	3.956976	2.219466

		6	7	8
6	B	0.000000		
7	B	2.914057	0.000000	
8	Rh	3.525608	3.371855	0.000000

Rh8-H-B2 Rh8-H 1.76 B2-H 1.34
B1-H-B6 B1-H 1.32 B6-H 1.33
B1-H-B7 B1-H 1.33 B7-H 1.32
B5-H-B6 B5-H 1.33 B6-H 1.31

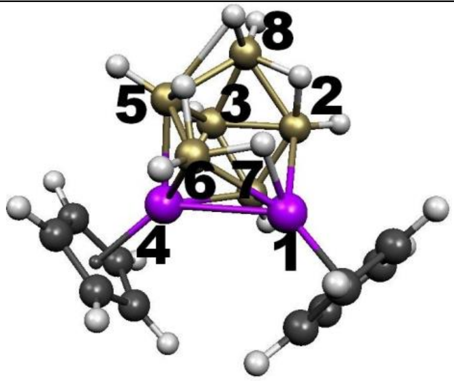

4. -763.368056 +2.4 C_1
WBI 0.33

		1	2	3	4	5
1	Rh	0.000000				
2	B	2.279408	0.000000			
3	B	3.125058	1.831446	0.000000		
4	Rh	2.670182	3.175661	2.214541	0.000000	
5	B	3.309200	2.813845	1.756947	2.157075	0.000000
6	B	2.250130	3.092953	2.893863	2.100091	1.822548
7	B	2.121307	1.724808	1.725643	2.077863	2.936537
8	B	3.516975	1.843100	1.760873	3.507886	1.947771

		6	7	8
6	B	0.000000		
7	B	3.069182	0.000000	
8	B	3.041502	2.991230	0.000000

Rh1-H-B6 Rh1-H 1.69 B6-H 1.34
B2-H-B8 B2-H 1.29 B8-H 1.33
B5-H-B6 B5-H 1.32 B6-H 1.30
B5-H-B8 B5-H 2.10 B8-H 1.20

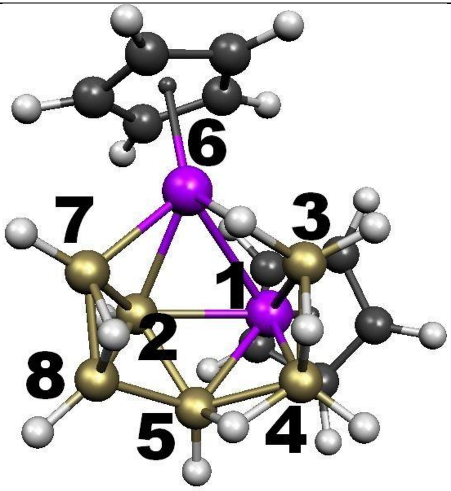

5. -763.364186 +4.8 C_1
WBI 0.32

```
                 1          2          3          4          5
    1  Rh   0.000000
    2  B    2.243805   0.000000
    3  B    2.111232   3.041411   0.000000
    4  B    2.087159   3.014550   1.799676   0.000000
    5  B    2.188508   1.841483   2.927588   1.815430   0.000000
    6  Rh   2.672925   2.218441   2.236230   3.474453   3.438702
    7  B    3.559526   1.748799   3.286636   3.639808   2.856019
    8  B    3.424465   1.711082   3.605791   3.096290   1.768035
                 6          7          8
    6  Rh   0.000000
    7  B    2.140960   0.000000
    8  B    3.286088   1.639995   0.000000
```

Rh6-H-B3   Rh6-H 1.69   B3-H 1.36
B3-H-B4   B3-H 1.34   B4-H 1.31
B4-H-B5   B4-H 1.31   B5-H 1.31
B7-H-B8   B7-H 1.35   B7-H 1.32

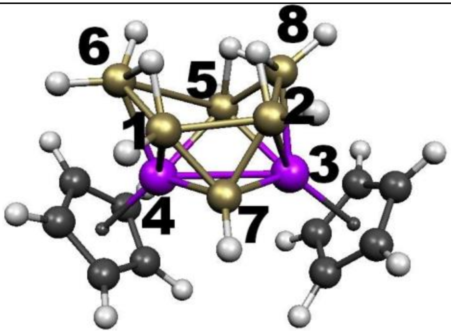

6. -763.363317 +5.3 C_1
WBI 0.30

```
                 1          2          3          4          5
    1  B    0.000000
    2  B    1.994837   0.000000
    3  Rh   3.266712   2.195736   0.000000
    4  Rh   2.196970   3.099394   2.680897   0.000000
    5  B    3.045579   2.836343   2.106935   2.100667   0.000000
    6  B    1.802650   3.196271   3.951149   2.196016   2.641172
    7  B    1.719852   1.720264   2.091886   2.091557   2.960315
    8  B    3.026630   1.811679   2.096492   3.278347   1.796214
                 6          7          8
    6  B    0.000000
    7  B    3.131595   0.000000
    8  B    3.232970   2.950510   0.000000
```

B1-H-B6   B1-H 1.28   B6-H 1.36
B2-H-B8   B2-H 1.30   B8-H 1.32
B5-H-B8   B5-H 1.35   B8-H 1.28
B6-H 1.20

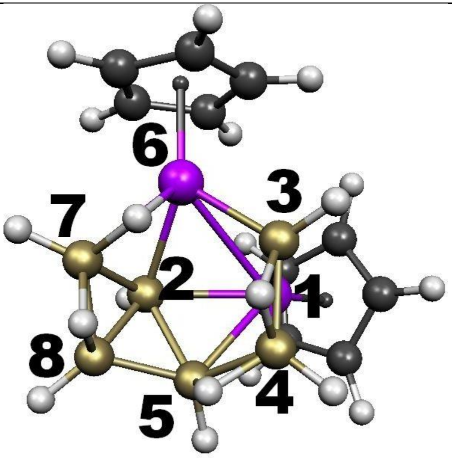

```
                 1          2          3          4          5
    1  Rh   0.000000
    2  B    2.231225   0.000000
    3  B    2.075369   3.004657   0.000000
    4  B    2.099551   2.982543   1.783037   0.000000
    5  B    2.185922   1.862426   2.952627   1.825739   0.000000
    6  Rh   2.692613   2.208698   2.126597   3.356955   3.424242
    7  B    3.592310   1.782769   3.301743   3.548246   2.838441
    8  B    3.429110   1.704874   3.719761   3.124196   1.758816
                 6          7          8
    6  Rh   0.000000
    7  B    2.178147   0.000000
```

7. -763.362044 +6.1 C_1 WBI 0.29	8 B 3.327711 1.667987 0.000000 Rh6-H-B7 Rh6-H 1.65 B7-H 1.43 B3-H-B4 B3-H 1.35 B4-H 1.31 B4-H-B5 B4-H 1.31 B5-H 1.31 B7-H-B8 B7-H 1.35 B8-H 131
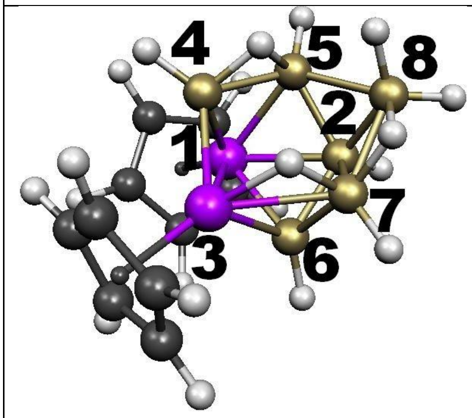 8. -763.361669 +6.3 C_1 WBI 0.31	1 2 3 4 5 1 Rh 0.000000 2 B 2.180035 0.000000 3 Rh 2.659384 3.079591 0.000000 4 B 2.070474 2.870662 2.120690 0.000000 5 B 2.159269 1.769526 3.213864 1.813884 0.000000 6 B 2.093785 1.733043 2.094606 3.010963 2.944286 7 B 3.216807 1.828938 2.322081 3.063778 2.749397 8 B 3.551956 1.768190 3.644369 3.185000 1.944411 6 7 8 6 B 0.000000 7 B 1.802190 0.000000 8 B 3.082533 1.891339 0.000000 Rh3-H-B7 Rh3-H 1.66 B7-H 1.40 B4-H-B5 B4-H 1.30 B5-H 1.32 B7-H-B8 B7-H 1.32 B8-H 1.31 B8-H 1.20
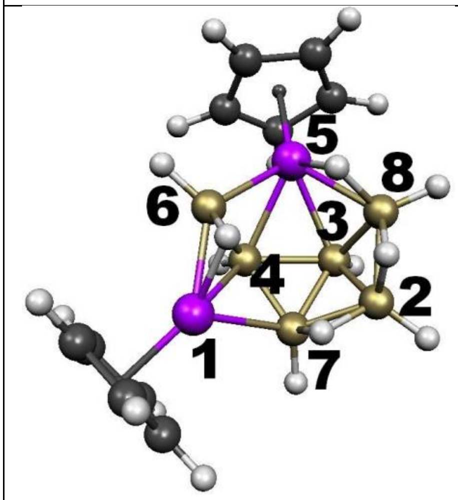 9. -763.360683 +7.0 C_1 WBI 0.10	1 2 3 4 5 1 Rh 0.000000 2 B 3.497292 0.000000 3 B 3.461531 1.746580 0.000000 4 B 2.181124 2.915404 1.817584 0.000000 5 Rh 3.796891 3.332857 2.205007 2.198666 0.000000 6 B 2.056251 3.663297 3.075419 1.816415 2.166808 7 B 2.203658 1.779003 1.775443 1.763819 3.345377 8 B 4.097917 1.726758 1.763932 2.994242 2.159605 6 7 8 6 B 0.000000 7 B 2.956002 0.000000 8 B 3.305486 2.871268 0.000000 Rh1-H-B6 Rh1-H 1.76 B6-H 133 Rh5-H-B8 Rh5-H 1.70 B8-H 1.36 B2-H-B7 B2-H 1.35 B7-H 1.31 B2-H-B8 B2-H 1.31 B8-H 1.35

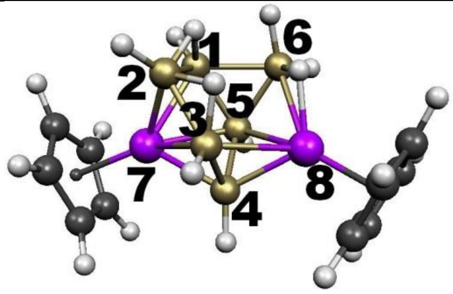

10. -763.359328 +7.8 C_1
WBI 0.09

```
              1          2          3          4          5
    1  B    0.000000
    2  B    1.831988   0.000000
    3  B    2.803455   1.807712   0.000000
    4  B    2.962238   3.000603   1.794386   0.000000
    5  B    1.759620   2.868238   2.662140   1.793367   0.000000
    6  B    1.901127   3.036183   3.218679   3.133509   1.761875
    7  Rh   2.159866   2.082634   2.215133   2.043519   2.237527
    8  Rh   3.304493   3.440181   2.305490   2.049432   2.268490
              6          7          8
    6  B    0.000000
    7  Rh   3.526432   0.000000
    8  Rh   2.309451   3.612619   0.000000
```

Rh8-H-B6   Rh8-H 1.69   B6-H 1.35
B1-H-B2   B1-H 1.34   B2-H 1.28
B2-H-B3   B2-1.32   B3-H 1.30
B6-H 1.21

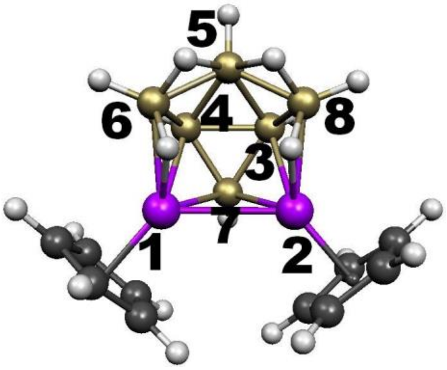

11. -763.358198 +8.5 C_S
WBI 0.38

```
              1          2          3          4          5
    1  Rh   0.000000
    2  Rh   2.764718   0.000000
    3  B    3.176797   2.237030   0.000000
    4  B    2.237804   3.174273   1.836748   0.000000
    5  B    3.304432   3.306827   1.820616   1.825502   0.000000
    6  B    2.227610   3.666826   2.929214   1.724083   1.803636
    7  B    2.119507   2.110114   1.728035   1.726745   2.945469
    8  B    3.676484   2.239576   1.723980   2.940724   1.808974
              6          7          8
    6  B    0.000000
    7  B    3.033938   0.000000
    8  B    3.071629   3.039884   0.000000
```

Rh1-H-B6   Rh1-H 1.72   B6-H 1.34
Rh2-H-B8   Rh2-H 1.72   B8-H 1.34
B5-H-B6   B5 1.47   B6-H 1.24
B5-H-B8   B5-H 1.50   B8-H 1.24

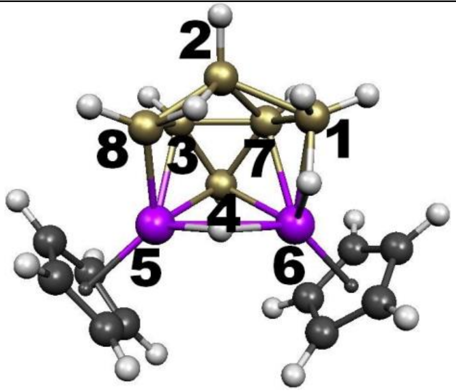

```
              1          2          3          4          5
    1  B    0.000000
    2  B    1.910058   0.000000
    3  B    3.082929   1.786538   0.000000
    4  B    3.201523   2.921447   1.723407   0.000000
    5  Rh   3.820212   3.213568   2.238300   2.068822   0.000000
    6  Rh   2.331479   3.287880   3.214598   2.159531   2.791561
    7  B    1.775620   1.764822   1.802962   1.769557   3.119703
    8  B    3.175015   1.746431   1.698054   2.930895   2.103987
              6          7          8
    6  Rh   0.000000
```

12. -763.356708 +9.5 C_1
WBI 0.26 2.791

7	B	2.235920	0.000000	
8	B	3.598986	2.820188	0.000000

Rh5-H- Rh6   Rh5-H 1.68   Rh6-H 1.84
Rh6-H-B1   Rh6-H 1.70   B1-H 1.35
B2-H-B8   B2-H 1.32   B8-H 1.30
B1-H 1.20

Table 91. Distance table for the lowest-lying $Cp_2Ir_2B_6H_{10}$ structures after M06L/6-311G(d,p) optimization. Included are the ZPcorrected E (a.u.), relative energy (kcal/mol), symmetry and WBI.

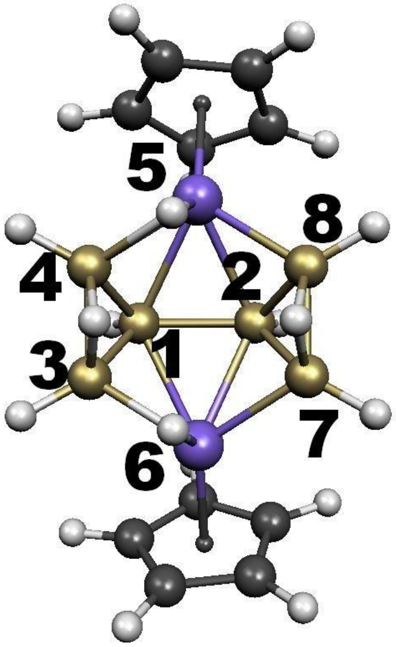

1. -751.000127 0.0 C_S
WBI 0.07

		1	2	3	4	5
1	B	0.000000				
2	B	1.877866	0.000000			
3	B	1.744933	3.044935	0.000000		
4	B	1.744933	3.044935	1.686910	0.000000	
5	Ir	2.235595	2.228373	3.336351	2.140256	0.000000
6	Ir	2.235595	2.228373	2.140256	3.336351	3.883160
7	B	3.040167	1.738880	3.313814	3.714227	3.318735
8	B	3.040167	1.738880	3.714227	3.313814	2.129805

		6	7	8
6	Ir	0.000000		
7	B	2.129805	0.000000	
8	B	3.318735	1.668212	0.000000

Ir5-H-B4   Ir5-H 1.62   B4-H 1.65
Ir6-H-B3   Ir6-H 1.62   B3-H 1.65
B3-H-B4   B3-H 1.34   B4-H 1.34
B7-H-B8   B7-H 1.34   B8-H 1.34

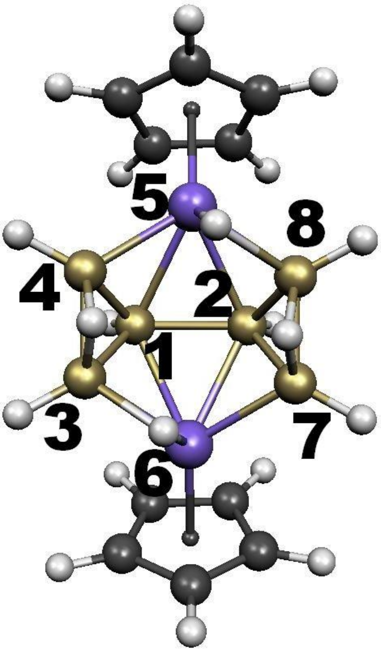

2. -750.999430 +0.4 C_2
WBI 0.07

```
              1          2          3          4          5
    1  B    0.000000
    2  B    1.881119   0.000000
    3  B    1.751145   3.046667   0.000000
    4  B    1.734969   3.042847   1.678499   0.000000
    5  Ir   2.241091   2.226183   3.314893   2.123919   0.000000
    6  Ir   2.226183   2.241091   2.147367   3.340924   3.884295
    7  B    3.042847   1.734969   3.314353   3.751165   3.340924
    8  B    3.046667   1.751145   3.676387   3.314353   2.147367
              6          7          8
    6  Ir   0.000000
    7  B    2.123919   0.000000
    8  B    3.314893   1.678499   0.000000
```

Ir5-H-B8   Ir5-H 1.63   B8-H 1.65
Ir6-H-B3   Ir6-H 1.63   B3-H 1.56
B3-H-B4   B3-H 1.35   B4-H 1.33
B7-H-B8   B7-H 1.35   B8-H 1.33

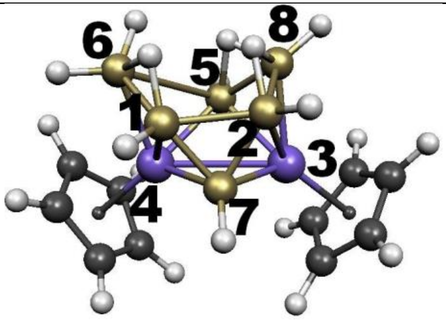

3. -750.995275 +3.0 C1
WBI 0.34

```
              1          2          3          4          5
    1  B    0.000000
    2  B    1.985827   0.000000
    3  Ir   3.291144   2.208252   0.000000
    4  Ir   2.209082   3.114341   2.735297   0.000000
    5  B    3.088801   2.862468   2.125693   2.112014   0.000000
    6  B    1.814127   3.198869   4.005616   2.206008   2.707879
    7  B    1.725589   1.729953   2.105056   2.115875   2.980136
    8  B    3.037317   1.825490   2.111209   3.286711   1.808223
              6          7          8
    6  B    0.000000
    7  B    3.153851   0.000000
    8  B    3.248243   2.965800   0.000000
```

B1-H-B6   B1-H 1.28   B6-H 1.36
B2-H-B8   B2-H 1.30   B8-H 1.32
B5-H-B8   B5-H 1.35   B8-H 1.28
B6-H 1.2

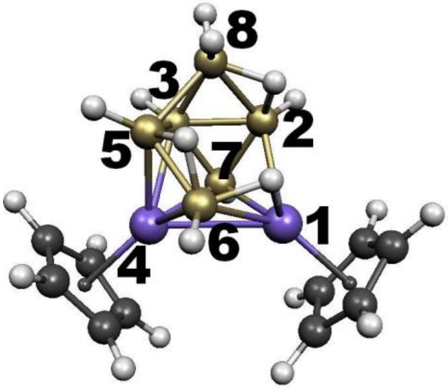

4. -750.993755 +4.0 C1
WBI 0.36

		1	2	3	4	5	6	7	8
1	Ir	0.000000							
2	B	2.278792	0.000000						
3	B	3.151989	1.844142	0.000000					
4	Ir	2.730062	3.207949	2.233842	0.000000				
5	B	3.323346	2.816857	1.763711	2.162116	0.000000			
6	B	2.246851	3.088953	2.902233	2.104855	1.829768	0.000000		
7	B	2.136237	1.730849	1.729912	2.097199	2.931937	3.050349	0.000000	
8	B	3.536390	1.856018	1.769097	3.535359	1.954407	3.061630	3.001203	0.000000

Ir1-H-B6 Ir1-H 1.67 B6-H 1.42
B2-H-B8 B2-H 1.30 B8-H 1.33
B5-H-B6 B5-H 1.32 B6-H 1.30
B8-H 1.20

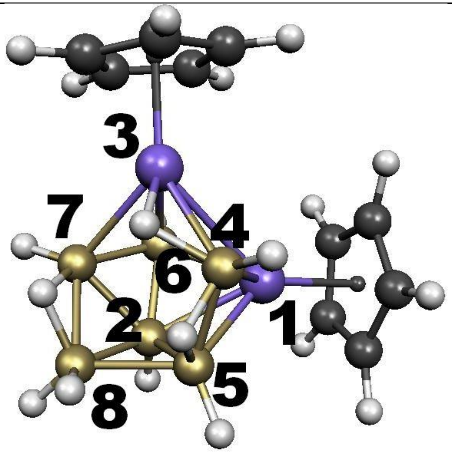

5. -750.993672 +4.1 C1
WBI 0.36

		1	2	3	4	5	6	7	8
1	Ir	0.000000							
2	B	2.232646	0.000000						
3	Ir	2.731780	3.152531	0.000000					
4	B	2.108130	2.902114	2.249847	0.000000				
5	B	2.163581	1.764064	3.324922	1.828841	0.000000			
6	B	2.095495	1.730744	2.133512	3.049652	2.932086	0.000000		
7	B	3.206823	1.844898	2.276570	3.086055	2.815118	1.731397	0.000000	
8	B	3.536215	1.770865	3.537148	3.060296	1.954350	3.002253	1.855310	0.000000

Ir3-H-B4 Ir3-H 1.67 B4-H 1.42
B4-H-B5 B4-H 1.30 B5-H 1.32
B7-H-B8 B7-H 1.30 B8-H 1.33
B8-H 1.20

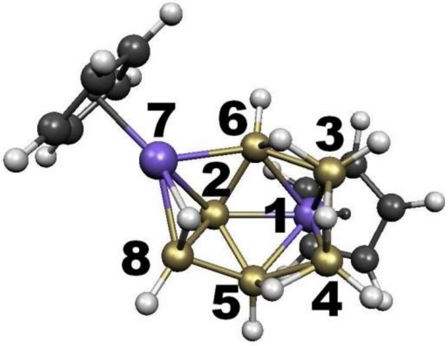

		1	2	3	4	5	6	7	8
1	Ir	0.000000							
2	B	2.218005	0.000000						
3	B	2.104910	2.999870	0.000000					
4	B	2.094088	2.955659	1.811858	0.000000				
5	B	2.165735	1.771938	2.939283	1.826213	0.000000			
6	B	2.203133	1.844104	1.842245	2.926226	2.890843	0.000000		
7	Ir	3.966967	2.182479	3.569122	4.064964	3.368836			
8	B	3.489841	1.751498	3.608670	3.108675	1.860654			

6. -750.991834 +5.2 C1 WBI 0.07	7 Ir 2.221761 0.000000 8 B 2.915439 2.027747 0.000000 Ir7-H-B8 Ir7-H 1.72 B8-H 1.42 B3-H-B4 B3-H 1.33 B4-H 1.33 B3-H-B6 B3-H 1.29 B6-H 1.35 B4-H-B5 B4-H 1.34 B5-H 1.32
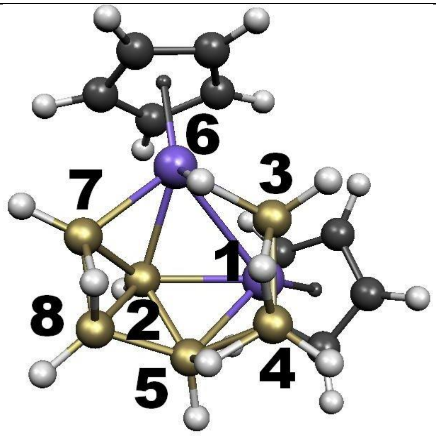 7. -750.988322 +7.4 C1 WBI 0.35	1 2 3 4 5 1 Ir 0.000000 2 B 2.261366 0.000000 3 B 2.115174 3.039839 0.000000 4 B 2.103349 3.026992 1.811105 0.000000 5 B 2.209325 1.859841 2.943491 1.825608 0.000000 6 Ir 2.733212 2.231624 2.229861 3.486333 3.463681 7 B 3.602701 1.759998 3.315631 3.652561 2.861952 8 B 3.443207 1.719078 3.631358 3.106315 1.759961 6 7 8 6 Ir 0.000000 7 B 2.152336 0.000000 8 B 3.297187 1.641791 0.000000 Ir6-H-B3 Ir6-H 1.67 B3-H 1.45 B3-H-B4 B3-H 1.35 B4-H 1.31 B4-H-B5 B4-H 1.31 B5-H 1.31 B7-H-B8 B7-H 1.35 B8-H 1.32
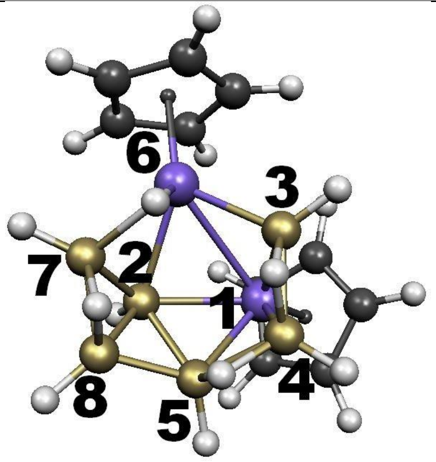 8. -750.987747 +7.8 C1 WBI 0.33	1 2 3 4 5 1 Ir 0.000000 2 B 2.240941 0.000000 3 B 2.096965 3.036476 0.000000 4 B 2.113732 3.013107 1.797870 0.000000 5 B 2.207049 1.877003 2.970452 1.836356 0.000000 6 Ir 2.746044 2.242496 2.149420 3.388229 3.448230 7 B 3.605071 1.763224 3.357790 3.607795 2.843432 8 B 3.438860 1.717430 3.729131 3.136427 1.752109 6 7 8 6 Ir 0.000000 7 B 2.167068 0.000000 8 B 3.322265 1.656019 0.000000 Ir6-H-B7 Ir6-H 1.62 B7-H 1.67 B3-H-B4 B3-H 1.35 B4-H 1.31 B4-H-B5 B4-H 1.32 B5-H 1.31 B7-H-B8 B7-H 1.36 B8-H 1.31

<table>
<tr>
<td>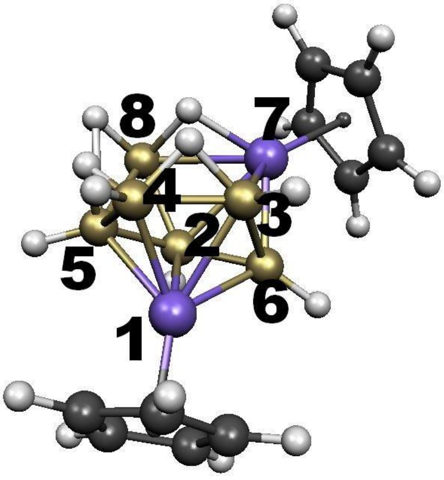
9. -750.986944 +8.3 C1
WBI 0.09</td>
<td>
<table>
<tr><td></td><td></td><td>1</td><td>2</td><td>3</td><td>4</td><td>5</td></tr>
<tr><td>1</td><td>Ir</td><td>0.000000</td><td></td><td></td><td></td><td></td></tr>
<tr><td>2</td><td>B</td><td>2.255108</td><td>0.000000</td><td></td><td></td><td></td></tr>
<tr><td>3</td><td>B</td><td>2.235640</td><td>2.670586</td><td>0.000000</td><td></td><td></td></tr>
<tr><td>4</td><td>B</td><td>2.096500</td><td>2.890251</td><td>1.828412</td><td>0.000000</td><td></td></tr>
<tr><td>5</td><td>B</td><td>2.164262</td><td>1.763121</td><td>2.804823</td><td>1.836292</td><td>0.000000</td></tr>
<tr><td>6</td><td>B</td><td>2.057124</td><td>1.808814</td><td>1.824411</td><td>3.042584</td><td>2.979495</td></tr>
<tr><td>7</td><td>Ir</td><td>3.625350</td><td>2.281404</td><td>2.291751</td><td>3.468598</td><td>3.323167</td></tr>
<tr><td>8</td><td>B</td><td>3.538150</td><td>1.760157</td><td>3.198841</td><td>3.045767</td><td>1.915629</td></tr>
<tr><td></td><td></td><td>6</td><td>7</td><td>8</td><td></td><td></td></tr>
<tr><td>6</td><td>B</td><td>0.000000</td><td></td><td></td><td></td><td></td></tr>
<tr><td>7</td><td>Ir</td><td>2.059678</td><td>0.000000</td><td></td><td></td><td></td></tr>
<tr><td>8</td><td>B</td><td>3.143340</td><td>2.312493</td><td>0.000000</td><td></td><td></td></tr>
</table>
Ir7-H-B8 Ir7-H 1.66 B8-H 1.44
B3-H-B4 B3-H 1.31 B4-H 1.31
B4-H-B5 B3-H 1.28 B5-H 1.34
B8-H 1.2
</td>
</tr>
<tr>
<td>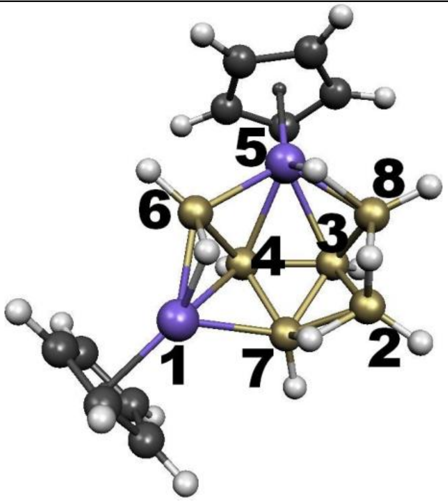
10. -750.983120 +10.7 C1
WBI 0.09</td>
<td>
<table>
<tr><td></td><td></td><td>1</td><td>2</td><td>3</td><td>4</td><td>5</td></tr>
<tr><td>1</td><td>Ir</td><td>0.000000</td><td></td><td></td><td></td><td></td></tr>
<tr><td>2</td><td>B</td><td>3.561987</td><td>0.000000</td><td></td><td></td><td></td></tr>
<tr><td>3</td><td>B</td><td>3.471599</td><td>1.748991</td><td>0.000000</td><td></td><td></td></tr>
<tr><td>4</td><td>B</td><td>2.175672</td><td>2.937396</td><td>1.815220</td><td>0.000000</td><td></td></tr>
<tr><td>5</td><td>Ir</td><td>3.802067</td><td>3.331065</td><td>2.232369</td><td>2.214077</td><td>0.000000</td></tr>
<tr><td>6</td><td>B</td><td>2.058670</td><td>3.691515</td><td>3.096486</td><td>1.836811</td><td>2.168865</td></tr>
<tr><td>7</td><td>B</td><td>2.202191</td><td>1.792807</td><td>1.787936</td><td>1.785865</td><td>3.360540</td></tr>
<tr><td>8</td><td>B</td><td>4.157774</td><td>1.720875</td><td>1.747048</td><td>2.995155</td><td>2.143276</td></tr>
<tr><td></td><td></td><td>6</td><td>7</td><td>8</td><td></td><td></td></tr>
<tr><td>6</td><td>B</td><td>0.000000</td><td></td><td></td><td></td><td></td></tr>
<tr><td>7</td><td>B</td><td>2.960974</td><td>0.000000</td><td></td><td></td><td></td></tr>
<tr><td>8</td><td>B</td><td>3.342622</td><td>2.873264</td><td>0.000000</td><td></td><td></td></tr>
</table>
Ir1-H-B6 Ir1-H 1.72 B6-H 1.42
Ir5-H-B8 Ir5-H 1.67 B8-H 1.50
B2-H-B7 B2-H 1.32 B7-H 1.32
B2-H B8 B2-H 1.31 B8-H 1.36
</td>
</tr>
<tr>
<td>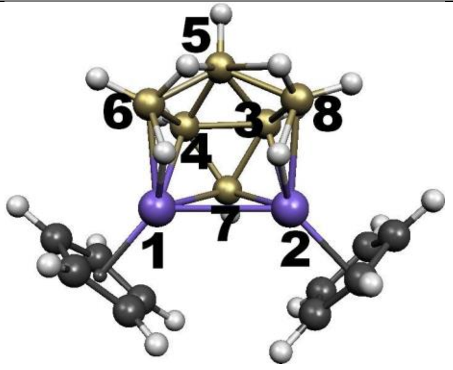
11. -750.980590 +12.3 C1</td>
<td>
<table>
<tr><td></td><td></td><td>1</td><td>2</td><td>3</td><td>4</td><td>5</td></tr>
<tr><td>1</td><td>Ir</td><td>0.000000</td><td></td><td></td><td></td><td></td></tr>
<tr><td>2</td><td>Ir</td><td>2.814666</td><td>0.000000</td><td></td><td></td><td></td></tr>
<tr><td>3</td><td>B</td><td>3.167053</td><td>2.239197</td><td>0.000000</td><td></td><td></td></tr>
<tr><td>4</td><td>B</td><td>2.263650</td><td>3.226899</td><td>1.835778</td><td>0.000000</td><td></td></tr>
<tr><td>5</td><td>B</td><td>3.275825</td><td>3.351725</td><td>1.752689</td><td>1.785606</td><td>0.000000</td></tr>
<tr><td>6</td><td>B</td><td>2.192041</td><td>3.673783</td><td>2.845842</td><td>1.719818</td><td>1.753523</td></tr>
<tr><td>7</td><td>B</td><td>2.124600</td><td>2.107063</td><td>1.756210</td><td>1.735171</td><td>2.911711</td></tr>
<tr><td>8</td><td>B</td><td>3.728966</td><td>2.291728</td><td>1.768082</td><td>3.051911</td><td>1.919394</td></tr>
<tr><td></td><td></td><td>6</td><td>7</td><td>8</td><td></td><td></td></tr>
<tr><td>6</td><td>B</td><td>0.000000</td><td></td><td></td><td></td><td></td></tr>
<tr><td>7</td><td>B</td><td>2.991264</td><td>0.000000</td><td></td><td></td><td></td></tr>
</table>
</td>
</tr>
</table>

WBI 0.41	8 B 3.086219 3.119057 0.000000 Ir1-H-B6 Ir1-H 1.67 B6-H 1.45 Ir2-H-B8 Ir2-H 1.67 B8-H 1.44 B5-H-B6 B5-H 1.32 B6-H 1.29 B8-H 1.20
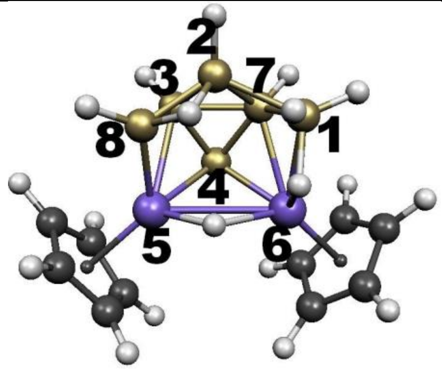 12. -750.980454 +12.4 C1 WBI 0.29	1 2 3 4 5 1 B 0.000000 2 B 1.913233 0.000000 3 B 3.078148 1.781392 0.000000 4 B 3.194556 2.921839 1.728858 0.000000 5 Ir 3.834844 3.223874 2.251667 2.090979 0.000000 6 Ir 2.344629 3.321139 3.242667 2.165398 2.851136 7 B 1.773343 1.771954 1.807917 1.771666 3.147688 8 B 3.176951 1.746542 1.708628 2.944860 2.111840 6 7 8 6 Ir 0.000000 7 B 2.248916 0.000000 8 B 3.649628 2.837379 0.000000 Ir5-H- Ir6 Ir5-H 1.69 Ir6-H 1.90 Ir6-H-B1 Ir6-H 1.70 B1-H 1.39 B2-H-B8 B2-H 1.32 B8-H 1.30 B1-H 1.2

6.1.4.3 Cp$_2$M$_2$B$_6$H$_{10}$ (M=Ru,Os) systems

Table 92. Distance table for the lowest-lying Cp$_2$Ru$_2$B$_6$H$_{10}$ structures after M06L/6-311G(d,p) optimization. Included are the ZPcorrected E (a.u.), relative energy (kcal/mol), symmetry and WBI.

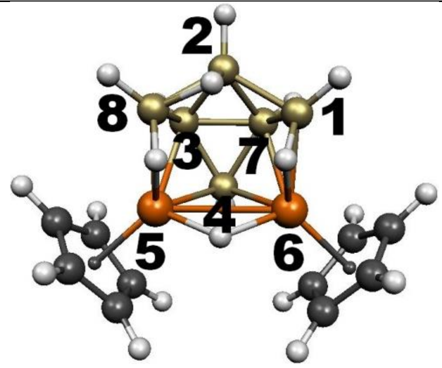 **1. -732.059181 0.0 $C_1(C_S)$** **WBI 0.30**	1 2 3 4 5 1 B 0.000000 2 B 1.878122 0.000000 3 B 2.920416 1.754423 0.000000 4 B 2.990508 2.925232 1.762375 0.000000 5 Ru 3.657106 3.297785 2.256927 2.108907 0.000000 6 Ru 2.104612 3.299788 3.210588 2.129996 2.878859 7 B 1.716428 1.743955 1.778322 1.755989 3.182620 8 B 3.004220 1.787314 1.742497 3.000225 2.167546 6 7 8 6 Ru 0.000000 7 B 2.259252 0.000000 8 B 3.611493 2.852062 0.000000 Ru5-H-Ru6 Ru5-H 1.75 Ru6-H 1.77 Ru5-H-B8 Ru5-H 1.72 B8-H 1.34

Ru6-H-B1   Ru6-H 1.73   B1-H 1.33
B1-H-B8   B1-H 1.97   B8-H 1.48

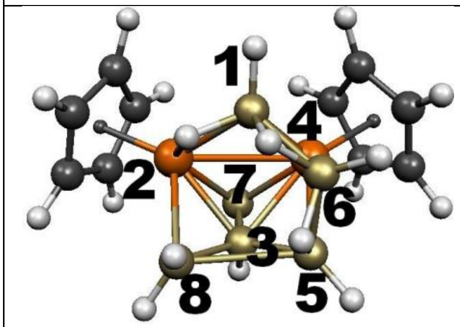

2. -732.054804 +2.8 C_1
WBI 0.36

```
                1          2          3          4          5
   1  B    0.000000
   2  Ru   2.253411   0.000000
   3  B    2.881311   2.162256   0.000000
   4  Ru   2.139317   2.754069   2.185674   0.000000
   5  B    2.914627   3.398043   1.666316   2.181579   0.000000
   6  B    1.813501   3.454977   2.789113   2.160371   1.774751
   7  B    3.346019   2.134109   1.631204   2.145884   2.964950
   8  B    3.172015   2.295777   1.696017   3.533923   2.548005
                6          7          8
   6  B    0.000000
   7  B    3.778513   0.000000
   8  B    3.261433   3.012647   0.000000
```

Ru2-H-B1   Ru2-H 1.71   B1-H 1.33
B1-H-B5   B1-H 1.38   B5-H 1.28
B5-H-B6   B5-H 1.32   B6-H 1.31
B8-H 1.19

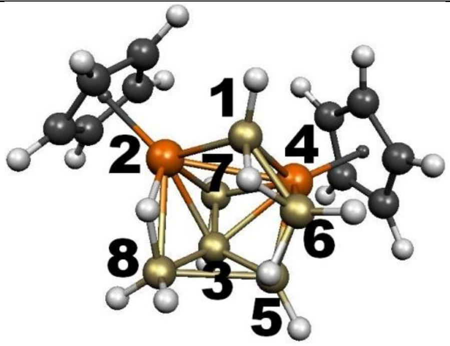

3. -732.052362 +4.3 C_1
WBI 0.34

```
                1          2          3          4          5
   1  B    0.000000
   2  Ru   2.114768   0.000000
   3  B    2.925697   2.163147   0.000000
   4  Ru   2.128775   2.747244   2.173036   0.000000
   5  B    2.892798   3.279104   1.688441   2.174467   0.000000
   6  B    1.792962   3.306178   2.858112   2.157814   1.791268
   7  B    3.247127   2.117690   1.620502   2.148506   3.028034
   8  B    3.192151   2.403785   1.701839   3.461714   2.248721
                6          7          8
   6  B    0.000000
   7  B    3.780876   0.000000
   8  B    3.090495   3.085237   0.000000
```

Ru2-H-B8   Ru2-H 1.71   B8-H 1.37
B1-H-B6   B1-H 1.38   B6-H 1.28
B6-H-B5   B6-H 1.30   B5-H 1.32
B8-H 1.20

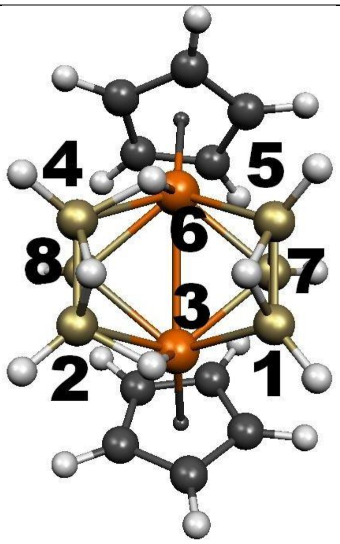

4. -732.051435 +4.9 C_S
WBI 0.39

		1	2	3	4	5	6	7	8
1	B	0.000000							
2	B	3.196827	0.000000						
3	Ru	2.218327	2.232395	0.000000					
4	B	3.618723	1.719322	3.120502	0.000000				
5	B	1.672562	3.618773	3.089626	3.196815	0.000000			
6	Ru	3.089615	3.120536	2.765088	2.232383	2.218327	0.000000		
7	B	1.695899	3.683067	2.154241	3.683036	1.695889	2.154233	0.000000	
8	B	3.646405	1.729633	2.139151	1.729629	3.646419	2.139165	3.283696	0.000000

B1-H-B5 B1-H 1.32 B5-H 1.32
B2-H-B4 B2-H 1.32 B4-H 1.32
B1-H-B2 B1-H 2.96 B2-H 1.38
B5-H-B4 B5-H 2.96 B4-H 1.38

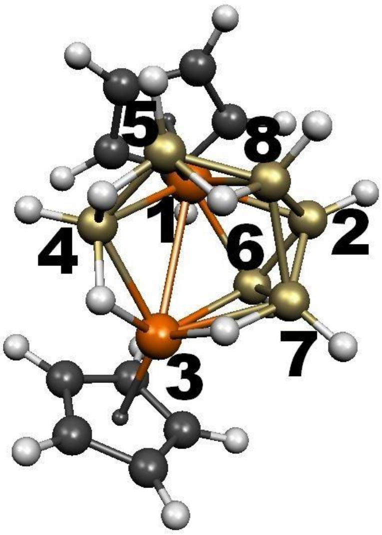

5. -732.045722 +8.5 C_1
WBI 0.37

		1	2	3	4	5	6	7	8
1	Ru	0.000000							
2	B	2.185211	0.000000						
3	Ru	2.784750	3.237329	0.000000					
4	B	2.137091	3.649066	2.225068	0.000000				
5	B	2.139550	3.091821	3.347353	1.792131	0.000000			
6	B	2.184221	1.686798	2.102179	3.296202	3.621081	0.000000		
7	B	2.927297	1.657475	2.364241	3.399209	3.213726	1.803530	0.000000	
8	B	2.241073	1.679632	3.367920	2.945804	1.749360	2.825612	2.029666	0.000000

Ru3-H-B4 Ru3-H 1.69 B4-H 1.36
Ru3-H-B7 Ru3-H 1.73 B7-H 1.33
B4-H-B5 B4-H 1.37 B5-H 1.29
B5-H-B8 B5-H 1.39 B8-H 1.28

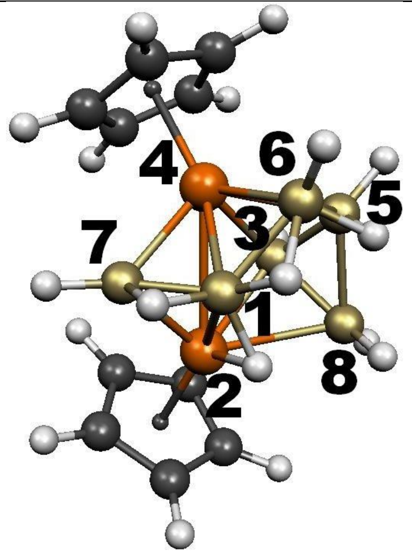 6. -732.043495 +9.8 C_1 WBI 0.34	1 2 3 4 5 1 B 0.000000 2 Ru 2.200288 0.000000 3 B 2.922397 2.128808 0.000000 4 Ru 2.168869 2.752277 2.142239 0.000000 5 B 2.740379 3.191876 1.719249 2.242495 0.000000 6 B 1.801221 3.464700 2.965535 2.085841 1.795285 7 B 1.688314 2.130248 3.242691 2.108213 3.736983 8 B 2.998873 2.390549 1.704115 3.327046 1.926284 6 7 8 6 B 0.000000 7 B 3.080160 0.000000 8 B 3.085647 3.947668 0.000000 Ru2-H-B1 Ru2-H 1.73 B1-H 1.33 B1-H-B6 B1-H 1.28 B6-H 1.41 B6-H-B5 B6-H 1.31 B5-H 1.32 B8-H 1.19
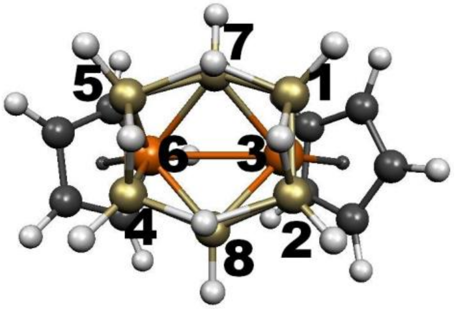 7. -732.040397 +11.8 C_{2V} WBI 0.54	1 2 3 4 5 1 B 0.000000 2 B 1.772894 0.000000 3 Ru 2.065174 2.027876 0.000000 4 B 3.379600 2.908688 3.440425 0.000000 5 B 2.913094 3.435184 3.450531 1.771562 0.000000 6 Ru 3.438541 3.445301 2.639056 2.059861 2.022649 7 B 1.830708 2.927897 2.146069 2.944552 1.868673 8 B 2.940918 1.858491 2.156485 1.838430 2.934056 6 7 8 6 Ru 0.000000 7 B 2.161152 0.000000 8 B 2.149333 2.939369 0.000000 B1-H-B2 B1-H 1.33 B2-H 1.35 B4-H-B5 B4-H 1.33 B5-H 1.35 (B1-B7-B5)-H B1-H 1.48 B7-H 1.34 B5-H 1.69 (B2-B8-B4)-H B2-H 1.65 B8-H 1.33 B4-H 1.51
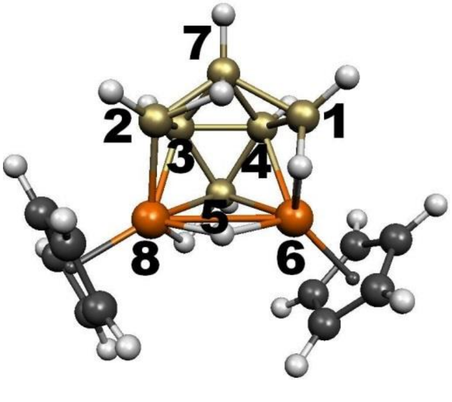	1 2 3 4 5 1 B 0.000000 2 B 2.921452 0.000000 3 B 2.932734 1.720354 0.000000 4 B 1.717363 2.783534 1.788513 0.000000 5 B 3.039528 2.965309 1.780470 1.757084 0.000000 6 Ru 2.108596 3.473325 3.213508 2.252423 2.184768 7 B 1.852874 1.764950 1.763242 1.741190 2.946247 8 Ru 3.720805 2.083184 2.265538 3.220463 2.203500 6 7 8 6 Ru 0.000000

8. -732.038415 +13.0 C_1 WBI 0.28	7 B 3.268551 0.000000 8 Ru 2.933372 3.312131 0.000000 Ru6-H- Ru8 Ru6-H 1.80 Ru8-H 1.74 Ru6-H-B1 Ru6-H 1.72 B1-H 1.33 B1-H-B7 B1-H 1.83 B7-H 1.27 Ru8-H-B5 Ru8-H 1.66 B5-H 1.36
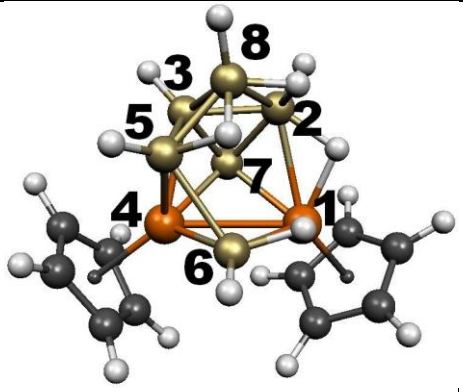 9. -732.038367 +13.1 C_1 WBI 0.39	1 2 3 4 5 1 Ru 0.000000 2 B 2.344627 0.000000 3 B 3.205953 1.833604 0.000000 4 Ru 2.737778 3.188884 2.219611 0.000000 5 B 3.440067 2.830129 1.760460 2.068185 0.000000 6 B 2.193231 3.201783 3.081320 1.999607 2.138691 7 B 2.144694 1.830822 1.751187 2.062716 2.936883 8 B 3.480747 1.851034 1.739449 3.301963 1.761249 6 7 8 6 B 0.000000 7 B 3.041589 0.000000 8 B 3.075431 3.003529 0.000000 Ru1-H-B2 Ru1-H 167 B2-H 1.42 Ru1-H-B6 Ru6-H 170 B6-H 1.36 B2-H-B8 B2-H 1.37 B8-H 1.27 B5-H-B8 B5-H 1.40 B8-H 1.29
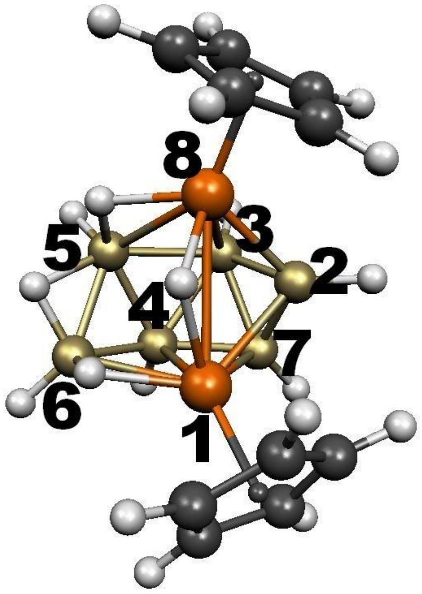 10. -732.038074 +13.2 C_1 WBI 0.30	1 2 3 4 5 1 Ru 0.000000 2 B 2.262190 0.000000 3 B 2.918789 1.750532 0.000000 4 B 2.253377 2.717593 1.848061 0.000000 5 B 2.989020 3.083020 1.913777 1.799985 0.000000 6 B 2.316213 3.675590 3.072928 1.688424 1.829250 7 B 2.218033 1.707001 1.714297 1.663237 2.962676 8 Ru 2.880776 2.065828 2.218374 3.205120 2.317040 6 7 8 6 B 0.000000 7 B 3.121496 0.000000 8 Ru 3.387149 3.244384 0.000000 Ru1-H-Ru8 Ru1-H 1.87 Ru8-H 1.70 Ru1-H-B5 Ru1-H 1.75 B5-H 1.31 Ru8-H-B5 Ru8-H 1.67 B5-H 1.36 B5-H-B6 B5-H 1.43 B6-H 1.26

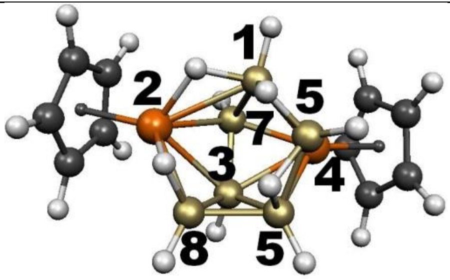

11. -732.038011 +13.3 C_1
WBI 0.14

```
              1          2          3          4          5
    1  B    0.000000
    2  Ru   2.451317   0.000000
    3  B    2.741491   2.304988   0.000000
    4  Ru   2.200701   3.617195   2.175109   0.000000
    5  B    2.839840   3.304386   1.742557   2.146432   0.000000
    6  B    1.833258   3.510651   2.869566   2.075619   1.815123
    7  B    1.926994   2.146884   1.792475   2.008019   2.981698
    8  B    3.157003   2.128736   1.694799   3.404408   1.883789
              6          7          8
    6  B    0.000000
    7  B    3.076439   0.000000
    8  B    2.978767   3.020373   0.000000
```

Ru2-H-B1 Ru2-H 1.70 B1-H 1.37
Ru2-H-B8 Ru2-H 1.71 B8-H 1.35
B1-H-B6 B1-H 1.36 B6-H 1.29
B5-H-B6 B5-H 1.32 B6-H 1.37

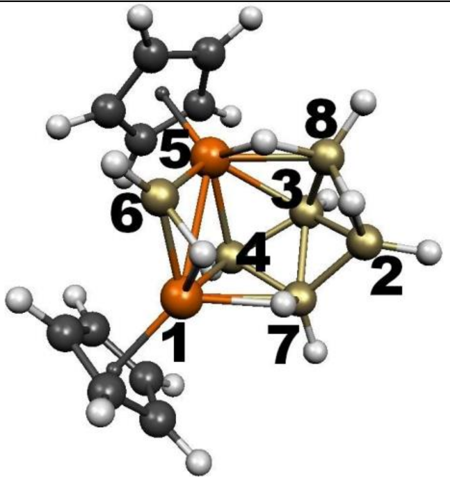

12. -732.036866 +14.0 C_1
WBI 0.35

```
              1          2          3          4          5
    1  Ru   0.000000
    2  B    3.529084   0.000000
    3  B    3.269794   1.724306   0.000000
    4  B    2.131897   2.918448   1.746804   0.000000
    5  Ru   2.783245   3.328330   2.259909   2.164467   0.000000
    6  B    2.024768   3.968648   3.675880   3.148902   2.086399
    7  B    2.389828   1.718380   1.790234   1.749449   3.169512
    8  B    3.696437   1.715365   1.739799   3.042930   2.260599
              6          7          8
    6  B    0.000000
    7  B    3.634981   0.000000
    8  B    3.268606   2.783595   0.000000
```

Ru1-H-B6 Ru1-H 1.73 B6-H 1.37
Ru1-H-B7 Ru1-H 1.87 B7-H 1.29
Ru5-H-B8 Ru5-H 1.70 B8-H 1.37
B2-H-B8 B2-H 1.31 B8-H 1.34

Table 93. Distance table for the lowest-lying $Cp_2Os_2B_6H_{10}$ structures after M06L/6-311G(d,p) optimization. Included are the ZPcorrected E (a.u.), relative energy (kcal/mol), symmetry and WBI.

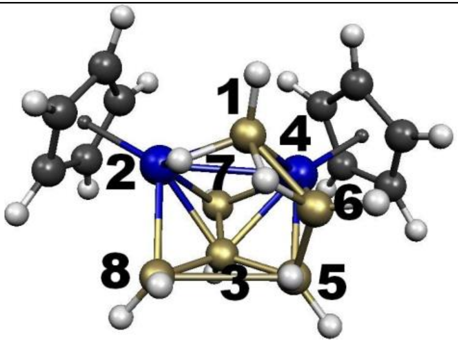

1. -723.660528 0.0 C_1
WBI 0.38

		1	2	3	4	5
1	B	0.000000				
2	Os	2.261078	0.000000			
3	B	2.888017	2.192192	0.000000		
4	Os	2.153623	2.797386	2.217297	0.000000	
5	B	2.930030	3.434570	1.670030	2.186844	0.000000
6	B	1.824559	3.477223	2.790645	2.178759	1.780729
7	B	3.341572	2.149113	1.644803	2.158334	2.964288
8	B	3.182113	2.283530	1.711428	3.580112	2.616933

		6	7	8
6	B	0.000000		
7	B	3.783149	0.000000	
8	B	3.293078	3.014809	0.000000

Os2-H-B1 Os2-H1.72 B1-H 1.36
B1-H-B6 B1-H 1.38 B6-H 1.28
B5-H-B6 B5-H 1.33 B6-H 1.30
B8-H 1.19

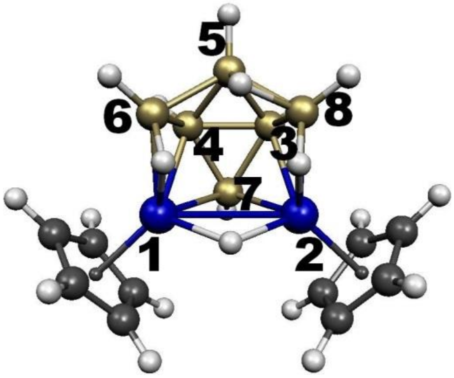

2. -723.660041 +0.3 $C_1(C_S)$
WBI 0.33

		1	2	3	4	5
1	Os	0.000000				
2	Os	2.921903	0.000000			
3	B	3.234959	2.273800	0.000000		
4	B	2.275001	3.210760	1.784490	0.000000	
5	B	3.314563	3.313866	1.756333	1.746346	0.000000
6	B	2.115273	3.678927	2.922017	1.718928	1.872116
7	B	2.148172	2.132182	1.766546	1.759395	2.926690
8	B	3.636512	2.172377	1.739759	2.858532	1.789769

		6	7	8
6	B	0.000000		
7	B	2.993691	0.000000	
8	B	3.006786	3.001834	0.000000

Os1-H- Os2 Os1-H 1.80 Os2-H 1.78
Os1-H-B6 Os1-H 1.74 B6-H 1.36
Os2-H-B8 Os2-H 1.73 B8-H 1.36
B5-H-B8 B5-H 1.26 B8-H 1.49

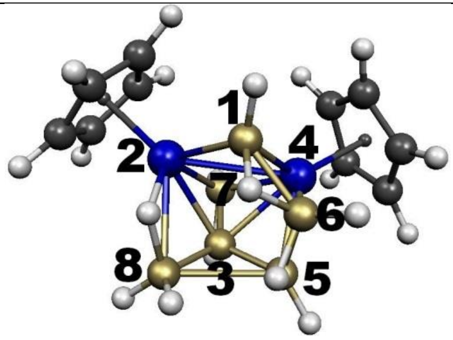 3. -723.658252 +1.4 C_1 WBI 0.37	1 2 3 4 5 1 B 0.000000 2 Os 2.132707 0.000000 3 B 2.923842 2.196868 0.000000 4 Os 2.157325 2.790438 2.204565 0.000000 5 B 2.913918 3.352269 1.699963 2.165886 0.000000 6 B 1.803172 3.347564 2.850141 2.178996 1.793908 7 B 3.263288 2.136999 1.633365 2.160819 3.019815 8 B 3.183397 2.397417 1.704512 3.511728 2.372762 6 7 8 6 B 0.000000 7 B 3.786742 0.000000 8 B 3.128332 3.076882 0.000000 Os2-H-B8 Os2-H 1.71 B8-H 1.41 B1-H-B6 B1-H 1.38 B6-H 1.28 B5-H-B6 B5-H 1.33 B6-H 1.29 B8-H 1.20
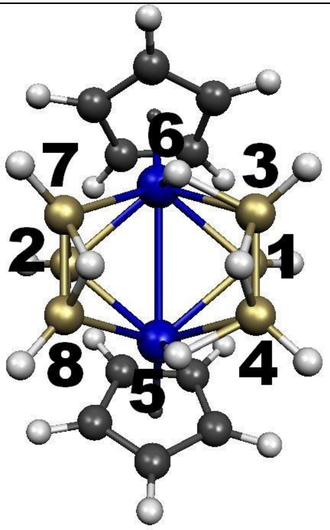 4. -723.656592 +2.5 C_{2V} WBI 0.41	1 2 3 4 5 1 B 0.000000 2 B 3.297626 0.000000 3 B 1.720199 3.688689 0.000000 4 B 1.720199 3.688689 1.712232 0.000000 5 Os 2.167826 2.171051 3.136838 2.239073 0.000000 6 Os 2.167826 2.171051 2.239073 3.136838 2.818720 7 B 3.674015 1.701995 3.221916 3.641192 3.118429 8 B 3.674015 1.701995 3.641192 3.221916 2.233276 6 7 8 6 Os 0.000000 7 B 2.233276 0.000000 8 B 3.118429 1.680578 0.000000 Os5-H-B4 Os5-H 1.68 B4-H 1.48 Os6-H-B3 Os6-H 1.68 B3-H 1.48 B3-H-B4 B3-H 1.33 B4-H 1.32 B7-H-B8 B7-H 1.32 B8-H 1.32
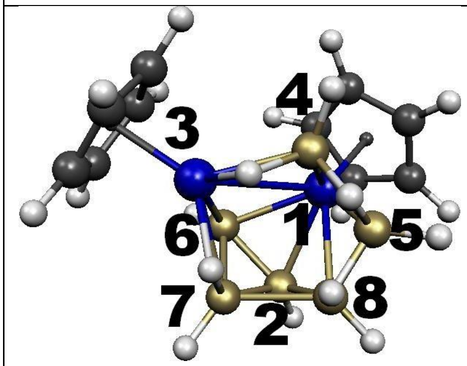 5. -723.651239 +5.8 C_1	1 2 3 4 5 1 Os 0.000000 2 B 2.203943 0.000000 3 Os 2.837560 3.259596 0.000000 4 B 2.147176 3.655882 2.233751 0.000000 5 B 2.155299 3.104706 3.364723 1.803845 0.000000 6 B 2.203549 1.686272 2.126008 3.293116 3.628390 7 B 2.956399 1.659857 2.369094 3.409082 3.228511 8 B 2.257820 1.684651 3.381109 2.954106 1.756024 6 7 8 6 B 0.000000 7 B 1.799837 0.000000

WBI 0.39	8 B 2.825586 2.036913 0.000000 Os3-H-B4 Os3-H 1.70 B4-H 1.41 Os3-H-B7 Os3-H 1.74 B7-H 1.35 B4-H-B5 B4-H 1.37 B5-H 1.29 B5-H-B8 B5-H 1.39 B8-H 1.29
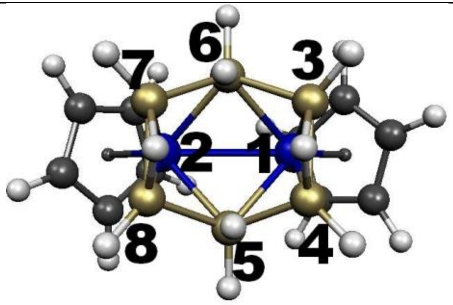 6. -723.650372 +6.4 C_2 WBI 0.58	1 2 3 4 5 1 Os 0.000000 2 Os 2.676462 0.000000 3 B 2.045762 3.486665 0.000000 4 B 2.082962 3.477610 1.778241 0.000000 5 B 2.173155 2.185816 2.944301 1.843434 0.000000 6 B 2.186139 2.172622 1.873604 2.954366 2.951220 7 B 3.475937 2.084110 2.935214 3.400335 2.952622 8 B 3.484979 2.047157 3.462096 2.934975 1.870800 6 7 8 6 B 0.000000 7 B 1.841682 0.000000 8 B 2.943484 1.778561 0.000000 B3-H-B4 B3-H 1.35 B4-H 1.33 B7-H-B8 B7-H 1.33 B8-H 1.35 (B3-B6-B7)-H B3-H 1.69 B6-H 1.33 B7-H 1.49 (B4-B5-B8)-H B4-H 1.50 B5-H 1.33 B8-H 1.68
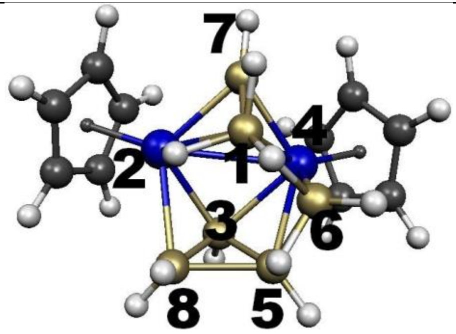 7. -723.648126 +7.8 C_1 WBI 0.37	1 2 3 4 5 1 B 0.000000 2 Os 2.224288 0.000000 3 B 2.930875 2.149574 0.000000 4 Os 2.187495 2.800458 2.167142 0.000000 5 B 2.758248 3.223896 1.718530 2.261611 0.000000 6 B 1.809714 3.495898 2.970938 2.100127 1.804839 7 B 1.697639 2.150811 3.259133 2.128973 3.760608 8 B 3.001311 2.399030 1.708749 3.354698 1.937603 6 7 8 6 B 0.000000 7 B 3.100907 0.000000 8 B 3.087444 3.958165 0.000000 Os2-H-B1 Os2-H 1.73 B1-H 1.37 B1-H-B6 B1-H 1.27 B6-H 1.43 B1-H-B7 B1-H 1.25 B7-H 1.54 B5-H-B6 B5-H 1.32 B6-H 1.32

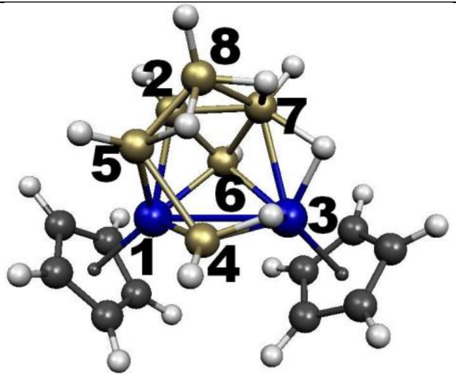

8. -723.642946 +11.0 C_1
WBI 0.42

		1	2	3	4	5
1	Os	0.000000				
2	B	2.248441	0.000000			
3	Os	2.796317	3.248620	0.000000		
4	B	2.013795	3.113857	2.206926	0.000000	
5	B	2.087968	1.764492	3.497356	2.194362	0.000000
6	B	2.088484	1.754546	2.171640	3.045424	2.945567
7	B	3.188272	1.834078	2.326209	3.186574	2.831290
8	B	3.312806	1.741076	3.483715	3.086435	1.762417

		6	7	8
6	B	0.000000		
7	B	1.800869	0.000000	
8	B	2.987771	1.845973	0.000000

Os3-H-B4 Os3-H 1.70 B4-H 1.40
Os3-H-B7 Os3-H 1.65 B7-H 1.60
B5-H-B8 B5 1.40 B8-H 1.29
B7-H-B8 B7-H 1.36 B8-H 1.27

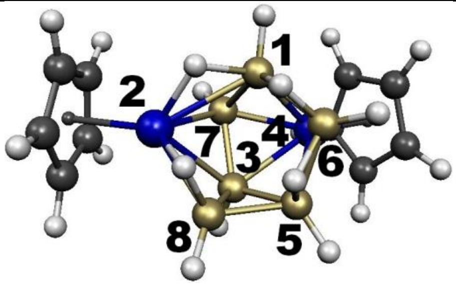

9. -723.640568 +12.5 C_1
WBI 0.13

		1	2	3	4	5
1	B	0.000000				
2	Os	2.441489	0.000000			
3	B	2.720152	2.326943	0.000000		
4	Os	2.213565	3.665246	2.197758	0.000000	
5	B	2.836929	3.327009	1.746664	2.167143	0.000000
6	B	1.835523	3.523544	2.875080	2.091405	1.828019
7	B	1.906316	2.165170	1.804839	2.041465	3.001904
8	B	3.116305	2.139087	1.699824	3.413668	1.865179

		6	7	8
6	B	0.000000		
7	B	3.086997	0.000000	
8	B	2.951566	3.025527	0.000000

Os2-H-B1 Os2-H 1.69 B1-H 1.47
Os2-H-B8 Os2-H 1.72 B8-H 1.39
B1-H-B6 B1-H 1.36 B6-H 1.30
B5-H-B6 B5-H 1.31 B6-H 1.40

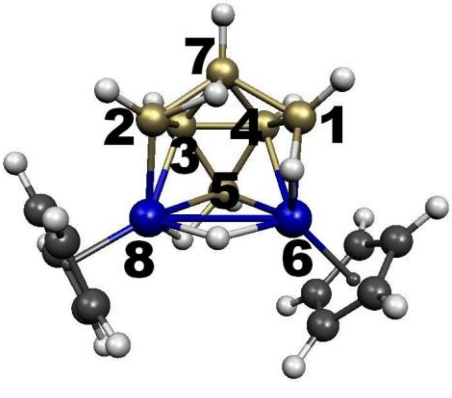

		1	2	3	4	5
1	B	0.000000				
2	B	2.923700	0.000000			
3	B	2.936033	1.727026	0.000000		
4	B	1.716438	2.790275	1.793274	0.000000	
5	B	3.030373	2.966064	1.780992	1.762430	0.000000
6	Os	2.116427	3.512249	3.241252	2.269737	2.189110
7	B	1.855299	1.763264	1.766573	1.740345	2.943382
8	Os	3.740095	2.099948	2.286731	3.252107	2.219110

		6	7	8
6	Os	0.000000		

10. -723.640239 +12.7 C_S WBI 0.30	7 B 3.292353 0.000000 8 Os 2.983729 3.331344 0.000000 Os6-H- Os8 Os6-H 1.81 Os8-H 1.77 Os6-H-B1 Os6-H 1.73 B1-H 1.36 Os8-H-B5 Os8-B5 1.68 B5-H 1.40 B2-H-B7 B2-H 1.49 B7-H 1.27
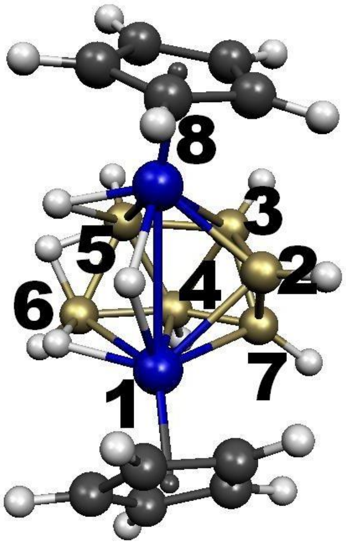 11. -723.639870 +13.0 C_1 WBI 0.32	1 2 3 4 5 1 Os 0.000000 2 B 2.258288 0.000000 3 B 2.939495 1.755394 0.000000 4 B 2.297124 2.731782 1.855972 0.000000 5 B 3.016625 3.030906 1.851826 1.813219 0.000000 6 B 2.330038 3.612330 3.004386 1.682381 1.790427 7 B 2.217266 1.693913 1.715399 1.675130 2.932096 8 Os 2.930923 2.133823 2.240082 3.231369 2.232539 6 7 8 6 B 0.000000 7 B 3.100671 0.000000 8 Os 3.271954 3.280153 0.000000 Os1-H- Os8 Os1-H 1.89 Os8-H 1.74 Os1-H-B6 Os1-H 1.74 B6-H 1.36 Os8-H-B5 Os8-H 1.62 B5-H 2.1 B5-H-B6 B5-H 1.38 B6-H 1.26
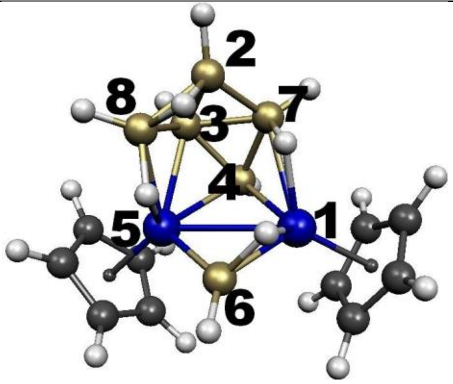 12. -723.638820 +13.6 C_1 WBI 0.38	1 2 3 4 5 1 Os 0.000000 2 B 3.564162 0.000000 3 B 3.299328 1.729782 0.000000 4 B 2.149880 2.919311 1.744808 0.000000 5 Os 2.829791 3.356608 2.277648 2.188660 0.000000 6 B 2.043545 4.040375 3.718494 3.163076 2.108760 7 B 2.412194 1.709385 1.796566 1.757518 3.198147 8 B 3.725553 1.712338 1.739096 3.040774 2.277134 6 7 8 6 B 0.000000 7 B 3.674412 0.000000 8 B 3.331525 2.771230 0.000000 Os1-H-B6 Os1-H 1.72 B6-H 1.44 Os1-H-B7 Os1-H 1.84 B7-H 1.31 Os5-H-B8 Os5-H 1.72 B8-H 1.40 B1-H-B8 B1-H 1.31 B8-H 1.34

6.1.4.4 $Cp_2Re_2B_6H_{10}$ systems

Table 94. Distance table for the lowest-lying $Cp_2Re_2B_6H_{10}$ structures after M06L/6-311G(d,p) optimization. Included are the ZPcorrected E (a.u.), relative energy (kcal/mol), symmetry and WBI.

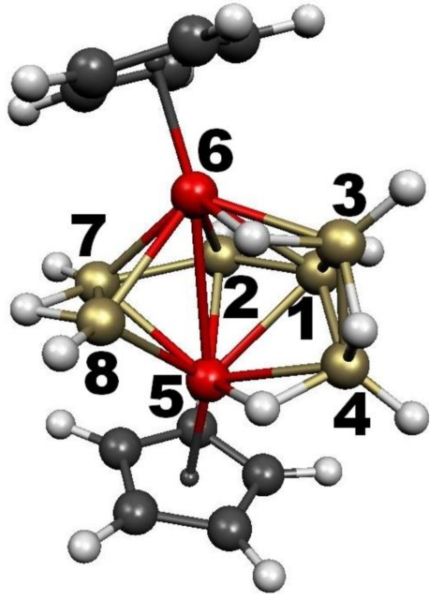

1. -698.862295 0.0 C_S
WBI 0.47

		1	2	3	4	5	6	7	8
1	B	0.000000							
2	B	1.815252	0.000000						
3	B	1.739077	3.192039	0.000000					
4	B	1.739096	3.192085	1.764457	0.000000				
5	Re	2.275687	2.109637	3.182850	2.264670	0.000000			
6	Re	2.275753	2.109575	2.264725	3.182815	2.834620	0.000000		
7	B	3.290423	2.066365	3.964337	3.964187	2.191805	2.192066	0.000000	
8	B	3.444603	3.081505	3.427140	3.427094	2.242156	2.241997	1.671745	0.000000

Re6-H-B3 Re6-H 1.79 B3-H 1.35
Re5-H-B4 Re5-H 1.79 B4-H 1.35
B3-H-B4 B3-H 1.32 B4-H 1.32
B7-H-B8 B7-H 1.34 B8-H 1.31

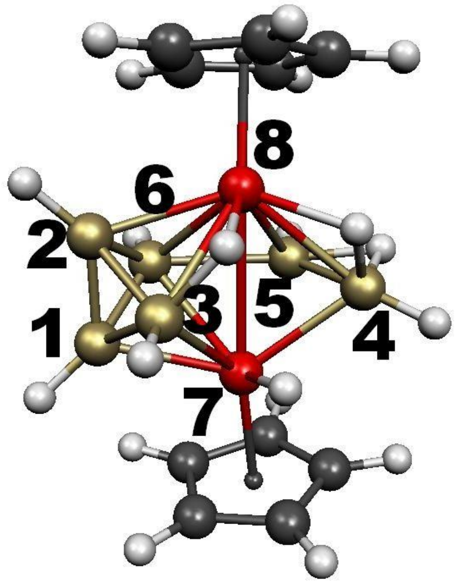

2. -698.858390 +2.5 C_1
WBI 0.46

		1	2	3	4	5	6	7	8
1	B	0.000000							
2	B	1.630153	0.000000						
3	B	1.743256	1.735140	0.000000					
4	B	3.513788	3.449852	2.203980	0.000000				
5	B	4.080925	3.996965	3.358923	1.736390	0.000000			
6	B	1.781719	1.748522	2.558999	3.492121	3.310573	0.000000		
7	Re	2.263619	3.090048	2.249808	2.201456	2.353717	2.348839	0.000000	
8	Re	3.104629	2.208340	2.266766	2.141025	2.227315	2.308736	2.819020	0.000000

Re8-H-B3 Re8-H 1.75 B3-H 1.42
Re8-H-B4 Re8-H 1.79 B4-H 1.35
B4-H-B5 B4-H 1.27 B5-H 1.45

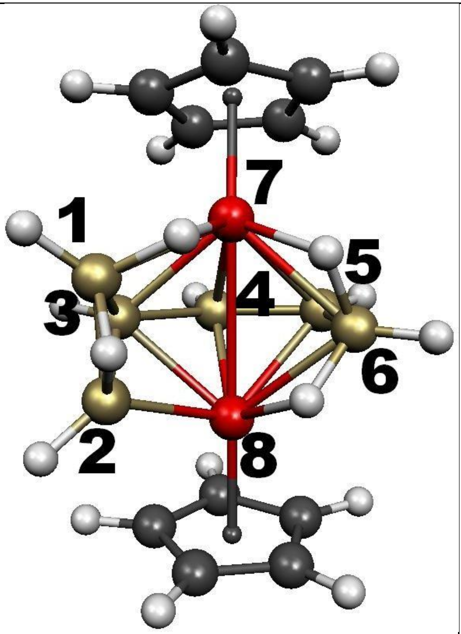

3. -698.842471 +12.4 C_1
WBI 0.47

		1	2	3	4	5	6	7	8
1	B	0.000000							
2	B	1.713806	0.000000						
3	B	1.746330	1.747373	0.000000					
4	B	3.347171	3.227471	1.914234	0.000000				
5	B	3.998181	3.909407	3.151745	1.745678	0.000000			
6	B	3.699988	3.617289	3.537624	2.955096	1.645526	0.000000		
7	Re	2.325375	3.187520	2.254590	2.221323	2.249919	2.375425	0.000000	
8	Re	3.148773	2.158077	2.250767	2.096381	2.242229	2.326223	2.928573	0.000000

Re7-H-B1 Re7-H 1.76 B1-H 1.36
Re7-H-B6 Re7-H 1.80 B6-H 1.36
Re8-H-B6 Re7-H 1.81 B6-H 1.36
B1-H-B2 B1-H 1.30 B2-H 1.34

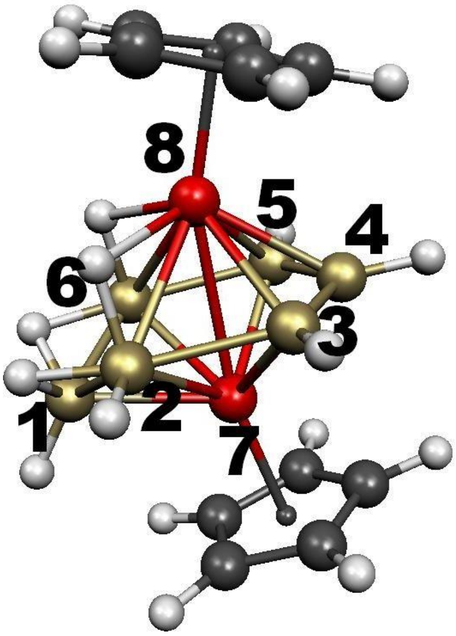

4. -698.842364 +12.5 C_S
WBI 0.47

		1	2	3	4	5	6	7	8
1	B	0.000000							
2	B	1.836526	0.000000						
3	B	3.504513	2.113453	0.000000					
4	B	4.005226	3.241486	1.659707	0.000000				
5	B	3.504267	3.513614	2.878800	1.659613	0.000000			
6	B	1.836593	2.737100	3.513498	3.241057	2.112897	0.000000		
7	Re	2.209951	2.194672	2.177139	2.232894	2.177394	2.194824	0.000000	
8	Re	3.177986	2.404889	2.235677	2.229901	2.235867	2.404889	2.803613	0.000000

Re8-H-B2 Re8-H 1.80 B2-H 1.34
Re8-H-B6 Re8-H 1.80 B6-H 1.34
B1-H-B2 B1-H 1.27 B2-H 1.43
B1-H-B6 B1-H 1.27 B6-H 1.43

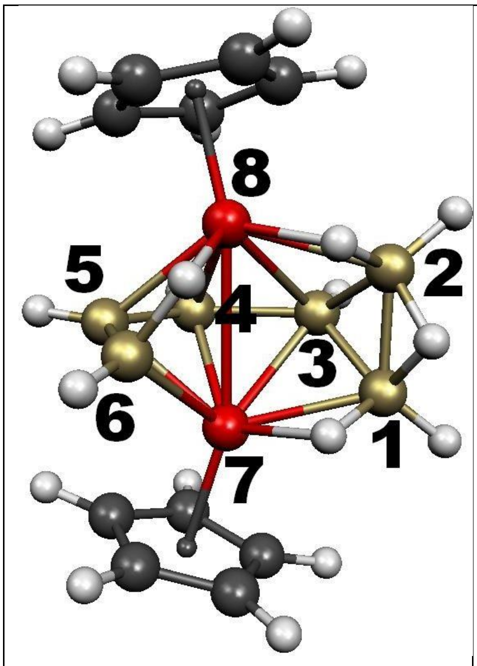

5. -698.841258 +13.2 C_1
WBI 0.46

		1	2	3	4	5	6	7	8
1	B	0.000000							
2	B	1.745412	0.000000						
3	B	1.746541	1.735426	0.000000					
4	B	3.245822	3.290558	1.867933	0.000000				
5	B	4.002058	4.033490	3.152394	1.747586	0.000000			
6	B	3.718708	3.823065	3.550874	2.923406	1.623709	0.000000		
7	Re	2.240841	3.190474	2.254398	2.122472	2.257500	2.235806	0.000000	
8	Re	3.193847	2.305667	2.287900	2.223556	2.242879	2.370792	2.879525	0.000000

Re7-H-B1 Re7-H 1.79 B1-H 1.37
Re8-H-B2 Re8-H 1.78 B2-H 1.35
Re8-H-B6 Re8-H 1.78 B6-H 1.37
B1-H-B2 B1-H 1.36 B2-H 1.30

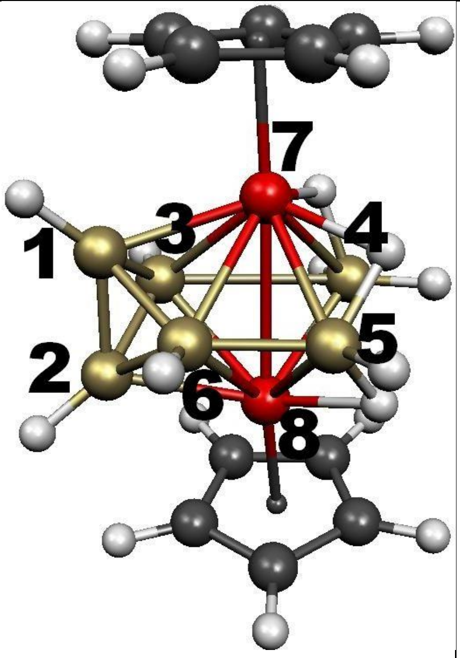

6. -698.838612 +14.9 C_1 (C_s)
WBI 0.52

		1	2	3	4	5	6	7	8
1	B	0.000000							
2	B	1.661933	0.000000						
3	B	1.729565	1.747200	0.000000					
4	B	3.877635	3.808497	2.670956	0.000000				
5	B	3.213578	3.199513	3.397578	3.054294	0.000000			
6	B	1.773948	1.773773	2.554948	3.687191	1.776088	0.000000		
7	Re	2.210297	3.095944	2.257082	2.446084	2.256828	2.300146	0.000000	
8	Re	3.053902	2.169602	2.235223	2.253042	2.229339	2.276173	2.803829	0.000000

Re7-H-B4 Re7-H 1.78 B4-H 1.32
Re7-H-B5 Re7-H 1.74 B5-H 1.38
Re8-H-B5 Re8-H 1.78 B5-H 1.31

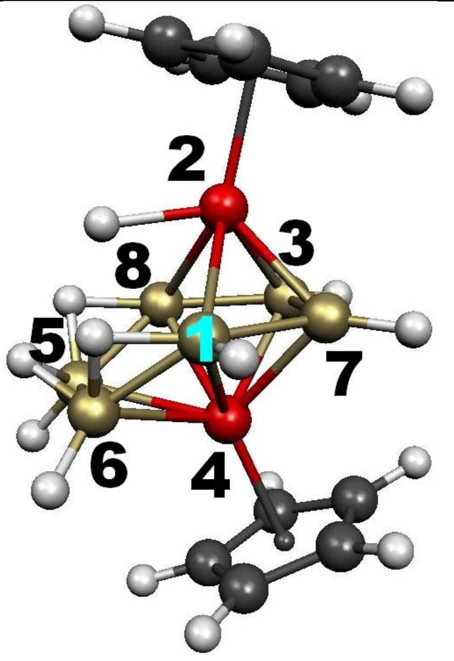

7. -698.836395 +16.3 C_S
WBI 0.46

		1	2	3	4	5
1	B	0.000000				
2	Re	2.275425	0.000000			
3	B	3.145084	2.065045	0.000000		
4	Re	2.233479	2.918596	2.143506	0.000000	
5	B	3.006967	3.282031	3.261301	2.189547	0.000000
6	B	1.793477	3.282932	3.780956	2.187434	1.817817
7	B	1.864533	2.064859	2.002183	2.139499	3.780746
8	B	3.211052	2.286554	1.855315	2.231855	1.789773

		6	7	8
6	B	0.000000		
7	B	3.267173	0.000000	
8	B	3.008667	3.144060	0.000000

B1-H-B6   B1-H 1.36   B6-H 1.29
B8-H-B5   B8-H 1.35   B5-H 1.29
B5-H-B6   B5-H 1.33   B6-H 1.33
Re2-H 1.66

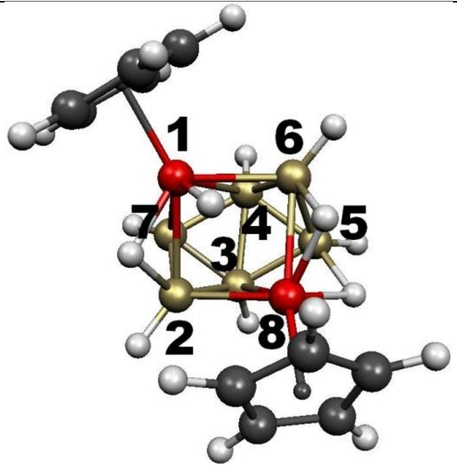

8. -698.831204 +19.5 C_2
WBI 0.44

		1	2	3	4	5
1	Re	0.000000				
2	B	2.239399	0.000000			
3	B	3.032073	1.777812	0.000000		
4	B	2.331194	2.741647	1.881924	0.000000	
5	B	3.323946	3.041293	1.791208	1.717353	0.000000
6	B	2.193953	3.105097	2.788710	1.775582	1.791250
7	B	2.165777	1.736491	1.697424	1.757147	2.908118
8	Re	2.962746	2.223212	2.375545	3.037931	2.207425

		6	7	8
6	B	0.000000		
7	B	3.018652	0.000000	
8	Re	2.279312	3.313948	0.000000

Re1-H-B2   Re1-H 1.68   B2-H 1.60
Re8-H-B6   Re8-H 1.68   B6-H 1.61
Re8-H-B5   Re8-H 1.68   B5-H 1.46
Re1-H 1.68

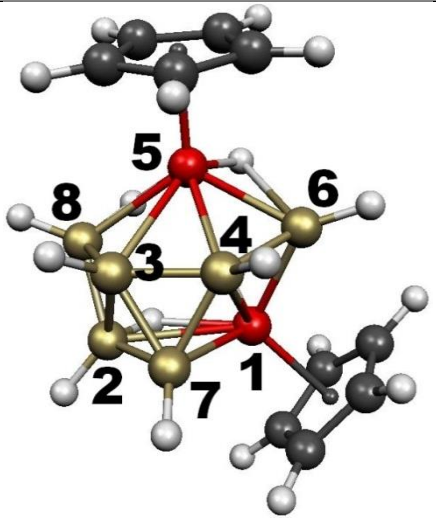

9. -698.829722 +20.4 C_1
WBI 0.42

```
                1          2          3          4          5
    1  Re   0.000000
    2  B    2.474806   0.000000
    3  B    2.970028   1.778650   0.000000
    4  B    2.252360   2.763759   1.746117   0.000000
    5  Re   2.946644   3.195763   2.348431   2.258377   0.000000
    6  B    2.069101   3.774842   3.205286   1.810324   2.140206
    7  B    2.182780   1.708254   1.727446   1.732951   3.369955
    8  B    3.230563   1.731044   1.773540   3.042040   2.237004
                6          7          8
    6  B    0.000000
    7  B    3.139555   0.000000
    8  B    3.765130   2.924499   0.000000
```

Re5-H-B8   Re5-H 1.77   B8-H 1.35
Re1-H-B2   Re1-H 1.90   B2-H 1.30
Re1-H 1.68
Re5-H 1.67

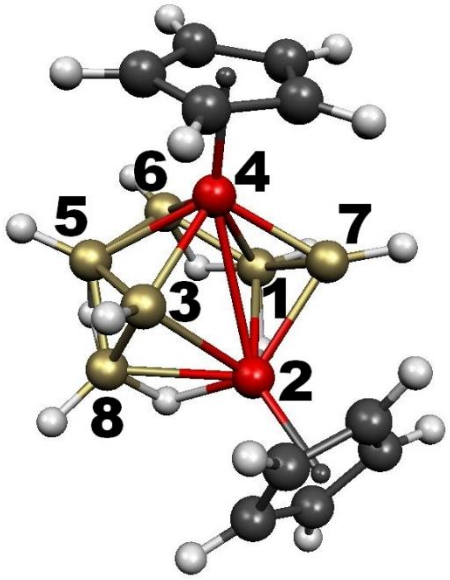

10. -698.826988 +22.2 C_1
WBI 0.42

```
                1          2          3          4          5
    1  B    0.000000
    2  Re   2.353788   0.000000
    3  B    3.215848   2.252221   0.000000
    4  Re   2.243561   2.896009   2.140597   0.000000
    5  B    2.962386   3.161958   1.765426   2.255739   0.000000
    6  B    1.817165   3.440385   3.071208   2.038307   1.911746
    7  B    1.892999   2.150180   3.071332   2.045675   3.726167
    8  B    3.208844   2.300568   1.732329   3.223659   1.747444
                6          7          8
    6  B    0.000000
    7  B    3.173009   0.000000
    8  B    3.042917   3.847992   0.000000
```

Re2-H-B1   Re2-H 1.75   B1-H 1.41
Re2-H-B8   Re2-H 1.77   B8-H 1.33
B1-H-B6   B1-H 1.32   B6-H 1.36
B5-H-B8   B5-H 1.29   B8-H 1.38

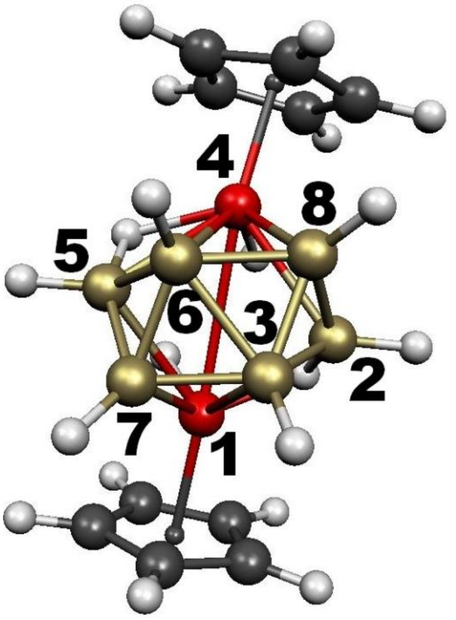

11. -698.824088 +24.0 C_2
WBI 0.43

```
                 1          2          3          4          5
    1  Re   0.000000
    2  B    2.244965   0.000000
    3  B    2.325506   1.779038   0.000000
    4  Re   3.026887   2.351674   3.055378   0.000000
    5  B    2.355413   3.229049   2.823121   2.230733   0.000000
    6  B    3.050466   2.819648   1.921116   2.324695   1.772020
    7  B    2.155049   3.038169   1.768454   3.275816   1.751192
    8  B    3.276525   1.741253   1.696121   2.152668   3.030978
                 6          7          8
    6  B    0.000000
    7  B    1.688798   0.000000
    8  B    1.770193   2.851928   0.000000
```

Re1-H-B2   Re1-H 1.73   B2-H 1.37
Re4-H-B5   Re4-H 1.72   B5-H 1.40
Re1-H 1.66
Re4-H 1.66

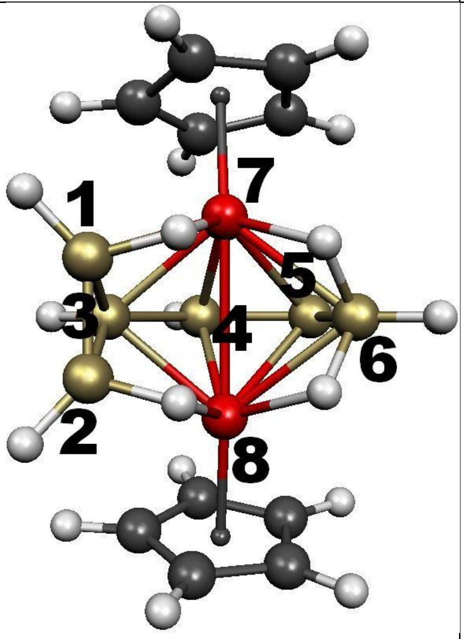

12. -698.819197 +27.0 C_S
WBI 0.49

```
                 1          2          3          4          5
    1  B    0.000000
    2  B    1.610700   0.000000
    3  B    1.807103   1.807084   0.000000
    4  B    3.380215   3.380166   1.886149   0.000000
    5  B    4.106289   4.106227   3.162210   1.749778   0.000000
    6  B    3.880289   3.880191   3.613357   2.971377   1.630070
    7  Re   2.379854   3.207308   2.242118   2.145665   2.249942
    8  Re   3.207430   2.379785   2.242164   2.145736   2.250083
                 6          7          8
    6  B    0.000000
    7  Re   2.377320   0.000000
    8  Re   2.377387   2.870600   0.000000
```

Re7-H-B1   Re7-H 1.86   B1-H 1.30
Re7-H-B6   Re7-H 1.81   B6-H 1.34
Re8-H-B2   Re8-H 1.86   B2-H 1.30
Re8-H-B6   Re8-H 1.81   B6-H 1.34

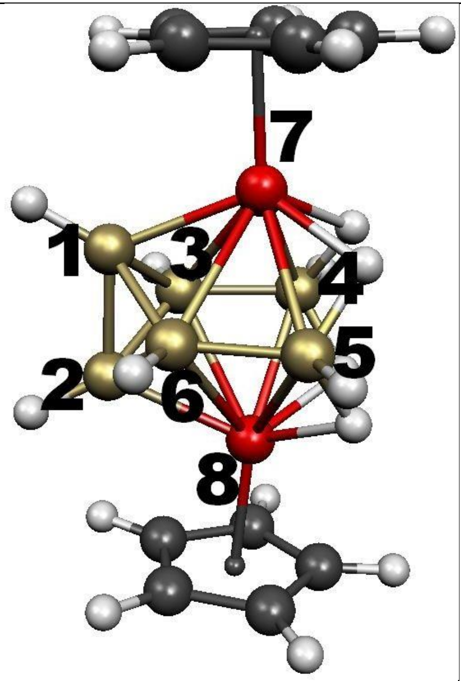

13. -698.815848 +29.2 C_{2V}
WBI 0.10

		1	2	3	4	5
1	B	0.000000				
2	B	1.761200	0.000000			
3	B	1.738265	1.738265	0.000000		
4	B	3.071639	3.071639	1.697455	0.000000	
5	B	3.070020	3.070020	3.128877	2.864247	0.000000
6	B	1.739287	1.739287	2.418658	3.135773	1.698921
7	Re	2.131258	3.266902	2.374025	2.343395	2.331629
8	Re	3.266902	2.131258	2.374025	2.343395	2.331629

		6	7	8
6	B	0.000000		
7	Re	2.368693	0.000000	
8	Re	2.368693	3.480800	0.000000

Re7-H-B4	Re7-H 1.78	B4-H 1.32
Re7-H-B5	Re7-H 1.78	B5-H 1.32
Re8-H-B4	Re7-H 1.78	B4-H 1.32
Re8-H-B5	Re7-H 1.78	B5-H 1.32

6.1.4.5 $Cp_2M_2B_6H_{10}$ (M=Mo,W) systems

Table 95. Distance table for the lowest-lying $Cp_2Mo_2B_6H_{10}$ structures after M06L/6-311G(d,p) optimization. Included are the ZPcorrected E (a.u.), relative energy (kcal/mol), symmetry and WBI.

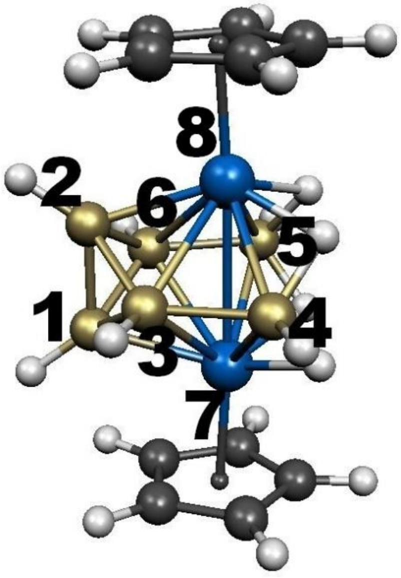

Mo2B6-1 -678.656321 0.0 C_{2V}
WBI 0.60

		1	2	3	4	5
1	B	0.000000				
2	B	1.672086	0.000000			
3	B	1.776439	1.776439	0.000000		
4	B	3.211782	3.211782	1.803332	0.000000	
5	B	3.211782	3.211782	3.457237	3.306792	0.000000
6	B	1.776439	1.776439	2.631094	3.457237	1.803332
7	Mo	2.153890	3.091205	2.312384	2.283475	2.283475
8	Mo	3.091205	2.153890	2.312384	2.283475	2.283475

		6	7	8
6	B	0.000000		
7	Mo	2.312384	0.000000	
8	Mo	2.312384	2.940224	0.000000

Mo7-H-B4	Mo7-H 1.80	B4-H 1.32
Mo7-H-B5	Mo7-H 1.80	B5-H 1.32
Mo8-H-B4	Mo8-H 1.80	B4-H 1.32
Mo8-H-B5	Mo8-H 1.80	B5-H 1.32

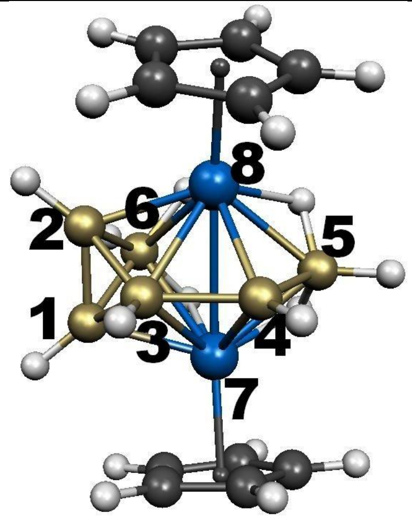

Mo2B6-2 -678.650743 +3.5 C_S
WBI 0.62

```
               1          2          3          4          5
    1  B    0.000000
    2  B    1.643834   0.000000
    3  B    1.765174   1.765267   0.000000
    4  B    3.190512   3.190574   1.814735   0.000000
    5  B    3.906038   3.906222   3.171893   1.827607   0.000000
    6  B    1.847864   1.847738   2.679272   3.413079   3.272075
    7  Mo   2.195092   3.104344   2.271905   2.156168   2.259545
    8  Mo   3.104313   2.195150   2.271843   2.156021   2.259945
               6          7          8
    6  B    0.000000
    7  Mo   2.379412   0.000000
    8  Mo   2.379372   2.931136   0.000000
```

Mo7-H-B5	Mo7-H 1.84	B5-H 1.31
Mo7-H-B6	Mo7-H 1.81	B6-H 1.36
Mo8-H-B5	Mo8-H 1.84	B5-H 1.31
Mo8-H-B6	Mo8-H 1.81	B6-H 1.36

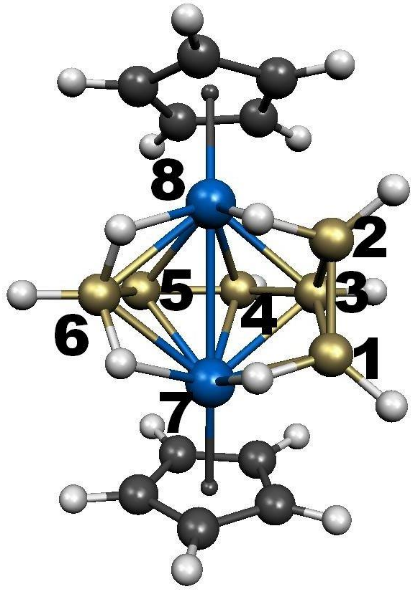

Mo2B6-3 -678.644902 +7.2 C_S
WBI 0.58

```
               1          2          3          4          5
    1  B    0.000000
    2  B    1.738546   0.000000
    3  B    1.752675   1.752706   0.000000
    4  B    3.198250   3.198242   1.755769   0.000000
    5  B    3.943218   3.943169   3.039023   1.731802   0.000000
    6  B    3.748003   3.747903   3.548517   3.020412   1.727889
    7  Mo   2.271989   3.194023   2.260590   2.169892   2.205731
    8  Mo   3.194155   2.271964   2.260641   2.169926   2.205813
               6          7          8
    6  B    0.000000
    7  Mo   2.325939   0.000000
    8  Mo   2.326016   2.899163   0.000000
```

Mo7-H-B1	Mo7-H 1.90	B1-H 1.28
Mo7-H-B6	Mo7-H 1.86	B6-H 1.29
Mo8-H-B2	Mo8-H 1.90	B2-H 1.28
Mo8-H-B6	Mo8-H 1.86	B6-H 1.29

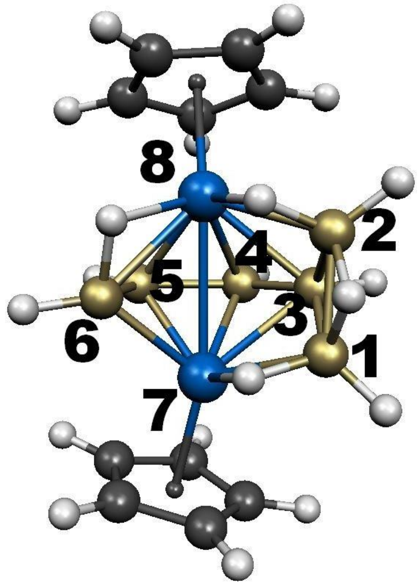 Mo2B6-4 -678.635658 +13.0 C_S WBI 0.60	1 2 3 4 5 1 B 0.000000 2 B 1.817265 0.000000 3 B 1.771665 1.755708 0.000000 4 B 3.179702 3.189247 1.723899 0.000000 5 B 3.913637 3.955533 3.023016 1.767351 0.000000 6 B 3.540208 3.670933 3.452379 3.060720 1.830346 7 Mo 2.296284 3.268451 2.292204 2.168168 2.135590 8 Mo 3.235834 2.334148 2.317006 2.214394 2.161984 6 7 8 6 B 0.000000 7 Mo 2.130854 0.000000 8 Mo 2.284248 2.874455 0.000000 Mo7-H-B1 Mo7-H 1.91 B1-H 1.28 Mo8-H-B2 Mo8-H 1.91 B2-H 1.27 Mo8-H-B6 Mo8-H 1.81 B6-H 1.32 B1-H-B2 B1-H 1.32 B2-H 1.31
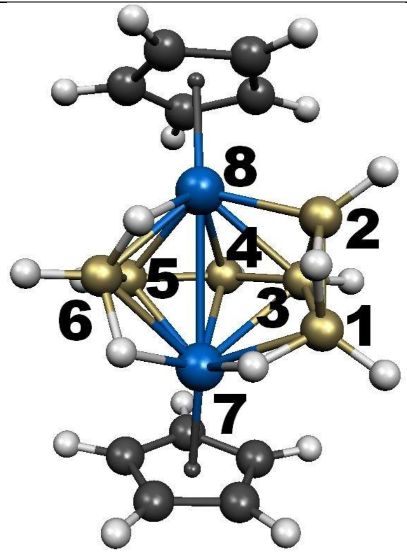 Mo2B6-5 -678.634305 +13.8 C_S WBI 0.64	1 2 3 4 5 1 B 0.000000 2 B 1.762377 0.000000 3 B 1.752957 1.736143 0.000000 4 B 3.209835 3.096677 1.750327 0.000000 5 B 3.910540 3.859142 3.062036 1.786830 0.000000 6 B 3.580208 3.577460 3.503827 3.064262 1.788133 7 Mo 2.345438 3.253954 2.282446 2.188104 2.165167 8 Mo 3.167225 2.199710 2.323254 2.143793 2.170162 6 7 8 6 B 0.000000 7 Mo 2.330170 0.000000 8 Mo 2.244137 2.931617 0.000000 Mo7-H-B1 Mo7-H 1.85 B1-H 1.29 Mo7-H-B6 Mo7-H 1.81 B6-H 1.33 Mo8-H-B6 Mo8-H 1.87 B6-H 1.29 B1-H-B2 B1-H 1.34 B2-H 1.29

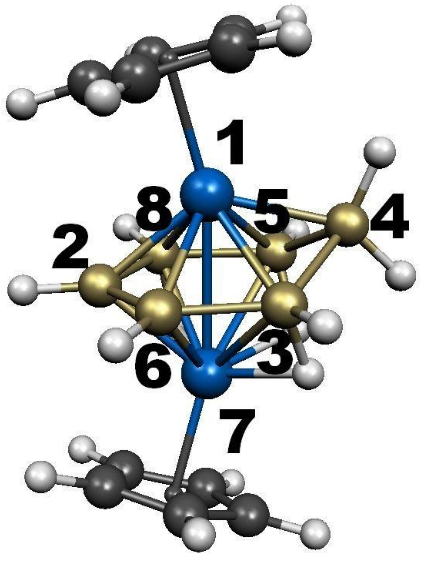

Mo2B6-6 -678.624361 +20.1
(C_1-C_S) WBI 0.59

		1	2	3	4	5
1	Mo	0.000000				
2	B	2.156447	0.000000			
3	B	2.202000	3.044323	0.000000		
4	B	2.161029	3.868232	1.913576	0.000000	
5	B	2.194101	3.140083	2.799460	1.894273	0.000000
6	B	2.151168	1.733946	1.782012	3.298320	3.432287
7	Mo	2.848438	2.186937	2.358881	3.192148	2.407012
8	B	2.163529	1.807719	3.475852	3.390869	1.922998

		6	7	8
6	B	0.000000		
7	Mo	2.220154	0.000000	
8	B	3.037683	2.295141	0.000000

Mo7-H-B3 Mo7-H 1.83 B3-H 1.32
Mo7-H-B5 Mo7-H 1.86 B5-H 1.32
Mo7-H-B8 Mo7-H 1.83 B8-H 1.32
B4-H 1.20

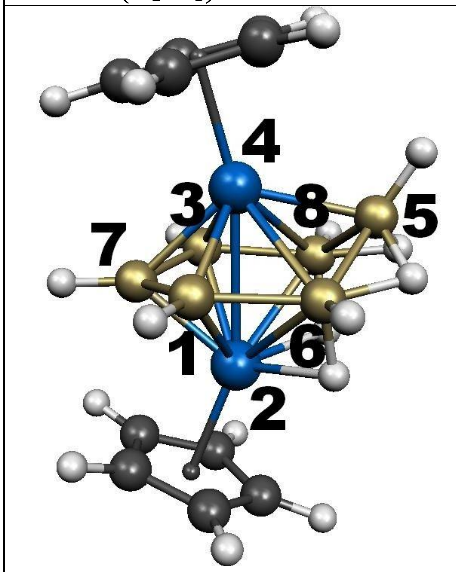

Mo2B6-7 -678.613777 +26.7 C_S
WBI 0.55

		1	2	3	4	5
1	B	0.000000				
2	Mo	2.262391	0.000000			
3	B	3.046203	2.262336	0.000000		
4	Mo	2.098773	2.877141	2.098785	0.000000	
5	B	3.261356	3.240054	3.261360	2.204981	0.000000
6	B	1.905277	2.386807	3.451369	2.347929	1.865976
7	B	1.814621	2.088975	1.814635	2.166323	3.865299
8	B	3.451380	2.386784	1.905266	2.347930	1.865986

		6	7	8
6	B	0.000000		
7	B	3.172970	0.000000	
8	B	2.718771	3.172978	0.000000

Mo2-H-B6 Mo2-H 1.87 B6-H 1.28
Mo2-H-B8 Mo2-H 1.87 B8-H 1.28
B5-H-B6 B5-H 1.27 B6-H 1.40
B5-H-B8 B5-H 1.27 B8-H 1.40

Table 96. Distance table for the lowest-lying $Cp_2W_2B_6H_{10}$ structures after M06L/6-311G(d,p) optimization. Included are the ZPcorrected E (a.u.), relative energy (kcal/mol), symmetry and WBI.

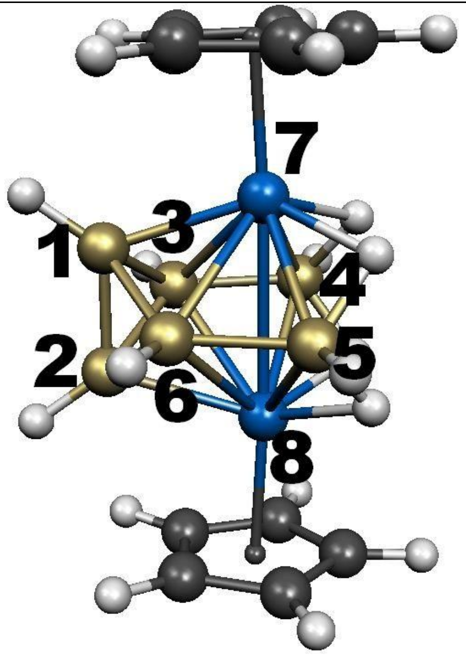

W2B6-1 -676.467791 0.0 C_{2v}
WBI 0.62

```
                 1          2          3          4          5
     1  B    0.000000
     2  B    1.671900   0.000000
     3  B    1.781671   1.781625   0.000000
     4  B    3.210036   3.210062   1.802943   0.000000
     5  B    3.210229   3.210151   3.459029   3.293800
 0.000000
     6  B    1.781614   1.781567   2.645400   3.458878
 1.803130
     7  W    2.163298   3.106109   2.329125   2.288129
 2.288311
     8  W    3.106117   2.163233   2.329073   2.288283
 2.288206
                 6          7          8
     6  B    0.000000
     7  W    2.329092   0.000000
     8  W    2.329040   2.971600   0.000000
```

W7-H-B4 W7-H 1.81 B4-H 1.34
W7-H-B5 W7-H 1.81 B5-H 1.34
W8-H-B4 W7-H 1.81 B4-H 1.34
W8-H-B5 W7-H 1.81 B5-H 1.34

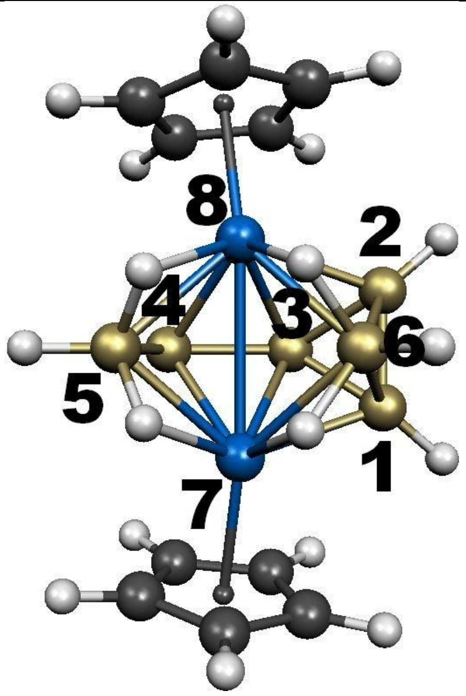

W2B6-2 -676.462405 +3.4 C_S
WBI 0.63

```
                 1          2          3          4          5
     1  B    0.000000
     2  B    1.649000   0.000000
     3  B    1.773660   1.773660   0.000000
     4  B    3.201474   3.201474   1.811511   0.000000
     5  B    3.912007   3.912007   3.155326   1.809635
 0.000000
     6  B    1.839751   1.839751   2.656109   3.392420
 3.260607
     7  W    2.206345   3.123870   2.286419   2.179214
 2.269914
     8  W    3.123870   2.206345   2.286419   2.179214
 2.269914
                 6          7          8
     6  B    0.000000
     7  W    2.363984   0.000000
     8  W    2.363984   2.965800   0.000000
```

W7-H-B5 W7-H 1.85 B5-H 1.32
W7-H-B6 W7-H 1.80 B6-H 1.43
W8-H-B4 W8-H 1.85 B4-H 1.32
W8-H-B6 W8-H 1.80 B6-H 1.43

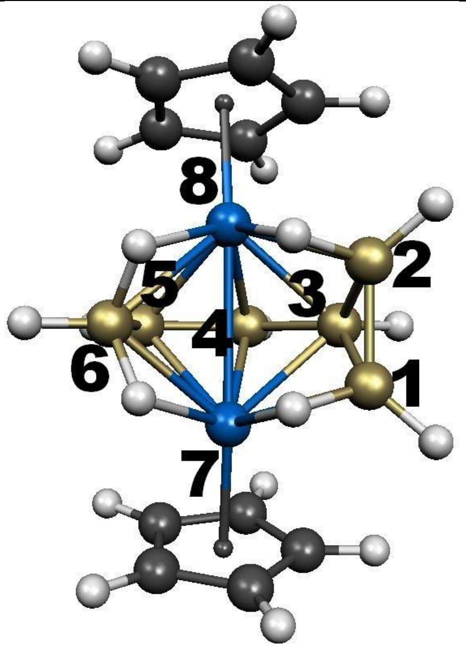

W2B6-3 -676.457141 +6.7 C_S
WBI 0.61

```
                1          2          3          4          5
    1  B    0.000000
    2  B    1.725900   0.000000
    3  B    1.761783   1.761832   0.000000
    4  B    3.218056   3.218083   1.763900   0.000000
    5  B    3.961638   3.961616   3.043706   1.727253
0.000000
    6  B    3.745176   3.745153   3.534569   3.004066
1.722645
    7  W    2.282287   3.201672   2.268487   2.187035
2.224795
    8  W    3.201682   2.282225   2.268508   2.187112
2.224849
                6          7          8
    6  B    0.000000
    7  W    2.320204   0.000000
    8  W    2.320314   2.921400   0.000000
```

W7-H-B1   W7-H 1.90   B1-H 1.29
W7-H-B6   W7-H 1.85   B6-H 1.32
W8-H-B2   W8-H 1.90   B2-H 1.29
W8-H-B6   W8-H 1.85   B6-H 1.32

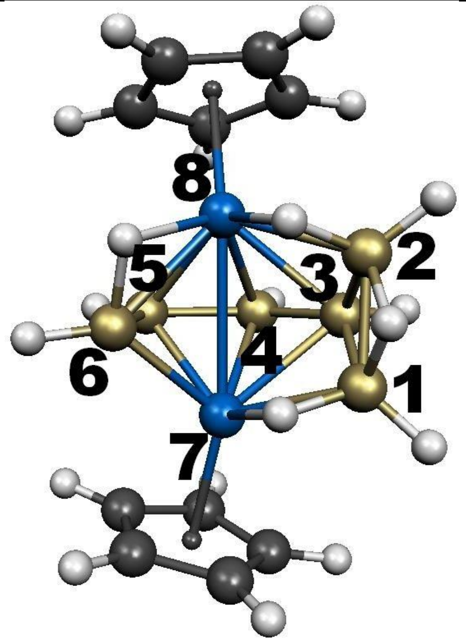

W2B6-4 -676.444631 +14.5 C_1
WBI 0.63

```
                1          2          3          4          5
    1  B    0.000000
    2  B    1.824519   0.000000
    3  B    1.772324   1.759450   0.000000
    4  B    3.190619   3.195910   1.735423   0.000000
    5  B    3.929940   3.961394   3.036919   1.768313
0.000000
    6  B    3.543260   3.659476   3.453992   3.060638
1.839151
    7  W    2.301632   3.276239   2.304945   2.184530
2.156480
    8  W    3.250004   2.326824   2.323466   2.219044
2.179843
                6          7          8
    6  B    0.000000
    7  W    2.137434   0.000000
    8  W    2.298206   2.903122   0.000000
```

W7-H-B1   W7-H 1.91   B1-H 1.29
W8-H-B2   W8-H 1.91   B2-H 1.28
W8-H-B6   W8-H-1.81   B6-H 1.39
B1-H-B2   B1-H 1.32   B2-H 1.31

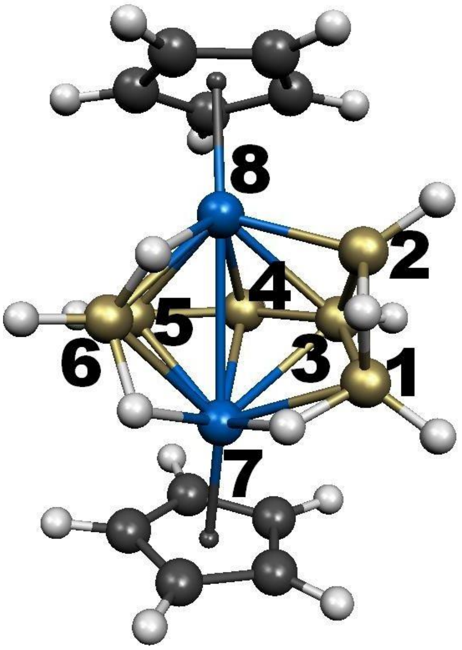

W2B6-5 -676.444242 +14.8 C_1
WBI 0.66

```
                 1          2          3          4          5
    1  B    0.000000
    2  B    1.768727   0.000000
    3  B    1.753884   1.749688   0.000000
    4  B    3.216739   3.117619   1.760686   0.000000
    5  B    3.921928   3.870882   3.070681   1.782785
0.000000
    6  B    3.576577   3.563021   3.492232   3.046883
1.781834
    7  W    2.344842   3.263903   2.293954   2.199429
2.184567
    8  W    3.184106   2.201204   2.331994   2.160653
2.192917
                 6          7          8
    6  B    0.000000
    7  W    2.326197   0.000000
    8  W    2.250325   2.964911   0.000000
```

W7-H-B1   W7-H 1.86   B1-H 1.30
W7-H-B6   W7-H 1.82   B6-H 1.35
W8-H-B6   W8-H 1.86   B6-H 1.31
B1-H-B2   B1-H 1.34   B2-H 1.29

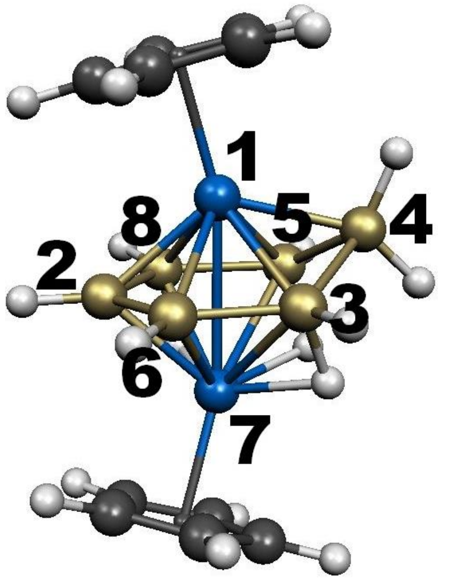

W2B6-6 -676.439278 +17.9 (Cs)
WBI 0.60

```
                 1          2          3          4          5
    1  W    0.000000
    2  B    2.177469   0.000000
    3  B    2.213157   3.044702   0.000000
    4  B    2.172640   3.881327   1.922756   0.000000
    5  B    2.201020   3.139598   2.801857   1.899014
0.000000
    6  B    2.170491   1.735464   1.781970   3.311618
3.434308
    7  W    2.891065   2.199925   2.368461   3.214048
2.425640
    8  B    2.178582   1.803690   3.475817   3.402223
1.924428
                 6          7          8
    6  B    0.000000
    7  W    2.230204   0.000000
    8  B    3.036641   2.311726   0.000000
```

W7-H-B8   W7-H 1.83   B8-H 1.34
W7-H-B3   W7-H 1.84   B3-H 1.33
W7-H-B5   W7-H 1.86   B5-H 1.34

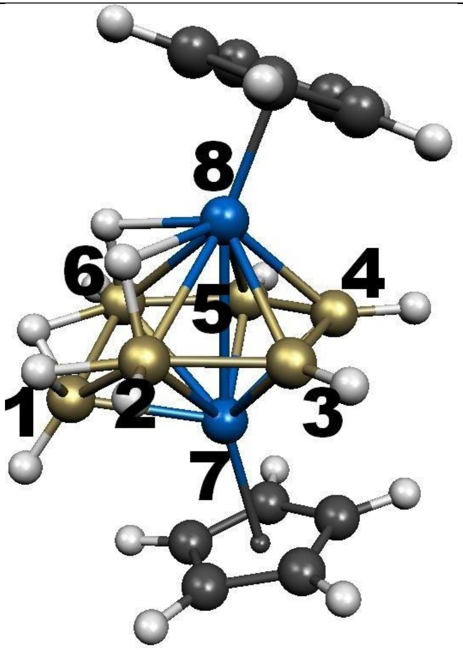

W2B6-7 -676.419185 +30.5 C_S
WBI 0.59

		1	2	3	4	5	6	7	8
1	B	0.000000							
2	B	1.880979	0.000000						
3	B	3.284178	1.900851	0.000000					
4	B	3.882236	3.166488	1.817043	0.000000				
5	B	3.284239	3.452267	3.057300	1.816862	0.000000			
6	B	1.880939	2.716400	3.452299	3.166476	1.900940	0.000000		
7	W	2.218037	2.353631	2.123447	2.180884	2.123514	2.353633	0.000000	
8	W	3.266404	2.389133	2.274090	2.108820	2.273914	2.389118	2.914892	0.000000

W8-H-B2	W8-H 1.87	B2-H 1.29
W8-H-B6	W8-H 1.87	B6-H 1.29
B1-H-B2	B1-H 1.26	B2-H 1.41
B1-H-B6	B1-H 1.26	B6-H 1.41

6.1.4.6 $Cp_2Ta_2B_6H_{10}$ systems

Table 97. Distance table for the lowest-lying $Cp_2Ta_2B_6H_{10}$ structures after M06L/6-311G(d,p) optimization. Included are the ZPcorrected E (a.u.), relative energy (kcal/mol), symmetry and WBI.

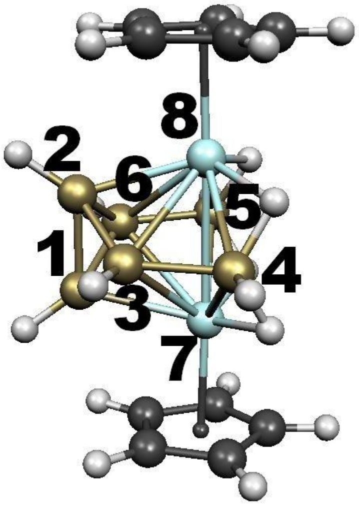

Ta2B6-1 -656.282274 0.0 C_{2v}
WBI 0.87

		1	2	3	4	5	6	7	8
1	B	0.000000							
2	B	1.704970	0.000000						
3	B	1.735147	1.735423	0.000000					
4	B	3.204740	3.204264	1.803970	0.000000				
5	B	3.204920	3.205085	3.615394	3.730209	0.000000			
6	B	1.736273	1.737028	2.634750	3.619864	1.806617	0.000000		
7	Ta	2.266155	3.170308	2.428033	2.374321	2.372335	2.430765	0.000000	
8	Ta	3.175887	2.266964	2.433309	2.379681	2.377986	2.435800	2.892289	0.000000

Ta7-H-B4	Ta7-H 1.90	B4-H 1.27
Ta7-H-B5	Ta7-H 1.90	B5-H 1.27
Ta8-H-B4	Ta8-H 1.90	B4-H 1.28
Ta8-H-B5	Ta8-H 1.90	B5-H 1.28

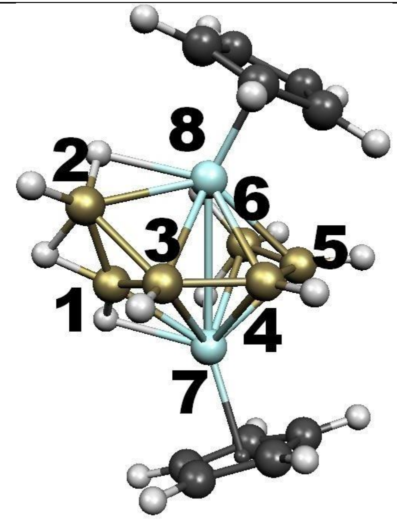

Ta2B6-2 -656.281971 +0.2 C_1
WBI 0.51

		1	2	3	4	5
1	B	0.000000				
2	B	1.691211	0.000000			
3	B	1.691322	1.914779	0.000000		
4	B	2.870056	3.290242	1.730522	0.000000	
5	B	3.388683	4.108860	3.054328	1.738363	0.000000
6	B	3.159796	4.045916	3.689684	3.097780	1.763604
7	Ta	2.153103	3.608871	2.445391	2.282573	2.199760
8	Ta	2.524916	2.320734	2.368806	2.255513	2.294977

		6	7	8
6	B	0.000000		
7	Ta	2.399663	0.000000	
8	Ta	2.400882	3.080422	0.000000

Ta7-H-B1 Ta7-H 1.99 B1-H 1.27
Ta7-H-B6 Ta7-H 2.04 B6-H 1.26
Ta8-H-B2 Ta8-H 1.99 B2-H 1.27
Ta8-H-B6 Ta8-H 2.03 B6-H 1.26
B1-H-B2 B1-H 1.28 B2-H 1.36

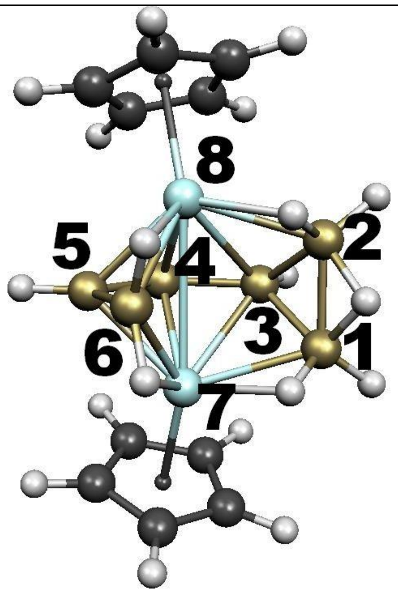

Ta2B6-3 -656.279641 +1.7 C_S
WBI 0.49

		1	2	3	4	5
1	B	0.000000				
2	B	1.827638	0.000000			
3	B	1.774861	1.774862	0.000000		
4	B	3.235189	3.235149	1.761857	0.000000	
5	B	4.011379	4.011306	3.059464	1.746471	0.000000
6	B	3.455233	3.455088	3.220227	2.825678	1.732908
7	Ta	2.388587	3.387999	2.378371	2.254476	2.268798
8	Ta	3.388115	2.388556	2.378357	2.254400	2.268796

		6	7	8
6	B	0.000000		
7	Ta	2.158813	0.000000	
8	Ta	2.158785	3.159082	0.000000

Ta7-H-B1 Ta7-H 1.99 B1-H 1.27
Ta7-H-B6 Ta7-H 2.03 B6-H 1.26
Ta8-H-B2 Ta8-H 1.99 B2-H 1.27
Ta8-H-B6 Ta8-H 2.03 B6-H 1.26
B1-H-B2 B1-H 1.32 B2-H 1.32

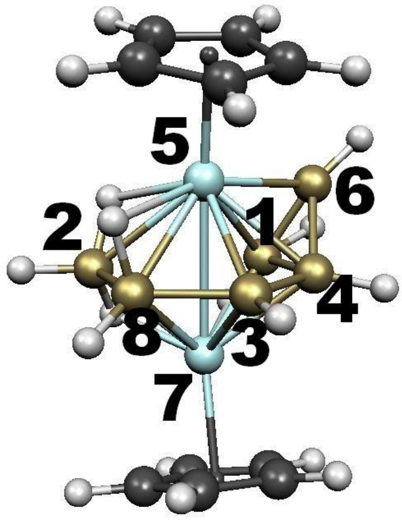

Ta2B6-4. -656.271684 +6.7 C_1
WBI 0.68

```
                1          2          3          4          5
    1  B    0.000000
    2  B    3.071508   0.000000
    3  B    2.921497   3.183835   0.000000
    4  B    1.745608   3.705251   1.728996   0.000000
    5  Ta   2.367778   2.451160   2.258783   2.367538   0.000000
    6  B    1.587758   4.055655   3.249542   1.891749   2.282130
    7  Ta   2.185263   2.367141   2.259139   2.341074   2.989620
    8  B    3.464313   1.848704   1.834943   3.139213   2.318660
                6          7          8
    6  B    0.000000
    7  Ta   3.516419   0.000000
    8  B    4.152740   2.283558   0.000000
```

Ta5-H-B2   Ta5-H 1.98   B2-H 1.29
Ta7-H-B2   Ta7-H 1.96   B2-H 1.28
Ta7-H-B1   Ta7-H 2.01   B1-H 1.25
B1-H-B6   B1-H 1.29   B6-H 1.34

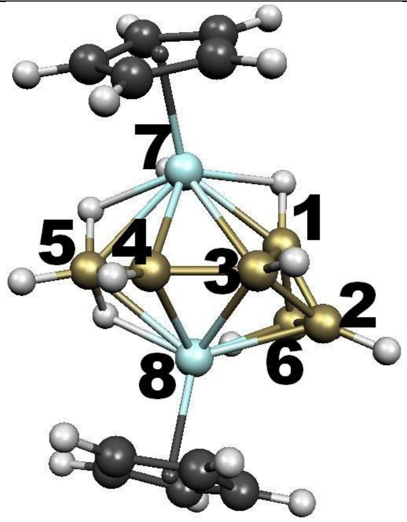

Ta2B6-5 -656.270661 +7.3 C_1
WBI 0.36

```
                1          2          3          4          5
    1  B    0.000000
    2  B    1.611652   0.000000
    3  B    1.738816   1.773327   0.000000
    4  B    2.877910   3.248669   1.748754   0.000000
    5  B    3.406556   4.138960   3.118249   1.777865   0.000000
    6  B    1.764424   1.742879   2.939322   3.882486   4.005400
    7  Ta   2.187118   3.562197   2.458651   2.282931   2.377220
    8  Ta   2.486451   2.327161   2.300327   2.261262   2.378228
                6          7          8
    6  B    0.000000
    7  Ta   3.623774   0.000000
    8  Ta   2.276204   3.250313   0.000000
```

Ta7-H-B1   Ta7-H 1.97   B1-H 1.26
Ta7-H-B5   Ta7-H 1.92   B5-H 1.29
Ta7-H 1.80
Ta8-H-B5   Ta8-H 1.96   B5-H 1.31
Ta8-H-B6   Ta8-H 1.93   B6-H 1.29

<table>
<tr>
<td>
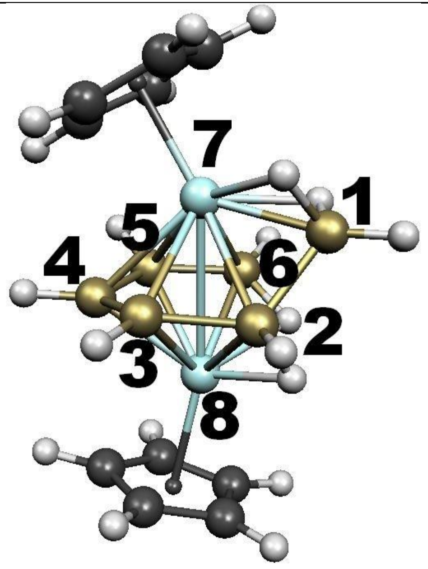

Ta2B6-6 -656.260665 +13.6 C_1
WBI 0.49
</td>
<td>
<table>
<tr><th></th><th></th><th>1</th><th>2</th><th>3</th><th>4</th><th>5</th></tr>
<tr><td>1</td><td>B</td><td>0.000000</td><td></td><td></td><td></td><td></td></tr>
<tr><td>2</td><td>B</td><td>1.801192</td><td>0.000000</td><td></td><td></td><td></td></tr>
<tr><td>3</td><td>B</td><td>3.136180</td><td>1.773092</td><td>0.000000</td><td></td><td></td></tr>
<tr><td>4</td><td>B</td><td>4.064570</td><td>3.027652</td><td>1.702995</td><td>0.000000</td><td></td></tr>
<tr><td>5</td><td>B</td><td>4.041606</td><td>3.545385</td><td>2.993127</td><td>1.723665</td><td>0.000000</td></tr>
<tr><td>6</td><td>B</td><td>3.434330</td><td>3.400260</td><td>3.700210</td><td>3.065612</td><td>1.667102</td></tr>
<tr><td>7</td><td>Ta</td><td>2.194491</td><td>2.382471</td><td>2.267651</td><td>2.426174</td><td>2.448390</td></tr>
<tr><td>8</td><td>Ta</td><td>3.552433</td><td>2.340509</td><td>2.373376</td><td>2.207811</td><td>2.215024</td></tr>
<tr><td></td><td></td><td>6</td><td>7</td><td>8</td><td></td><td></td></tr>
<tr><td>6</td><td>B</td><td>0.000000</td><td></td><td></td><td></td><td></td></tr>
<tr><td>7</td><td>Ta</td><td>2.699073</td><td>0.000000</td><td></td><td></td><td></td></tr>
<tr><td>8</td><td>Ta</td><td>2.294880</td><td>3.071491</td><td>0.000000</td><td></td><td></td></tr>
</table>

Ta7-H1-B1 Ta7-H1-1.97 B1-H 1.29
Ta7-H2-B1 Ta7-H2-1.96 B1-H 1.29
Ta8-H-B2 Ta8-H 1.90 B2-H 1.30
Ta8-H-B6 Ta8-H 1.97 B6-H 1.26
</td>
</tr>
<tr>
<td>
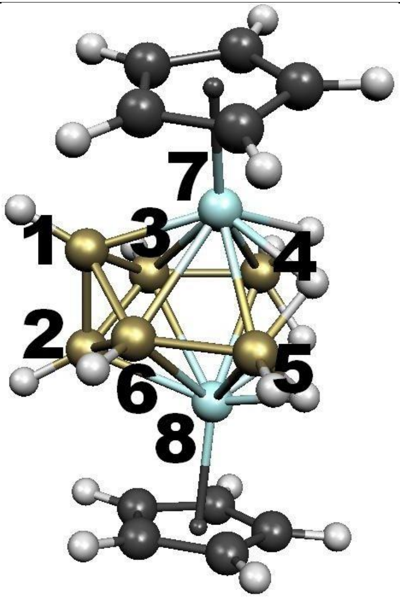

Ta2B6-7 -656.260421 +13.7 C_{2v}
WBI 0.50
</td>
<td>
<table>
<tr><th></th><th></th><th>1</th><th>2</th><th>3</th><th>4</th><th>5</th></tr>
<tr><td>1</td><td>B</td><td>0.000000</td><td></td><td></td><td></td><td></td></tr>
<tr><td>2</td><td>B</td><td>1.697411</td><td>0.000000</td><td></td><td></td><td></td></tr>
<tr><td>3</td><td>B</td><td>1.761178</td><td>1.761958</td><td>0.000000</td><td></td><td></td></tr>
<tr><td>4</td><td>B</td><td>3.211861</td><td>3.213238</td><td>1.847040</td><td>0.000000</td><td></td></tr>
<tr><td>5</td><td>B</td><td>3.237584</td><td>3.236100</td><td>3.418441</td><td>3.155521</td><td>0.000000</td></tr>
<tr><td>6</td><td>B</td><td>1.804213</td><td>1.802799</td><td>2.614038</td><td>3.398829</td><td>1.824722</td></tr>
<tr><td>7</td><td>Ta</td><td>2.178761</td><td>3.209936</td><td>2.416395</td><td>2.377476</td><td>2.352115</td></tr>
<tr><td>8</td><td>Ta</td><td>3.208863</td><td>2.179057</td><td>2.413291</td><td>2.375076</td><td>2.350024</td></tr>
<tr><td></td><td></td><td>6</td><td>7</td><td>8</td><td></td><td></td></tr>
<tr><td>6</td><td>B</td><td>0.000000</td><td></td><td></td><td></td><td></td></tr>
<tr><td>7</td><td>Ta</td><td>2.378140</td><td>0.000000</td><td></td><td></td><td></td></tr>
<tr><td>8</td><td>Ta</td><td>2.378263</td><td>3.271222</td><td>0.000000</td><td></td><td></td></tr>
</table>

Ta7-H-B4 Ta7-H 1.92 B4-H 1.31
Ta7-H-B5 Ta7-H 1.86 B5-H 1.33
Ta8-H-B4 Ta8-H 1.92 B4-H 1.31
Ta8-H-B5 Ta8-H 1.86 B5-H 1.33
</td>
</tr>
</table>

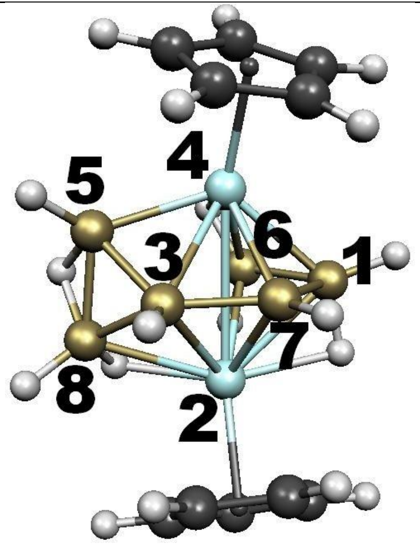

Ta2B6-8 -656.249076 +20.8 C_1
WBI 0.43

		1	2	3	4	5	6	7	8
1	B	0.000000							
2	Ta	2.339636	0.000000						
3	B	3.177224	2.349399	0.000000					
4	Ta	2.297090	3.138257	2.391764	0.000000				
5	B	3.982813	3.345846	1.756853	2.249003	0.000000			
6	B	1.837461	2.221582	3.243536	2.146918	3.312481	0.000000		
7	B	1.868728	2.259428	1.767759	2.224119	3.141150	2.911940	0.000000	
8	B	4.078273	2.423549	1.759165	3.285238	1.768481	3.356208	3.251159	0.000000

Ta2-H-B6   Ta2-H 2.12   B6-H 1.24
Ta2-H-B8   Ta2-H 1.92   B8-H 1.29
Ta4-H-B6   Ta4-H 2.03   B6-H 1.23
B5-H-B8   B5-H 1.30   B8-H 1.34

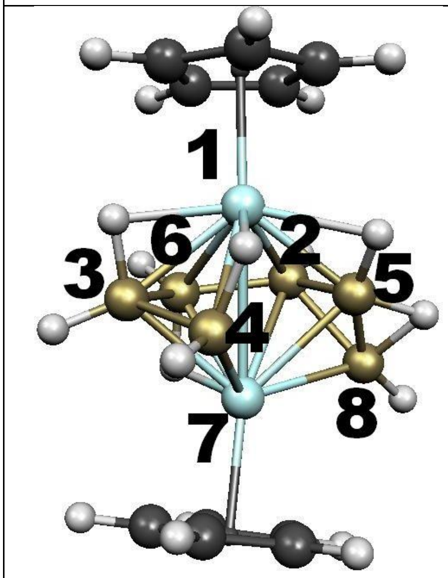

Ta2B6-9 -656.244505 +23.7 C_1
WBI 0.57

		1	2	3	4	5	6	7	8
1	Ta	0.000000							
2	B	2.290006	0.000000						
3	B	2.243921	3.162441	0.000000					
4	B	2.364723	3.555218	1.939866	0.000000				
5	B	2.221826	1.738735	3.507307	2.884920	0.000000			
6	B	2.367965	1.801974	1.874310	3.184017	3.017317	0.000000		
7	Ta	2.978552	2.437645	2.386539	2.198016	2.356600	2.283129	0.000000	
8	B	3.504147	1.858543	4.171710	3.836247	1.590706	3.209647	2.284705	0.000000

Ta1-H-B3   Ta1-H 1.96   B3-H 1.25
Ta1-H-B4   Ta1-H 1.89   B4-H 1.33
Ta1-H-B5   Ta1-H 2.08   B5-H 1.25
B5-H-B8   B5-H 1.28   B8-H 1.35

6.2 Molecular orbital analysis of the high-spin ferric substrate-free models of the Ssulfite reductase active site.

6.2.1 Heme, siroheme and cubane frontier orbitals

6.2.1.1 Cubane: vacuum vs. solvated MOs

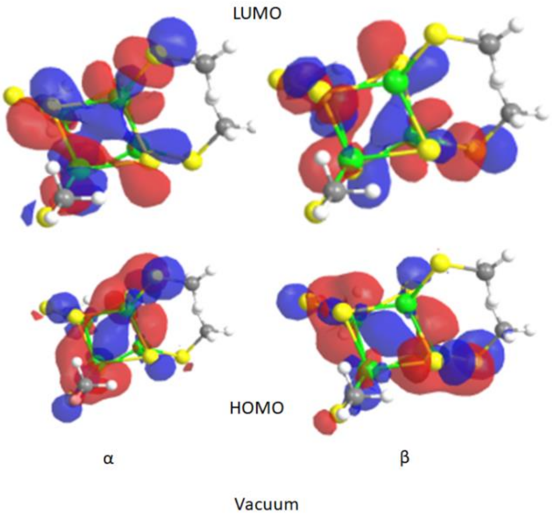

Figure 88. Cubane HOMO-LUMO orbitals computed in vacuum conditions.

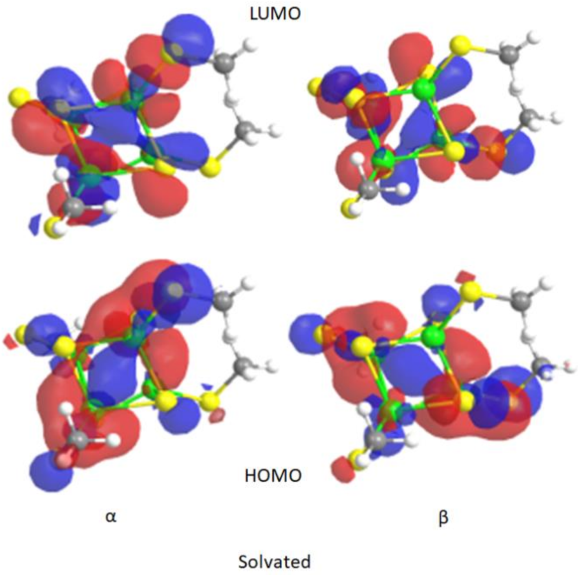

Figure 89. Cubane HOMO-LUMO orbitals computed in solvation conditions.

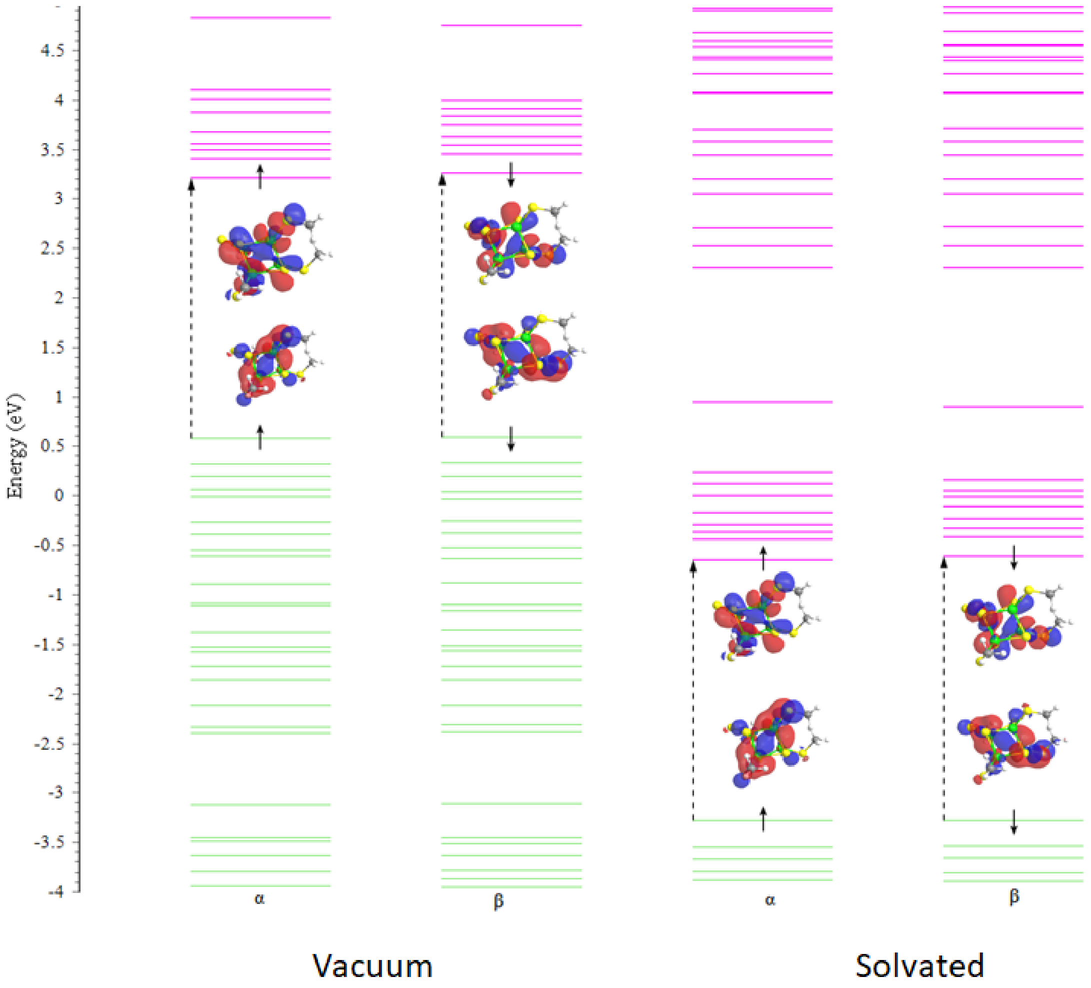

Figure 90. Cubane molecular orbitals computed in vacuum and solvation conditions.

The HOMOs are of metallic character, with the α-HOMO being localized on the two iron ions of one face of the cubane, while the β-HOMO on the other two iron ions localized on the opposing face of the cubane. The corresponding LUMOs are localized on the same iron ions but now they become of antibonding character with respect to the metal-metal bond. Solvation stabilizes the cubane MOs, but does not influence the shape of the orbitals. The HOMO-LUMO transition is degenerated in four channels:α->α, α -> β, β->β, β->α.

6.2.1.2 Heme: vacuum vs. solvated MOs

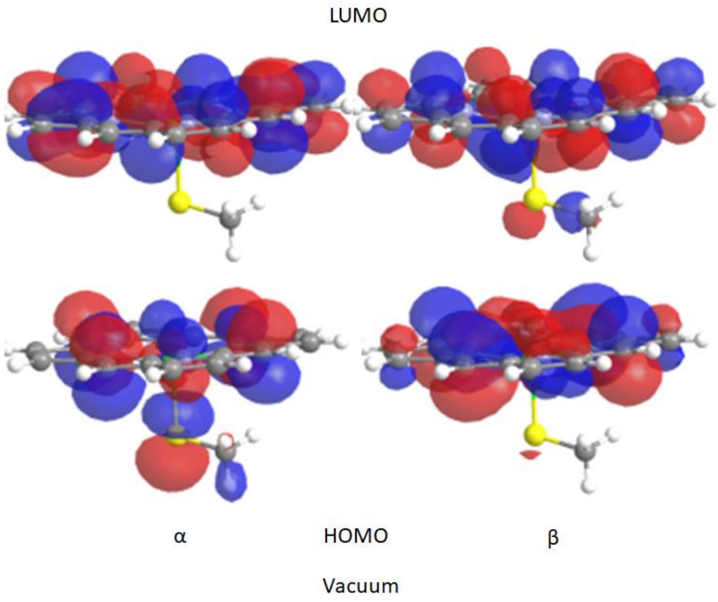

Figure 91. Heme frontier MOs computed in vacuum conditions.

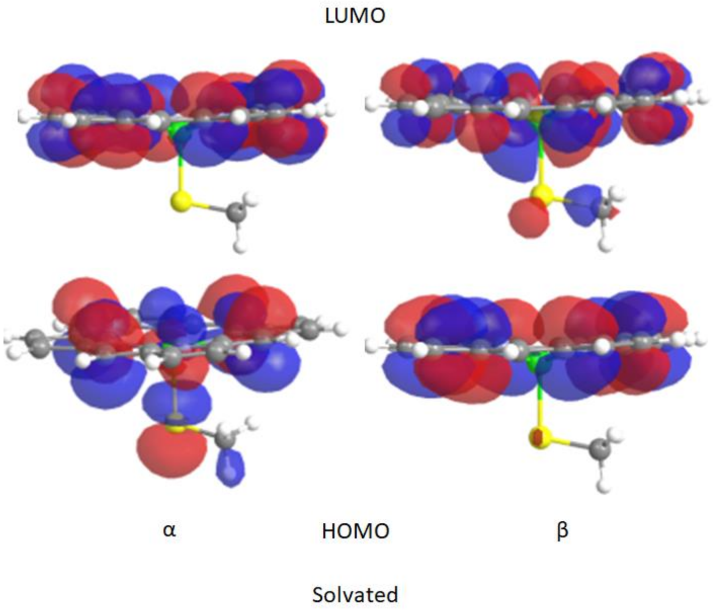

Figure 92. Heme frontier MOs computed in solvation conditions.

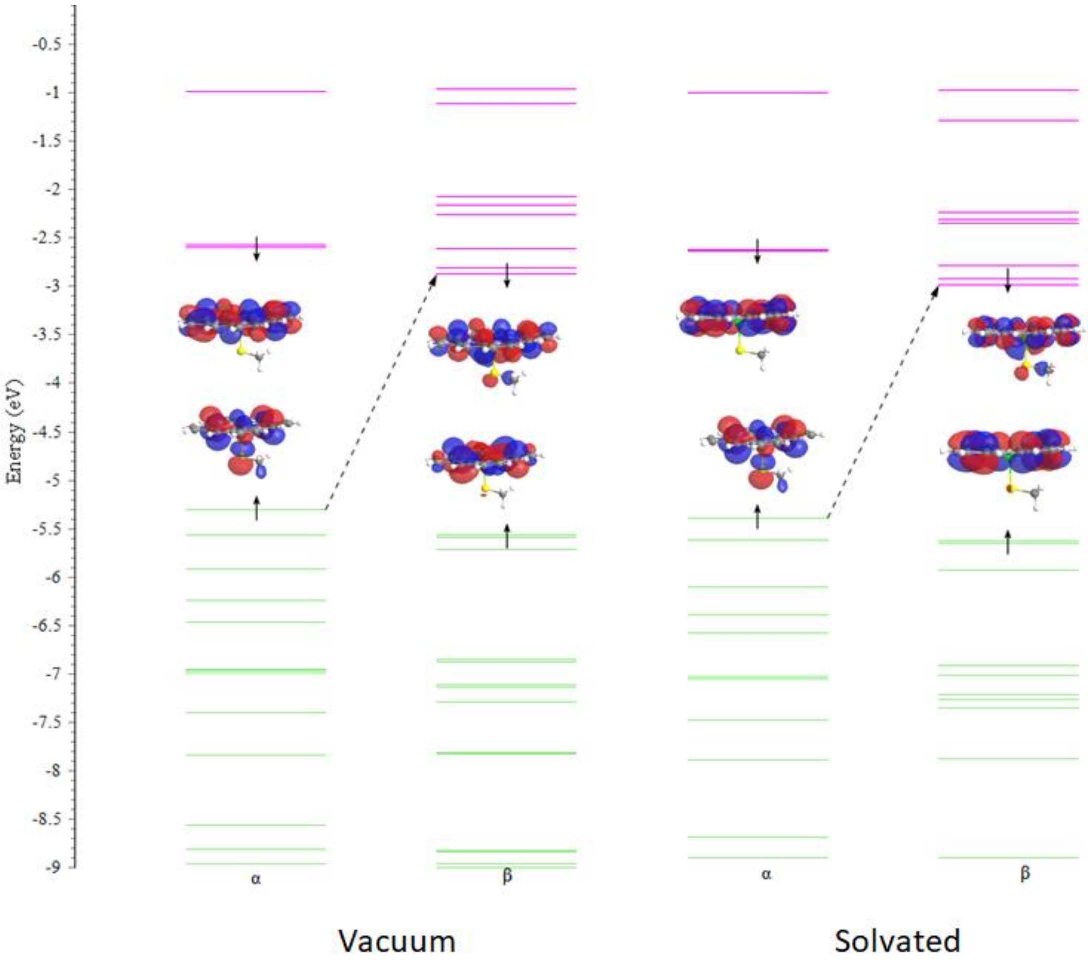

Figure 93. Heme molecular orbitals computed in vacuum and solvation conditions.

Solvation induces a small stabilizing effect on the heme frontier orbitals, but has no effect on the shape of the orbitals. The α-HOMO is predominantly localized on the porphyrin ring, but also extends to the methylthiolate fragment. The phase of this orbital emphasizes the antibonding character that it adds to the iron-sulfur bond. The α-LUMO is delocalized on the porphyrin. The opposite is valid for the β frontier orbitals: the HOMO is mainly localized on the porphyrin ring while the LUMO extends from the porphyrin to the methylthiolate fragment. This β-LUMO also manifests an antibonding effect on the iron-sulfur bond. The HOMO-LUMO transition occurs via an α->β channel.

6.2.1.3 Siroheme: vacuum vs. solvated MOs

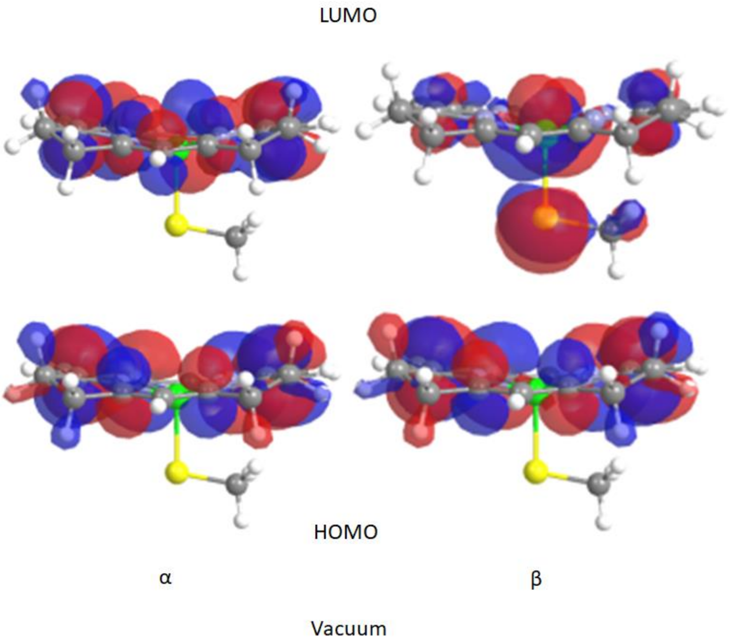

Figure 94. Siroheme frontier MOs computed in vacuum conditions.

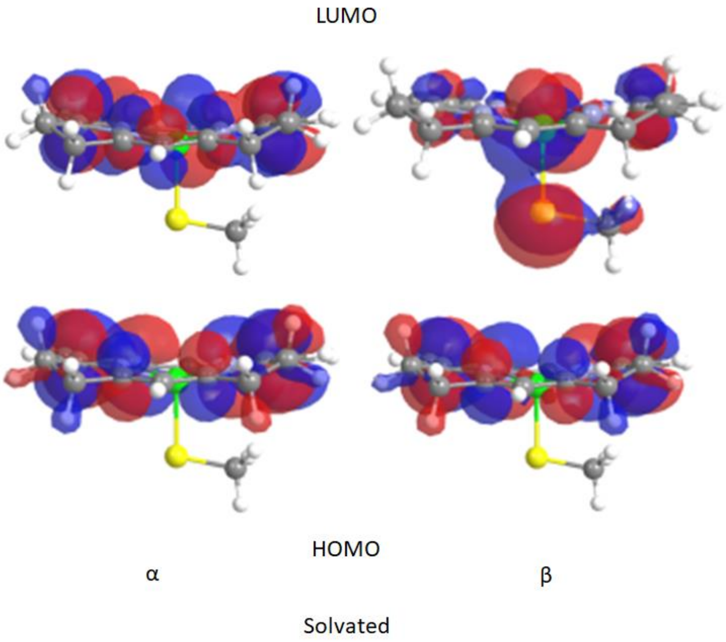

Figure 95. Siroheme frontier MOs computed in solvation conditions.

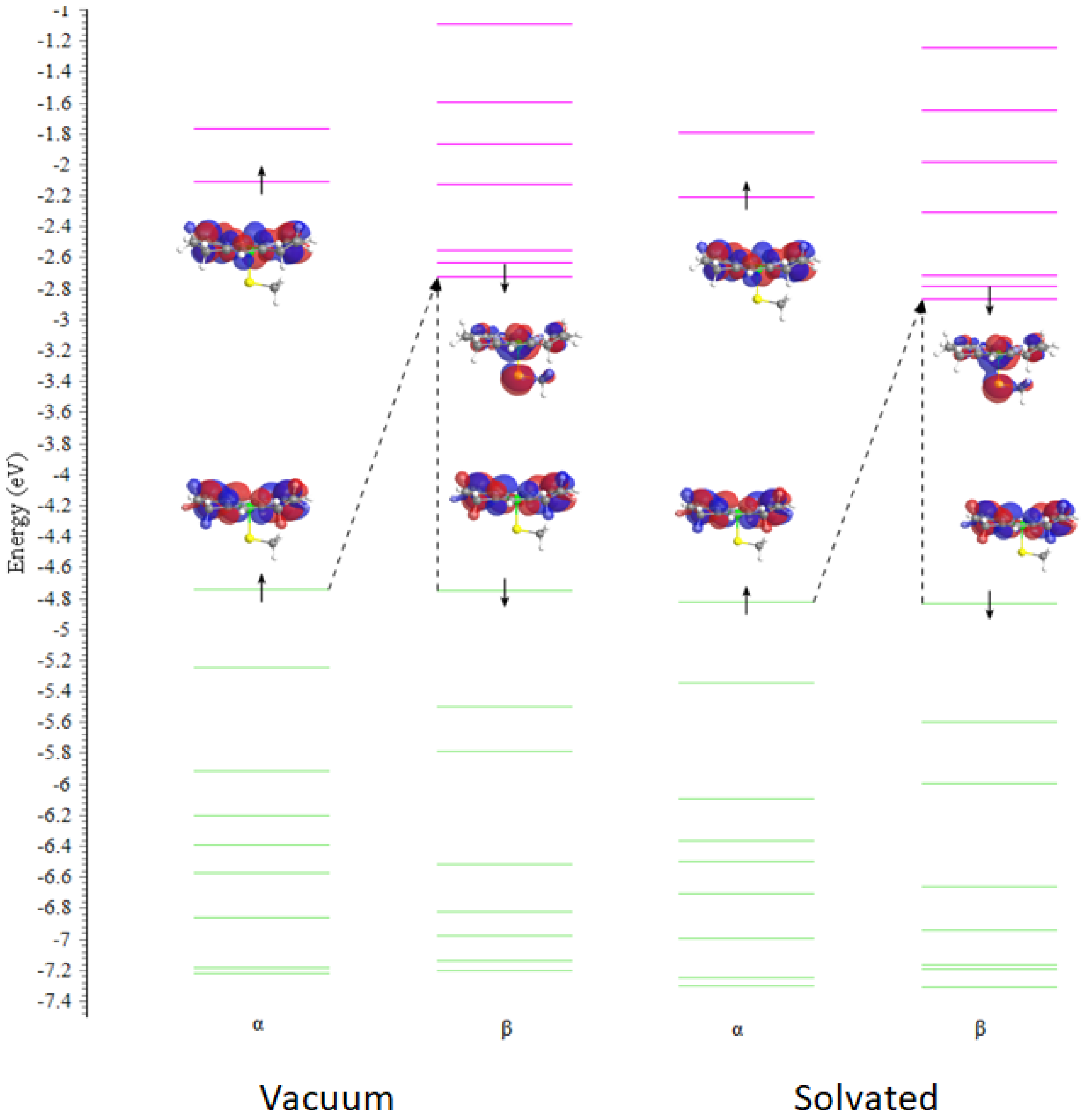

Figure 96. Siroheme molecular orbitals computed in vacuum and solvation conditions.

Both α-HOMO and α-LUMO are localized on the porphyrin ring. The β-HOMO is also porphyrin-localized, but the β-LUMO extends from the porphyin over the methylthiolate fragment and adds antibonding character to the iron-sulfur bond. Solvation slightly stabilizes the MOs. The HOMO-LUMO transition is possible through two degenerate channels: α->β and β->β.

6.2.1.4 Heme vs. siroheme

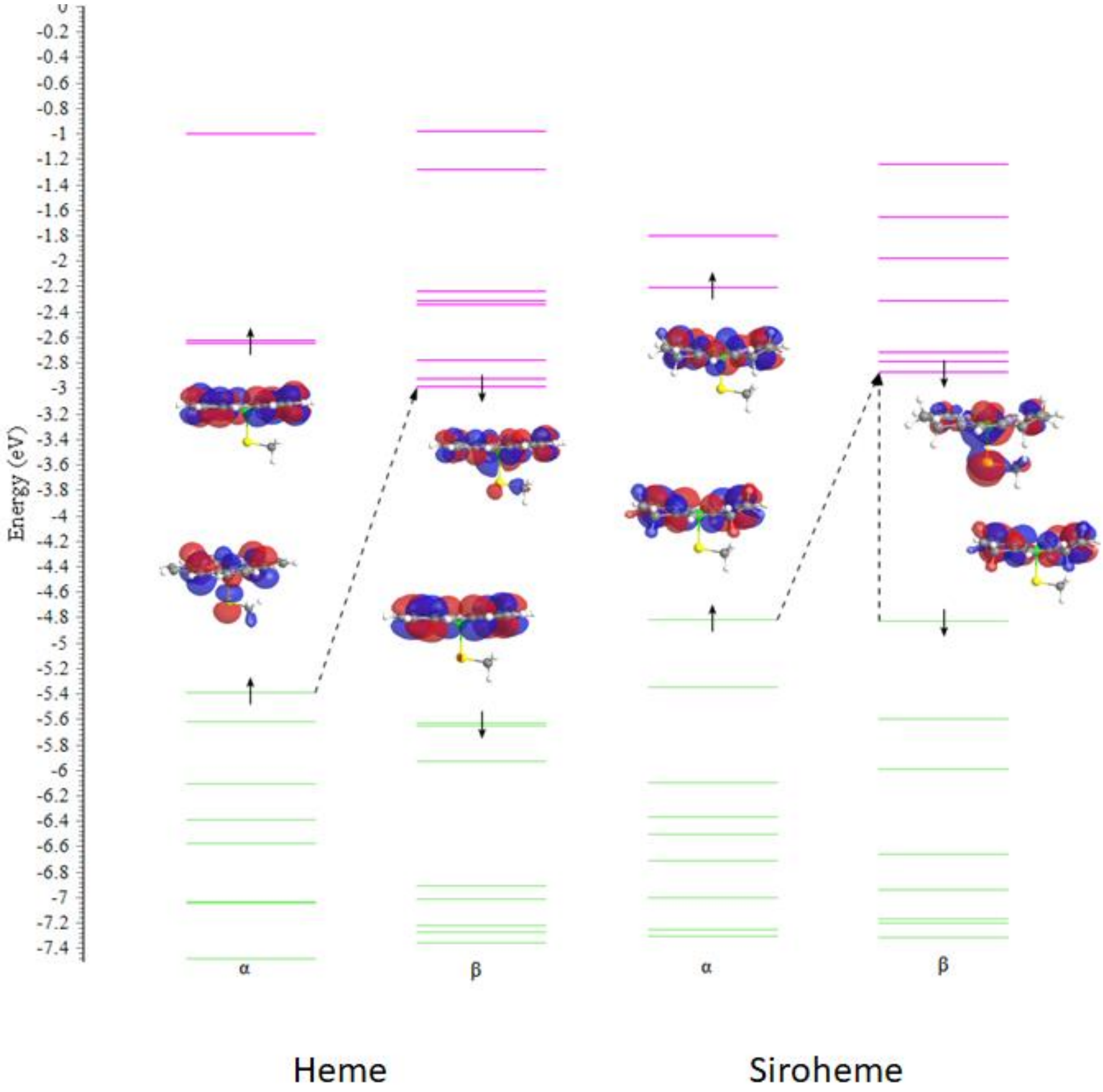

Figure 97. Heme and siroheme molecular orbitals computed solvation conditions.

When changing the porphyrin structure from the heme to the siroheme variant, the α and β HOMO become degenerated and, having the β-LUMO lower-lying that the α-LUMO, the α->β and β->β HOMO-LUMO transitions are possible. Furthermore, siroheme has a slight destabilizing effect on the unoccupied orbitals and strong destabilizing effect on the occupied ones – which leads to a decrease of the HOMO-LUMO gap.

The siroheme HOMO does not have an antibonding character with regard to the iron-sulfur bond, as opposed to the heme HOMO.

6.2.1.5 SiR active site as an electronic transport device

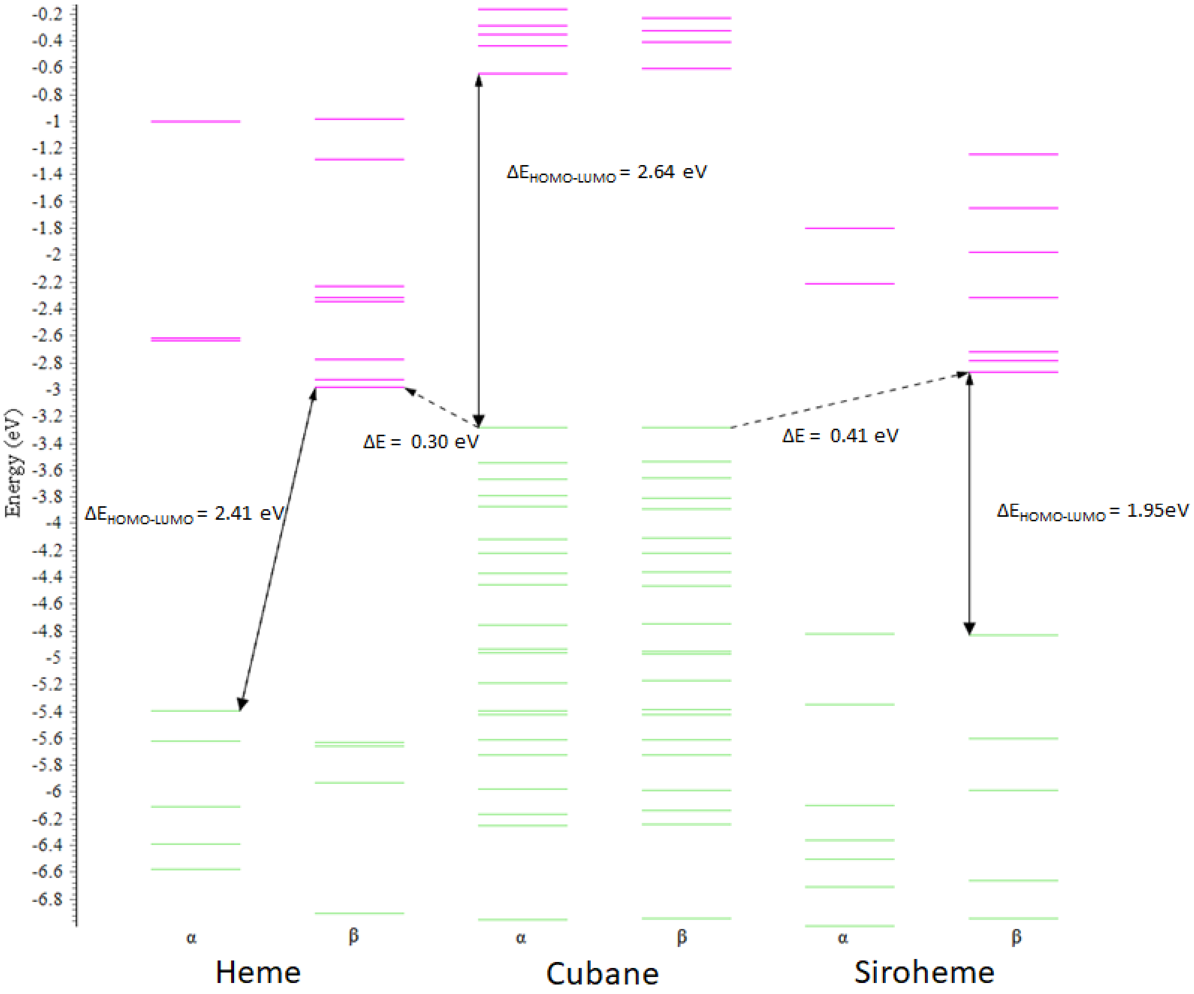

Figure 98. Heme, cubane and siroheme MOs computed in solvation conditions.

The cubane LUMOs lie at a much higher energy than the both heme and siroheme LUMOs. When connected, a transition from the cubane HOMO will occur on a (siro)heme localized LUMO. The heme LUMO is with 0.1 eV more stable than the siroheme LUMO, but for the latter case, the HOMO-LUMO gaps is 0.46 eV smaller.

6.2.1.6 Conclusions

Solvation brings a strong MO stabilization in the cubane model, a modest one in the (siro)heme models and does not change the overall shape of the orbitals.

Having an energetically lower-lying LUMO, the (siro)heme fragment can be regarded as the acceptor part of a donor-acceptor molecule comprised of the (siro)heme and cubane fragments.

6.2.2 (Siro)heme-Cubane MO analysis

6.2.2.1 Heme-Cubane systems

6.2.2.1.1 Ferromagnetic coupled

6.2.2.1.1.1 Solvation influence on the vertical MOs

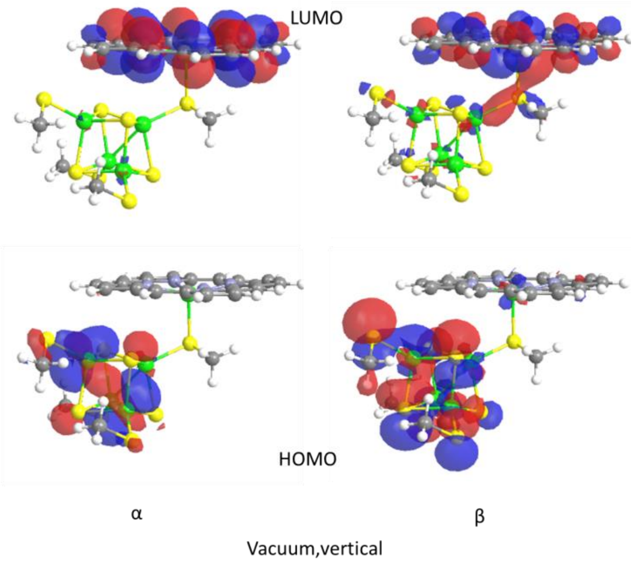

Figure 99. Frontier MOs of the ferromagnetically coupled heme-cubane MOs computed in vertical and vacuum conditions.

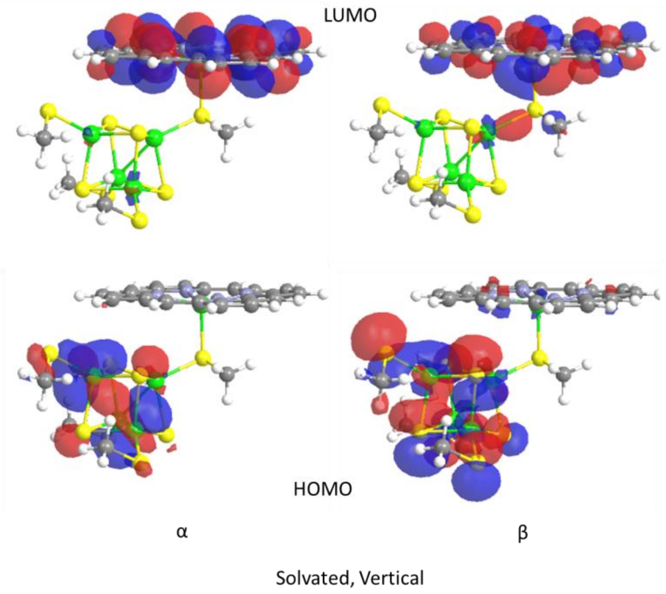

Figure 100. Frontier MOs of the ferromagnetically coupled heme-cubane MOs computed in vertical and solvation conditions.

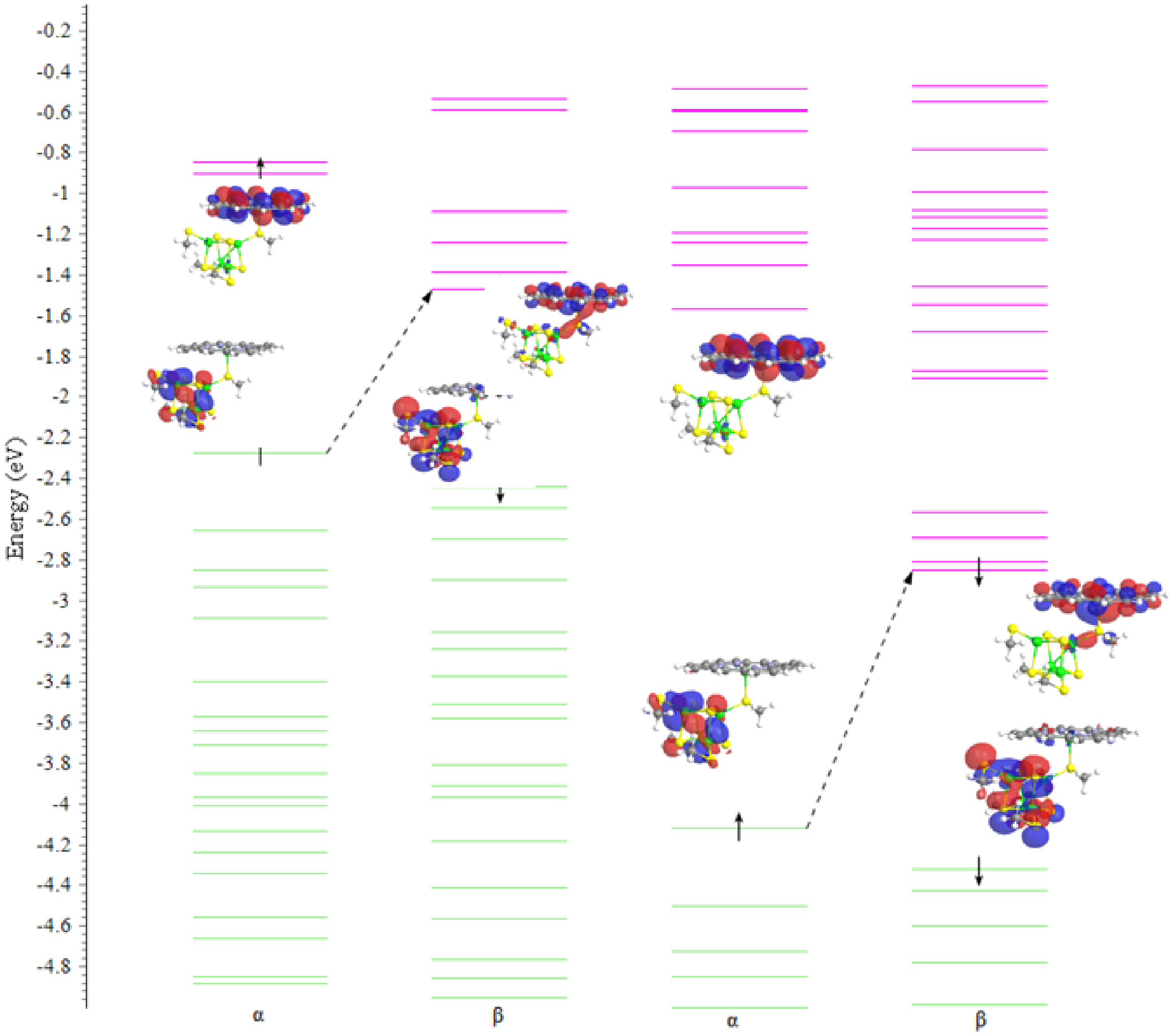

Figure 101. Ferromagnetically coupled heme-cubane vertical MOs computed in vacuum and solvation conditions.

For both the vacuum and the solvated case, the HOMOs reside on the cubane fragment, while the LUMOs are localized on the heme part of the molecule. The β-HOMO, however, is extended over the bridging methylthiolate fragment. Solvation brings strong stabilization of the MOs. The HOMO-LUMO transition is, in both vacuum and solvent, associated with an α->β excitation that delocalizes charge density from the cubane fragment to the to the bridging methylthiolate and heme fragment.

6.2.2.1.1.2 Solvation influence on the relaxed MOs

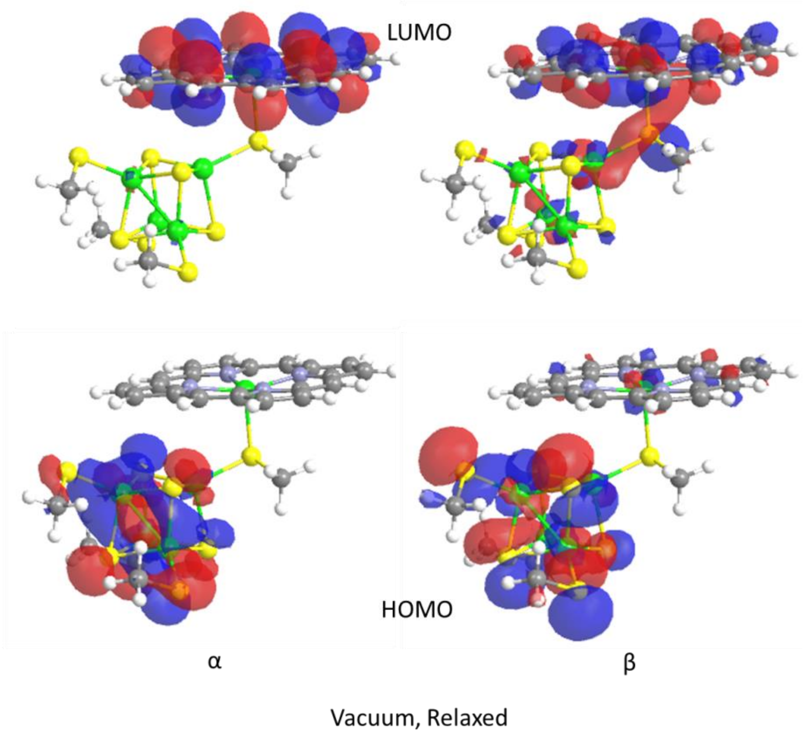

Figure 102. Frontier MOs of the ferromagnetically coupled heme-cubane system computed in relaxed and vacuum conditions.

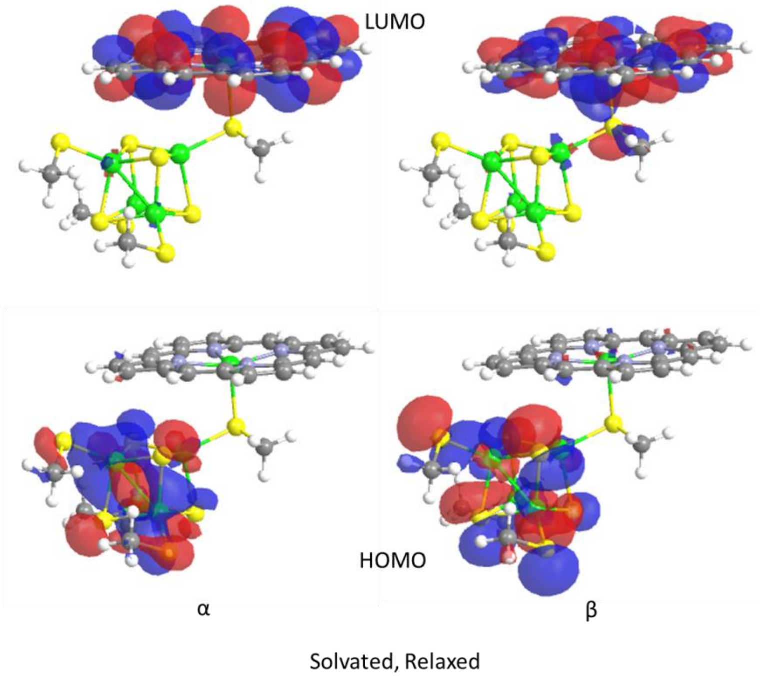

Figure 103. Frontier MOs of the ferromagnetically coupled heme-cubane system computed in relaxed and solvation conditions.

The behavior is similar to the vacuum case, with regard to the localization of the frontier orbitals and the stabilizing effect induced by solvation. The β-HOMO, however, is delocalized and now the HOMO-LUMO occurs via a β->β channel, as opposed to the α->β channel occurring in vacuum.

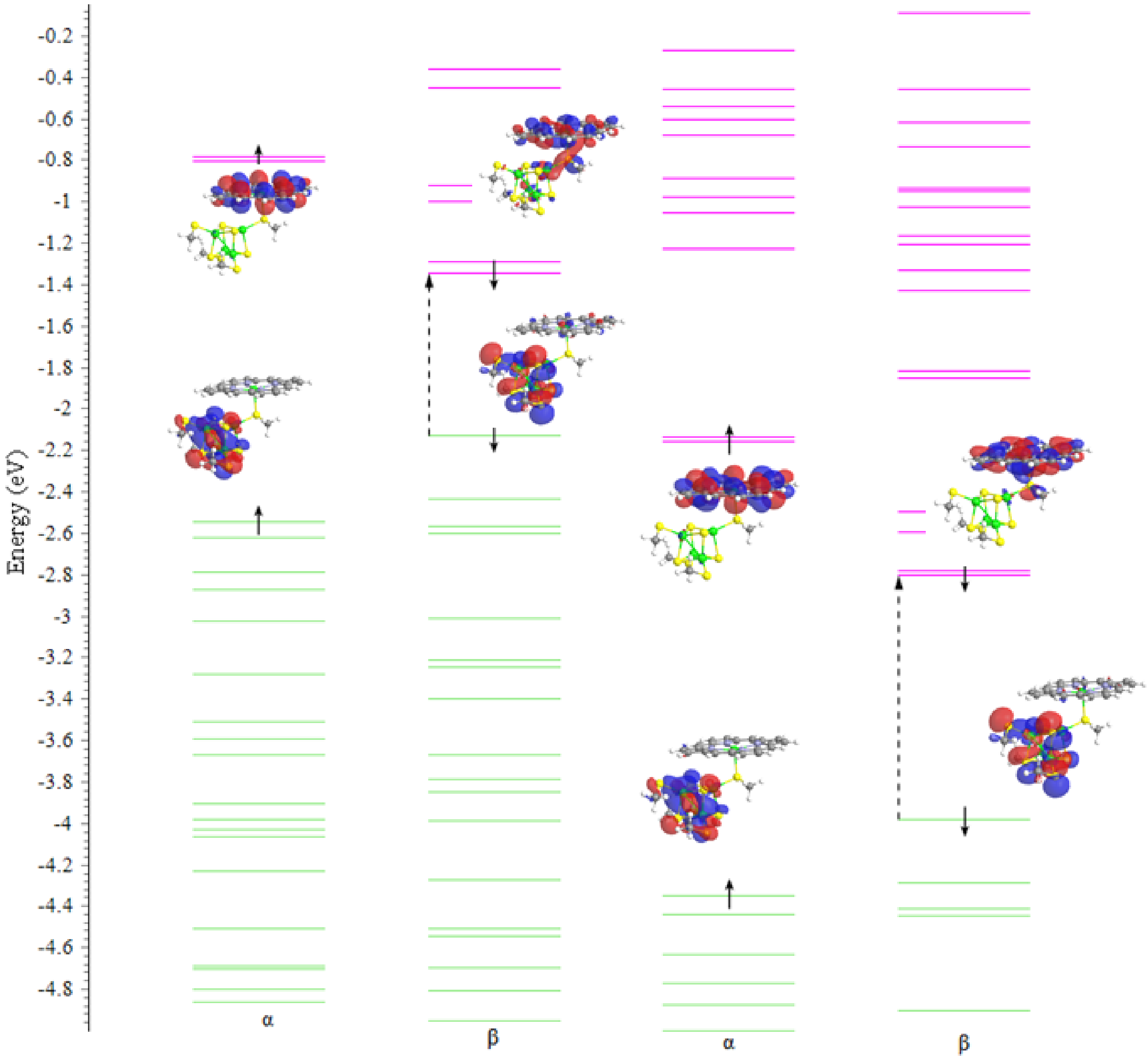

Figure 104. Ferromagnetically coupled heme-cubane relaxed MOs computed in vacuum and solvation conditions.

6.2.2.1.1.3 *Relaxation effects*

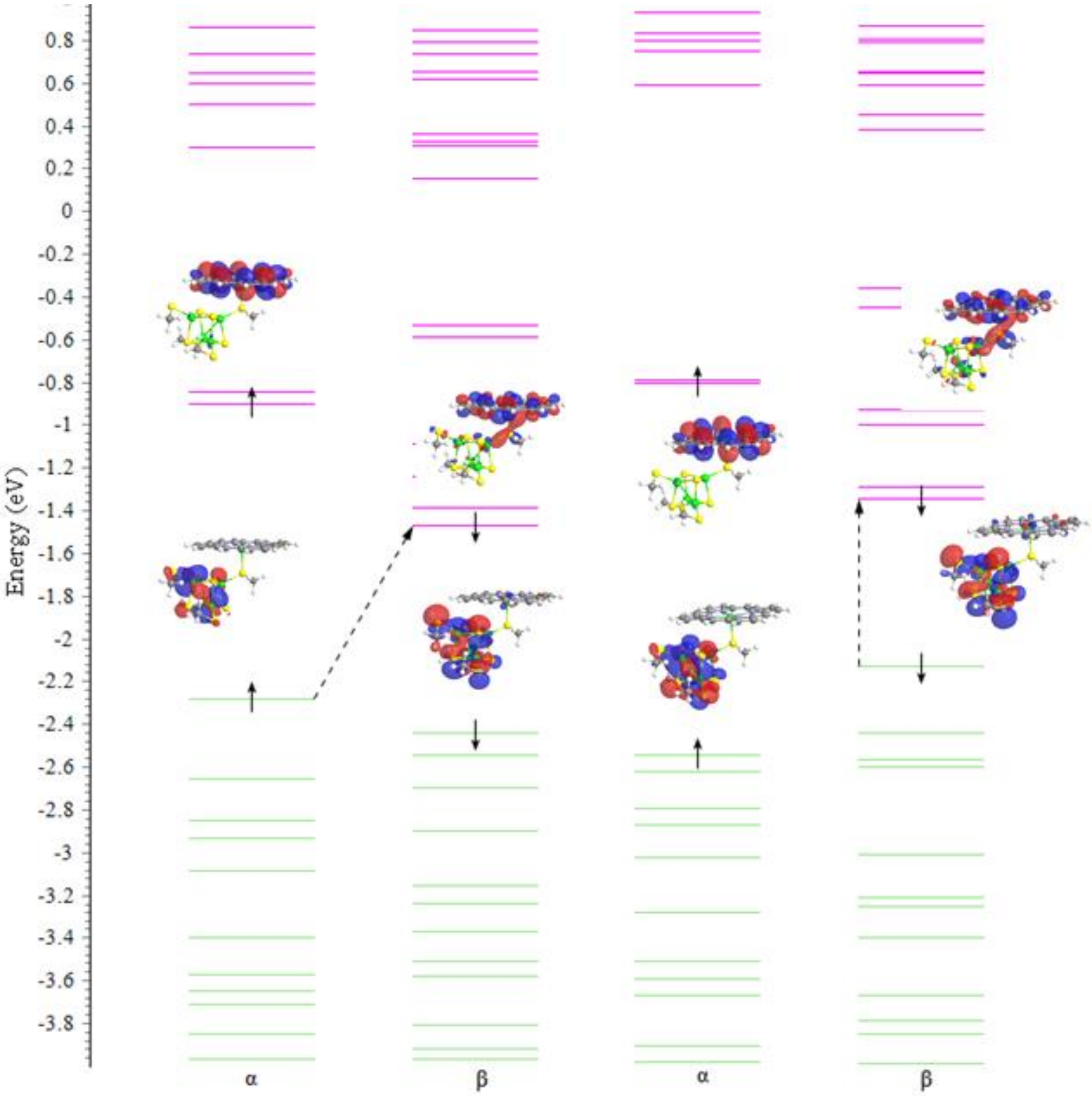

Figure 105. Vertical and relaxed ferromagnetic heme-cubane relaxed MOs computed in vacuum conditions.

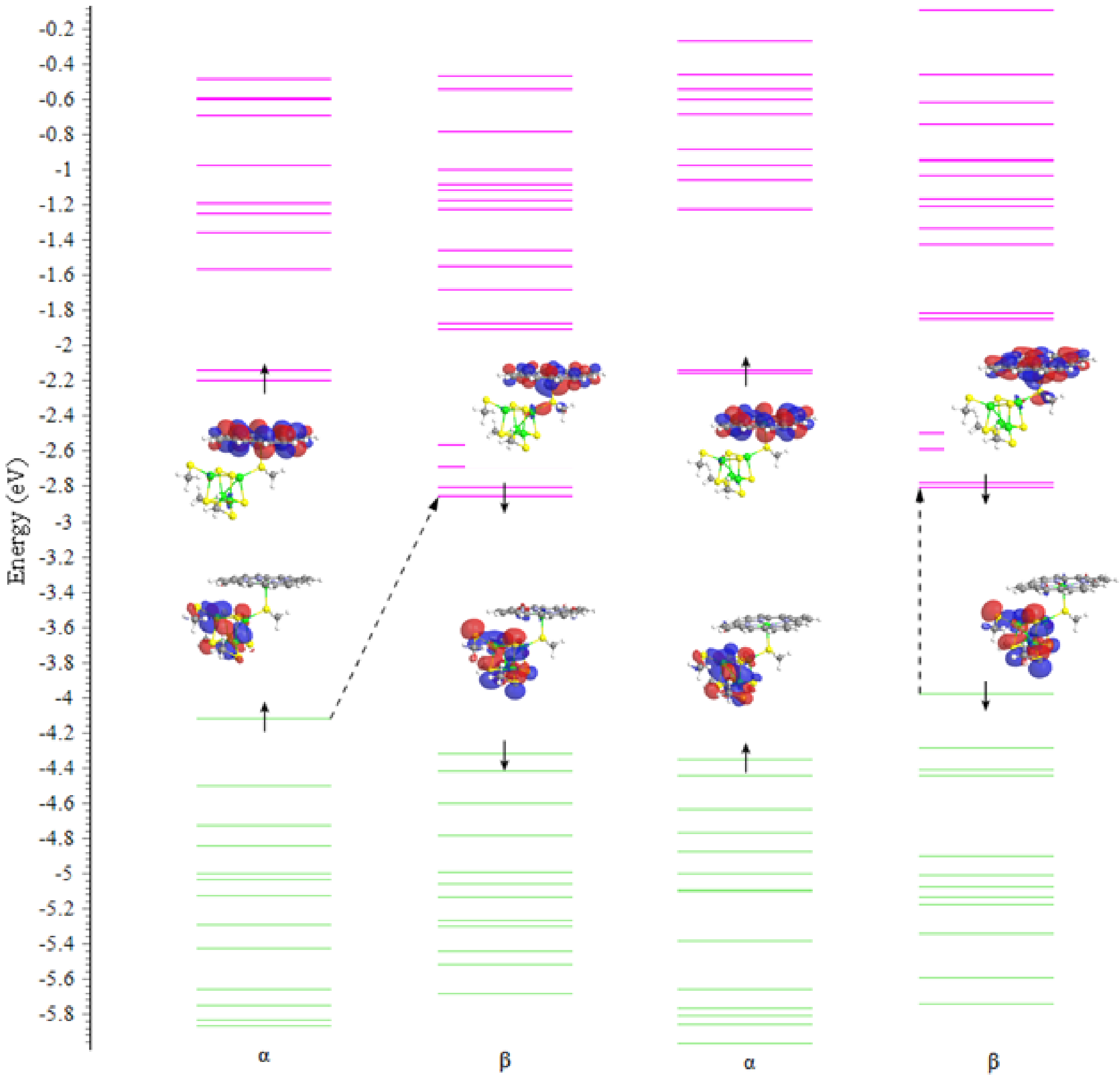

Figure 106. Vertical and relaxed ferromagnetic heme-cubane relaxed MOs computed in solvent conditions.

In vacuum as well as in solvent, relaxation stabilizes the α-HOMO and destabilizes the β-HOMO, while preserving the LUMO energetic levels. Thus relaxation changes the channel of transition from α->β to β->β.

6.2.2.1.2 Antiferromagnetic coupled

6.2.2.1.2.1 Solvation influence on the vertical MOs

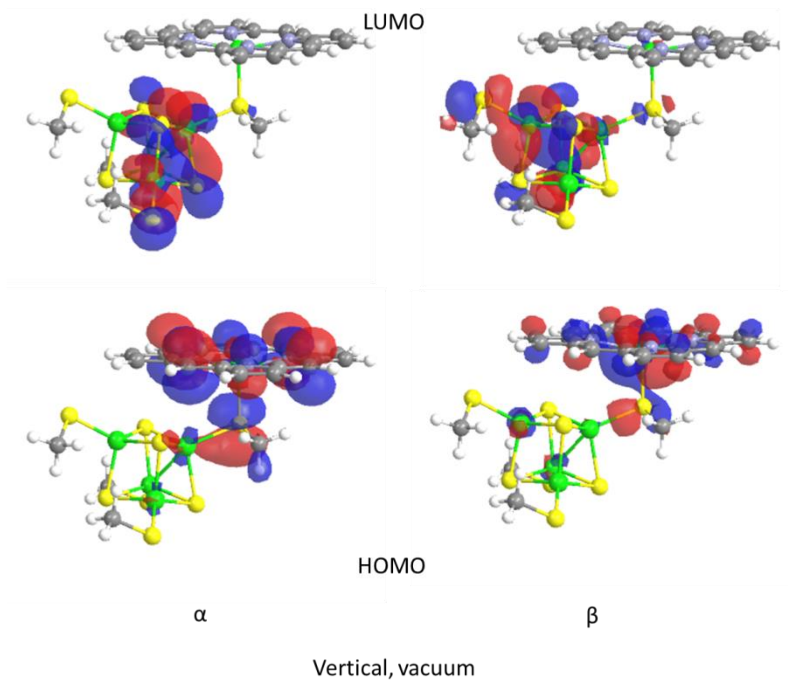

Figure 107. Frontier MOs of the antiferromagnetically coupled heme-cubane MOs computed in vertical and vacuum conditions.

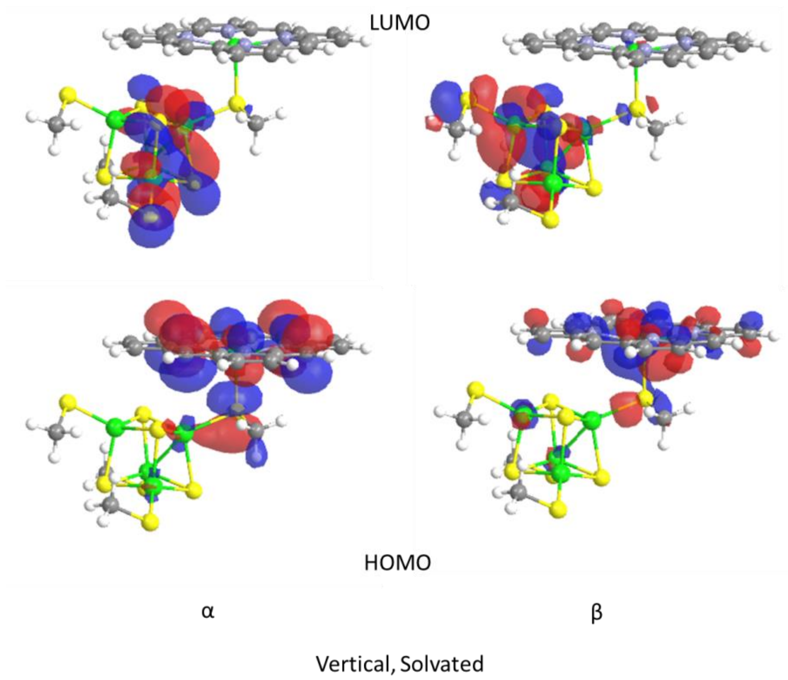

Figure 108. Frontier MOs of the antiferromagnetically coupled heme-cubane MOs computed in vertical and solvation conditions.

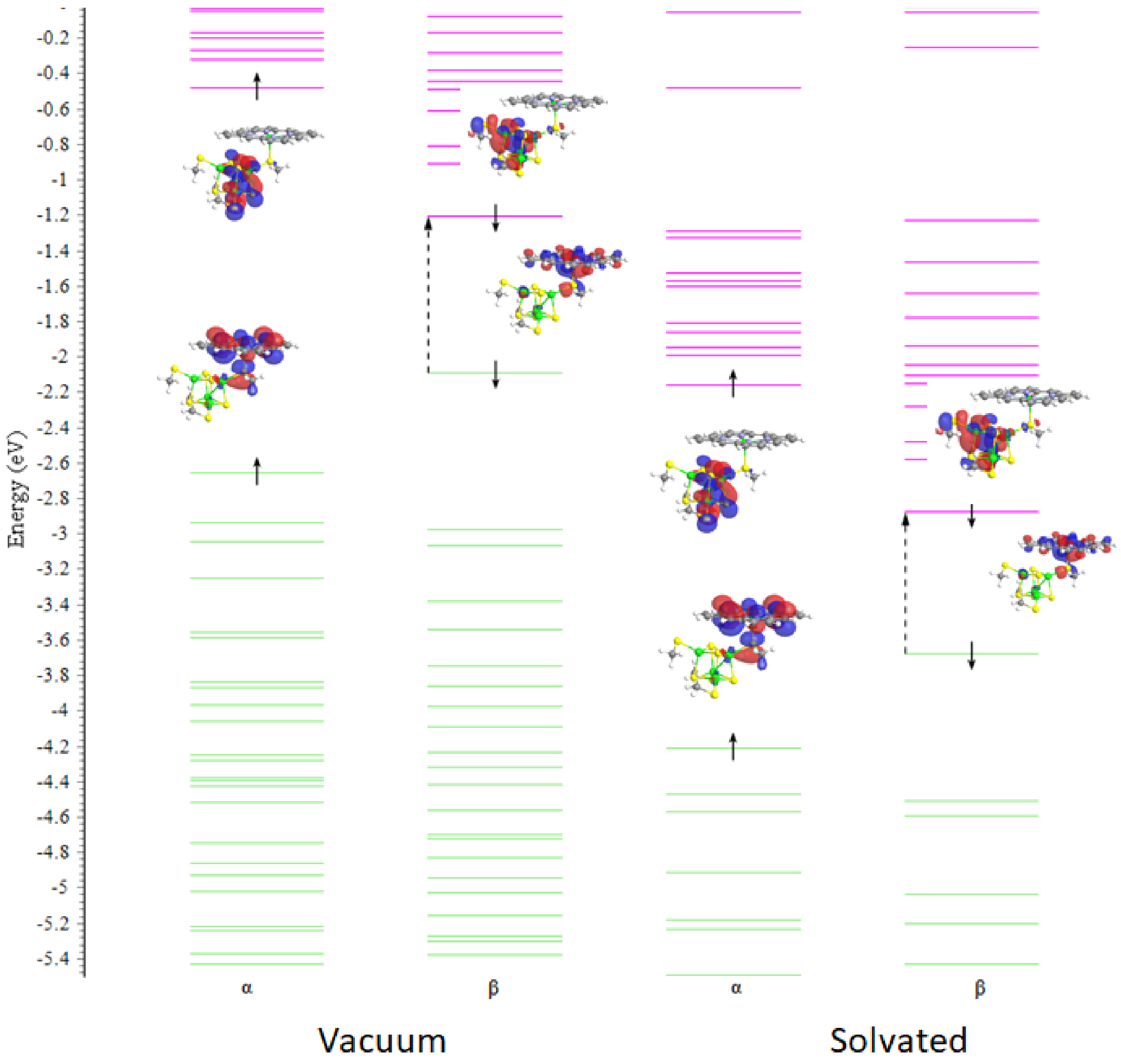

Figure 109. Antierromagnetically coupled heme-cubane vertical MOs computed in vacuum and solvation conditions.

Upon changing the magnetic coupling, the HOMOs become mainly localized on the heme fragment and on the bridging methyltiolate, while the LUMOs localize on the cubane fragment. Solvation stabilizes the MOs, but does not change the β->β.

6.2.2.1.2.2 Solvation influence on the relaxed MOs

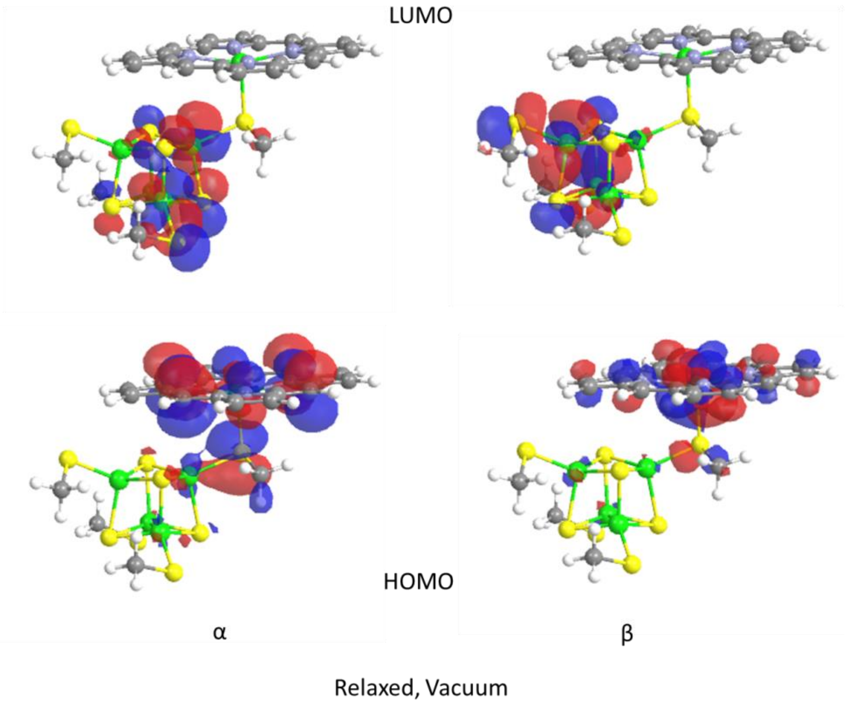

Figure 110. Frontier MOs of the antiferromagnetically coupled heme-cubane MOs computed in vertical and solvation conditions.

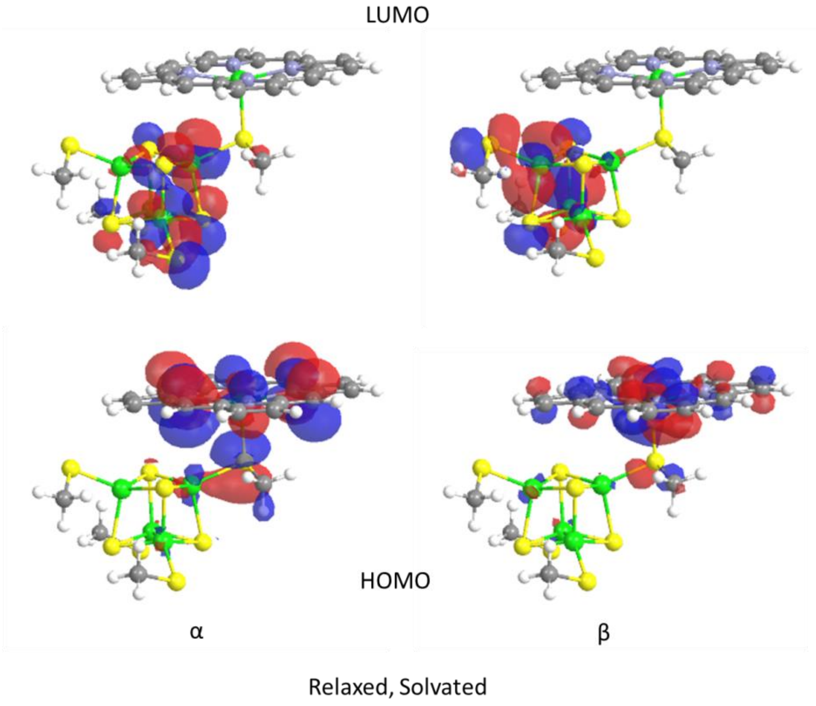

Figure 111. Frontier MOs of the antiferromagnetically coupled heme-cubane MOs computed in relaxed and solvation conditions.

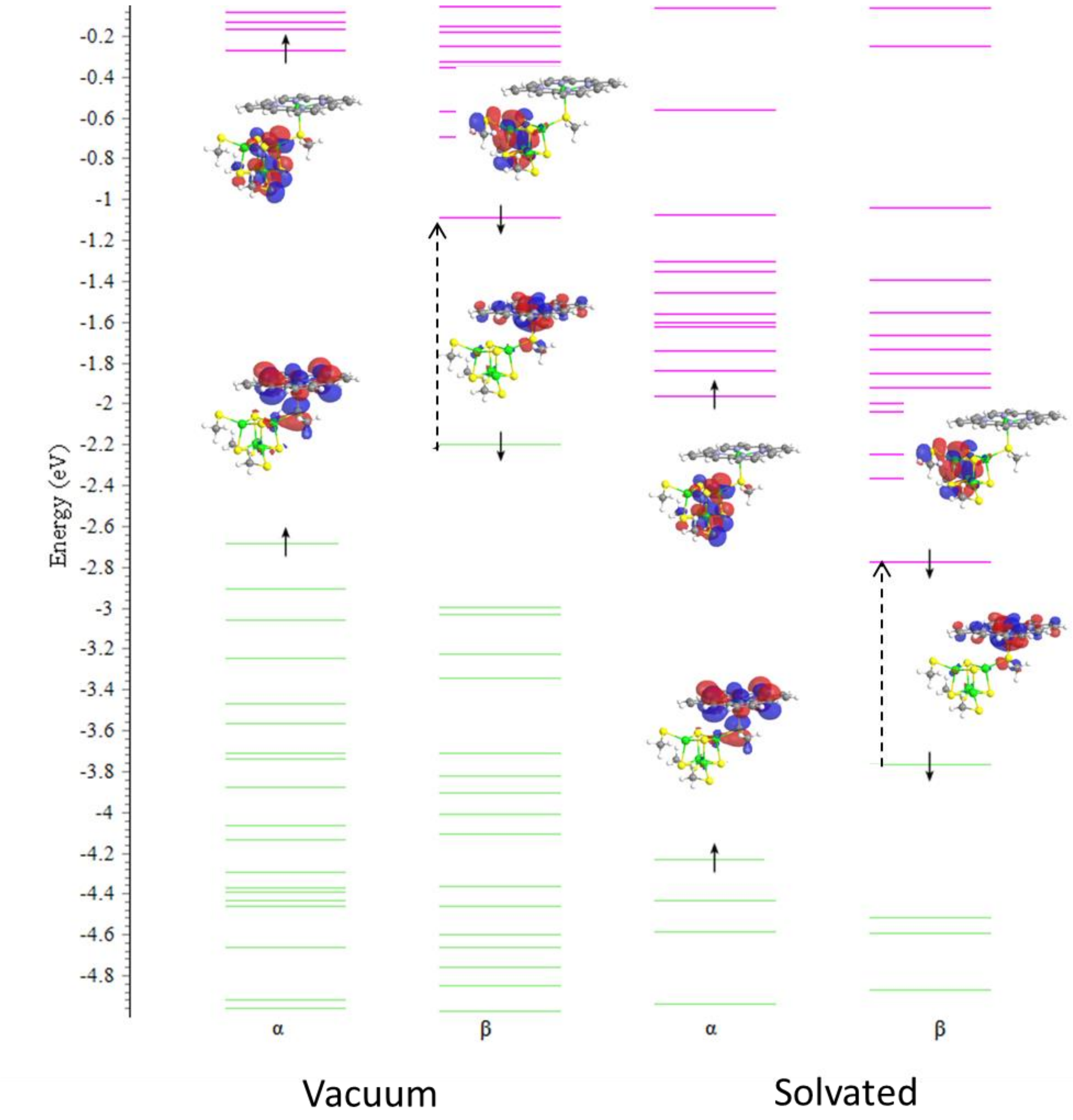

Figure 112. Antierromagnetic coupled heme-cubane vertical MOs computed in relaxed and solvation conditions.

The shape and position of the frontier orbitals remain unchanged.

6.2.2.1.2.3 Relaxation effects

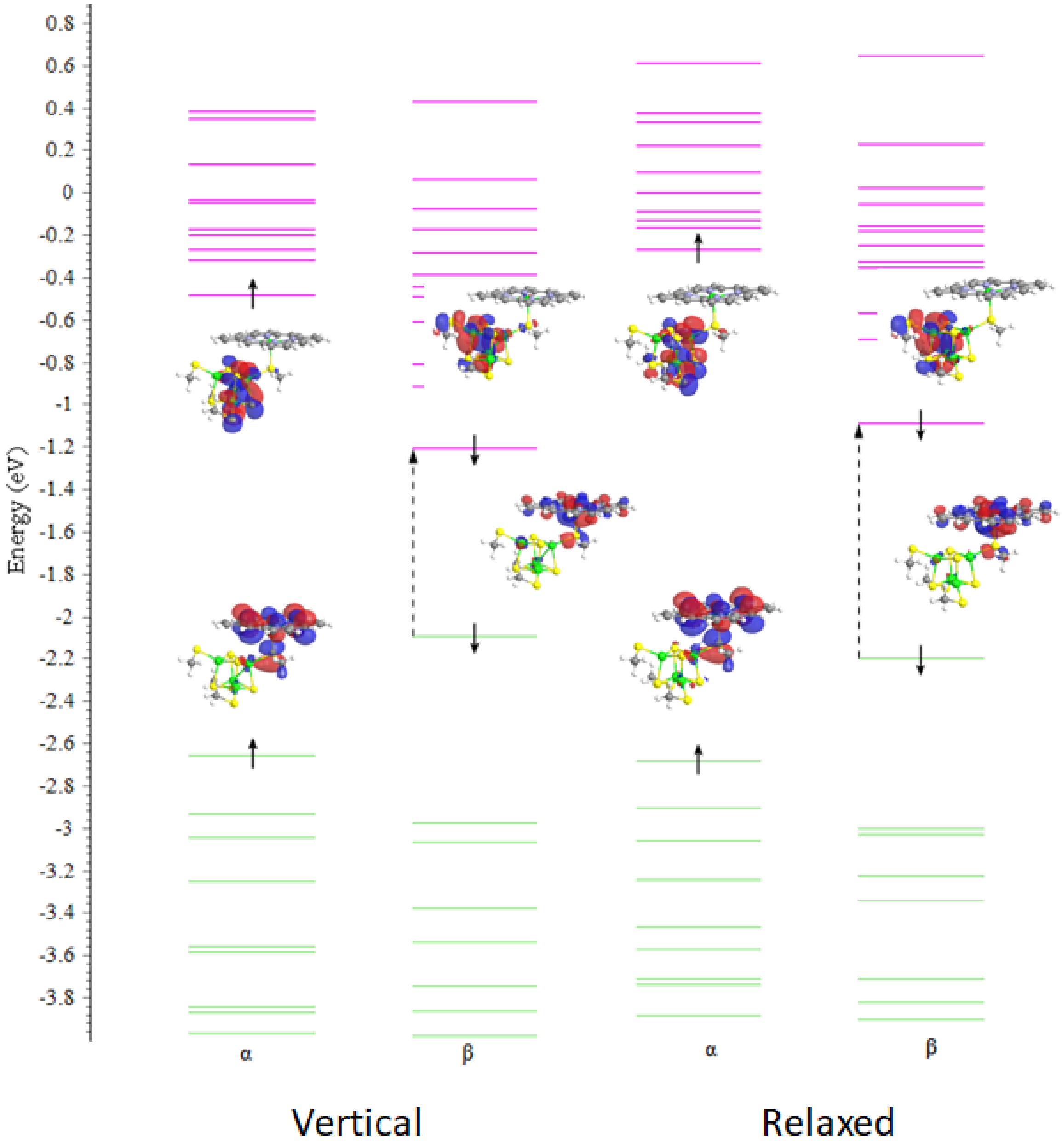

Figure 113. Antiferromagnetically coupled heme-cubane vertical and relaxed MOs computed in vacuum conditions.

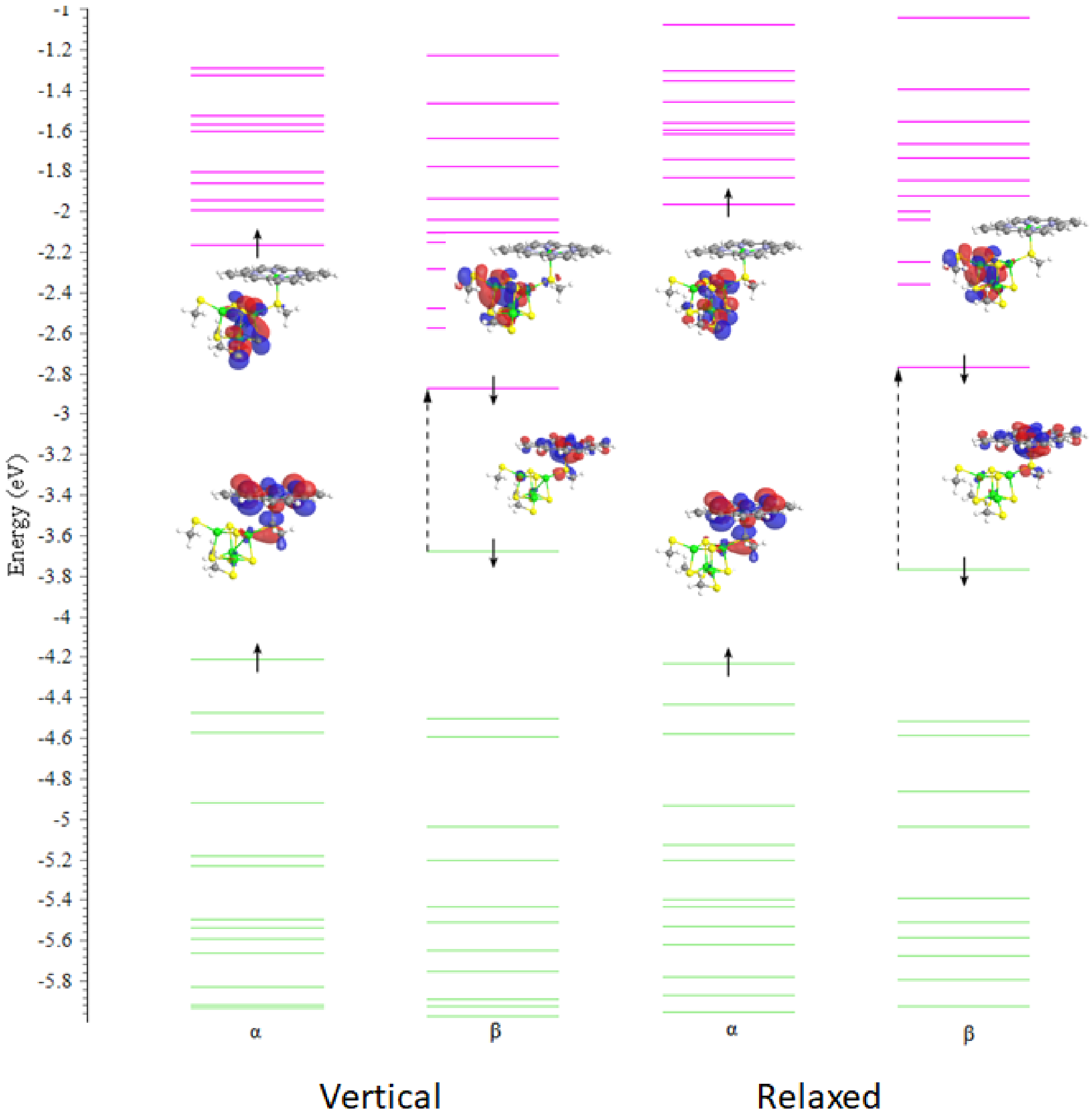

Figure 114 Antiferromagnetically coupled heme-cubane vertical and relaxed MOs computed in vacuum conditions.

Relaxation does not bring significant changes.

6.2.2.1.3 Ferromagnetic vs. Antiferromagnetic coupled systems

A HOMO-LUMO excitation occurring in the ferromagnetic coupled regime is associated with a charge transfer from the cubane to the heme fragment. The same excitation performed in the antiferromagnetic regime is responsible with the inverse charge transfer, i.e. from heme to cubane.

6.2.2.1.4 Conclusions

In heme-cubane high-spin ferric models the magnetic coupling regime employed (i.e. anti- or ferromagnetic) modulates the direction of the heme ←→ cubane charge transfer associated with the HOMO-LUMO excitation.

6.2.2.2 Siroheme-Cubane systems

6.2.2.2.1 Ferromagnetic coupled

6.2.2.2.1.1 Solvation influence on the vertical MOs

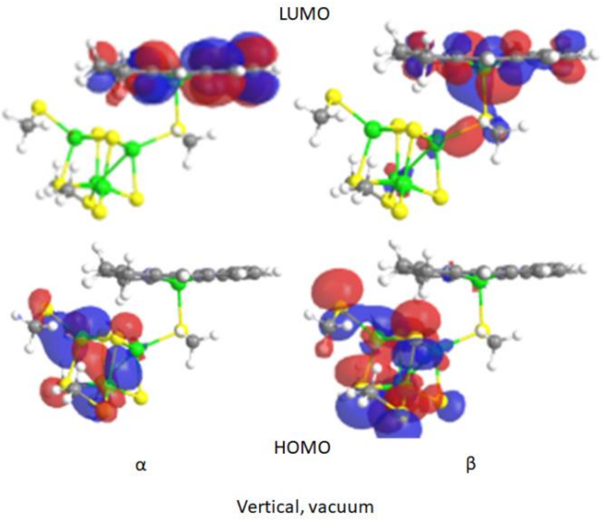

Figure 115. Frontier MOs of the ferromagnetically coupled siroheme-cubane MOs computed in vertical and vacuum conditions.

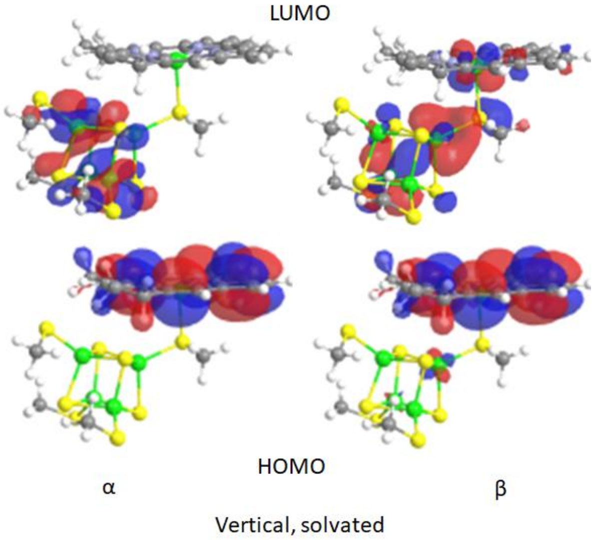

Figure 116. Frontier MOs of the ferromagnetically coupled siroheme-cubane MOs computed in vertical and solvation conditions.

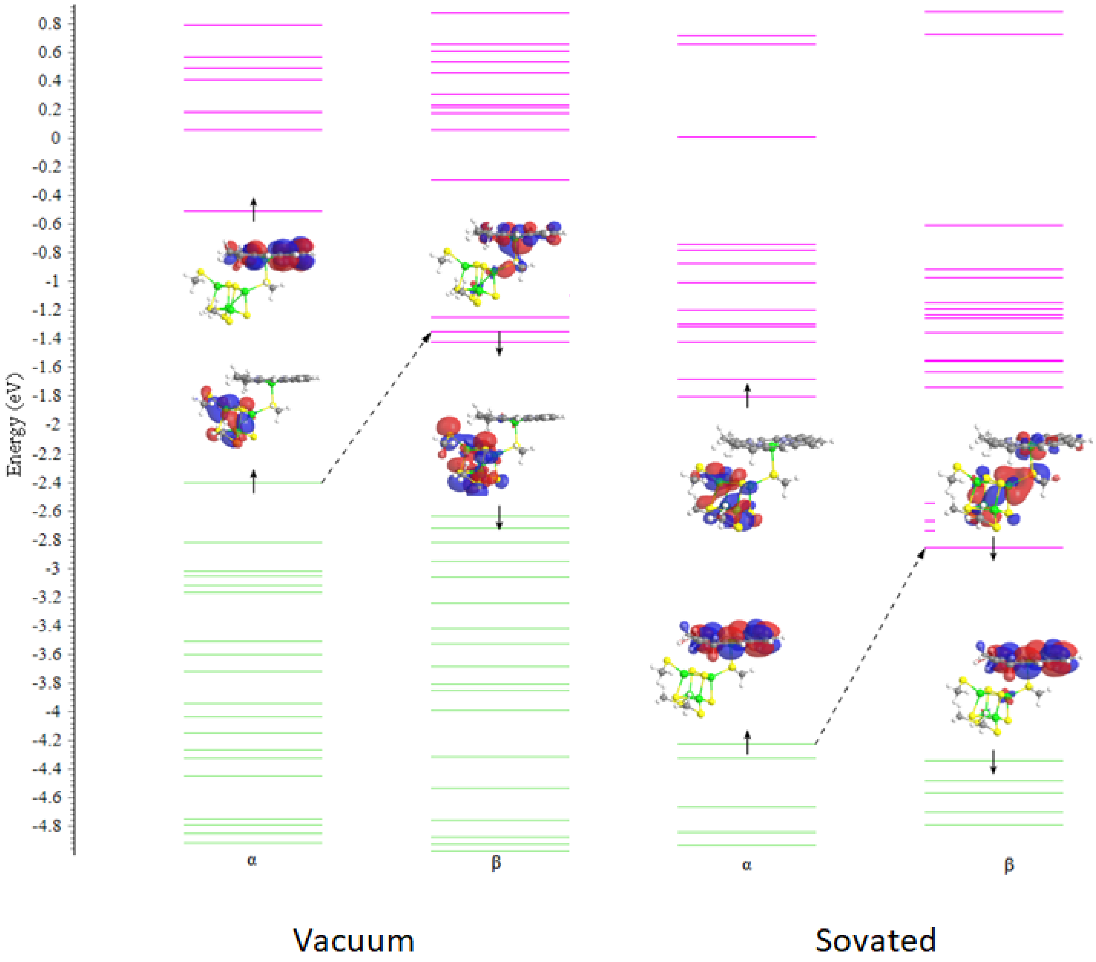

Figure 117. Ferromagnetically coupled siroheme-cubane vertical MOs computed in vacuum and solvation conditions.

Similar to the heme-cubane correspondent, the HOMOs reside on the cubane fragment and LUMOs on the bridging methylthiolate and siroheme fragment. In solvent, however, the HOMOs become localized on the siroheme fragment while the α-LUMO on the cubane and the β-LUMO delocalize over both fragments.

6.2.2.2.1.2 Solvation influence on the relaxed MOs

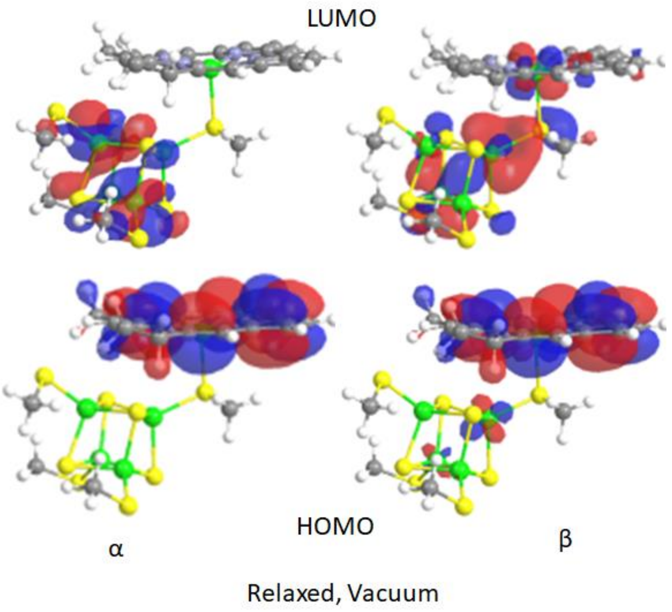

Figure 118. Frontier MOs of the ferromagnetically coupled siroheme-cubane MOs computed in relaxed and vacuum conditions.

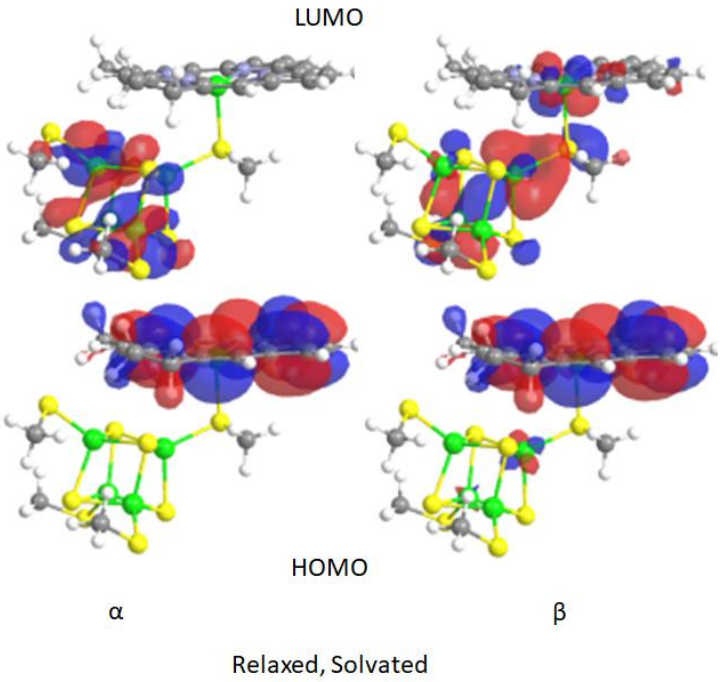

Figure 119. Frontier MOs of the ferromagnetically coupled siroheme-cubane MOs computed in relaxed and solvation conditions.

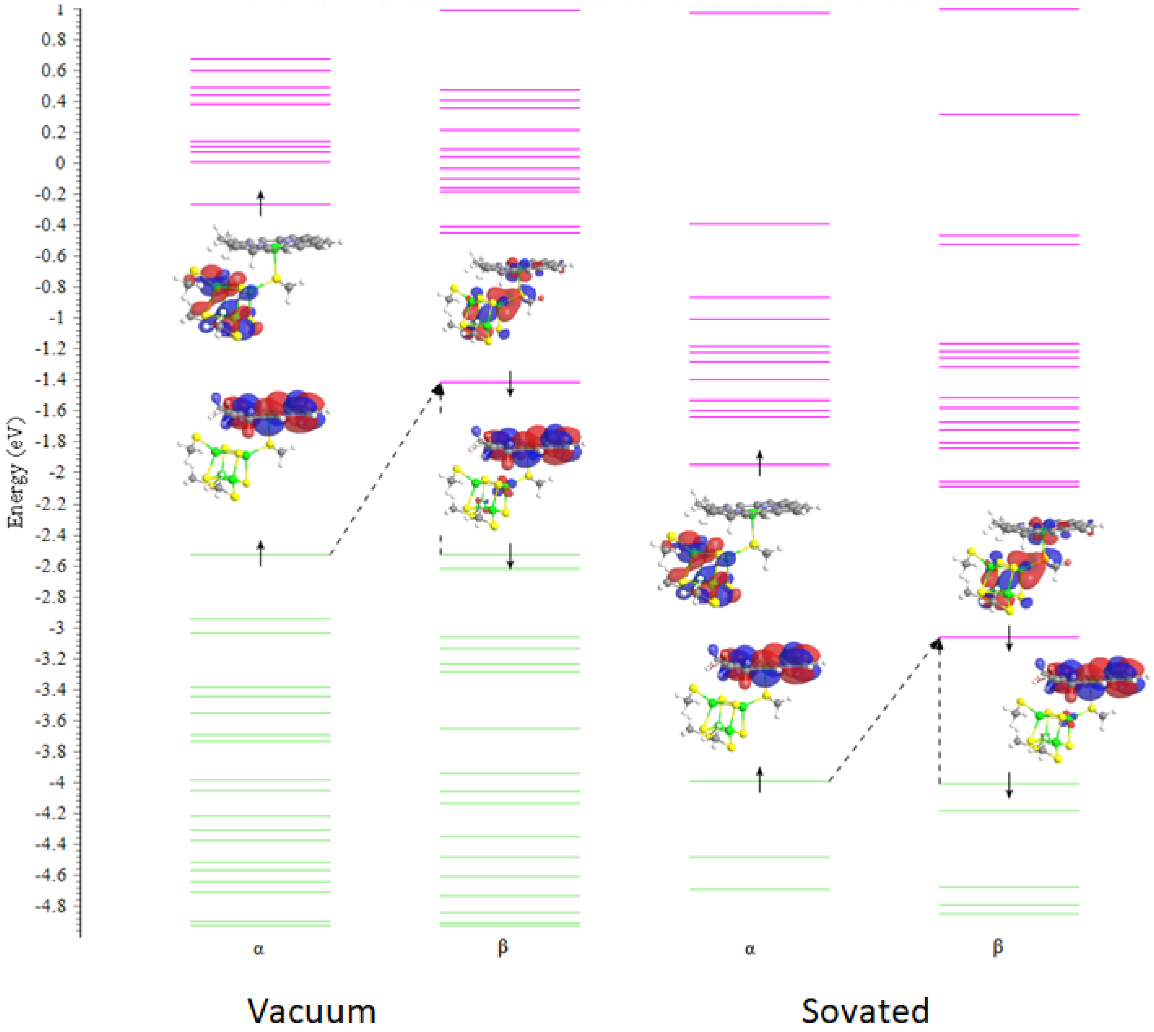

Figure 120. Ferromagnetically coupled siroheme-cubane relaxed MOs computed in vacuum and solvation conditions.

6.2.2.2.1.3 Relaxation effects

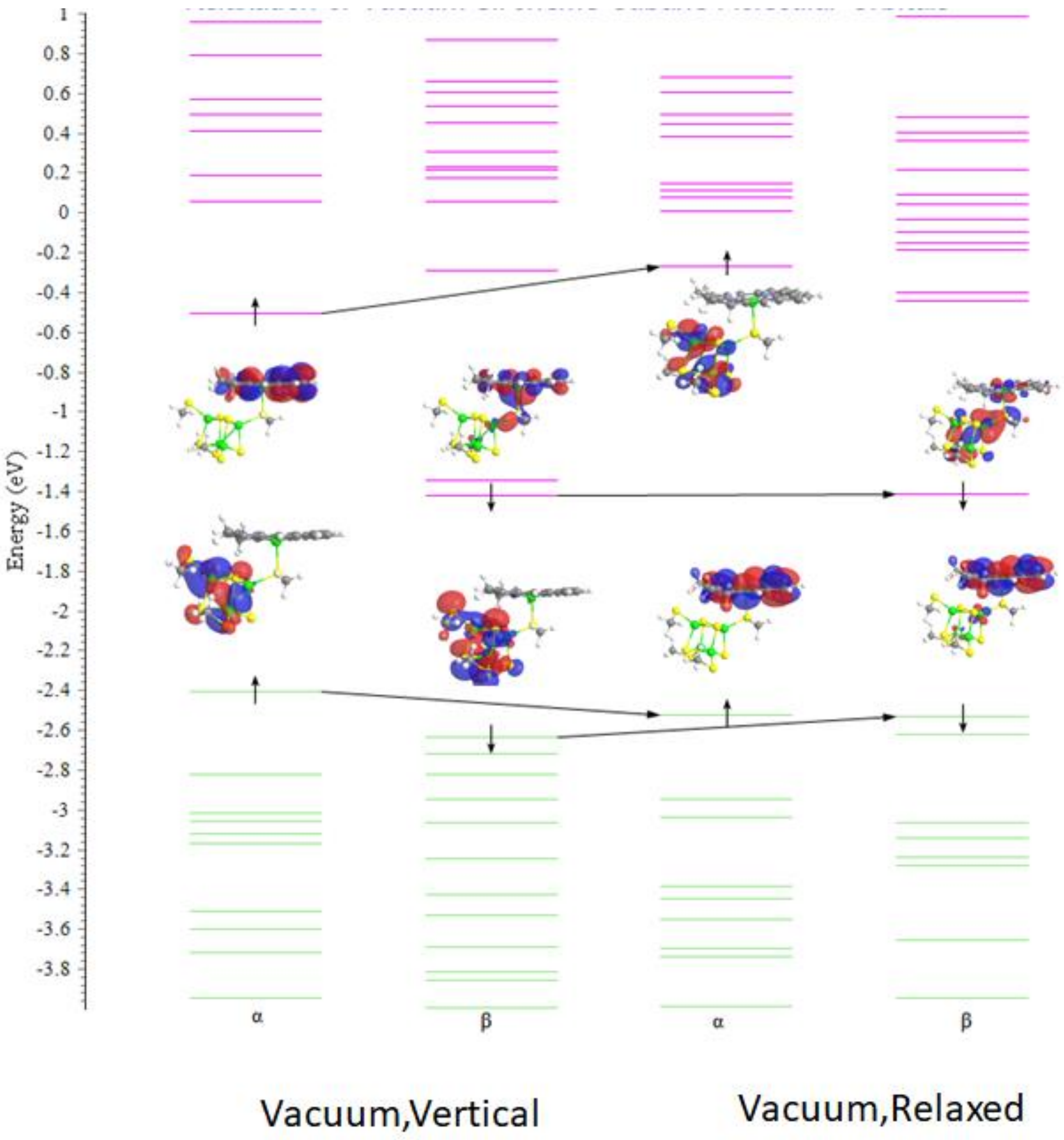

Figure 121. Vertical and relaxed ferromagnetic siroheme-cubane relaxed MOs computed in vacuum conditions.

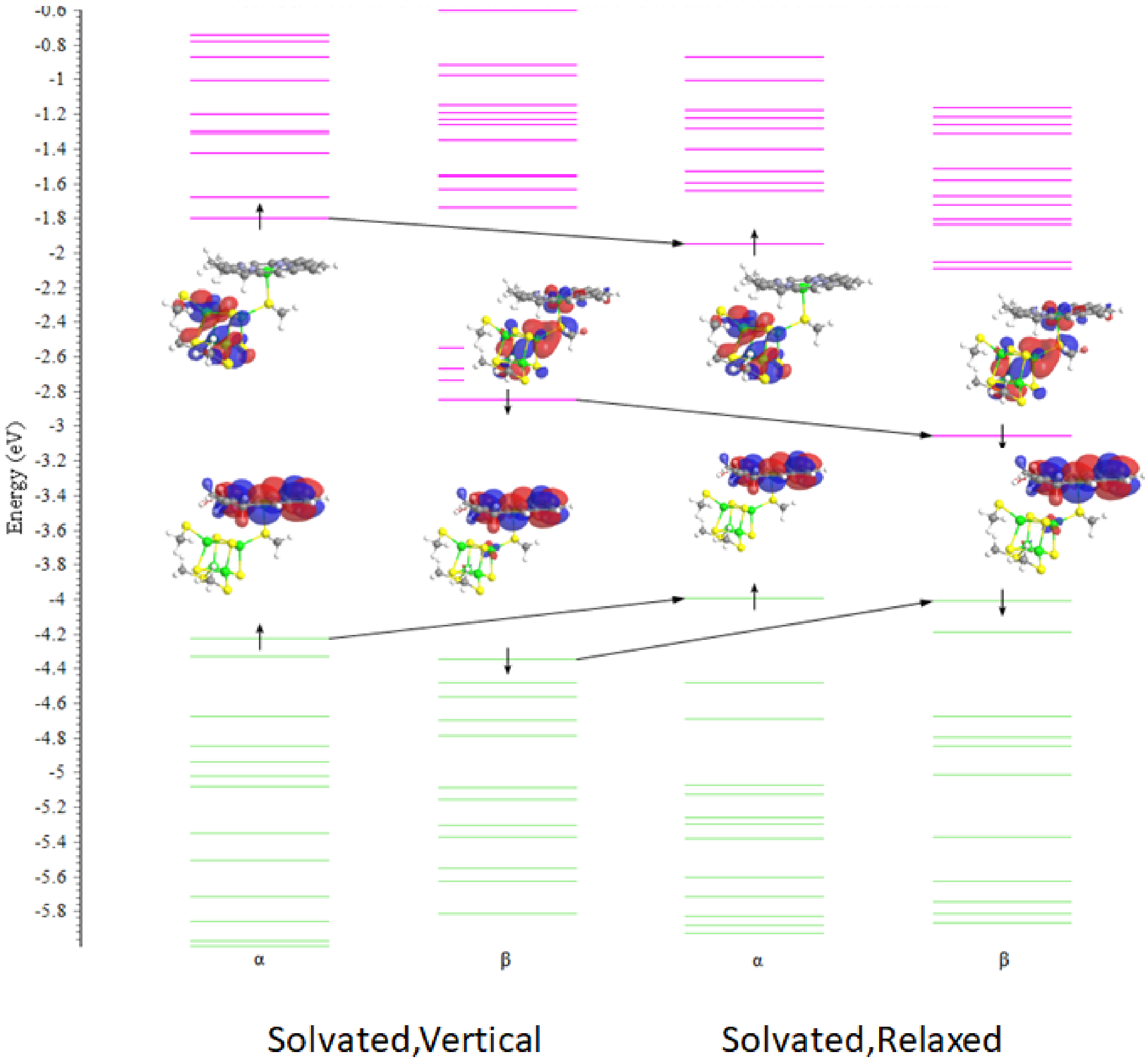

Figure 122. Vertical and relaxed ferromagnetic siroheme-cubane relaxed MOs computed in solvation conditions.

In vacuum, the relaxation process stabilizes the α-HOMO, destabilizes the α-LUMO and the β-HOMO while leaving the β-LUMO unaffected. Furthermore, the HOMOs change their localisation from the cubane to the siroheme fragment.

When relaxed in solvent, the HOMOs are destabilized and LUMOs stabilized, and thus a decrease in HOMO-LUMO gap is obtained.

Relaxation modifies the excitation channel from the α→β found in vacuum to the double degenerated channel α→β and β→β present in solvent.

6.2.2.2.2 Antiferromagnetic coupled

6.2.2.2.2.1 Solvation influence on the vertical MOs

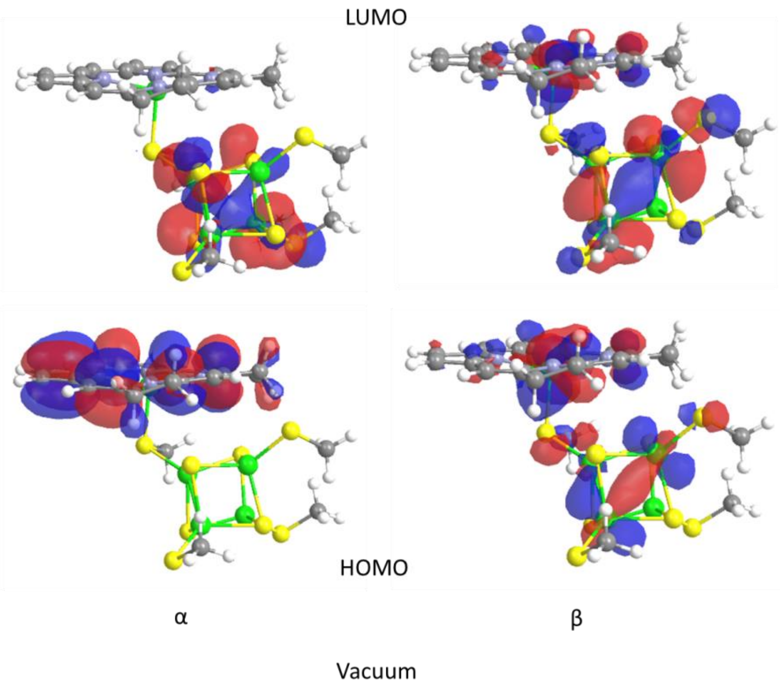

Figure 123. Frontier MOs of the antiferromagnetically coupled siroheme-cubane MOs computed in vertical and vacuum conditions.

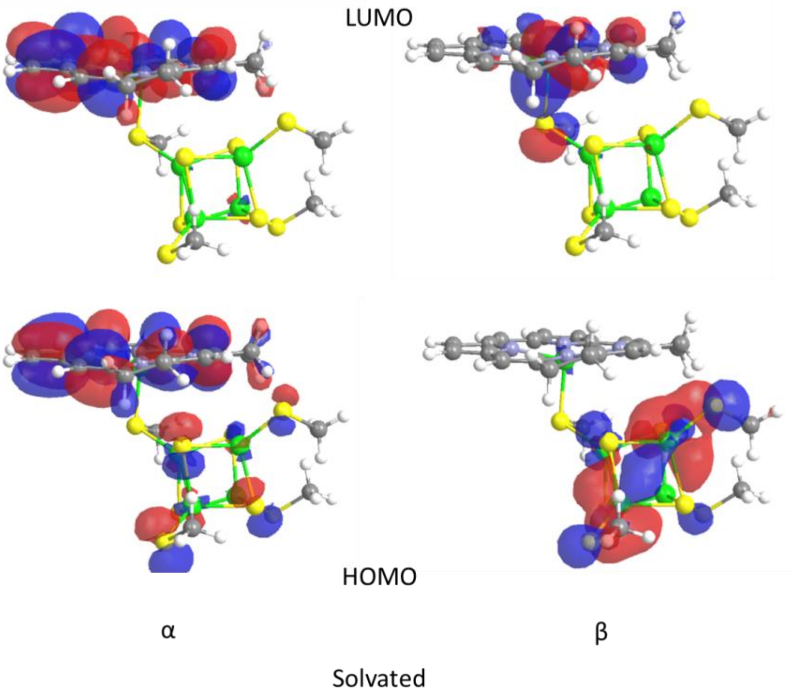

Figure 124 . Frontier MOs of the antiferromagnetically coupled siroheme-cubane MOs computed in vertical and solvation conditions.

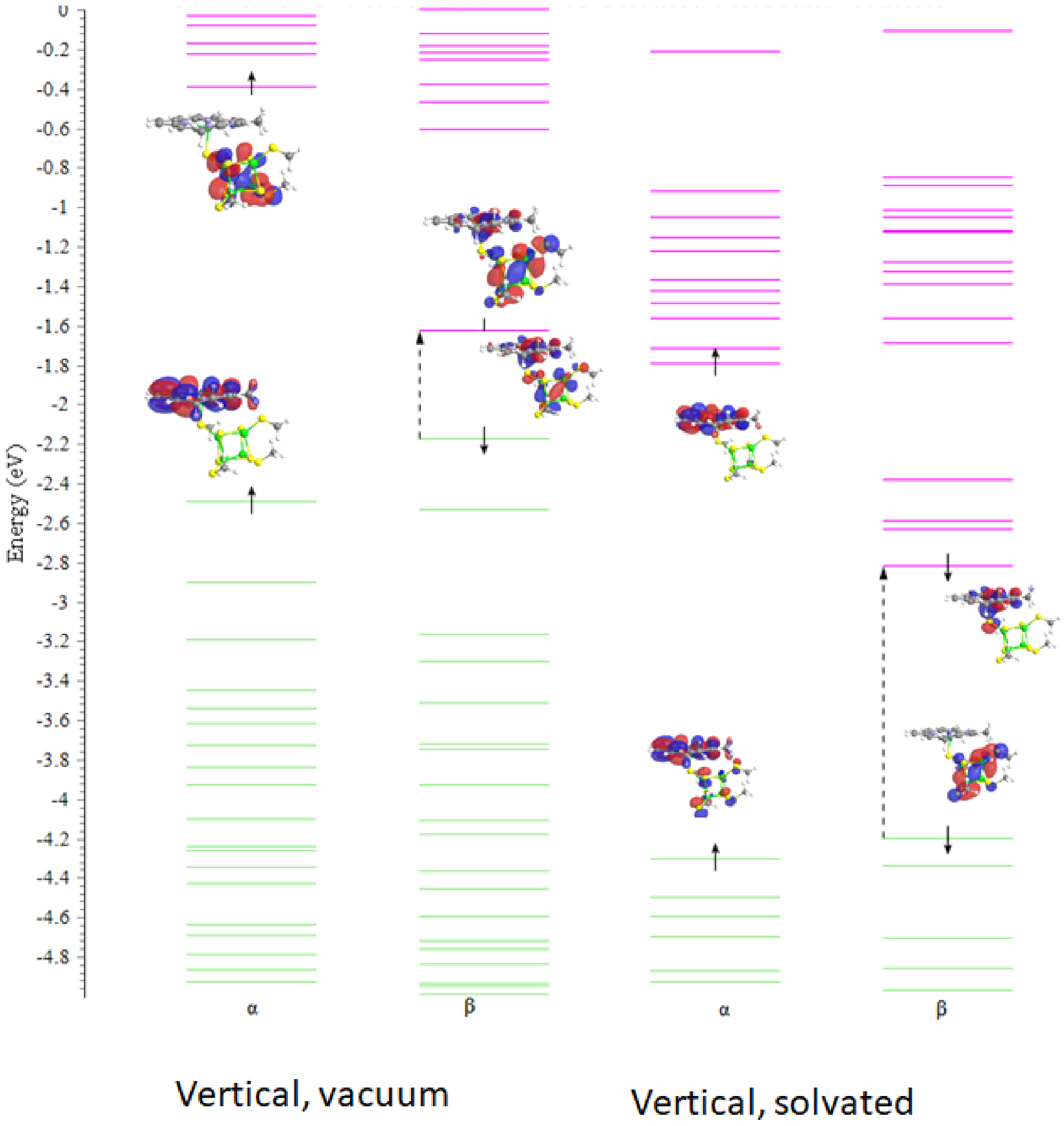

Figure 125. Ferromagnetically coupled siroheme-cubane vertical MOs computed in vacuum and solvation conditions.

In vacuum, the α-HOMO is localized on the siroheme fragment and the α-LUMO on the cubane. The HOMO-LUMO excitation, however, is associated with a β→β transition, a channel that by having both β-HOMO and β-LUMO delocalised on the two fragments does not transfer charge from one part of the system to the other. Upon solvation, the HOMO-LUMO channel remains of β→β type, with the HOMO localized on the cubane fragment and the LUMO on the siroheme. Again, solvation stabilizes the MOs.

6.2.2.2.2.2 Solvation influence on the relaxed MOs

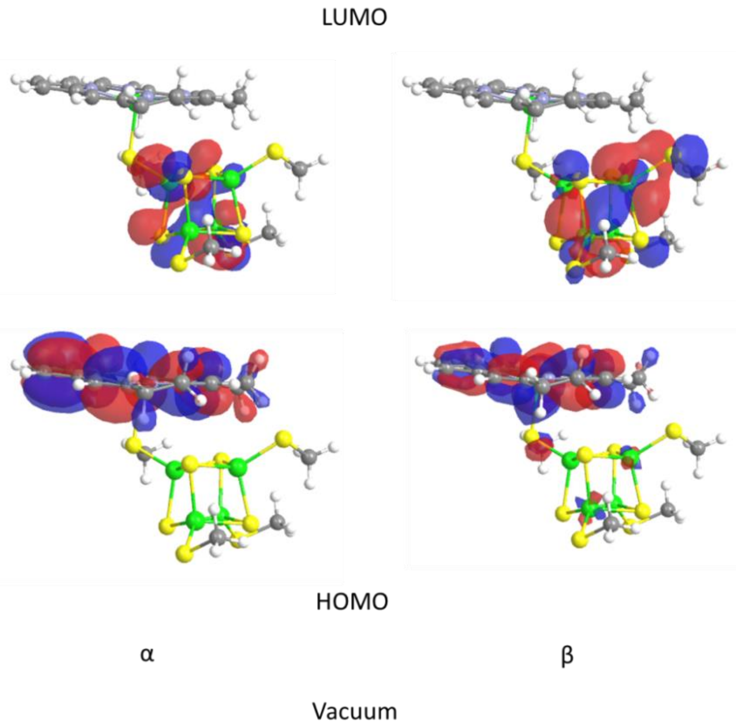

Figure 126. Frontier MOs of the antiferromagnetically coupled siroheme-cubane MOs computed in relaxed and vacuum conditions.

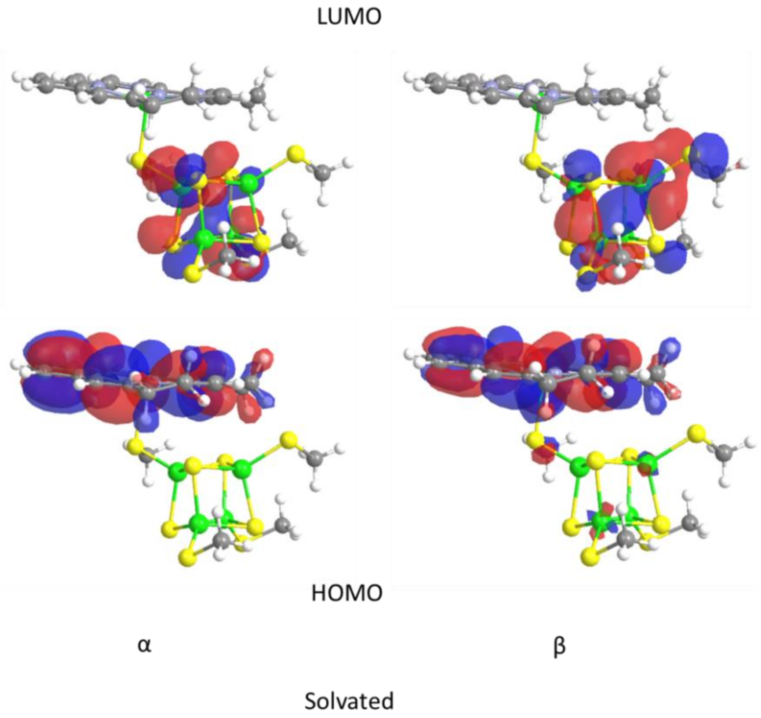

Figure 127. Frontier MOs of the antiferromagnetic coupled siroheme-cubane MOs computed in relaxed and solvated conditions.

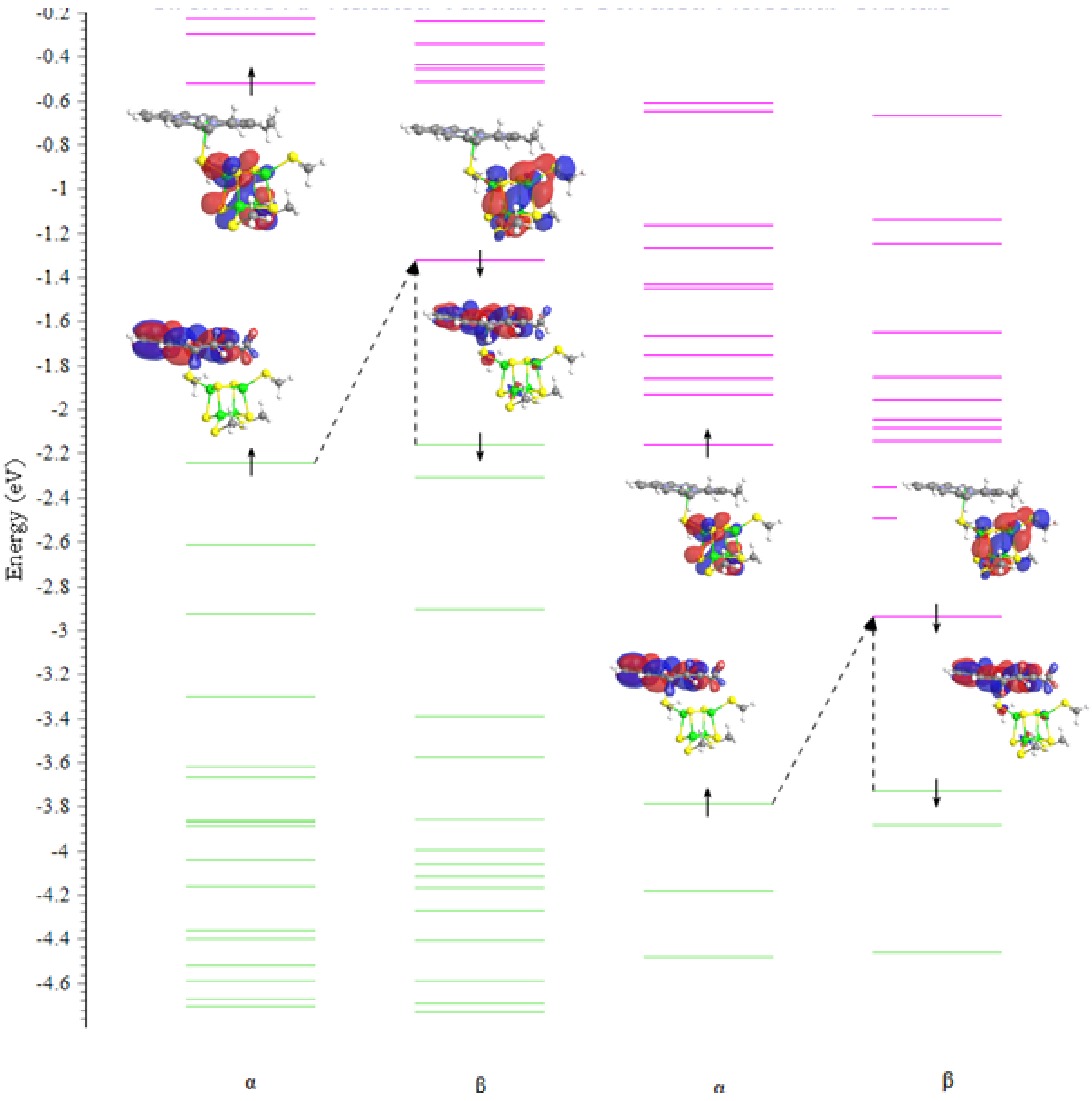

Figure 128. Antiferromagnetically coupled siroheme-cubane relaxed MOs computed in vacuum and solvation conditions.

After relaxation, the HOMOs become localized on the siroheme and LUMOs on the cubane in both the vacuum and the solvated cases.

6.2.2.2.2.3 Relaxation effects

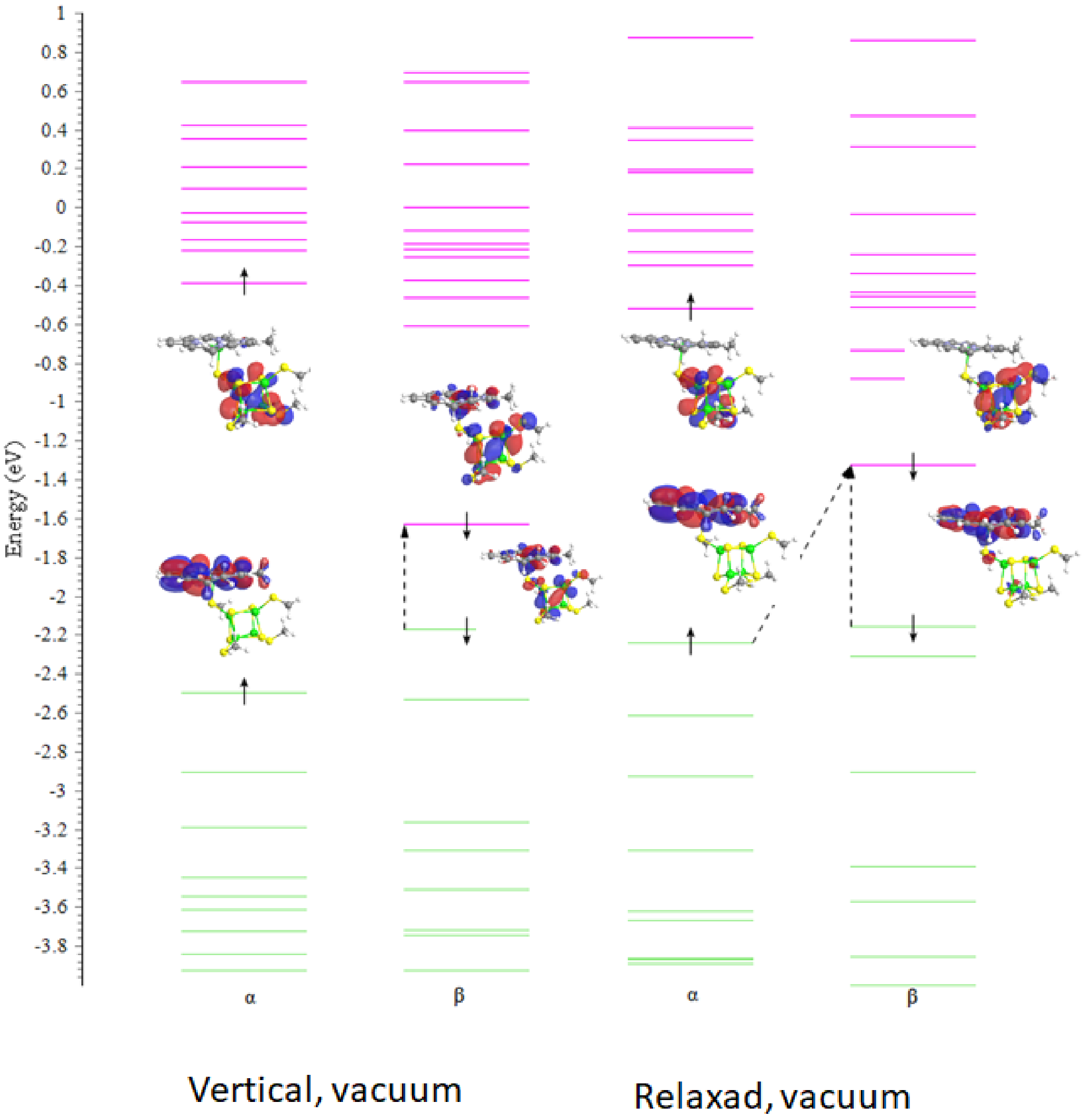

Figure 129. Vertical and relaxed antiferromagnetic siroheme-cubane relaxed MOs computed in vacuum conditions.

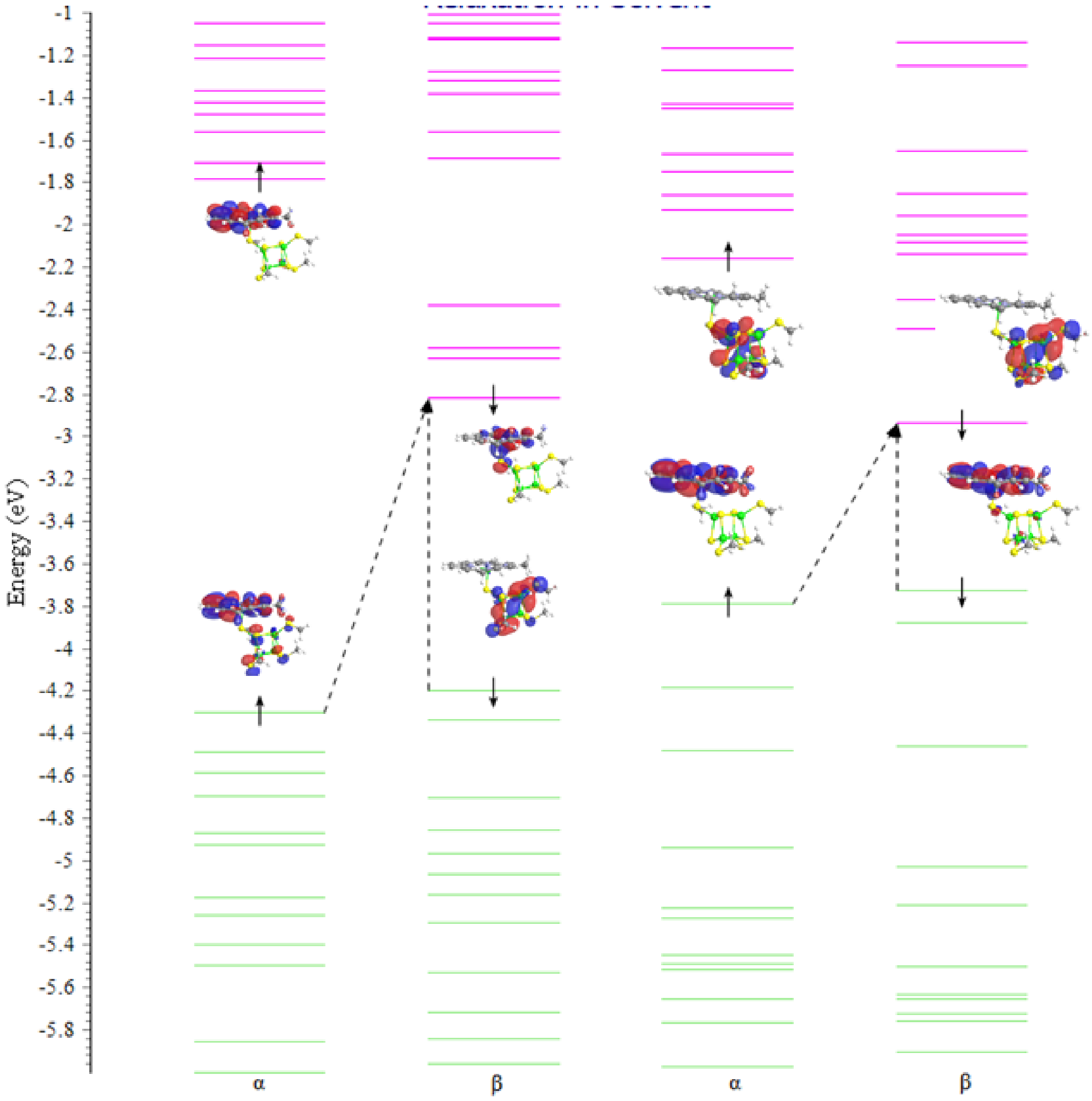

Figure 130. . Vertical and relaxed antiferromagnetic siroheme-cubane relaxed MOs computed in solvation conditions.

In vacuum, relaxation increases the HOMO-LUMO gap and changes the excitation channel from an α→β transition to a quasidegenerated α→β and β→β channel. The relaxation process induces a localization of the previously delocalized frontier orbitals. Thus, the HOMO becomes localized on the siroheme fragment and the LUMO on the cubane.

In solvent, the relaxation process induces a decrease of the HOMO-LUMO gap. Again, this process delocalizes the HOMO from the cubane fragment to the siroheme and vice versa with the LUMO.

6.2.2.2.3 Ferromagnetic vs. Antiferromagnetic coupled systems

With regard to the type of HOMO-LUMO transition and charge transfer associated with it, when computed in the vertical regime the switching of the magnetic coupling from ferromagnetic to antiferromagnetic affects the vacuum-computed frontier orbitals by changing the α-HOMO localized on the cubane to a β-HOMO delocalized on both fragments, and the β-LUMO localized on the siroheme to a β-LUMO delocalized on the two fragments. In the relaxed regime, the antiferromagnetic coupling localizes on the cubane the delocalized LUMO found in the ferromagnetic case.

In solvated vertical models, ferromagnetic coupling is associated with a HOMO-LUMO partial charge transfer from the cubane to the siroheme. In the relaxed regime, the charge transfer flows from the siroheme to the cubane fragment in both couplings.

6.2.2.2.4 Conclusions

Switching from ferromagnetic to antiferromagnetic coupling does not have a straightforward association with a specific direction of charge flow from one fragment to the other upon HOMO-LUMO excitation.

6.2.3 Heme vs. Siroheme in Cubane connected models

Table 98. Charge flow associated with a HOMO-LUMO excitation

Configuration			Heme		Siroheme	
			Charge flow		Charge flow	
Coupling	Regime	Medium	Direction	Type	Direction	Type
F	Vertical	Vacuum	cubane -> heme	α->β	cubane -> siroheme	α->β
		Solvent	cubane -> heme	α->β	siroheme -> delocalized	α->β
	Relaxed	Vacuum	cubane -> heme	β->β	siroheme -> delocalized	α->β , β->β
		Solvent	cubane -> heme	β->β	siroheme -> delocalized	α->β , β->β
AF	Vertical	Vacuum	heme -> cubane	β->β	delocalized -> delocalized	β->β
		Solvent	heme -> cubane	β->β	cubane -> siroheme	β->β
	Relaxed	Vacuum	heme -> cubane	β->β	siroheme -> cubane	α->β , β->β
		Solvent	heme -> cubane	β->β	siroheme -> cubane	α->β , β->β

The direction of charge flow associated with an HOMO-LUMO excitation is modulated by magnetic coupling employed.

In the heme-cubane system, the ferromagnetic coupling is always associated with a cubane-to-heme charge transfer while the antiferromagnetic coupling is associated with a heme-to-cubane transfer. In the vertical regime, the former is performed through an α->β channel while the latter through a β->β channel. After relaxation, the charge transfer in heme-cubane occurs through a β->β channel regardless of magnetic coupling.

The siroheme-cubane frontier orbitals behave differently. In ferromagnetic coupling, the cubane-to-siroheme transfer occurs only in vacuum in the vertical regime. For the rest of the ferromagnetic cases the HOMO is always localized on the siroheme fragment and the HOMO-LUMO excitation leads to a delocalization of charge among both fragments. In the antiferromagnetic case, the cubane-to-siroheme charge transfer is found in the vertical regime when computed in solvent environment (in vacuum, both frontier orbitals are delocalized on the two fragments) and performed through a β->β channel. After relaxation, the charge transfer flows in the opposite direction, i.e. siroheme→cubane, through a degenerated α->β, β->β channel.

6.2.3.1 Conclusions

In the heme-cubane system, charge will flow from one fragment to the other depending on the magnetic coupling employed between the two fragments. Siroheme disturbs this behaviour and allows charge transfer from the cubane to the siroheme only in the antiferromagnetic coupling assuming the vertical regime employed (the similar ferromagnetic vacuum case is neglected in this discussion due to its unrealistic character). Among the two magnetic coupling situations, we have shown that in the siroheme-cubane system the antiferromagnetic state is more stable than the ferromagnetic one. Thus, these coinciding results suggest that charge transfer occurs in the SiR active site from cubane to siroheme in the vertical regime and after relaxation it occurs in the opposite direction, from the siroheme to the cubane. This can be interpreted as an initial electron transfer from the cubane to the siroheme that can be used to reduce the substrate. In the event of the absence of the substrate, the system has enough time to relax and now, if excitation will occur, the electron will be transferred back to the cubane. (there is no need to bring another electron on the siroheme if the substrate has not ligated to the siroheme).

6.2.4 General conclusions

The (siro)heme-cubane system can be regarded as an acceptor-donor molecule that transfers electrons from the cubane fragment to the (siro)heme.

Although the heme variant behaves symmetrically in terms of the direction of the charge flow associated with the magnetic coupling, for the more stable antiferromagnetic coupling the charge transfer occurs from the heme to the cubane fragment. This problem is removed by the siroheme and now, if assuming that charge transfer occurs in the vertical regime, the electron will move from the cubane to the siroheme upon HOMO-LUMO excitation. This is done at the cost of losing the symmetrical magnetic modulation of the direction of charge flow.

6.3 Sulfite Reductase

6.3.1 Correlation of bond parameters in two-parameters plots

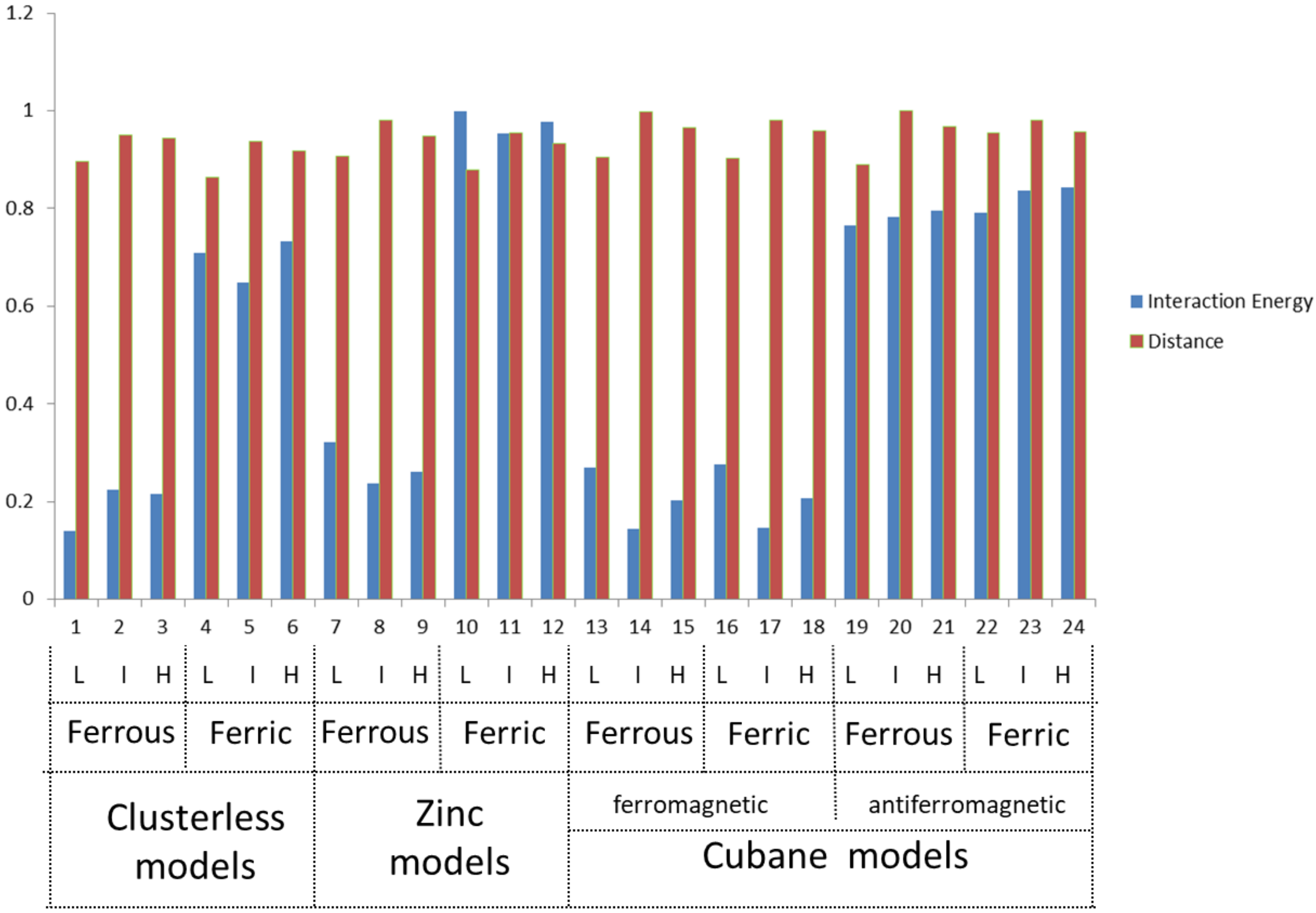

Figure 131. Plot of normalized ΔE_{tot} and the Fe–S bond length for the $\mathrm{Fe}_{\mathrm{(siro)heme}}$–$\mathrm{S}_{\mathrm{Cys}}$ bond in the heme models. L stands for low-spin, I for intermediate-spin and H for high-spin systems.

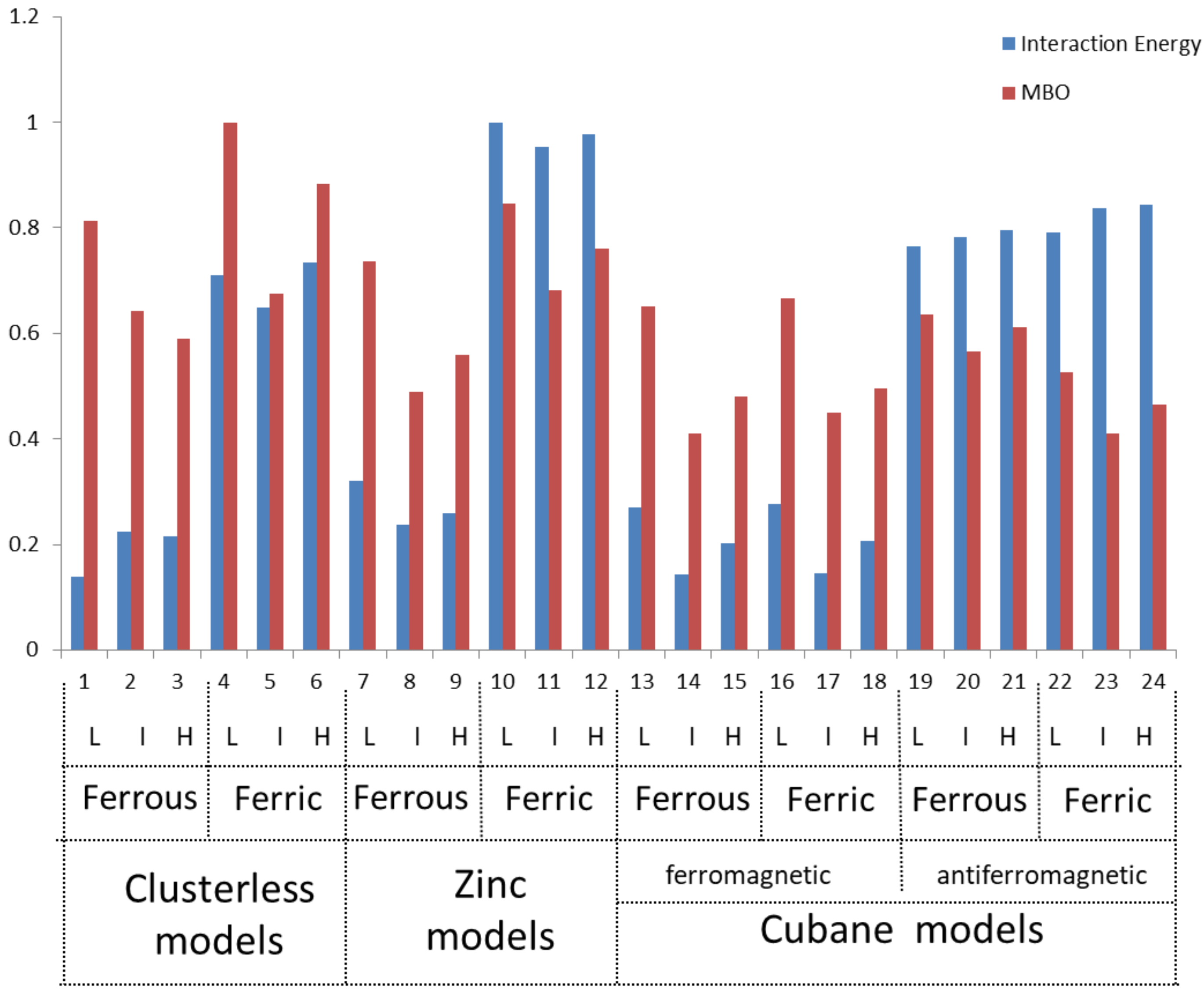

Figure 132. Plot of the interfactor bond energies vs MBO in heme models. L stands for low-spin, I for intermediate-spin and H for high-spin systems.

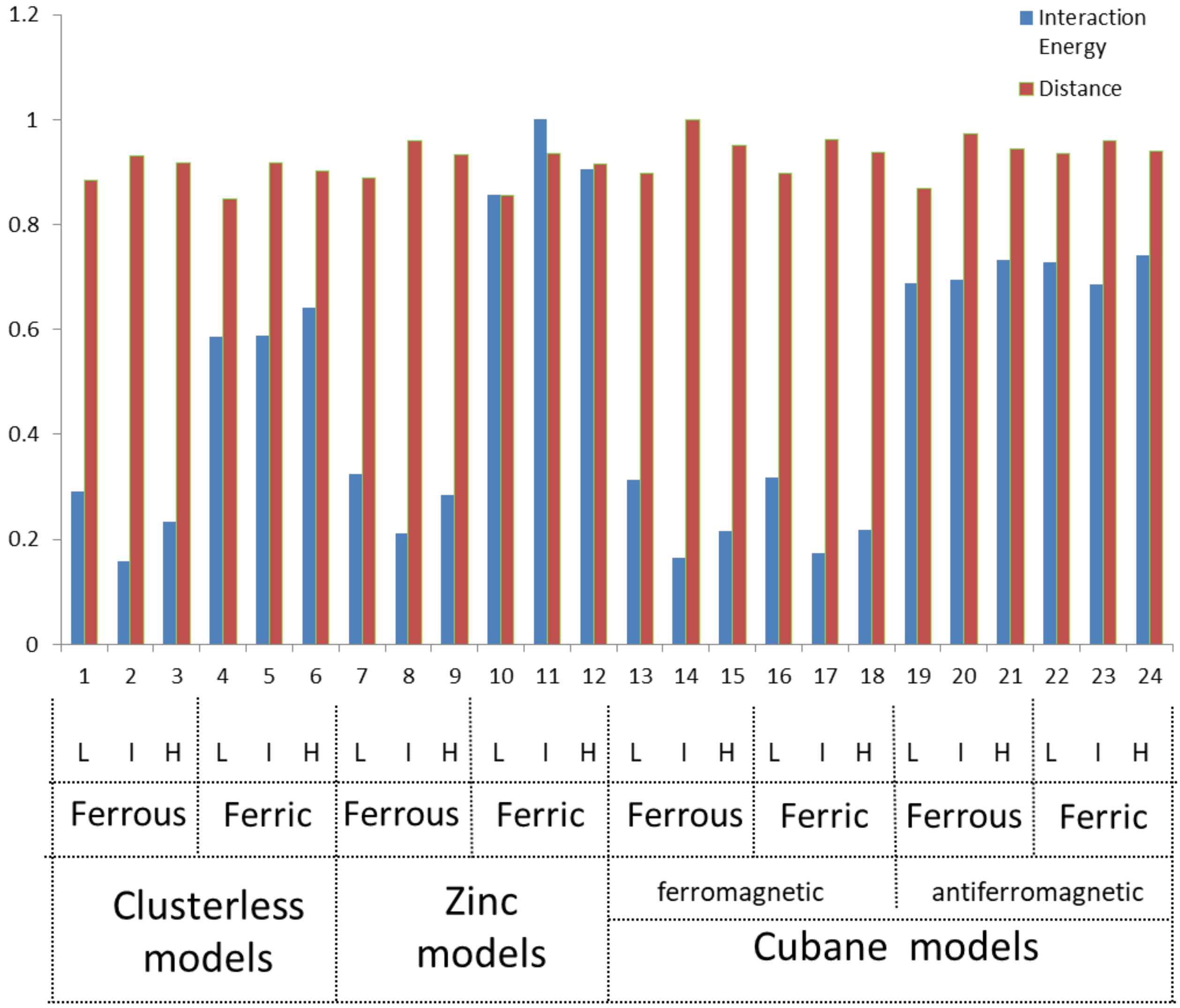

Figure 133. Plot of the interfactor bond energy vs length in siroheme models. L stands for low-spin, I for intermediate-spin and H for high-spin systems.

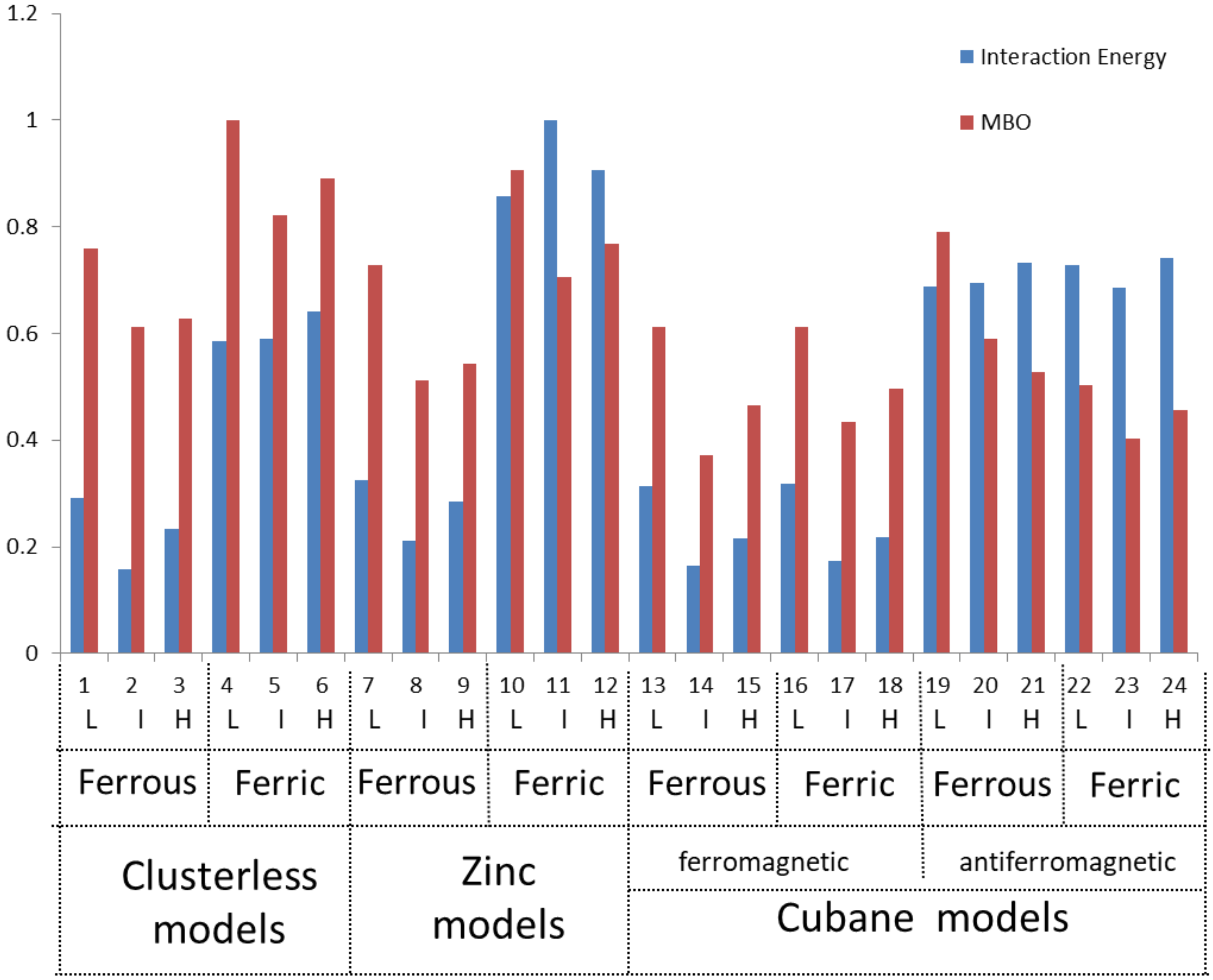

Figure 134. Plot of the interfactor bond energy vs length in siroheme models. L stands for low-spin, I for intermediate-spin and H for high-spin systems.

6.3.2 Electron conductance in various conformers of SiR active site models

The conductance of the investigated routes was computed in several different orientations of the (siro)heme cofactor relative to the cubane (cf. Figure 135):

1) The geometry of the active site as found in the crystal structure (pdb 1AOP) was used. This conformation is dubbed "Crystal, vertical geometry" in Figure 135. Models are depicted in Figure 136 and results are given in Table 99.
2) The geometry of the active was optimized. This conformation is dubbed "Crystal, relaxed geometry" in Figure 135. Models are depicted in Figure 137 while the results are collected in Table 100. This geometry was further employed in the calculations reported in the main body of the article.
3) The geometry of the active site (as found in the crystal structure) was changed by orienting the two siroheme-specific saturated bonds towards the cubane cofactor. This conformation is dubbed "Facing, vertical geometry" in Figure 135. The distances between the two cofactors were kept as in the crystal structure. Models are depicted in Figure 138 and results are in Table 101.
4) The geometry of 3) was optimized. This conformation is dubbed "Facing, relaxed geometry" in Figure 135. Models are depicted in Figure 139 and results are collected in Table 102.

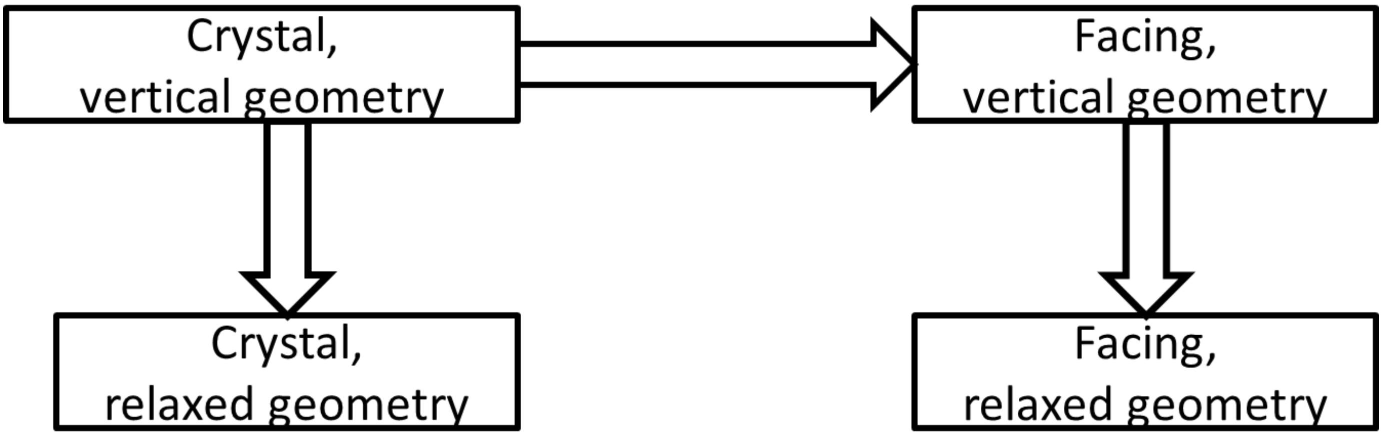

Figure 135. Scheme of the conformers used.

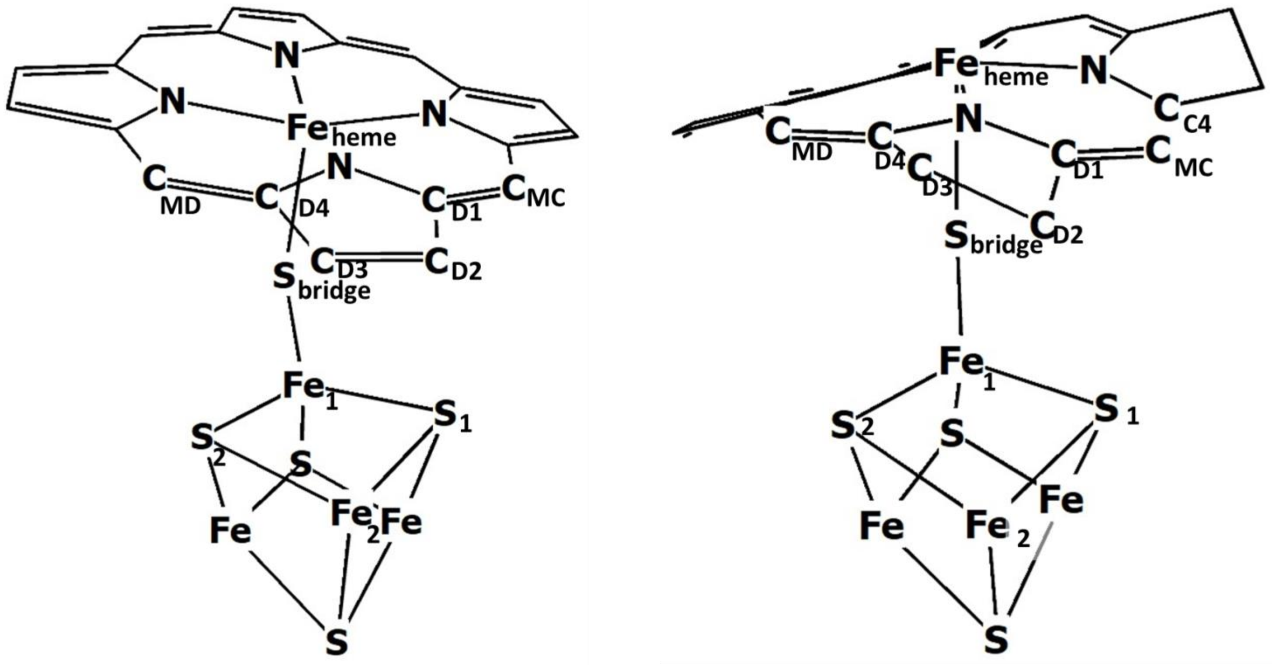

Figure 136. Heme–cubane (left) and siroheme–cubane (right) models in the “Crystal, vertical geometry” conformation.

Table 99. Computed conductance (*G*) for the investigated routes in the (siro)heme–cubane systems in the “Crystal, vertical geometry” conformation. Atom numbers are given in Figure 136, *d* represents the distance (in Å) between the two atoms.

Route	Heme-cubane				Siroheme-cubane			
	Atoms		*d*	*G*	Atoms		*d*	*G*
	#1	#2	(Å)		#1	#2	(Å)	
bridged	Fe_1	S_{bridge}	2.2	**2.2**	Fe_1	S_{bridge}	2.2	**2.3**
	S_{bridge}	Fe_{heme}	2.8	**1.6**	S_{bridge}	Fe_{heme}	2.8	**0.9**
direct	S_1	C_{MC}	3.6	0.3	S_1	C_{C4}	4.3	0.3
		C_{D1}	3.6	0.5		C_{MC}	3.6	0.3
		C_{D2}	3.8	0.5		C_{D1}	3.8	0.3
	Total			**1.3**	Total			**0.8**
direct	S_2	C_{D3}	3.8	0.2	S_2	C_{D3}	4.5	0.1
		C_{D4}	3.6	0.3		C_{D4}	4.1	0.2
		C_{MD}	3.7	0.4		C_{MD}	4.1	0.2
	Total			**0.8**	Total			**0.5**
direct	Fe_2	C_{D2}	3.8	0.1	Fe_2	C_{D2}	4.2	0.0
		C_{D3}	3.9	0.1		C_{D3}	5.0	0.1
	Total			**0.2**	Total			**0.1**
Total direct routes				**2.3**	Total direct routes			**1.4**

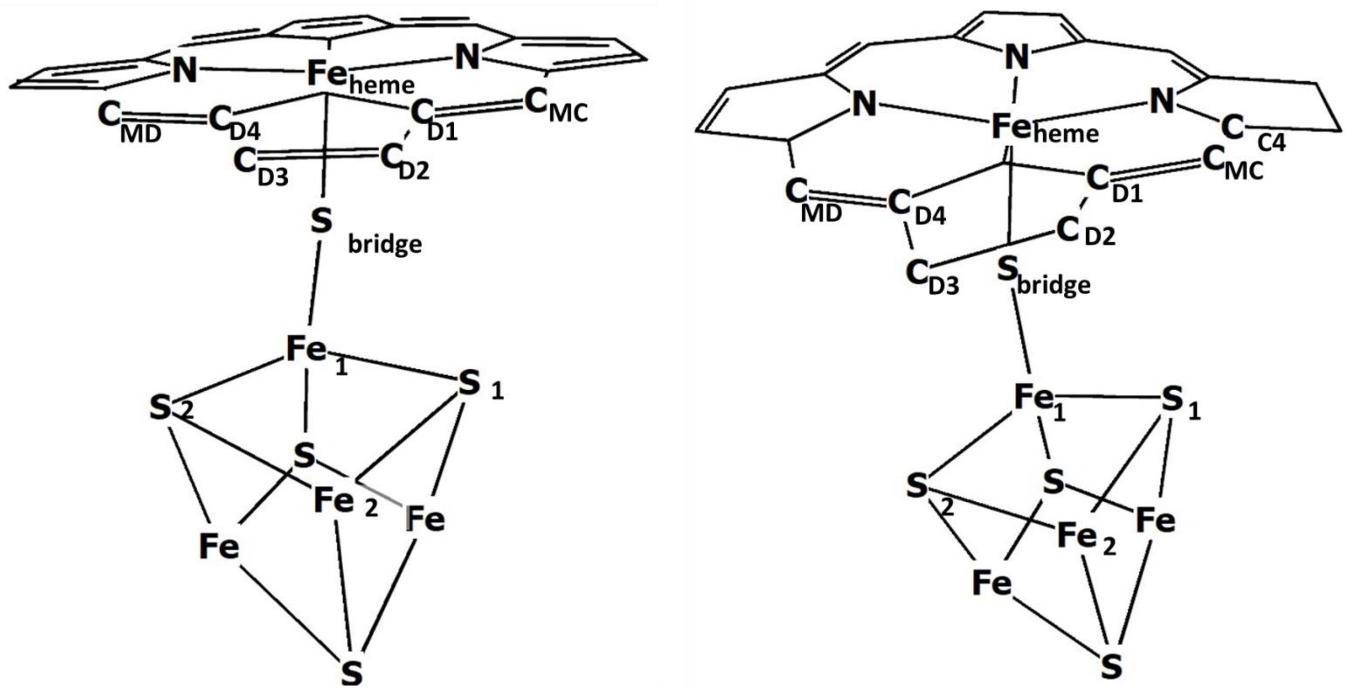

Figure 137. Heme–cubane (left) and siroheme–cubane (right) models in the "Crystal, relaxed geometry" conformation. Corresponds to the conformation used in section 4.2.3.4 .

Table 100. Computed conductance (*G*) for the investigated routes in the (siro)heme–cubane systems in the "Crystal, relaxed geometry" conformation. Atom numbers are given in Figure 137 and *d* represents the distance (in Å) between the two atoms.

Route	Heme-cubane				Siroheme-cubane			
	Atoms		*d* (Å)	*G*	Atoms		*d* (Å)	*G*
	#1	#2			#1	#2		
bridged	Fe_1	S_{bridge}	2.4	**2.0**	Fe_1	S_{bridge}	2.3	1.9
	S_{bridge}	Fe_{heme}	2.2	**0.7**	S_{bridge}	Fe_{heme}	2.4	1.0
direct	S_1	C_{MC}	3.4	0.9	S_2	C_{C4}	3.6	0.2
		C_{D1}	3.3	1.3		C_{MC}	3.2	0.1
		C_{D2}	3.4	1.5		C_{D1}	3.4	0.1
	Total			**3.6**	Total			**0.4**
direct	S_2	C_{D3}	3.4	0.9	S_1	C_{D3}	3.7	0.3
		C_{D4}	3.4	0.9		C_{D4}	3.7	0.1
		C_{MD}	3.4	0.3		C_{MC}	4.0	0.2
	Total			**2.2**	Total			**0.6**
direct	Fe_2	C_{D3}	3.7	0.2	Fe_2	C_{D2}	4.0	0.2
		C_{D2}	3.7	0.1		C_{D3}	3.9	**0.1**
	Total			**0.3**	Total			**0.3**
Total direct routes				**6.1**	Total direct routes			**1.4**

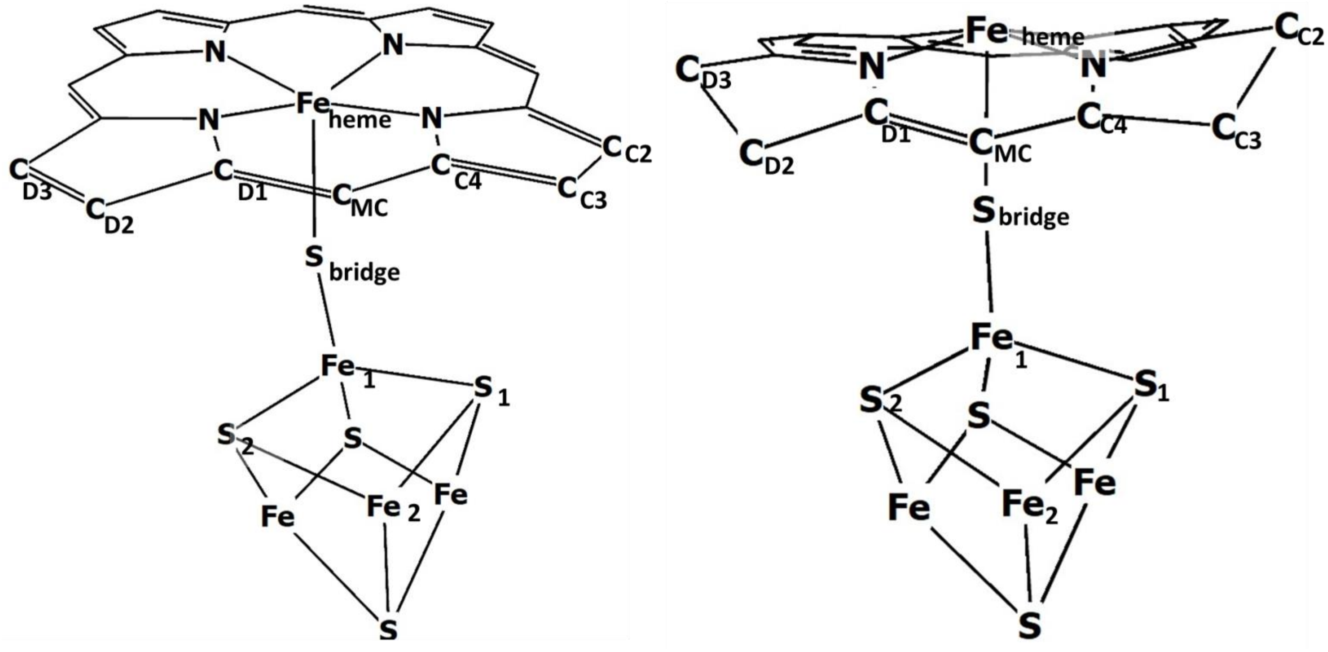

Figure 138. Heme–cubane (left) and siroheme–cubane (right) models in the "Facing, vertical geometry" conformation.

Table 101. Computed conductance (*G*) for the investigated routes in the (siro)heme–cubane systems in the "Facing,vertical geometry" conformation. Atom numbers are given in Figure 138 and *d* represents the distance (in Å) between the two atoms.

Route	Heme-cubane				Siroheme-cubane			
	Atoms		*d* (Å)	*G*	Atoms		*d* (Å)	*G*
	#1	#2			#1	#2		
bridged	Fe_1	S_{bridge}	2.2	**2.2**	Fe_1	S_{bridge}	2.2	**2.4**
	S_{bridge}	Fe_{heme}	2.8	**1.5**	S_{bridge}	Fe_{heme}	2.8	**0.6**
direct	S_1	C_{C2}	3.8	0.2	S_1	C_{C2}	4.8	0.1
		C_{C3}	3.5	0.6		C_{C3}	3.9	0.1
		C_{C4}	3.6	0.6		C_{C4}	3.8	0.6
	Total			**1.4**	Total			**0.8**
direct	S_2	C_{D1}	3.7	0.5	S_2	C_{D1}	3.8	0.4
		C_{D2}	3.7	0.3		C_{D2}	3.7	0.4
		C_{D3}	4.2	0.2		C_{D3}	4.8	0.1
	Total			**1.0**	Total			**0.9**
direct	Fe_2	C_{MC}	4.0	**0.2**	Fe_2	C_{MC}	4.4	**0.1**
Total direct routes				**2.6**	Total direct routes			**1.8**

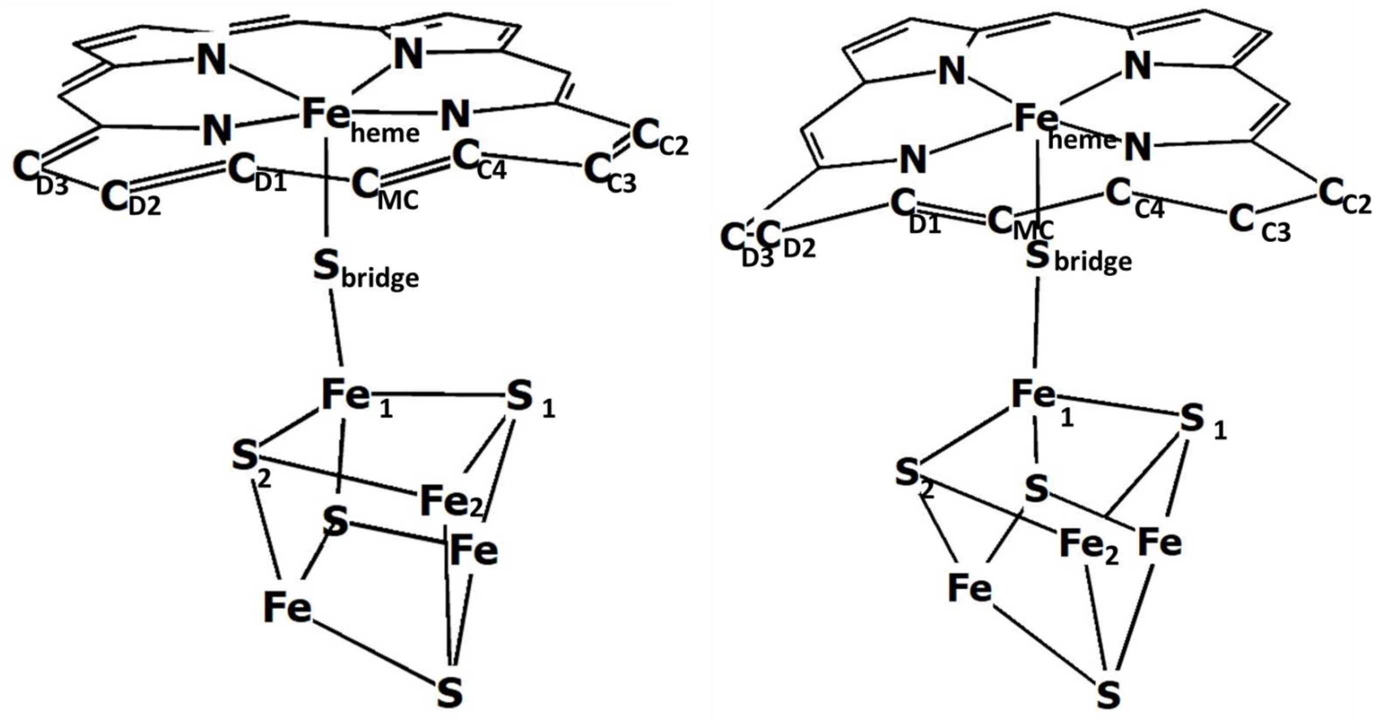

Figure 139. Heme–cubane (left) and siroheme–cubane (right) models in the “Facing, relaxed geometry” conformation.

Table 102. Computed conductance (*G*) for the investigated routes in the (siro)heme–cubane systems in the “Facing, relaxed geometry” conformation. Atom numbers are given in Figure 139 and *d* represents the distance (in Å) between the two atoms.

Route	Heme-cubane				Siroheme-cubane			
	Atoms		*d*	*G*	Atoms		*d*	*G*
	#1	#2	(Å)		#1	#2	(Å)	
bridged	Fe$_1$	S$_{bridge}$	2.3	**1.9**	Fe$_1$	S$_{bridge}$	2.3	**2.2**
	S$_{bridge}$	Fe$_{heme}$	2.4	**0.9**	S$_{bridge}$	Fe$_{heme}$	2.3	**0.8**
direct	S$_1$	C$_{C2}$	3.6	0.2	S$_1$	C$_{C2}$	3.4	0.2
		C$_{C3}$	3.4	0.4		C$_{C3}$	3.4	0.3
		C$_{C4}$	3.4	0.3		C$_{C4}$	3.3	0.6
	Total			**0.9**	Total			**1.1**
direct	S$_2$	C$_{D1}$	3.3	0.5	S$_2$	C$_{D1}$	3.3	0.6
		C$_{D2}$	3.4	0.4		C$_{D2}$	3.4	0.1
		C$_{D3}$	4.0	0.5		C$_{D3}$	3.6	0.1
	Total			**1.3**	Total			**0.8**
direct	Fe$_2$	C$_{MC}$	3.6	**0.4**	Fe$_2$	C$_{MC}$	3.8	**0.1**
Total direct routes				**2.6**	Total direct routes			**2.0**

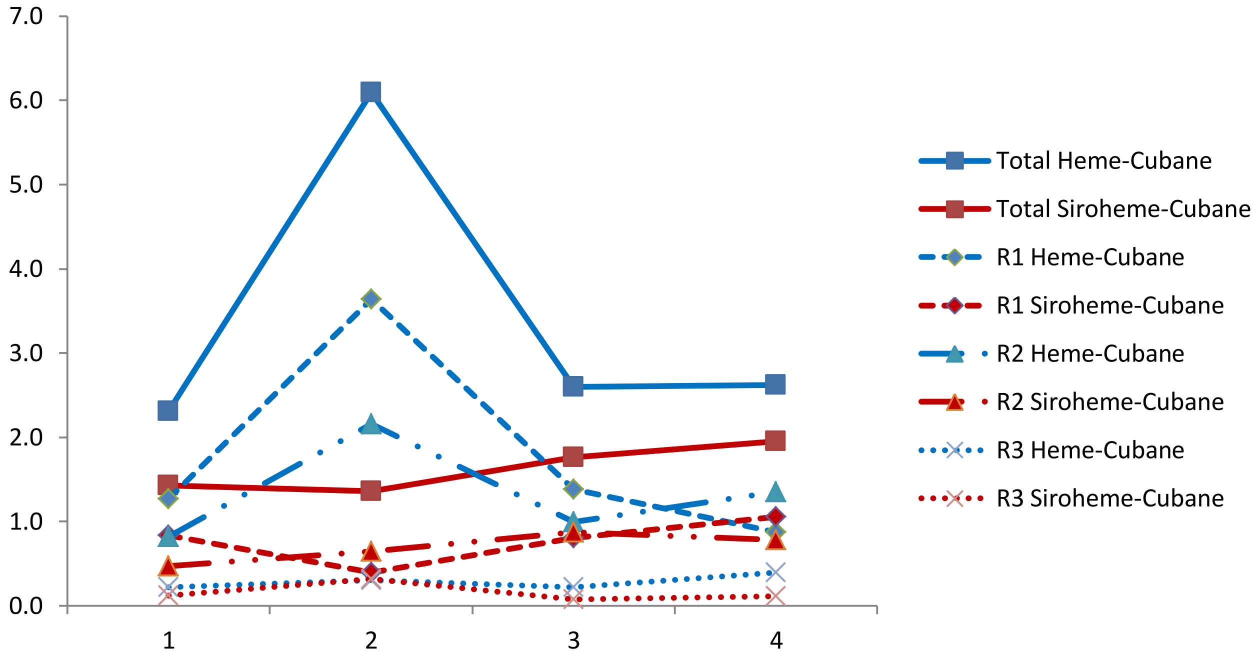

Figure 140. Conductance in direct routes: 1= crystal, vertical geometry, 2= crystal, relaxed geometry, 3=facing, vertical geometry, 4= facing relaxed geometry.

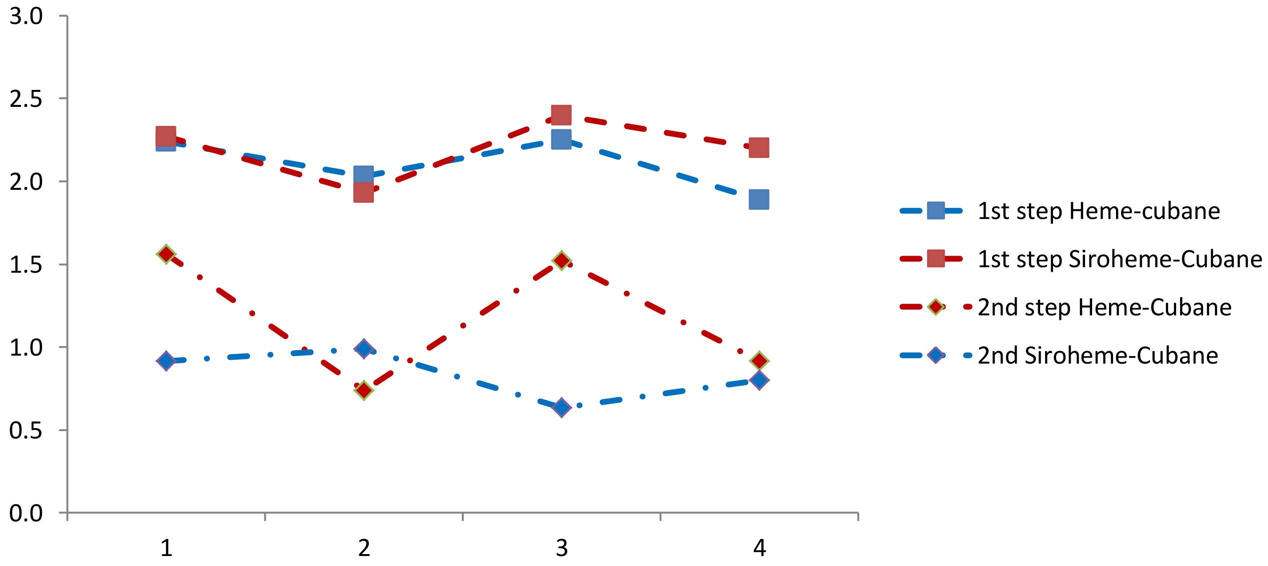

Figure 141. Conductance in bridged route: 1= crystal, vertical geometry, 2= crystal, relaxed geometry, 3=facing, vertical geometry, 4= facing relaxed geometry.

Table 103. Energies of SiR active site different possible adopted geometries.

System	Geometry	Energy kcal/mol
Siroheme–Cubane	crystal vertical	0.0
	crystal relaxed	-74.0
	facing vertical	-78.1
	facing relaxed	-80.2

6.3.3 Bond distances within substrate-including models

Table 104. Critical bond distances within substrate-including models of the Sulfite Reductase active site.

Substrate bonded via S atom								Substrate bonded via O atom				
				Distances (A)					Distances (A)			
Inter.	Model	*S*	Observation	S proximal	N average	S distal	S-O substrate	Observation	S proximal	N average	O distal	S-O substrate
1	SCH3	1/2		2.24	2.01	2.37	1.50		2.23	2.02	1.98	1.58
		3/2		2.24	2.10	2.40	1.50		2.36	2.08	2.00	1.59
		5/2	substrate detached	2.36	2.12	2.72	1.51		2.42	2.12	2.06	1.58
	Zn	1/2		2.26	2.03	2.35	1.50		2.26	2.04	1.98	1.58
		3/2	cluster detached		0.00				2.54	2.05	2.15	1.57
		5/2	substrate detached	2.40	2.11	2.72	1.51		2.46	2.11	2.06	1.58
	Fe4S4	1/2		2.36	2.06	2.68	1.50/1.49		2.44	2.06	2.18	1.57
		3/2		2.58	2.03	2.67	1.50		2.68	2.05	2.05	1.58
		5/2		2.49	2.10	2.67	1.50		2.65	2.11	1.99	1.59
2	SCH3	1/2		2.17	2.01	2.38	1.47		2.17	2.00	2.12	1.52
		3/2	substrate detached	2.32	2.01	4.10	1.49		2.35	2.03	2.44	1.51
		5/2	substrate detached	2.27	2.12	3.63	1.49		2.31	2.12	2.38	1.51
	Zn	1/2		2.21	2.03	2.28	1.48		2.19	2.04	2.15	1.52
		3/2	substrate detached	2.36	2.03	3.54	1.49		2.36	2.03	2.47	1.50
		5/2	substrate detached	2.31	2.13	3.70	1.49		2.36	2.12	2.43	1.51
	Fe4S4	1/2	substrate detached	2.22	2.01	3.80	1.48		2.24	2.04	2.09	1.52
		3/2	substrate detached	2.49	2.03	3.54	1.48		2.54	2.04	2.39	1.51
		5/2	substrate detached	2.38	2.12	3.62	1.48		2.50	2.12	2.31	1.52
3	SCH3	1/2		2.16	1.99	2.66	1.50		2.18	2.00	2.02	1.54
		3/2	substrate detached	2.30	2.01	2.85	1.50		2.27	2.00	2.00	1.57
		5/2	substrate detached	2.28	2.11	3.09	1.49		2.29	2.11	2.63	1.50

Substrate bonded via S atom								Substrate bonded via O atom				
				Distances (A)					Distances (A)			
Inter.	Model	*S*	Observation	S proximal	N average	S distal	S-O substrate	Observation	S proximal	N average	O distal	S-O substrate
	Zn	1/2		2.29	2.02	2.16	1.50		2.20	2.03	1.99	1.55
		3/2	model breaks	2.49	2.01	2.76	1.50		2.52	2.11	2.05	1.55
		5/2	cluster breaks	2.84	2.09	2.36	1.52		2.54	2.11	2.05	1.55
	Fe4S4	1/2	substrate detached	2.25	2.03	2.80	1.50		2.31	2.04	2.27	1.53
		3/2		2.56	2.02	2.69	1.50		2.60	2.04	2.13	1.55
		5/2	substrate detached	2.43	2.10	2.82	1.50		2.67	2.10	2.02	1.55
4	SCH3	1/2		2.28	2.02	2.17	1.50		2.25	2.01	1.91	1.55
		3/2		2.26	2.00	2.55	1.52		2.24	2.01	2.02	1.58
		5/2		2.31	2.11	2.67	1.50		2.26	2.11	2.04	1.57
	Zn	1/2		2.29	2.03	2.15	1.50		2.27	2.03	1.92	1.55
		3/2	cluster breaks	N/A	N/A	N/A	N/A		2.27	2.05	2.24	1.56
		5/2		2.37	2.11	2.76	1.51		2.43	2.11	2.11	1.55
	Fe4S4	1/2		2.34	2.03	2.11	1.50		2.30	2.03	1.91	1.57
		3/2	substrate detached	2.49	2.03	2.70	1.51		2.47	2.05	2.20	1.55
		5/2	substrate detached	2.44	2.11	2.73	1.50		2.55	2.11	2.07	1.55
5	SCH3	0		2.19	2.00	2.33	1.51		2.17	2.02	1.91	1.56
		1		2.20	1.99	2.44	1.51		2.19	2.00	2.03	1.55
		2		2.29	2.10	2.67	1.51		2.34	2.02	2.62	1.52
	Zn	0		2.21	2.03	2.29	1.51		2.20	2.03	1.93	1.59
		1		2.34	2.02	2.29	1.52		2.26	2.03	1.95	1.58
		2		2.30	2.11	2.59	1.52		2.42	2.04	2.32	1.55
	Fe4S4	0		2.71	2.05	2.42	1.52		2.41	2.03	1.89	1.61
		1		2.76	2.04	2.32	1.51		2.79	2.05	1.92	1.61
		2		2.47	2.11	2.50	1.51		2.66	2.11	2.01	1.58

Substrate bonded via S atom								Substrate bonded via O atom				
				Distances (A)					Distances (A)			
Inter.	Model	*S*	Observation	S proximal	N average	S distal	S-O substrate	Observation	S proximal	N average	O distal	S-O substrate
6	SCH3	0		2.16	2.01	2.34	1.68		-	-	-	-
		1		2.21	1.98	2.31	1.69/1.65		-	-	-	-
		2	substrate detached	2.34	2.02	2.92	1.68		-	-	-	-
	Zn	0		2.33	2.00	2.23	1.69		-	-	-	-
		1		2.23	2.02	2.31	1.67		-	-	-	-
		2	substrate detached	2.43	2.01	2.85	1.68/1.67		-	-	-	-
	Fe4S4	0	substrate detached	2.22	2.05	2.78	1.65/1.68		-	-	-	-
		1	substrate detached	2.28	2.03	2.79	1.65/1.68		-	-	-	-
		2	substrate detached	2.49	2.02	2.77	1.65/1.68		-	-	-	-
7	SCH3	0		2.29	1.99	2.13	1.52		2.21	2.00	1.86	1.57
		1		2.27	2.02	2.22	1.53		2.20	2.00	1.92	1.57
		2		2.51	1.98	2.82	1.55		2.18	2.01	2.02	1.56
	Zn	0		2.47	1.99	2.08	1.52		2.26	2.02	1.83	1.60
		1		2.41	2.02	2.14	1.53		2.25	2.00	1.94	1.58
		2		2.32	2.01	2.32	1.55		2.34	2.02	1.87	1.59
	Fe4S4	0		2.56	2.08	2.02	1.51	substrate detached	2.23	2.03	2.30	1.55
		1		2.48	2.02	2.10	1.53		2.04	2.03	2.26	1.56
		2		2.46	2.09	2.21	1.53	substrate detached	2.50	2.02	2.35	
8	SCH3	1/2		2.29	2.00	2.23	1.53		2.21	2.00	1.89	1.58
		3/2		2.28	2.10	2.34	1.53		2.19	2.00	1.99	1.57
		5/2		2.27	2.09	2.43	1.54		2.35	2.01	2.49	1.54
	Zn	1/2		2.35	2.03	2.17	1.55		2.40	2.02	1.85	1.62
		3/2	cluster breaks	2.50	2.02	2.24	1.55	cluster breaks	2.41	1.99	1.83	1.62
		5/2		2.55	2.11	2.30	1.55		2.62	2.02	2.16	1.59

Substrate bonded via S atom								Substrate bonded via O atom				
				Distances (A)					Distances (A)			
Inter.	Model	*S*	Observation	S proximal	N average	S distal	S-O substrate	Observation	S proximal	N average	O distal	S-O substrate
	Fe4S4	1/2		2.78	2.04	2.05	1.53		2.38	2.03	1.82	1.61
		3/2		2.44	2.02	2.27	1.55		2.35	2.03	1.85	1.60
		5/2		2.59	2.10	2.28	1.54		2.58	2.10	2.07	1.58
9	SCH3	0		2.33	2.02	2.11	1.55		2.28	2.02	1.83	1.63
		1		2.28	2.01	2.33	1.57		2.28	2.01	1.89	1.62
		2		2.31	2.14	2.36	1.56		2.42	2.04	2.23	1.59
	Zn	0		2.37	2.04	2.10	1.55		2.28	2.04	1.82	1.63
		1		2.32	2.11	2.27	1.56		2.31	2.03	1.86	1.62
		2		2.33	2.14	2.34	1.56		2.50	2.05	2.19	1.60
	Fe4S4	0		2.41	2.04	2.13	1.55		2.34	2.03	1.87	1.62
		1		2.45	2.02	2.28	1.56		2.36	2.03	1.84	1.61
		2		2.47	2.10	2.29	1.55		2.59	2.11	1.90	1.61
10	SCH3	1/2		2.41	2.00	2.27	1.58		2.42	2.00	2.28	1.58
		3/2		2.46	2.13	2.27	1.57		2.32	2.02	2.31	1.57
		5/2		2.57	2.10	2.31	1.57		2.38	2.13	2.41	1.57
	Zn	1/2		2.49	2.00	2.23	1.58		2.46	2.01	1.89	1.66
		3/2		2.57	2.11	2.23	1.58		2.77	2.04	1.97	1.64
		5/2		2.67	2.12	2.54	1.59		2.76	2.13	1.88	1.64
	Fe4S4	1/2		2.79	2.04	2.17	1.57		N/A	N/A	N/A	N/A
		3/2		2.79	2.04	2.18	1.57		N/A	N/A	N/A	N/A
		5/2		2.76	2.11	2.46	1.59		N/A	N/A	N/A	N/A
11	SCH3	1/2		2.30	2.02	2.23	1.74		-	-	-	-
		3/2		2.30	2.11	2.24	1.73		-	-	-	-
		5/2		2.42	2.12	2.47	1.73		-	-	-	-

Substrate bonded via S atom								Substrate bonded via O atom				
				Distances (A)					Distances (A)			
Inter.	Model	*S*	Observation	S proximal	N average	S distal	S-O substrate	Observation	S proximal	N average	O distal	S-O substrate
	Zn	1/2		2.34	2.04	2.21	1.74		-	-	-	-
		3/2		2.73	2.06	2.14	1.73		-	-	-	-
		5/2		2.47	2.12	2.46	1.72		-	-	-	-
	Fe4S4	1/2		2.41	2.04	2.16	1.72		-	-	-	-
		3/2		2.69	2.05	2.43	1.72		-	-	-	-
		5/2		2.59	2.12	2.42	1.71		-	-	-	-
12	SCH3	1/2		2.32	2.02	2.08	-		-	-	-	-
		3/2		2.36	2.01	2.12	-		-	-	-	-
		5/2		2.37	2.11	2.11	-		-	-	-	-
	Zn	1/2		2.43	2.04	2.09	-		-	-	-	-
		3/2		2.42	2.04	2.10	-		-	-	-	-
		5/2		2.54	2.12	2.08	-		-	-	-	-
	Fe4S4	1/2		2.75	2.05	2.06	-		-	-	-	-
		3/2		2.59	2.11	2.07	-		-	-	-	-
		5/2		2.60	2.11	2.07	-		-	-	-	-
13	SCH3	0		2.30	2.02	2.16	-		-	-	-	-
		1		2.38	2.03	2.13	-		-	-	-	-
		2		2.39	2.11	2.12	-		-	-	-	-
	Zn	0		2.33	2.04	2.15	-		-	-	-	-
		1		2.41	2.04	2.11	-		-	-	-	-
		2		2.48	2.13	2.11	-		-	-	-	-
	Fe4S4	0		2.46	2.04	2.10	-		-	-	-	-
		1		2.71	2.06	2.08	-		-	-	-	-
		2		2.55	2.12	2.09	-		-	-	-	-

Substrate bonded via S atom								Substrate bonded via O atom				
				Distances (A)					Distances (A)			
Inter.	Model	*S*	Observation	S proximal	N average	S distal	S-O substrate	Observation	S proximal	N average	O distal	S-O substrate
14	SCH3	0		2.20	2.02	2.23	-		-	-	-	-
		1		2.26	2.00	2.27	-		-	-	-	-
		2		2.27	2.08	2.28	-		-	-	-	-
	Zn	0		2.19	2.03	2.24	-		-	-	-	-
		1	cluster breaks	2.38	2.03	2.24	-		-	-	-	-
		2		2.32	2.10	2.28	-		-	-	-	-
	Fe4S4	0		2.75	2.05	2.20	-		-	-	-	-
		1		2.75	2.05	2.20	-		-	-	-	-
		2		2.56	2.10	2.24	-		-	-	-	-
15	SCH3	1/2		2.26	1.99	2.33	-		-	-	-	-
		3/2		2.29	2.10	2.31	-		-	-	-	-
		5/2		2.45	2.12	2.45	-		-	-	-	-
	Zn	1/2		2.32	2.03	2.30	-		-	-	-	-
		3/2		2.35	2.11	2.32	-		-	-	-	-
		5/2		2.58	2.12	2.46	-		-	-	-	-
	Fe4S4	1/2		2.71	2.06	2.24	-		-	-	-	-
		3/2		N/A	0.00	N/A	-		-	-	-	-
		5/2		2.67	2.11	2.39	-		-	-	-	-
16	SCH3	1/2		2.17	2.00	2.54	-		-	-	-	-
		3/2	substrate detached	2.33	2.03	3.12	-		-	-	-	-
		5/2	substrate detached	2.30	2.11	3.11	-		-	-	-	-
	Zn	1/2		2.18	2.03	2.51	-		-	-	-	-
		3/2	substrate detached	2.36	2.02	3.61	-		-	-	-	-
		5/2	substrate detached	2.31	2.13	3.63	-		-	-	-	-

Substrate bonded via S atom								Substrate bonded via O atom				
				Distances (A)					Distances (A)			
Inter.	Model	*S*	Observation	S proximal	N average	S distal	S-O substrate	Observation	S proximal	N average	O distal	S-O substrate
	Fe4S4	1/2	substrate detached	2.23	2.04	2.79	-		-	-	-	-
		3/2	substrate detached	2.47	2.02	4.13	-		-	-	-	-
		5/2	substrate detached	2.39	2.11	3.68	-		-	-	-	-
18	SCH3	1/2		2.18	1.99	2.48	1.50		2.23	1.98	1.90	1.59
		3/2		2.19	1.99	2.48	1.50		2.17	2.00	2.06	1.65
		5/2		2.27	2.10	2.66	1.50		2.34	2.02	2.47	1.69
	Zn	1/2		2.47	1.99	2.24	1.70		2.22	1.99	2.05	1.55
		3/2		2.31	2.02	2.33	1.73		2.25	1.99	1.96	1.57
		5/2		2.37	2.10	2.61	1.68		2.40	2.10	2.14	1.55
	Fe4S4	1/2		2.36	2.05	2.73	1.52		2.23	2.04	2.29	1.54
		3/2		2.75	2.03	2.40	1.51		2.33	2.01	1.93	1.58
		5/2	geo opt failure				1.67		2.52	2.03	2.30	1.54
19	SCH3	0		2.35	2.00	2.33	1.51		2.32	1.98	2.07	1.55
		1	substrate detached	2.38	2.03	N/A	N/A		2.25	2.03	2.01	1.57
		2	substrate detached	2.33	2.13	N/A	N/A	comp not done	2.44	2.12	2.23	1.54
	Zn	0		2.41	2.01	2.28	1.50/1.51		2.36	2.00	2.04	1.56
		1		2.30	2.04	2.39	1.50	cluster detached	2.71	2.02	2.25	1.55
		2	geo opt failure	N/A	N/A	N/A	N/A	comp not done	2.55	2.11	2.19	1.56
	Fe4S4	0		2.39	2.02	2.26	1.50		2.32	2.05	2.24	1.56
		1		2.71	2.03	2.62	1.50/1.51		2.76	2.04	2.14	1.56
		2		2.63	2.10	2.63	1.51		2.81	2.11	2.06	1.57
20	SCH3	0		2.32	2.01	2.16	1.49		2.27	1.99	2.18	1.52
		1	substrate breaks	2.24	2.00	2.51	N/A	substrate detached	2.35	2.03	2.76	1.50
		2	substrate detached	2.30	2.13	N/A	N/A	substrate detached	2.33	2.13	2.62	1.50

Substrate bonded via S atom								Substrate bonded via O atom				
				Distances (A)					Distances (A)			
Inter.	Model	*S*	Observation	S proximal	N average	S distal	S-O substrate	Observation	S proximal	N average	O distal	S-O substrate
	Zn	0	substrate breaks	2.27	2.03	2.19	N/A		2.29	2.02	2.14	1.51
		1	substrate detached	2.38	2.04	3.35	N/A	substrate detached	2.40	2.04	2.77	1.50
		2	substrate detached	2.33	2.14	3.66	N/A	substrate detached	2.45	2.04	2.34	1.52
	Fe4S4	0		2.34	2.03	2.16	1.67/1.68		2.29	2.03	2.11	1.52
		1	substrate detached	2.46	2.03	N/A	N/A	substrate detached	2.56	2.04	2.53	1.50
		2	substrate detached	2.37	2.13	N/A	N/A	substrate detached	2.46	2.12	2.42	1.51
21	SCH3	1/2		2.22	2.01	2.25	1.67		-	-	-	-
		3/2		2.22	2.01	2.26	1.67		-	-	-	-
		5/2		2.22	2.10	2.28	1.66		-	-	-	-
	Zn	1/2		2.37	2.03	2.16	1.70		-	-	-	-
		3/2		2.38	2.02	2.18	1.70		-	-	-	-
		5/2		2.38	2.09	2.20	1.70		-	-	-	-
	Fe4S4	1/2		2.43	2.02	2.15	1.70		-	-	-	-
		3/2		2.44	2.02	2.16	1.70		-	-	-	-
		5/2		2.45	2.09	2.17	1.70		-	-	-	-
22	SCH3	0		2.23	2.02	2.15	1.69		-	-	-	-
		1		2.23	2.01	2.26	1.68		-	-	-	-
		2		2.23	2.10	2.28	1.67		-	-	-	-
	Zn	0		2.25	2.04	2.15	1.70		-	-	-	-
		1		2.37	2.03	2.16	1.72		-	-	-	-
		2		2.38	2.11	2.17	1.72		-	-	-	-
	Fe4S4	0		2.76	2.05	2.12	1.72		-	-	-	-
		1		2.76	2.05	2.13	1.72		-	-	-	-
		2		2.56	2.11	2.36	1.70		-	-	-	-

6.3.4 Mulliken charge and spin analysis of the SiR intermediates

Table 105. Mulliken charge and spin populations of models of the SiR intermediates.

Inter.	Bond isomer	*S*	Fragment	Cluster model					
				SCH3		Zn		Fe4S4	
				Charge	Spin	Charge	Spin	Charge	Spin
1	S	1/2	S bridge	-0.19	0.10	-0.13	0.05	-0.32	0.22
			Fe	0.26	1.01	0.26	1.03	0.48	1.31
			Porphyrin	-0.57	-0.08	-0.65	-0.05	-0.57	-0.06
			Cluster	-	-	-1.49	0.00	-1.04	-0.31
			Substrate	-0.50	-0.02	-0.49	-0.02	-0.56	-0.10
		3/2	S bridge	-0.19	-0.04	N/A		N/A	
			Fe	0.41	3.03				
			Porphyrin	-0.74	0.10				
			Cluster	-	-				
			Substrate	-0.48	-0.10				
		5/2	S bridge	N/A		N/A		-0.32	0.22
			Fe					0.72	4.15
			Porphyrin					-0.64	0.46
			Cluster					-1.15	-0.04
			Substrate					-0.60	0.20
	O	1/2	S bridge	-0.21	0.05	-0.14	0.00	-0.32	0.22
			Fe	0.46	1.03	0.48	1.06	0.60	1.26
			Porphyrin	-0.65	-0.08	-0.71	-0.09	-0.60	-0.08
			Cluster	-	-	-1.52	0.00	-1.06	-0.35
			Substrate	-0.61	0.00	-0.60	0.00	-0.62	-0.02
		3/2	S bridge	-0.31	0.08	-0.31	0.22	-0.34	0.20
			Fe	0.62	2.87	0.68	2.76	0.73	2.85
			Porphyrin	-0.67	0.00	-0.62	-0.07	-0.49	-0.05
			Cluster	-	-	-1.56	0.00	-1.27	-0.09
			Substrate	-0.63	0.05	-0.70	0.08	-0.63	0.13
		5/2	S bridge	-0.34	0.34	-0.25	0.25	-0.33	0.21
			Fe	0.79	4.19	0.80	4.21	0.86	4.25
			Porphyrin	-0.80	0.29	-0.84	0.35	-0.70	0.44
			Cluster	-	-	-1.55	0.00	-1.24	-0.07
			Substrate	-0.65	0.09	-0.65	0.11	-0.58	0.16
2	S	1/2	S bridge	-0.07	0.10	-0.02	0.13	N/A	
			Fe	0.43	0.98	-0.23	0.00		
			Porphyrin	-0.45	-0.08	-0.50	-0.03		
			Cluster	-	-	-1.35	0.10		
			Substrate	0.09	0.00	0.19	-0.02		
		3/2	S bridge	N/A		N/A		N/A	

Inter.	Bond isomer	*S*	Fragment	Cluster model					
				SCH3		Zn		Fe4S4	
				Charge	Spin	Charge	Spin	Charge	Spin
			Fe						
			Porphyrin						
			Cluster						
			Substrate						
		5/2	S bridge	N/A		N/A		N/A	
			Fe						
			Porphyrin						
			Cluster						
			Substrate						
	O	1/2	S bridge	-0.07	0.10	-0.04	0.03	-0.25	-0.17
			Fe	0.43	0.98	-0.23	0.00	-0.23	0.00
			Porphyrin	-0.45	-0.08	-0.53	-0.09	-0.76	-0.02
			Cluster	-	-	-1.39	0.02	-0.56	0.47
			Substrate	0.09	0.00	0.07	0.00	0.07	0.00
		3/2	S bridge	-0.25	0.42	-0.20	0.31	-0.24	-0.17
			Fe	0.61	2.63	-0.24	0.00	-0.23	0.00
			Porphyrin	-0.38	-0.09	-0.49	-0.06	-0.78	-0.14
			Cluster	-	-	-1.44	0.06	-0.65	0.62
			Substrate	0.03	0.01	0.02	0.01	0.01	0.01
		5/2	S bridge	-0.16	0.47	-0.18	0.36	-0.22	-0.18
			Fe	0.74	4.13	-0.21	0.00	-0.22	0.00
			Porphyrin	-0.60	0.29	-0.70	0.29	-0.90	0.12
			Cluster	-	-	-1.35	0.13	-0.63	0.62
			Substrate	0.02	0.02	0.00	0.02	-0.01	0.02
3	S	1/2	S bridge	-0.02	0.05	-0.14	0.00	N/A	
			Fe	0.33	1.04	-0.43	0.06		
			Porphyrin	-0.20	-0.09	-0.31	0.45		
			Cluster	-	-	-1.15	0.53		
			Substrate	-0.11	0.00	-0.07	0.00		
		3/2	S bridge	N/A		N/A		0.07	0.00
			Fe					-0.38	0.21
			Porphyrin					-0.56	-0.06
			Cluster					-0.58	0.67
			Substrate					-0.21	-0.05
		5/2	S bridge	N/A		N/A		N/A	
			Fe						
			Porphyrin						
			Cluster						
			Substrate						
	O	1/2	S bridge	-0.07	0.09	-0.05	0.03	0.04	0.00
			Fe	0.42	1.02	-0.44	0.00	-0.41	0.10

Inter.	Bond isomer	*S*	Fragment	Cluster model					
				SCH3		Zn		Fe4S4	
				Charge	Spin	Charge	Spin	Charge	Spin
			Porphyrin	-0.28	-0.01	-0.25	0.32	-0.34	-0.25
			Cluster	-	-	-1.32	0.16	-0.82	-0.56
			Substrate	-0.07	-0.12	-0.30	-0.56	-0.12	0.23
		3/2	S bridge	-0.04	0.20	-0.25	0.14	0.06	0.00
			Fe	0.48	2.27	-0.24	-0.54	-0.34	0.20
			Porphyrin	-0.17	-0.11	-0.83	0.30	-0.65	-0.09
			Cluster	-	-	-0.82	-0.98	-0.53	0.63
			Substrate	-0.27	0.63	-0.42	-0.62	-0.27	0.48
		5/2	S bridge	-0.16	0.44	-0.44	0.00	0.08	0.00
			Fe	0.73	4.11	0.00	0.00	-0.36	0.21
			Porphyrin	-0.53	0.37	-0.83	0.30	-0.75	0.30
			Cluster	-	-	-1.87	-0.26	-0.58	0.72
			Substrate	-0.04	0.02	-0.82	-0.98	-0.34	-0.53
4	S	1/2	S bridge	-0.29	0.00	-0.18	0.00	0.03	0.00
			Fe	-0.27	0.00	-0.47	0.00	-0.43	0.10
			Porphyrin	-0.72	0.00	-0.82	0.00	-0.70	0.00
			Cluster	-	0.00	-1.54	0.00	-1.12	-0.23
			Substrate	-0.16	0.00	-0.14	0.00	-0.02	0.00
		3/2	S bridge	-0.26	0.11	N/A		0.03	0.00
			Fe	0.35	1.32			-0.43	0.11
			Porphyrin	-0.61	-0.07			-0.68	-0.07
			Cluster	-	-			-1.23	-0.19
			Substrate	-0.48	0.62			-0.26	0.18
		5/2	S bridge	-0.37	0.25	-0.29	0.17	0.03	0.00
			Fe	0.61	3.91	-0.47	0.00	-0.43	0.11
			Porphyrin	-0.87	0.18	-0.92	0.20	-0.86	0.18
			Cluster	-	-	-1.56	0.00	-1.23	-0.13
			Substrate	-0.37	-0.39	-0.37	-0.40	-0.24	-0.20
	O	1/2	S bridge	-0.29	0.00	-0.19	0.00	0.03	0.00
			Fe	0.45	0.00	-0.47	0.00	-0.41	0.11
			Porphyrin	-0.72	0.00	-0.90	0.00	-0.65	0.09
			Cluster	-	0.00	-1.56	0.00	-1.07	-0.21
			Substrate	-0.32	0.00	-0.31	0.00	-0.48	0.85
		3/2	S bridge	-0.23	0.07	-0.15	-0.03	0.02	0.00
			Fe	0.46	1.07	-0.46	0.00	-0.42	0.11
			Porphyrin	-0.65	-0.09	-0.75	-0.10	-0.70	-0.09
			Cluster	-	-	-1.52	0.00	-1.14	-0.29
			Substrate	-0.58	0.94	-0.60	0.86	-0.44	0.68
		5/2	S bridge	-0.22	-0.09	-0.27	0.22	-1.54	0.28
			Fe	0.61	3.16	-0.47	0.00	0.00	0.00
			Porphyrin	-0.88	0.09	-0.93	0.27	-0.70	-0.09

Inter.	Bond isomer	*S*	Fragment	Cluster model					
				SCH3		Zn		Fe4S4	
				Charge	Spin	Charge	Spin	Charge	Spin
			Cluster	-	-	-1.57	0.00	-5.29	0.81
			Substrate	-0.51	0.83	-0.52	-0.72	-1.14	-0.29
5	S	1	S bridge	0.01	0.00	0.00	0.00	-0.20	0.31
			Fe	0.23	0.00	-0.44	0.00	0.46	-1.66
			Porphyrin	-0.24	0.00	-0.36	0.00	-0.61	0.10
			Cluster	-	0.00	-1.31	0.00	-0.59	0.63
			Substrate	0.00	0.00	-0.02	0.00	-0.06	0.57
		2	S bridge	-0.06	0.19	-0.18	0.00	-0.20	0.31
			Fe	0.27	1.00	-0.41	0.00	0.44	1.58
			Porphyrin	-0.27	0.13	-0.60	-0.07	-0.59	-0.08
			Cluster	-	-	-0.79	0.99	-0.59	0.66
			Substrate	0.06	0.68	-0.21	-0.09	-0.06	-0.45
		3	S bridge	-0.14	0.47	-0.14	0.28	-0.19	0.32
			Fe	0.61	4.01	-0.44	0.01	0.60	3.62
			Porphyrin	-0.54	0.30	-0.63	0.38	-0.85	0.08
			Cluster	-	-	-1.31	0.19	-0.55	0.66
			Substrate	0.07	-0.82	0.03	-0.78	-0.01	-0.72
	O	1	S bridge	-0.23	0.00	0.10	0.00	-0.23	0.24
			Fe	-0.34	0.00	-0.42	0.00	0.54	1.15
			Porphyrin	-6.58	0.00	-0.64	0.00	-0.56	-0.08
			Cluster	-	0.00	-1.09	0.00	-0.39	-1.27
			Substrate	0.53	0.00	-0.29	0.00	-0.35	-0.04
		2	S bridge	-0.07	0.11	-0.13	0.02	-0.20	0.32
			Fe	0.42	1.04	-0.42	0.09	0.65	1.39
			Porphyrin	-0.43	-0.07	-0.29	0.32	-0.62	-0.08
			Cluster	-	-	-1.26	0.28	-0.56	0.63
			Substrate	0.08	0.89	-0.28	0.33	-0.27	-0.27
		3	S bridge	-0.25	0.42	-0.22	0.30	-0.24	0.23
			Fe	0.60	2.62	-0.45	0.01	0.82	4.10
			Porphyrin	-0.38	-0.05	-0.43	0.04	-0.81	0.23
			Cluster	-	-	-1.42	0.12	-0.52	-1.15
			Substrate	0.02	1.00	-0.04	0.86	-0.24	0.57
6	S	1	S bridge	1.22	0.00	-0.20	0.00	N/A	
			Fe	-0.61	0.00	0.26	0.00		
			Porphyrin	-11.51	0.00	-0.03	0.00		
			Cluster	-	0.00	-0.76	0.00		
			Substrate	0.43	0.00	0.27	0.00		
		2	S bridge	0.26	0.05	-0.06	-0.01	-0.18	0.30
			Fe	0.21	-0.04	0.29	1.08	0.48	1.26
			Porphyrin	0.26	1.96	-0.39	-0.05	-0.28	-0.03
			Cluster	-	-	-0.67	0.99	-0.20	0.49

Inter.	Bond isomer	*S*	Fragment	Cluster model					
				SCH3		Zn		Fe4S4	
				Charge	Spin	Charge	Spin	Charge	Spin
			Substrate	0.28	0.00	0.35	-0.03	0.18	-0.02
		3	S bridge	N/A		N/A		-0.18	0.30
			Fe					0.62	2.78
			Porphyrin					-0.20	0.04
			Cluster					-0.39	0.82
			Substrate					0.14	0.07
7	S	1	S bridge	0.19	0.00	-0.21	0.00	-0.16	0.34
			Fe	0.11	0.00	-0.09	0.00	0.24	-1.00
			Porphyrin	0.76	0.00	0.23	0.00	0.33	-0.85
			Cluster	-	0.00	-0.74	0.00	-0.49	0.61
			Substrate	0.43	0.00	0.07	0.00	0.08	0.92
		2	S bridge	0.09	0.56	-0.20	0.00	-0.14	0.35
			Fe	0.24	1.64	-0.26	0.46	0.23	1.08
			Porphyrin	0.63	0.86	0.23	0.81	0.36	0.88
			Cluster	-	-	-0.69	1.06	-0.46	0.63
			Substrate	0.04	-1.08	-0.06	-1.00	0.02	-0.95
		3	S bridge	0.16	0.06	-0.15	0.02	-0.15	0.34
			Fe	0.57	2.39	-0.24	0.44	0.44	3.32
			Porphyrin	0.44	-0.06	0.20	0.80	0.12	1.06
			Cluster	-	-	-0.66	1.04	-0.44	0.66
			Substrate	-0.17	1.58	-0.17	1.02	0.03	-1.40
	O	1	S bridge	0.25	0.00	-0.12	0.00	-0.15	0.31
			Fe	0.41	0.00	-0.31	0.00	0.52	-1.17
			Porphyrin	0.64	0.00	0.42	0.00	-0.21	0.33
			Cluster	-	0.00	-0.94	0.00	-0.13	-1.26
			Substrate	0.22	0.00	-0.28	0.00	-0.04	1.78
		2	S bridge	0.00	0.18	-0.07	0.06	-0.16	0.31
			Fe	0.43	0.98	-0.24	0.46	0.57	1.24
			Porphyrin	0.57	1.00	-0.07	0.54	-0.20	0.14
			Cluster	-	-	-0.69	1.00	-0.16	-1.44
			Substrate	0.00	-0.18	-0.13	1.50	-0.05	1.75
		3	S bridge	0.01	0.16	-0.15	-0.03	-0.17	0.30
			Fe	0.43	1.01	-0.25	0.46	0.71	2.79
			Porphyrin	0.46	0.92	0.14	0.83	-0.14	0.16
			Cluster	-	-	-0.69	1.04	-0.36	-1.09
			Substrate	0.09	1.88	-0.32	1.28	-0.03	1.85
8	S	1/2	S bridge	-0.04	0.39	-0.19	0.04	-0.20	0.31
			Fe	0.22	1.85	-0.35	0.25	0.29	-1.12
			Porphyrin	-0.18	-0.09	-0.17	0.44	-0.51	0.15
			Cluster	-	-	-1.21	0.43	-0.60	0.63
			Substrate	-0.01	-1.13	-0.15	-1.00	0.01	1.03

Inter.	Bond isomer	*S*	Fragment	Cluster model					
				SCH3		Zn		Fe4S4	
				Charge	Spin	Charge	Spin	Charge	Spin
		3/2	S bridge	-0.07	0.47	N/A		-0.19	0.31
			Fe	0.48	3.80			0.33	1.15
			Porphyrin	-0.48	0.22			-0.49	0.02
			Cluster	-	-			-0.50	0.60
			Substrate	0.07	-1.53			-0.15	0.93
		5/2	S bridge	-0.08	0.43	-0.26	0.00	-0.20	0.31
			Fe	0.50	3.83	-0.26	0.46	0.54	3.57
			Porphyrin	-0.43	0.36	-0.82	0.12	-0.73	0.15
			Cluster	-	-	-0.83	0.98	-0.55	0.65
			Substrate	0.02	0.34	-0.12	0.30	-0.06	0.29
	O	1/2	S bridge	-0.07	0.14	-0.19	-0.03	-0.20	-0.27
			Fe	0.44	1.10	-0.26	0.44	0.55	-1.08
			Porphyrin	-0.24	0.04	-0.61	-0.05	-0.56	0.08
			Cluster	-	-	-0.81	0.98	-0.40	1.29
			Substrate	-0.13	-0.28	-0.41	-1.00	-0.40	0.96
		3/2	S bridge	-0.06	0.12	N/A		-0.28	0.24
			Fe	0.43	1.08			0.55	1.03
			Porphyrin	-0.32	0.06			-0.06	0.52
			Cluster	-	-			-0.89	-0.05
			Substrate	-0.04	1.71			-0.32	1.26
		5/2	S bridge	-0.27	0.41	-0.31	0.10	-0.23	0.24
			Fe	0.64	2.62	-0.27	0.46	0.85	4.10
			Porphyrin	-0.33	0.07	-0.61	-0.08	-0.79	0.29
			Cluster	-	-	-0.83	0.99	-0.52	-1.13
			Substrate	-0.03	1.88	-0.45	1.37	-0.31	1.50
9	S	1	S bridge	-0.21	0.00	-0.25	0.00	N/A	
			Fe	0.17	0.00	-0.46	0.00		
			Porphyrin	-0.71	0.00	-0.80	0.00		
			Cluster	-	0.00	-1.57	0.00		
			Substrate	0.08	0.00	-0.08	0.00		
		2	S bridge	-0.30	0.07	-0.22	-0.01	-0.33	0.21
			Fe	0.29	1.04	-0.47	0.00	0.35	1.22
			Porphyrin	-0.65	-0.04	-0.93	0.05	-0.60	-0.04
			Cluster	-	-	-1.57	0.00	-1.20	-0.26
			Substrate	-0.35	0.94	-0.19	-1.26	-0.22	0.88
		3	S bridge	-0.33	0.00	-0.24	-0.02	-0.34	0.20
			Fe	0.47	3.27	-0.45	0.00	0.49	3.43
			Porphyrin	-0.89	0.07	-0.97	0.08	-0.84	0.16
			Cluster	-	-	-1.54	0.00	-1.19	-0.24
			Substrate	-0.25	0.62	-0.23	0.59	-0.13	0.45
	O	1	S bridge	-0.16	0.00	-0.18	0.00	N/A	

Inter.	Bond isomer	*S*	Fragment	Cluster model					
				SCH3		Zn		Fe4S4	
				Charge	Spin	Charge	Spin	Charge	Spin
			Fe	0.47	0.00	-0.46	0.00		
			Porphyrin	-0.72	0.00	-0.79	0.00		
			Cluster	-	0.00	-1.55	0.00		
			Substrate	-0.27	0.00	-0.45	0.00		
		2	S bridge	-0.29	0.05	-0.20	0.01	-0.33	0.21
			Fe	0.49	1.03	-0.46	0.00	0.54	0.99
			Porphyrin	-0.66	-0.08	-0.76	-0.08	-0.65	-0.07
			Cluster	-	-	-1.53	0.00	-1.12	-0.25
			Substrate	-0.55	1.01	-0.52	1.03	-0.44	1.11
		3	S bridge	-0.44	0.27	-0.33	0.18	-0.34	0.20
			Fe	0.67	2.58	-0.47	0.00	0.84	4.12
			Porphyrin	-0.68	-0.13	-0.75	-0.12	-0.83	0.30
			Cluster	-	-	-1.58	0.00	-1.26	-0.11
			Substrate	-0.55	1.27	-0.53	1.29	-0.41	-0.55
10	S	1/2	S bridge	-0.57	0.00	-0.37	0.00	-0.40	0.16
			Fe	0.30	0.27	-0.47	0.00	0.35	0.21
			Porphyrin	-1.21	-0.18	-1.24	-0.09	-1.13	-0.06
			Cluster	-	-	-1.72	0.00	-1.39	-0.19
			Substrate	-0.52	0.91	-0.50	0.90	-0.43	0.87
		3/2	S bridge	-0.60	0.04	-0.38	0.01	-0.37	0.21
			Fe	0.50	3.42	-0.50	0.00	0.34	0.21
			Porphyrin	-1.31	-0.12	-1.32	-0.05	-1.12	-0.09
			Cluster	-	-	-1.75	0.00	-1.43	1.72
			Substrate	-0.59	-0.36	-0.56	-0.35	-0.42	0.90
		5/2	S bridge	-0.37	0.59	-0.44	0.04	-0.39	0.16
			Fe	0.52	3.51	-0.50	0.00	0.67	3.85
			Porphyrin	-1.76	0.21	-1.39	0.00	-1.24	0.02
			Cluster	-	-	-1.70	0.00	-1.41	-0.16
			Substrate	-0.40	0.68	-0.67	1.07	-0.63	1.08
	O	1/2	S bridge	-0.57	0.00	-0.36	0.00	N/A	
			Fe	0.31	0.25	-0.50	0.00		
			Porphyrin	-1.21	-0.17	-1.22	-0.04		
			Cluster	-	-	-1.70	0.00		
			Substrate	-0.52	0.91	-0.74	0.84		
		3/2	S bridge	-0.38	0.03	-0.46	0.05	N/A	
			Fe	0.31	1.10	-0.52	0.00		
			Porphyrin	-1.55	0.92	-1.21	-0.26		
			Cluster	-	-	-1.76	0.00		
			Substrate	-0.38	0.93	-0.81	0.98		
		5/2	S bridge	-0.57	0.14	-0.45	0.04	N/A	
			Fe	0.57	3.91	-0.49	0.00		

Inter.	Bond isomer	*S*	Fragment	Cluster model					
				SCH3		Zn		Fe4S4	
				Charge	Spin	Charge	Spin	Charge	Spin
			Porphyrin	-1.38	-0.12	-1.33	0.05		
			Cluster	-	-	-1.75	0.00		
			Substrate	-0.62	1.06	-0.87	0.93		
11	S	1/2	S bridge	-0.32	0.04	-0.22	0.00	-0.34	0.21
			Fe	0.28	0.98	-0.47	0.00	0.31	0.91
			Porphyrin	-0.70	-0.10	-0.77	-0.07	-0.67	-0.05
			Cluster	-	-	-1.57	0.00	-1.17	-0.25
			Substrate	-0.26	0.08	-0.23	0.11	-0.12	0.21
		3/2	S bridge	-0.30	-0.06	-0.28	-0.02	-0.35	0.20
			Fe	0.42	3.05	-0.35	0.00	0.60	2.62
			Porphyrin	-0.89	0.06	-1.44	0.91	-0.62	-0.07
			Cluster	-	-	-1.06	0.99	-1.30	-0.13
			Substrate	-0.23	-0.08	-0.14	0.08	-0.34	0.41
		5/2	S bridge	-0.40	0.29	-0.31	0.18	-0.35	0.20
			Fe	0.67	4.09	-0.47	0.00	0.69	4.09
			Porphyrin	-0.90	0.22	-0.95	0.23	-0.83	0.28
			Cluster	-	-	-1.57	0.00	-1.26	-0.11
			Substrate	-0.38	0.35	-0.35	0.42	-0.25	0.51
12	S	1/2	S bridge	-0.05	-0.42	-0.20	-0.04	-0.23	0.25
			Fe	0.23	1.19	0.50	0.02	0.38	1.34
			Porphyrin	-0.04	-0.58	-0.24	-0.56	-0.47	-0.08
			Cluster	-	-	-1.14	-0.57	-0.51	-1.27
			Substrate	-0.15	0.78	-0.22	0.89	-0.17	0.80
		3/2	S bridge	-0.14	0.27	-0.20	-0.02	-0.23	0.24
			Fe	0.25	1.24	0.50	-0.01	0.48	3.41
			Porphyrin	0.06	0.48	-0.23	0.32	-0.62	0.11
			Cluster	-	-	-1.15	0.56	-0.45	-1.27
			Substrate	-0.17	1.01	-0.21	0.90	-0.19	0.52
		5/2	S bridge	-0.21	-0.04	-0.20	-0.06	-0.19	0.31
			Fe	0.41	3.30	0.51	-0.02	0.48	3.41
			Porphyrin	0.05	0.99	-0.71	0.14	-0.59	0.10
			Cluster	-	-	-0.85	1.00	-0.52	0.62
			Substrate	-0.25	0.74	-0.22	0.53	-0.18	0.50
13	S	1	S bridge	-0.26	0.00	-0.17	0.00	N/A	
			Fe	0.30	0.00	0.50	0.00		
			Porphyrin	-0.65	0.00	-0.73	0.00		
			Cluster	-	0.00	-1.54	0.00		
			Substrate	-0.39	0.00	-0.36	0.00		
		2	S bridge	-0.35	0.00	-0.24	-0.02	-0.34	0.20
			Fe	0.30	1.28	0.51	0.00	0.39	1.39
			Porphyrin	-0.62	-0.09	-0.71	-0.10	-0.56	-0.08

Inter.	Bond isomer	*S*	Fragment	Cluster model					
				SCH3		Zn		Fe4S4	
				Charge	Spin	Charge	Spin	Charge	Spin
			Cluster	-	-	-1.57	0.00	-1.26	-0.25
			Substrate	-0.33	0.85	-0.30	0.83	-0.22	0.78
		3	S bridge	-0.30	-0.12	-0.21	-0.13	-0.33	0.21
			Fe	0.44	3.35	0.50	0.00	0.48	3.42
			Porphyrin	-0.80	0.11	-0.87	0.13	-0.73	0.14
			Cluster	-	-	-1.56	0.00	-1.17	-0.30
			Substrate	-0.34	0.64	-0.32	0.58	-0.25	0.53
14	S	1	S bridge	0.02	0.00	0.05	0.00	N/A	
			Fe	0.27	0.00	-0.43	0.00		
			Porphyrin	-0.22	0.00	-0.41	0.00		
			Cluster	-	0.00	-1.22	0.00		
			Substrate	-0.07	0.00	-0.14	0.00		
		2	S bridge	0.00	0.21	N/A		-0.20	0.31
			Fe	0.28	1.76			0.46	1.10
			Porphyrin	-0.17	-0.07			-0.56	-0.08
			Cluster	-	-			-0.57	0.62
			Substrate	-0.11	0.10			-0.14	0.02
		3	S bridge	0.04	0.08	-0.16	-0.06	-0.20	0.31
			Fe	0.42	3.59	-0.35	0.24	0.56	3.05
			Porphyrin	-0.39	0.25	-0.32	0.70	-0.68	0.07
			Cluster	-	-	-1.23	0.33	-0.51	0.63
			Substrate	-0.07	0.01	-0.25	-0.06	-0.17	-0.06
15	S	1/2	S bridge	-0.18	0.64	-0.25	0.02	-0.34	0.20
			Fe	0.33	-0.65	-0.46	0.00	0.49	1.14
			Porphyrin	-0.77	1.04	-0.80	-0.08	-0.68	-0.11
			Cluster	-	-	-1.53	0.00	-1.26	-0.25
			Substrate	-0.39	0.00	-0.34	0.02	-0.21	0.00
		3/2	S bridge	-0.28	-0.07	-0.22	-0.07	N/A	
			Fe	0.49	3.05	-0.46	0.00		
			Porphyrin	-0.88	0.07	-0.95	0.06		
			Cluster	-	-	-1.54	0.00		
			Substrate	-0.33	-0.05	-0.32	-0.07		
		5/2	S bridge	-0.40	0.30	-0.33	0.21	-0.34	0.20
			Fe	0.70	4.15	-0.46	0.00	0.75	4.18
			Porphyrin	-0.85	0.26	-0.94	0.28	-0.78	0.35
			Cluster	-	-	-1.56	0.00	-1.28	-0.10
			Substrate	-0.45	0.25	-0.43	0.28	-0.34	0.33
16	S	1/2	S bridge	-0.08	0.10	-0.05	0.04	-0.28	0.24
			Fe	0.35	0.99	-0.45	0.00	0.48	1.27
			Porphyrin	-0.49	-0.08	-0.61	-0.09	-0.48	-0.12
			Cluster	-	-	-1.41	0.01	-0.88	-0.38

Inter.	Bond isomer	*S*	Fragment	Cluster model					
				SCH3		Zn		Fe4S4	
				Charge	Spin	Charge	Spin	Charge	Spin
			Substrate	0.21	-0.01	0.23	-0.01	0.17	0.00
		3/2	S bridge	N/A	0.00	N/A		-0.20	0.32
			Fe		0.00			0.60	2.16
			Porphyrin		0.00			-0.76	-0.10
			Cluster	-	0.00			-0.65	0.60
			Substrate		0.00			0.00	0.00
		5/2	S bridge	N/A	0.00	N/A		-0.20	0.31
			Fe		0.00			0.74	3.91
			Porphyrin		0.00			-0.88	0.20
			Cluster	-	0.00			-0.65	0.53
			Substrate		0.00			0.00	0.00
18	S	1/2	S bridge	0.02	-0.02	0.26	0.01	-0.15	0.35
			Fe	0.28	1.03	-0.35	0.00	0.50	-1.70
			Porphyrin	0.60	0.72	-0.46	-0.07	0.11	1.01
			Cluster	-	-	-0.55	0.00	-0.42	0.59
			Substrate	0.10	-0.75	0.01	-0.37	-0.04	0.73
		3/2	S bridge	0.02	0.24	-0.14	0.02	-0.15	0.34
			Fe	0.28	0.96	-0.38	0.05	0.48	1.72
			Porphyrin	0.57	1.07	0.19	0.81	0.20	0.80
			Cluster	-	-	-0.67	1.04	-0.52	0.69
			Substrate	0.13	0.73	-0.15	-0.02	-0.01	-0.55
		5/2	S bridge	-0.05	0.56	-0.18	0.17	N/A	
			Fe	0.60	3.97	-0.39	0.02		
			Porphyrin	0.32	1.27	-0.36	0.58		
			Cluster	-	-	-0.67	1.03		
			Substrate	0.13	-0.81	0.10	-0.81		
	O	1/2	S bridge	0.32	-0.03	-0.04	-0.04	-0.17	0.29
			Fe	0.39	0.42	-0.40	0.00	0.51	-1.17
			Porphyrin	0.33	-0.01	-0.35	-0.11	-0.27	0.27
			Cluster	-	-	-0.66	0.99	-0.13	0.71
			Substrate	-0.04	0.62	0.14	-0.94	0.05	0.88
		3/2	S bridge	0.00	0.15	-0.06	0.00	-0.14	0.35
			Fe	0.41	0.97	-0.40	0.00	0.51	1.07
			Porphyrin	0.45	0.92	-0.23	0.14	0.03	0.48
			Cluster	-	-	-0.67	1.00	-0.31	0.60
			Substrate	0.14	0.95	0.03	0.71	-0.09	0.49
		5/2	S bridge	-0.19	0.48	-0.17	0.19	-0.15	-0.23
			Fe	0.62	2.59	-0.24	0.47	0.69	2.84
			Porphyrin	0.46	0.91	-0.47	0.40	-0.20	0.00
			Cluster	-	-	-0.67	1.06	-0.42	1.38
			Substrate	0.10	1.00	0.07	-0.80	0.08	1.02

Inter.	Bond isomer	*S*	Fragment	Cluster model					
				SCH3		Zn		Fe4S4	
				Charge	Spin	Charge	Spin	Charge	Spin
19	S	1	S bridge	-0.51	0.00	-0.33	0.00	N/A	
			Fe	0.28	0.00	0.28	0.00		
			Porphyrin	-1.12	0.00	-1.16	0.00		
			Cluster	-	0.00	-1.68	0.00		
			Substrate	-0.66	0.00	-0.63	0.00		
		2	S bridge	N/A		-0.18	0.00	-0.39	0.17
			Fe			0.32	1.11	0.57	2.06
			Porphyrin			-1.51	0.88	-1.00	-0.14
			Cluster			-1.61	0.00	-1.39	-0.15
			Substrate			-0.55	-0.03	-0.79	0.04
		3	S bridge	N/A		N/A		-0.38	0.17
			Fe					0.69	3.82
			Porphyrin					-1.16	0.07
			Cluster					-1.37	-0.14
			Substrate					-0.78	0.04
	O	1	S bridge	-0.50		-0.30	0.00	N/A	
			Fe	0.47		0.48	0.00		
			Porphyrin	-1.27		-1.28	0.00		
			Cluster	-	-	-1.68	0.00		
			Substrate	-0.70		-0.73	0.00		
		2	S bridge	0.01		-0.43	0.04	-0.39	0.16
			Fe	1.07		0.64	2.15	0.67	2.11
			Porphyrin	0.90		-1.24	-0.24	-1.11	-0.19
			Cluster	-	-	-1.74	0.00	-1.40	-0.14
			Substrate	0.00		-0.77	0.02	-0.77	0.04
		3	S bridge	N/A		N/A		-0.39	0.16
			Fe					0.78	3.86
			Porphyrin					-1.24	0.04
			Cluster					-1.41	-0.15
			Substrate					-0.74	0.05
20	S	1	S bridge	-0.40	0.00	N/A		N/A	
			Fe	0.19	0.00				
			Porphyrin	-0.83	0.00				
			Cluster	-	0.00				
			Substrate	0.04	0.00				
		2	S bridge	N/A		-0.35	0.11	-0.34	0.20
			Fe			-0.25	0.01	0.51	2.01
			Porphyrin			-1.00	-0.10	-0.82	-0.09
			Cluster			-1.60	0.00	-1.29	-0.13
			Substrate			-0.07	0.00	-0.06	0.00
		3	S bridge	-0.51	0.14	N/A		-0.33	0.21

Inter.	Bond isomer	*S*	Fragment	Cluster model					
				SCH3		Zn		Fe4S4	
				Charge	Spin	Charge	Spin	Charge	Spin
			Fe	0.66	3.77			0.70	3.78
			Porphyrin	-1.10	0.09			-0.99	0.14
			Cluster	-	-			-1.25	-0.15
			Substrate	-0.06	0.00			-0.13	0.00
	O	1	S bridge	-0.41	0.00	-0.29	0.00	-0.35	0.20
			Fe	0.44	0.00	-0.26	0.00	0.46	0.03
			Porphyrin	-1.05	0.00	-1.08	0.00	-0.95	0.00
			Cluster	-	0.00	-1.58	0.00	-1.19	-0.22
			Substrate	0.01	0.00	0.01	0.00	0.02	0.00
		2	S bridge	-0.51	0.18	N/A		-0.35	0.19
			Fe	0.57	2.04			0.62	2.07
			Porphyrin	-0.99	-0.24			-0.91	-0.16
			Cluster	-	-			-1.33	-0.14
			Substrate	-0.07	0.00			-0.03	0.00
		3	S bridge	-0.50	0.15	-0.20	0.23	-0.35	0.20
			Fe	0.69	3.81	-0.23	0.00	0.74	3.82
			Porphyrin	-1.11	0.01	-0.30	-0.05	-1.04	0.10
			Cluster	-	-	-0.70	1.00	-1.29	-0.15
			Substrate	-0.08	0.00	0.07	0.02	-0.06	0.00
21	S	1/2	S bridge	0.02	0.30	-0.18	0.00	-0.15	0.35
			Fe	0.22	0.64	-0.22	0.55	0.28	-0.88
			Porphyrin	0.48	0.93	0.16	1.04	0.29	1.06
			Cluster	-	-	-0.68	1.06	-0.43	0.63
			Substrate	0.27	-0.90	-0.05	-0.20	0.01	-0.19
		3/2	S bridge	0.02	0.25	-0.18	0.00	-0.15	0.35
			Fe	0.22	1.09	-0.22	0.55	0.29	0.91
			Porphyrin	0.54	0.92	0.16	0.81	0.29	0.89
			Cluster	-	-	-0.68	1.07	-0.43	0.61
			Substrate	0.21	0.72	-0.07	0.16	0.00	0.21
		5/2	S bridge	0.03	-0.03	-0.17	-0.05	-0.15	0.35
			Fe	0.38	3.16	-0.22	0.55	0.44	3.12
			Porphyrin	0.36	1.09	-0.01	0.98	0.11	1.07
			Cluster	-	-	-0.67	1.06	-0.42	0.61
			Substrate	0.23	0.74	-0.05	-0.14	0.02	-0.16
22	S	1	S bridge	-0.03	0.00	-0.01	0.00	-0.24	0.23
			Fe	0.19	0.00	-0.42	0.00	0.37	0.97
			Porphyrin	-0.29	0.00	-0.48	0.00	-0.58	-0.08
			Cluster	-	0.00	-1.24	0.00	-0.51	-1.24
			Substrate	0.12	0.00	0.09	0.00	-0.04	0.15
		2	S bridge	-0.05	0.18	-0.20	-0.01	-0.27	0.24
			Fe	0.23	1.26	-0.26	0.55	0.37	1.00

Inter.	Bond isomer	*S*	Fragment	Cluster model					
				SCH3		Zn		Fe4S4	
				Charge	Spin	Charge	Spin	Charge	Spin
			Porphyrin	-0.30	-0.05	-0.66	-0.06	-0.19	0.40
			Cluster	-	-	-0.80	0.99	-0.87	0.23
			Substrate	0.12	0.61	-0.12	0.16	-0.04	0.13
		3	S bridge	-0.03	-0.05	-0.19	-0.06	-0.24	0.22
			Fe	0.39	3.21	-0.26	0.52	0.66	4.06
			Porphyrin	-0.51	0.13	-0.83	0.08	-0.76	0.26
			Cluster	-	-	-0.81	0.99	-0.48	-1.14
			Substrate	0.16	0.68	-0.09	-0.10	-0.17	0.57

6.3.5 SiR reaction mechanism in vacuum

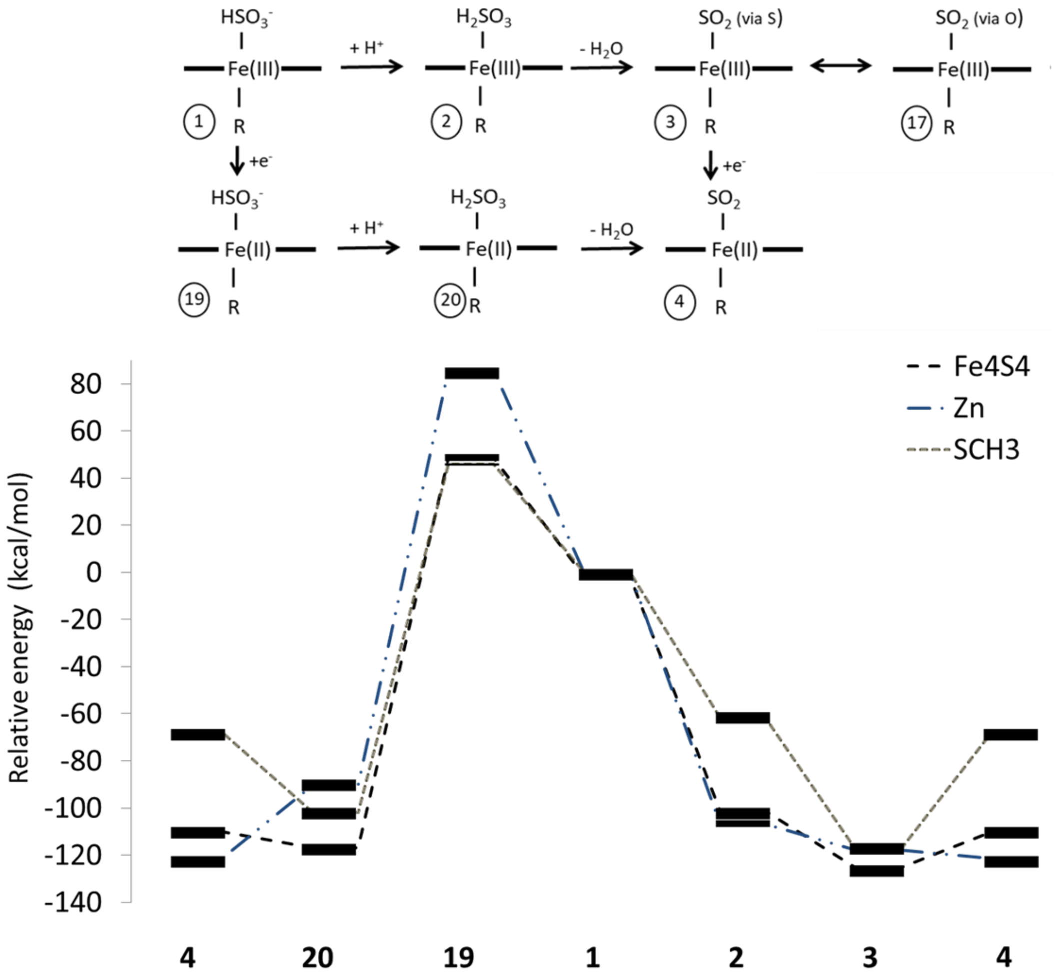

Figure 142. The **1-2-3-4** and **1-19-20-1** pathways computed in vacuum.

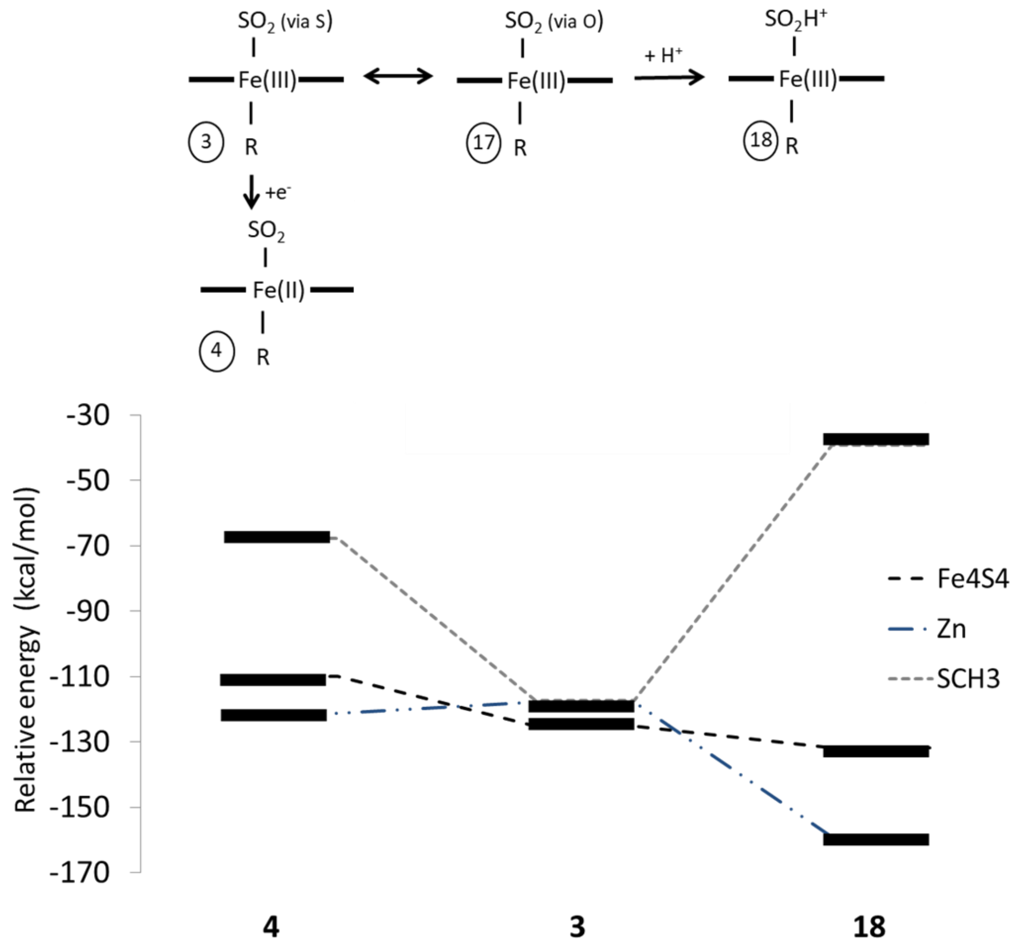

Figure 143. Intermediate **3** as a crossroad (computed in vacuum).

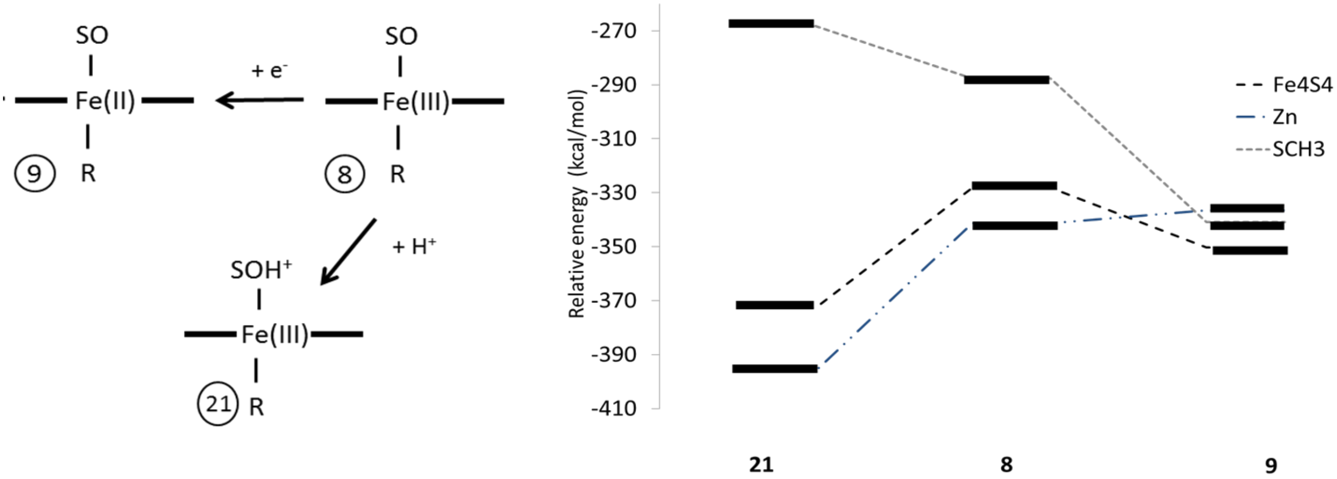

Figure 144. Intermediate **8** as a crossroad (computed in vacuum).

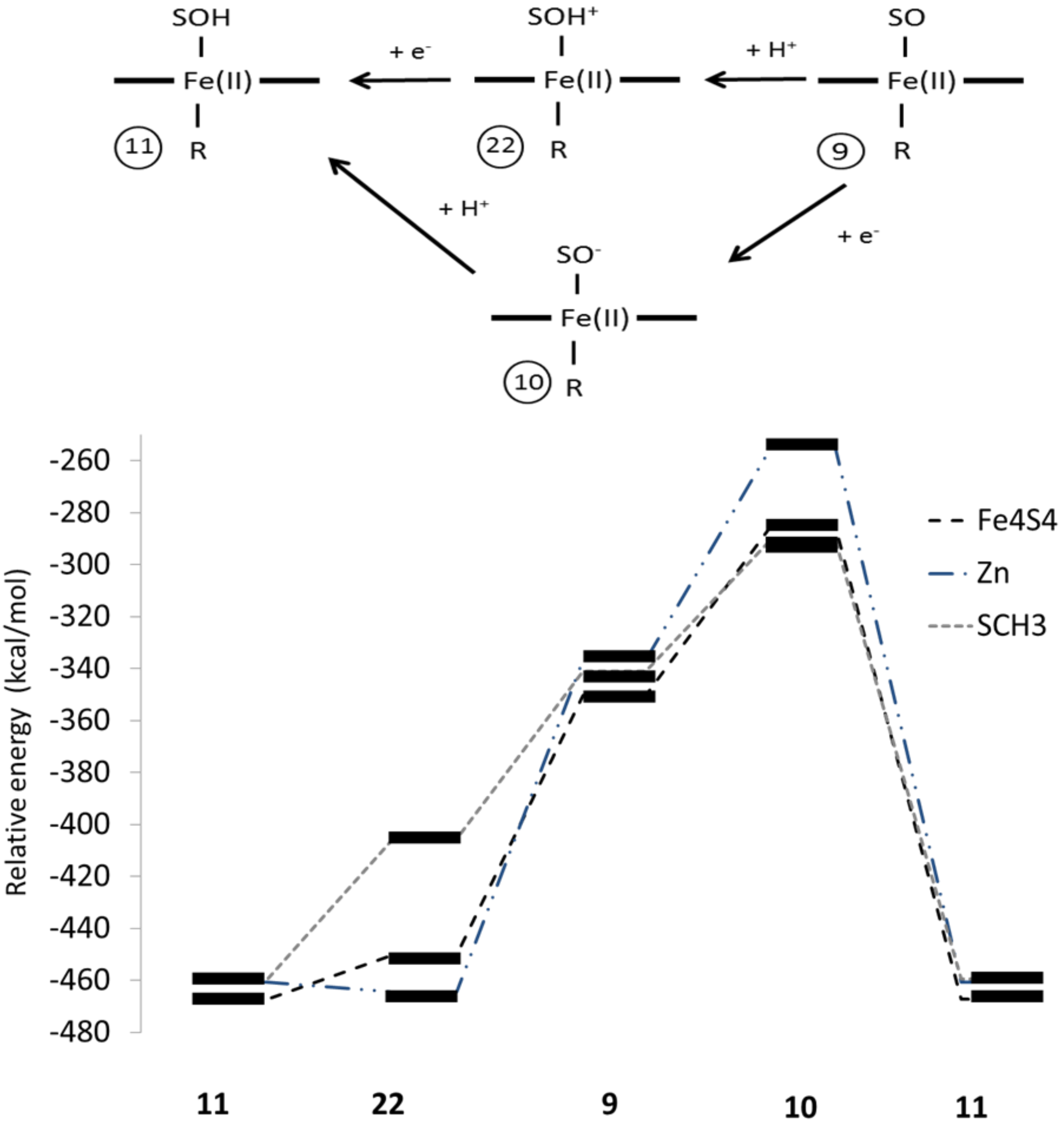

Figure 145. The **9-10-11** and **9-22-11** pathways computed in vacuum.

7 References

Motto:

"I will never be ashamed to cite a bad author

if he says something good."[*]

Seneca

---

[*] Personal translation from "Costa Ioana, *Asta a spus Seneca. Tu ce spui? – Carte de citate,* ed. Seneca Lucius Annaeus, Bucharest, 2018, pag. 129.

1. B. E. Sernelius, *Int. J. Mod. Phys. A*, **2009**, 24, 1804–1812.
2. D. Frauchiger and R. Renner, *Nat. Commun.*, **2018**, 9, 1–10.
3. V. R. I. Kaila, *J. R. Soc. Interface*, **2018**, 15.
4. P. Pyykko and J. P. Desclaux, *Acc. Chem. Res.*, **1979**, 12, 276–281.
5. G. Gamow, *Nature*, **1928**, 122, 805–806.
6. R. B. King, *Chem. Rev.*, **2001**, 101, 1119–1152.
7. A. Stock, *Hydrides of boron and silicon*, Cornell University Press, Ithaca, NY, **1933**.
8. W. Dilthey, *Zeitschrift für Angew. Chemie*, **1921**, 34, 596.
9. H. C. Longuet-Higgins, *Proc. Roy. Soc.*, **1945**, 183, 357.
10. W. N. Lipscomb, *Boron Hydrides*, W. A. Benjamin, New York, **1963**.
11. K. Hedberg and V. Schomaker, *J. Am. Chem. Soc.*, **1951**, 73, 1482–1487.
12. K. S. Pitzer, *J. Am. Chem. Soc.*, **1945**, 67, 1126–1132.
13. W. H. Eberhardt, B. Crawford and W. N. Lipscomb, *J. Chem. Phys.*, **1954**, 22, 989–1001.
14. R. E. Williams, *Inorg. Chem.*, **1971**, 10, 210–214.
15. H. C. Longuet-Higgins and M. de V. Roberts, *Proc. R. Soc. London. Ser. A. Math. Phys. Sci.*, **1955**, 230, 110–119.
16. A. R. Pitochelli and M. F. Hawthorne, *J. Am. Chem. Soc.*, **1960**, 82, 3228–3229.
17. M. F. Hawthorne and A. R. Pitochelli, *J. Am. Chem. SOC*, **1959**, 81, 5519.
18. J. A. Wunderlich and W. N. Lipscomb, *J. Am. Chem. Soc.*, **1960**, 82, 4427–4428.
19. A. Kaczmarczyk, R. D. Dobrott and W. N. Lipscomb, *Proc. Natl. Acad. Sci.*, **1962**, 48, 729–733.
20. F. Klanberg, D. R. Eaton, L. J. Guggenberger and E. L. Muetterties, *Inorg. Chem.*, **1967**, 6, 1271.

21. R. B. King and A. J. W. Duijvestijn, *Inorganica Chim. Acta*, **1990**, 178, 55–57.

22. I. Shapiro, D. C. Good and R. E. Williams, **1962**, 84, 3837.

23. I. Shapiro, R. E. Williams and D. C. Good, *J. Am. Chem. Soc.*, **1963**, 3167–3171.

24. R. B. King and D. H. Rouvray, *J. Am. Chem. Soc.*, **1977**, 99, 7834–7840.

25. J. Aihara, *J. Am. Chem. Soc.*, **1978**, 100, 3339–3342.

26. A. J. Stone and M. J. Alderton, *Inorg. Chem.*, **1982**, 21, 2297–2302.

27. K. Wade, *Chem. Commun.*, **1971**.

28. D. M. P. Mingos, *Acc. Chem. Res.*, **1984**, 17, 311–319.

29. R. Hoffman, *Angew. Chem. Int. Ed.*, **1982**, 27, 711–800.

30. J. D. Kennedy, *The Borane-Carborane-Carbocation Continuum*, Wiley, New York, **1998**.

31. S. Ghosh, M. Shang, Y. Li and T. P. Fehlner, *Angew. Chem. Int. Ed*, **2001**, 40, 1125–1128.

32. R. B. King, *Inorg. Chem.*, **2006**.

33. S. H. Vosko, L. Wilk and M. Nusair, *Can. J. Phys.*, **1980**, 58, 1200–1211.

34. A. D. Becke, *J. Chem. Phys.*, **1993**, 98, 5648–5652.

35. C. Lee, W. Yang and R. G. Parr, *Phys. Rev. B*, **1988**, 37, 785–789.

36. D. Andrae, U. Häußermann, M. Dolg, H. Stoll and H. Preuß, *Theor. Chim. Acta*, **1990**, 77, 123–141.

37. Y. Zhao and D. G. Truhlar, *Theor. Chem. Acc.*, **2008**, 120, 215–241.

38. P. J. Stephens, F. J. Devlin, C. F. Chabalowski and M. J. Frisch, *J. Phys. Chem.*, **1994**, 98, 11623–11627.

39. 2013 Frisch, M. J. et al. Gaussian 09, Revision E.01, Gaussian, Inc., Wallingford CT, .

40. F. Weinhold and C. R. Landis, *Valency and Bonding: A Natural Bond Order Donor-*

Acceptor Perspective, Cambridge University Press, Cambridge, **2005**.

41. A. Lupan and R. Bruce King, *Inorganica Chim. Acta*, **2013**, 397, 83–87.

42. H. Wang, Y. Xie, R. B. King and H. F. Schaefer, *J. Am. Chem. Soc.*, **2006**, 128, 11376–11384.

43. E. A. McNeill, K. L. Gallaher, F. R. Scholer and S. H. Bauer, *Inorg. Chem.*, **1973**, 12, 2108.

44. P. T. Brain, D. Hnyk, D. W. H. Rankin, M. Bühl and P. von Ragué Schleyer, *Polyhedron*, **1994**.

45. H. Yan, A. M. Beatty and T. P. Fehlner, *Organometallics*, **2002**, 21, 5029–5037.

46. A. Lupan and R. B. King, *Inorg. Chem.*, **2012**, 51, 7609–7616.

47. A. Lupan and R. B. King, *Organometallics*, **2013**, 32, 4002–4008.

48. X. Lei, M. Shang and T. P. Fehlner, *Chem. - A Eur. J.*, **2006**, 6, 2653.

49. X. Lei, M. Shang and T. P. Fehlner, *Organometallics*, **2000**, 19, 118–120.

50. X. Lei, M. Shang and T. P. Fehlner, *J. Am. Chem. Soc.*, **1999**, 121, 1275–1287.

51. R. Mason, K. M. Thomas and D. M. P. Mingos, **1973**, 95, 3802–3804.

52. S. Ghosh, M. Shang and T. P. Fehlner, *J. Organomet. Chem.*, **2000**, 614–615, 92–98.

53. R. E. Williams, *Chem. Rev.*, **1992**, 92, 177–207.

54. H. Janet Bullick, P. D. Grebenik, M. L. H Green, A. K. Hughes, C. B. John LeachC and P. C. McGowanb, *J. CHEM. SOC. Dalt. TRANS*, **1995**, 67–75.

55. D. Y. Kim and G. S. Girolami, *J. Am. Chem. Soc.*, **2006**, 128, 10969–10977.

56. A. S. Weller, M. Shang and T. P. Fehlner, *Organometallics*, **1988**, 18, 53–64.

57. D. K. Roy, S. K. Bose, R. S. Anju, V. Ramkumar and S. Ghosh, *Inorg. Chem.*, **2012**, 51, 10715–10722.

58. S. K. Bose, S. Ghosh, B. C. Noll, J.-F. Halet, J.-Y. Saillard and A. Vega, *Organometallics*, **2007**, 26, 5377–5385.

59. A. M. V. Brânzanic, A. Lupan and R. B. King, *Dalt. Trans.*, **2015**, 44, 7355–7363.

60. A. M. V. Brânzanic, A. Lupan and R. B. King, *Organometallics*, **2014**, 33, 6433–6451.

61. S. Aldridge, H. Hashimoto, K. Kawamura, M. Shang and T. P. Fehlner, *Inorg. Chem.*, **1998**, 37, 928–940.

62. A. M. V Brânzanic, A. Lupan and R. B. King, *J. Organomet. Chem.*, **2015**, 792, 74–80.

63. A. M. V. Brânzanic, A. Lupan and R. B. King, *Dalt. Trans.*, **2016**, 45, 9354–9362.

64. R. Borthakur, S. Kar, S. K. Barik, S. Bhattacharya, G. Kundu, B. Varghese and S. Ghosh, *Inorg. Chem.*, **2017**, 56, 1524–1533.

65. B. Mondal, R. Bag and S. Ghosh, *Organometallics*, **2018**, 37, 2419–2428.

66. S. Aldridge, M. Shang and T. P. Fehlner, *J. Am. Chem. SOC*, **1998**, 120, 2586–2598.

67. B. R. Crane, L. M. Siegel and E. D. Getzoff, *Biochemistry*, **1997**, 36, 12120–12137.

68. H. D. Peck, T. Lissolo and J. A. Cole, *Symposium of the Society of General Microbiology – The Nitrogen and Sulfur Cycles*, Cambridge University Press, Cambridge, **1988**.

69. A. Messerschimdt, R. Huber, T. Poulos and K. Wieghardt, *Handbook of Metalloproteins, Wiley ,2001*, John Wiley & Sons Ltd, Chichester, **2001**.

70. T. Akashi, T. Matsumura, T. Ideguchi, K. Iwakiri, T. Kawakatsu, I. Taniguchi and T. Hase, *J. Biol. Chem.*, **1999**, 274, 29399–29405.

71. K. Sekine, M. Fujiwara, M. Nakayama, T. Takao, T. Hase and N. Sato, *FEBS J.*, **2007**, 274, 2054–2069.

72. N. Sato, M. Nakayama and T. Hase, *FEBS Lett.*, **2001**, 487, 347–350.

73. K. Sekine, T. Hase and N. Sato, *J. Biol. Chem.*, **2002**, 277, 24399–24404.

74. G. C. Cannon, L. N. Ward, C. I. Case and S. Heinhorst, *Plant Mol. Biol.*, **1999**, 39, 835–845.

75. B. R. Crane, L. M. Siegel and E. D. Getzoff, *Science*, **1995**, 270, 59–67.

76. L. M. Siegel, D. C. Rueger, M. J. Barber, R. J. Krueger, N. R. Orme-Johnson and W. H. Orme-Johnson, *J. Biol. Chem.*, **1982**, 257, 6348–6350.

77. J. A. Christner, E. Munch, P. A. Janick and L. M. Siegel, *J. Biol. Chem.*, **1981**, 256, 2089–2101.

78. B. R. Crane, L. M. Siegel and E. D. Getzoff, *Biochemistry*, **1997**, 36, 12101–12119.

79. M. Surducan, D. Lup, A. Lupan, S. V. Makarov and R. Silaghi-Dumitrescu, *J. Inorg. Biochem.*, **2013**, 118, 13–20.

80. M. Surducan, A. M. V. Brânzanic and R. Silaghi-Dumitrescu, *Int. J. Quantum Chem.*, **2018**, 118, 2–10.

81. M. Surducan, S. V Makarov and R. Silaghi-Dumitrescu, *Eur. J. Inorg. Chem.*, **2014**, 34, 5827–5837.

82. R. Silaghi-Dumitrescu and S. V. Makarov, *Int. J. Quantum Chem.*, **2012**, 112, 900–908.

83. E. Sigfridsson, M. H. M. Olsson and U. Ryde, *J. Phys. Chem. B*, **2001**, 105, 5546–5552.

84. E. Sigfridsson, M. H. M. Olsson and U. Ryde, *Inorg. Chem.*, **2001**, 40, 2509–2519.

85. J. Ballmann, A. Albers, S. Demeshko, S. Dechert, E. Bill, E. Bothe, U. Ryde and F. Meyer, *Angew. Chemie - Int. Ed.*, **2008**, 47, 9537–9541.

86. J. Ballmann, S. Dechert, E. Bill, U. Ryde and F. Meyer, *Inorg. Chem.*, **2008**, 47, 1586–1596.

87. M. G. G. Fuchs, F. Meyer and U. Ryde, *J. Biol. Inorg. Chem.*, **2010**, 15, 203–212.

88. M. G. G. Fuchs, S. Dechert, S. Demeshko, U. Ryde and F. Meyer, *Inorg. Chem.*, **2010**, 49, 5853–5858.

89. C. Greco, M. Bruschi, J. Heimdal, P. Fantucci, L. De Gioia and U. Ryde, *Inorg. Chem.*, **2007**, 46, 7256–7258.

90. U. Ryde, C. Greco and L. De Gioia, *J Am Chem Soc*, 132, 4512–4513.

91. M. Bruschi, C. Greco, M. Kaukonen, P. Fantucci, U. Ryde and L. De Gioia, *Angew. Chemie - Int. Ed.*, **2009**, 48, 3503–3506.

92. C. Greco, P. Fantucci, L. De Gioia, R. Suarez-Bertoa, M. Bruschi, J. Talarmin and P. Schollhammer, *Dalt. Trans*, 39, 7320–7329.

93. C. Greco, M. Bruschi, P. Fantucci, U. Ryde and L. Dea Gioia, *Chem. - A Eur. J.*, **2011**, 17, 1954–1965.

94. K. Haufschildt, S. Schmelz, T. M. Kriegler, A. Neumann, J. Streif, H. Arai, D. W. Heinz and G. Layer, *J. Mol. Biol.*, **2014**, 426, 3272–3286.

95. H. L. Schubert, E. Raux, A. A. Brindley, H. K. Leech, K. S. Wilson, C. P. Hill and M. J. Warren, *EMBO J.*, **2002**, 21, 2068–2075.

96. M. E. Stroupe, H. K. Leech, D. S. Daniels, M. J. Warren and E. D. Getzoff, *Nat. Struct. Biol.*, **2003**, 10, 1064–1073.

97. B. Kushkuley and S. S. Stavrov, *Biophys J*, **1997**, 72, 899–912.

98. R. Schnell, T. Sandalova, U. Hellman, Y. Lindqvist and G. Schneider, *J. Biol. Chem.*, **2005**, 280, 27319–27328.

99. S. Nakano, M. Takahashi, A. Sakamoto, H. Morikawa and K. Katayanagi, *Protein Sci.*, **2012**, 21, 383–395.

100. T. F. Oliveira, C. Vonrhein, P. M. Matias, S. S. Venceslau, I. A. C. Pereira and M. Archer, *J. Biol. Chem.*, **2008**, 283, 34141–34149.

101. M. Jormakka, S. Törnroth, B. Byrne and S. Iwata, *Science (80-.).*, **2002**, 295, 1863–1868.

102. Zhou; Cai; Holm;, *Inorg. Chem.*, **1996**, 35, 2767.

103. L. Cai and R. H. Holm, *J. Am. Chem. Soc.*, **1994**, 116, 7177–7188.

104. E. N. Mirts, I. D. Petrik, P. Hosseinzadeh, M. J. Nilges and Y. Lu, *Science (80-.).*, **2018**, 361, 1098 LP – 1101.

105. K. Kitaura and K. Morokuma, **1976**, X, 325–340.

106. K. Morokuma, *J. Chem. Phys.*, **1971**, 55, 1236–1244.

107. I. Mayer, *Chem.Phys.Lett.*, **1983**, 97, 270–274.

108. B. a Wittenberg, L. Kampa, J. B. Wittenberg, W. E. Blumberg and J. Peisach, *J. Biol. Chem.*, **1968**, 243, 1854–1862.

109. B. a Wittenberg, L. Kampa, J. B. Wittenberg, W. E. Blumberg and J. Peisach, *J. Biol. Chem.*, **1968**, 243, 1863–1870.

110. J. Peisach, W. E. Blumberg, B. A. Wittenberg and J. B. Wittenberg, *J. Biol. Chem.*, **1968**, 243, 1871–1880.

111. M. D. Clay, C. A. Cosper, F. E. Jenney, M. W. Adams and M. K. Johnson, *Proc. Natl. Acad. Sci. USA*, **2003**, 100, 3796–3801.

112. P. A. M. Dirac, *R. Soc.*, **1929**, 123, 714-- 733.

113. J. C. Slater, *Phys. Rev.*, **1951**, 81, 385–390.

114. P. Hohenberg and W. Kohn, *Phys. Rev.*, **1964**, 136, B864–B871.

115. L. J. Sham and W. Kohn, *Phys. Rev.*, **1965**, 140, A1133–A1138.

116. J. P. Perdew and Y. Wang, *Phys. Rev. B*, **1992**, 45, 244–249.

117. A. D. Becke, *Phys. Rev. A*, **1988**, 38, 3098–3100.

118. R. Ahlrichs, M. Bär, M. Häser, H. Horn and C. Kölmel, *Chem. Phys. Lett.*, **1989**, 162, 165–169.

119. J. Tao, J. P. Perdew, V. N. Staroverov and G. E. Scuseria, *Phys. Rev. Lett.*, **2003**, 91, 146401–146404.

120. S. Grimme, *J. Comput. Chem.*, **2006**, 27, 1787–1799.

121. A. V. Krukau, G. E. Scuseria, J. P. Perdew and A. Savin, *J. Chem. Phys.*, **2008**, 129, 1–8.

122. J. P. Perdew, M. Ernzerhof and K. Burke, *J. Chem. Phys.*, **1996**, 105, 9982–9985.

123. A. D. Becke, *J. Chem. Phys.*, **1993**, 98, 1372–1377.

124. S. Grimme, *J. Chem. Phys.*, **2006**, 124, 034108.

125. O. Treutler and R. Ahlrichs, *J. Chem. Phys.*, **1995**, 102, 346–354.

126. K. Eichkorn, M. Htiser, R. Ahlrichs, K. Eichkorn, O. Treutler, H. Marco and R. Ahlrichs, *Chem. Phys. Lett.*, **1995**, 240, 283–290.

127. K. Eichkorn, F. Weigend, O. Treutler and R. Ahlrichs, *Theor. Chem. Accounts Theory, Comput. Model. (Theoretica Chim. Acta)*, **1997**, 97, 119–124.

128. A. Schäfer, H. Horn and R. Ahlrichs, *J. Chem. Phys.*, **1992**, 97, 2571–2577.

129. S. Grimme, J. Antony, S. Ehrlich and H. Krieg, *J. Chem. Phys.*, **2010**, 132.

130. A. Schäfer, H. Horn and R. Ahlrichs, *J. Chem. Phys.*, **1994**, 100, 5821–5835.

131. P. Deglmann, K. May, F. Furche and R. Ahlrichs, *Chem. Phys. Lett.*, **2004**, 384, 103–107.

132. A. Klamt and G. Schüürmann, *J. Chem. Soc., Perkin Trans. 2*, **1993**, 799–805.

133. A. Klamt, V. Jonas, T. Bürger and J. C. W. Lohrenz, *J. Phys. Chem. A*, **1998**, 102, 5074–5085.

134. E. Sigfridsson and U. Ryde, *J. Comput. Chem.*, **1998**, 19, 377–395.

135. L. Noodleman, *J. Chem. Phys.*, **1981**, 74, 5737.

136. L. Noodleman, T. Lovell, T. Liu, F. Himo and R. A. Torres, *Curr. Opin. Chem. Biol.*, **2002**, 6, 259–273.

137. S. I. Gorelsky, *J. Chem. Theory Comput.*, **2012**, 8, 908–914.

138. T. Lu and F. Chen, *J. Comput. Chem.*, **2012**, 33, 580–592.

139. L. Noodleman, W.-G. Han Du, J. A. Fee, A. W. Götz, R. C. Walker, W.-G. H. Du, J. A. Fee, A. W. Götz and R. C. Walker, *Inorg. Chem.*, **2014**, 53, 6458–6472.

140. P. Su and H. Li, *J. Chem. Phys.*, **2009**, 131.

141. T. Ziegler and A. Rauk, *Theor. Chim. Acta*, **1977**, 46, 1–10.

142. M. Mitoraj and A. Michalak, *J. Mol. Model.*, **2007**, 13, 347–355.

143. M. P. Mitoraj, A. Michalak and T. Ziegler, *J. Chem. Theory Comput.*, **2009**, 5, 962–975.

144. A. Michalak, M. Mitoraj and T. Ziegler, *J. Phys. Chem. A*, **2008**, 112, 1933–1939.

145. P. A. Janick and L. M. Siegel, *Biochemistry*, **1983**, 22, 504–515.

146. H. Nagao, M. Nishino, Y. Shigeta, T. Soda, Y. Kitagawa, T. Onishi, Y. Yoshioka and K. Yamaguchi, *Coord. Chem. Rev.*, **2000**, 198, 265–295.

147. E. Koch, in *Correlated Electrons. From Models to Materials*, eds. E. Pavarini, E. Koch, F. Anders and M. Jarell, Forschungszentrum Jülich GmbH Institute for Advanced Simulation, Julich, **2012**, p. 31.

148. M. Swart and M. Costas, *Spin States in Biochemistry and Inorganic Chemistry: Influence on Structure and Reactivity*, **2015**.

149. L. Noodleman, D. A. Case, J.-M. Mouesca and B. Lamotte, *J. Biol. Inorg. Chem.*, **1996**, 1, 177–182.

150. L. Pauling, *The Nature of the Chemical Bond*, Cornell University Press, New York, **1960**.

151. R. Dronskowski, *Computational Chemistry of Solid State Materials*, Wiley, Weinheim, **2005**.

152. M. Kaupp, B. Metz and H. Stoll, *Angew. Chem., Int. Ed.*, **2000**, 39, 4607–4609.

153. M. Boggio-Pasqua, A. I. Voronin, P. Halvick and J. C. Rayez, *J. Mol. Struct. THEOCHEM*, **2000**, 531, 159–167.

154. A. Zerr, G. Miehe, G. Serghiou, M. Schwarz, E. Kroke, R. Riedel, H. Fueß, P. Kroll and R. Boehler, *Lett. to Nat.*, **1999**, 400, 340–342.

155. A. Pecchia, G. Penazzi, L. Salvucci and A. Di Carlo, *New J. Phys.*, **2008**, 10.

156. A. Pecchia and A. Di Carlo, *Reports Prog. Phys.*, **2004**, 67, 1497–1561.

157. J. C. Cuevas and E. Scheer, *Molecular Electronics. An Introduction to Theory and Experiment*, World Scientific, Singapore, **2010**.

158. K. Yoshizawa, *Acc. Chem. Res.*, **2012**, 45, 1612–1621.

159. S. Priyadarshy, S. S. Skourtis, S. M. Risser and D. N. Beratan, *J. Chem. Phys.*, **1996**, 104, 9473–9481.

160. A. Nitzan, *J. Phys. Chem. A*, **2001**, 105, 2677–2679.

161. B. Delley, *J. Chem. Phys.*, **1990**, 92, 508–517.

162. 2017 Dassault Systèmes BIOVIA, Materials Studio, 2017, San Diego: Dassault Systèmes.

163. 2017. L.V. Skripnikov, Chemissian Version 4.53, Visualization Computer Program, www.chemissian.com, .

164. F. T. J. C. C. 2004 O.-12. http://www. rbvi. ucsf. edu/chimer. . UCSF Chimera--a visualization system for exploratory research and analysis. Pettersen EF, Goddard TD, Huang CC, Couch GS, Greenblatt DM, Meng EC, .

165. L. Noodleman and D. A. Case, *Adv. Inorg. Chem.*, **1992**, 38, 423.

166. J. P. Launay and M. Verdaguer, *Electrons in Molecules*, Oxford University Press, Oxford, revised ed., **2018**.

167. J. J. Warren, M. E. Ener, A. Vlček, J. R. Winkler and H. B. Gray, *Coord. Chem. Rev.*, **2012**, 256, 2478–2487.

168. J. Geng, K. Dornevil, V. L. Davidson and A. Liu, *Proc. Natl. Acad. Sci.*, **2013**, 110, 9639–9644.

169. N. A. Tarboush, L. M. R. Jensen, E. T. Yukl, J. Geng, A. Liu, C. M. Wilmot and V. L. Davidson, *Proc. Natl. Acad. Sci.*, **2011**, 108, 16956–16961.

170. P. L. Dutton, C. C. Page, C. C. Moser and X. Chen, *Nature*, **1999**, 402, 47–52.

171. C. C. Moser, S. E. Chobot, C. C. Page and P. L. Dutton, *Biochim. Biophys. Acta - Bioenerg.*, **2008**, 1777, 1032–1037.

172. R. Pietri, E. Román-Morales and J. López-Garriga, *Antioxid. Redox Signal.*, **2010**, 15, 393–404.

173. B. B. Ríos-González, E. M. Román-Morales, R. Pietri and J. López-Garriga, *J. Inorg. Biochem.*, **2014**, 133, 78–86.

174. H. D. Arbelo-Lopez, N. A. Simakov, J. C. Smith, J. Lopez-Garriga and T. Wymore, *J. Phys. Chem. B*, **2016**, 120, 7319–7331.

175. J. A. Berzofsky, J. Peisach and J. A. Alben, *J. Biol. Chem.*, **1972**, 247, 3774–3782.

176. P. R. O. de Montellano, *Curr. Opin. Chem. Biol.*, **2000**, 221–227.

177. A. M. V Brânzanic, U. Ryde and R. Silaghi-dumitrescu, *J. Inorg. Biochem.*, **2020**, 203, 110928.

178. R. Silaghi-Dumitrescu, *Stud. Univ. Babes-Bolyai, Chem.*, **2007**, 52, 127–130.

179. R. Silaghi-Dumitrescu, *J. Biol. Inorg. Chem.*, **2004**, 9, 471–476.

180. A. M. V. Brânzanic, U. Ryde and R. Silaghi-Dumitrescu, *Chem. Commun.*, **2019**, 55, 14047–14049.

181. D. A. Bryant, C. N. Hunter and M. J. Warren, *J. Biol. Chem.*, **2020**, 295, 6888–6925.

182. G. Frenking and A. Krapp, *J. Comput. Chem.*, **2007**, 28, 15–24.

List of Publications

1. **A. M. V. Brânzanic**, A. Lupan and R. B. King, *Organometallics*, **2014**, 33, 6433–6451.

2. **A. M. V Brânzanic**, A. Lupan and R. B. King, *J. Organomet. Chem.*, **2015**, 792, 74–80.

3. **A. M. V. Brânzanic**, A. Lupan and R. B. King, *Dalt. Trans.*, **2015**, 44, 7355–7363.

4. **A. M. V. Brânzanic**, A. Lupan and R. B. King, *Dalt. Trans.*, **2016**, 45, 9354–9362.

5. M. Surducan, **A. M. V. Brânzanic** and R. Silaghi-Dumitrescu, *Int. J. Quantum Chem.*, **2018**, 118, 2–10.

6. **A. M. V. Brânzanic**, U. Ryde and R. Silaghi-Dumitrescu, *Chem. Commun.*, **2019**, 55, 14047–14049.

7. A. A. A. Attia, **A. M. V. Brânzanic**, A. Munõz-Castro, A. Lupan and R. B. King, *Phys. Chem. Chem. Phys.*, **2019**, 21, 17779–17785.

8. I. A. Dereven’kov, L. Hannibal, P. A. Molodtsov, **A. M. V. Brânzanic**, R. Silaghi-Dumitrescu and S. V. Makarov, *Inorganica Chim. Acta*, **2020**, 499, 119215.

9. **A. M. V Brânzanic**, U. Ryde and R. Silaghi-Dumitrescu, *J. Inorg. Biochem.*, **2020**, 203, 110928.